

UNCLASSIFIED

AD NUMBER

AD812266

LIMITATION CHANGES

TO:

Approved for public release; distribution is unlimited.

FROM:

Distribution authorized to U.S. Gov't. agencies and their contractors; Critical Technology; MAR 1967. Other requests shall be referred to Rome Air Development Center, Attn: EMLI, Griffiss AFB, NY 13441-5700. This document contains export-controlled technical data.

AUTHORITY

RADC ltr, 14 Jul 1969

THIS PAGE IS UNCLASSIFIED

RADC-TR-66-606, Volume I
Final Report



HIGH VOLTAGE POWER LINE SITING CRITERIA
Volume I. High Voltage Power Line Test Results,
Analysis and Appendices

W. E. Pakala
E. R. Taylor, Jr.
R. T. Harrold

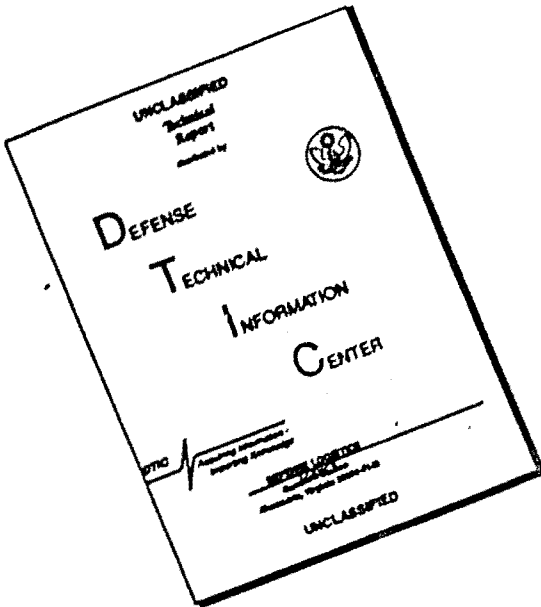
Westinghouse Electric Corp.

TECHNICAL REPORT NO. RADC-TR-66-606
March 1967

This document is subject to special
export controls and each transmittal
to foreign governments, foreign na-
tionalis or representatives thereto may
be made only with prior approval of
RADC (EMLI), GAFB, N.Y. 13440

Rome Air Development Center
Research and Technology Division
Air Force Systems Command
Griffiss Air Force Base, New York

DISCLAIMER NOTICE



**THIS DOCUMENT IS BEST
QUALITY AVAILABLE. THE COPY
FURNISHED TO DTIC CONTAINED
A SIGNIFICANT NUMBER OF
PAGES WHICH DO NOT
REPRODUCE LEGIBLY.**

When US Government drawings, specifications, or other data are used for any purpose other than a definitely related government procurement operation, the government thereby incurs no responsibility nor any obligation whatsoever; and the fact that the government may have formulated, furnished, or in any way supplied the said drawings, specifications, or other data is not to be regarded, by implication or otherwise, as in any manner licensing the holder or any other person or corporation, or conveying any rights or permission to manufacturer, use, or sell any patented invention that may in any way be related thereto.

Do not return this copy. Retain or destroy.

HIGH VOLTAGE POWER LINE SITING CRITERIA

Volume I. High Voltage Power Line Test Results,
Analysis and Appendices

W. E. Pakala

E. R. Taylor, Jr.

R. T. Harrold

Westinghouse Electric Corp.

This document is subject to special
export controls and each transmittal
to foreign governments, foreign na-
tionals or representatives thereto may
be made only with prior approval of
RADC (EMLI), GAFB, N.Y. 13440

FOREWORD

This final report was prepared by W. E. Pakala, E. R. Taylor, Jr., and R. T. Harrold of Westinghouse Electric Corporation, Electric Utility Headquarters Department, Pittsburgh, Pennsylvania, under Contract AF30 (602)-3822, project number 4540, task number 4540C2. Secondary report number is 66-8E0-RADIO-RI. RADC project engineer is Jacob Scherer (EMCVI-1).

Document contains information embargoed from release to Sino-Soviet Bloc Countries by AFR 400-10, "Strategic Trade Control Program."

This report has been reviewed and is approved.

Approved: *Jacob J. Scherer*
JACOB SCHERER
Interf Anal & Control Sec
Vulnerability Reduction Br

Approved: *Richard M. CoSEL*
RICHARD M. COSEL
Colonel, USAF
Chief, Communications Division

FOR THE COMMANDER:

Irving J. Gabelman
IRVING J. GABELMAN
Chief, Advanced Studies Group

Abstract

The purpose of this contract on High Voltage Power Line Siting Criteria is to determine the various factors involved and their effects on radio noise from power lines so that a communication site can be selected which will not be seriously affected by radio interference from existing lines or from proposed lines in the vicinity of the communication site.

Field strength measurements were made from 60 cycles to 1000 Mc/s on both wood pole and steel tower lines from 2.4 kV to 345 kV inclusive. Some measurements were attempted below 60 cycles without success. Measurements were also made with an artificial gap connected to a phase conductor at the tower. This was done in order to have a controllable and powerful radio noise generator for the measurement of spectra at various distances from the line. These measurements have been applied to estimation or prediction of radio noise with respect to the most important factors of distance from line and the frequency and to other factors such as line height, and antenna height and polarization.

The report also includes (1) laboratory measurements of conductor corona type radio noise with conductors of different diameters and different surface conditions. (These measurements are applicable in the estimation of the magnitude of radio noise generation by extra high voltage line conductor corona) (2) laboratory measurements of the frequency spectra of artificial gap-type radio noise generator and corona. (3) A bibliography of American and Foreign literature of importance to the problem of radio noise from power lines. (4) Application of antenna theory to radiation from lines and measurements with different antenna heights.

The field measurements were made on 18 lines (2.4 - 345 kV) in six different states of the United States of America. During these measurements several local sources were found which in these cases would determine how far away from line a communication site should be. It can be concluded that all lines, if they have these local sources, can produce radio noise several miles away from the line at certain frequencies. Some lines may have sources on each pole which will cause radio noise all along the line. In most cases these local sources can be found and eliminated. These powerful local sources do occur occasionally on lines above 70 kV, however, they are much more prevalent on lines below 70 kV. With respect to lines from 110 kV to 345 kV the radio noise generation is nearly always due to corona on conductors, hardware, and insulators. These types exist all along the line and cannot be completely eliminated. It would not be economical to build lines free of conductor corona at all times in all types of weather. In this report the results are applied and predictions are

made on radio noise from power lines for the two voltage ranges, 2.4 - 70 kV and 110 - 345 kV.

CONTENTS

	<u>Page No.</u>
Foreword	ii
List of Figures	ix
Scope	1
1. Introduction	2
2. Generation of Radio Noise by Power Lines	3
2.1 Electrical Characteristics of Gap Type Discharges	4
2.2 Electrical Characteristics of the Corona Discharge	4
3. Instrumentation	6
3.1 The Principal Instruments	6
3.2 Antennas Used	7
3.3 Calibration of Instruments	7
4. Methods of Measurement	8
4.1 The Artificial Gap-Type Radio Noise Generator	8
4.2 Power Lines Measured for Radio Noise	9
4.3 Laboratory Measurements	10
4.3.1 Conducted Measurements	10
4.3.2 Artificial Gap Spectrum	10
4.3.3 Corona Source Spectrum	10
5. Discussion of Measurements with Power Lines Normal	11
5.1 Frequency Spectrum for 2.4 kV Line	11
5.2 Frequency Spectrum for 4.16 kV Line	11
5.3 Frequency Spectrum for 8 kV Line	12
5.4 Frequency Spectrum for 12.5 kV Line	12
5.5 Frequency Spectrum for 12.5-34.5 kV Dual Line	12
5.6 Frequency Spectrum for 34.5 kV Line	13
5.7 Frequency Spectra for 46 kV Line-- Local Source Found	13
5.7.1 Frequency Spectrum at Local Source	13
5.7.2 Test Location at Single Circuit 46 kV Line	13
5.8 Frequency Spectrum of 69 kV Line	14

	<u>Page No.</u>
5.9 Frequency Spectrum of 110 kV Line	14
5.10 Frequency Spectrum of 138 kV Line	14
5.11 Frequency Spectrum of 161 kV Line	14
5.12 Frequency Spectrum of 244 kV Line	15
5.13 Frequency Spectra of 345 kV HCST Line	15
5.14 Frequency Spectra of 345 kV VCDC Line	15
5.15 Frequency Spectrum of 345 kV VCSC Line	15
5.16 Frequency Spectra of 345 kV HCWP Line	16
5.16.1 Test Location at T119	15
5.16.2 Test Location at T192	16
5.16.3 Test Location at T101	17
5.17 Frequency Spectrum near 46 kV Sub-station	17
6. Conductor Gradients of the Power Lines Tested	17
7. Analysis and Discussion of Data and Conclusions for Lines Normal	18
7.1 Analysis of Test Results for Low Voltage Lines Normal	18
7.2 Analysis of Test Results for High Voltage Lines Normal	21
7.2.1 Sub-Audio Measurements (3 to 45 cycles)	21
7.2.2 Low Frequency Measurements on HV Lines	22
7.2.3-7.2.12 Measurements in Range of 0.015 - 1000 Mc/s	22-24
8. Discussion of Tests with the Artificial Gap	24
8.1 Measurements with Artificial Gap on 345 kV HCST Line	24
8.1.1 Lateral Profiles of Field Strength with Artificial Gap at T129	25
8.1.2 Frequency Spectra with Artificial Gap at T129	26
8.1.3 Effect of Distance from Line on Field Strength	26
8.1.4 Attenuation Down the Line	27
8.2 Measurements with Artificial Gap on 345 kV VCDC Line	27
8.2.1 Lateral Profiles of Field Strength with Artificial Gap at Tower 473	28
8.2.2 Procedure in the Measurement of Frequency Spectra	28
8.2.3 Frequency Spectra with Artificial Gap	29

	<u>Page No.</u>
8.3 Measurements with Artificial Gap on 345 kV Wood Pole Line	30
8.4 Measurements with Artificial Gap on 244 kV HCST Line	30
8.4.1 The Lateral Profiles	30
8.4.2 Frequency Spectra at Several Distances	30
8.4.3 Comparison of Frequency Spectra on Opposite Sides of Tower	31
8.4.4 Effect of Distance from 244 kV Line	31
8.5 Measurements with Artificial Gap on 161 kV HCST Line	31
8.5.1 Lateral Profiles	31
8.5.2 Frequency Spectra for 161 kV Line at Several Distances	31
8.5.3 Effect of Lateral Distances from Line Tower	32
8.6 Measurements with Artificial Gap on 110 kV Wood Pole Line	32
8.7 Measurements on 345 kV Wood Pole Line with Natural Gap	33
8.7.1 Frequency Spectra near Tower 192	33
8.7.2 Lateral Profiles near Tower 119	33
9. Conclusions from Tests with Artificial Gap	33
10. Corrections for Antenna Height for Frequencies 25 Mc/s and Higher	34
11. Recommendations	35
Appendix I Analysis of Laboratory Tests to Determine the Effect of Conductor Diameter and the Shape and Size of Conductor Protrusions on Radio Noise Generation.	136
Appendix II Calculation of Electric Field near a Transmission Line.	157
Appendix III Radio Noise - High Voltage Transmission Line Conductor Gradient Calculations	162
Appendix IV Application of Antenna Theory to Radiation From Lines.	177
Appendix V Effect of Antenna Height	290

Page No.

Appendix VI Low Frequency Measurements, 60 cps
 to 15 kc.

313

LIST OF FIGURES

	<u>Page No.</u>
Fig. 1 Frequency Spectrum of 5/16" Gap in Air as Measured in Laboratory.	36
Fig. 2 Corona on High Voltage Conductors and the Ground Wires on a Test Line at 10,700 Foot Altitudes.	37
Fig. 3 Frequency Spectrum of Corona Radio Noise Voltage for Conical Rivet.	38
Fig. 4 Ionization by Collision (Electrons in Air at Atmospheric Pressure).	39
Fig. 5 Photograph of Van with Antenna on Roof.	40
Fig. 6 Artificial Gap Type Radio Noise. Generator, 18 kV _{rms} B.D. Voltage (Floating) Approx. to 1/4 scale.	41
Fig. 7 Corona and Gap Type Radio Noise Generators.	42
Fig. 8 Test Location at 2.4 kV Wood Pole Line.	43
Fig. 9 Test Location at 4.16 kV Wood Pole Line.	44
Fig. 10 Test Location at 8 kV Wood Pole Line.	45
Fig. 11 Test Locations at 12.5 kV Wood Pole Line.	46
Fig. 12 Test Location at 34.5 and 12.5 kV Wood Pole Line.	47
Fig. 13 Test Location at 34.5 kV Wood Pole Line.	48
Fig. 14 Test Location on Double Circuit 46 kV Line.	49
Fig. 15 Test Location on Single Circuit 46 kV Line.	50
Fig. 16 Test Locations at 69 kV Horizontal Line.	51
Fig. 17 Test Locations at 115 kV H-Frame Wood Pole Line.	52
Fig. 18 Test Locations at 138 kV Wood Pole Line.	53
Fig. 19 Test Locations at 161 kV Horizontal Line.	54

	<u>Page No.</u>
Fig. 20 Test Locations at 244 kV Steel Tower Line.	55
Fig. 21 Test Locations Along 345 kV Horizontal Line.	56
Fig. 22 Test Locations 345 kV Vertical Line.	57
Fig. 23 Test Locations at 345 kV Single Circuit Vertical Line.	58
Fig. 24 Test Locations at Tower 119 on 345 kV Wood Pole Line.	59
Fig. 25 Test Locations at 345 kV Wood Tower Line Where Natural Gap-Type Discharge was Found.	60
Fig. 26 Test Locations at Tower 101 on 345 kV Wood Pole Line.	61
Fig. 27 Photographs of 2.4, 4.16, and 8 kV Lines and Local Source.	62
Fig. 28 Photographs of 12.5 and 34.5 kV Lines Measured.	63
Fig. 29 Photographs of 46 and 69 kV Lines and 46 kV Substation.	64
Fig. 30 Photographs of 115, 138, 161, and 244 kV Lines Measured.	65
Fig. 31 Photographs of Four 345 kV Lines Measured.	66
Fig. 32 2.4 kV WP Line Frequency Spectrum at 50 ft. Laterally From Pole.	67
Fig. 33 4.16 kV WP Line Frequency Spectrum at 50 ft. Laterally From Pole.	68
Fig. 34 8 kV WP Line Frequency Spectrum at 50 ft. Laterally From Pole.	69
Fig. 35 12.5 kV WP Normal Line Frequency Spectrum at 50 ft. From Pole.	70
Fig. 36 12.5-34.5 kV Dual Circuit Wood Pole Line with Natural Local Source.	71
Fig. 37 34.5 kV Single Circuit Wood Pole-Normal Line Spectrum.	72

	<u>Page No.</u>
Fig. 38 46 kV WP Line With and Without Source at Pole.	73
Fig. 39 46 kV WP Normal Line Frequency Spectra.	74
Fig. 40 69 kV HCWP Normal Line Frequency Spectrum at 200 Feet From Tower.	75
Fig. 41 110 kV WP Normal Line in Light Rain at 66 ft. From Center Line at Tower.	76
Fig. 42 138 kV HCWP Line Frequency Spectra.	77
Fig. 43 161 kV HCST Normal Line Frequency Spectrum at 200 ft. From Tower.	78
Fig. 44 244 kV HCST Normal Line Frequency Spectra in Fair Weather and With Snow and Sleet.	79
Fig. 45 345 kV HCST Line Frequency Spectra in Fair Weather and in Rain.	80
Fig. 46 345 kV VCDCST Normal Line Frequency Spectra 200 ft. From Tower.	81
Fig. 47 345 VCSC Normal Line Frequency Spectra in Air Weather and Rain.	82
Fig. 48 345 kV HCWP Line Frequency Spectrum 200 ft. From Tower 119.	83
Fig. 49 345 kV HCWP Line Frequency Spectra at 200 ft. North with Natural Gap.	84
Fig. 50 345 kV HCWP Line Frequency Spectra Near Tower 101.	85
Fig. 51 Maximum Conductor Gradient to Voltage of Lines Tested.	86
Fig. 52 Conductor Critical Gradient and Line Conductor Gradients.	87
Fig. 53 Radio Noise Near 46 kV Substation.	88
Fig. 54 345 kV HCST Line Lateral Profiles at 0.154 Mc/s with Artificial Gap.	89

	<u>Page No.</u>
Fig. 55 345 kV HCST Line Lateral Profiles at 0.5 Mc/s with Artificial Gap.	90
Fig. 56 345 kV HCST Line Lateral Profiles at 1.03 Mc/s with Artificial Gap.	91
Fig. 57 345 kV HCST Line Lateral Profiles at 3.05 Mc/s with Artificial Gap.	92
Fig. 58 345 kV HCST Line Lateral Profiles at 10.05 Mc/s with Artificial Gap.	93
Fig. 59 345 kV HCST Line Lateral Profiles at 22.3 Mc/s with Artificial Gap.	94
Fig. 60 345 kV HCST Line Lateral Profiles at Mid-Span Near T129.	95
Fig. 61 345 kV HCST Line Frequency Spectra at Several Lateral Distances with Artificial Gap.	96
Fig. 62 345 kV HCST Line at 0.15-24 Mc at Several Lateral Distances with Artificial Gap.	97
Fig. 63 345 kV HCST Line at 24-390 Mc at Several Lateral Distances with Artificial Gap.	98
Fig. 64 345 kV Line at 24-400 Mc at Several Lateral Distances with Artificial Gap. (Dipole Vertical).	99
Fig. 65 345 kV HCST Line Frequency Spectra at Several Longitudinal Distances From Artificial Gap.	100
Fig. 66 345 kV VCST DC Line Lateral Profiles at Mid-Span Near Gap on Top Conductor T473.	101
Fig. 67 345 kV VCST DC Line Lateral Profiles at Mid-Span 3.85 Mile From Artificial Gap.	102
Fig. 68 345 kV VCST DC Line Lateral Profiles at Mid-Span Near Tower with Gap on Bottom Conductor at Tower 473.	103
Fig. 69 345 kV VCST DC Line Lateral Profiles at Mid-Span 3.85 Mile From Artificial Gap.	104

	<u>Page No.</u>
Fig. 70 345 kV VCST DC Line Lateral Profiles at Mid-Span with Line Normal (T472-473).	105
Fig. 71 345 kV VCDC Line - Comparison at Frequency Spectra with Artificial Gap at Different Heights.	106
Fig. 72 345 kV VCDS Line Spectra 3.85 Miles Down the Line From Artificial Gap.	107
Fig. 73 345 kV VCDGST Line Attenuation for 3.85 Miles 24-125 Mc with Artificial Gap.	108
Fig. 74 345 kV VCDGST Line Lateral Attenuation 0.15 ⁴ -22.3 Mc with Gap on Center Phase.	109
Fig. 75 345 kV VCDGST Line Lateral Attenuation 0.15-24 Mc with Gap on Center Phase.	110
Fig. 76 345 kV VCDGST Line Lateral Attenuation 24-1000 Mc with Gap on Center Phase.	111
Fig. 77 345 kV VCDGST Line Lateral Attenuation 24-1000 Mc with Gap on Top Phase.	112
Fig. 78 345 kV VCDC Line Frequency Spectra 0.15-24 Mc with Artificial Gap at Tower on Center Phase.	113
Fig. 79 345 kV HCWP Line Lateral Attenuation 0.15 ⁴ -24 Mc with Artificial Gap at T119.	114
Fig. 80 Recording of Field Strength Variation with Distance from Tower.	115
Fig. 81 244 kV HCST Line Lateral Profiles at Tower with Artificial Gap on East Phase.	116
Fig. 82 244 kV HCST Line Lateral Profiles Near Mid-Span by Tower with Artificial Gap.	117
Fig. 83 244 kV HCST Line Lateral at Mid-Span 8.23 Mile from Tower with Artificial Gap.	118
Fig. 84 244 kV HCST Normal Line Lateral Profiles Near Mid-Span.	119
Fig. 85 244 kV HCST Line Lateral Profiles at Tower 161.	120

	<u>Page No.</u>
Fig. 86 244 kV HCST Line Frequency Spectra with Artificial Gap.	121
Fig. 87 244 kV HCST Line Frequency Spectra on East and West Side of Tower with Artificial Gap on East Phase.	122
Fig. 88 244 kV HCST Line Lateral Attenuation .015-0.25 Mc with Artificial Gap.	123
Fig. 89 244 kV HCST Line Lateral Attenuation 0.15-24 Mc Range with Artificial Gap on East Phase.	124
Fig. 90 161 kV HCST Line Lateral Profiles from Tower with Artificial Gap on No. Phase.	125
Fig. 91 161 kV HCST Line Frequency Spectra with Artificial Gap on North Phase.	126
Fig. 92 161 kV HCST Line Spectra 0.154-24 Mc at Towers and Mid-Span with Artificial Gap.	127
Fig. 93 161 kV HCST Line Attenuation 0.015-0.25 Mc with Artificial Gap on North Phase.	128
Fig. 94 161 kV HCST Line Lateral Attenuation Range 0.154-24 Mc with Artificial Gap.	129
Fig. 95 110 kV HCWP Line Spectra with Artificial Gap.	130
Fig. 96 345 kV HCWP Line Lateral Profiles at 9 ft. East of T119.	131
Fig. 97 345 kV HCWP Line Lateral Profiles at Mid-Span with Line Normal (T118-119).	132
Fig. 98 345 kV HCWP Line Spectra From 200-21000 Feet Lateral to Tower with Natural Gap.	133
Fig. 99 345 kV HCWP Line Lateral Attenuation 0.154-24 Mc with Natural Gap at T192.	134
Fig. 100 345 kV HCWP Line Lateral Attenuation 10-250 Mc with Line Normal.	135

EVALUATION

This effort has developed simplified procedures which can be used to determine the field strength of noise generated by high voltage transmission and distribution lines. The procedures are applicable for lines in the voltage range of 2.4 to 350 kilovolts (kV), and for a frequency range of noise from 60 hertz to 1 GHz.

The procedures will be used to develop siting criteria for Air Force C&E installations when located in the vicinity of these lines. This effort is a part of an R&D program to develop good engineering standards for siting AF C&E installations.

Jacob Scherer
JACOB SCHERER
Project Engineer

Volume I

Scope

This Volume I, of the complete report consisting of three volumes, includes Foreword and Abstract for the complete report and describes instrumentation, test methods and includes results of field strength measurements of radio noise near high voltage power lines and discussion and analysis of these results. Several appendices are included which are necessary in the analysis and in the development of the method of prediction described and used in Volume II of the report on high voltage power line siting criteria.

1. Introduction

The purpose of the radio noise measurements and analysis described is to determine the various radio noise factors of ac power transmission lines from 2.4 to 345 kilovolts and to develop techniques for use in the selection of a communication site which will not be seriously affected by radio interference from existing or proposed power transmission lines. The frequency range of measurements was 60 cycles to 1000 Mc/s.

Power line radio noise can be generated by line components such as hardware, insulators, conductors, line apparatus etc. In many cases the generation is because of faulty components, corrosion between metal parts, discharges between unbonded or floating metal parts and hardware, and between neutral conductors and ground and pole guys and because of conductor corona. Most of the possible generation sources mentioned, can be found and, except for conductor corona, can be and have been eliminated on their lines by electric utilities. Radio noise from conductor corona is the principal problem on extra high voltage lines (EHV) (345-1000 kV) and to a lesser extent on lines down to 100 kV. A great deal of radio noise testing and analysis has been done in many countries of the world in the EHV transmission field, especially in the frequency range from about 0.2 to 1.6 Mc/s. The developments in this field of EHV transmission are given in "Status Report on EHV Transmission Design" by J. K. Dillard, IEEE Transactions on Power Apparatus and Systems," June, 1966/Vol. PAS-85/No. 6. It is stated that transmission line voltages have risen to 500 kV and 750 kV in North America and plans are for about 1200 miles of 700 kV transmission, 9000 miles of 500 kV, 6000 miles of new 345 kV, and 1500 miles of high voltage direct current transmission. The extent of this field and work is obvious from this status report and from a review of the bibliography included in this report.

In this report power lines will be considered in two classes, (1) lines below 70 kV, and (2) lines from 110-345 kV. This separation is based on the fact that all lines below 70 kV can be made free of conductor corona generation under normal conditions and that higher voltage lines, especially EHV lines, generate radio noise and cannot be constructed free of radio noise for economic reasons. For these lines a prediction technique is developed which is based on laboratory measurements on conductors and the comparison of radio noise levels of lines will be based on field measurements and line parameters such as the conductor diameter and gradient, height, and phase spacing.

The radio noise field strengths in the vicinity of lines were measured under three conditions with respect to radio noise. These were (1) under normal conditions, (2) with natural gap in line, and (3) with artificial gap connected to one phase conductor at a time.

The artificial gap was used as a measurement tool to increase the radio noise level from a line so that the field strength could be measured farther away and at the higher frequencies with the radio noise meters and amplifiers available. In one case a natural source at a tower could be detected several miles away at some frequencies.

It was found that the measured field strength decreases away from the line approximately inversely as the first, second, or third power of the distance from the line depending on the frequency and that the field strength is not the same on both sides of line or tower when the antenna is not too far from a local source, such as a natural gap or the artificial gap. As the antenna is moved along the line the field strength on the two sides of the line becomes more symmetrical, as would be expected.

This report includes bibliography, laboratory tests and analysis, calculation of field strength near lines and far away, calculation of line conductor gradients, comparison of dipole antenna at different heights, and lateral distances from the line, field strength measurements on lines from 2.4 - 345 kV and application of results to the estimation of the radio noise level as a function of the lateral distance to the line and frequency.

2. Generation of Radio Noise by Power Lines

Radio noise on power lines is caused by partial electrical discharges, such as corona, by electrical discharges at small gaps in insulators, between hardware parts due to excessive electric stress across wood or due to corrosion between metal parts, at small gaps between neutrals and hardware, ground wires and hardware, and by many types of corona or gap sources in electrical apparatus if defective or damaged, or if improper design, mounting and or use.

Interference was discovered in the early days of radio and measures were taken by electric utilities and electrical manufacturers to reduce or eliminate radio noise from lines and apparatus. Radio-free pintype insulators were developed and lines with these insulators were found to be quite free of radio noise whereas lines with comparable size plain pintype insulators were not nearly as good. Laboratory and shop test methods for radio noise were developed and adopted as standard for high voltage apparatus as early as 1938. Radio influence voltage (RIV) limits were later established for high voltage apparatus by the National Electrical Manufacturers Association (NEMA).

With the advent of extra high voltage lines (EHV) it was found early at the Tidd Project (Ref. 37, App. VII, Part 3) that conductor corona formed at conductor gradients well below the

theoretical critical gradient and that EHV line design would require consideration of radio noise and corona loss.

2.1 Electrical Characteristics of Gap Type Discharges

The gap-type radio noise source is a more or less complete electrical discharge mainly in air between two metal parts. The type of discharge permits very low (μ) cycles currents, since one or both of the electrodes concerned have a high 60 cycle impedance to line conductors or to ground. These gap-type discharges may be localized or they may be distributed along the line. They are the principal cause of radio noise occurring on low voltage lines, below 70 kV. The artificial gap-type radio noise generator had an electrode spacing of 5/16 inches and was used on some of the lines tested. It was used with one electrode connected to the line conductor and the other electrode was left floating. This gap-type radio noise generator will produce broadband radio noise which can be measured up to 1000 Mc/s with dipole antenna 200 feet from line. The frequency spectrum of this gap as measured in the laboratory is shown on Fig. 1.

2.2 Electrical Characteristics of the Corona Discharge

The generation of radio noise by conductor corona is by means of the electrical discharge, usually called corona, occurring at or near the conductor surface. Figure 2 shows how intense conductor corona can be at excessive gradients on the conductors including the ground wires. Corona is defined as "a luminous discharge due to ionization of the air surrounding a conductor around which exists a voltage gradient exceeding a certain critical value." Many aspects on lines are unknown, undefined, and a calculation of radio noise generation, at least for the conductor diameters used for EHV lines, is not possible with the present state of knowledge. A short resume of the known corona processes for the case of a conductor will be given.

The basic physical process is that of electron multiplication or avalanche formation. The electric gradient in the vicinity of the line conductor is the highest gradient, and if this gradient or electric stress is sufficiently high, any electrons in the air around the conductor will ionize the gas molecules, and electrons produced by this ionization will produce an avalanche. If an additional electron is formed in this gradient by some process from the original electron avalanche, a new avalanche is formed by this secondary process and a self-maintaining discharge is developed. Figure 4 shows how the efficiency of this process increases with the electric gradient.

In the case of the transmission line conductor, it is believed that the important secondary process is the ejection of electrons from gas molecules by high energy ultraviolet light (photoionization) generated by the original avalanche. It has been found by several investigators that the radio noise generated when the conductor is at positive potential is significantly greater, at the gradients generally used for line conductors, than it is with the conductor at negative potential. Ref. 45, App. VII, Pt. 2. In the case of a positive line conductor, the cathode is so far away that cathode emission is of no consequence, and as stated before, the only secondary process existing in this case is photoionization of the gas.

The positive corona which is the principal cause of radio interference is of the streamer type; that is, a compact and bright filament starting from the conductor and extending out and ending in a tree-like discharge array. This type of discharge can be heard by ear directly and readily photographed at night. Sharp current pulses occur and radio noise is produced. Some aspects of this streamer corona are known. These streamers propagate at very high velocities 2×10^7 to over 10^8 cm per sec. Also because of the electric field intensification by the streamer itself, it propagates into fields which are below the critical breakdown as based on the non-uniform field around the conductor with no ionization. Near the conductor surface, however, an opposite effect occurs in that the field is reduced which effect tends to inhibit the streamer. The current pulse formed is of the form $i = te^{-\alpha t}$. The positive corona pulse for a 5 cm advance of streamer at a velocity of 5×10^7 cm/sec. gives a rise time of 10^{-7} seconds. The measured spectrum of corona from a rivet mounted on the surface of a 1.05 inch diameter smooth tube is shown on Fig. 3.

When the conductor is at sufficiently high negative potential ionization occurs. In this case, the cathode emission process prevails and since this process is more efficient than the gas photoemission process with conductor positive, it is expected that negative corona starts at lower conductor gradients than does positive corona. The current pulses have longer rise times and their peak values will not reach the magnitude of the positive pulses. The negative corona pulses will give considerably lower readings as has been found by measurement using an oscilloscope in the radio noise meter peak detector output.

When streamer corona forms at a "point" on the conductor two pulse fields will exist. Near the streamer a localized or direct field is formed, and along the line the indirect field is developed due to the pulses traveling down the line. For design of EHV lines only the indirect field is considered and the most significant measurements are made at some distance from the streamer locations.

Gap-type sources can and do occur on EHV lines, however, they occur rarely and the cause can usually be eliminated when necessary. The principal radio noise source on EHV lines is the corona-type discharges which may form at hardware, insulators, at burrs and scratches on the conductor surface and by discharges of various kinds at towers. Since radio noise may be caused by particles, such as raindrops, snow, aerosols, dirt, vegetation and insects, that may pass within the near electric field of the conductor or be on the surface of the conductor, radio noise generation becomes variable and determination of the average radio noise level of a line is usually made by comparison methods based on long term recordings or several fair weather readings and on measurements made in rain. With respect to communication sites near lines the radio noise levels in rain are highest and therefore most important.

3. Instrumentation

3.1 The principal instruments used for the field strength measurements were:

<u>Frequency Range</u>	<u>Name</u>	<u>Manufacturer</u>
3-45 cps*	ET-1A Sub-Audio System	Electro-International Co.
30-15,000 cps	NM-40 Field Intensity Meter	Stoddart Electro-Systems
0.014-0.25 Mc/s	NM-10 Field Intensity Meter	Stoddart Electro-Systems
0.15-25 Mc/s	NM-20B Field Intensity Meter	Stoddart Electro-Systems
20-400 Mc/s	NM-30A Field Intensity Meter	Stoddart Electro-Systems
375-1000 Mc/s	NM-52A Field Intensity Meter	Stoddart Electro-Systems
30-300 Mc/s	AP-501R Low Noise Tunable Amp.	Electro-International Inc.
300-1000 Mc/s	AP-502R Low Noise Tunable Amp.	Electro-International Inc.
.010-1000 Mc/s	IG-115 Impulse Gen.	Empire Devices Inc.
	Signal Generator	Hewlett-Packard
	Signal Generator	General Radio Co.
	Signal Generator	Measurements Corp.

* No data or results are given in this report for this frequency range.

<u>Frequency Range</u>	<u>Name</u>	<u>Manufacturer</u>
0.55-220 Mc/s	Signal Generator Interference Locator M-500	Measurements Corp. Sprague Electric Inc.

These instruments and accessories were carried in a van, see Fig. 6 in Appendix V, equipped with antenna supports, shelves and straps for tying down the instruments.

3.2 Antennas Used

The antennas used were as follows:

<u>Frequency Range</u>	<u>Name</u>	<u>Manufacturer</u>
20-1,500 cps	Electric Probe	Stoddart Electro Systems
0.14-0.25 cps	2 Meter Vertical Rods	Stoddart Electro Systems
0.15-25 Mc/s	1 Meter Vertical Rod	Stoddart Electro Systems
20-1000 Mc/s	Dipole	Stoddart Electro Systems
88-350 Mc/s	BCA-902 Bi-Conical	Electro International Co.
375-1000 Mc/s	BCA-901 Bi-Triangle	Electro International Co.

3.3 Calibration of Instruments

The instruments were calibrated with signal generators and impulse generator. When pre-amplifiers were used they were calibrated with impulse generator in order to obtain amplifier gain factors for measurement frequencies. In this report practically all the data is in dB Peak above 1 μ V/m/Mc bandwidth and all calibrations are referred to rms value of sine wave. The overall general accuracy of measurements is estimated as no better than \pm 2 dB up to 25 Mc/s and \pm 3 dB from 25-1000 Mc/s.

4. Methods of Measurement

In the frequency range up to 24 Mc/s measurements of the field strength were made with receivers on the ground and antenna on the receiver or on a tripod. Above 24 Mc/s up to 1000 Mc/s practically all field strength measurements were made with receivers inside the van and the proper dipole antenna on the van roof bringing the dipole 20.5 feet above ground level. As many as three receivers were used at the same time at different distances from the line under test. All receivers were monitored by headphones and readings were taken even if only the meter residual was present. This was done in order to make sure that at the specific test location radio noise from the line could not be measured or heard in the headphones. All directional antennas were rotated for maximum signal with the aid of the remote indicating meter available with instruments. Readings were taken with dipole horizontal and vertical. The FI, Field Intensity, QP (Quasi-Peak), and Peak detector readings were taken on all meters at practically all test locations.

The antennas were setup on all lines at standard distances of 50 feet laterally from nearest phase conductor or from pole on low voltage lines and 200 feet laterally from center line of line opposite tower or at mid-span. Other standard distances used if possible were 300, 400, 600, 900, 1200 and 1500 feet. Locations farther away were in sight of line and were chosen depending on accessibility, trees, cultivation, other lines, auto and truck traffic, and on permission of the land owner. Measurements were made on both sides of towers on lines from 138 to 345 kV. For the investigations of the field strength across the line the lateral profiles were usually taken at distances 20 feet apart and to 200 feet on both sides of center line.

Measurements were also made on several lines at distances ranging from 0.64 to 8.23 miles down the line from a local source such as the artificial gap-type radio noise generator.

Various techniques were found useful in determining if a gap-type natural and local source was on the line. The sound in receiver headphones is the first clue. If this is confirmed by obtaining an extended frequency spectrum or an unsymmetrical lateral profile the local source is not too far away. Three natural gap-type sources were located on three different lines and measurements were then made near these local sources.

4.1 The Artificial Gap-Type Radio Noise Generator

The artificial gap-type radio noise generator simulates natural gaps on lines and it was used as an aid in the investigation of the radiation from lines and of the longitudinal and lateral propagation characteristics. A gap in air can be made to generate noise above the normal noise level of a line and it also extends the

normal line frequency spectrum to much higher frequencies.

The artificial gap can be placed on a line at the desired distance from end of line and at a place with suitable terrain and low ambient for investigation and for measurements. A natural gap on a line may generate just as much radio noise but it may be at a location unsuitable for the measurements required.

A drawing of the gap is shown on Fig. 6 and a photograph on Fig. 7d. The frequency spectrum of radio noise voltage of this gap is given by Fig. 1.

4.2 Power Lines Measured for Radio Noise

The following list of lines includes figure numbers for the test location plan, figure numbers of photograph of nearest tower or pole, conductor heights, conductor gradient and figure numbers of normal line frequency spectrum.

Line kV and Type*	Test Loc. Fig. No.	Photo Fig. No.	Ph. Cond. Height Feet	Cond. Gradient kV _{rms} /cm	RN Freq. Spectrum Fig. No.
2.4 HC	8	27c	34	0.77	32
4.16 HC	9	27b	34	1.13	33
8 HC	10	27a	33	2.1	34
12.5 HC	11	28d	32.5	3.6	35
34.5-12.5 HC	12	28b,c	34	8.85-3.11	36
34.5 HC	13	28a	35	6.18	37
46 VCDC	14	29c	35,40,45	8.52	38
46 TCSC	15	29b	35,39	----	39
69 HCWP	16	29a	36	9.11	40
110 HCWP	17	30d	39	15.6	41
138 HCWP	18	30c	48	13.06	42
161 HCST	19	30b	61	12.57	43
244 HCST	20	30a	56.5	14.45	44
345 HCST	21	31a	90	15.51	45
345 VCDC	22	31c	108,129.5,153	17	46
345 VCSC	23	31b	80,103,126	17.0	47
345 HCWP	24	31d	46	15.7	48
345 HCWP	25	31d	48	15.7	49
345 HCWP	26	31d	52	15.65	50

*In the above tabulation the abbreviations for the lines are:

HC = Horizontal Configuration of Line Conductors.
VCDC = Vertical Configuration Double Circuit.
TCSC = Triangle Configuration Single Circuit.

VCSC = Vertical Configuration Single Circuit.
HCWP = Horizontal Configuration Wood Pole.
ST = Steel Tower

These abbreviations have also been used on captions for related figures.

The original photographs were obtained with Polaroid black and white or on 35 mm film. The conductor heights were measured at the test location by means of a "Telehite" and tape measure and the conductor gradients were obtained by computer.

The effect of varying the receiver antenna height from 24 feet to 90 feet was measured at three locations 200, 600 and 2000 feet from a 345 kV line tower. These results are given in Appendix V.

4.3 Laboratory Measurements

4.3.1 Conducted radio noise measurements were made in the laboratory with the NEMA high voltage test circuit. These tests and results are described in Appendix I. Three sizes of round head rivets and three sizes of conical head rivets were mounted on twenty-foot lengths of aluminum tubing of different diameters. Corona plumes or streamers were produced at the rivets at conductor to ground voltages from 125 to 250 kV depending on the conductor diameter. These measurements were used as part of investigations to determine the effect of conductor diameter on magnitude of radio noise generation.

4.3.2 Artificial Gap Spectrum

The frequency spectrum of the artificial gap used on several lines was measured in the laboratory from 0.015 to 1000 Mc/s. The circuit used and the frequency spectrum are shown on Fig. 1. The output of the gap with the 150 ohm loading is 150 ± 2 dB above 1 μ V/MCBW up to 30 Mc/s. Beyond this frequency the output drops rapidly with marked fluctuations above 200 Mc/s. These fluctuations are probably due to impedance variations of the test circuit and gap which require appreciable physical dimensions for tests at 20 kV.

4.3.3 Corona Source Spectrum

The spectrum of corona was also obtained in the laboratory at relatively low voltage in order to maintain the same test circuit used for spectrum measurement of the artificial gap. The corona spectrum obtained is shown on Fig. 3. This spectrum begins to fall off at a lower frequency than the gap spectrum and the radio noise magnitude is lower. Further investigation is required to determine the effect of multiple corona sources.

5. Discussion of Measurements with Lines Normal

The curves of frequency spectra, Figures 32 to 50 inclusive, are for lines as found and are defined as normal. For each figure the radio noise magnitude has been corrected and then plotted for the frequency ranges given as follows:

<u>Frequency Range</u>	<u>Antenna Eff. Height</u>	<u>Ant. Factor</u>
0.015 - 0.25 Mc/s	1 Meter Vertical	0 dB
0.15 to 25 Mc/s	1/2 Meter Vertical	+6 dB

For dipole antennas on van roof, $h = 20.5$ feet, the values plotted are after correcting data to "standard" tripod heights according to instrument manufacturer's charts. This was done because correction data on effect of increasing antenna heights from 8-1/2 to 10 feet to 20.5 feet was not available for the 50 foot and 200 foot lateral distance from the line where practically all measurements were made with lines normal. The comparison of antenna on tripod and on van roof is discussed in detail in Appendix V. Actually at 200 feet from line the difference is less than 2.5 dB. At 500 feet and farther, the difference is nearly 6 dB and was found to be very nearly the same, as when the antennas on tripod and on van roof were compared on TV stations in a clear area more than 10 miles from TV stations.

The instrument residual has been corrected in the same manner as field strength readings in order to have residual points consistent with the ordinate of the frequency spectrum.

5.1 Frequency Spectrum for 2.4 kV Line

Lines of this voltage having any appreciable length between transformers and their secondaries are difficult to find and difficult to test because they are in populated areas and along roads where vehicle ignition noise and other noise sources are not too far away. In this case the nearest pole had a transformer, two arresters, and two fuse cut-outs.

The frequency spectrum obtained for this line is shown on Fig. 32. The test location and conductor configuration plan is on Fig. 8 and photograph of pole and line is on Fig. 27c. Radio noise of low level compared to the 4.16 kV line was measured. The sources of radio noise on this line are not known. However, rapid increase at the lower frequencies indicates that the source is far away since at these frequencies attenuation is lower than at the higher frequencies.

5.2 Frequency Spectrum for 4.16 kV Line

For this line the test location and conductor configuration

are on Fig. 9 and photograph on Fig. 27b. The frequency spectrum is shown on Fig. 33. This spectrum was obtained at a lateral distance of 50 feet from the pole.

In this case radio noise was measured above instrument residual over practically the whole frequency range. The magnitude falls off very approximately at the rate of 20 dB per decade and is approximately 15 dB higher than was found on the 2.4 kV and is higher than on any of the other low voltage line tested except the 12.5 - 34.5 kV line where a gap source was found.

5.3 Frequency Spectrum for 8 kV Line

The frequency spectrum of this line is shown on Fig. 34 and it was obtained at 50 feet from pole. See Fig. 10 and photograph on Fig. 27a. In this case radio noise was measured up to 250 Mc/s and the magnitude decreases approximately 20 dB per decade. The sources are not known. The form of the frequency spectra indicates that the sources are not as far away as they are on the 2.4 kV line.

5.4 Frequency Spectrum for 12.5 kV Line

The test location plan and conductor configurations are on Fig. 11 and photograph is on Fig. 28d and 50 feet from pole is shown on Fig. 35. This line is within 300 feet of salt water and runs over marsh land. The radio noise level was very low and could only be detected over meter residual below 0.25 Mc/s and in the 30 to 110 Mc/s range.

5.5 Frequency Spectrum of 12.5 - 34.5 kV Dual Line

Two natural sources were found on this dual line after measurements were made. One of them was between insulated pole guy wire and neutral at the measurement location and the other was about one-half mile away at loose pole guy. Both of these sources could be heard in headphones because the more intense source would go on and off occasionally.

The frequency spectrum shown in Fig. 36 was measured 50 feet from pole where the pole guy to neutral source was located. See Fig. 12 and photograph on Fig. 28b. The radio noise level is quite high. In fact it is about the same at low frequencies as 345 kV lines in rain. At the higher frequencies the radio noise level is higher than for 345 kV lines in rain. The form or shape of the spectrum is similar to those obtained on lines with the artificial gap. Both of the sources on this line were easily eliminated.

5.6 Frequency Spectrum of 34.5 kV Line

This line has post type insulators as can be seen on Fig. 28a. The measurements could not be made directly opposite pole because of terrain roughness. They were therefore made at a location as indicated on Fig. 13.

The frequency spectrum is shown on Fig. 37. Radio noise of low magnitude, compared to the previous line with local sources, was measured from 0.15 to 250 Mc/s.

5.7 Frequency Spectra of 46 kV Lines - Local Source Found

5.7.1 Test Location with Local Source

The 46 kV line was measured at two test locations. At one of the locations, Fig. 14 and photograph Fig. 29c, a radio noise source was found with the Sprague locator. The frequency spectra shown on Fig. 38 were obtained with the portable battery-operated NM-20C at 90 feet from the pole with the radio noise source. Measurements could not be made at 50 feet because of highway, or at 200 feet because of heavy woods. Fig. 38 shows the frequency spectrum before elimination of source and the spectrum after lineman tightened and bonded connections on pole. The repairs made were as follows:

1. Replaced burned aluminum tie wire on pin-type insulator.
2. Tightened through-bolt on top cross-arm.
3. Bonded two guy wires.
4. Drove new staples on metal pole cap over ground wire on metal cap.

After these repairs were made the radio noise level dropped considerably as shown by the lower curve on Fig. 38. It will be noted that the upper curve is quite flat as obtained from gap-type sources which are near the radio noise meter antenna.

5.7.2 Test Location at Single Circuit 46 kV Line

The second test location for 46 kV line was on single circuit line, see photograph Fig. 29b, 1.7 miles from the first test location and 1.1 miles from where double circuit split into two separate single circuit lines. The measurements were made at 100 feet and 200 feet from the line pole as shown on location Fig. 15. The frequency spectra are on Fig. 39 and were made before the local source 1.7 miles away was eliminated. The radio noise level is considerably lower than at the local source location 1.7 miles away and it decreases with frequency about 40 dB per decade from 0.015

to 0.1 Mc/s and about 20 dB per decade from 0.1 to 175 Mc/s.

5.8 Frequency Spectrum of 69 kV Line

Measurements were made on this line at 200 feet, see Fig. 16, from wood H-frame tower, see photograph Fig. 29a. The frequency spectrum curve is shown on Fig. 40. The radio noise level is appreciable below 0.1 Mc/s and is only a few dB above instrument residual from 0.15 to 25 Mc/s and decreases about 40 dB per decade below 0.15 Mc/s and about 10 dB per decade above 0.15 Mc/s.

5.9 Frequency Spectrum of 110 kV Line

This 110 kV line was used to compare dipole antenna on tripod with same antenna on van roof. See Appendix V. For these tests the 5/16 inch air-gap type radio noise generator was connected to one phase of the 110 kV line. Part of the time the gap stopped operating, because of rain, and the frequency spectrum shown on Fig. 41 was then obtained. Radio noise was measured over the frequency range of tests which was 0.015 to 24 Mc/s. The test location and conductor configuration diagrams are shown by Fig. 17, and a photograph of the line at test tower is on Fig. 30d.

5.10 Frequency Spectrum of 138 kV Line

This line is shown on photograph Fig. 30c and the test locations and conductor configuration are shown on Fig. 18. The frequency spectra, Fig. 42, was obtained at 50 feet and at 200 feet from tower. These spectra include data with varying amounts of rain and intermittent showers. The readings were higher in rain and decrease with frequency approximately 20 dB per decade. The spectra at 50 feet cannot be compared accurately to spectra at 200 feet because of the varying amounts of rain during the time taken for tests.

5.11 Frequency Spectra of 161 kV Normal Line

This line was investigated with and without the 5/16 inch gap-type radio noise generator. The line and tower are shown on photograph Fig. 30b and the test locations and conductor configuration are on Fig. 19. The frequency spectrum with line normal was taken at 200 feet laterally from center line of tower. This spectrum is shown on Fig. 43. The radio noise levels are only slightly above instrument residual above 0.1 Mc/s. Below this frequency the level rises at a rate of about 40 dB per decade.

5.12 Frequency Spectrum of 244 kV Line

This line was investigated with and without the 5/16 inch gap-type radio noise generator. Fig. 30a includes a photograph of this line and Fig. 20 gives the conductor configuration and shows the test locations used during investigation.

Measurements without gap (line normal) were obtained on this line with light snow and sleet as well as in fair weather. Fig. 44 shows the frequency spectra obtained. This line gives approximately a 20 dB decrease per frequency decade in both fair and foul weather.

5.13 Frequency Spectra of 345 kV HCST Line

This line, see Fig. 31a, has a two conductor bundle in a horizontal configuration. This line was investigated quite thoroughly with the 5/16 inch gap-type generator connected to the west phase at tower 129. The test locations and conductor configurations are shown on Fig. 21.

The frequency spectrum with line normal is shown on Fig. 45. This spectrum follows the 20 dB decrease per frequency decade. A few readings were obtained in heavy rain. The readings increased by as much as 7 to 14 dB below 3 Mc/s. From 30 to 300 Mc/s the rain had very little if any effect on this line.

5.14 Frequency Spectra of 345 kV VCDC Line

This line, see photograph Fig. 31c, is a vertical configuration double circuit line. Besides normal line tests the 5/16 inch gap-type radio noise generator was used extensively on all three vertically placed conductors on the east side circuit. The test locations and conductor configuration are shown on Fig. 22.

The frequency spectra with line normal are plotted on Fig. 46. Two spectra are shown. One is with clear and cold weather and the other with misty rain from 0.015 to 24 Mc/s. Both spectra follow approximately the 20 dB per decade curves.

5.15 Frequency Spectrum of 345 kV VCSC Line

This line has towers similar to those of line discussed in section 5.14. Only one vertical circuit is however, on the towers at the present time. The photograph of this line and tower is on Fig. 23. Because of heavy plowed field it was necessary to make measurements on this line at a distance of 420 feet laterally from tower instead of at 200 feet as was done on most other lines. Measurements were also made at 72 feet from center line of tower (50 feet laterally from point directly under outside phase conductor) from 0.015 to 20 Mc/s.

Field strength measurements at 420 feet were made in fair weather from 0.015 to 1000 Mc/s and with steady medium rain and with light rain from 0.15 to 1000 Mc/s. The frequency spectra obtained are shown on Fig. 47. It will be noted from Fig. 47 that rain gives considerably higher field strengths than fair weather. From 0.015 to 0.1 Mc/s the radio noise decreases about 40 dB per frequency decade and above 0.1 Mc/s it decreases at the rate of approximately 20 dB per decade. These measurements can be corrected to 200 feet by means of lateral attenuation curves given in Appendix IV.

5.16 Frequency Spectra of 345 kV HC Wood Pole Line

Measurements were made on this line at three locations. At tower 101, 119 and 192. From tower 101 to tower 119 it is 2.24 miles and then from tower 119 to tower 192 it is 9.3 miles. Photograph Fig. 31d shows a typical tower on this line.

5.16.1 Test Location at Tower 119

The measurement locations used near tower 119 are shown on Fig. 24. The frequency spectrum is given on Fig. 48. This spectrum indicates that gap-type radio noise was predominant since the spectrum is similar to spectra obtained with the artificial gap. Also the sound in headphones was characteristic for gaps. Radio noise was measured up to 350 Mc/s. Above this frequency the readings are near the instrument residual. The horizontal polarization of dipole gave somewhat higher readings at most frequencies than vertical polarization. Lateral profiles at tower 119 and at mid-span were measured and they have been plotted on Figures 96 and 97. Calculated curves are also shown using the method described in Appendix II.

5.16.2 Test Location at Tower 192

Measurements were made at this tower because a natural gap-type source was found at this tower. During tests at tower 119 a gap-type source was suspected. It was decided to explore the line and locate the gap-type source. After some exploration in the suspected area the gap on tower 192 was found. The exact location of this radio noise source on tower was found by visual observation at night to be between hardware on upper end of tower cross-brace and the ground wire coming down the pole. The location of this source is shown on photograph Fig. 27d and a night photograph of this discharge gap is shown by Fig. 7a.

The test locations and conductor configuration are given by Fig. 25. The frequency spectrum obtained is on Fig. 49. This spectrum is somewhat similar with respect to frequency to the one measured at tower 119. The magnitude of the radio noise field is,

however, approximately 20 dB higher. Measurements were made at several locations out to 20,000 feet as shown on Fig. 25. These measurements will be discussed later in detail in connection with lateral attenuation of power line radio noise radiation.

5.16.3 Test Location at Tower 101

The test locations at tower 101 are on Fig. 26. The frequency spectra is on Fig. 50 and is only from 0.16 to 200 Mc/s. It should be noted that these data are at 100 feet and 250 feet from tower and cannot be compared without distance correction with measurements made at towers 119 and 192. It can be said, however, that the radio noise level at tower 101 is lower than at tower 119 and approximately 10-30 dB lower, depending on the frequency, than at tower 192.

5.17 Frequency Spectrum Near 46 kV Sub-station

Measurements were made near a 46 kV sub-station. The results are on Fig. 53. The magnitude is about 10 dB higher than was measured on one of the 46 kV lines coming to the station, see Fig. 39. The reason for this higher level was not investigated. It is necessary to make measurements at more than one location around a sub-station to find the highest levels and to identify the principal radio noise sources. However the measurements do indicate that sub-stations require further investigation.

6. Conductor Gradients of the Power Lines Tested

The conductor gradient has an important bearing on radio noise from power lines because (1) it greatly affects the magnitude of radio noise generation if the ionization gradient for air is exceeded, and (2) it can affect or give rise to the local sources at poles or towers because of the gradient in the space around the conductors.

The conductor gradients of the lines tested were obtained from computer program. These gradients have been plotted on Fig. 51 for three phase voltages of the lines tested. It can be seen that the conductor gradients for the lines tested increases with increase in voltage rating.

The conductor surface gradient values calculated and shown on Fig. 51 are for smooth conductors. The critical gradient is that at which corona starts, and for smooth conductors it is from Peeks

*Dielectric Phenomena in High Voltage Engineering (book) by F. W. Peeks, Jr., McGraw-Hill Book Co. Inc., New York, 1926.

empirical relation for conductor radius r in cms and for relative air density = 1;

$$g = 21.1 \left(1 + \frac{0.3}{\sqrt{r}}\right) \text{kV}_{\text{rms}}/\text{cm} \quad (1)$$

The calculated critical gradient is considerably higher than any of the conductor gradient values for the power lines tested, as can be seen from Fig. 52. Because of the conductor surface conditions and gradients existing in practice all the lines above 110 kV will be in corona; whereas, all lines 70 kV and below are not expected to have conductor corona even in rain because their gradients are well below the curve shown on Fig. 52 for laboratory tests in the rain. The points for these curves were obtained at 1 Mc/s and are for the gradient values where the radio noise voltage generated was only 85 dB above 1 $\mu\text{V}/\text{MCBW}$ as measured with the NEMA-107-1964 test circuit. These gradients are lower than visual corona starting gradients, see Fig. 52, obtained by Peek for wet conductors.

7. Analysis and Discussion of Data and Conclusions for Lines Normal

7.1 Analysis of Test Results for Low-Voltage Lines Normal

7.1.1 Low-Frequency Measurements on Low-Voltage Lines

Appendix VI reports the low-frequency measurements 60 cps to 0.015 Mc/s for the 8-, 48-, and 69-kV lines (Figs. 12 and 13, 11, and 10, respectively, of Appendix VI for the electric field). As indicated in this appendix, levels measured in this frequency range are predominantly at the harmonics of the 60 cycle voltage (even with the artificial gap), and drop off about as the inverse of the frequency squared (40 dB per frequency decade) to about 2000 cps where the values generally level off. For some of the lines tested the harmonics were not measured above 2000 cps because of noise.

From these results, one can conclude that the 60 cycle field strength levels in the range of frequencies below 0.015 Mc/s can be taken proportional to the line voltage (Fig. 16 of Appendix VI) but are not uniquely determined by this voltage. The prediction of levels for a particular frequency in this range of frequencies can be made only if the harmonic percentages are accurately known. The percentages measured have been compared on Table I of Appendix VI to

values given in Table 6, page 772 of fourth edition of Electrical Transmission and Distribution Reference Book, Westinghouse Electric Corporation, 1950.

7.1.2 Measurements in the frequency range 0.015 to 1000 Mc/s were made on eight lines rated 2.4 kV to 69 kV. Figures 32 to 40 give the frequency spectra for these low-voltage lines tested in the as found or normal condition. On all curves, the values shown for the noise levels over the frequency range of 25 Mc/s to 1000 Mc/s, where the dipole antenna is used, are the highest values obtained regardless of dipole polarization or orientation, unless specifically noted otherwise. (See Section 7.2.1 for further discussion on dipole orientation).

7.1.3 Radio noise could be measured from all lines at the measurement location of 50 feet used for lines 2.4 to 34.5 kV and at the test location of 200 feet used for 46- kV lines and up. However, as shown by the figures, the magnitude of radio noise from these lower voltage lines was quite low, even at 50 feet, except on those lines where a radio noise source was found near the test location.

7.1.4 For the low voltage lines with no known sources, there is no correlation of radio noise levels with line voltage. The highest levels for the low voltage lines tested were measured on the 4.16- kV line at 50 feet.

7.1.5 All lines below 70 kV should not have conductor corona even in rain, because their operating gradients are so low (Fig. 52 and Section 6).

7.1.6 Correction of the data of Figures 39 and 40 for the 46- and 69- kV lines, respectively, to 50 feet indicates the levels for these lines are about equal to that for the 4.16- kV line, except below 0.1 Mc/s where the levels tend to rise. From the results of tests with artificial gaps on the line at some distance from the measurement position, (see Section 8.2), it can be assumed that a distant noise source was present on these two lines at a considerable distance from the point of measurement. For such a distance, the higher frequency energy will be attenuated before reaching the measurement position, but the energy in the lower frequencies will not be completely attenuated and may override that from the rest of the line.

7.1.7 The frequency spectra for the lines are not alike. The form of the spectra depends on the type or types of sources, and, as indicated previously, the distance from the source or sources, and on the lateral distance from the line where measurements are made. Also, the heights of the line and the receiver antenna influence this form. With no obvious sources, the frequency spectra falls off as the inverse of the frequency (20 dB per frequency decade). The

exception to this was the 34.5- kV line with post-type insulators, whose levels, although generally lower than those for the 4.16- kV line, fall off as the inverse of the square root of the frequency.

With the natural gap-type source the frequency spectra is quite flat into the higher range of the frequency spectra, how flat depending upon the distance from the source. Before elimination of the radio noise source at the pole near the measurement position for the 46- kV line (Fig. 38), the spectrum showed no tendency to fall off with the inverse of frequency. After removal of this source, the spectrum tended to fall off as the inverse of the square root of the frequency. However, it was noted that another source (or sources) existed elsewhere on the line, and the trend of this spectrum compares with that of the 12.5-, 34.5- kV dual-circuit line with known sources (Fig. 36), although of lower levels than those for this dual-circuit line.

7.1.8 It may be concluded that for low-voltage lines where no obvious gap source is present, the levels will be comparatively low, regardless of voltage, and will decrease as the inverse of frequency (20 dB per frequency decade). For higher voltages it can be assumed that gap sources are more probable, and where these do exist, the levels are higher and the spectrum is flatter over a greater frequency range. It is not possible to predict, from the data presented here, the maximum possible magnitudes of radio noise from gap-type sources.

7.1.9 Present-day line designs consider and are constructed to be normally free of radio noise. The low levels generally measured here bears this out. However, because of mechanical damage with time and because of stormy weather conditions, it is impossible to guarantee freedom from radio noise in the vicinity of these lines for 100 percent of the time. Where sources do exist or start, it may be necessary to locate and eliminate or reduce them so as to have insignificant interference to communications, or to place the communication site far from the line.

7.1.10 Measurements were taken in fine weather near one low-voltage line (12.5 kV, Fig. 35) which is within 300 feet of salt water and runs over marsh land. Although of older construction, noise levels from this line were as low or lower than the other low-voltage line levels. However, because of the limited sampling of such lines, no conclusion should be made concerning radio noise on lines near salt water or age of construction.

7.1.11 All measurement sites may be considered to be in rural or suburban areas. The study covered by this contract did not include the effect on noise levels of the location nor of whatever electric power utilization devices may be connected to these lines. These considerations and the previous remarks result in the conclusion that levels from any particular low-voltage line are not predictable.

However, the measured levels reported here may be considered "typical" of low-voltage lines taken as a group and the highest levels measured are recommended for use in the prediction technique to follow.

7.1.12 Radio noise from a sub-station was measured. Radio noise generated in a sub-station can propagate for great distances at the low frequencies, below 0.15 Mc/s. Transients, such as caused by switching at sub-station, may be important for some cases of radio noise prediction. This report does not cover to any useful extent, the effect of sub-stations and switching surges for the siting of communication systems.

7.2 Analysis of Test Results for High-Voltage Lines Normal

7.2.1 Sub-Audio Measurements (3 to 45 cycles/sec)

Unsuccessful attempts were made to determine and measure the presence of sub-audio frequencies (3 to 45 cycles/sec) in the vicinity of the 345-kV flat configuration line using the Electro International ET-1A Sub-Audio Detection Equipment. Measurements were attempted at three different locations using different power sources without obtaining reasonable data. Measurement difficulties near high voltage lines were attributed to both voltage and frequency instability of the portable unit used for the test instrumentation.

The Model ET-1A equipment is designed for a specific measurement application and operates but in a special sub-audio frequency shielded enclosure. The electrometer pickup device is a conventional vertical rod, which connects directly to the grid of the electrometer tube through a high impedance (6000 megohm glass enclosed resistor). It is intended that the sixty-cycle pickup on the grid be balanced out with a phase and amplitude shifter circuit whose supply voltage is derived from the 60 cycle power . However, while suitable in its intended environment, the electro-meter is subject to serious overloading where comparatively strong 60 cycle electric fields are present, such as near high-voltage power lines. Difficulty will be experienced, also, in cancelling out the 60 cycle grid pickup when a portable power supply is being used which is not in exact synchronism with the power line voltage.

No internal balancing-out circuitry is provided when using the magnetic loop. In the normal environment in the RFI laboratory, 60 cycle cancellation is accomplished by orienting the loop for minimum 60 cycle pickup and moving the test sample about the loop for maximum sub-audio frequency signal. In the high-voltage power line environment, it is impossible to place the loop for both 60 cycle rejection and maximum sub-audio pickup. Thus, the loop must be rotated for maximum sub-audio pickup, and the filter network should be capable of rejecting the 60 cycle component.

7.2.2 Low-Frequency Measurements on High-Voltage Lines

Measurements in the frequency range of 60 cps to 0.015 Mc/s are given in Appendix VI for 161-, 244-, and 345-kV lines (Figs. 9, 8, and 7, respectively, in Appendix VI). Levels measured in this frequency range are predominantly at harmonics of the 60 cycle voltage and fall off about as the inverse of the frequency squared (40 dB per frequency decade). Measurements on the 244-kV with and without a gap-type noise generator, indicate no difference in levels.

From the results of Appendix VI, one may conclude that the prediction of field-strength levels at 200 feet can be based on the 60 cycle line voltage, and the harmonics from the inverse-frequency-squared relationship. However, the lateral fall off of harmonic field strengths with distance (Fig. 14 of Appendix VI) cannot be defined nor can the level for a particular frequency be exactly predetermined from these curves because of possible variations in the harmonic content between measurement locations. It is recommended that for prediction of harmonic fields typical harmonic percentages be used and that the lateral attenuation be taken as $\frac{1}{d^3}$.

7.2.3 Measurements in the frequency range of 0.015 Mc/s to 1000 Mc/s were made on eight lines tested 110 kV and higher. Figures 41 to 52 give the frequency spectra for these high-voltage transmission lines. Again, on all these curves, the noise levels shown over the frequency range of 25 Mc/s to 1000 Mc/s are the highest obtained regardless of dipole polarization unless specifically noted.

Horizontal polarization of dipole antenna gave higher readings for about 60 percent of the measurements than did vertical polarization. The differences between values recorded for the two polarizations were from 0 to 10 dB.

With the horizontal polarization, the orientation of the dipole for a maximum reading varied from the dipole perpendicular to the line to an orientation parallel to the line, depending on the frequency and distance from the line. At 200 feet from a tower there were some lines tested where the horizontal dipole was perpendicular to the line for all maximum readings. At greater distances from the tower, the orientation sometimes varied from 0 to 90° from the perpendicular. On all the curves of Figures 41 to 52 the noise levels shown over the frequency range of 25 Mc/s to 1000 Mc/s are the highest obtained regardless of dipole orientation.

It can be shown from a theoretical consideration of the electric field vectors for the noise radiated from a horizontal conductor of uniform height or from its image, at a depth in the ground equal to the height of the conductor (see Appendix II), that

the perpendicular orientation of a horizontal dipole above ground gives a higher reading than that with parallel orientation. With the dipole perpendicular to the line, the electric field vectors from points along the conductor on both sides of the point on the conductor perpendicular to the dipole reinforce. With the dipole parallel to the line these vectors from points along the conductor cancel. (See also Appendix II).

It does not appear from the field results that antenna orientation can be considered as a useful factor in the general prediction of the radio noise level or in determining the best distance from the transmission line to the communication site. Calculations have, therefore, only been performed for the horizontal dipole perpendicular to the line.

7.2.4 The magnitude of radio noise on lines from 110 kV to 345 kV is more dependent on the conductor gradient, and on weather and other environment conditions than are the low-voltage lines discussed in the preceding sections. Figure 51 summarizes the gradients at which the lines tested operate for their rated voltage, and indicates the trend to higher gradients as voltage rating increases. These gradients are considerably above the corona-starting or critical gradient in rain (see Fig. 52). Lines rated above 110 kV are therefore expected to have radio noise due to conductor corona since usually the gradients exceed those found in the laboratory for rain tests.

7.2.5 Field tests show that rain or other foul weather can increase the levels as much as 26 dB, depending on the intensity of the precipitation.

7.2.6 It is not economically feasible to build lines rated above 110 kV which are free of conductor corona in rain. To achieve freedom from corona in rain, it would be necessary to operate the conductors at about one-fourth their critical gradient. This would require conductors with diameters about twice the present diameters or more, and correspondingly heavier and more costly towers.

7.2.7 No distinct difference in noise levels were noted between horizontal and vertical phase-conductor configurations. Appendices II and IV indicate the effect of height on lateral profiles of the noise field. Usually phase conductors will be higher for the vertical configurations so that the levels will not decrease as fast with distance lateral to the line as they would for lower conductors.

7.2.8 The frequency spectra shown on Figs. 41 to 50 for the high-voltage lines indicate that with no gap sources the levels vary inversely with frequency, or decrease 20 dB per frequency decade, whether the weather is fair or foul.

7.2.9 Figures 41, 43, 47 and 48 for fair weather for the 110-, 161-, and 345-kV lines, respectively, show an inverse-frequency-squared relationship of levels to frequency below about 0.2 Mc/s. Also, the frequency spectrum on Fig. 48 is flat between 0.1 and 10 Mc/s. As with the low-voltage lines (Section 7.1.5), these features are characteristic of gap-type sources at far distances from the measurement site, and audible noise, characteristic of distant sources, was detected in the instrument headphones for the lines with these frequency characteristics.

7.2.10 One high-voltage line tested, the 345-kV line of wood-pole construction, was found to have a gap source (Fig. 48). If gap-type sources exist on high-voltage lines, the radio noise levels can be higher especially at frequencies above 10 Mc/s, than from conductor corona in rain, and the frequency spectrum will be flatter.

7.2.11 Since levels are higher in rain than in fair weather for normal high-voltage lines (without gap-type sources), the communication siting distance will be based on the radio noise magnitudes and frequency spectra obtained in heavy rain from conductors operating at gradients comparable to the values given on Fig. 51 for lines above 110 kV.

7.2.12 In some areas rain is insignificant. However, in areas where sand or dirt will be blown on the conductors and the radio noise level will approach levels in rain as was found for dirt in laboratory tests (Appendix I). (See also Effect of Atmospheric Contamination on Generated Radio Influence Voltage by C. J. Miller, Jr. AIEE Conference Paper No. 56-1046).

8. Discussion of Tests with the Artificial Gap

As mentioned previously the artificial gap was used in order to obtain higher radio noise levels from overhead lines than normally exist, and over an extended frequency range so that the lateral attenuation characteristics of lines could be measured to greater distances. In addition, natural gap sources had been found or detected on the power lines measured. Tests with gaps of known characteristics are, therefore, of value in interpreting these measurements.

8.1 Measurements with Artificial Gap on 345 kV HCST Line

Fig. 31a is a photograph of tower 129 of this line. The line configuration and test locations are shown on Fig. 21. For all measurements the 5/16 inch artificial gap-type radio noise generator was connected to the west phase conductor at tower 129.

8.1.1 Lateral Profiles of Field Strength with 5/16 Inch Air Gap at Tower 129

These tests consist of lateral profile measurements at 0.154, 0.5, 1.03, 3.05, 10.05 and 22.3 Mc/s out to 200 feet each side of the line. These five frequencies were chosen because they were clear of station signals. Field strength measurements were made at mid-span and opposite tower 129 at location 0, and at approximately mid-span at distances of 0.64, 1.45, 3.08 and 5.6 miles down the line from tower 129.

The data obtained has been plotted for each test frequency on Figures 54, 55, 56, 57, 58 and 59. The curves show that as the distance from the source along the line increases:

8.1.1.1 The lateral profile tends to become more symmetrical (same on both sides of the line). However, complete symmetry for all test frequencies is not attained even at 5.6 miles away. This result indicates that lines of this type should be measured on both sides of center line in order more accurately to evaluate their radio noise level.

8.1.1.2 The field under the center of line dips down at the larger distance slightly at 0.154 and 0.5 Mc/s and very definitely at 1.03 and 3.05 Mc/s. This indicates a relative increase in the line to line mode of propagation. (See Appendix IV for discussion of modes of propagation).

8.1.1.3 The measured field decreases laterally in a manner similar to the calculated profiles except at the higher frequencies, especially 10.05 and 22.3 Mc/s where the electrostatic theoretical method of calculation as given in Appendix II, fails to give the measured field pattern, and calculations as described in Appendix IV become necessary.

8.1.1.4 The "attenuation" down the line has numerous values depending on what lateral distance is used for comparing the field strengths at the five locations. It is obvious that great care, especially as to test locations laterally from the line, is necessary in the measurement of transmission line attenuation at these frequencies.

8.1.1.5 The field strength measured opposite the tower on the west side where the gap is located is higher at 100-200 feet away than at mid-span for all frequencies, except for 3.05 Mc/s. Because of the higher conductor height at the tower it is apparent that measurements should be made opposite a line tower and on both sides of the tower.

8.1.2 Measurements of Frequency Spectra with Artificial Gap on Phase Conductor at Tower 129

The frequency spectrum measurement is the most important measurement to be made on a transmission line. These measurements were made at various distances from the line up to 3500 feet laterally from tower 129 (the gap location) and at 0.64, 1.45, 3.08 and 5.6 miles down the line from the tower with the artificial gap-type radio noise generator. The test locations for measurements of field strength were governed by accessibility, type of farm field, etc. The terrain is quite flat, only very slightly rolling, and tower 129 could be seen from all the lateral test locations.

Figure 61 shows several frequency spectra taken at 200, 1000, 2500 and 3500 feet laterally from the line near tower 129. Although the test locations are far from the line ends, 25 miles and more, there are large variations, up to 30 dB, in the neighborhood of 2 Mc/s, even 2500 feet from the line. The reason for these large variations in this frequency range are not known. The tower heights do correspond to approximately quarter-wavelength at 2 Mc/s. The same effects were found on the other two 345 kV lines tested and to be reported later.

The frequency spectra extend to 1000 Mc/s at 200 and 1000 feet away, and at 3500 feet the gap could be heard up to 500 Mc/s and a reading could be obtained. It is evident that a gap-type discharge in laboratory, see Fig. 1, and at a line tower can generate frequencies up to 1000 Mc/s and possibly higher. Figure 61 gives results obtained with vertical antennas below 24 Mc/s and vertical and horizontal dipoles above 24 Mc/s and at a height of 20.5 feet. Only one horizontal dipole curve is shown (at 200 ft.) on Figure 61 since readings were higher with the dipole vertical. The Figure 61 uses receiver antenna factors for the 8-1/2 and 10 foot heights used with the tripod on the ground. (Appendix V).

8.1.3 The Effect of Distance From the Line on the Field Strength

Since frequency spectra were obtained at several lateral distances from the line it is possible to obtain information as to the lateral attenuation. Figure 62 shows results of frequency spectra measurements taken in the frequency range 0.154 to 24 Mc at the several lateral test locations. The field strengths decrease as $\frac{1}{d^2}$ or $\frac{1}{d}$ depending on the frequency and distance from the line.

For instance, at 0.154 Mc and up to 600 feet away, (no reading could be obtained at 0.154 Mc beyond 600 feet) the field strength decreases as $\frac{1}{d^2}$. For frequencies above 24 Mc, Figures 63 and 64 show what field

strength measurements were obtained at the several lateral distances with the dipole antenna horizontal (Fig. 63) and with the dipole antenna vertical (Fig. 64). Here the field strength decreases approximately as $\frac{1}{d}$. From point to point, the decrease may be more or less than $\frac{1}{d}$. This variation is due to reflections and ground conditions which can be readily seen on continuous chart recordings of the field strength, see Fig. 80, as the dipole is moved away from the line. This has been done on the 345 kV wood pole line and will be reported later in more detail.

8.1.4 Attenuation Down the Line

At the time the lateral profile measurements were made (discussed in section 8.1.1) at 0, 0.64, 1.45, 3.08 and 5.6 miles down the line from tower with the artificial gap, frequency spectra were also measured at 200 feet west of the line center-line. These spectra, except for the one taken 1.4 miles away, have been plotted on Figure 65. By comparing these spectra it can be seen that the attenuation increases with the frequency. However, it is not possible readily to obtain the exact attenuation at any specific frequency. It is evident that in this frequency range the gap-type radio noise is carried several miles down the line and this effect should be considered in prediction analysis for these sources or in maintenance of a line in the vicinity of a communication site.

8.2 Measurements with Artificial Gap on 345 kV VCDC Line

This line has two vertical configuration circuits on steel towers as shown on Fig. 22 and photograph Fig. 31c. The artificial gap can be seen on Fig. 31c. It was connected in sequence to the top, center and bottom phase conductors and radio noise field strength measurements were made at test locations shown on Fig. 22.

Measurements were made on this line near tower 473 (gap location), at tower 488, 3.85 miles from tower 473, and at several lateral distances from the line up to 2.27 miles from tower 473.

The lateral profile measurements obtained with the line normal have been plotted on Figure 70 for the same frequencies measured with the gap at tower 473. The measurements at 0.154, 0.50 and 1.03 Mc/s follow part way all three of the calculated profiles which cross each other at 72, 94 and 130 feet. The values are considerably lower with line normal than obtained with the artificial gap (see Figure 66) except for the one point obtained at 20 feet west at 0.154 Mc/s. Near this location a conductor corona source could be heard directly by ear.

8.2.1 Lateral Profiles of the Field Strengths with 5/16" Air Gap at Tower 473

The lateral field strength profiles were made out to 200 feet East and West of center line at center of span and at two towers. Most of these measurements were made at the same frequencies and with the same instrument and by the same operator as those made for the horizontal configuration line discussed in Section 8.1.

The gap was placed on the top phase at tower 473 and lateral readings taken at center of span adjacent to tower 473 and 3.85 miles North at center of span adjacent to tower 488. These lateral field strength profiles are compared at several frequencies on Figure 66 and 67. On Figure 66 the form of the calculated field for the top conductor is shown by the dashed line. (Gap is on top conductor). On Figure 67, 3.85 miles away, the measured lateral profile follows the calculated center conductor profile rather than the calculated top conductor profile. This indicates a change in the mode of propagation between towers 473 and 488.

With the artificial gap on the bottom conductor the lateral field decreases more rapidly, see Figure 68, than it did with the gap on the top conductor, see Figure 66. The field pattern beyond 60 feet from the line follows most closely the calculated field pattern for the center conductors (B1 and B2). This occurs only at 0.154, 0.50 and 1.03 Mc/s. At the higher frequencies the measured field strength patterns are much more complicated, and the calculations by the method of Appendix II fail.

The lateral field patterns obtained between towers 488 and 489, which are 3.85 miles from the tower 473 with the gap on the bottom conductor, are shown on Figure 69. The lateral fields are now more symmetrical with respect to line center-line than they were near the gap. The measured fields at 0.154, 0.50 and 1.03 Mc/s follow the calculated field patterns more closely than they did near the tower with the gap on bottom conductor. By comparing Figures 68 and 69 at the higher frequencies one can readily see the effect of line attenuation. It is not possible to give any single attenuation figure from comparison of Figures 68 and 69.

These results indicate that it is possible to locate a single and strong radio noise source on a line by making careful lateral measurements at several locations until the lateral pattern becomes relatively flat and shifts over to the side of line where the source is located.

8.2.2 Procedure in the Measurements of Frequency Spectra

At the more distant lateral locations no field strength could be measured at all frequencies. In all cases, however, this

was checked by calibrating the instrument with its preamp, tuning the dipole antenna, rotating it and listening with headphones to make sure no noise from line was detectable. If no noise could be heard or read and the meter reading did not change when antenna was rotated and then disconnected, it was concluded that external noise was lower than the receiver system noise.

8.2.3 Frequency Spectra with Artificial Gap

The frequency spectrum was measured in part at 200 feet laterally from towers 473 (with 5/16 inch artificial gap) and 488, and 200 feet from center of line between towers 472 and 473 and between towers 488 and 489. Measurements were also made at several more distant locations laterally up to 2.27 miles from tower 473.

The most complete frequency spectra are shown in Figure 71 for the artificial gap located in sequence on the top, center and bottom conductors at tower 473. These spectra are quite flat, on the average, up to about 125 Mc/s. At 200 feet from tower 473, readings were obtained up to 1000 Mc/s. The attenuation effect of 3.85 miles of line can be seen by comparing Figure 71 with Figure 72 which gives data obtained 200 feet from tower 488. The spectra of Figure 72 are no longer flat because of the effect of line attenuation on the higher frequency range. The noise signal drops off rapidly at 50 Mc/s and could not be read above 125 Mc/s. The relative attenuation at the frequencies above 24 Mc/s can also be seen on Figure 73. It appears that at 50 Mc/s and above the line conducts or guides very little, if any energy, at least for the total distance of 3.85 miles, and direct radiation from the source becomes important. The effect of the gap location at tower 473 can also be seen from Figure 72; the attenuation down to tower 488 and up to 24 Mc/s is essentially the same regardless of which conductor the gap is connected to.

The attenuation laterally (perpendicular) to the line can be estimated from frequency spectrum measurements taken at various lateral distances from the line. These data have been plotted on Figures 74 and 75 for the frequency range of 0.154 to 24 Mc/s and on Figures 76 and 77 for the frequency range of 24 to 1000 Mc/s. The inverse distance relation (1) has been drawn on all these figures.

d

The test points follow the inverse distance law approximately. It is not possible to justify, on the average, any other relation from these data. It is necessary to compute the near-field relation to the far field for the lower frequencies because measurements cannot be always made at low frequencies except in the near-field. This has been done in Appendix IV.

Figure 78, as did Fig. 71, shows the large variations that occurred in the frequency spectra near 2 Mc/s. As noted previously, the tower height corresponds approximately a quarter wave of 2 Mc/s.

8.3 Measurements with Artificial Gap on 345 kV Wood Pole Line

This line has H-frame wood pole towers as shown on photograph Fig. 31d. The test locations used for all tests are on diagram Fig. 24.

The type of measurements made on this line with the artificial gap on the south phase conductor are plotted on Figures 79 and 80. Fig. 79 shows readings obtained over the 0.154 - 24 Mc/s frequency range at 200, 500, 1000, 2000 and 4000 feet south of tower with artificial gap, and indicates a lateral attenuation of $1/d$.

Figure 80 is a plot of a chart recording obtained at 30 Mc/s with the horizontal dipole perpendicular to the line, riding on the van roof as the van was driven away from the line. The standing wave effect is due to cancellation of the incident and reflected rays at the dipole location. It should be noted that the distance scale is not exactly linear and the effect of distance on the average or maximum radio noise is not exactly as $\frac{1}{d}$. For a more complete discussion of

the lateral near-field radiation see Appendix IV. Large variations in the frequency spectrum were not evident near 2 Mc/s for the wood pole line.

8.4 Measurements with Artificial Gap on 244 kV HCST Line

This line is shown on photograph of Fig. 30a, and its conductor configuration and test locations are on Fig. 20. In this case the 5/16 inch artificial gap-type radio noise generator was connected to the east phase conductor at the tower.

8.4.1 The Lateral Profiles to 200 feet east and 100 feet west at several distances along the line from the gap are on Figures 81 to 85. These profiles were made at the six selected frequencies used on the other lines tested and are similar to the results for previous lines.

8.4.2 Frequency Spectra at Several Distances

The frequency spectra taken at 78 feet from center of line (50 feet horizontally from under the east phase conductor) and at 200, 600 and 1600 feet east are shown on Fig. 86. Measurements were limited to 1600 feet because of woods. A few measurements are shown taken at 8.23 miles north of gap and at 78 and 200 feet from center line. In this case radio noise could be measured, near the tower with the gap, up to 1600 feet over the frequency range of 0.015 to 1000 Mc/s. Here again, as in the case of 345 kV ST lines, the large excursions in magnitude occur in the 2-4 Mc/s frequency range.

8.4.3 Comparison of Frequency Spectra on Opposite Sides of Tower

Measurements of frequency spectra were made on both east and west sides of tower with gap connected to the east phase conductor. These two spectra are compared on Fig. 87. It is evident that the radio noise level with the gap on the east side of tower is much higher on the east side of tower than on the west side of the tower for the lower range of frequencies. On lines of this type it is necessary to make measurements on both sides of a tower in order to make sure that the highest radio noise level of line is measured.

8.4.4 Effect of Distance from 244 kV Line

The lateral attenuation rate from the line depends on the frequency and the ground constants, etc. (See Appendix IV). Fig. 88 shows that in the frequency range of 0.015 to 0.25 Mc/s the radio noise field strength decreases as $\frac{1}{d^3}$. Fig. 89 is a plot of selected frequencies as shown for the frequency range of 0.15 to 24 Mc/s. These curves indicate a decrease in radio noise field strength with distance from line as $\frac{1}{d}$ or $\frac{1}{d^3}$ depending on the frequency.

8.5 Measurements with Artificial Gap on 161 kV HCST Line

This line and tower are shown on photograph Fig. 30b and the conductor configuration and test locations are on Fig. 19. The artificial gap was connected to the north phase conductor at tower 226.

8.5.1 Lateral Profiles

Lateral profile measurements were made at the six selected frequencies at the tower out to 200 feet north and 200 feet south of the center-line of tower. The lateral profiles measured and the frequencies of measurement are given on Fig. 90. As pointed out previously, it will be noted that the profile is unsymmetrical with the highest readings being on the north and gap side of the tower.

8.5.2 Frequency Spectra for 161 kV Line at Several Distances

The 0.015 to 1000 Mc/s frequency spectra taken at 200, 600 and 660 feet are on Fig. 91. These spectra show rapid variations of 10 dB and more in the 2 to 8 megacycle frequency range. Radio noise was measured out to 600 feet north of tower 226 from 0.015 to 1000 Mc/s. At 6600 feet radio noise could still be measured from 0.15 to 250 Mc/s. The characteristic flat spectrum of the gap in the frequency range of 0.15 to 100 Mc/s with fast attenuation beyond this range is evident in Fig. 91.

Four frequency spectra are shown on Fig. 92. These are all for lateral distance of 200 feet and the specific locations are given on the figure. The readings are highest at most test frequencies on the gap side of tower.

The rapid variations in magnitude from about 2 to 8 megacycles are evidently conducted by the line and persist out to tower 240 which is 2.75 miles from the gap tower 226. Measurements were made by means of 8 inch loop antenna at base of tower 226 on one corner about 14 inches above ground level. Variations in gap radio noise of type similar to those shown on frequency spectra in the 2 to 8 megacycle frequency range were measured. The maximums and minimums occurred at the same frequencies as at 100 feet north of tower.

8.5.3 Effect of Lateral Distance from Line Tower

The lateral attenuation trend can be seen from Fig. 93 for frequencies in the 0.015 to 0.25 Mc/s range. It appears that at these frequencies the attenuation varies approximately as $\frac{1}{d^3}$. The effect

of distance at frequencies from 0.154 to 24 Mc/s can be seen on Fig. 94. The points are from frequency spectra made at nine lateral distances from the line. The test frequency of the points is not identified and the true lateral attenuation in the near zone, especially for the lower frequencies, cannot be taken as proportional to $\frac{1}{d^3}$.

8.6 Measurements with Artificial Gap on 110 kV Wood Pole Line

The photograph of this line is Fig. 30d, and the conductor configuration and test locations are on Fig. 17.

The artificial gap was used on this line mainly to compare readings with the dipole antenna on the van roof with readings obtained with the more standard method, that is, with the dipole antenna mounted on a tripod. These comparisons were made at 77, 184 and 484 feet laterally from the conductor with the artificial gap and are described in Appendix V.

8.6.1 Frequency Spectra with Artificial Gap

The frequency spectra obtained at these distances are shown on Fig. 95. The large variations from 2 to 8 megacycles found on steel tower lines were not found on this line which has wood towers. A large decrease in radio noise is shown on the spectrum, occurring only at one frequency, 4.85 Mc, and a maximum occurring at 5.3 Mc. The phase conductors are 39 feet above ground level, which distance is less than one quarter the wave length at these frequencies.

8.7 Measurements on 345 kV Wood Pole Line with Natural Gap at Tower 192

As mentioned previously, a natural gap-type radio noise generator was found at tower 192. This is shown on photograph Fig. 27d and a night photograph of the discharge is shown on Fig. 7a. The test locations used near this tower are on Fig. 25.

8.7.1 Frequency Spectra Near Tower 192

The frequency spectra from 0.015 to 1000 Mc/s was measured at 200 feet from center line of tower. This spectrum is shown on Fig. 49 and was discussed in Sec. 5.16.2. Several frequency spectra were taken in the frequency range of 0.15 to 24 Mc/s. There are shown on Fig. 98 for distances of 200, 1000, 1600, 6000, 10,000 and 21,000 feet from the line. It can be seen that the radio noise at the lowest frequencies is depleted, with lateral distance, at a faster rate than are the higher frequencies. Also to be noted on Fig. 98 is the rapid change in levels at 2 to 6 Mc/s.

These same data have been plotted in another form on Fig. 99. This figure gives the trend with distance from line. These data cannot be used directly since the measurement points are not identified as to the frequency of measurement. It will be noted that the last group of points at 21,000 feet are somewhat higher than would be expected. This was due to a nearby single-phase low-voltage line which was apparently conducting the noise to some extent. It was found that the radio noise dropped when receiver was moved farther from this low voltage line.

8.7.2 Lateral Profiles Near Tower 119

Figures 96 and 97 are the lateral profiles for both sides of the line out to 200 feet with the line normal for frequencies up through 22.23 Mc/s. These indicate a slight dissymmetry about the center line.

Additional data as to effect of the lateral distance was obtained on this line at the higher frequencies, from 10 to 250 Mc/s, at Tower 119. These data are shown on Fig. 100 with the frequencies identified. These curves are similar to those obtained with artificial gap on other lines.

9. Conclusions from Tests with Artificial Gap

9.1 The lateral profile of radio noise field strength from an artificial gap on one phase conductor is unsymmetrical near the gap and becomes more symmetrical at the greater distances from the gap

location.

9.2 The frequency spectra are not the same on both sides of the line. This indicates that lines, especially lines above 110 kV which have appreciable phase spacings, should be measured on both sides of the tower in order to determine the maximum radio noise level.

9.3 Large variations, up to 30 dB, occur in the radio noise field strength in the frequency range of 2 to 8 Mc/s for all steel tower lines tested. For the wood pole line only one minimum (4.85 Mc/s) and only one maximum (5.3 Mc/s) were found.

9.4 The variations in field strength, measured near the tower where gap-type radio noise generator is located, persist laterally from the line and also they can be found several miles down the line from the tower with gap.

9.5 The lateral attenuation for frequencies above about 1.0 Mc/s can be taken as $1/d$ beyond 200 feet, regardless of antenna polarization. Below this frequency, the lateral profile may decrease as $1/d^2$ or $1/d^3$.

9.6 Attenuation longitudinal with distance to 3.85 miles along the line for 20 to 40 Mc/s is about as $1/f^{1/2}$, and for 50 to 125 Mc/s approximately as $1/f$. Although the higher frequencies attenuate rapidly with distance the associated levels may still be significant several miles away from a gap-type noise source.

10. Corrections for Antenna Height for Frequencies 25 Mc/s and Higher

The analysis and data given in the prediction technique for frequencies 25 Mc/s and higher are based on a receiving antenna height of 20 feet. Appendices IV and V discuss the effect of antenna height changes, and Appendix V shows measured and calculated variations resulting from changes in antenna height up to 90 feet for frequencies in the range of 30 to 200 Mc/s at three distances from a power line of 200, 600 and 1998 feet (Fig. 13 of Appendix V). Within this range of frequencies the maximum of the average increase of measured field strength with antenna heights was 12 dB referred to the field strength level at 24 foot height. Similar values from calculations at these three distances were 10 to 19 dB. At what frequency these maximums occur depends on the particular distance, and will vary because of the interaction (cancellation or reinforcement) between the direct field and ground reflections with height and distance. (See, for example, Fig. 16 and Section 10 of Appendix IV). Because of the variation in the way the direct field and ground reflections interact, curves similar to those of Fig. 13

of Appendix V at a particular distance other than the three given can only be obtained by measurement or calculation at that particular distance.

Therefore, it is proposed that if a correction for antenna height up to 90 feet be desired for distance 2000 feet or less for frequencies 25 Mc/s and higher that a value of 12 dB be used, regardless of actual antenna height. It should be recognized that slight changes in antenna height, particularly at the higher frequencies, can make significant changes in received levels (see Appendix V).

For distances beyond 2000 feet (where the received field strength begins to vary inversely with the square of distance) the literature indicates an increase of about 18 to 20 dB per decade of antenna height, or (again) about 12 dB from 24- to 90-foot antenna heights. (See Appendix IV, Section 2.9).

11. Recommendations

11.1 It is recommended that field strength measurements be made at 50 feet or 200 feet horizontally from the outside phase conductor.

11.2 It is desirable to improve field strength measurement techniques mainly to obtain the data in a shorter time. It may be possible to obtain useful data with recorders or spectrum analyzers.

11.3 The measurements reported should be extended to overhead ac power lines 500 to 750 kV and dc lines up to 800 kV and frequency should be extended to 10,000 Mc/s.

11.4 The effects of parallel lines and line cross-overs should be investigated by measurements.

11.5 There are means, such as adding conductors, or by using magnetic tape wrapping on conductors to increase attenuation, which will reduce radio noise. These means are to reduce radio noise generation and to increase attenuation even for EHV lines and lines coupled to noisier lines. Feasible methods may not be expensive since only a short length of the line will need to be modified in many cases. More complete information by experimentation is necessary in order to make more definite recommendations.

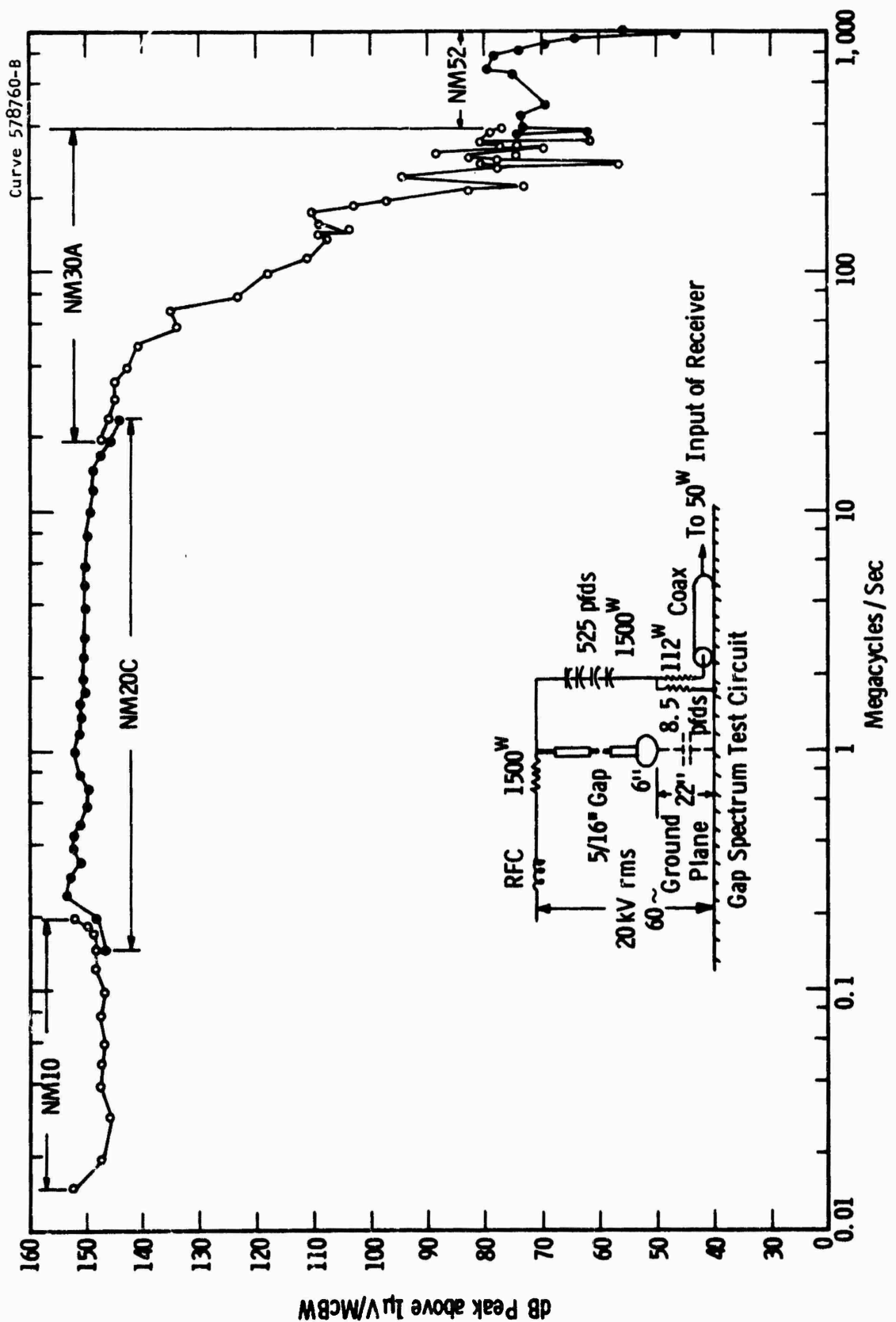


Fig. 1 —Frequency spectrum of 5/16" gap in air as measured in laboratory

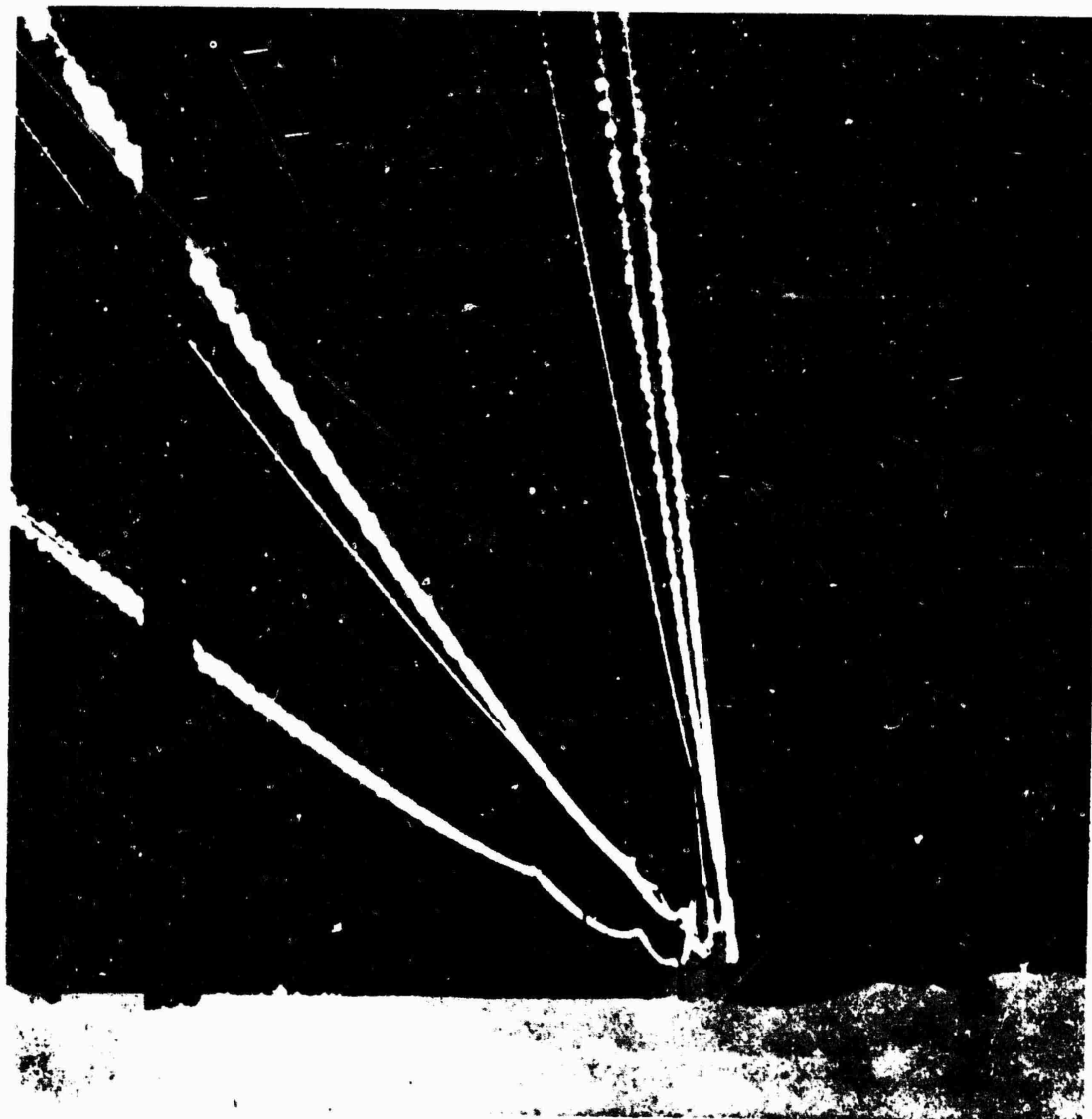


Fig. 2. Corona on high voltage conductors and the ground wires on a test line at 10,700 foot altitudes.

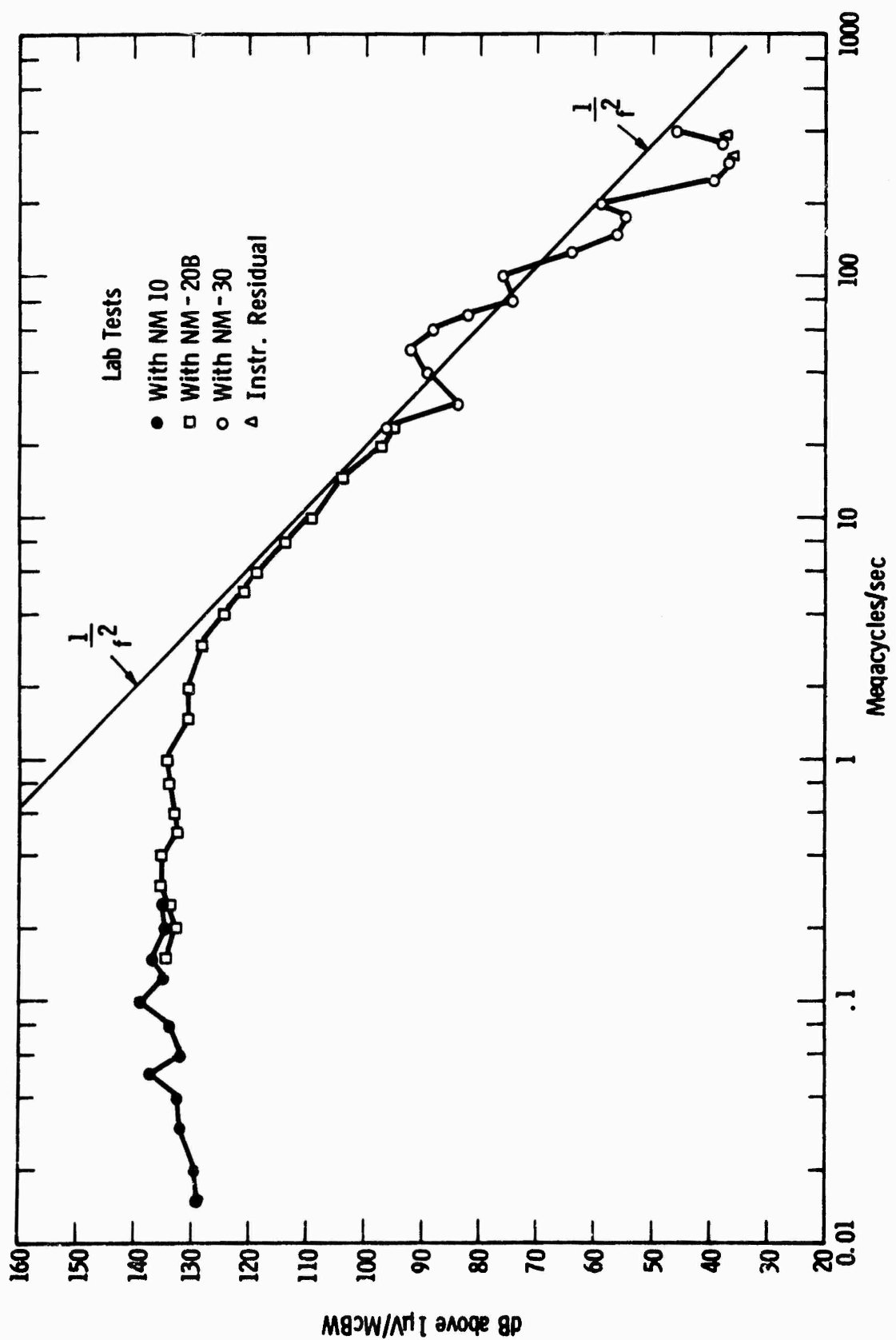


Fig. 3—Frequency spectrum of corona radio noise voltage from conical rivet

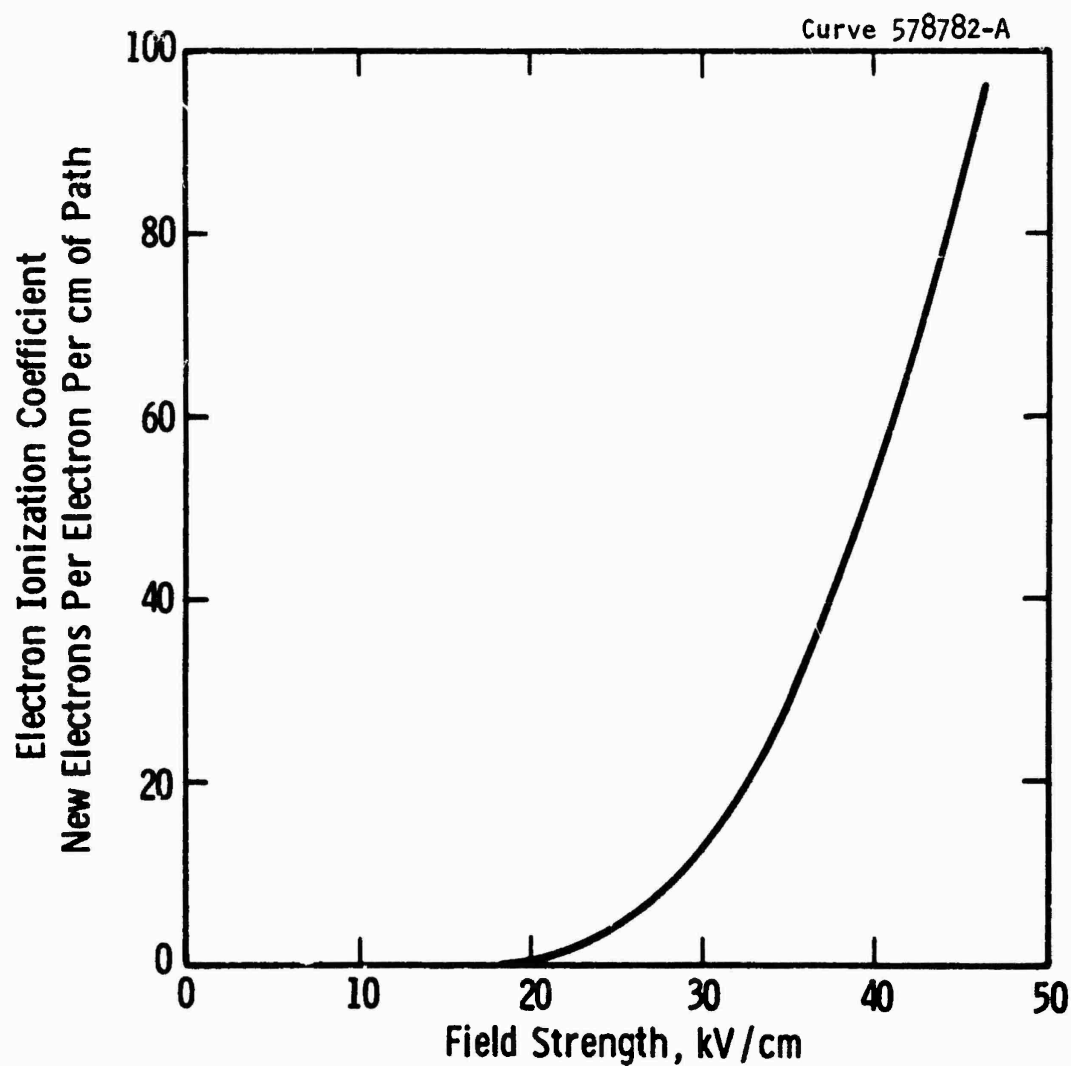
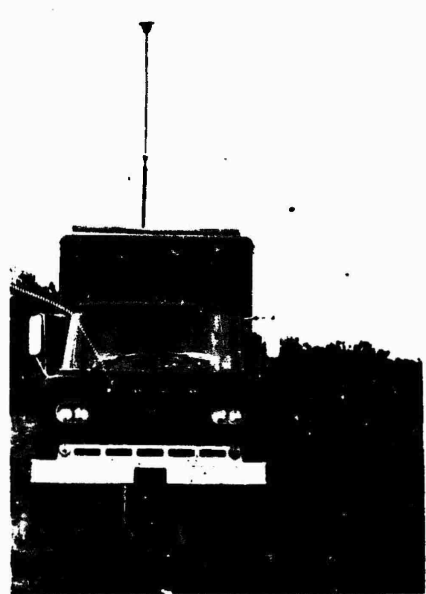
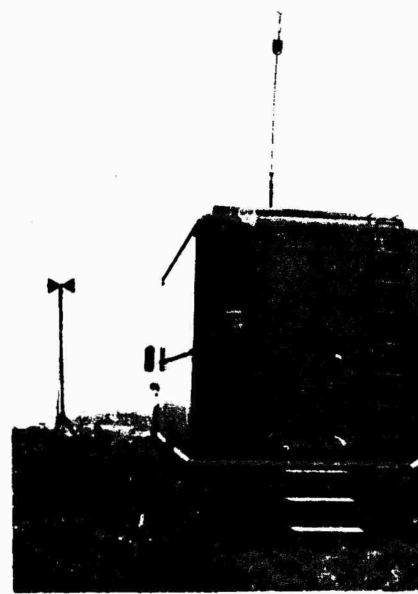


Fig. 4—Ionization by collision
(Electrons in air at atmospheric pressure)



(a) Tunable Dipole Antenna



(b) Broadband Antennas

Fig.5 . Van Used for Instruments and Antenna Mounting.

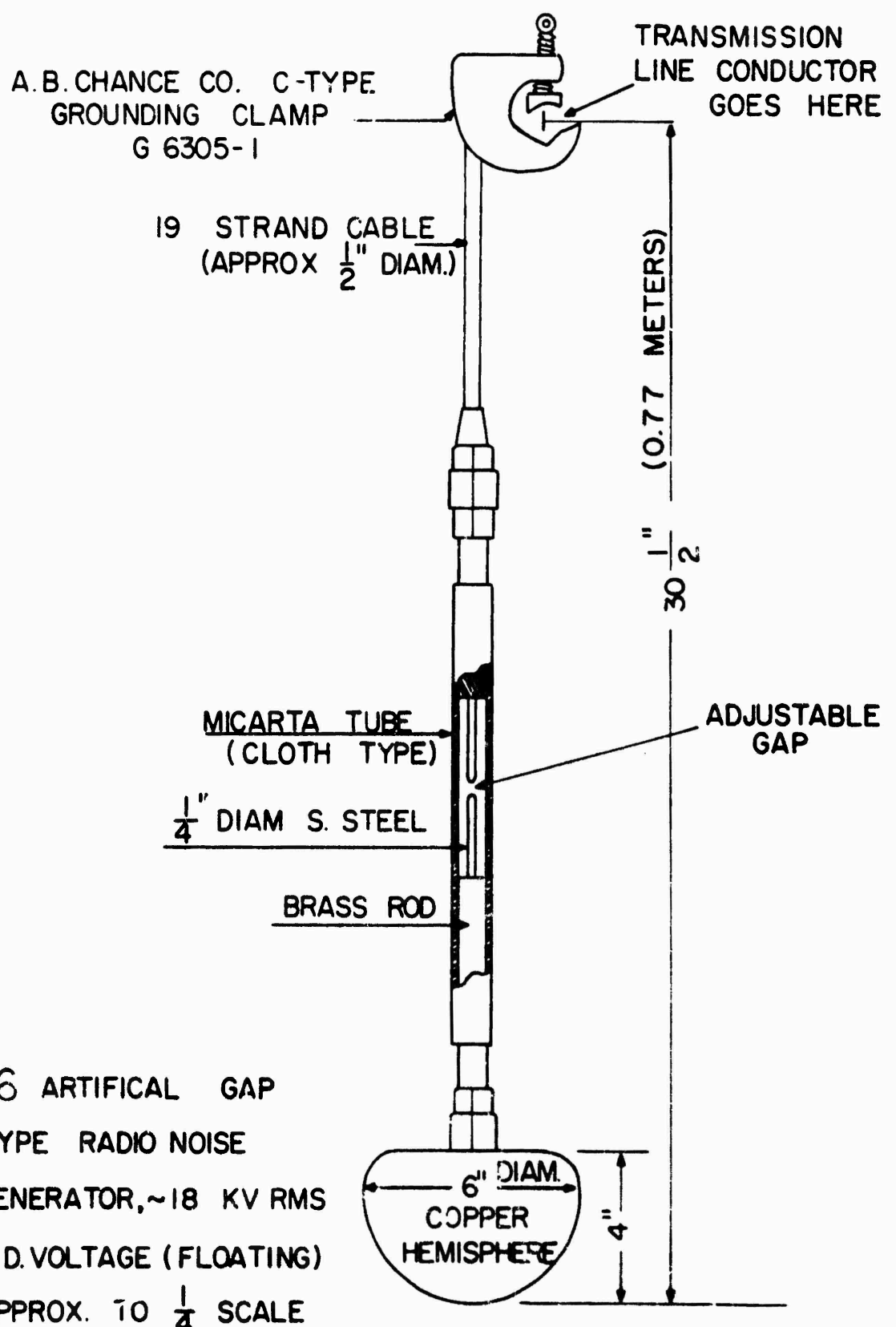
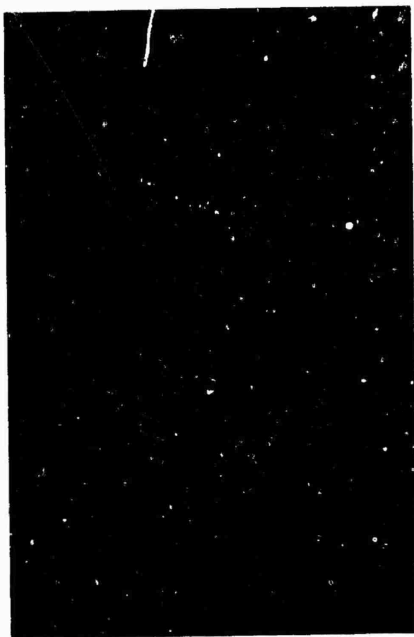
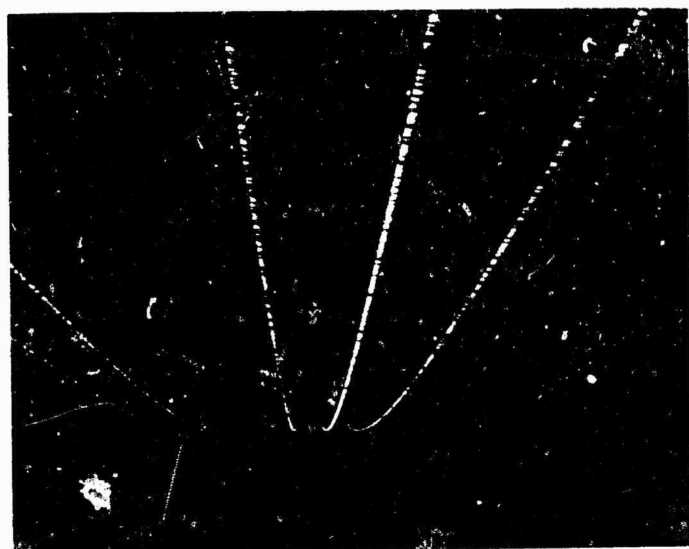


FIG. 6 ARTIFICAL GAP

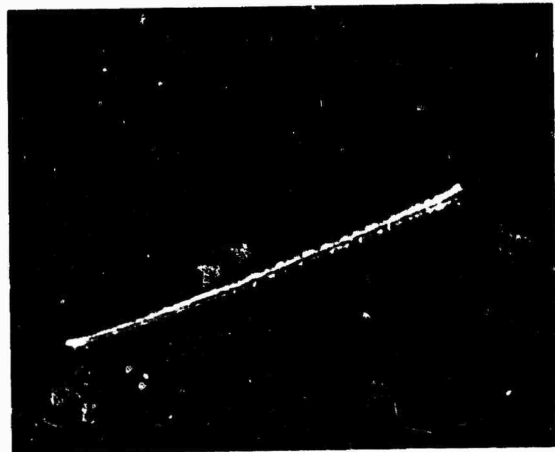
TYPE RADIO NOISE
 GENERATOR, ~18 KV RMS
 B.D. VOLTAGE (FLOATING)
 APPROX. TO $\frac{1}{4}$ SCALE



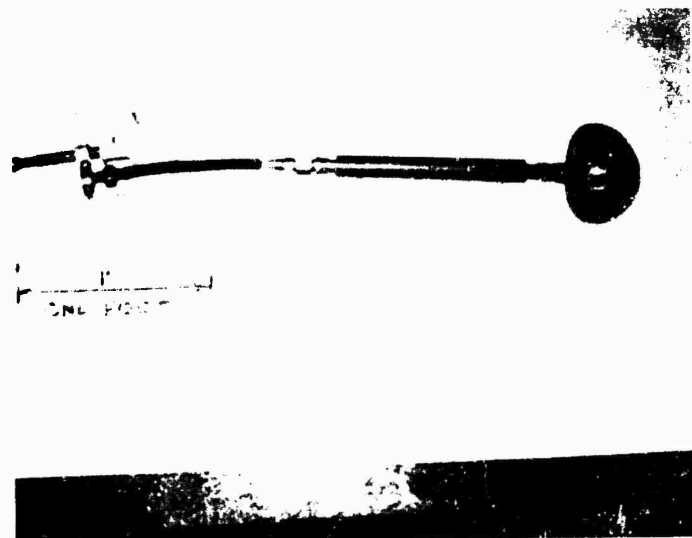
(a) Radio Noise Source (Bright Spot) taken at Night



(b) 230 kV Lines in Corona (Night Photo)



(c) Corona on 1.5 inch diam. Conductor in Artificial Rain, Lab. Tests

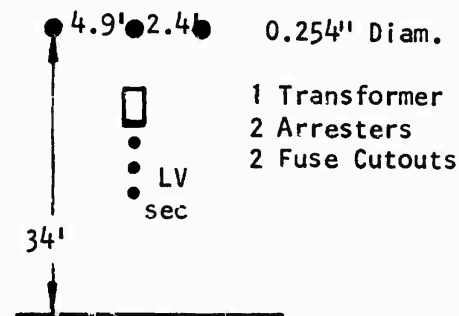


(d) Artificial Gap Type Radio Noise Generator

Fig. 7

Dwg. 851A984

2.4 KV



X 50' No.

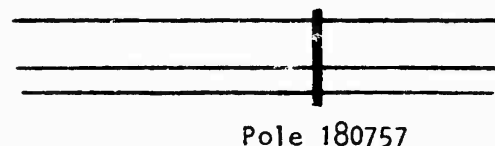


Fig. 8 —Test location at 2.4 KV wood pole line

Dwg. 851A985

4.16 KV

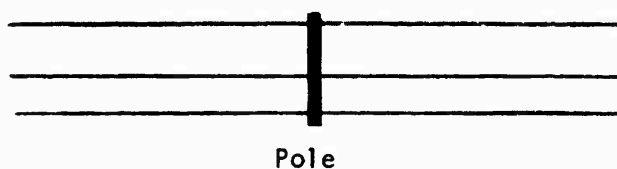
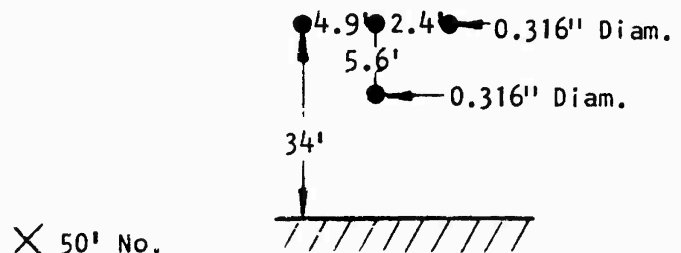
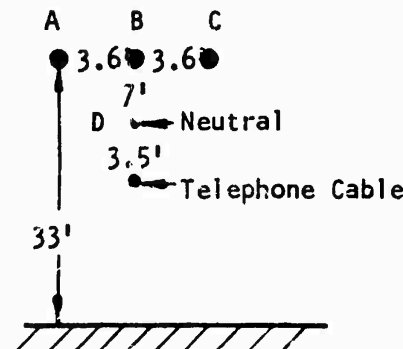


Fig. 9 -Test location at 4.16 KV wood pole line

Dwg. 851A986

8 KV



A and C 0.29" Diam.
B and D 0.316" Diam.

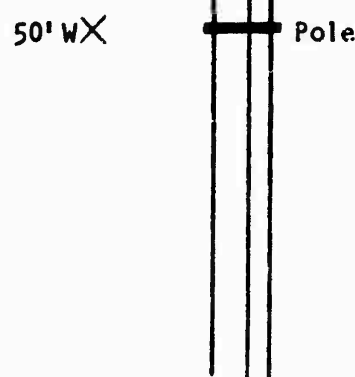


Fig. 10 -Test location at 8 KV wood pole line

Dwg. 851A987

12.5 KV

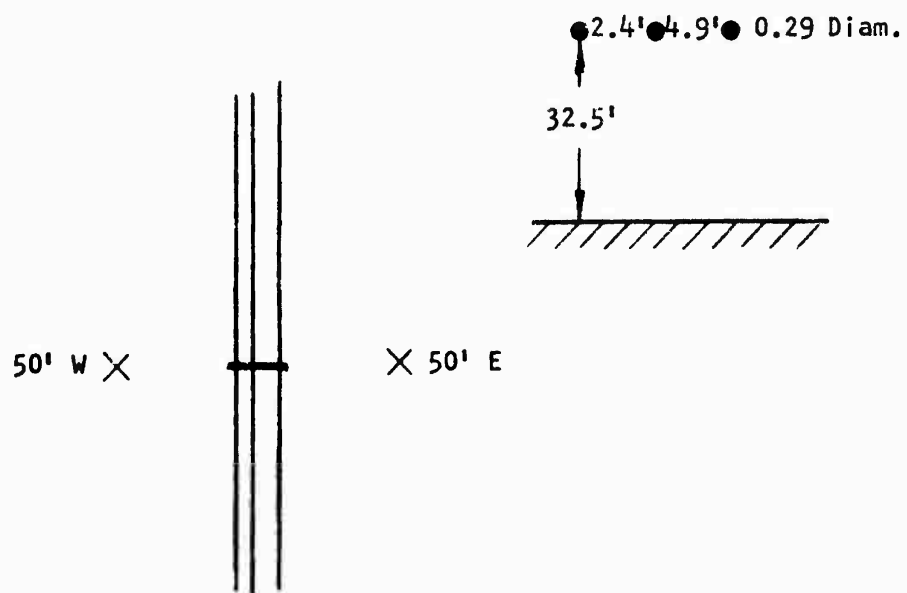


Fig. 11 -Test locations at 12.5 KV wood pole line

Dwg. 851A989

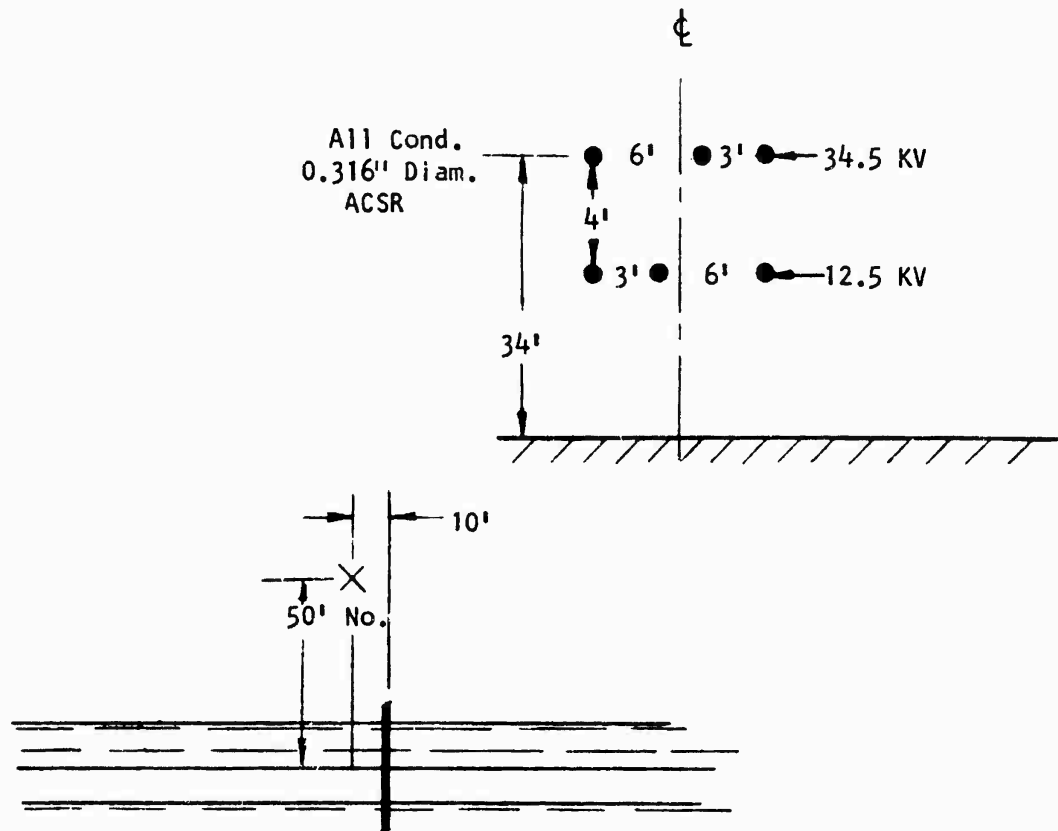


Fig. 12 -Test location at 34.5 and 12.5 KV wood pole line

Dwg. 851A988

34.5 KV

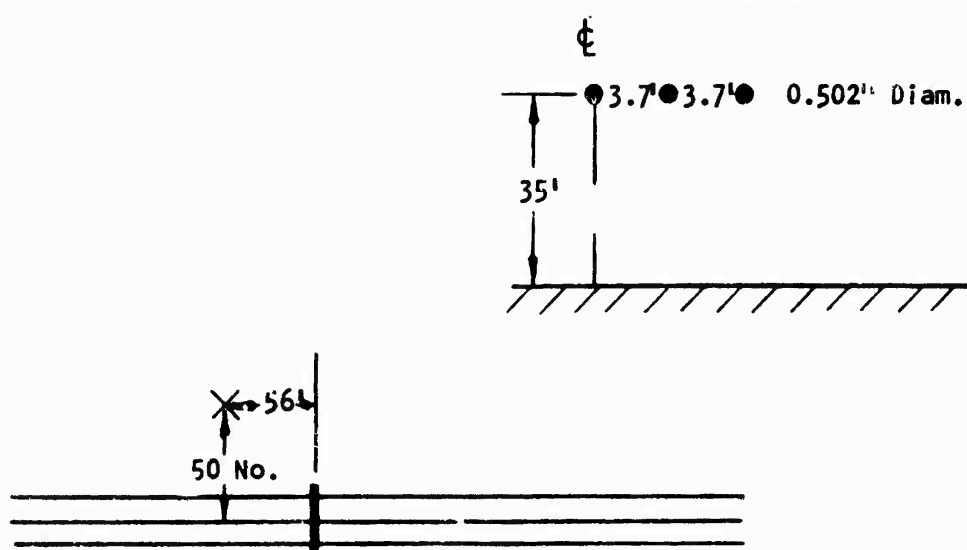


Fig. 13 -Test location at 34.5 KV wood pole line

Dwg. 851A990

46 KV

0.447" Diam. Conductors

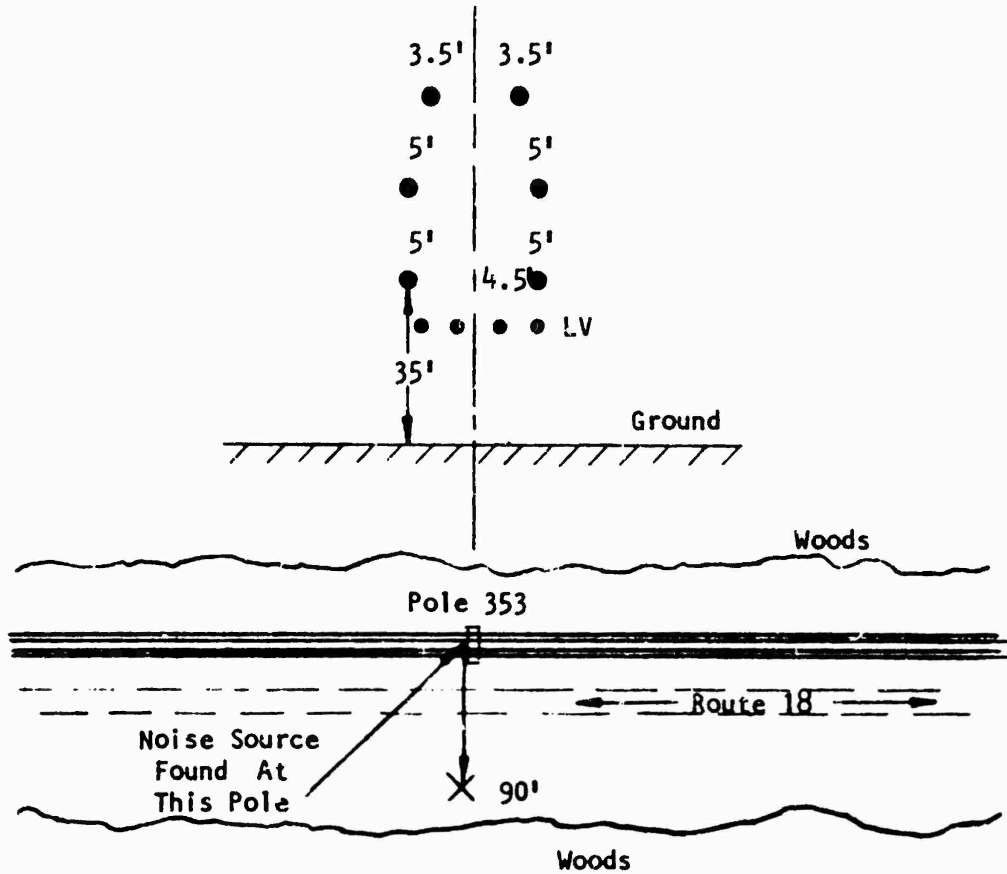


Fig. 14 -Test location on double circuit 46 KV line

Dwg. 851A.991

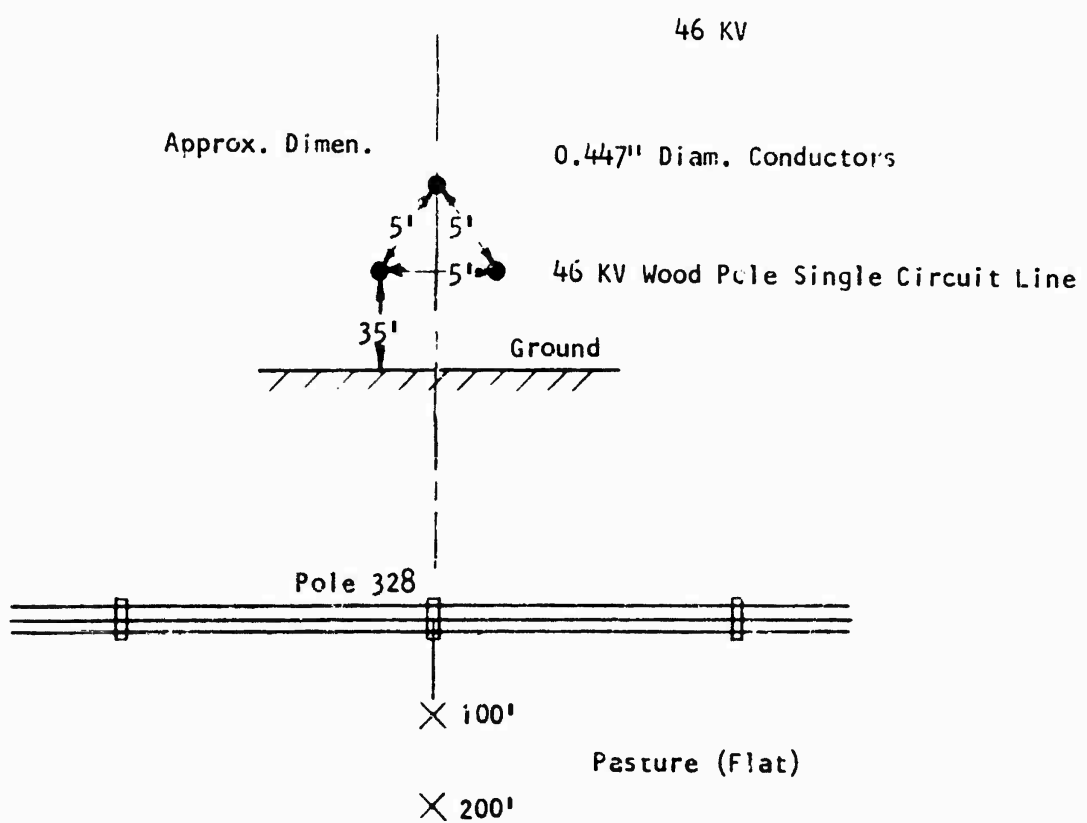
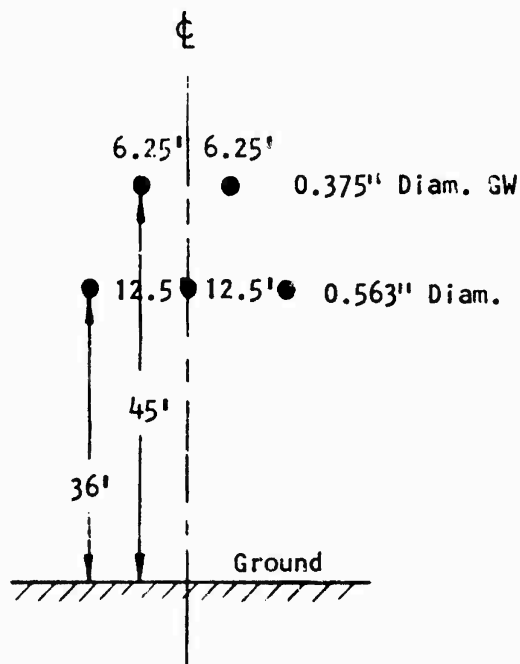


Fig. 15 --Test location on single circuit 46 KV line

Dwg. 851A992

69 KV



69 KV Wood Pole H-Frame Line

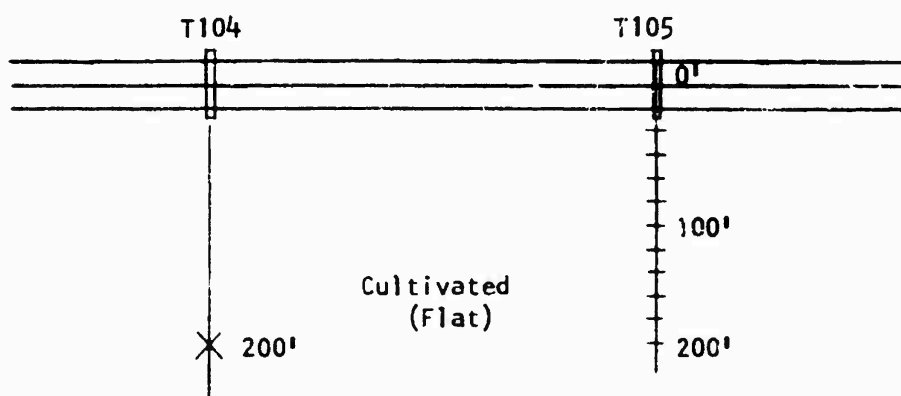


Fig. 16—Test locations at 69 KV horizontal line

Dwg. 851A993

115 KV

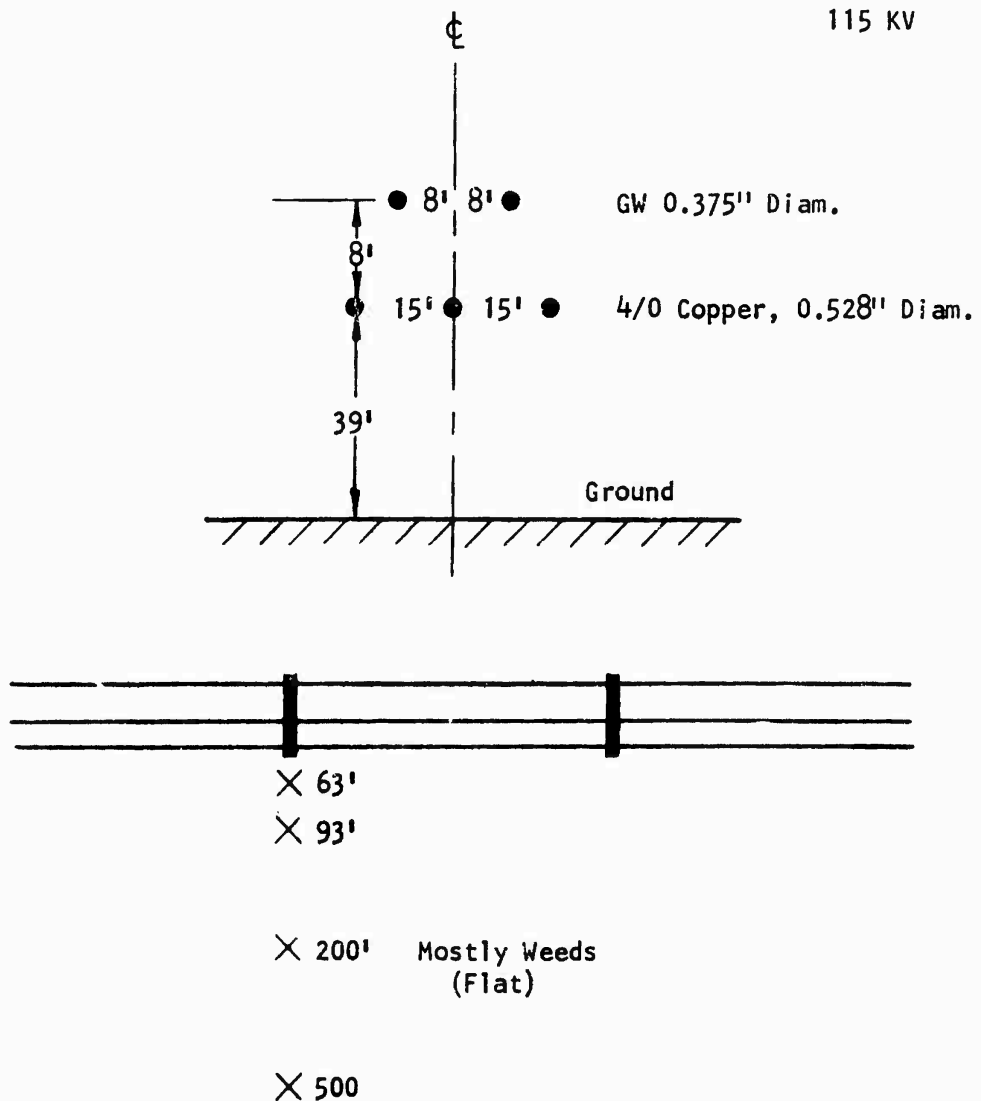


Fig. 17 -Test locations at 115 KV H-frame wood pole line

Dwg. 851A995

138 KV

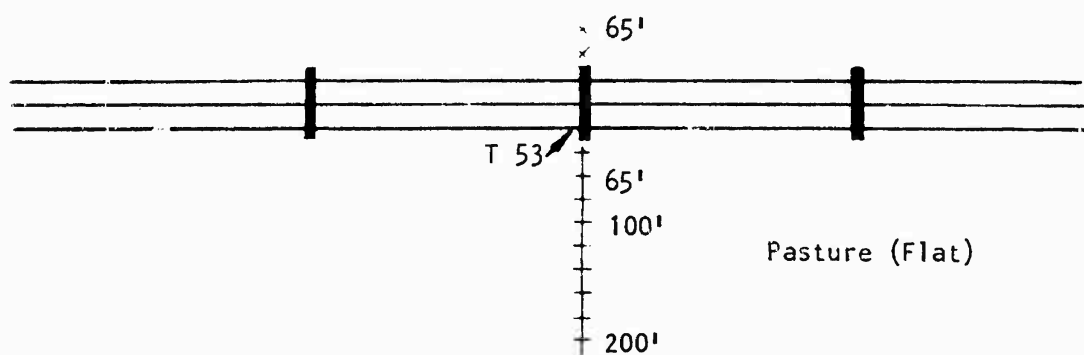
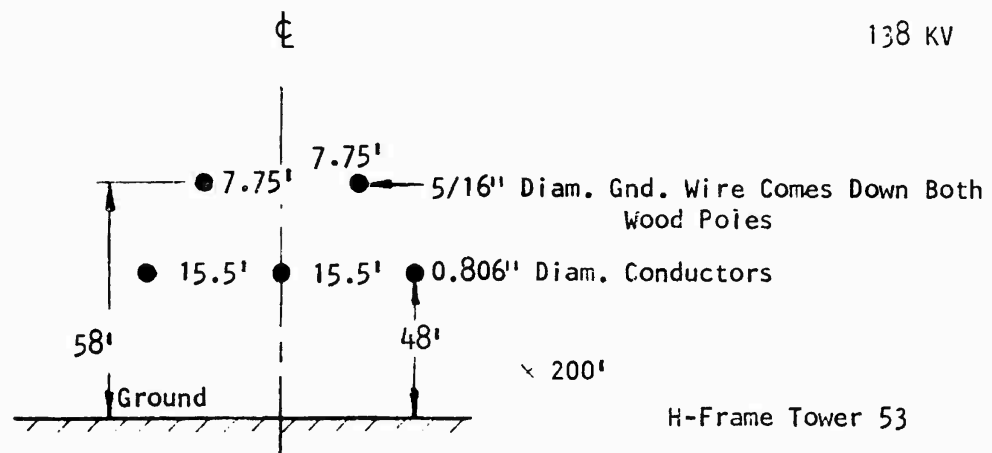


Fig. 18 -Test locations at 138 KV wood pole line

Dwg. 851A996

161 KV

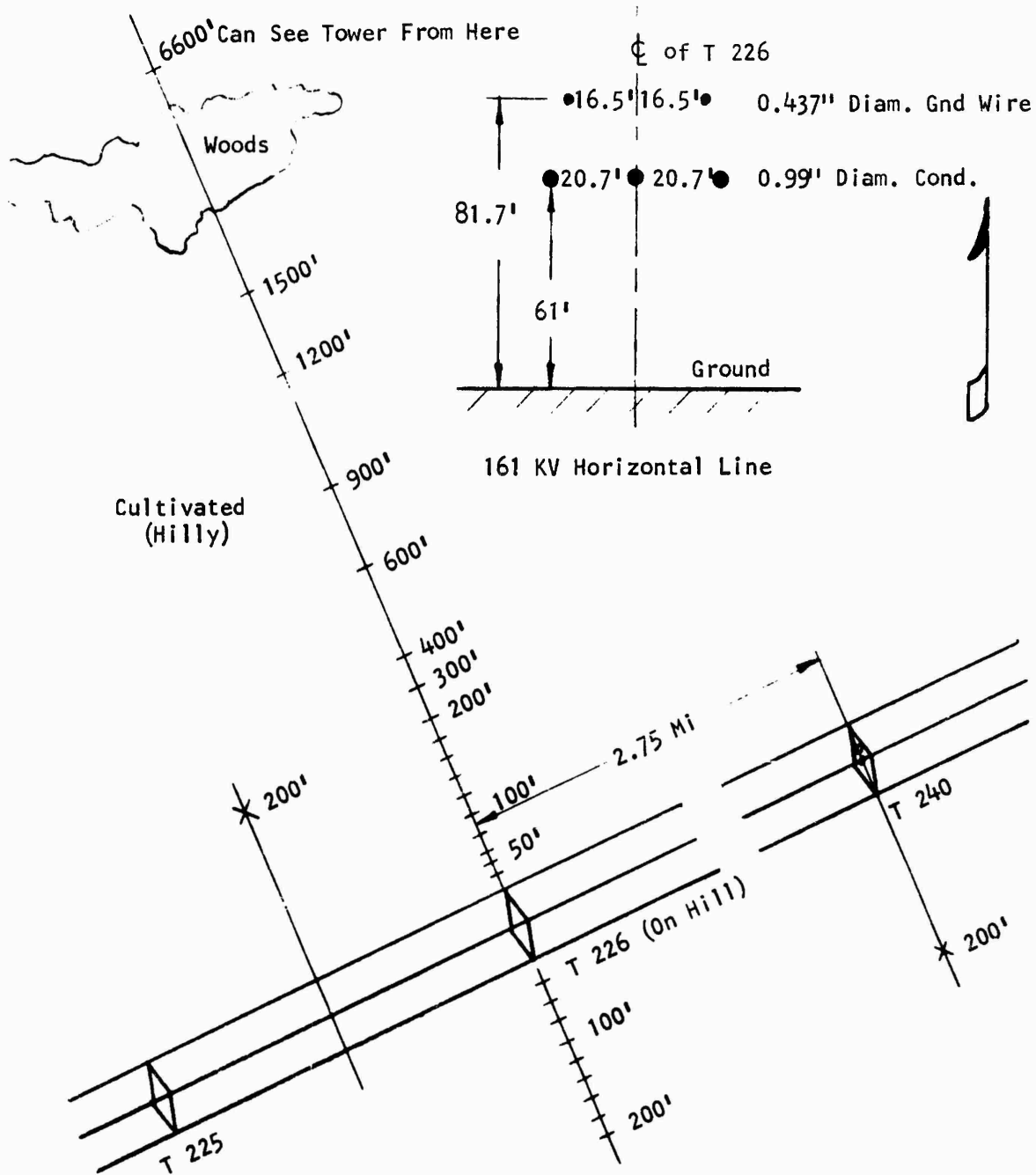


Fig. 19 -Test locations at 161 KV horizontal line

Dwg. 851A997

244 KV

of Tower

0.5" Diam. GW

1.246" Diam.
Conductors

20.34' 20.34'

28'

28'

56.5'

79.8'

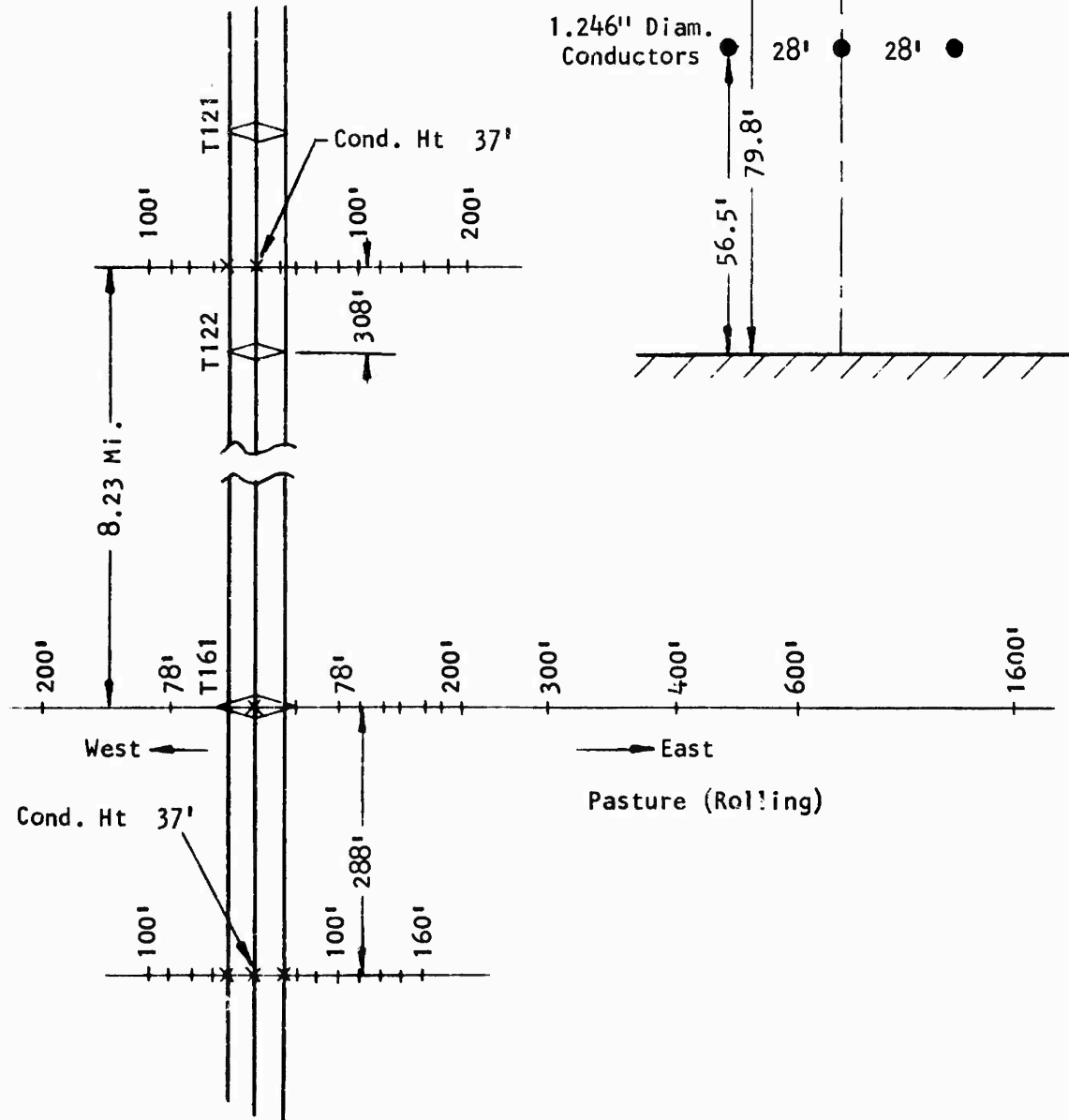


Fig. 20 -Test locations at 244 KV steel tower line

Dwg. 851A958

345 KV

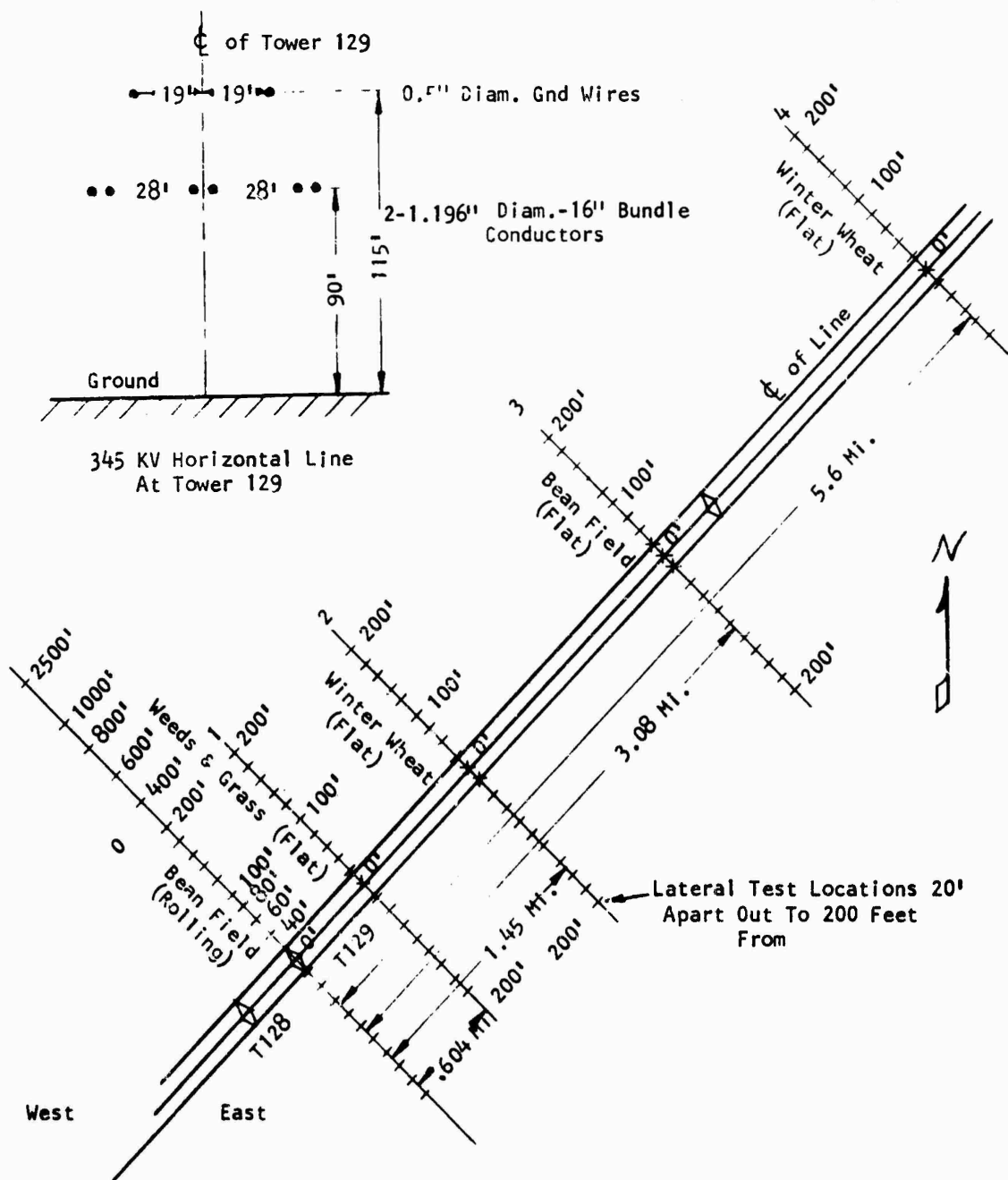


Fig. 21 –Test locations along 345 KV horizontal line

Dwg. 851A999

345 KV

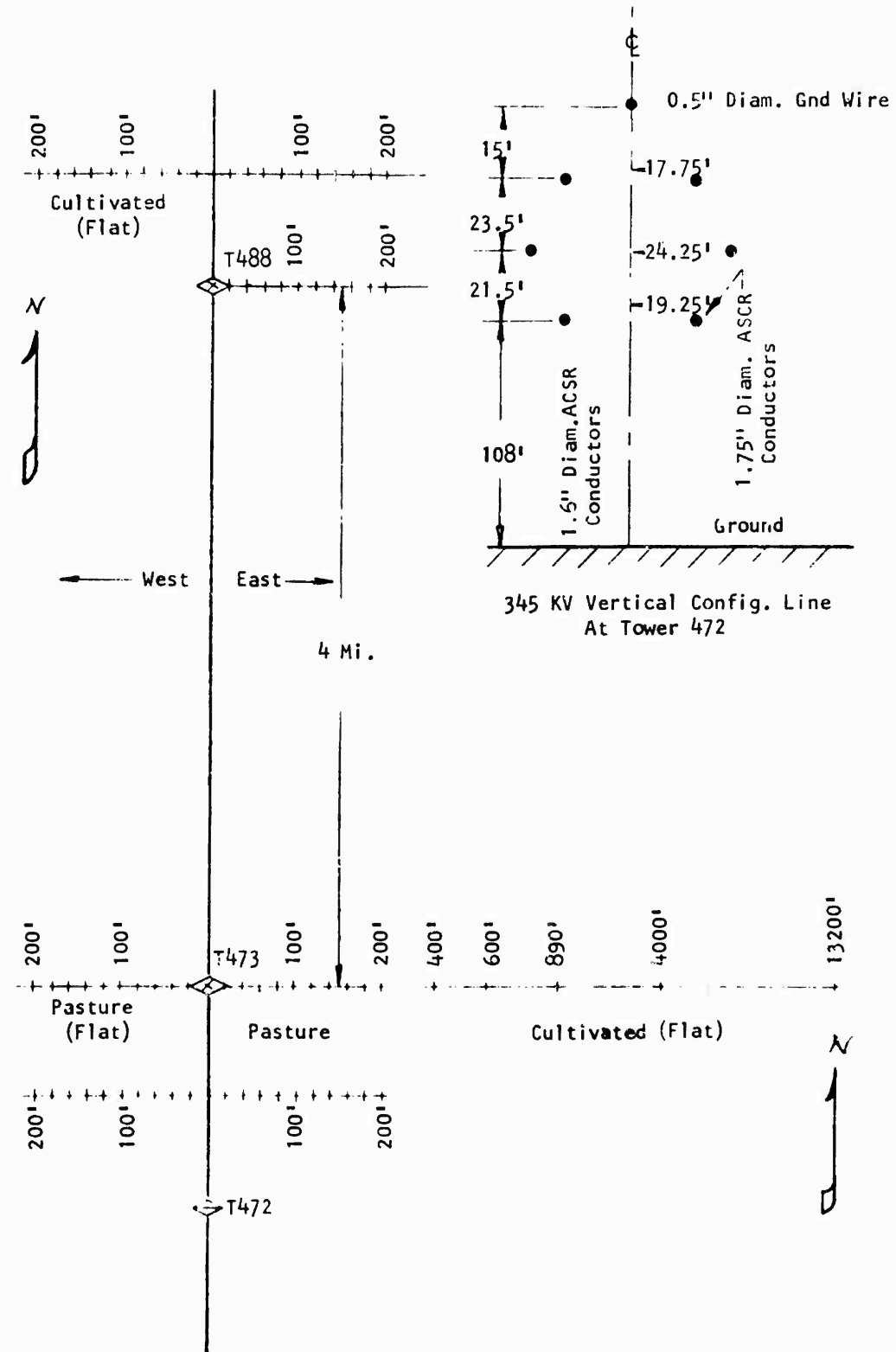


Fig. 22 -Test locations 345 KV vertical line

Dwg. 851A994
345 KV

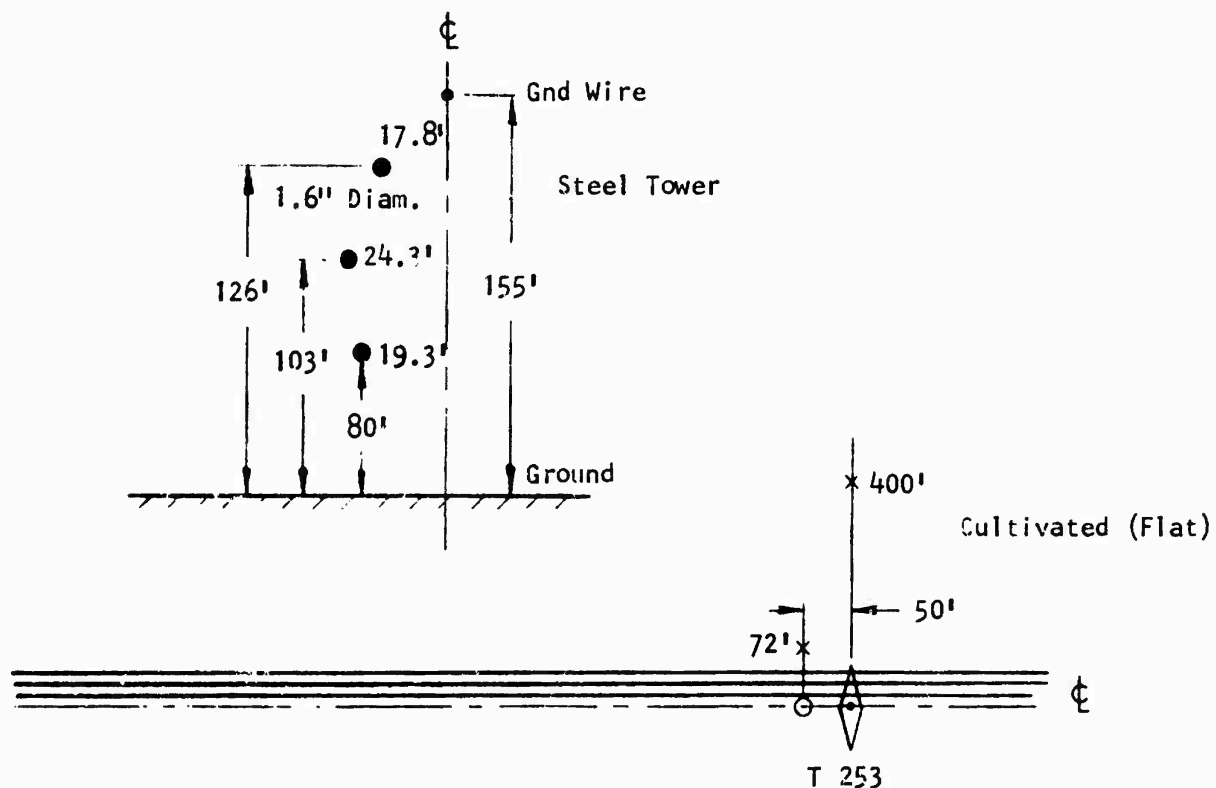


Fig. 23 -Test locations at 345 KV single circuit vertical line

Dwg. 852A003

345 KV

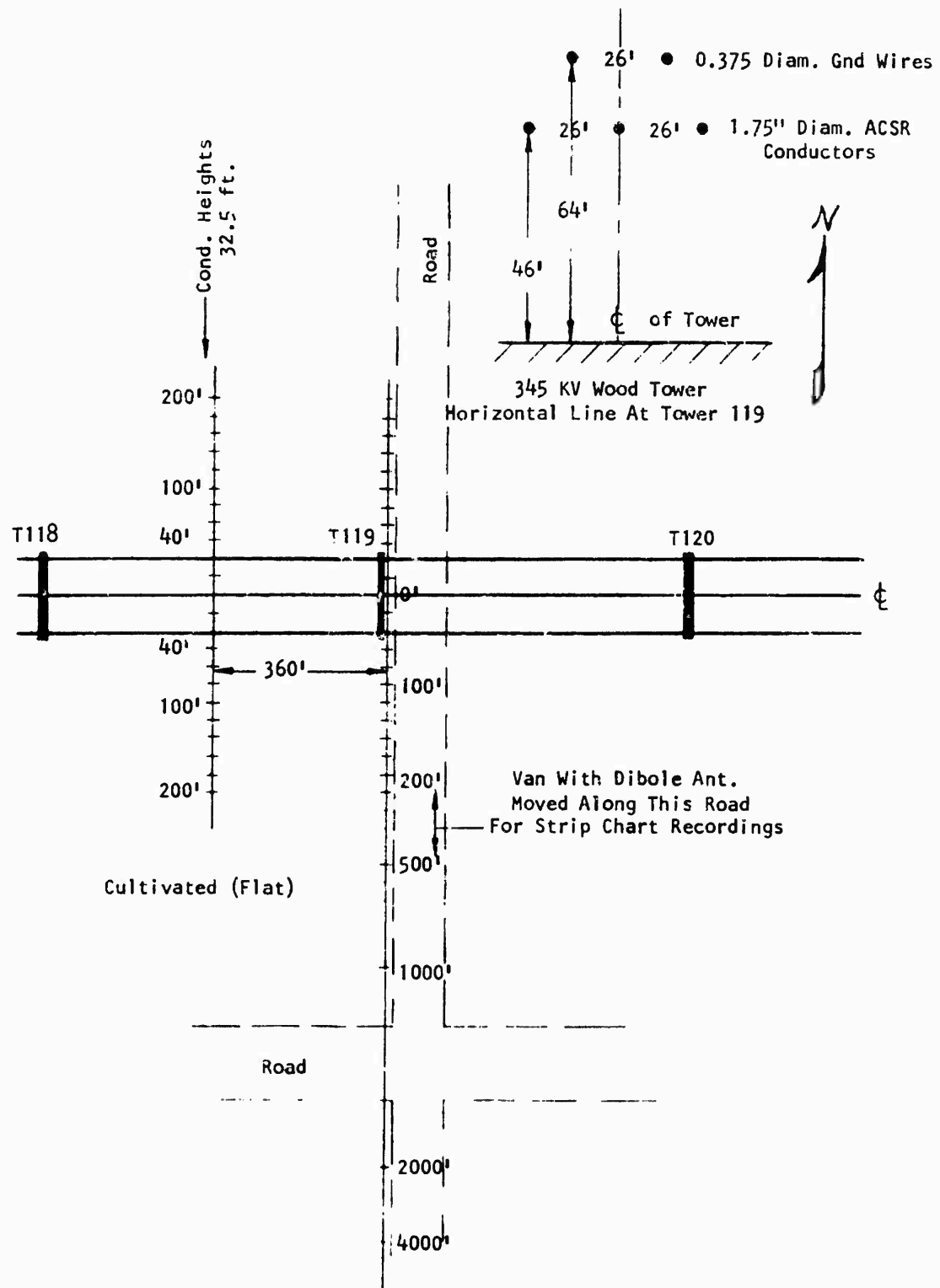


Fig. 24 - Test locations at tower 119 on 345 KV wood pole line

Dwg. 852A001

345 KV

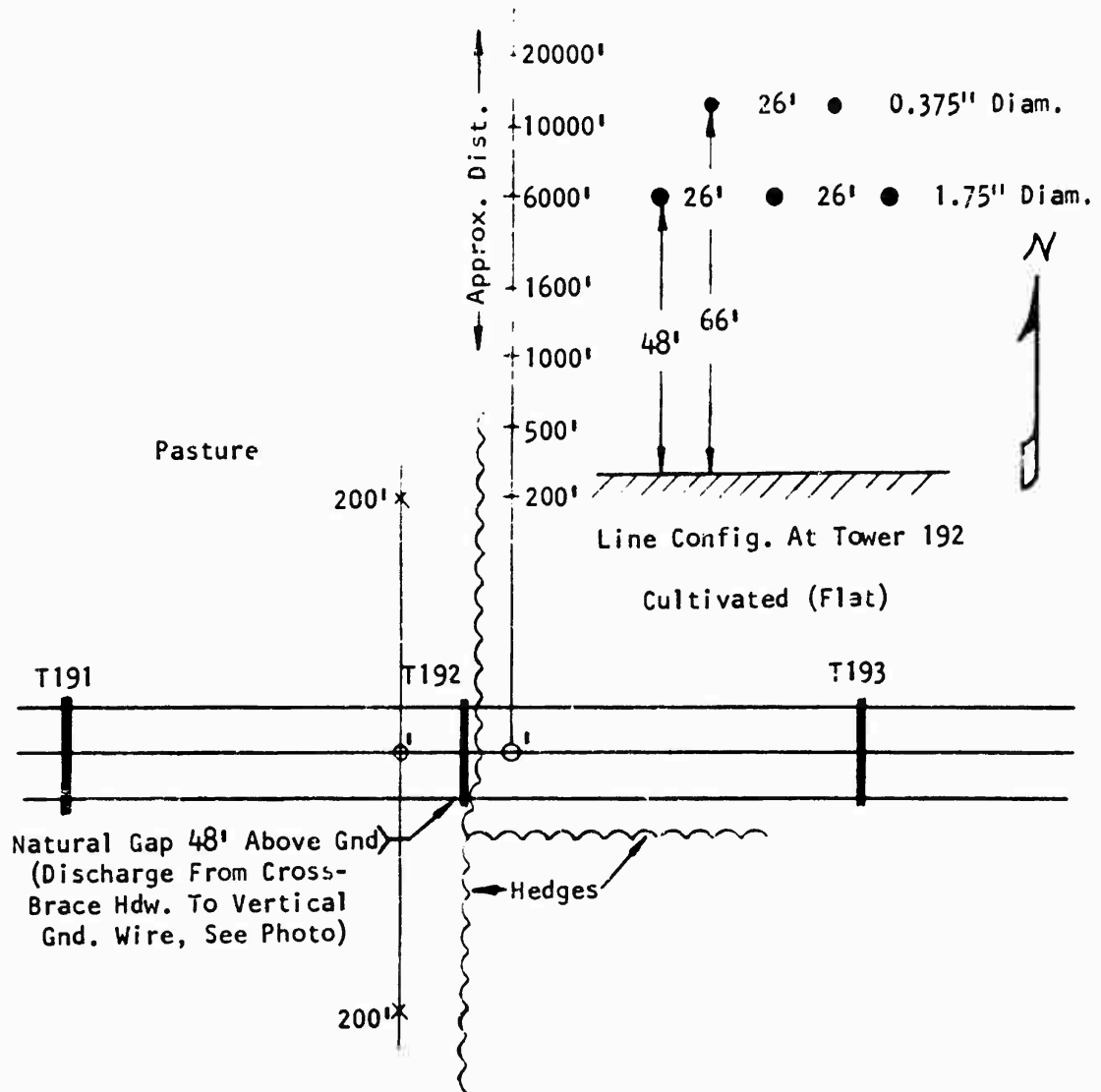


Fig. 25 -Test locations at 345 KV wood tower line where natural gap-type discharge was found

Dwg. 852A002

345 KV

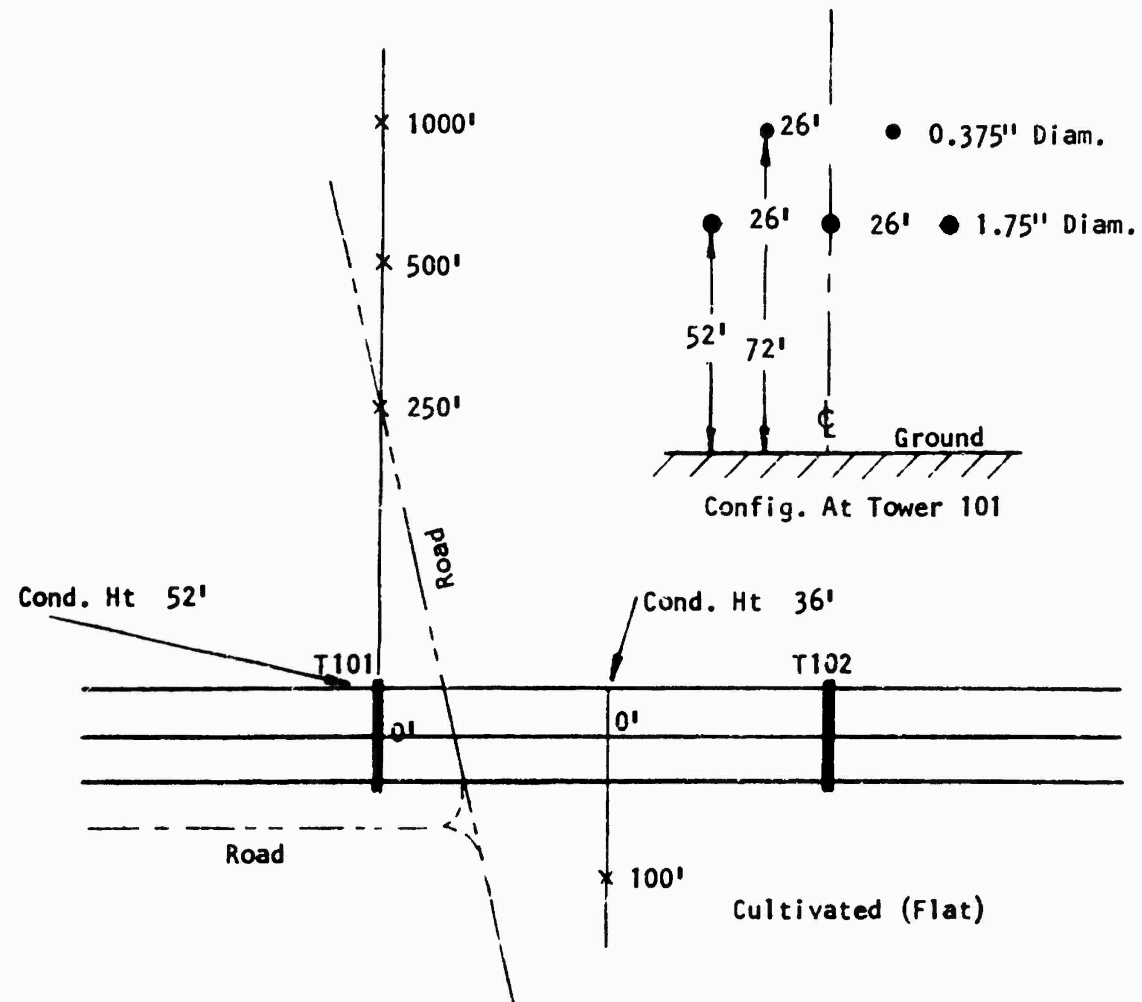


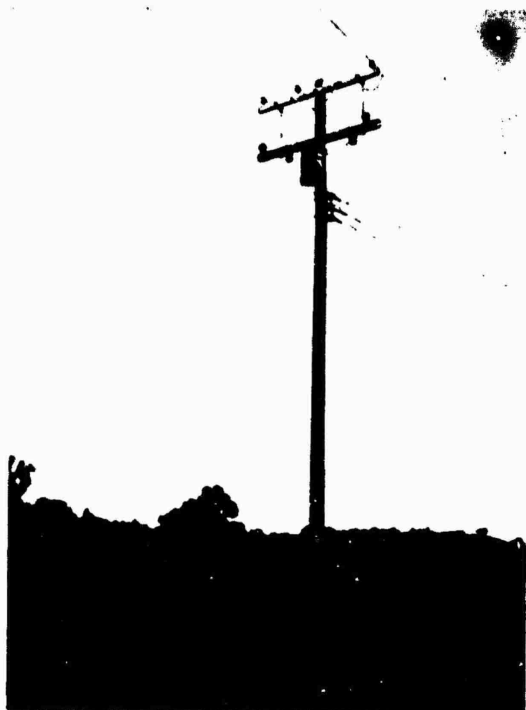
Fig. 26 -Test Locations at tower 101 on 345 KV wood pole line



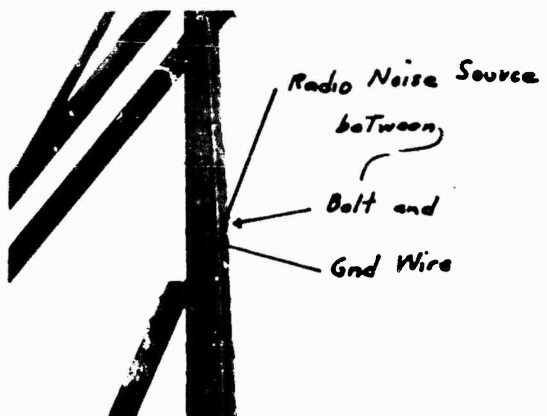
(a) 8 kV with Fuse Cutouts



(b) 4.16 kV Single Circuit



(c) 2.4 kV with Transformer,
Cutouts, and Arresters



(d) Radio Noise Source Found
Between Hardware and Gnd Wire

Fig. 27



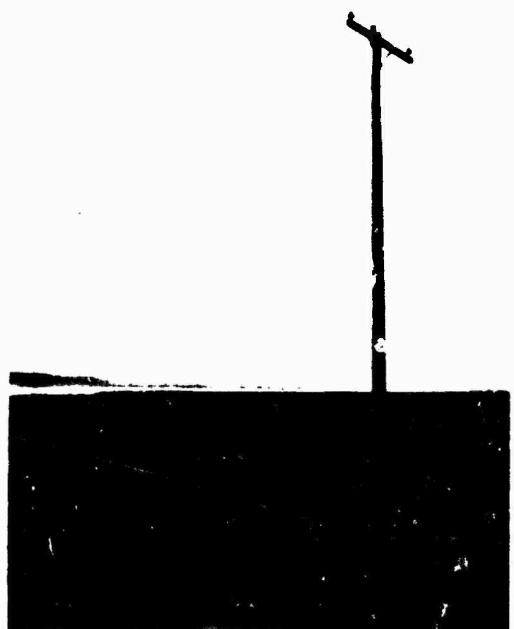
(a) 34.5 kV Single Circuit



(b) 34.5 kV and 12.5 kV Dual

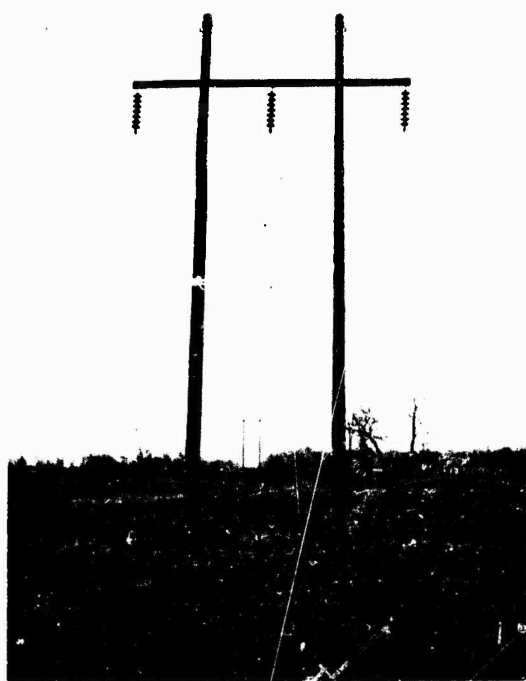


(c) 34.5 kV and 12.5 kV Dual



(d) 12.5 kV Single Circuit

Fig. 28



(a) 69 kV H-Frame Wood Pole



(b) 46 kV Single Circuit

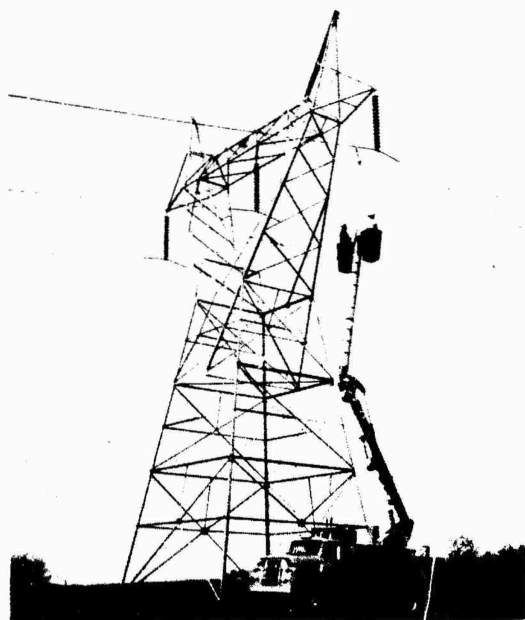


(c) 46 kV Double Circuit

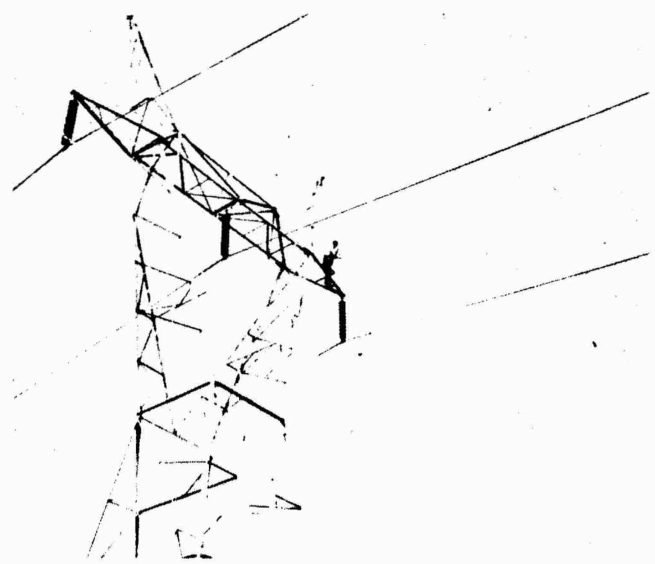


(d) 46 kV Substation

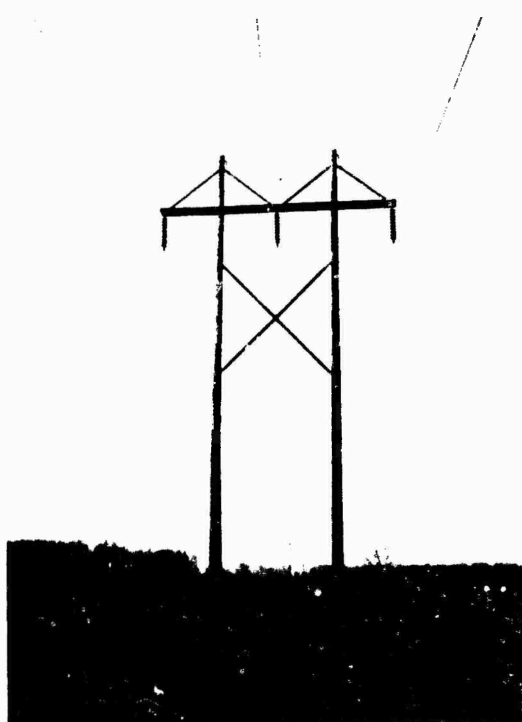
Fig. 29



(a) 244 kV Horizontal



(b) 161 kV Horizontal

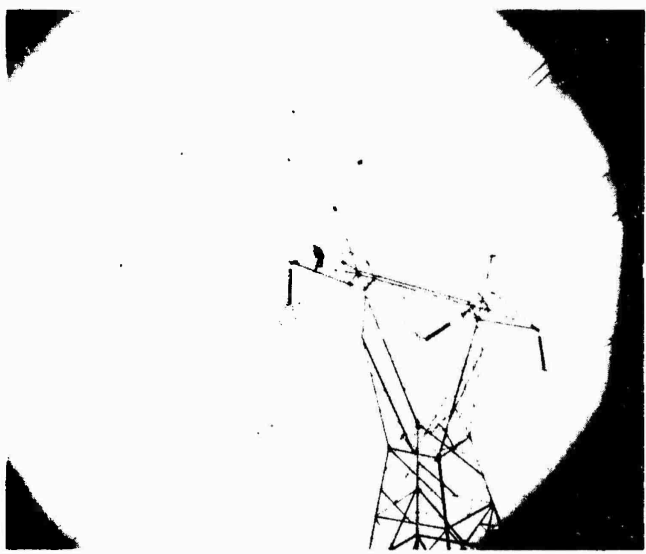


(c) 138 kV H-Frame Wood Pole

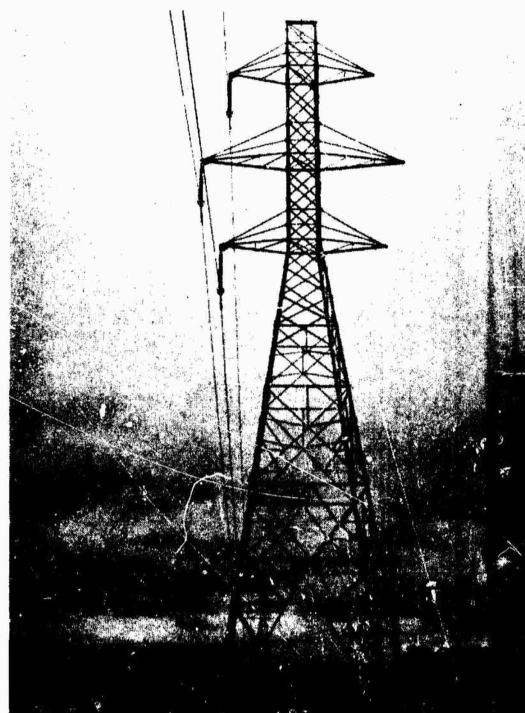


(d) 115 kV H-Frame Wood Pole

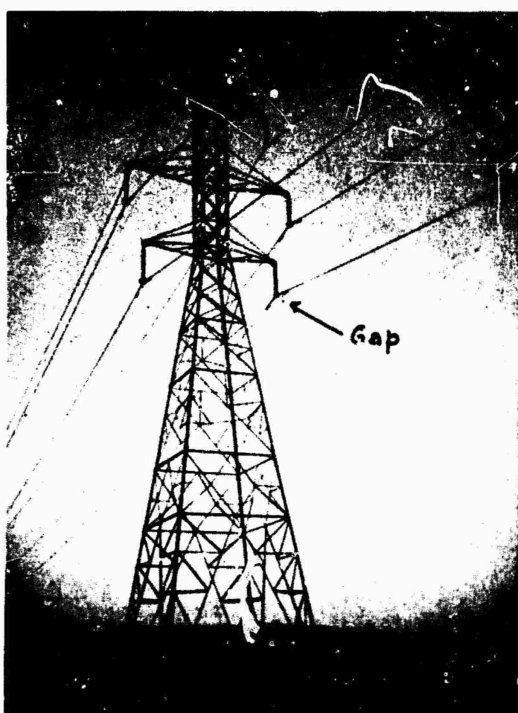
Fig. 30



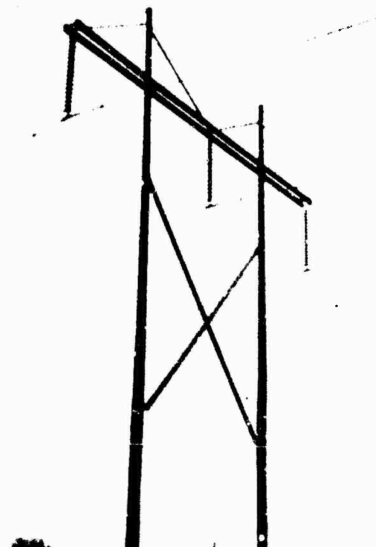
(a) 345 kV Horizontal



(b) 345 kV Single Circuit Vertical



(c) 345 kV Double Circuit Vertical



(d) 345 kV Horizontal (Wood Pole)

Fig. 31

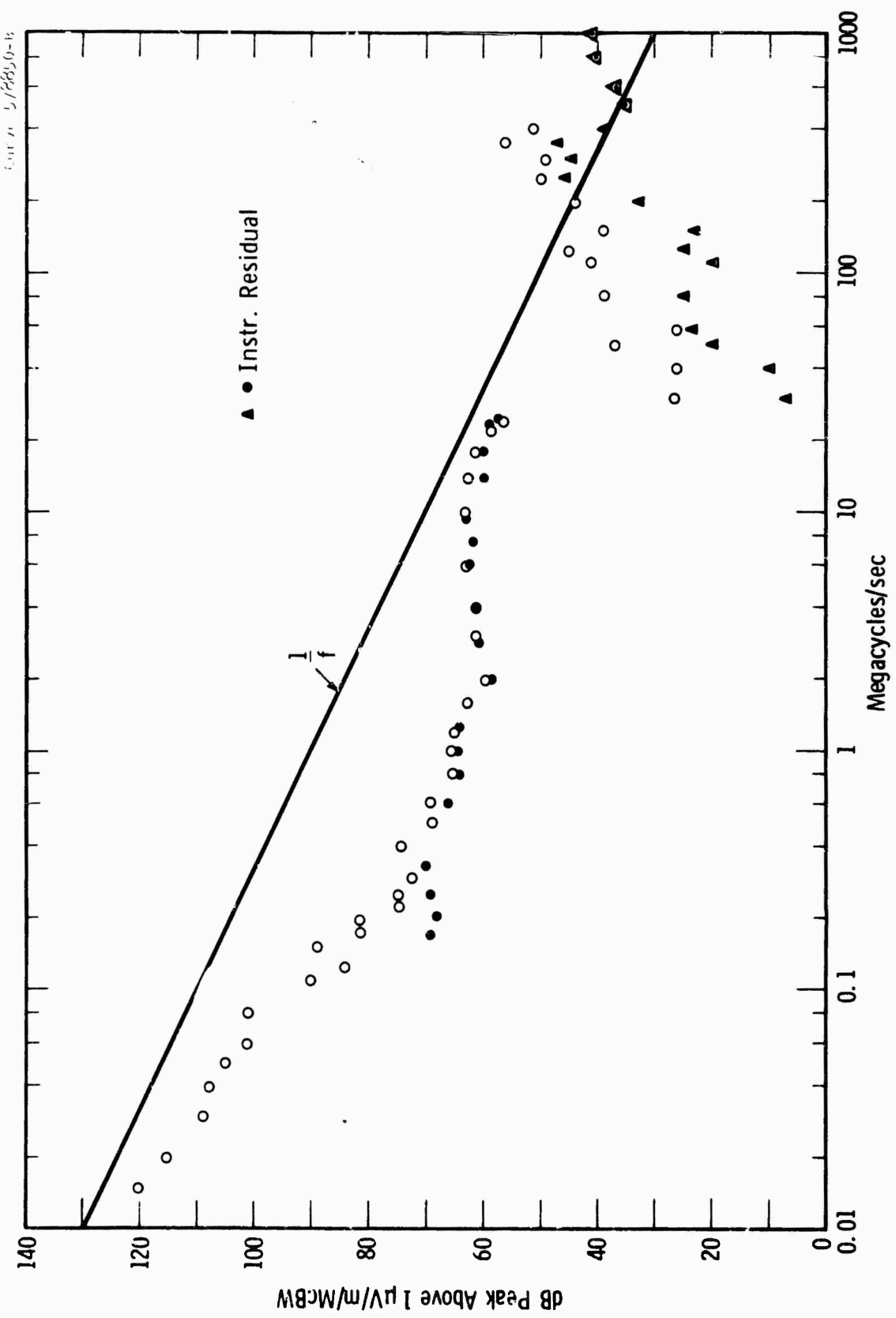


Fig. 32—2.4 kV WP line frequency spectrum at 50 ft. laterally from pole

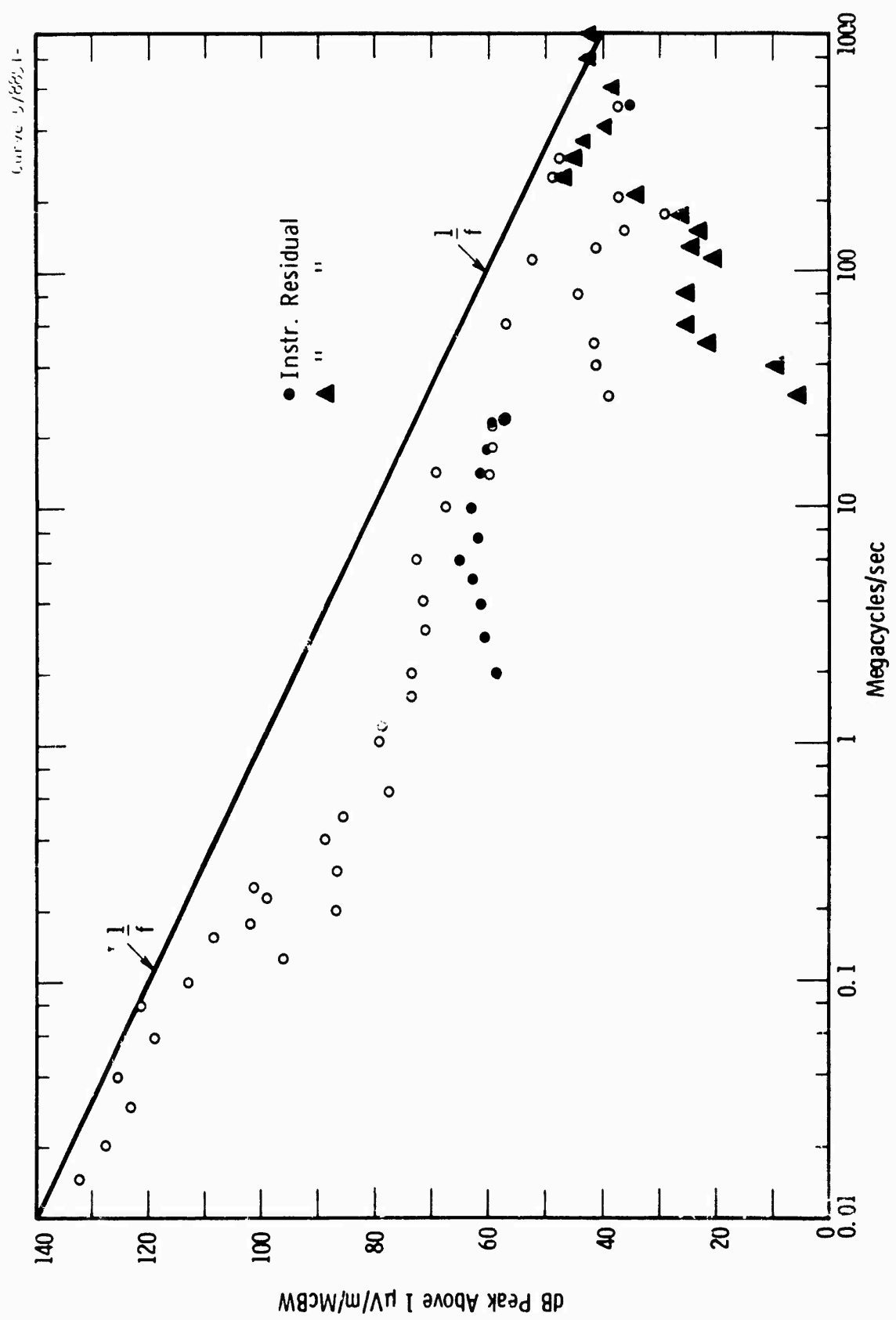


Fig. 33-4. 16 kV WP line frequency spectrum at 50 ft. laterally from pole

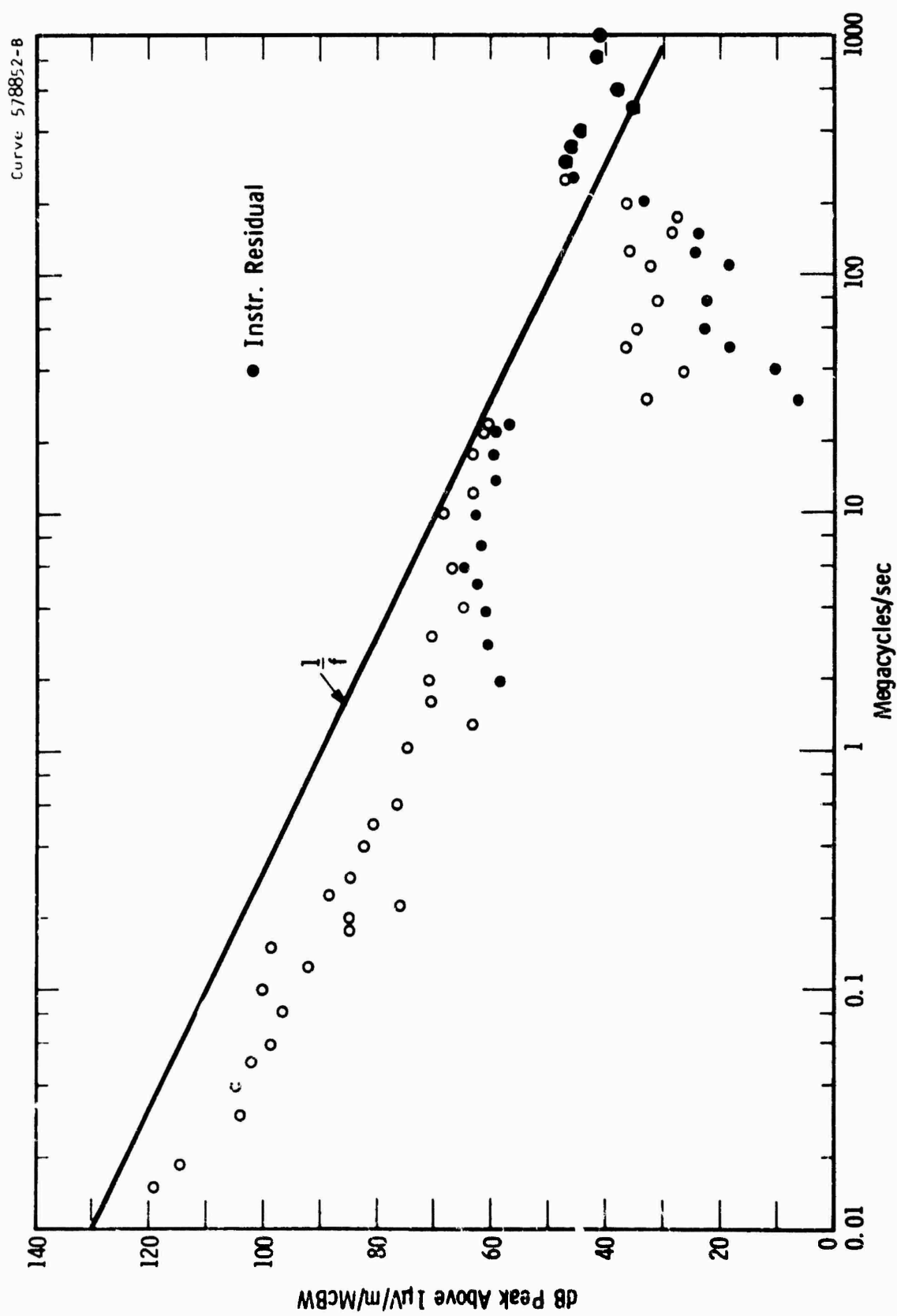


Fig. 34—8 kV WP line frequency spectrum at 50 ft. laterally from pole

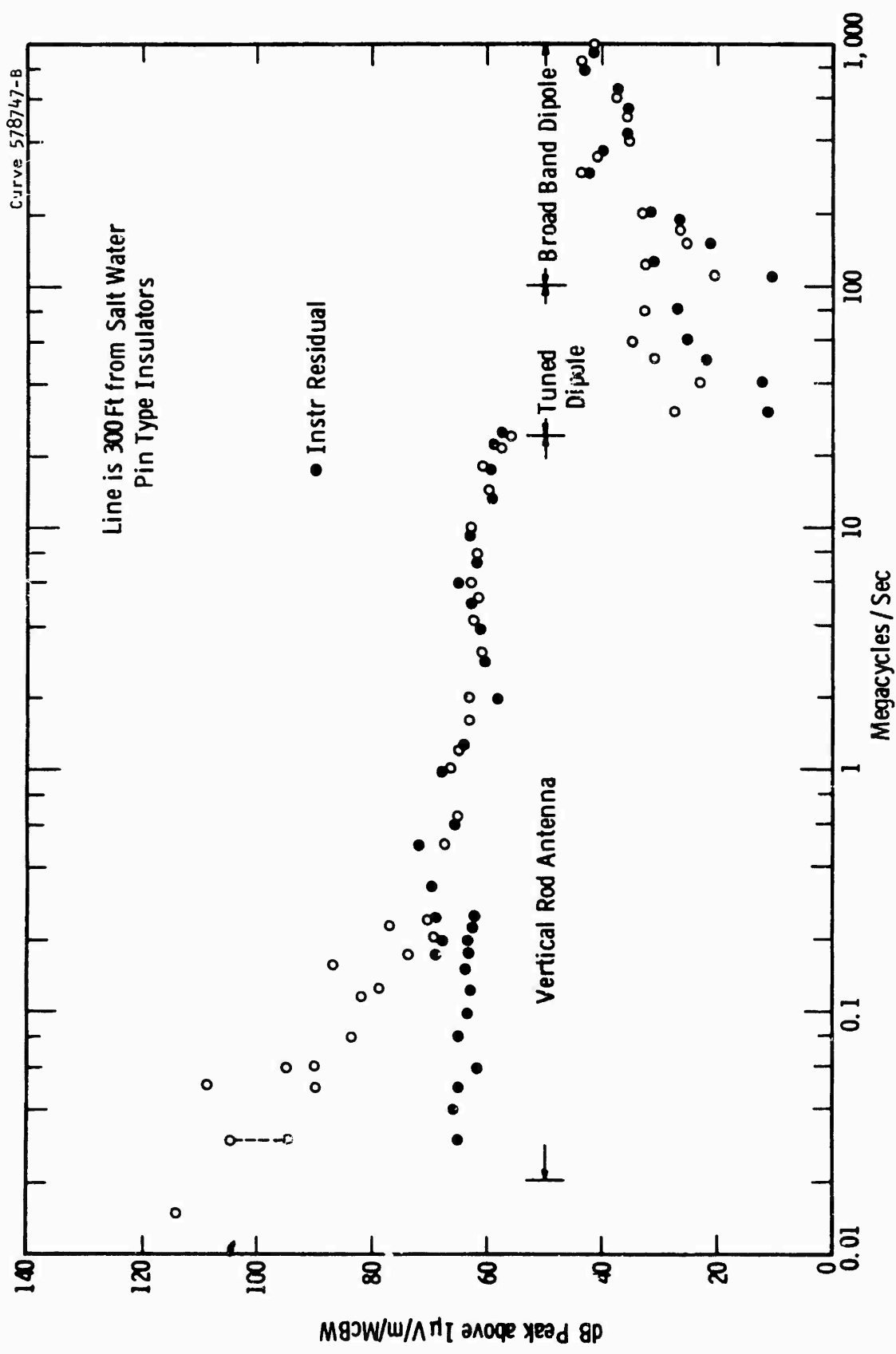


Fig. 35—12.5 KV WP normal line frequency spectrum at 50 feet from pole

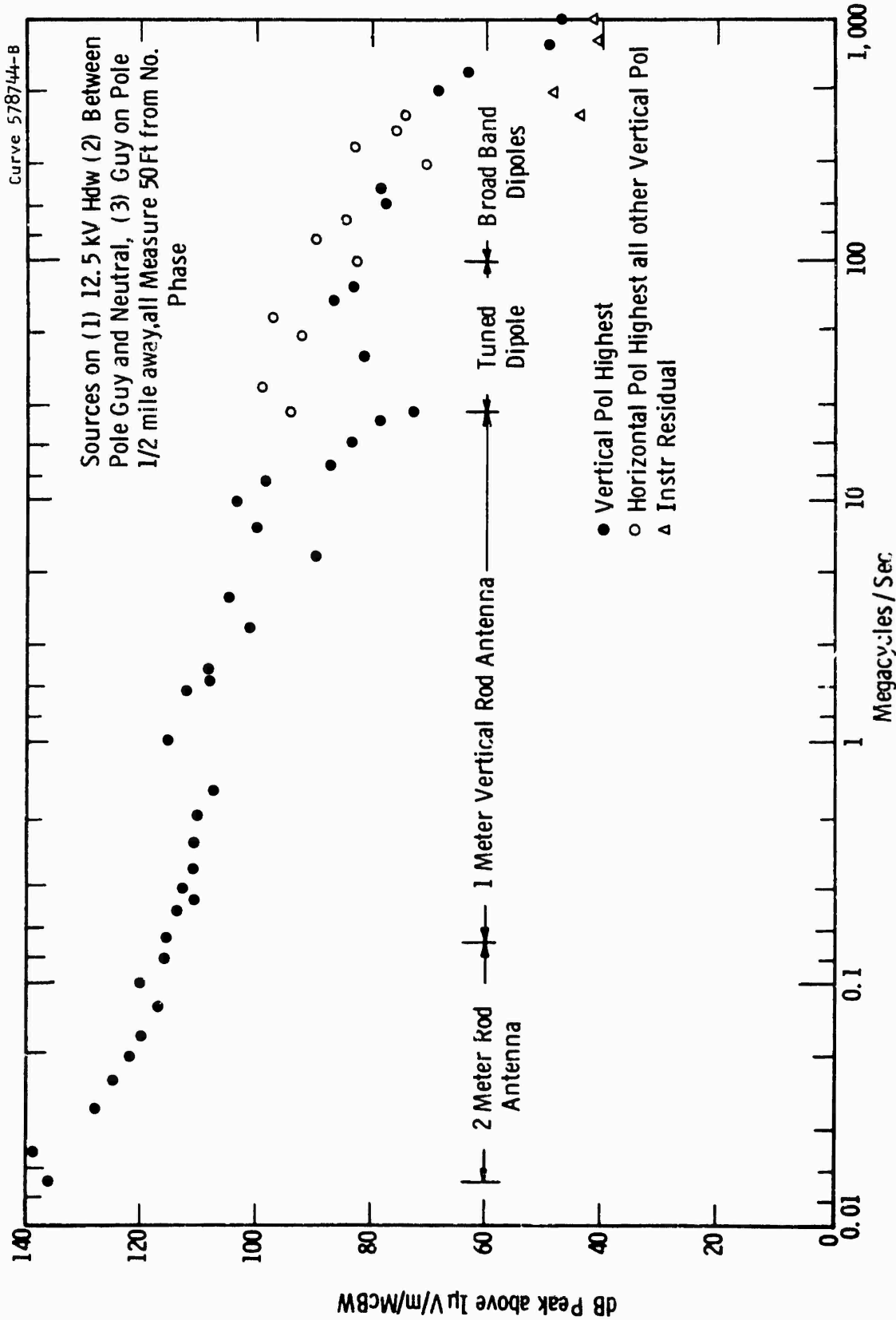


Fig. 36 - 12.5-34.5 kV dual circuit wood pole line with natural local source

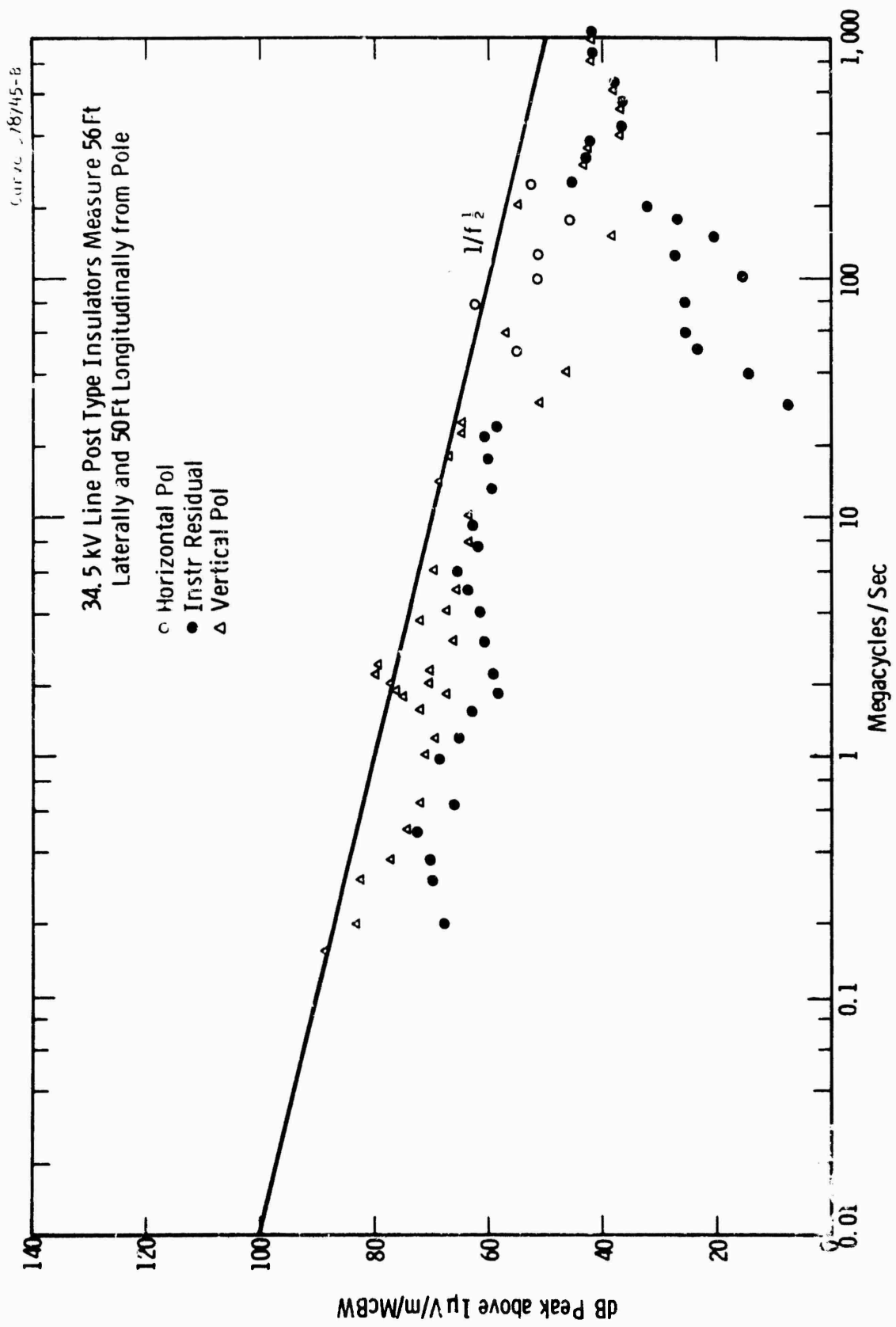


Fig. 37 -34.5 kV single circuit wood pole - normal line spectrum

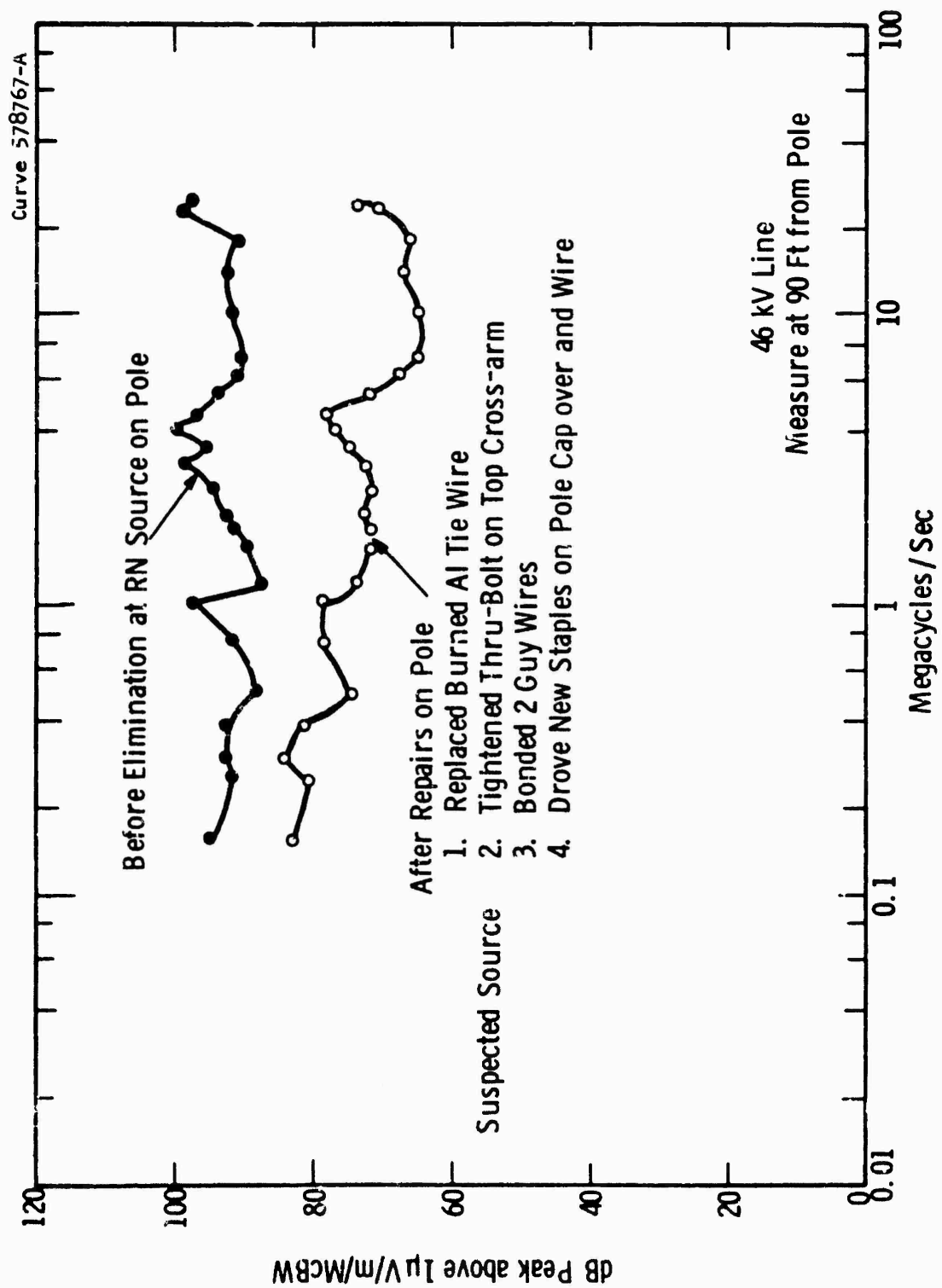


Fig. 38 — 46 kV WP line with and without source at pole

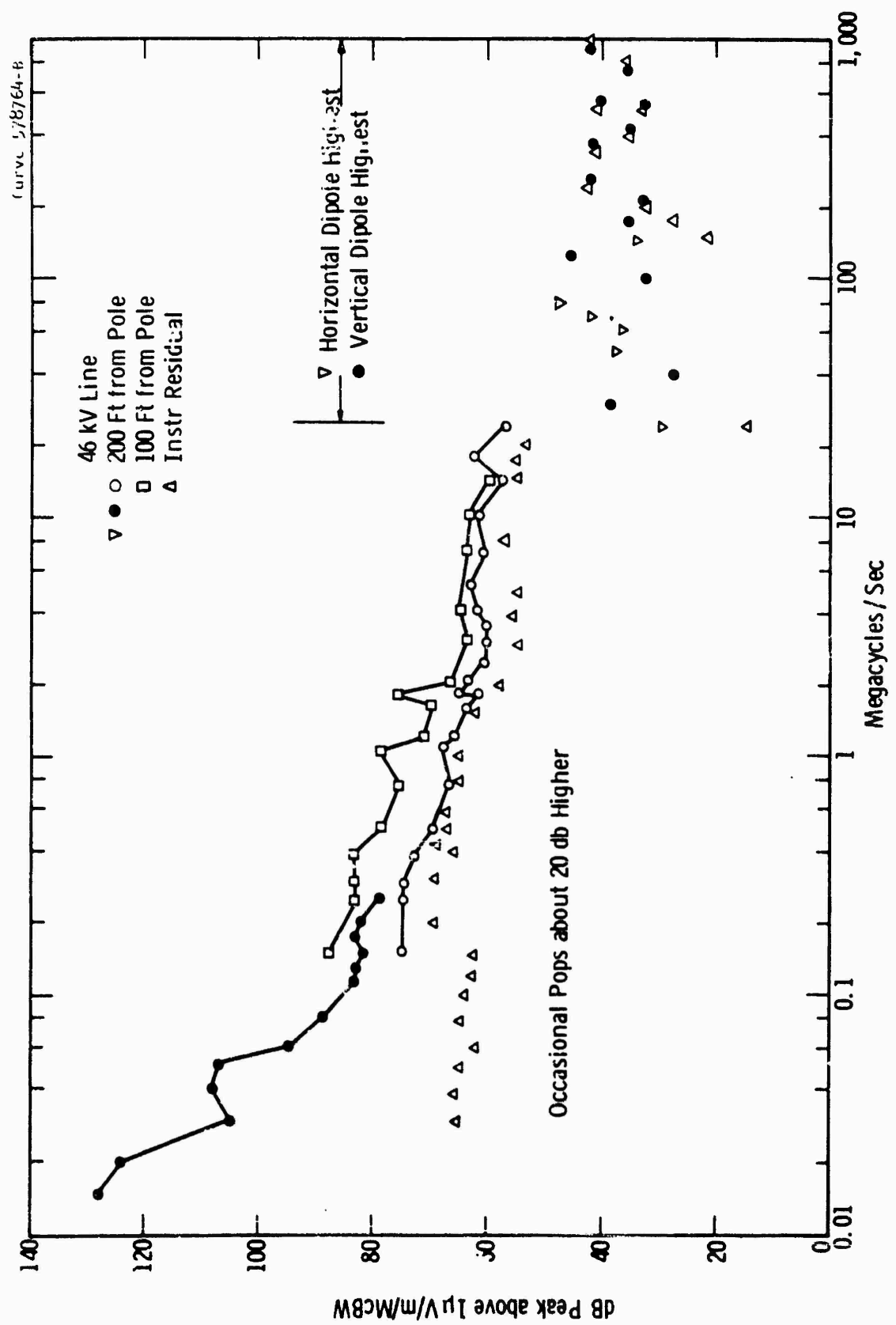


Fig. 39 -46 KV WP normal line frequency spectra

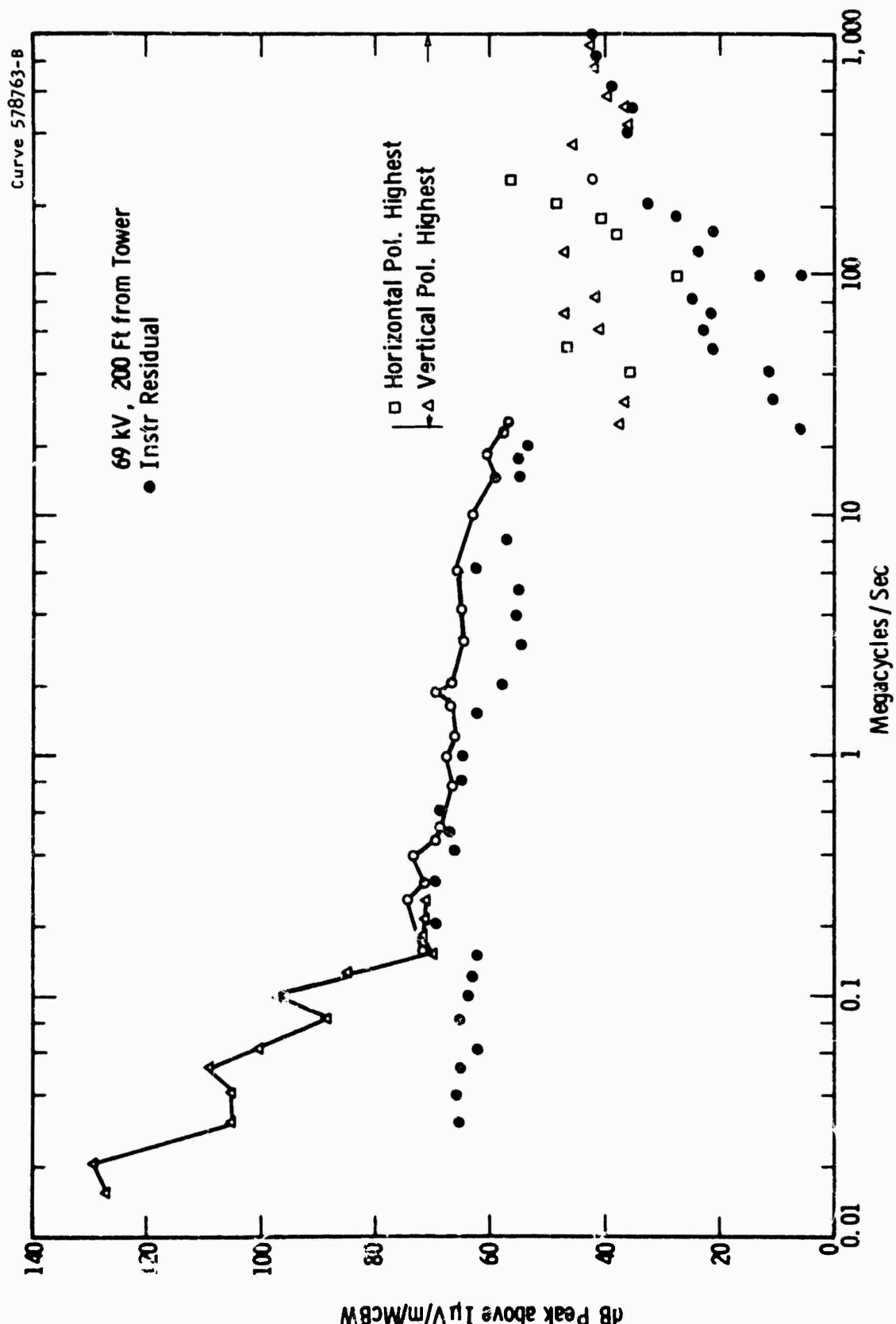


Fig. 40 - 69 KV HCWP normal line frequency spectrum at 200 feet from tower

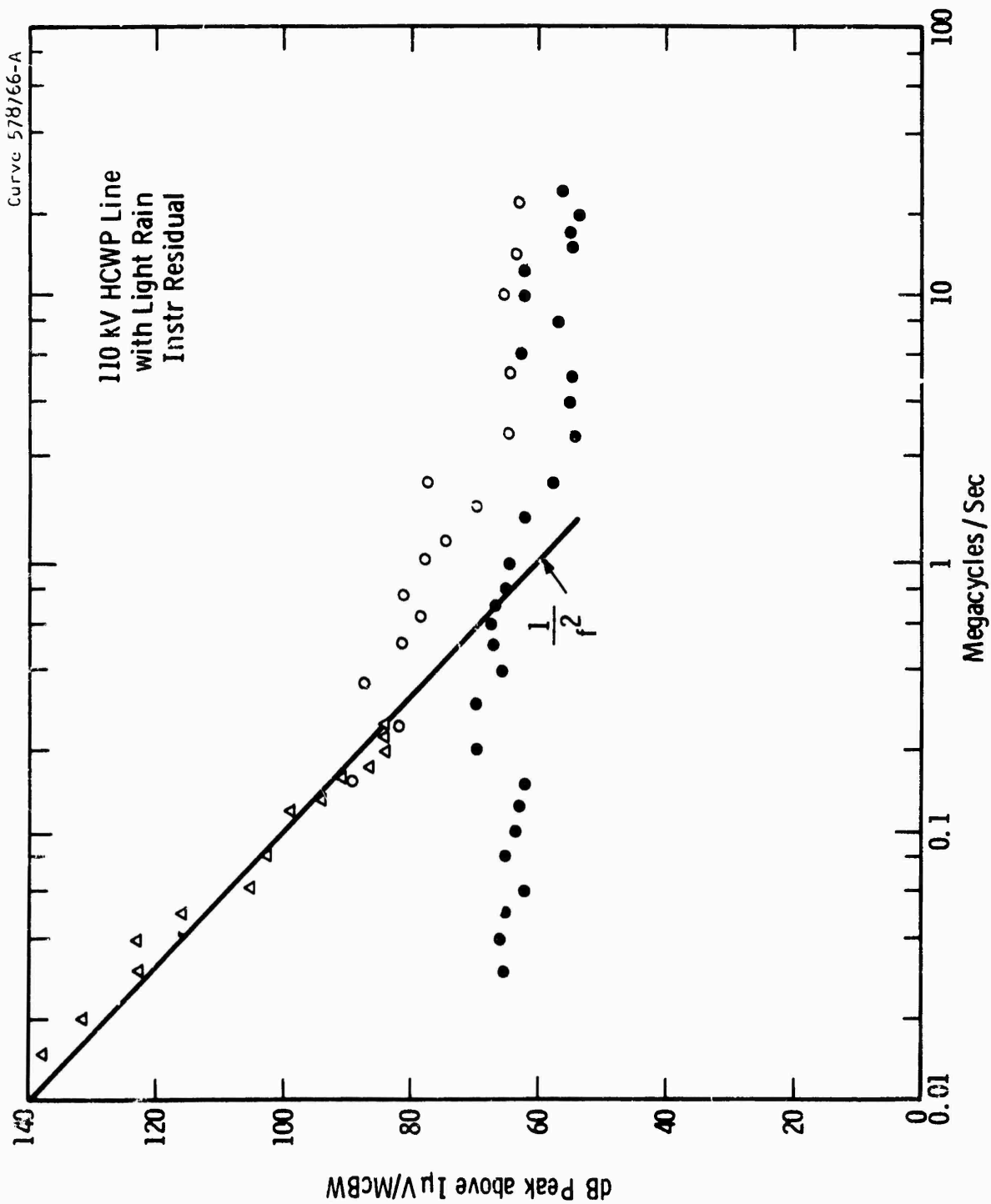


Fig. 41 — 110 KV WP normal line in light rain at 66 ft from center line at tower

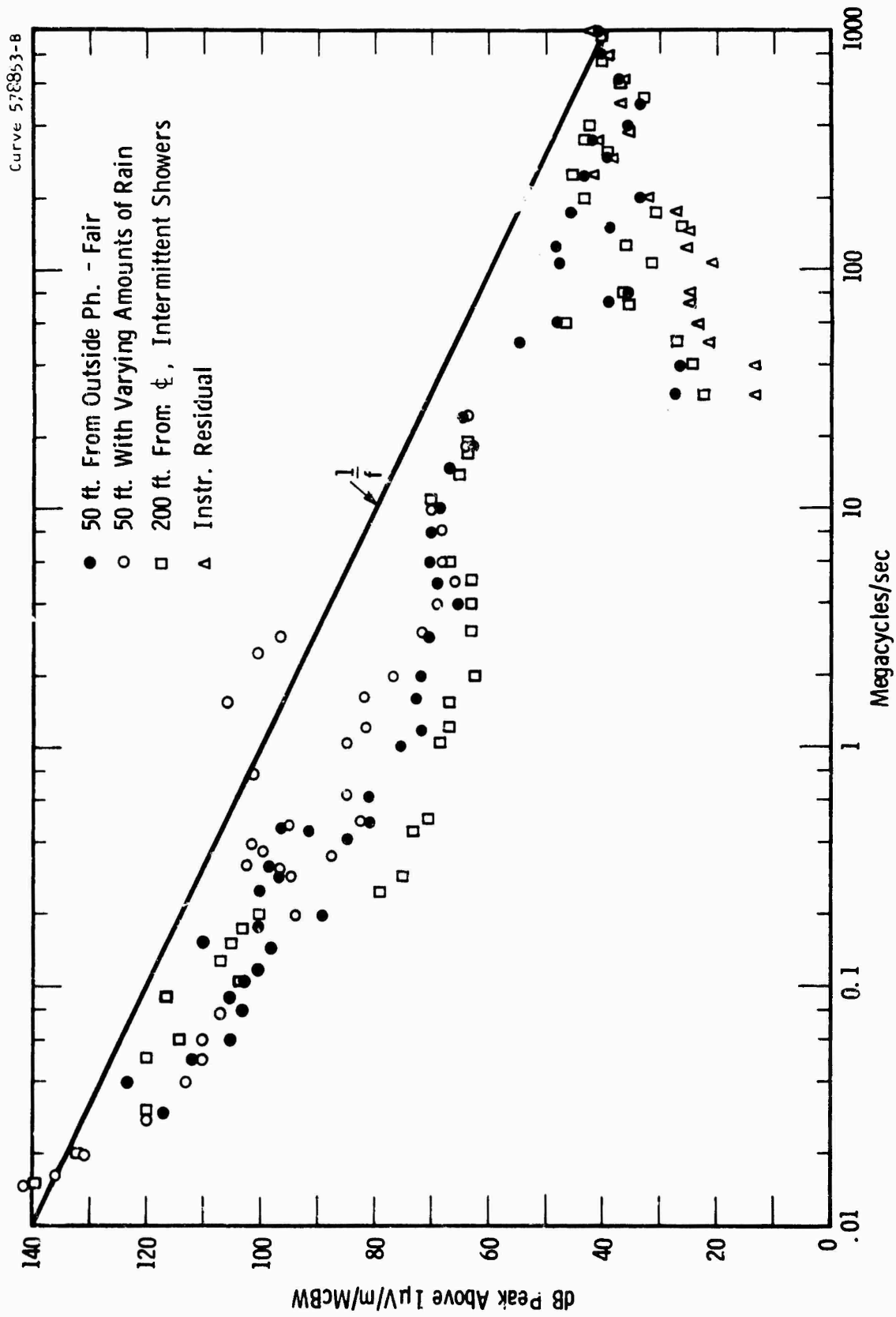
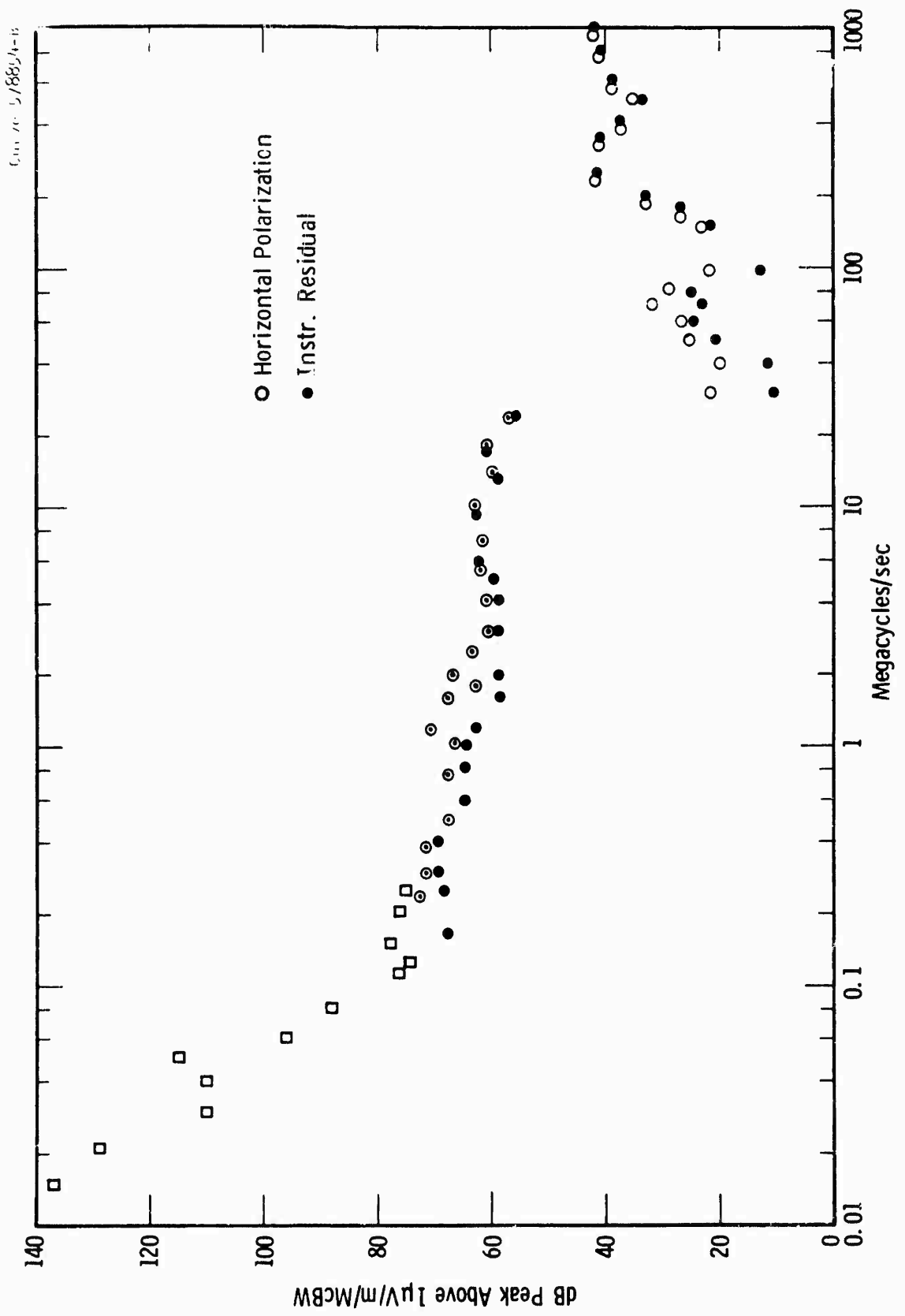


Fig. 42-138 kV HCWP line frequency spectra



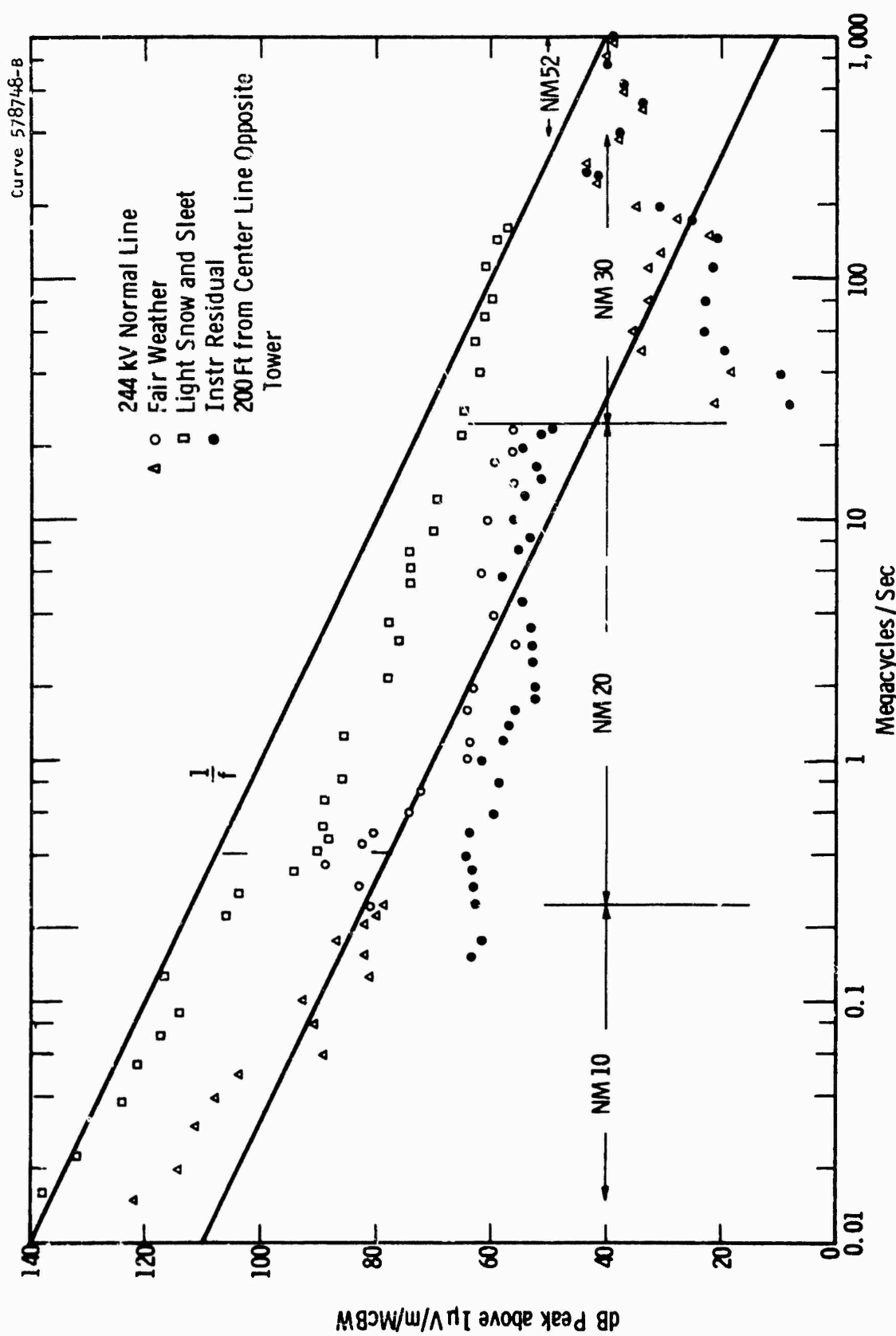


Fig. 44 - 244 KV HCST normal line frequency spectra in fair weather and with snow and sleet

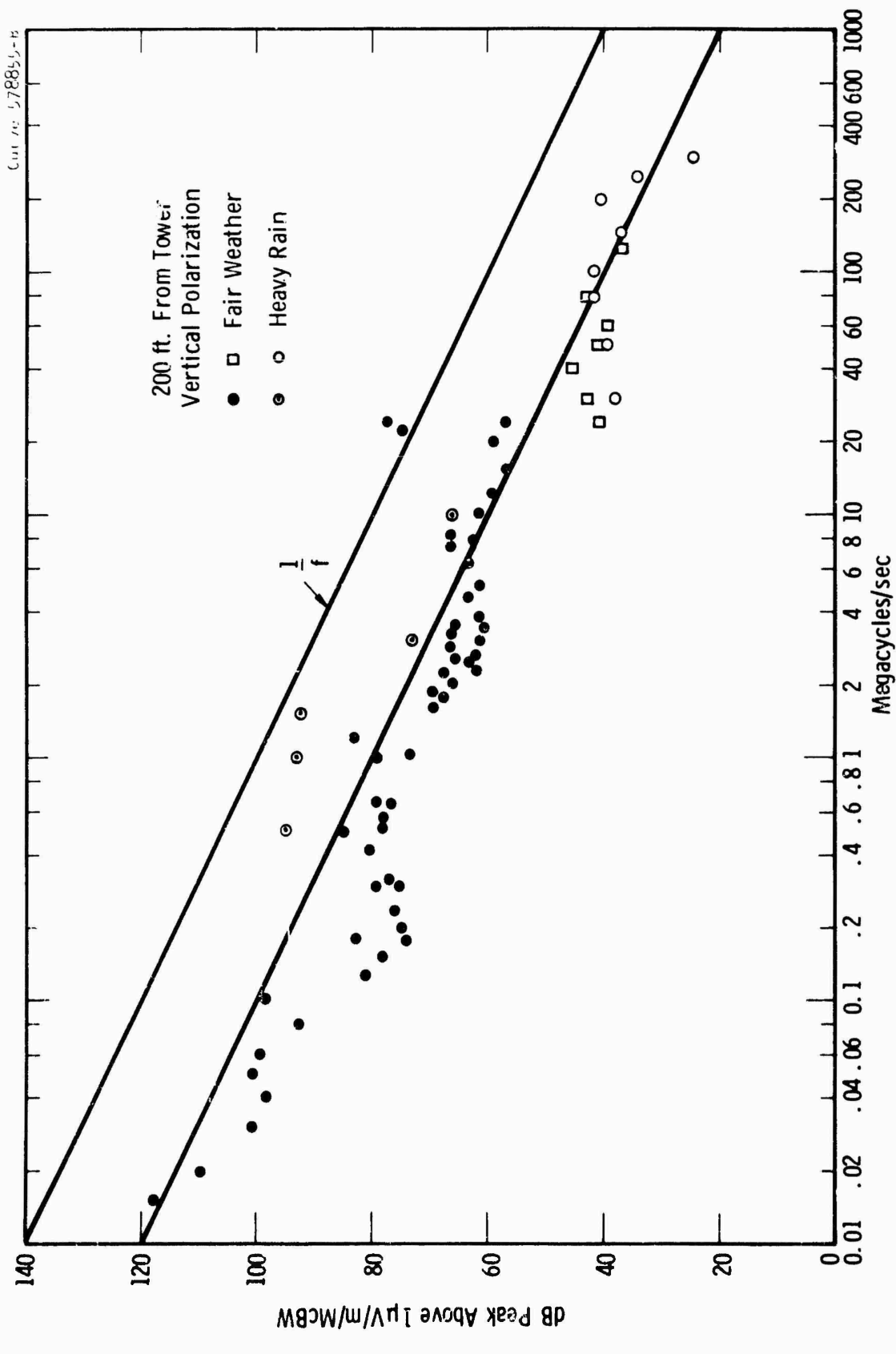


Fig. 45—45-345 kV HCST line frequency spectra in fair weather and in rain

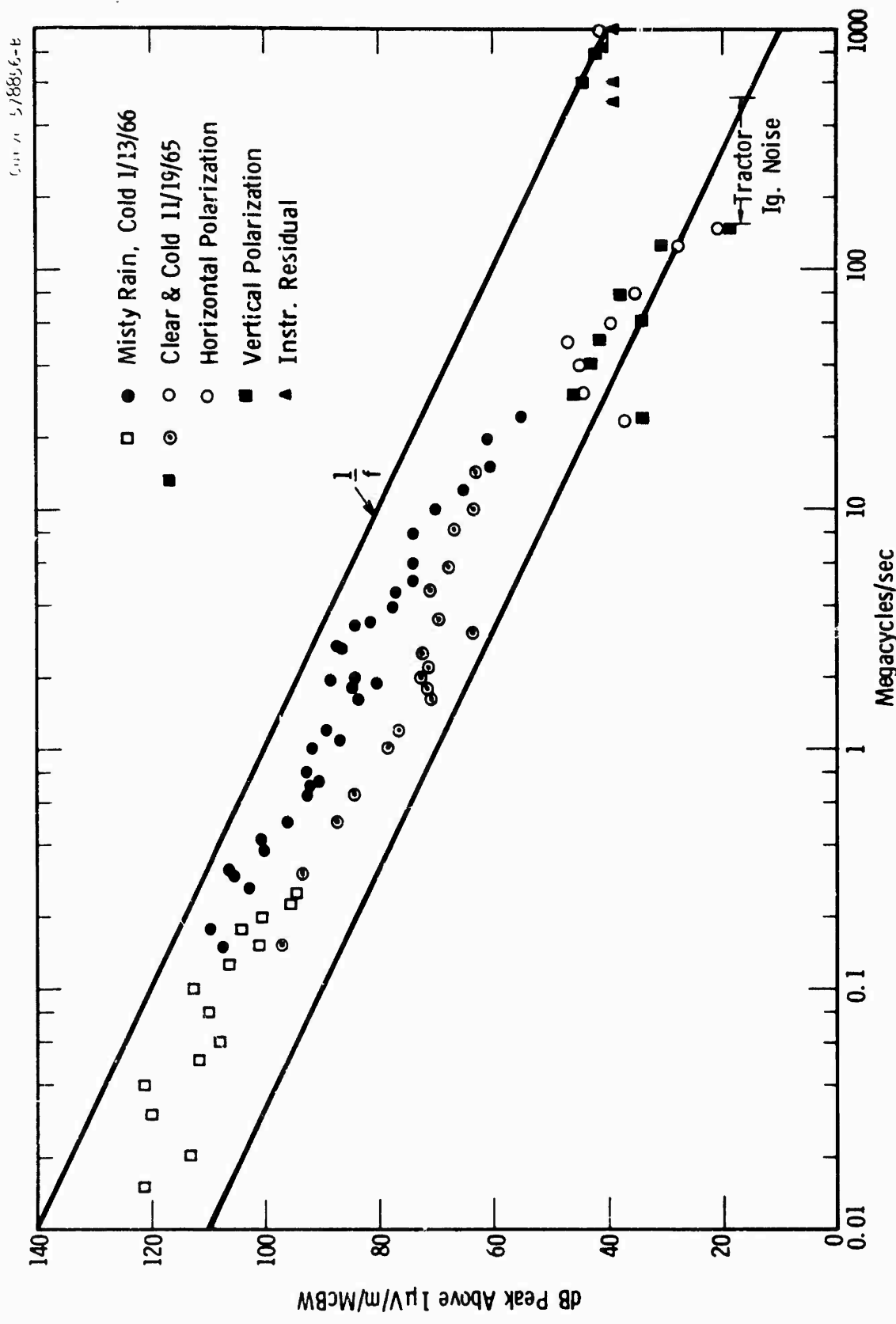


Fig. 46-345 kV VCD/CST normal line frequency spectra 200 ft. from tower

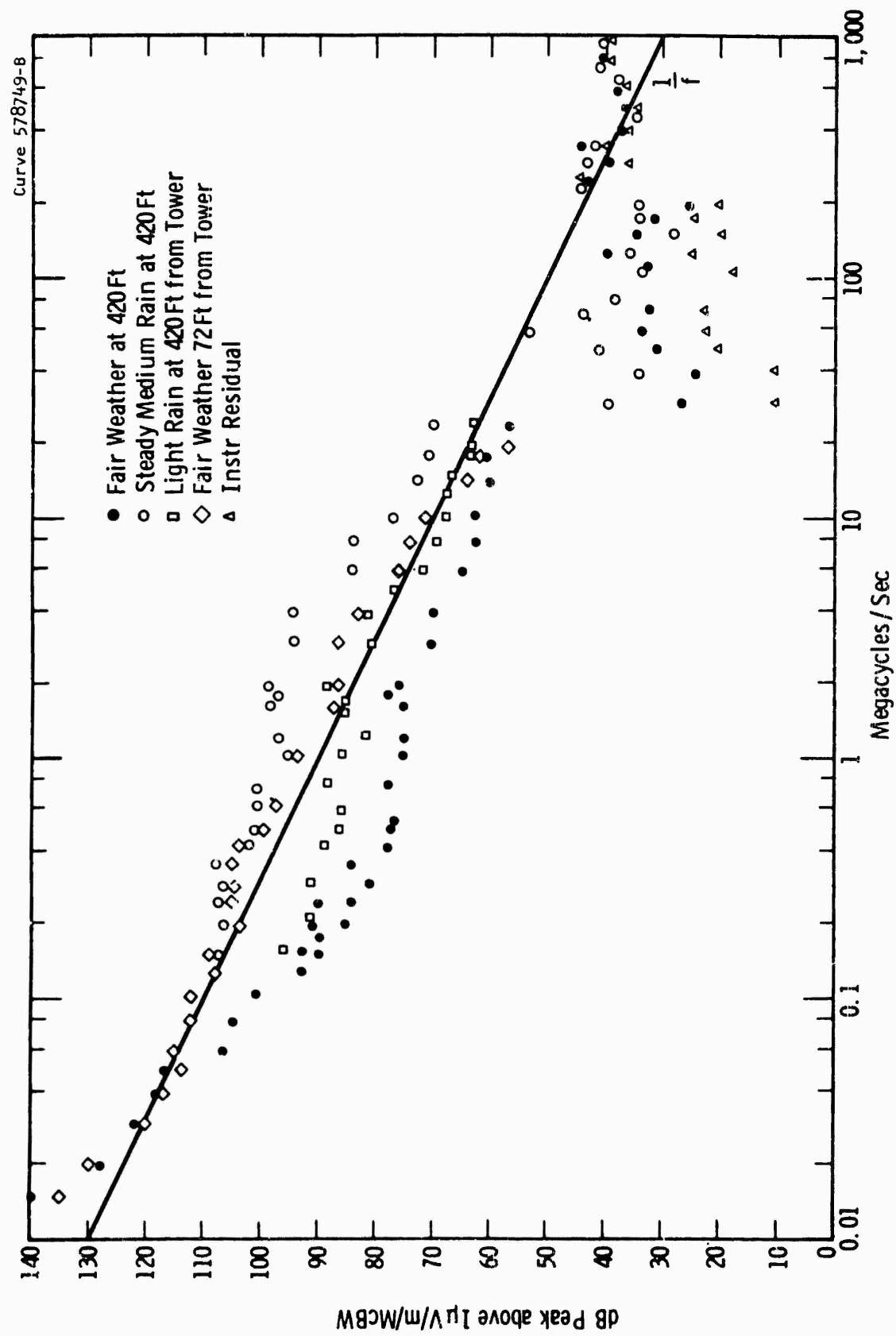


Fig. 47 -345 kV VCSSC normal line frequency spectra in fair weather and rain

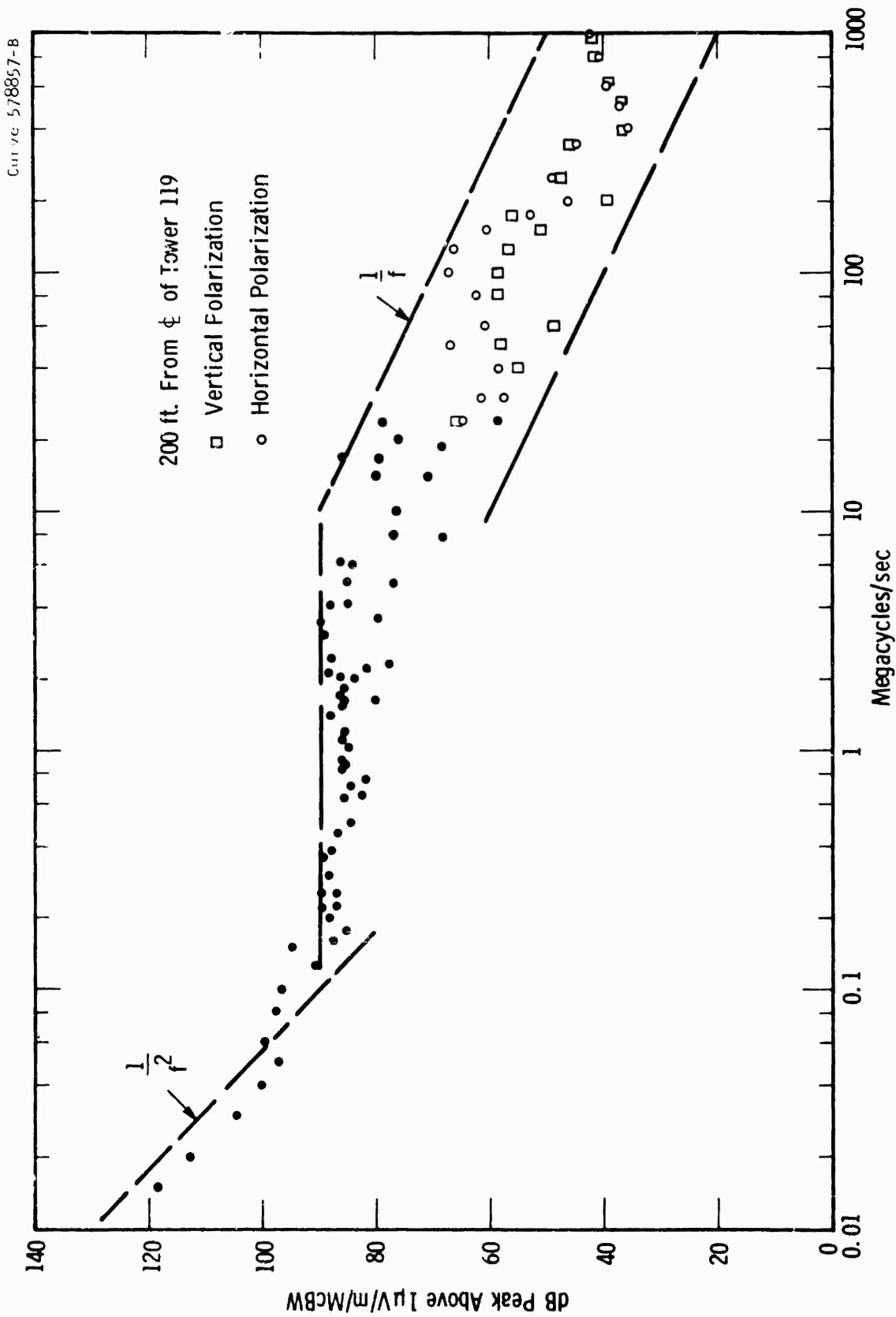


Fig. 48—345 kV HCWP line frequency spectrum 200 ft. from Tower 119

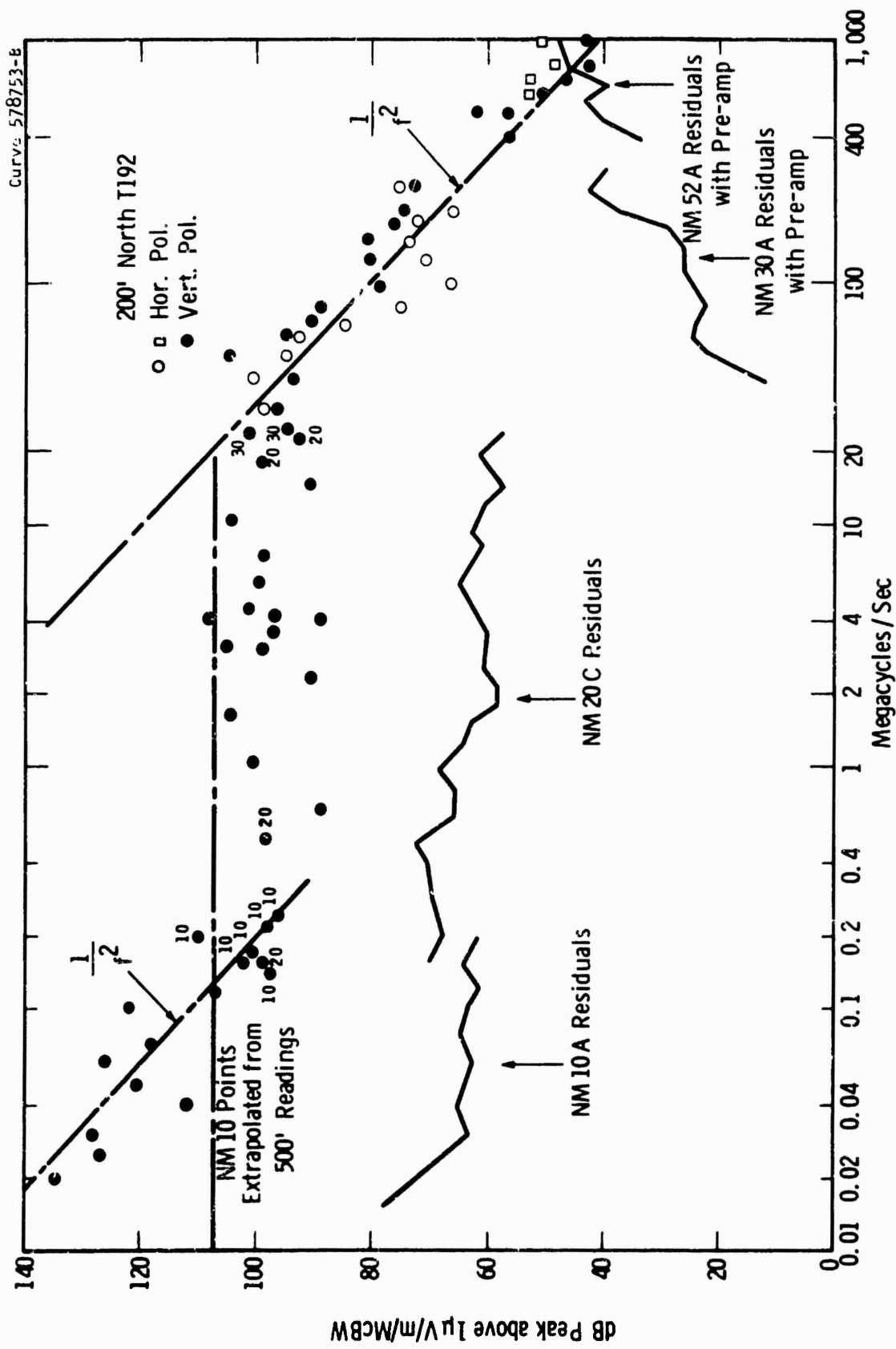


Fig. 49 - 345 kV HCWP line frequency spectra at 200 feet north with natural gap

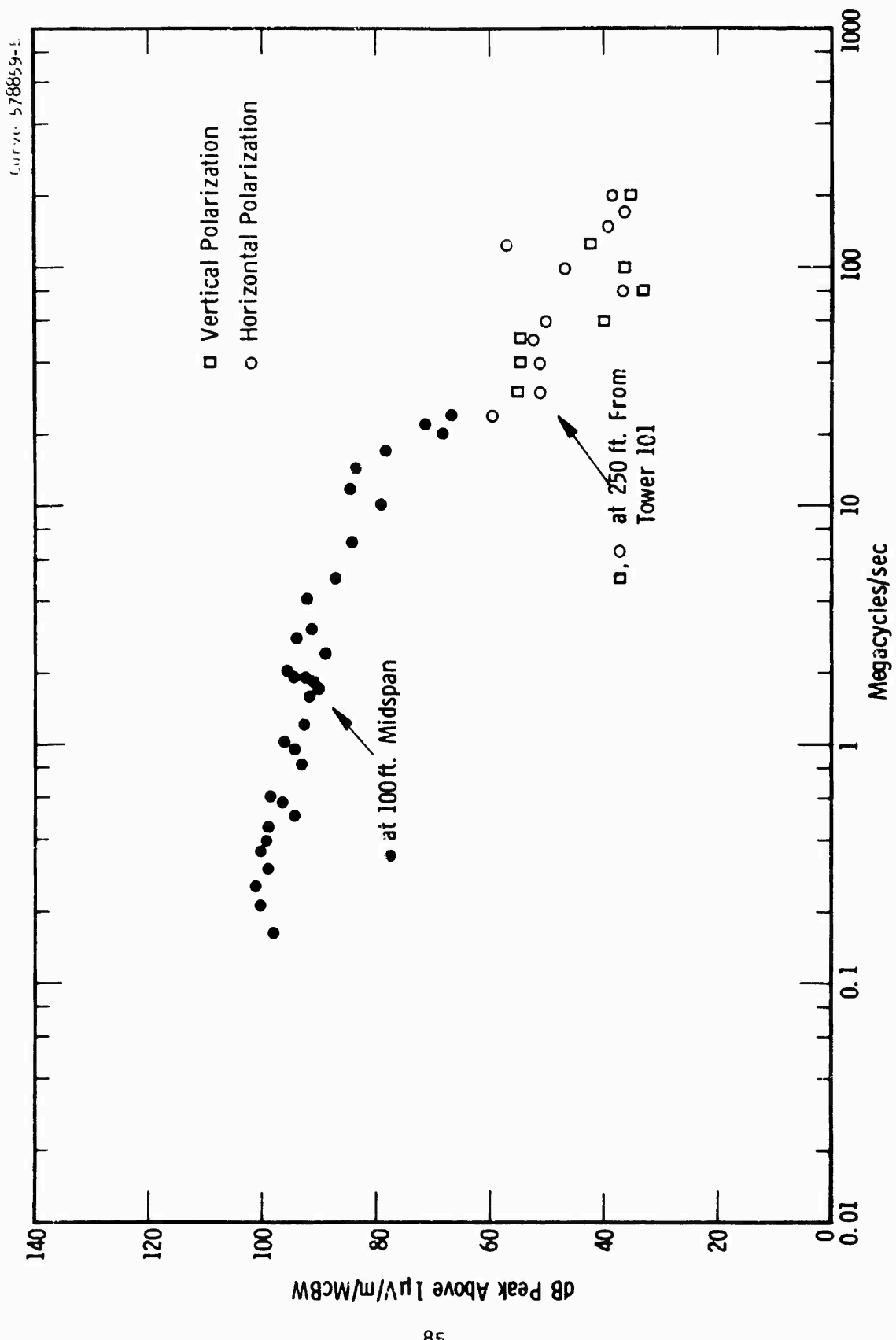


Fig. 50-345 kV HCWP line frequency spectra near Tower 101

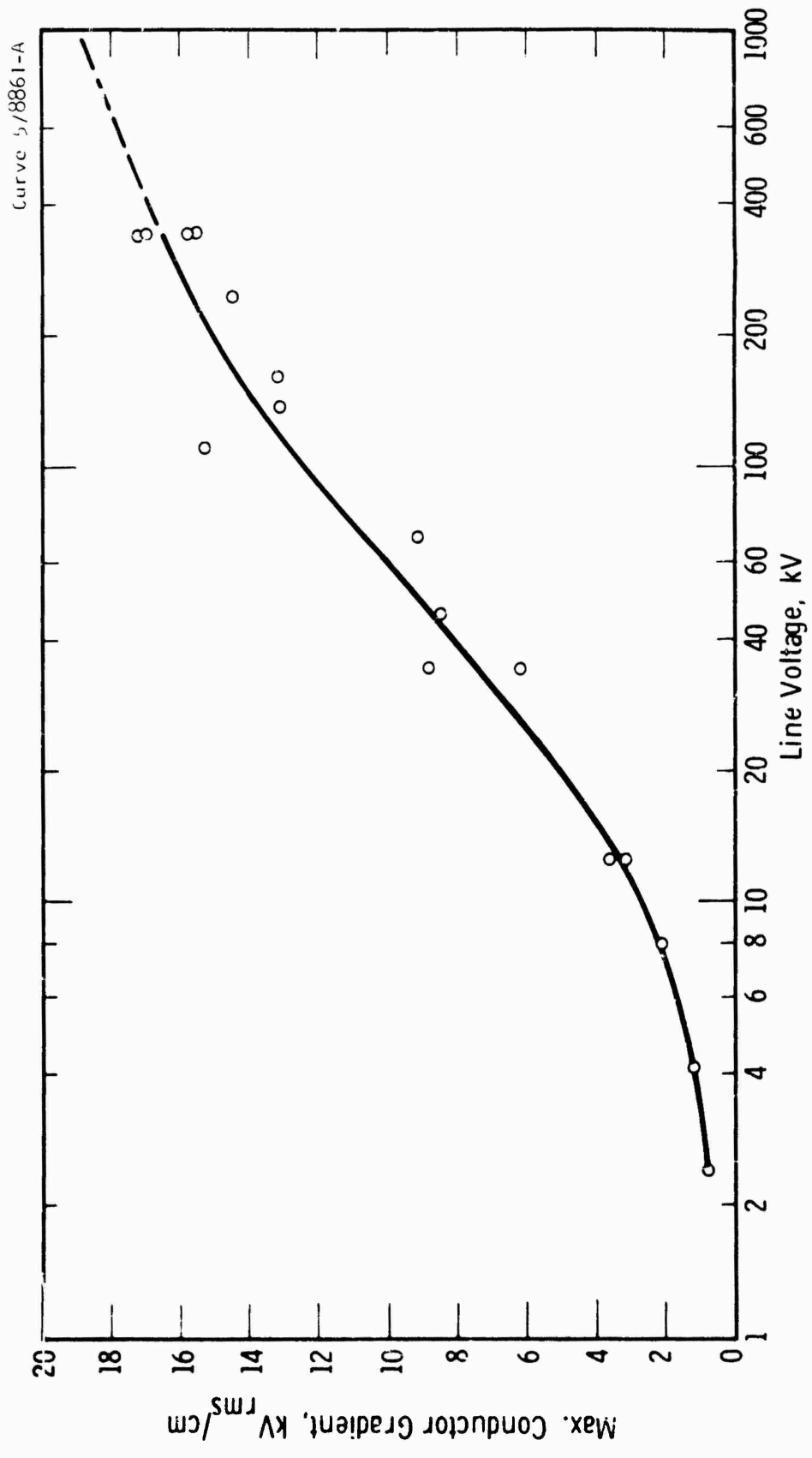


Fig. 51 — Maximum conductor gradient to voltage of lines tested

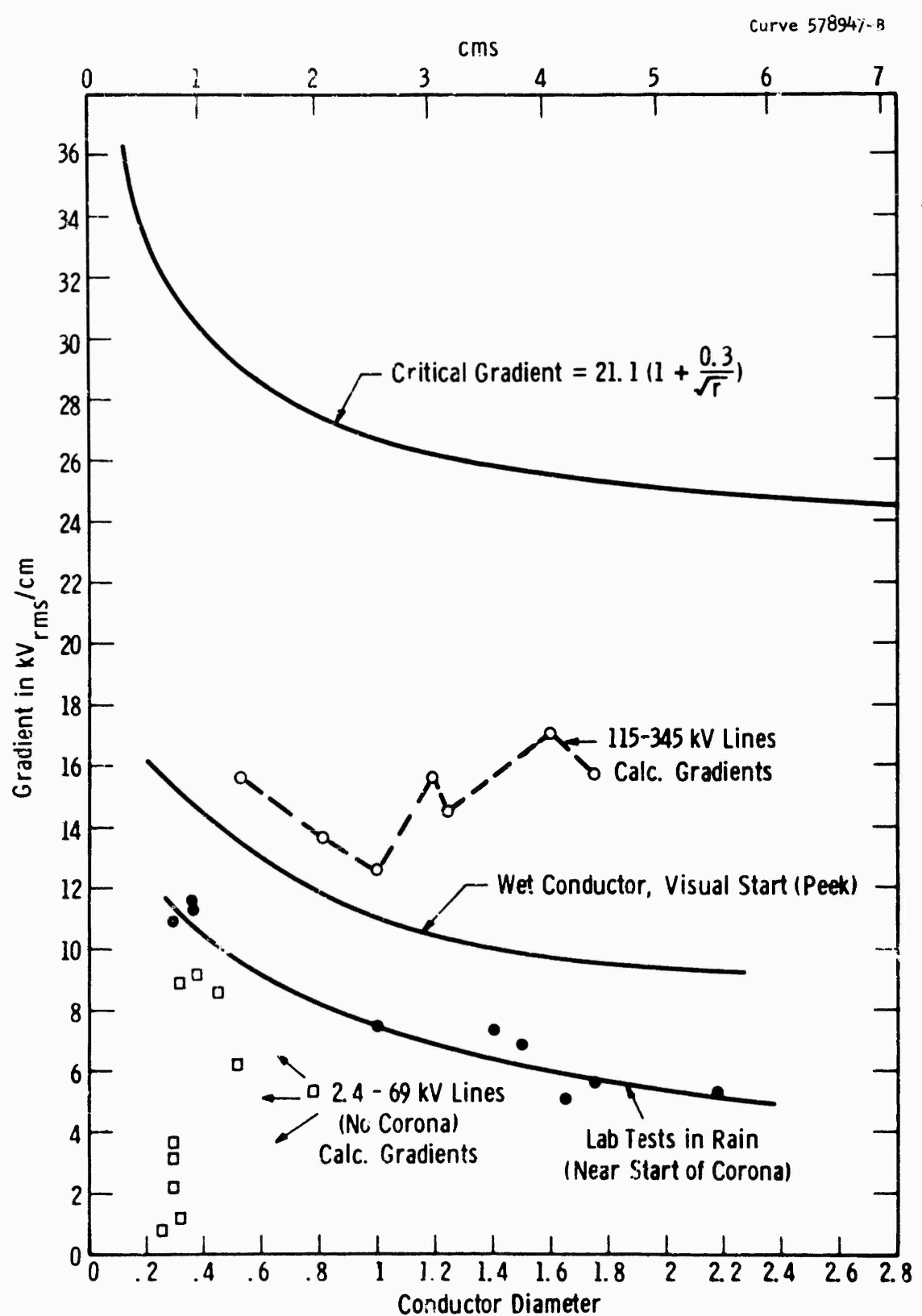


Fig. 52—Conductor critical gradient and line conductor gradients and gradients for start of corona in rain

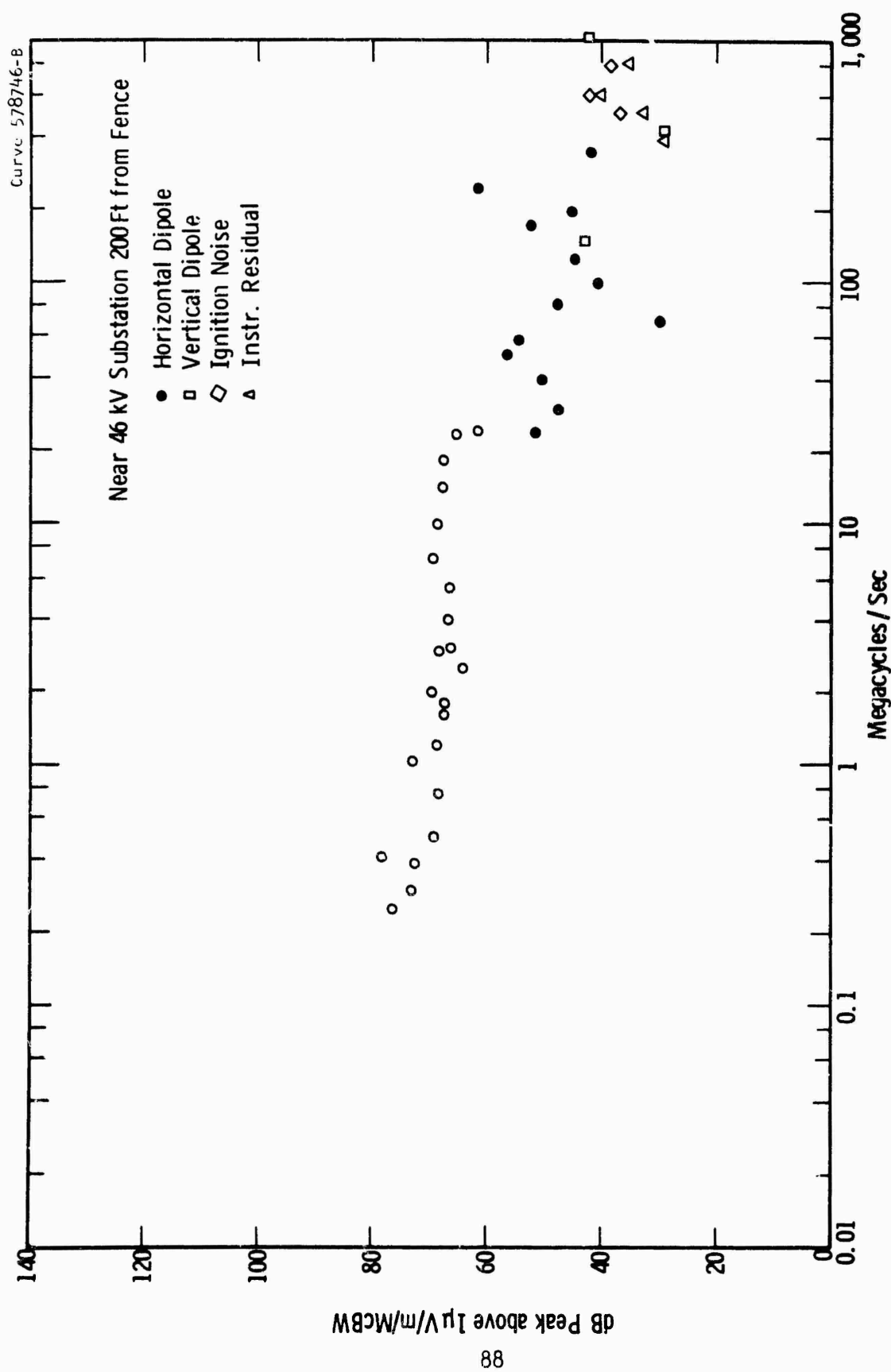


Fig. 53—Radio noise near 46 kV substation

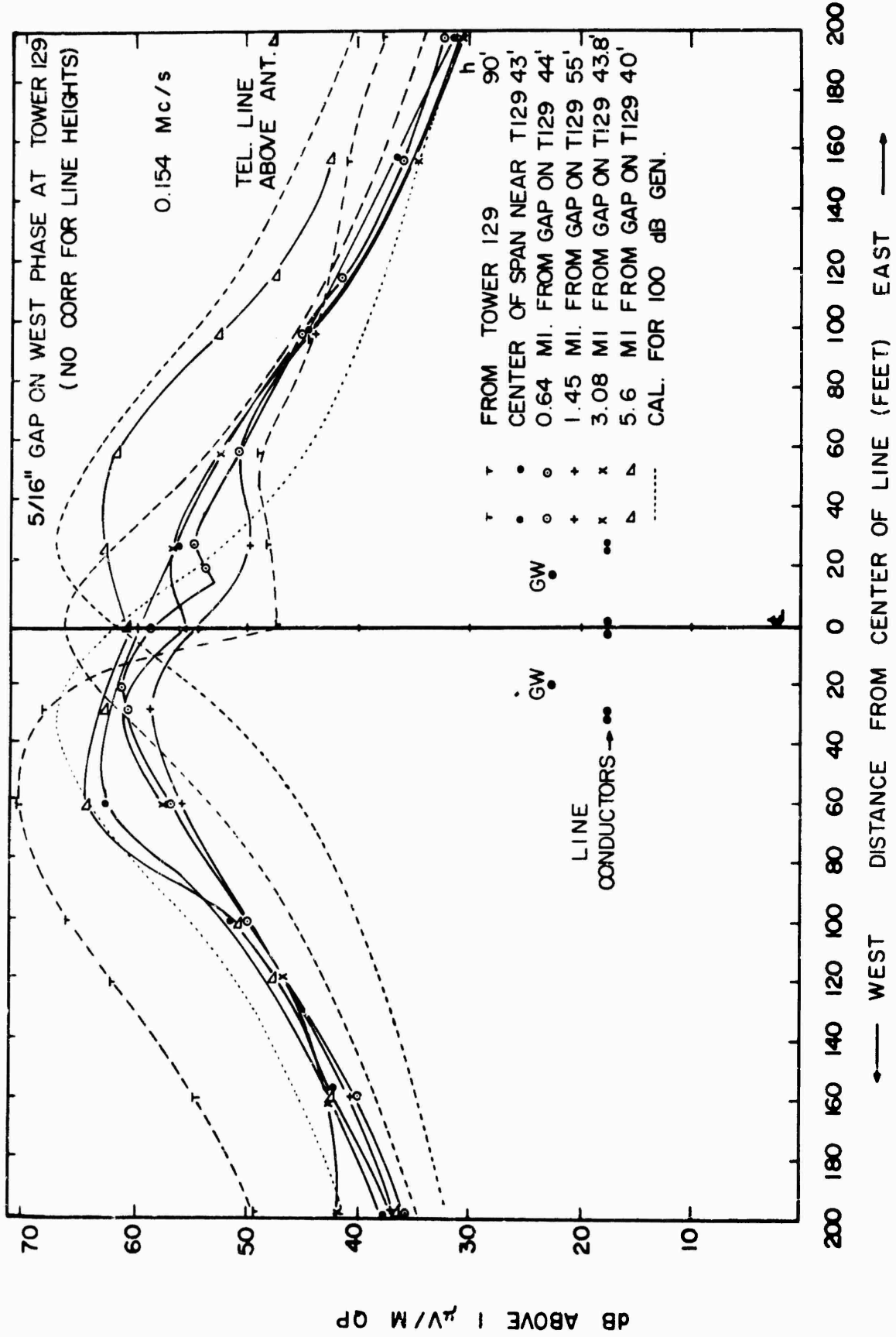


FIG. 54 345 KV HC ST LINE LATERAL PROFILES AT 0.154 Mc/s WITH ARTIFICIAL GAP.

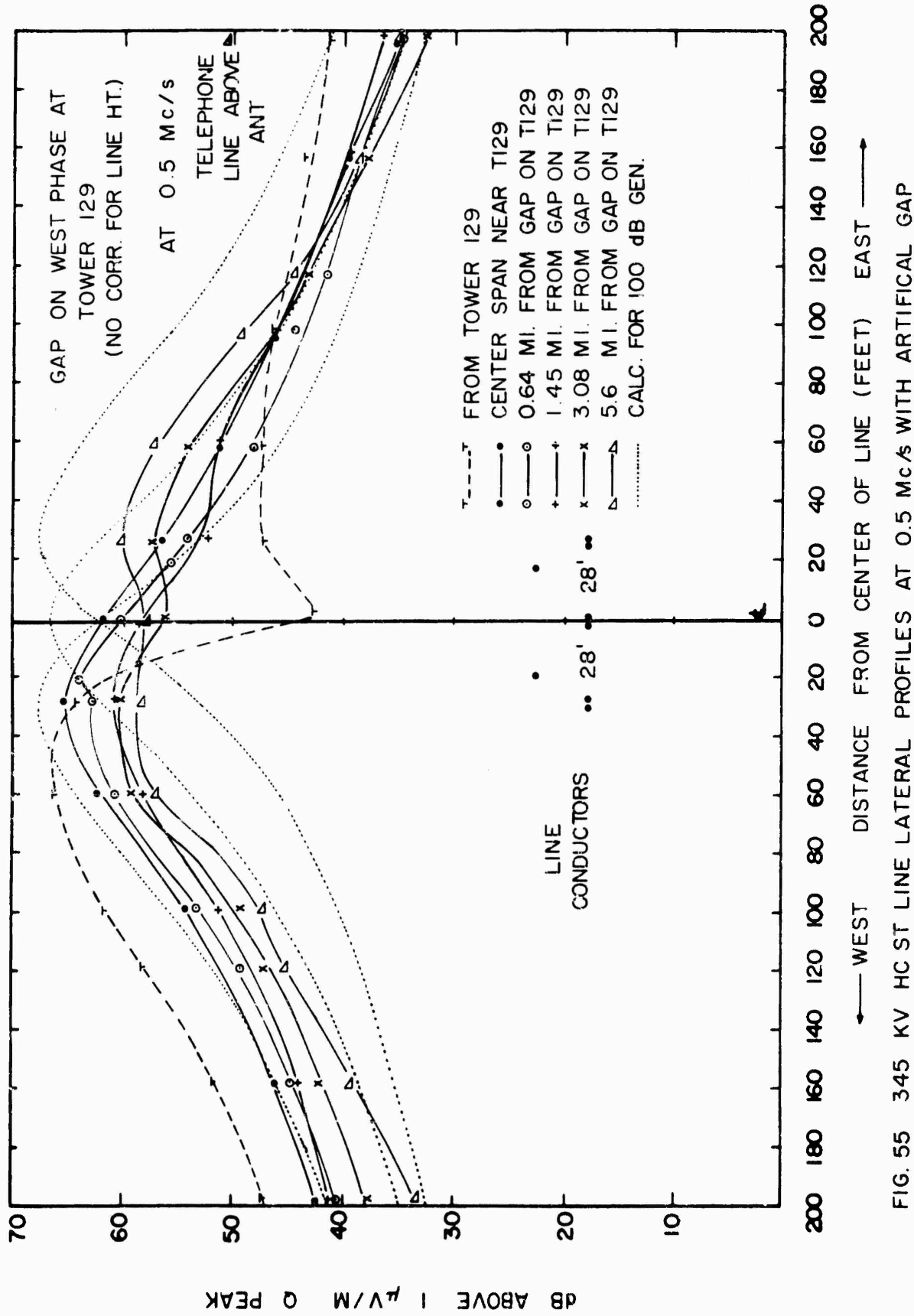


FIG. 55 345 KV HC ST LINE LATERAL PROFILES AT 0.5 MC/S WITH ARTIFICIAL GAP

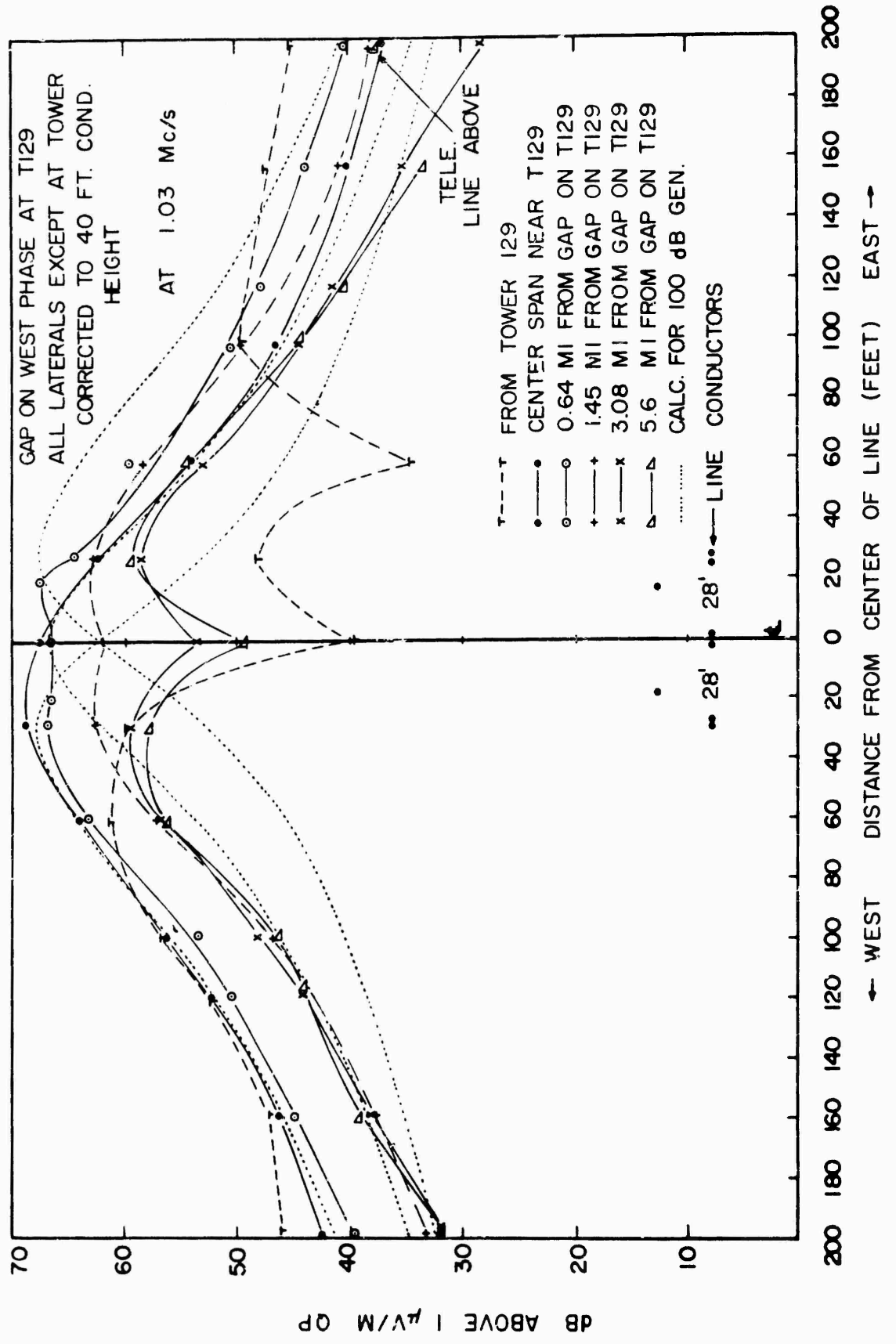


FIG. 56 345 KV HC ST LINE LATERAL PROFILES AT 1.03 Mc/s WITH ARTIFICIAL GAP

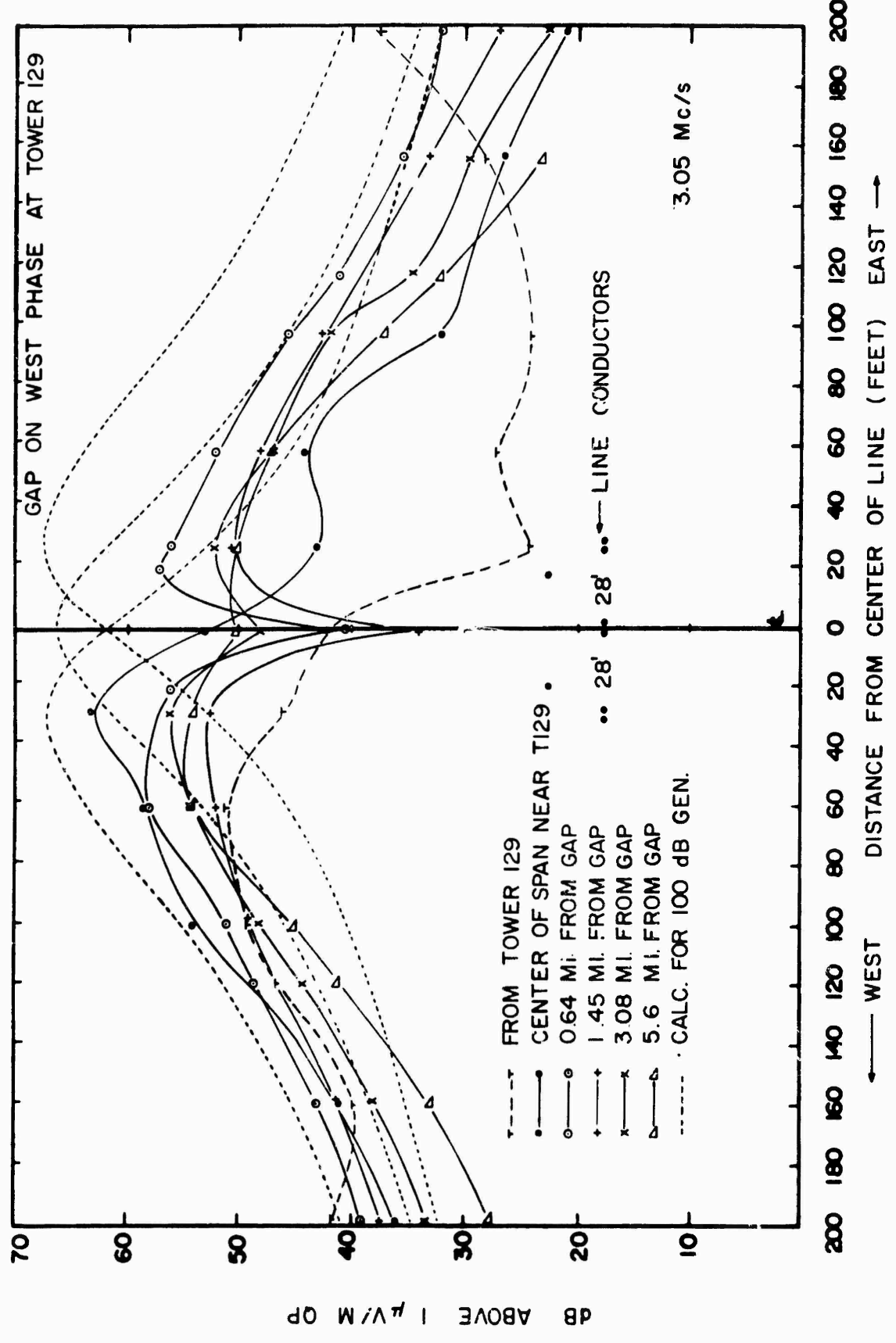
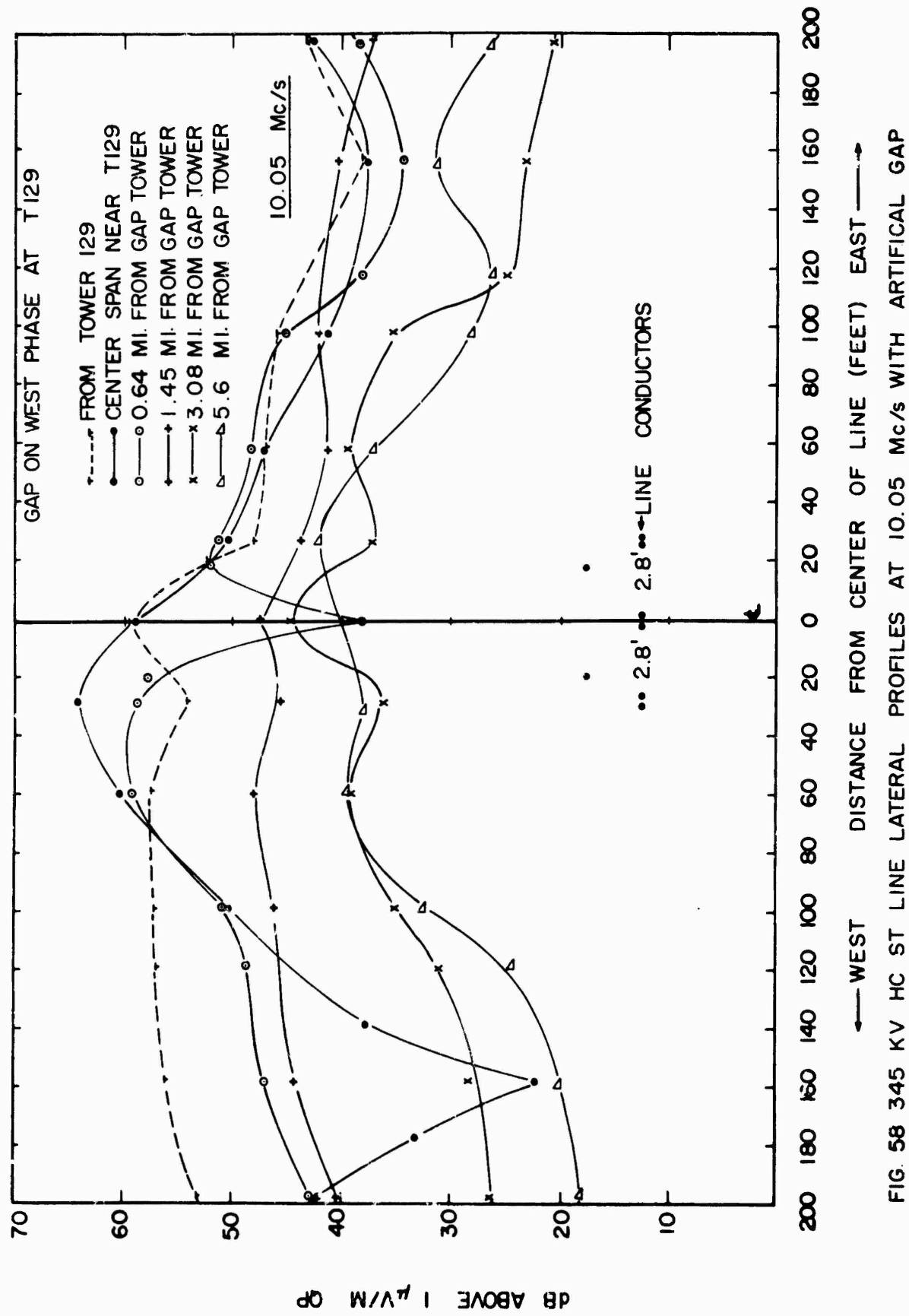
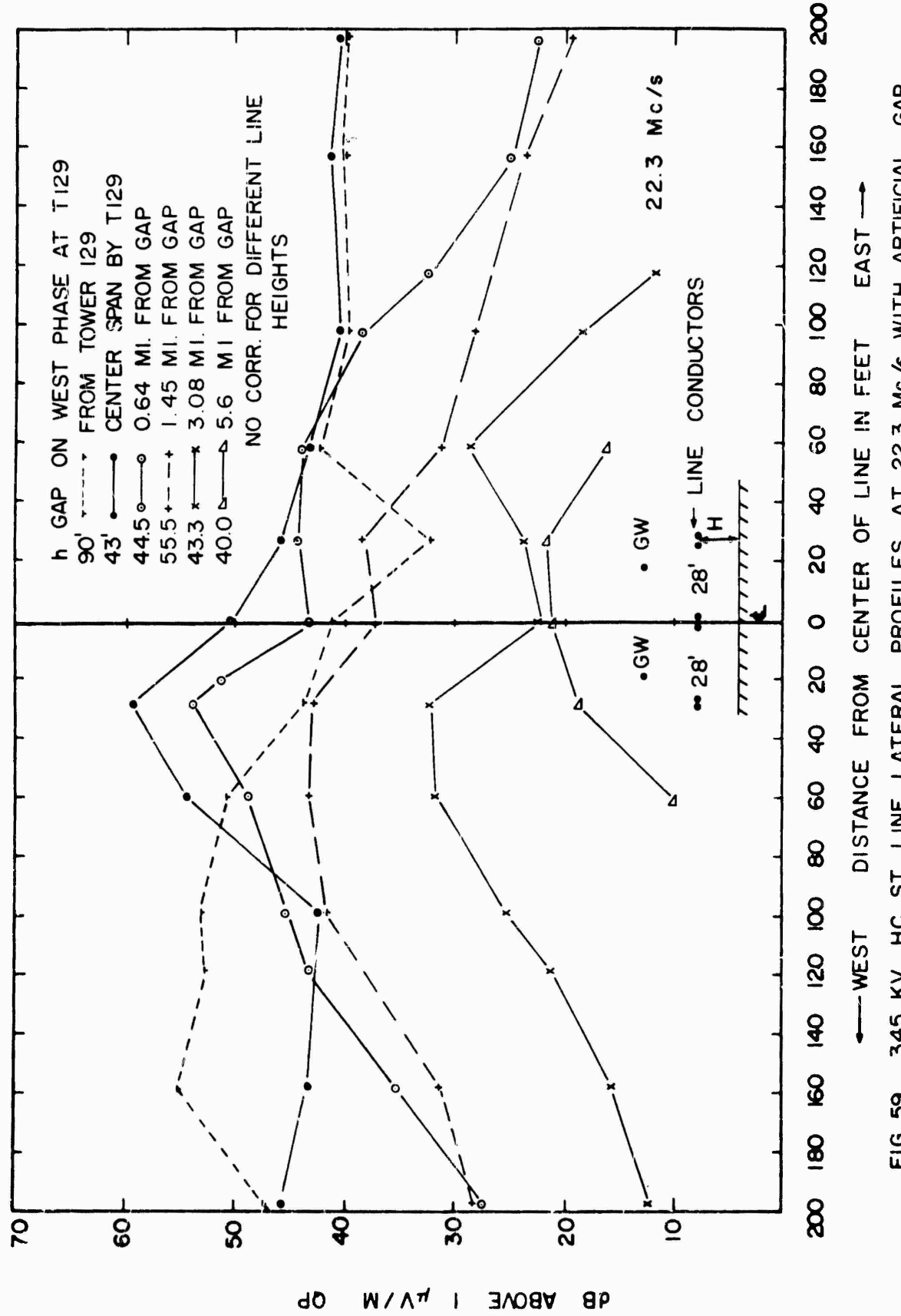


FIG. 57 345 KV HC ST LINE LATERAL PROFILE A 3.05 Mc/s WITH ARTIFICIAL GAP





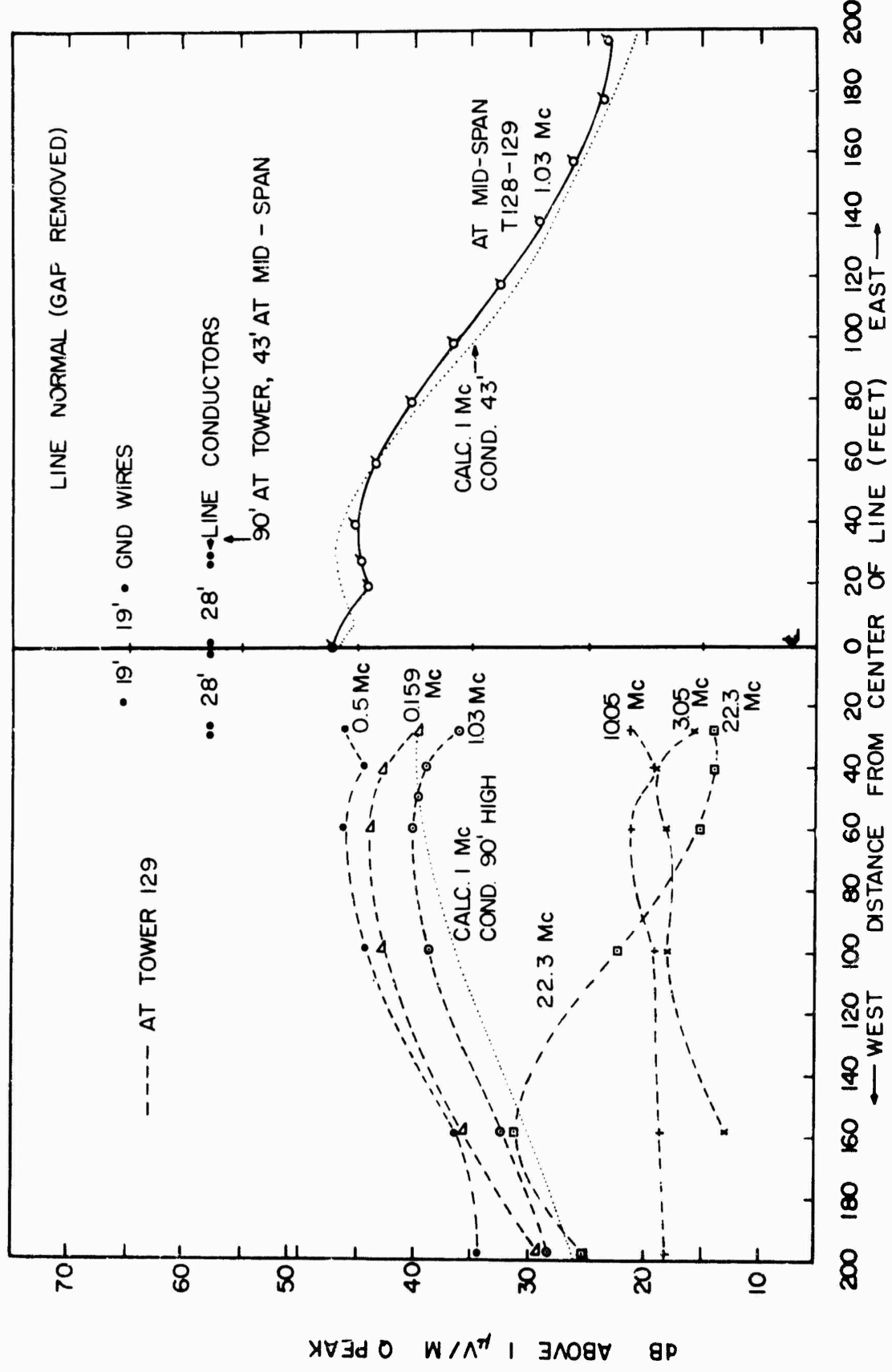


FIG. 60 345 KV HC ST LINE LATERAL PROFILES AT MID-SPAN NEAR T129

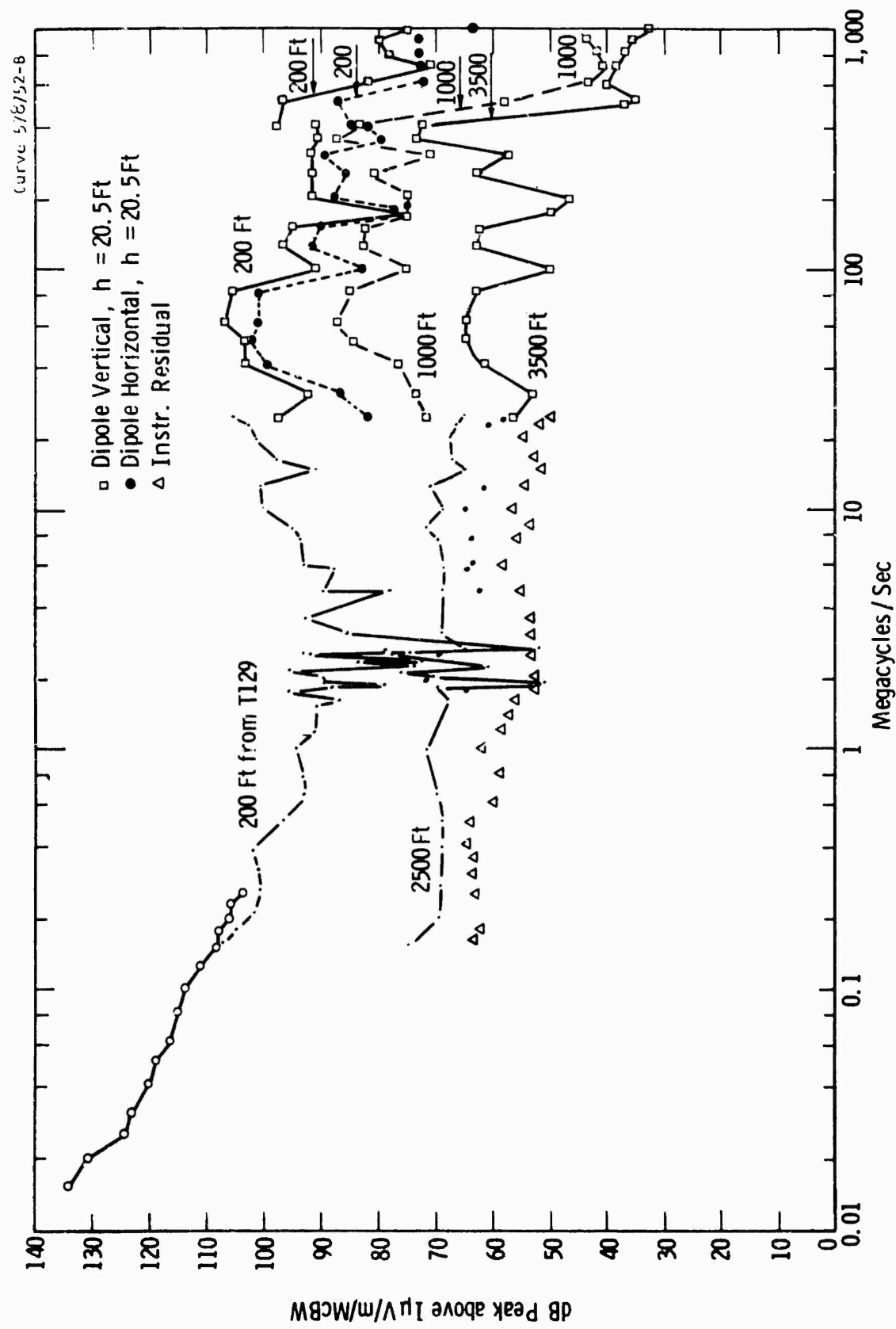


Fig. 61—345 kV HCST line frequency spectra at several lateral distances with artificial gap

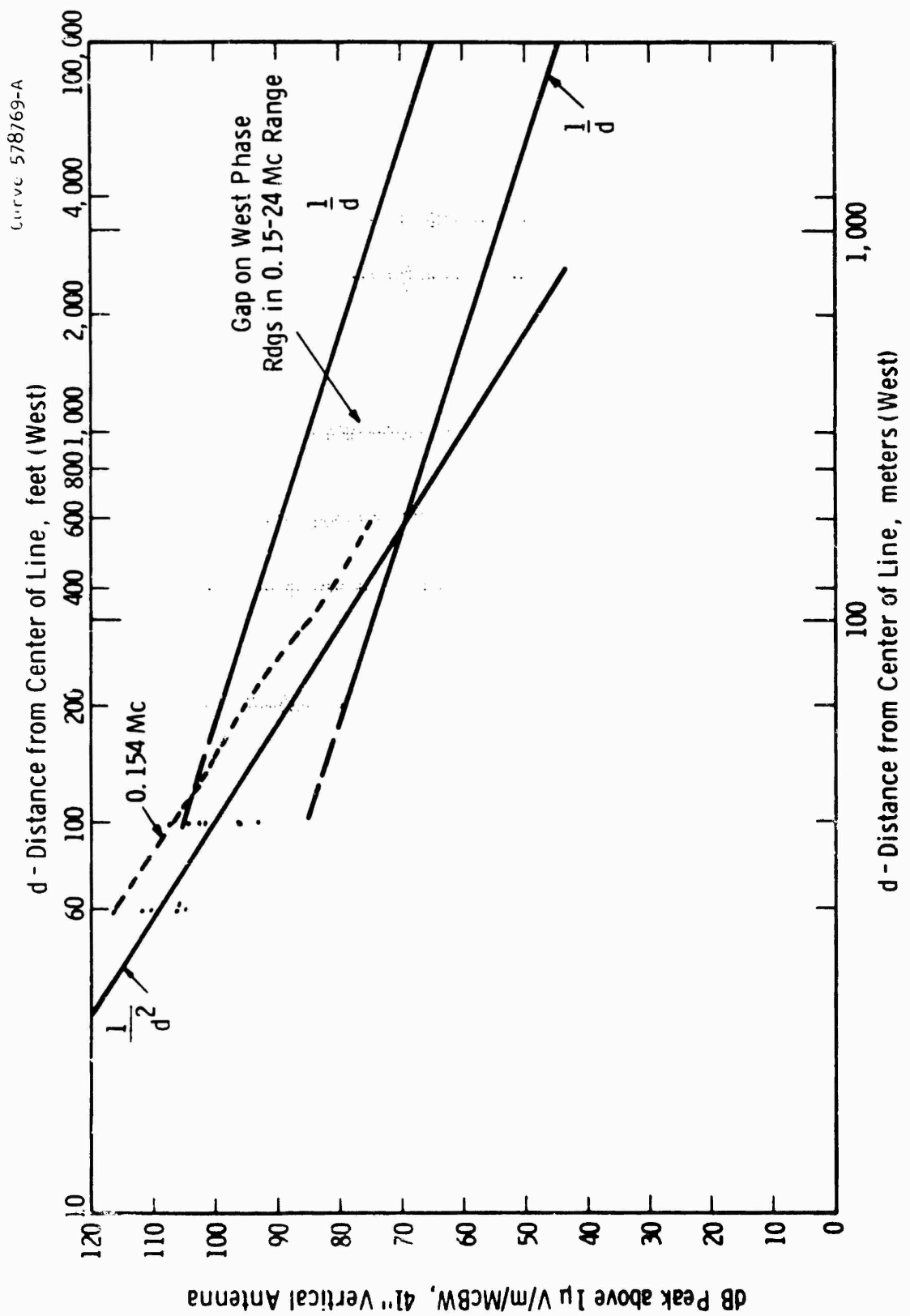


Fig. 62-345 kV HCST line at 0.15-24 Mc at several lateral distances with artificial gap

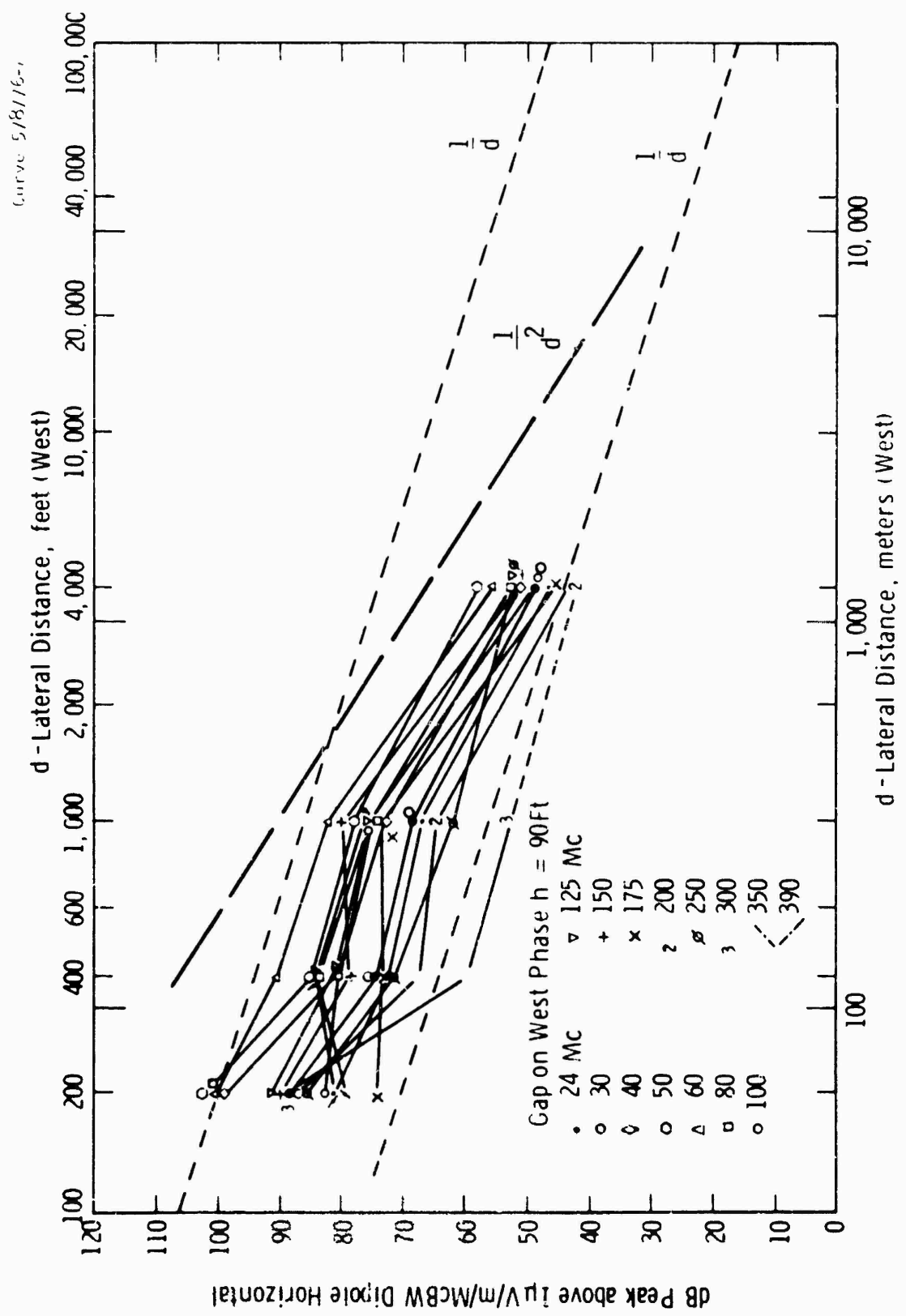


Fig. 63—345 KV HCST line at 24-390 Mc at several lateral distances with artificial gap. (Dipole Horizontal)

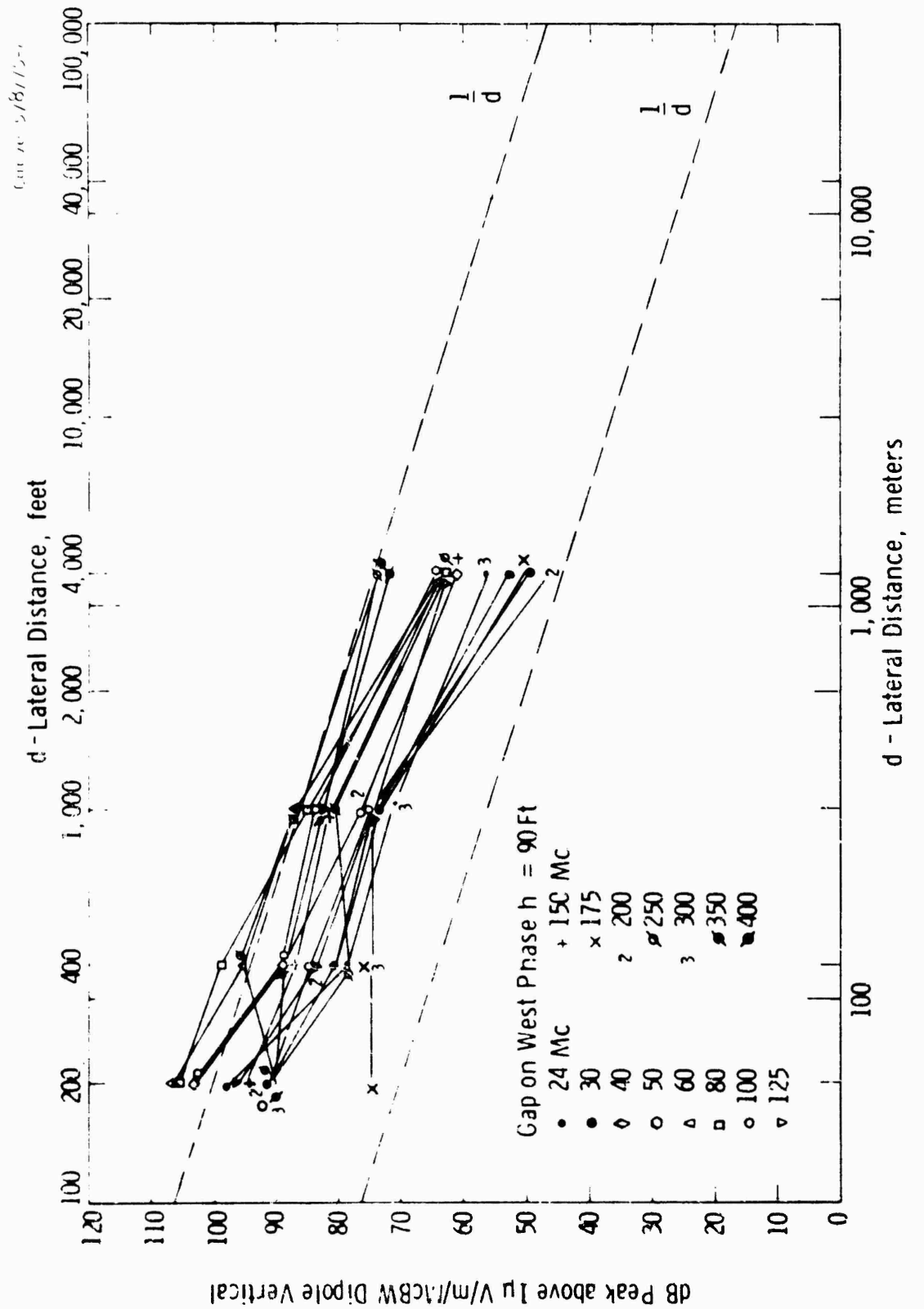


Fig. 64-345 kV HCST line at 24-400 Mc at several lateral distances with artificial gap. (Dipole Vertical)

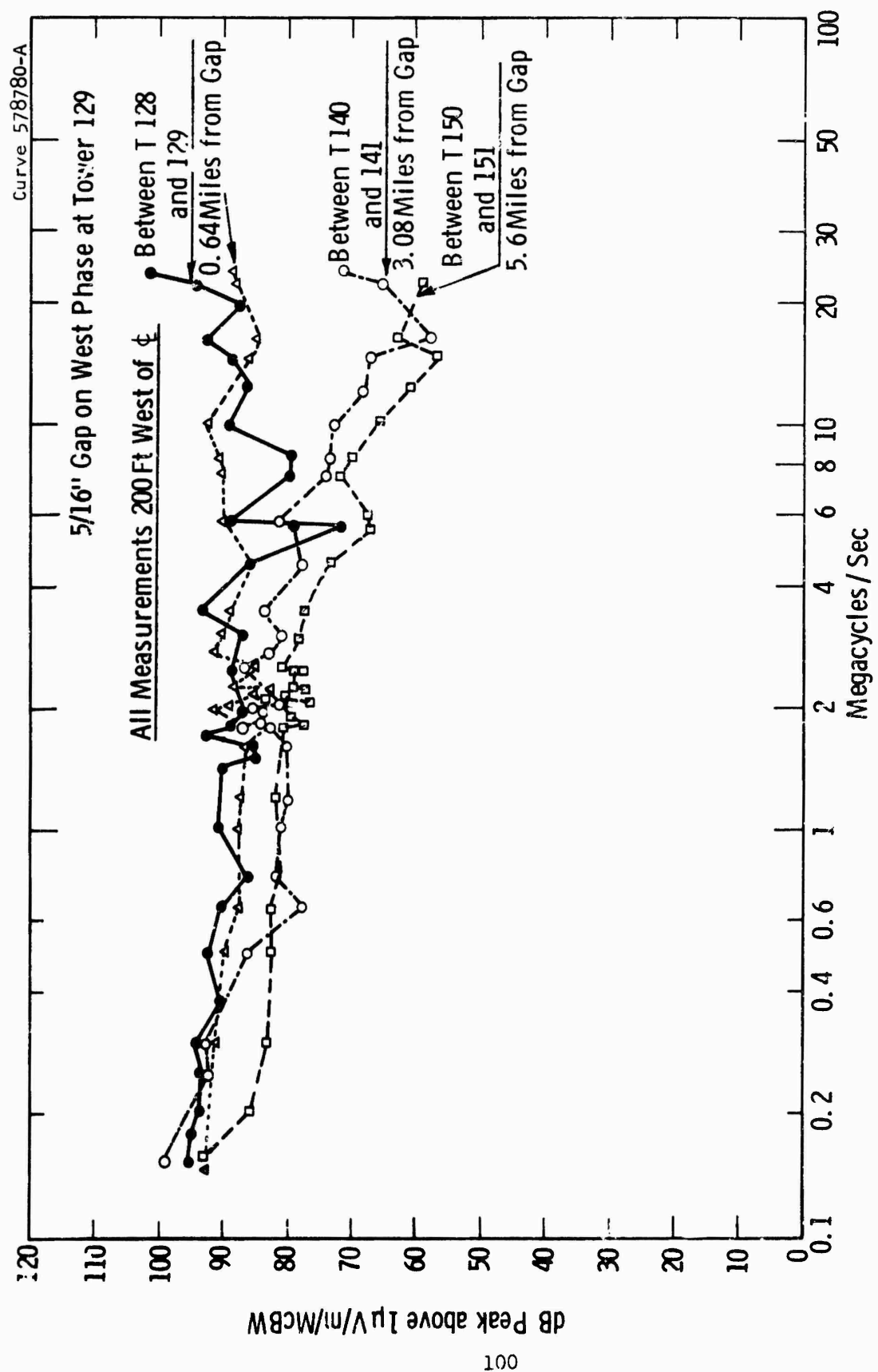


Fig. 65—345 kV HCST line frequency spectra at several longitudinal distances from artificial gap

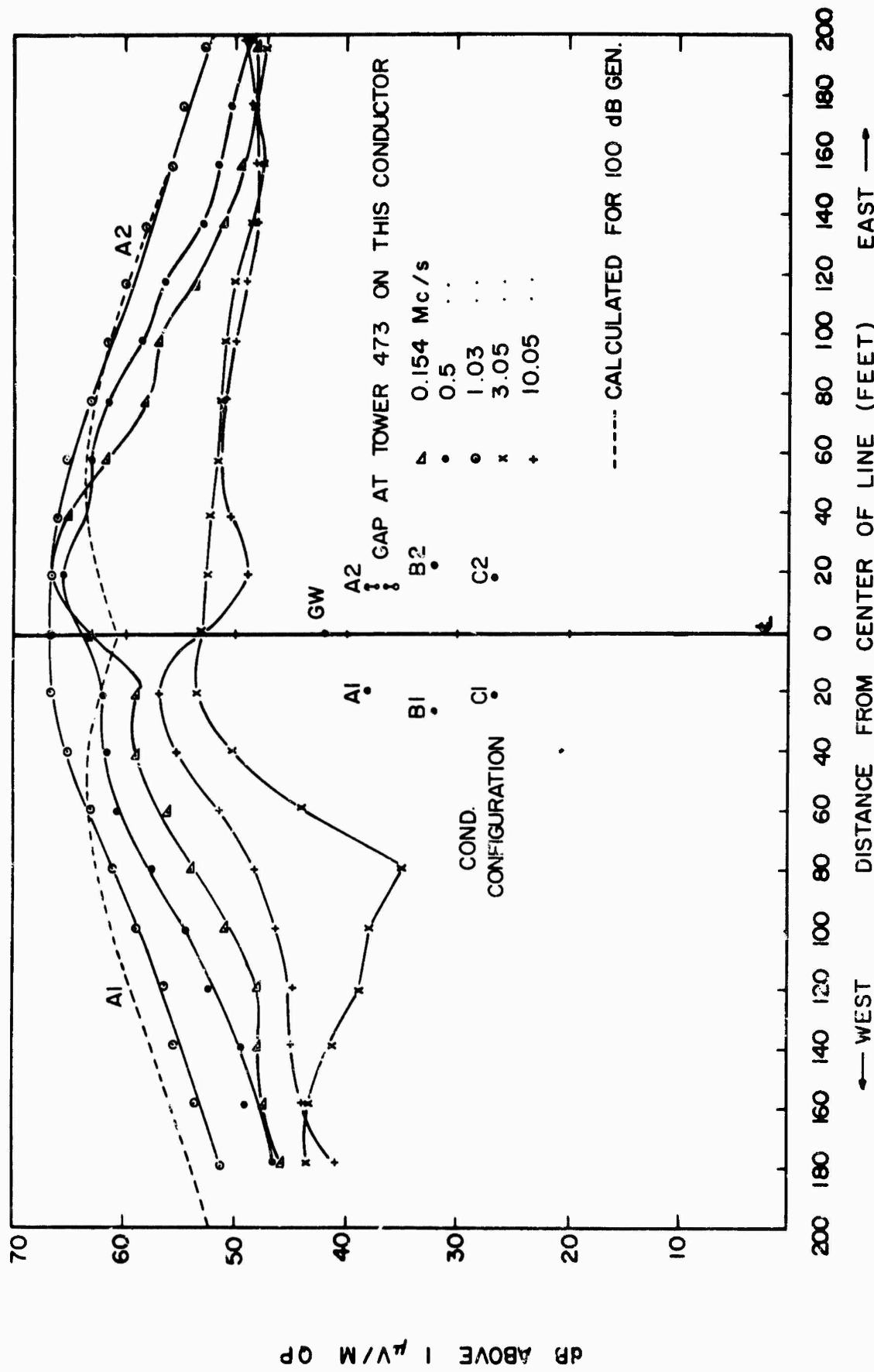


FIG. 66 345 KV VC ST DC LINE LATERAL PROFILES AT MID-SPAN NEAR TOWER WITH GAP ON TOP CONDUCTOR T 473

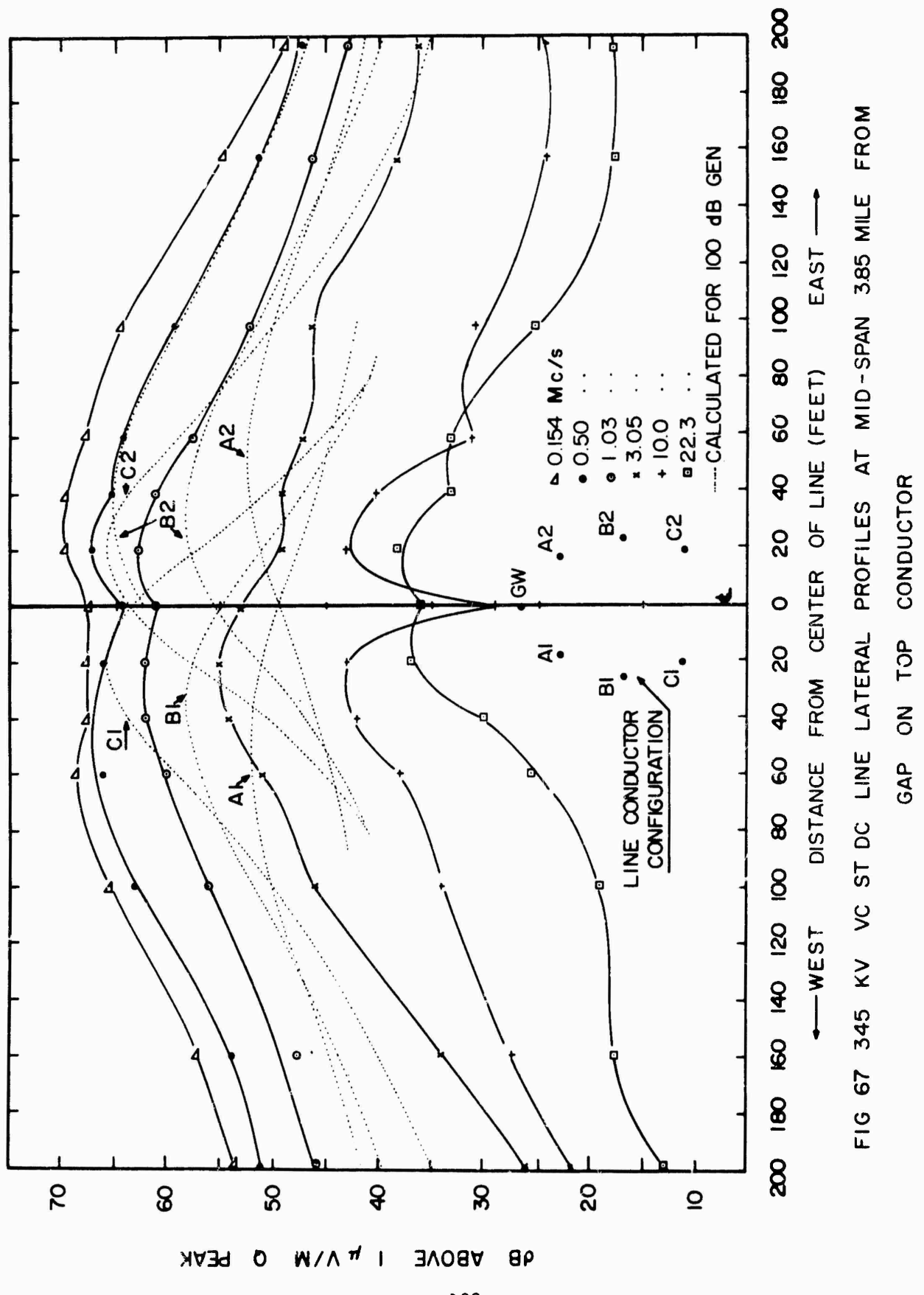


FIG 67 345 KV VC ST DC LINE LATERAL PROFILES AT MID-SPAN 385 MILE FROM GAP ON TOP CONDUCTOR

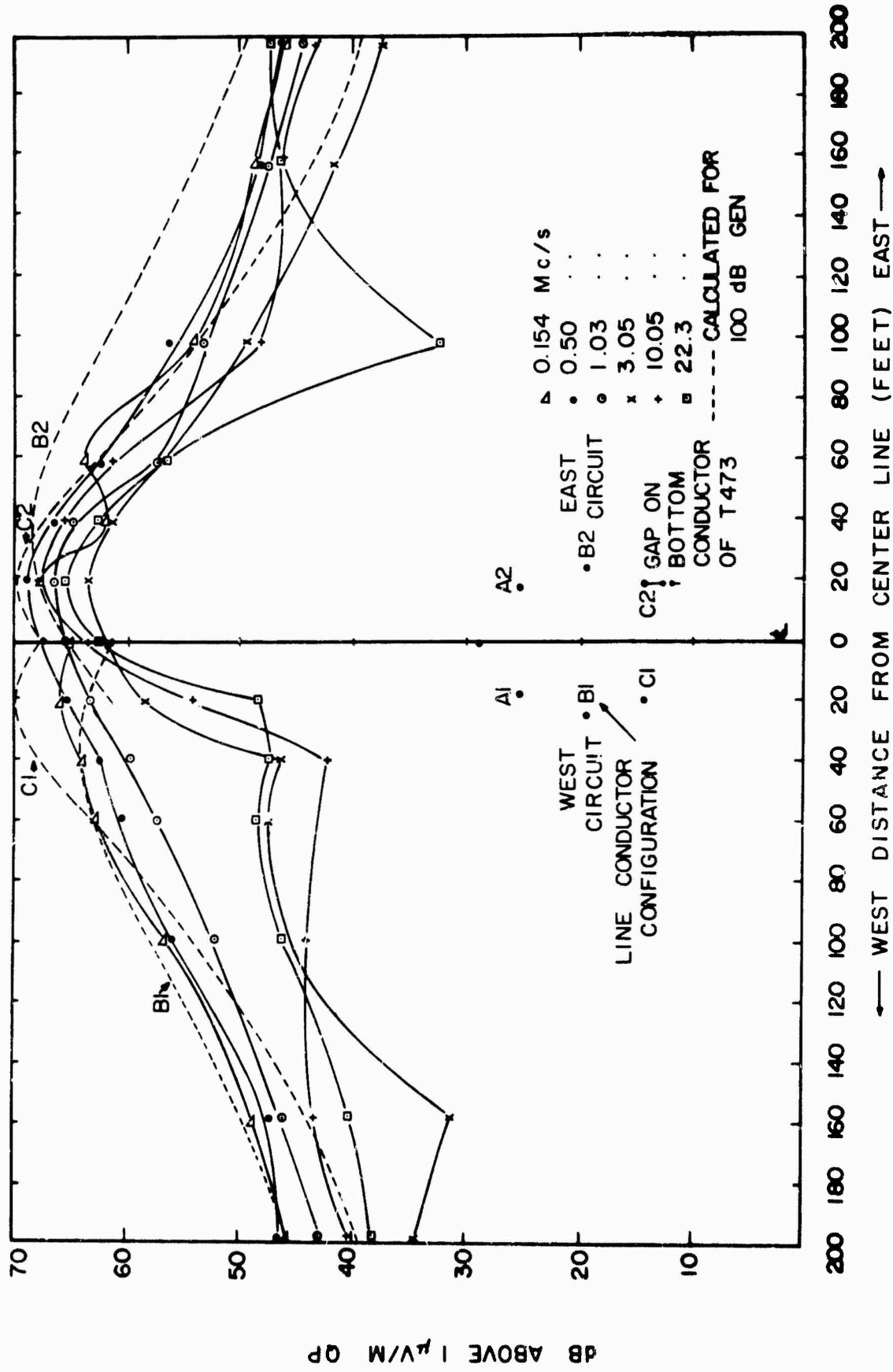


FIG. 68 345 KV VC ST DC LINE LATERAL PROFILES AT MID-SPAN NEAR TOWER WITH GAP ON BOTTOM CONDUCTOR AT TOWER 473

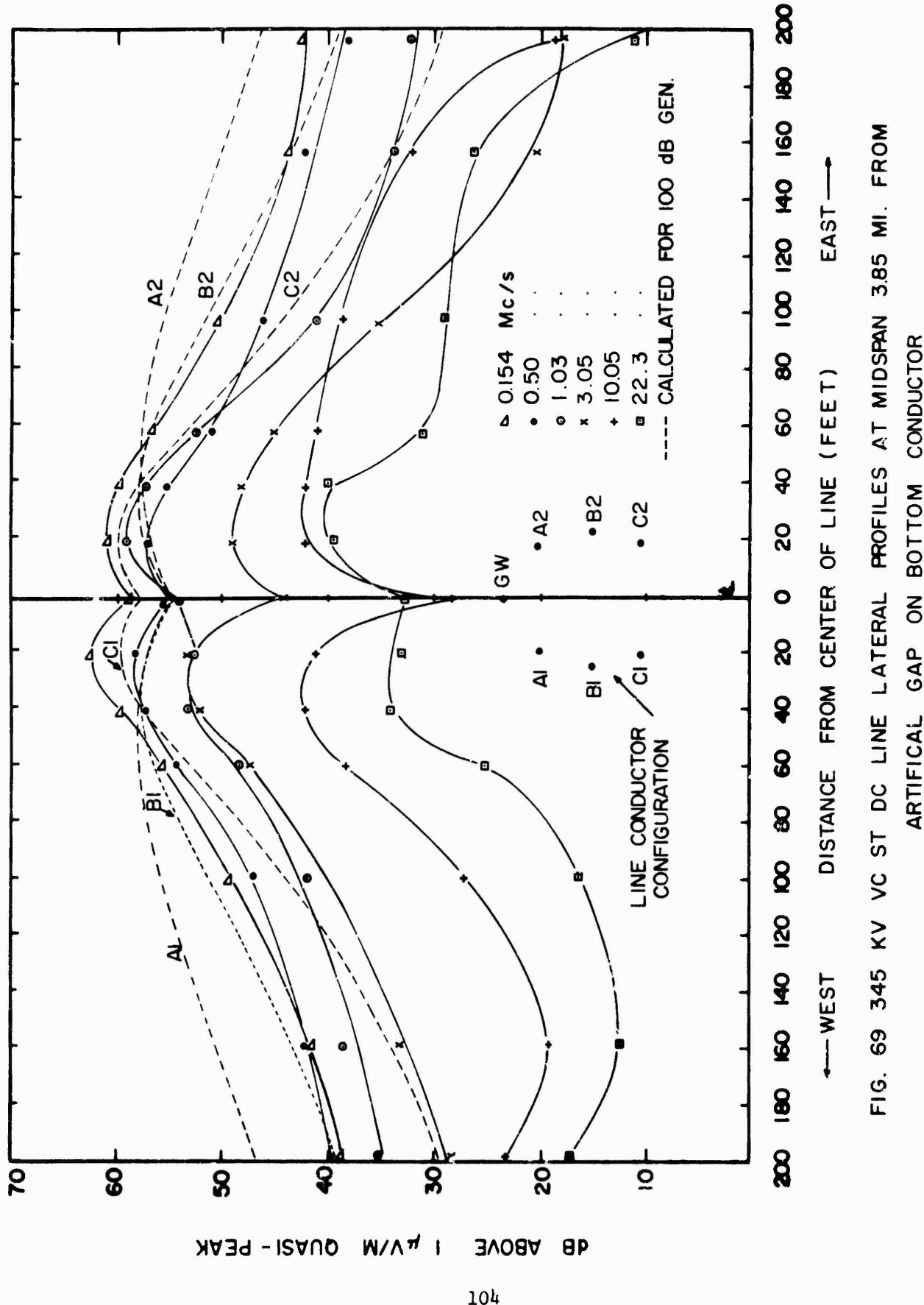
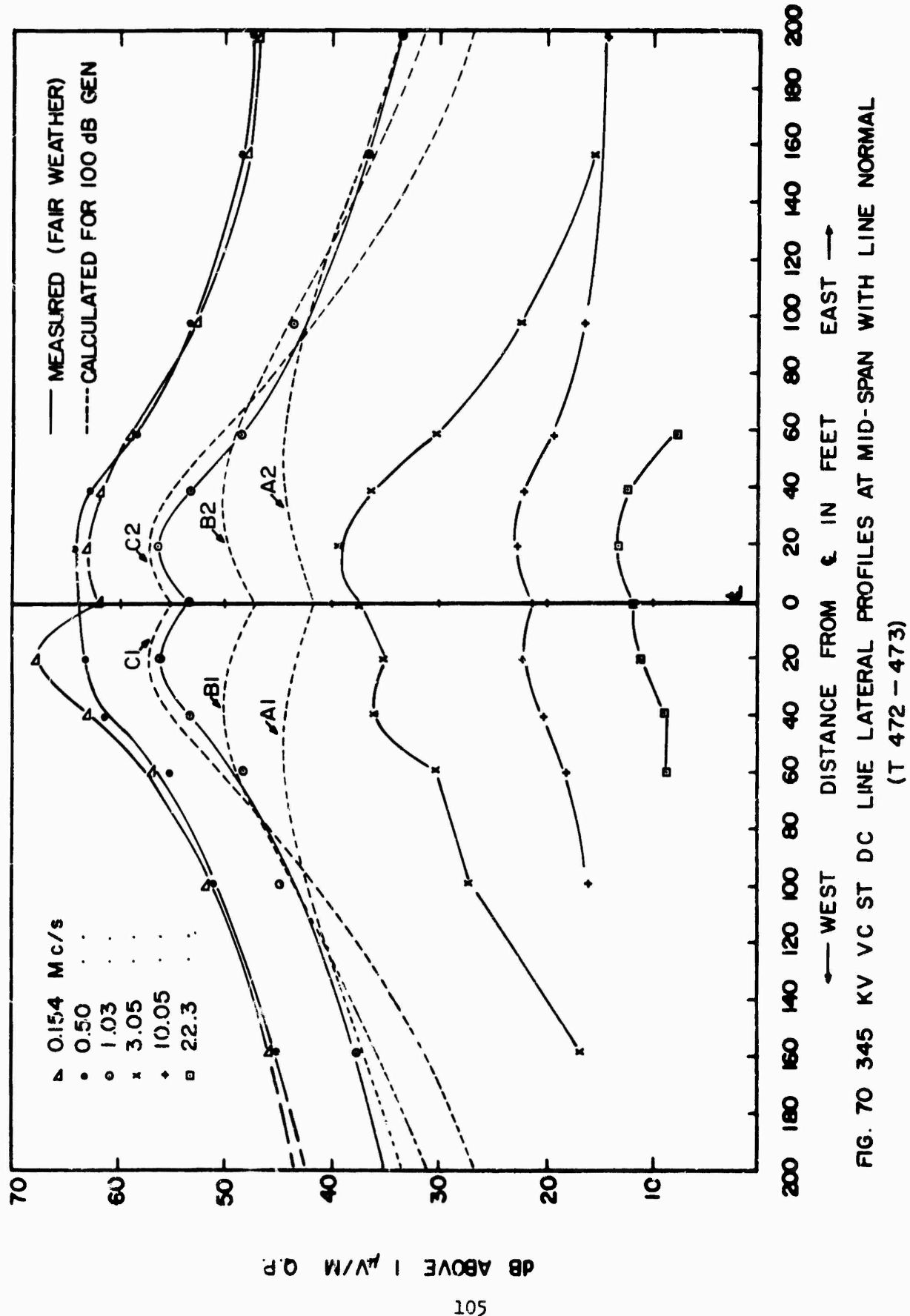


FIG. 69 345 KV ST DC LINE LATERAL PROFILES AT MIDSPAN 3.85 MI. FROM ARTIFICIAL GAP ON BOTTOM CONDUCTOR



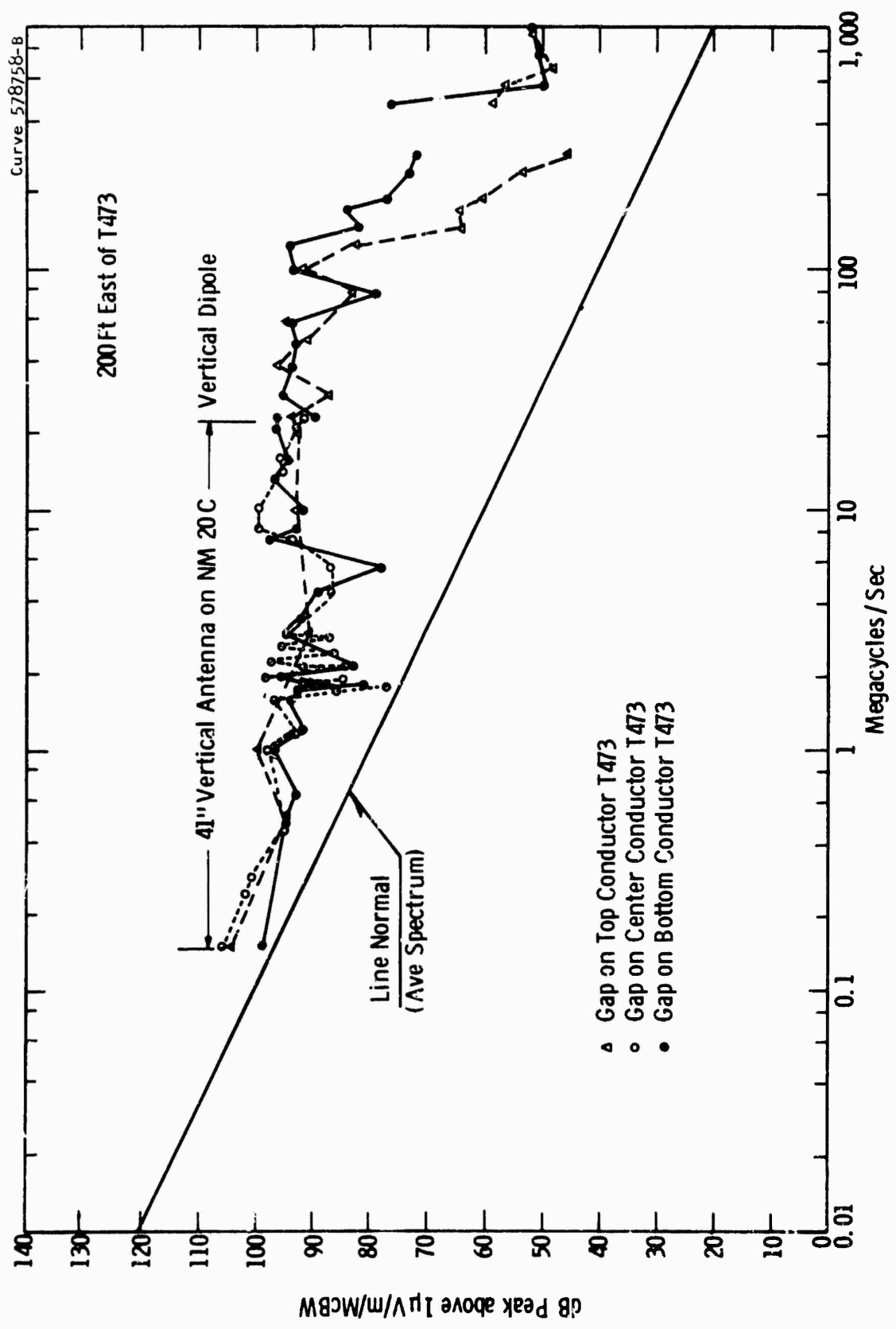


Fig. 71—345 kV VCD line - comparison of frequency spectra with artificial gap at different heights

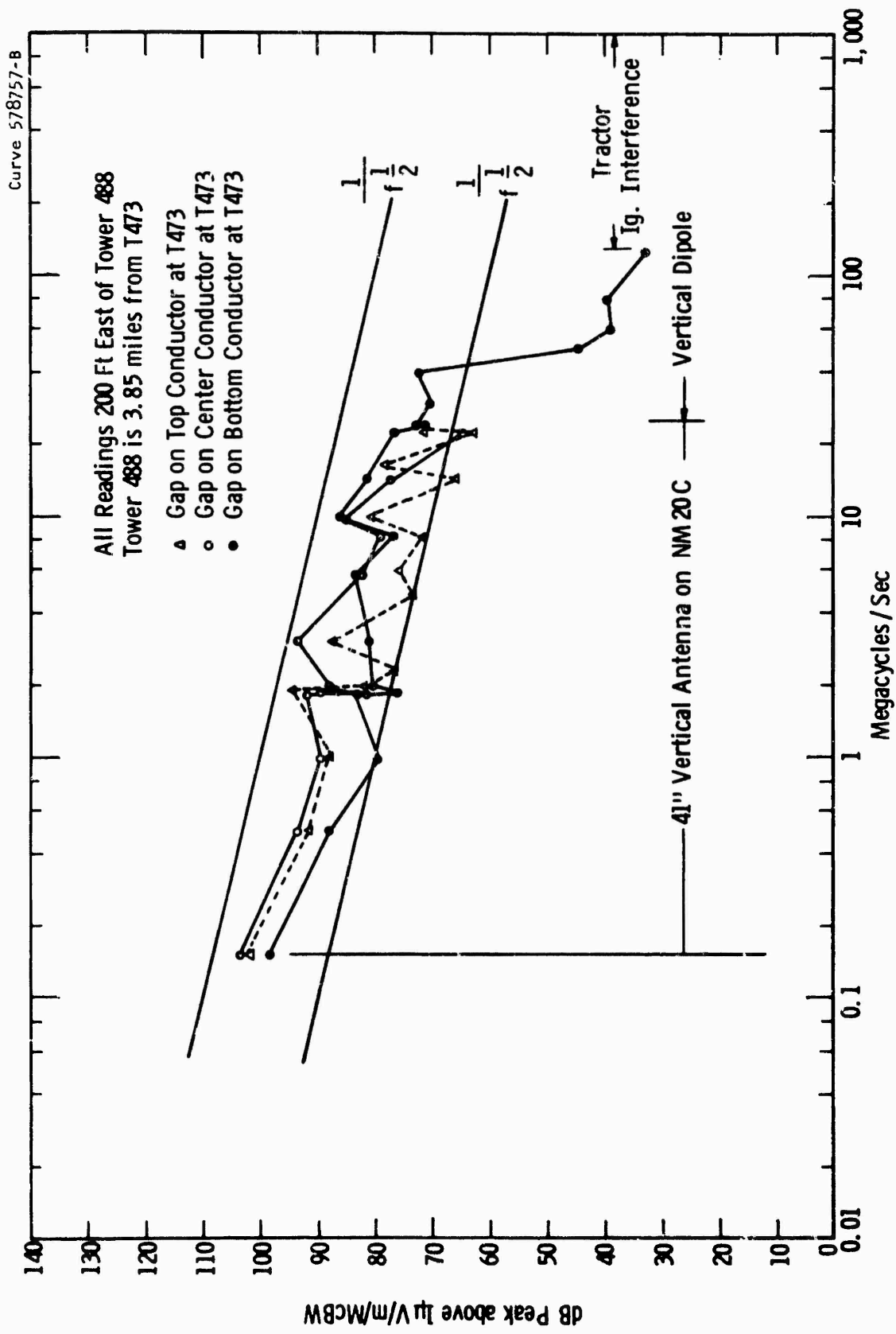


Fig. 72—345 kV VCDCSI line spectra 3.85 miles down the line from artificial gap

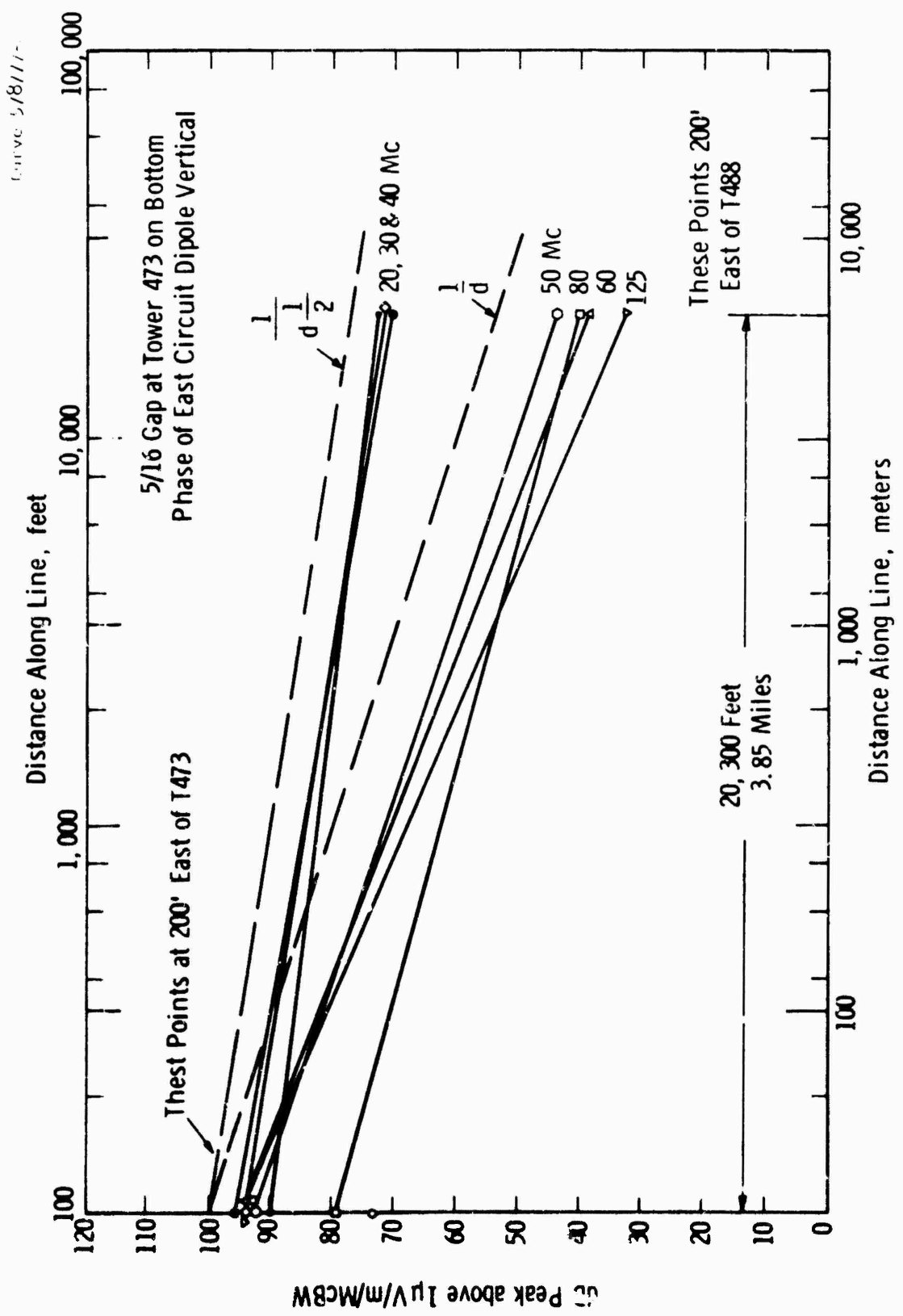


Fig. 73—345kV VCD CDT line attenuation for 3.85 miles 24-125 Mc with artificial gap

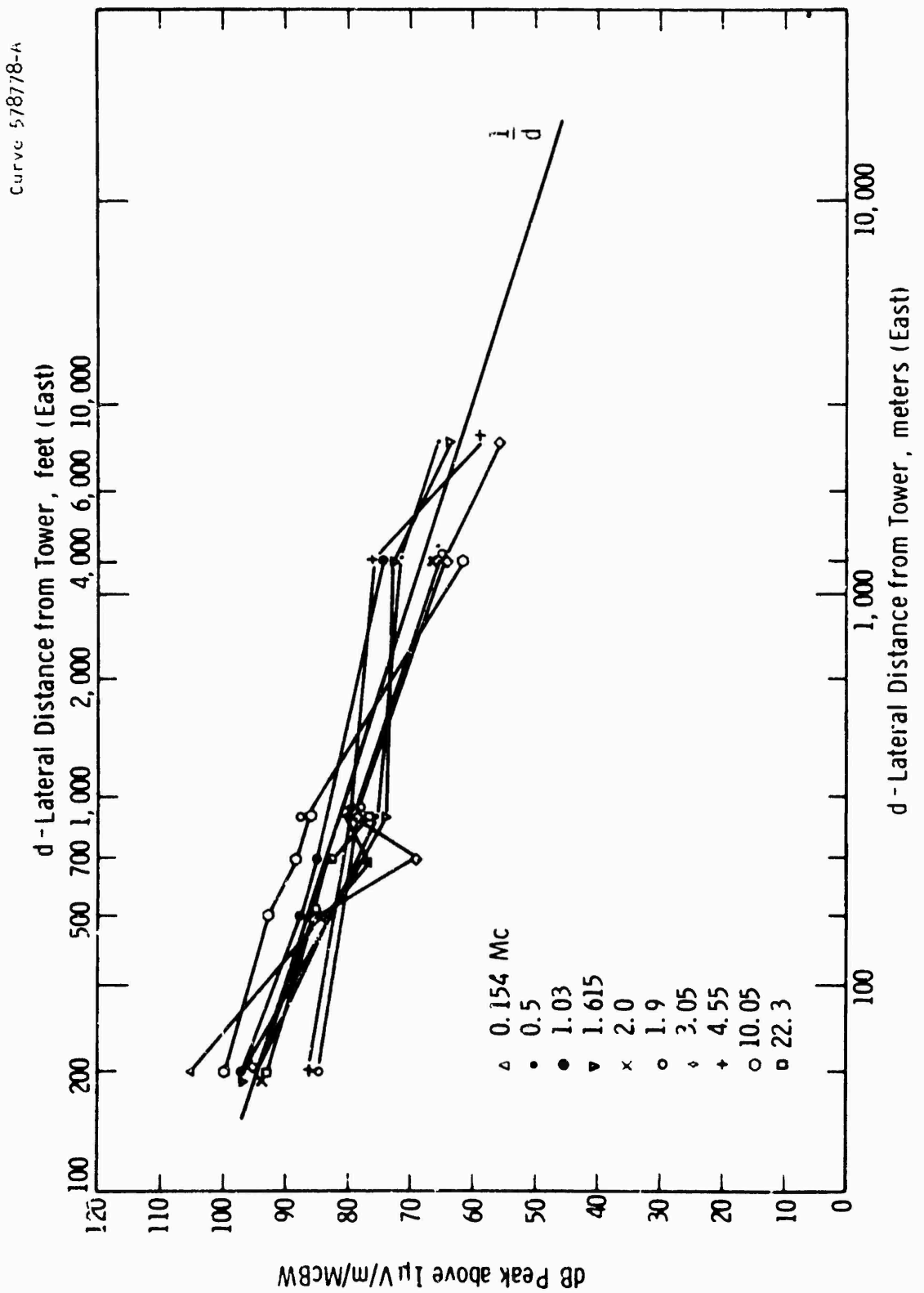


Fig. 74-345 kV VCDGST line lateral attenuation 0.154-22.3 Mc with gap on center phase

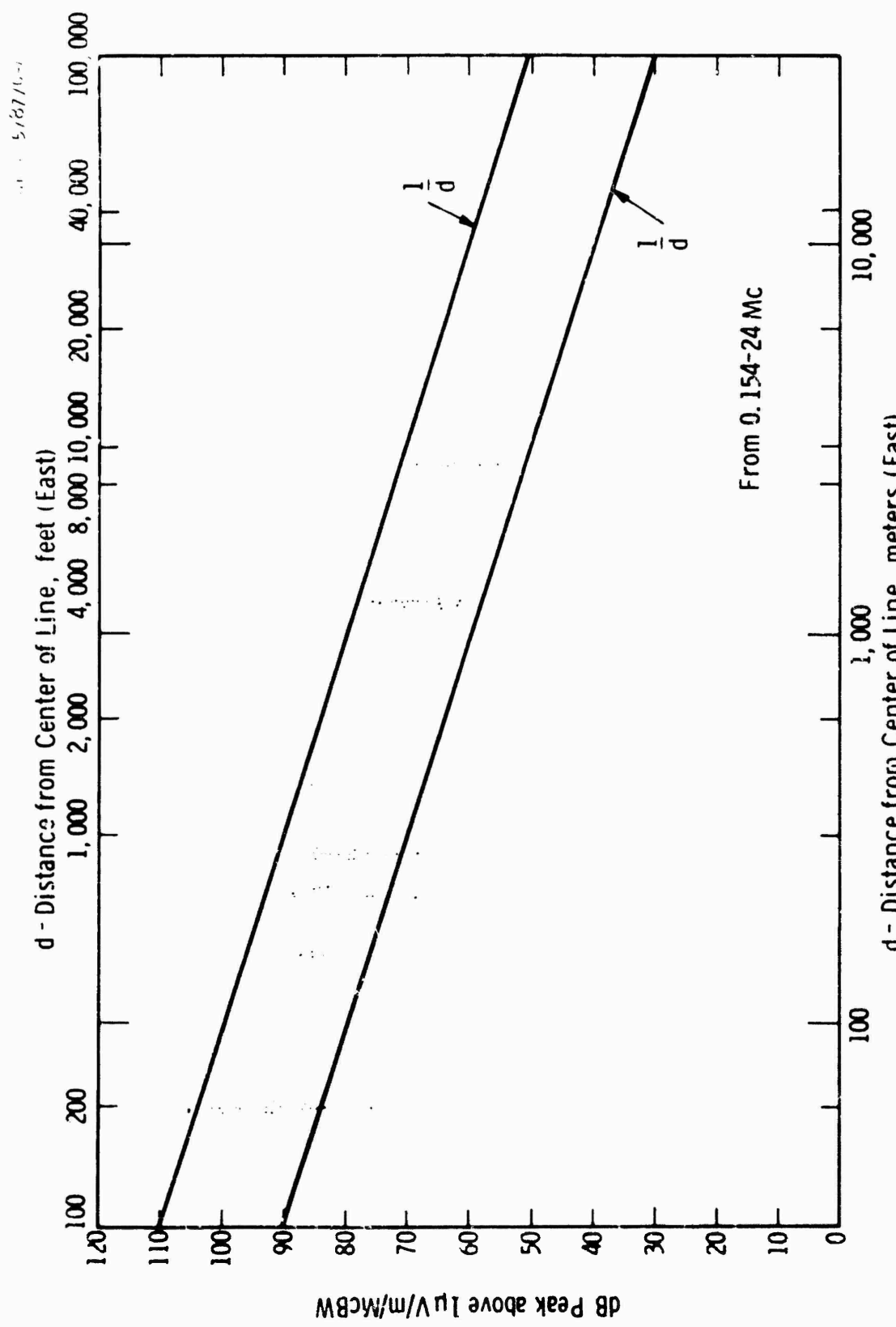


Fig. 75-345 kV VCDGST line lateral attenuation 0.15-24 Mc with gap on center phase

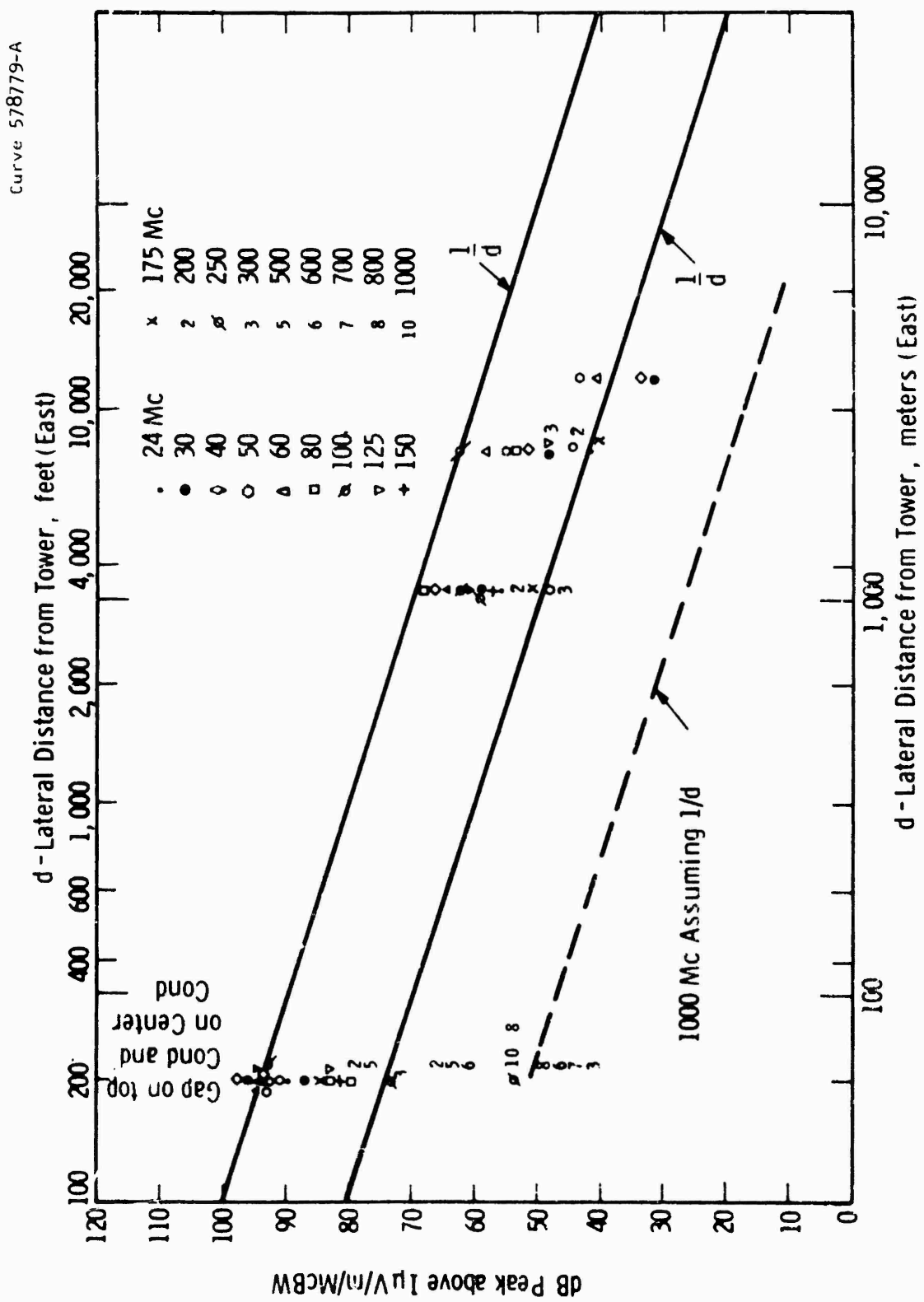


Fig. 76—345 kV VCDGST line lateral attenuation 24-1000 Mc with gap on center phase

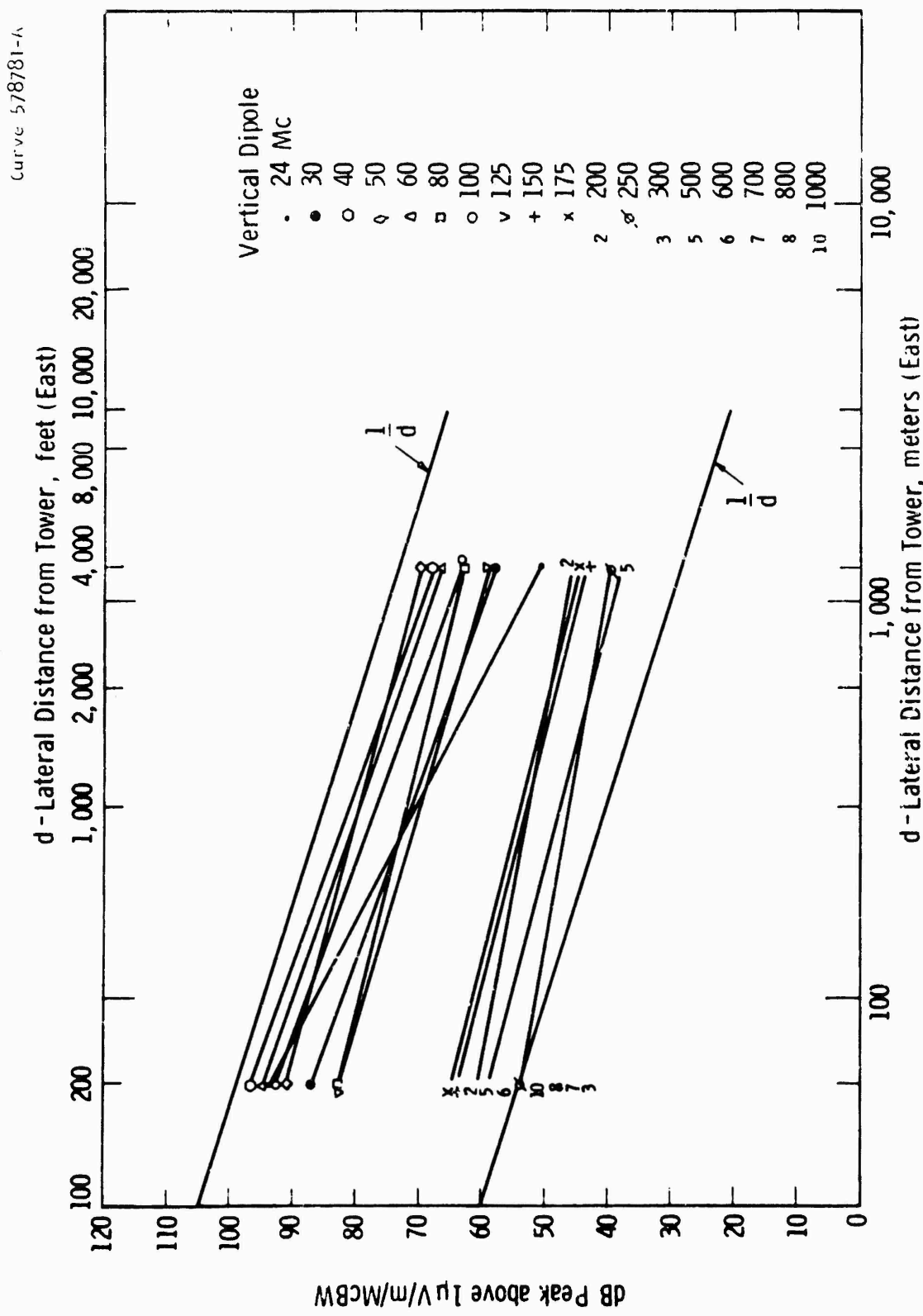


Fig. 77 – 345 kV VCD/CST line lateral attenuation 24-1000 Mc with gap on top phase

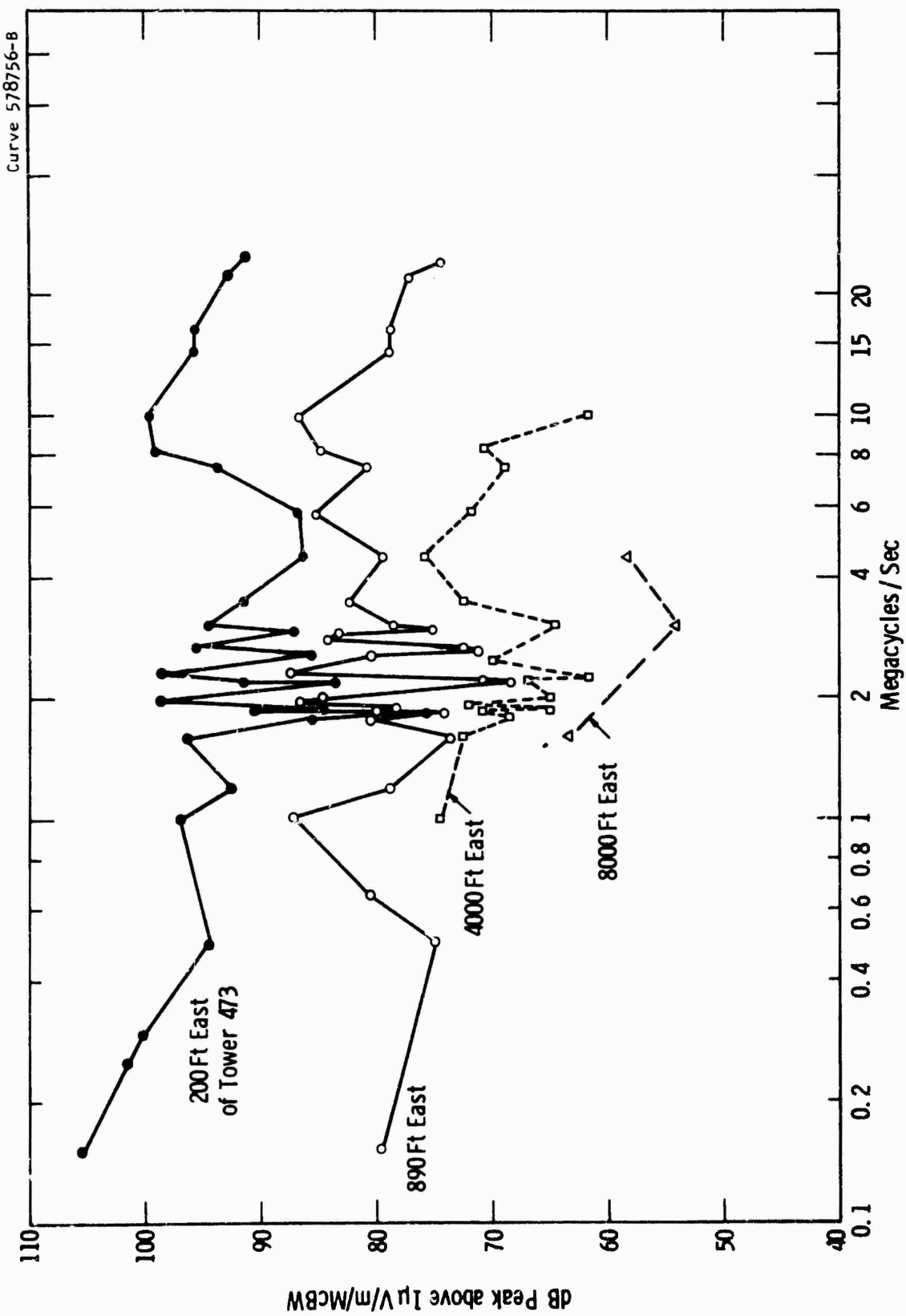


Fig. 78—345 KV VCDCSR line frequency spectra 0.15-24 Mc with artificial gap at tower on center phase

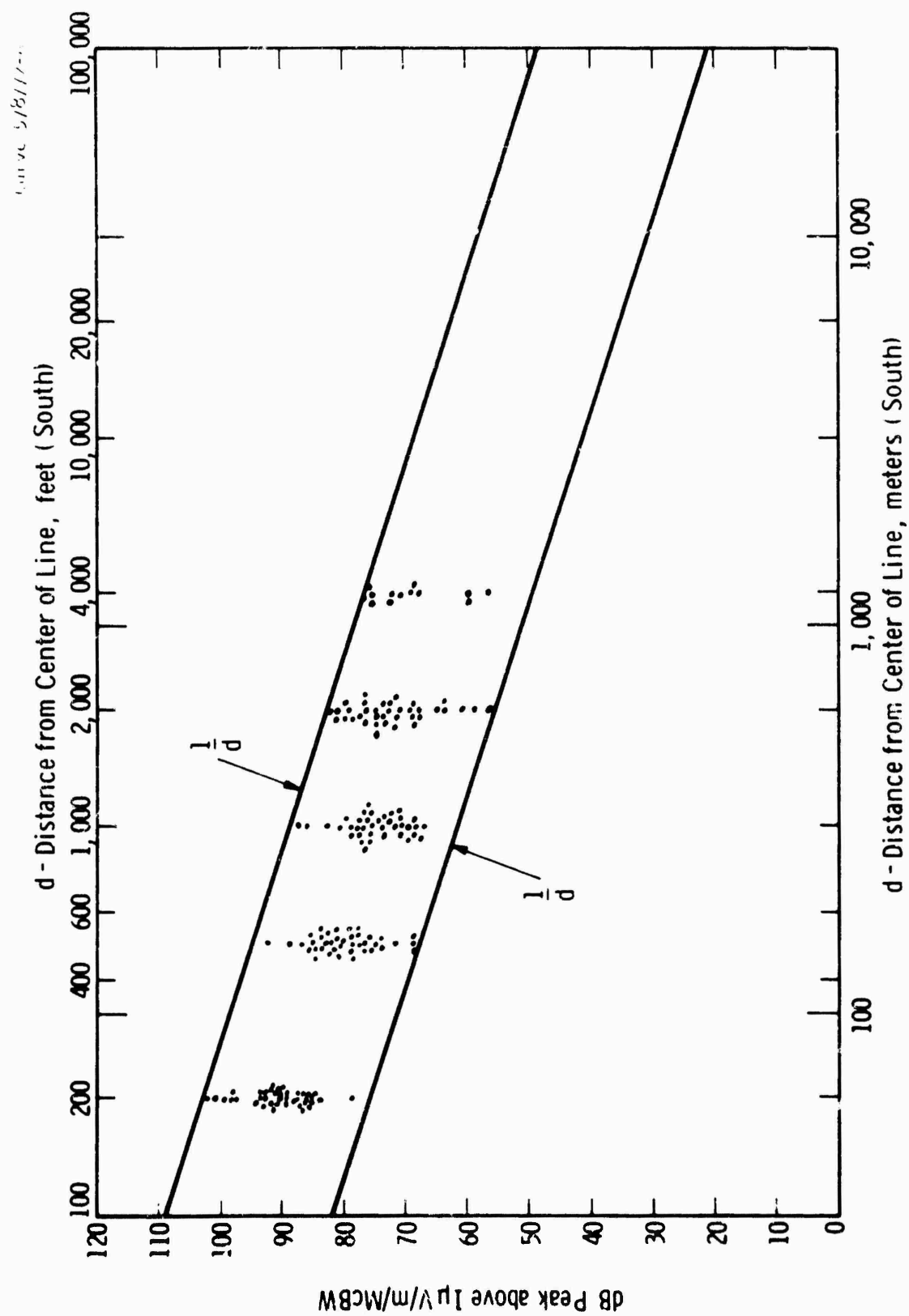


Fig. 79—345 kV HCWP line lateral attenuation 0.154-24 Mc with artificial gap at T119

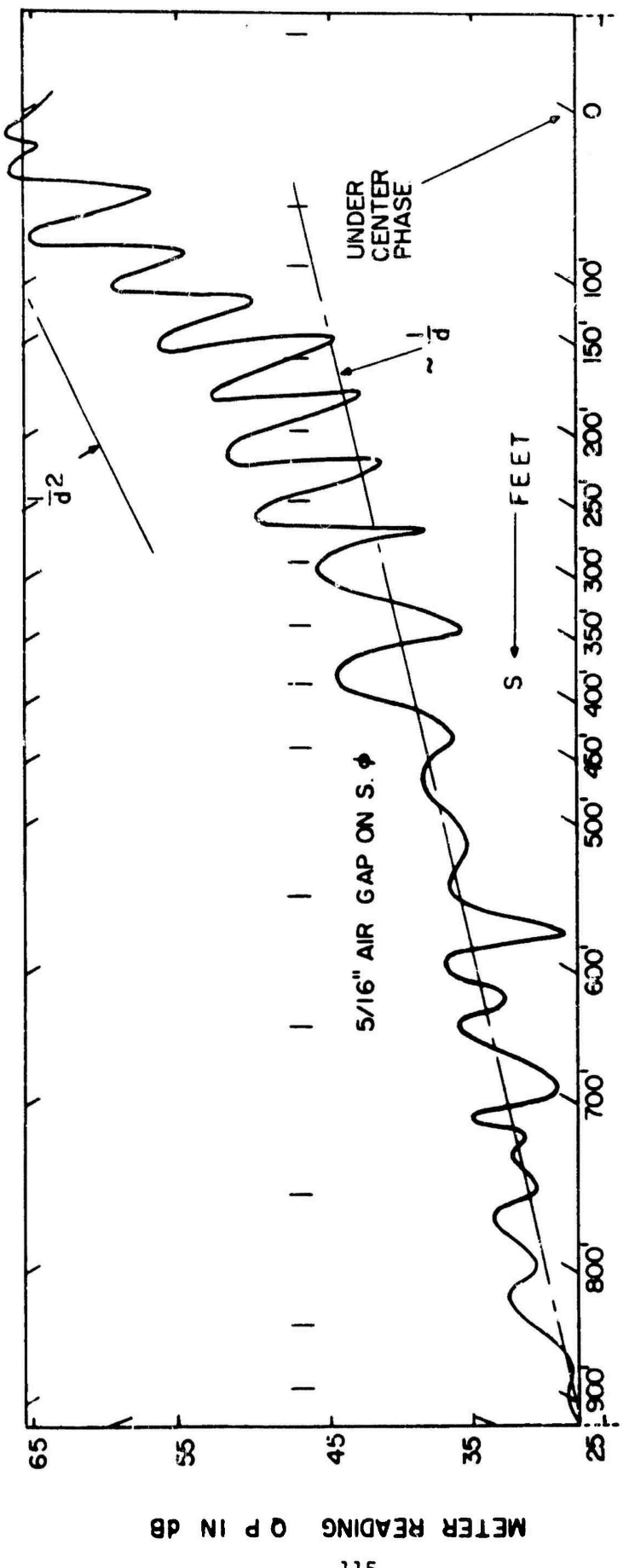


FIG. 80 345 KV WOOD POLE LINE FREQUENCY RECORDING AT 30 MC FROM CENTER PHASE TO 1,000' SOUTH ANTENNA HORIZONTAL

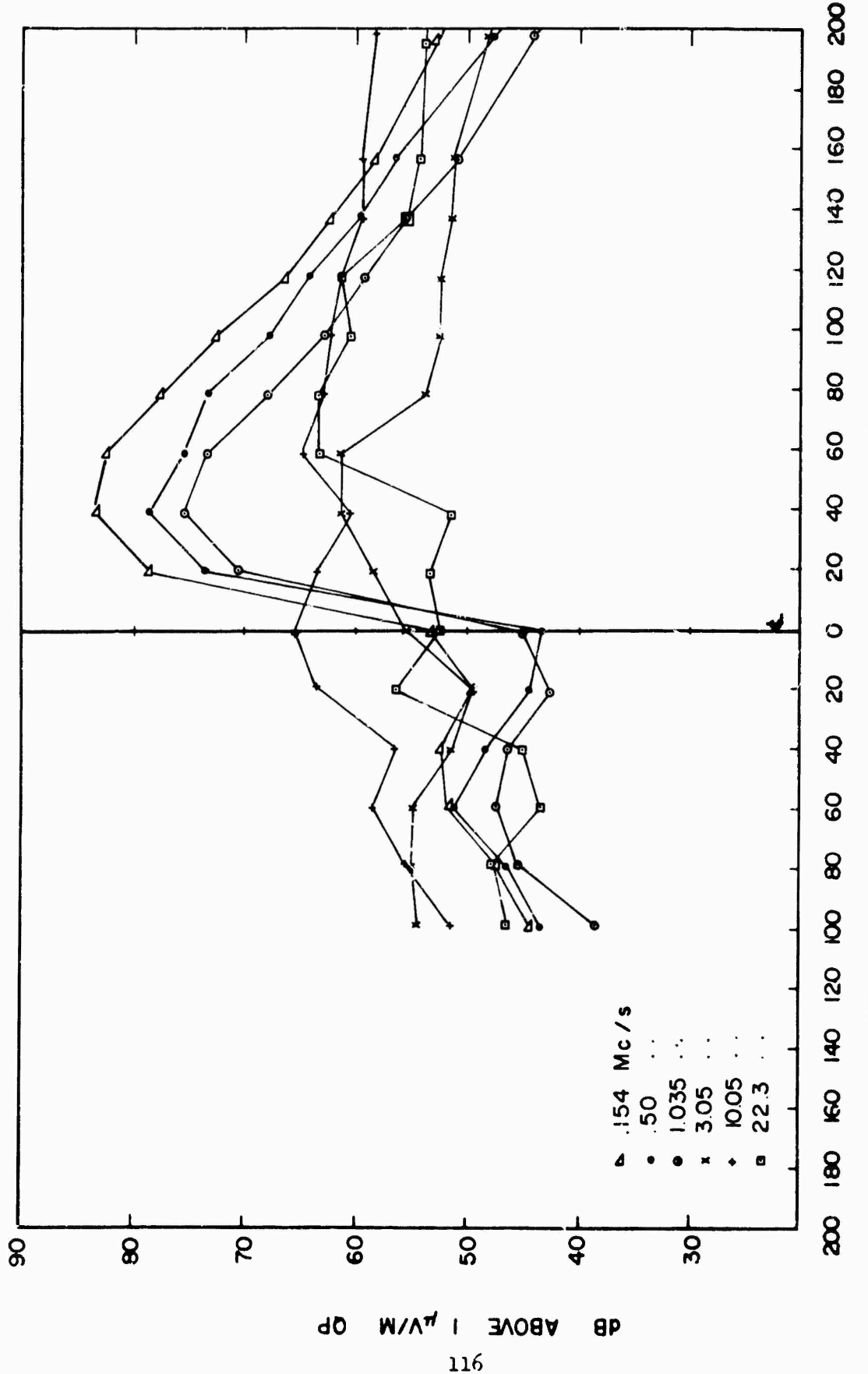


FIG. 81 244 KV HC ST LINE LATERAL PROFILES AT TOWER WITH ART. GAP ON EAST PHASE

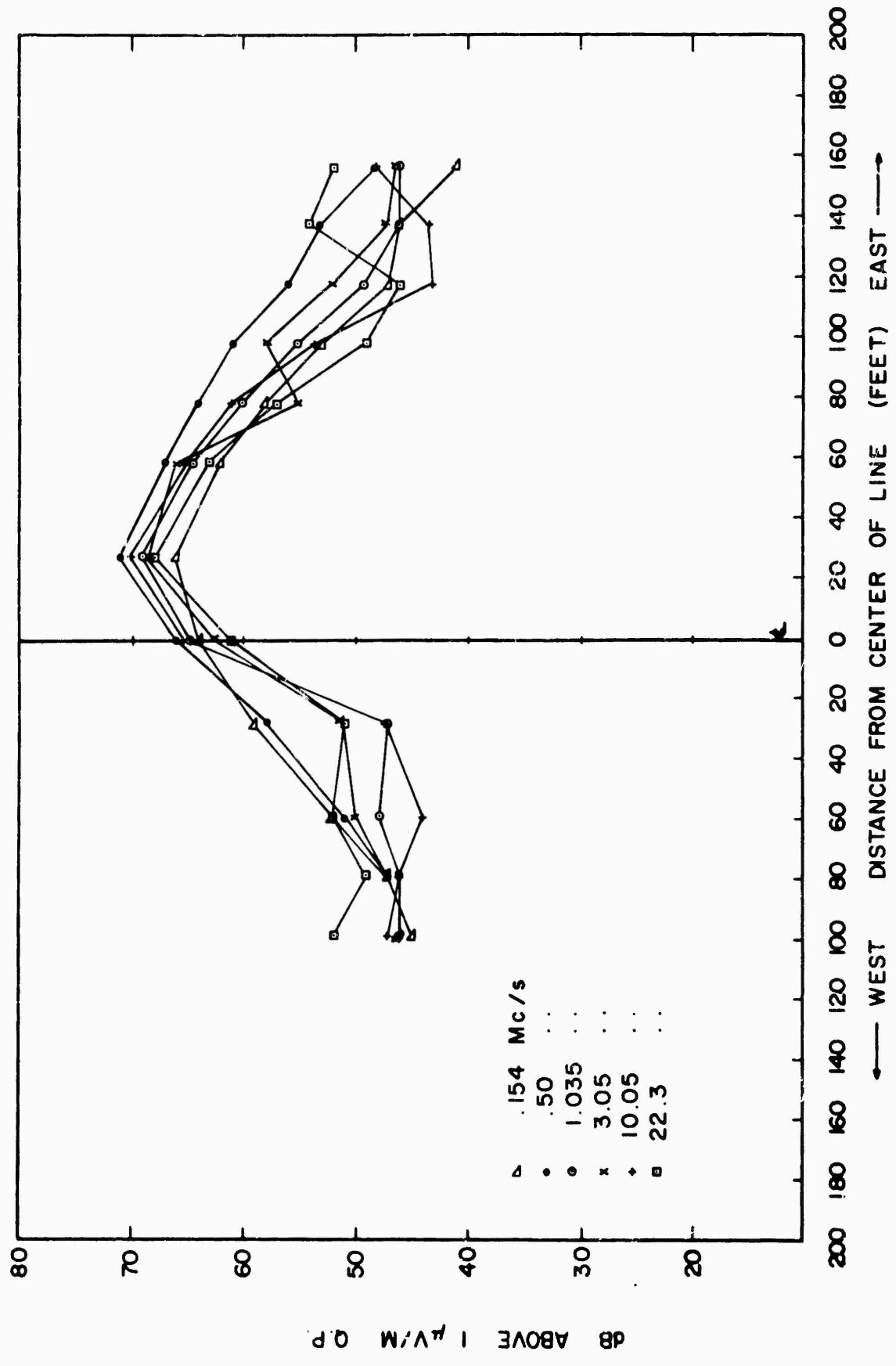


FIG. 82 244 KV HC ST LINE LATERAL PROFILES NEAR MIDSPAN BY TOWER WITH ART. GAP

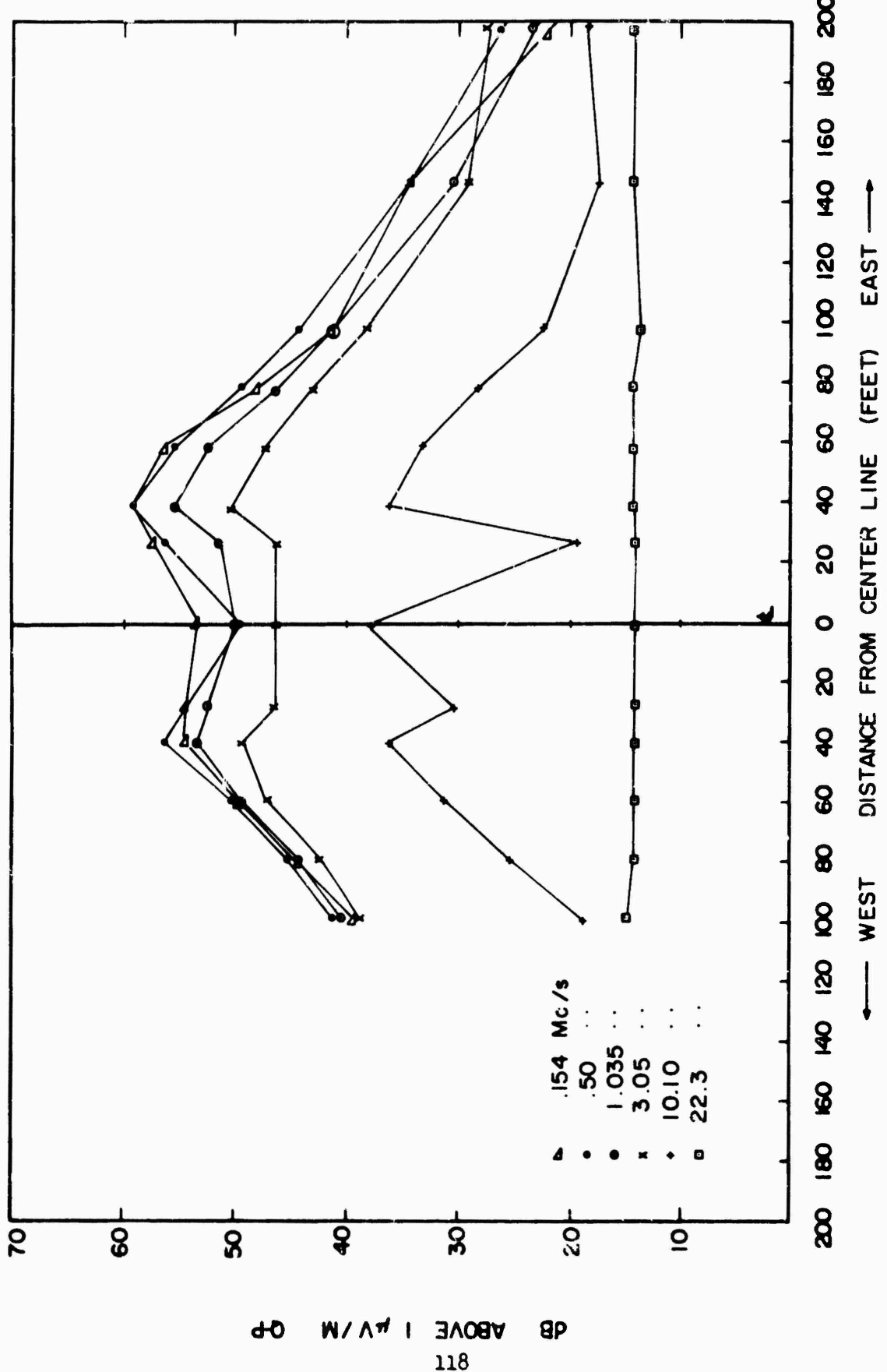


FIG. 83 244 KV HC ST LINE LATERAL AT MIDSPAN 8.23. MI. FROM TOWER WITH ART. GAP

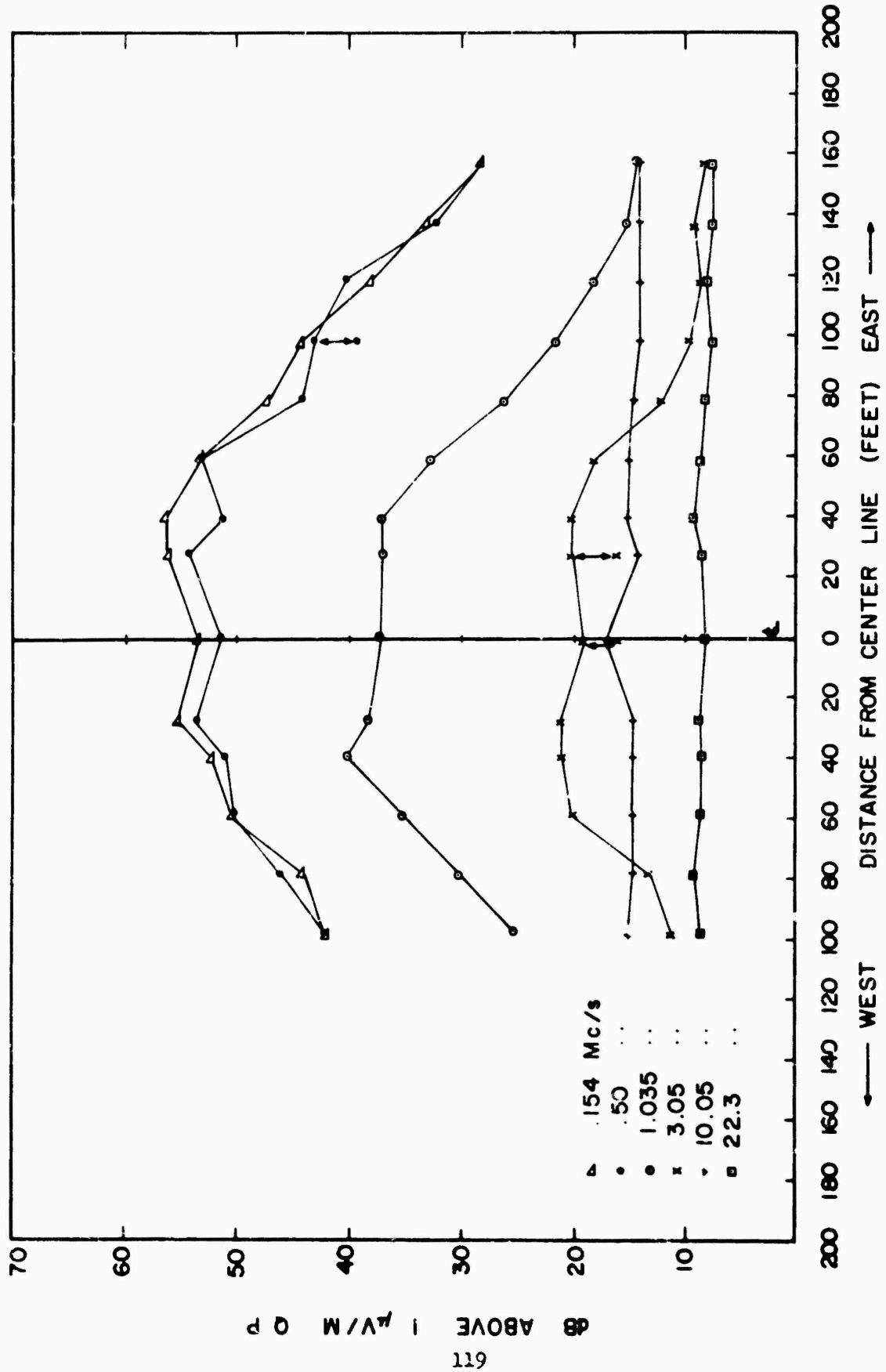


FIG. 84 244 KV HC ST NORMAL LINE LATERAL PROFILES NEAR MIDSPAN

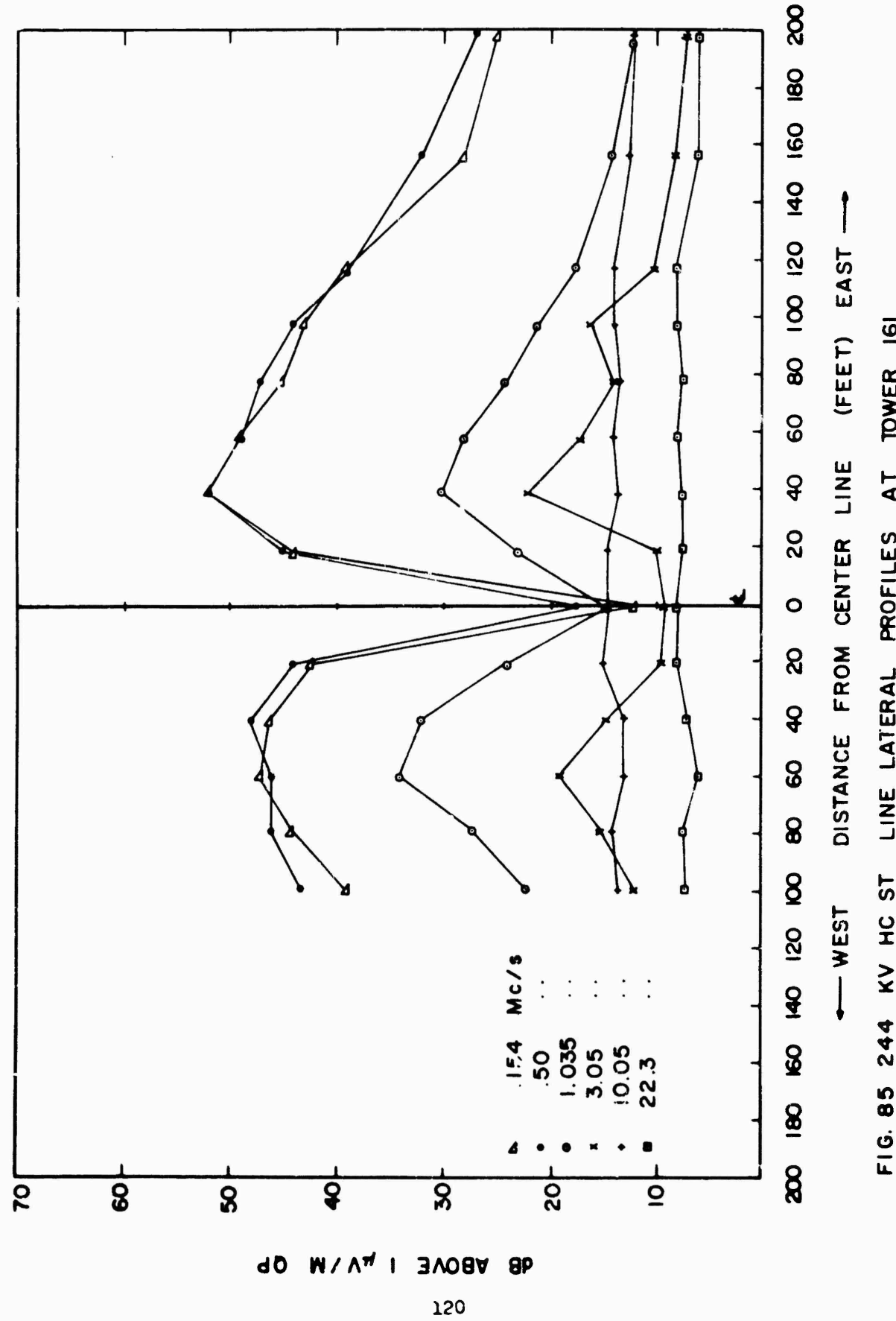


FIG. 85 244 KV HC ST LINE LATERAL PROFILES AT TOWER 16

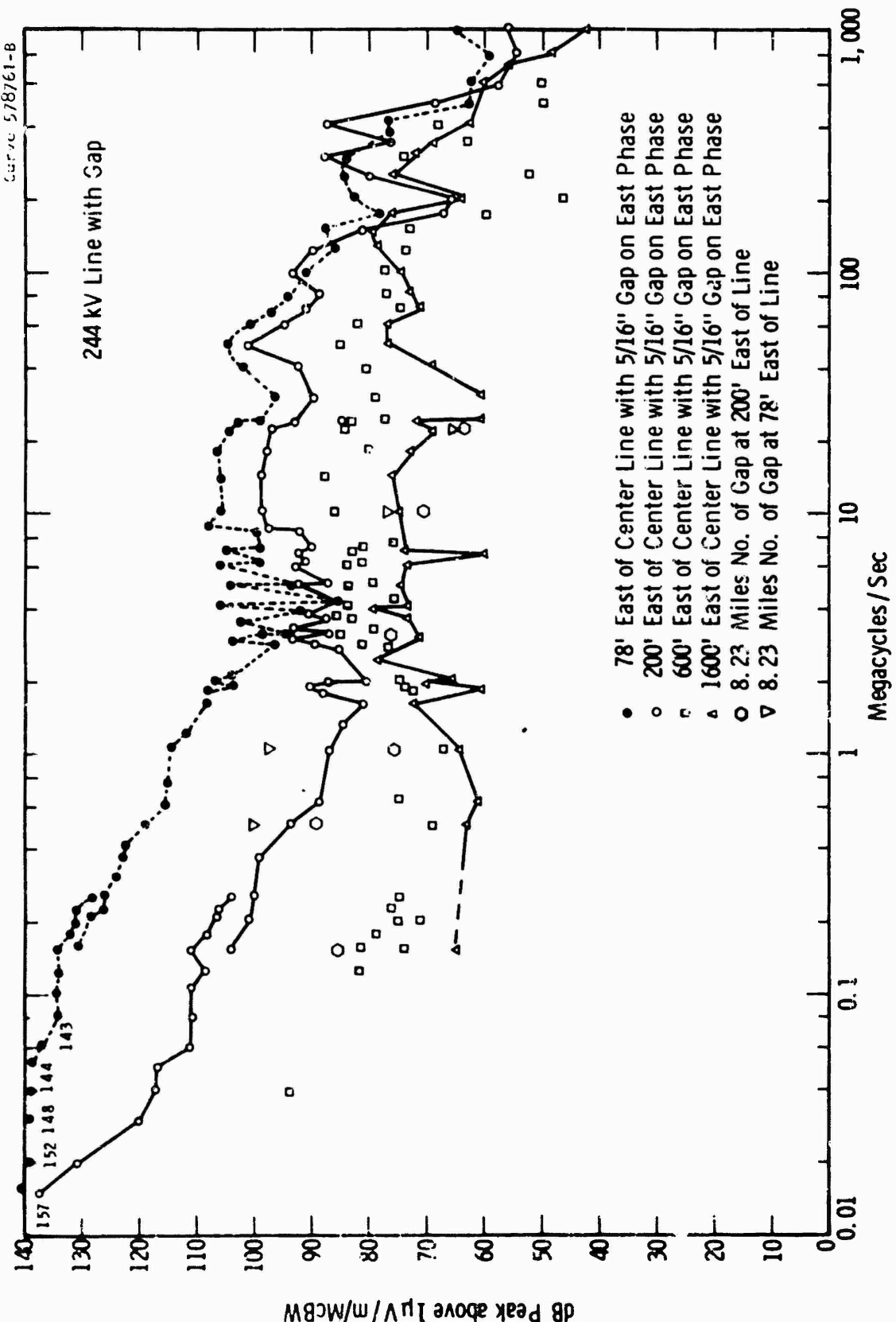


Fig. 86 - 244 KV HCST line frequency spectra with artificial gap

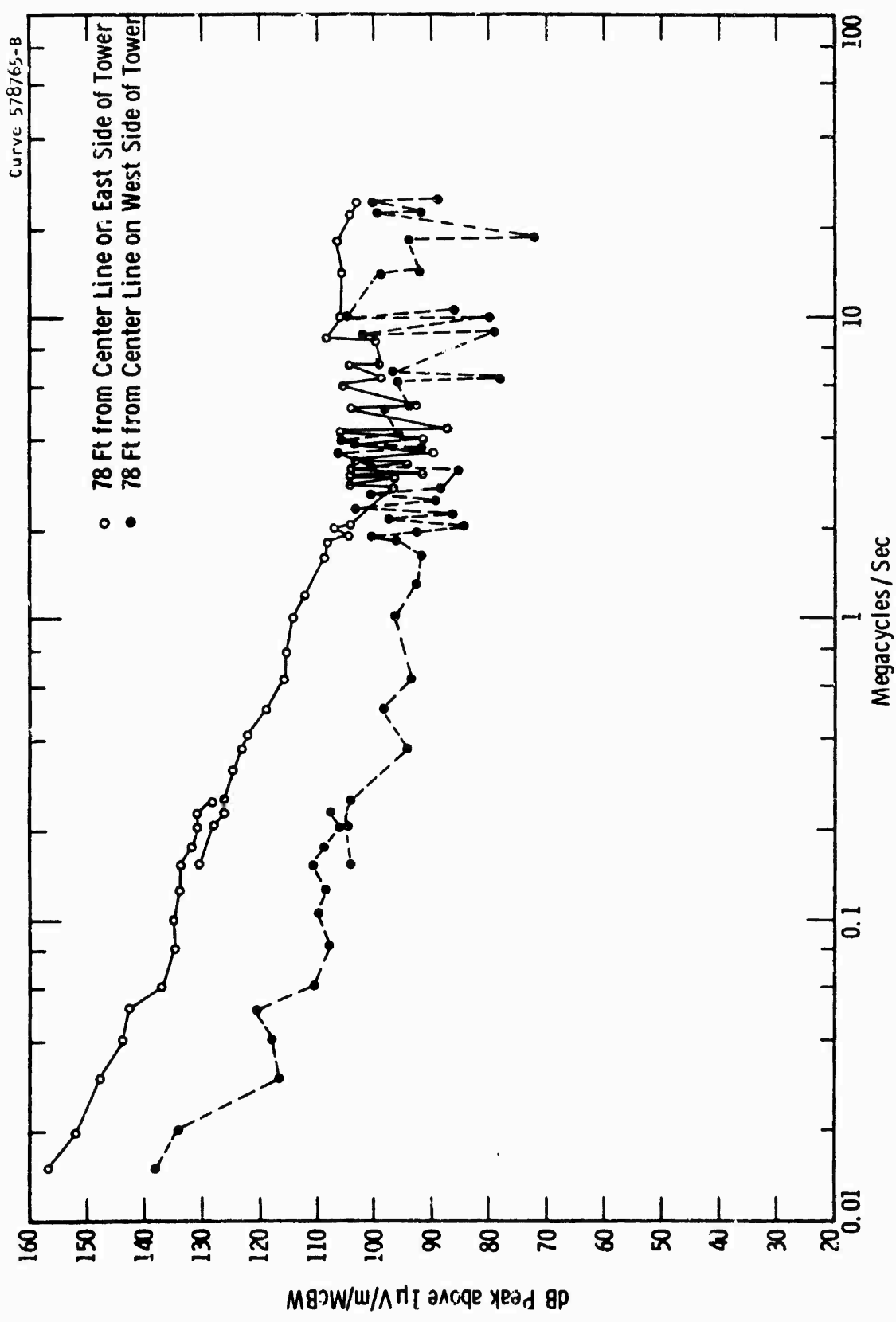


Fig. 87 -244 kV HCST line frequency spectra on east and west side of tower with artificial gap on east phase

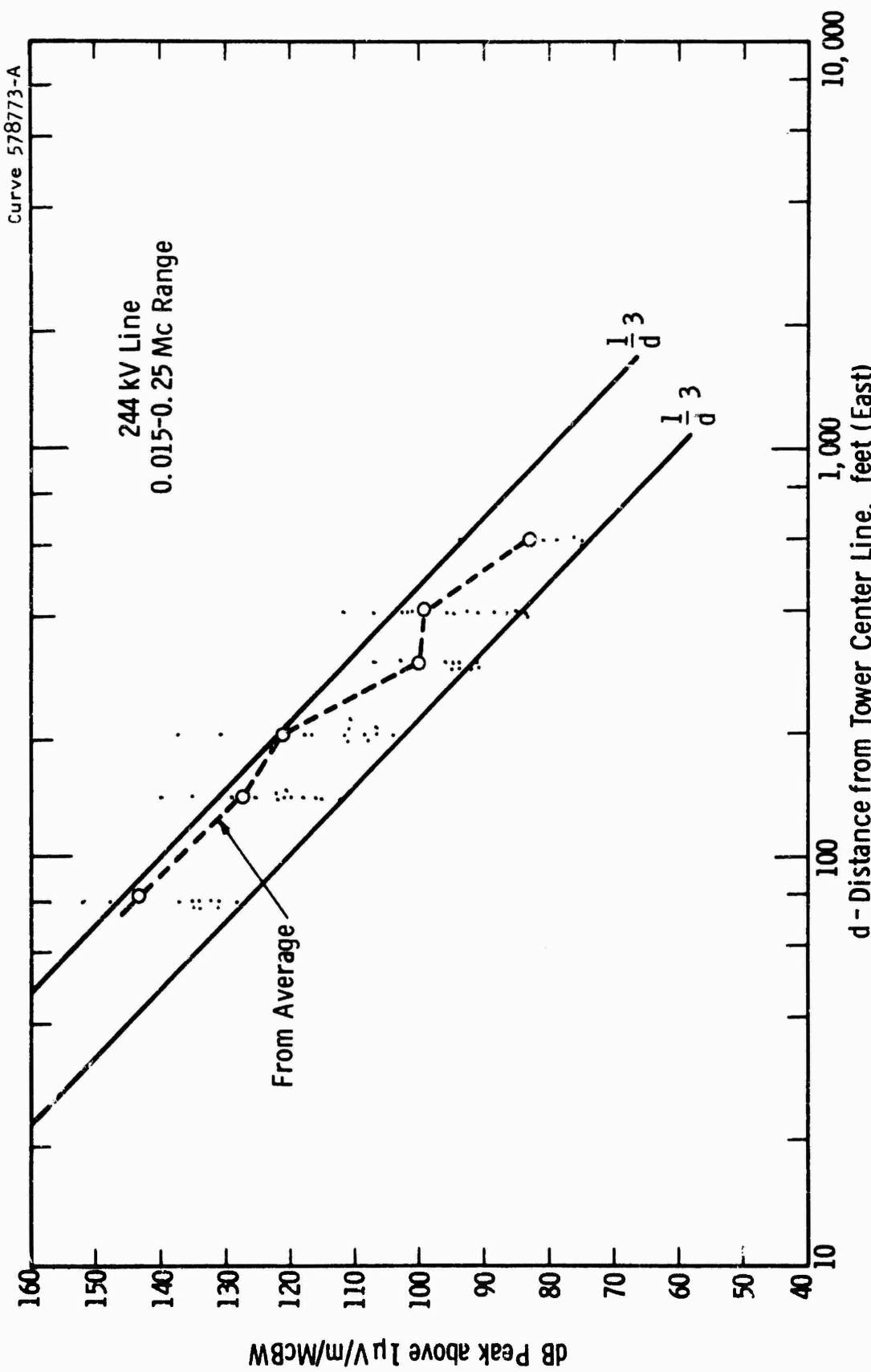


Fig.88 -244 KV HCST line lateral attenuation .015-0.25 Mc with artificial gap

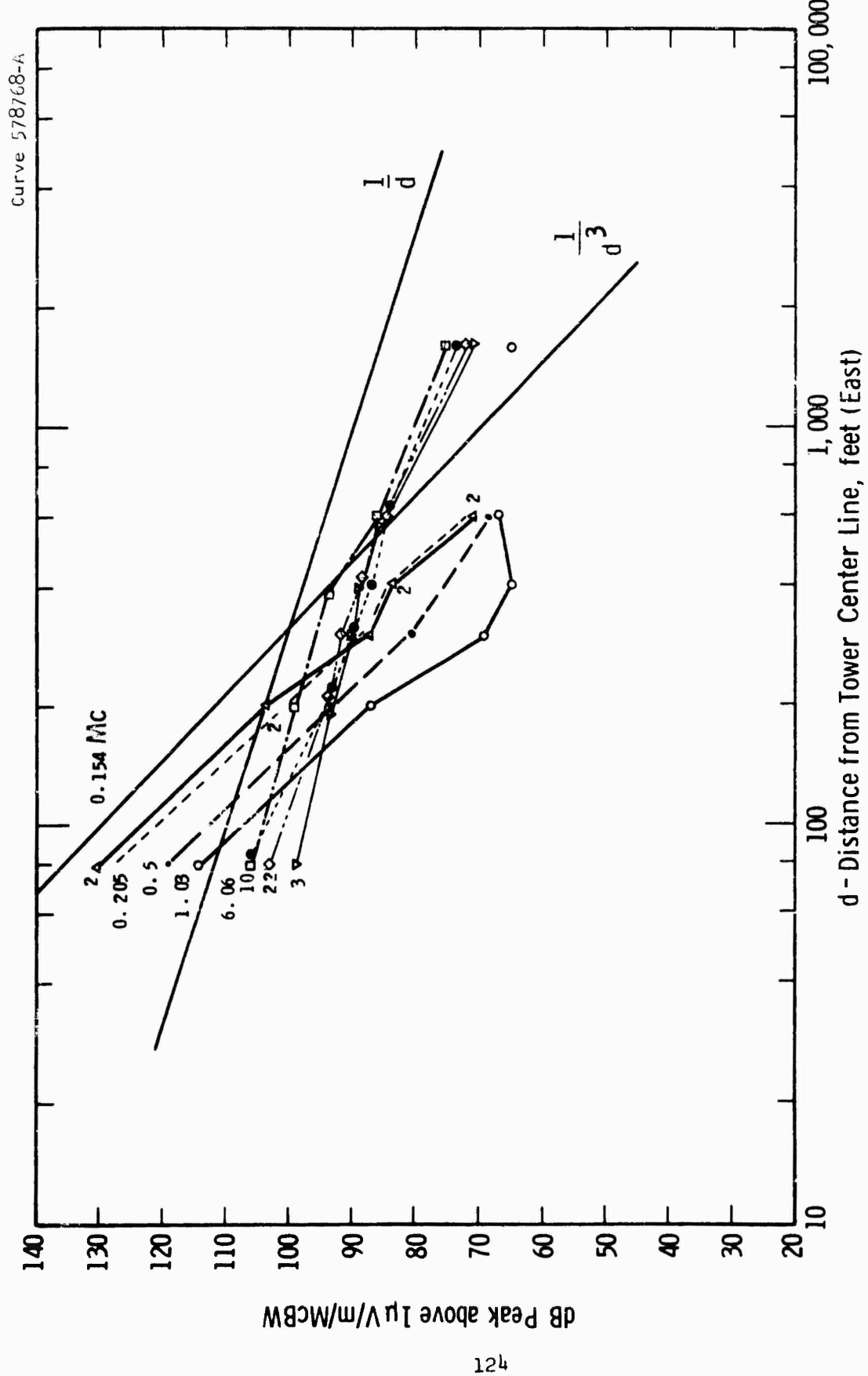


Fig. 89 - 244 kV HCST line lateral attenuation 0.15-24 Mc range with artificial gap on east phase

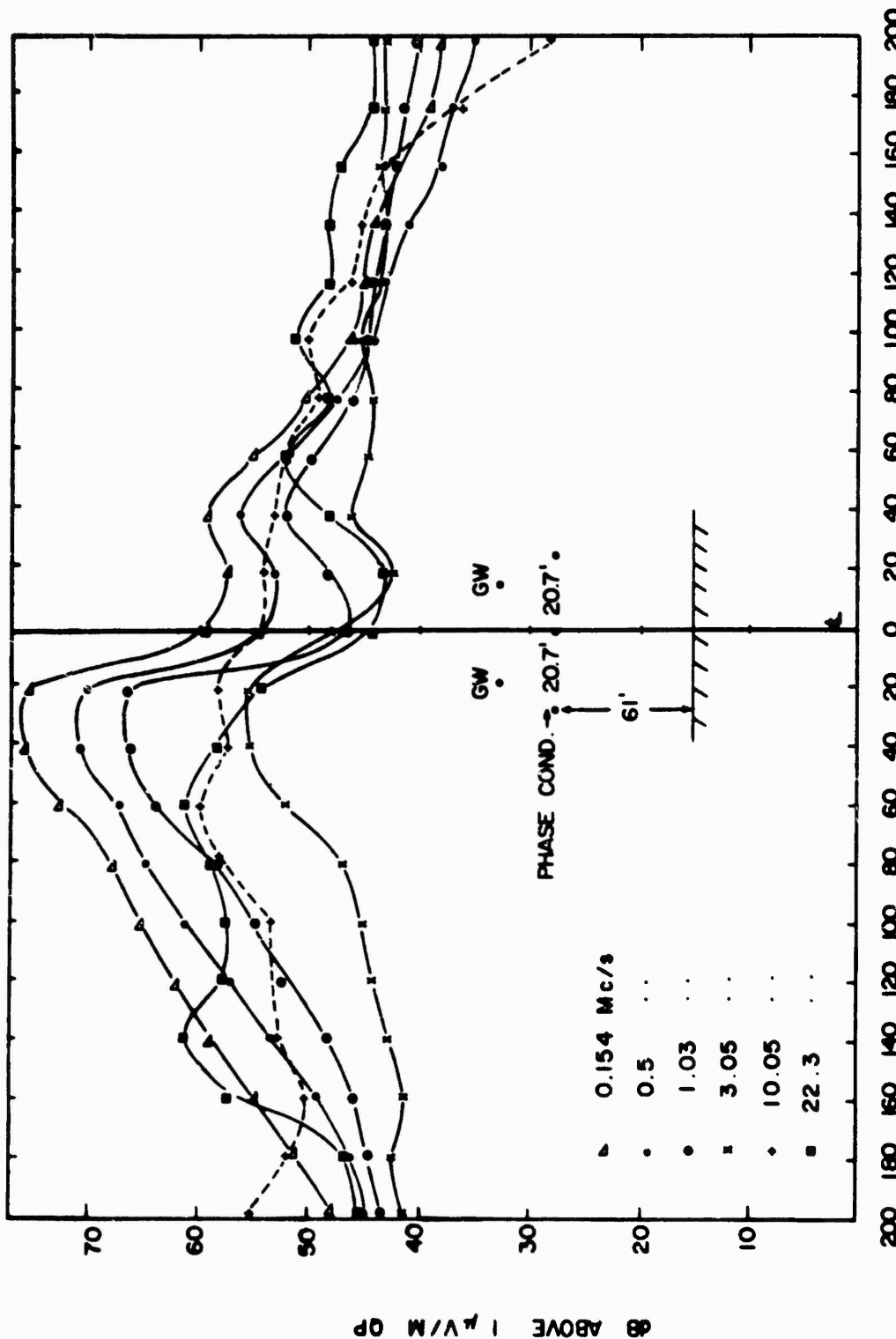


FIG. 90 161 KV HC ST LINE LATERAL PROFILES FROM TOWER WITH ARTIFICIAL GAP ON
NORTH PHASE

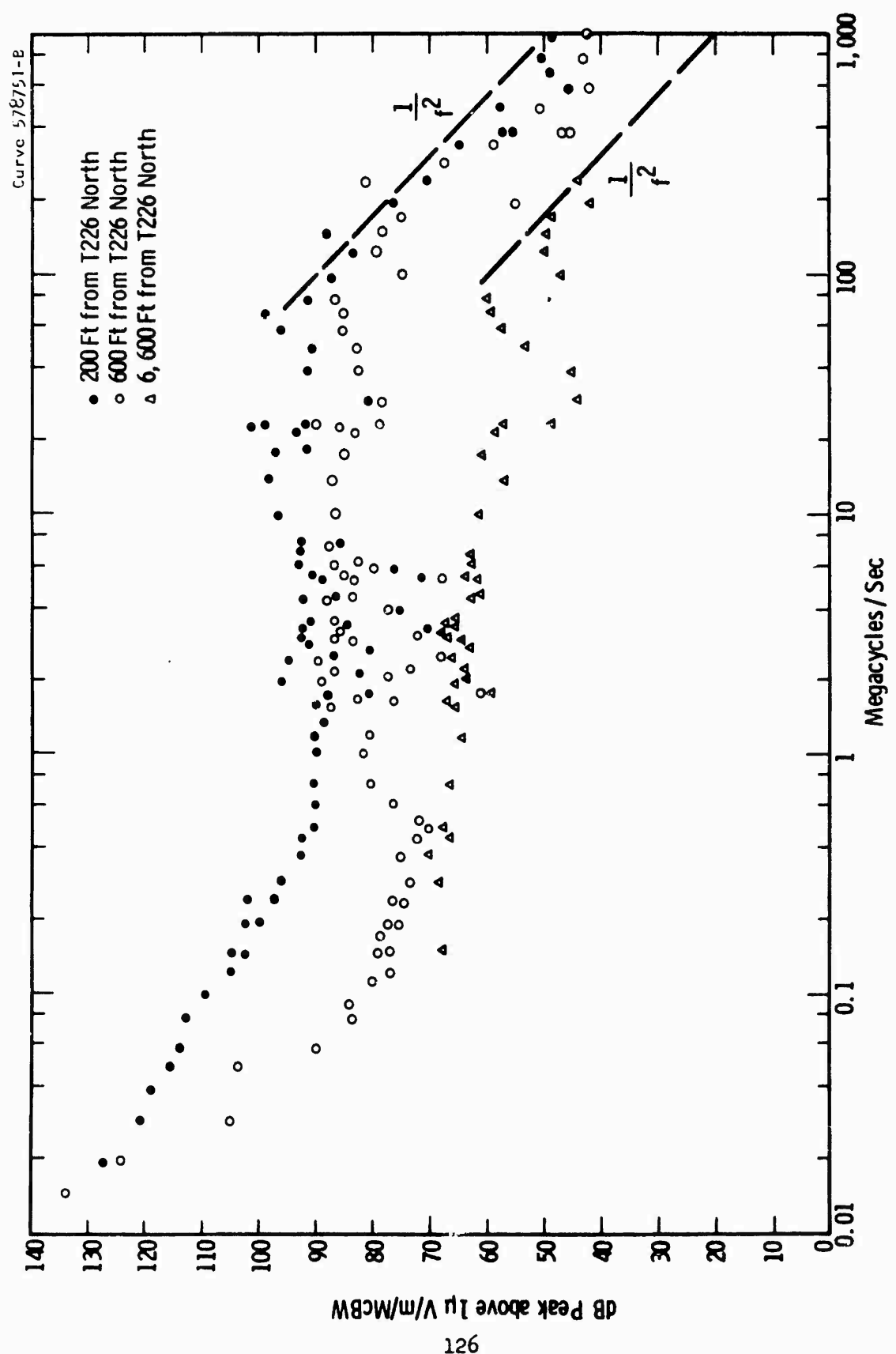


Fig. 91-161 kV HCST line frequency spectra with artificial gap on north phase

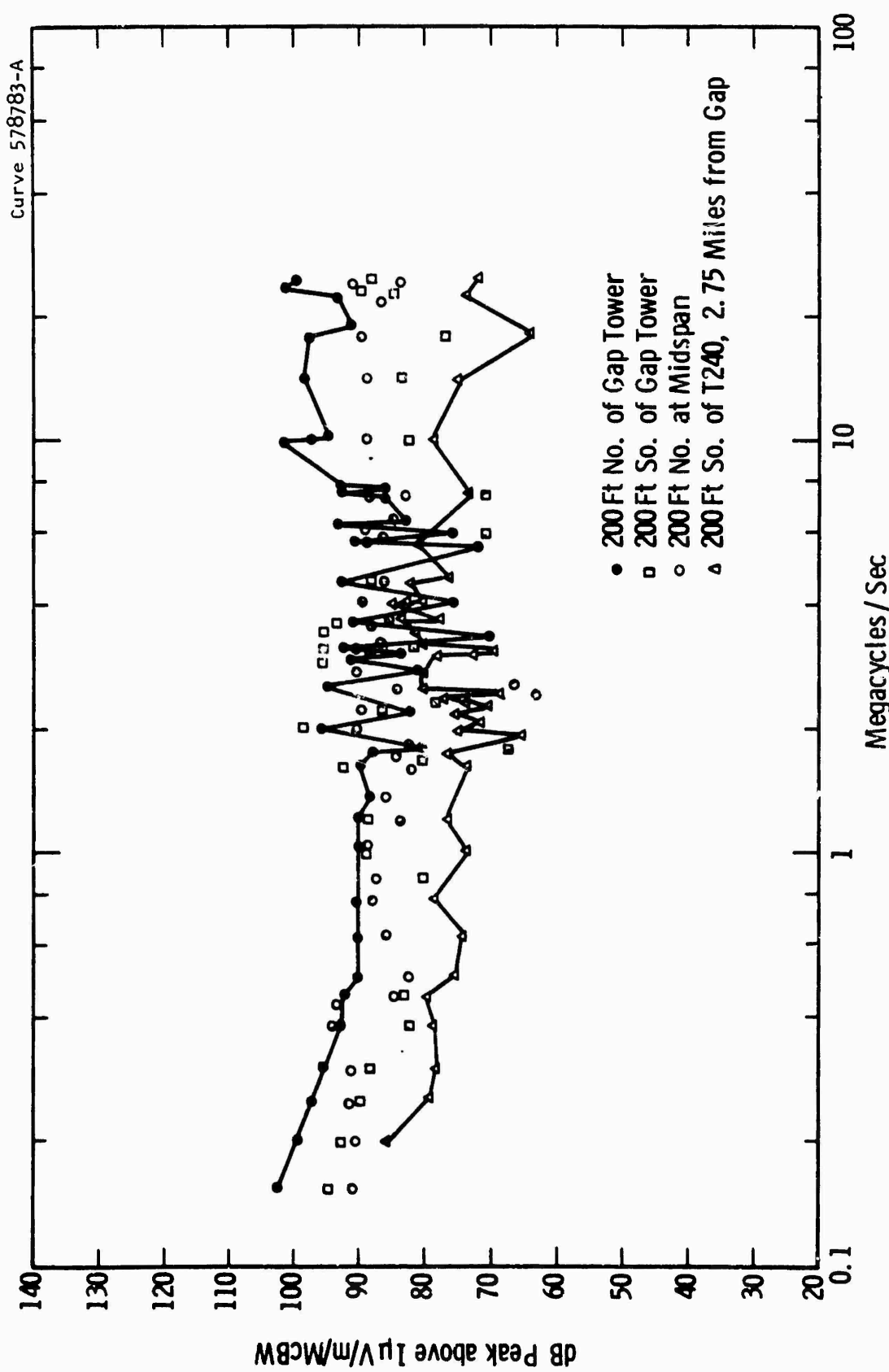


Fig. 92—161kV HCST line spectra 0.154-24 Mc at towers and midspan with artificial gap

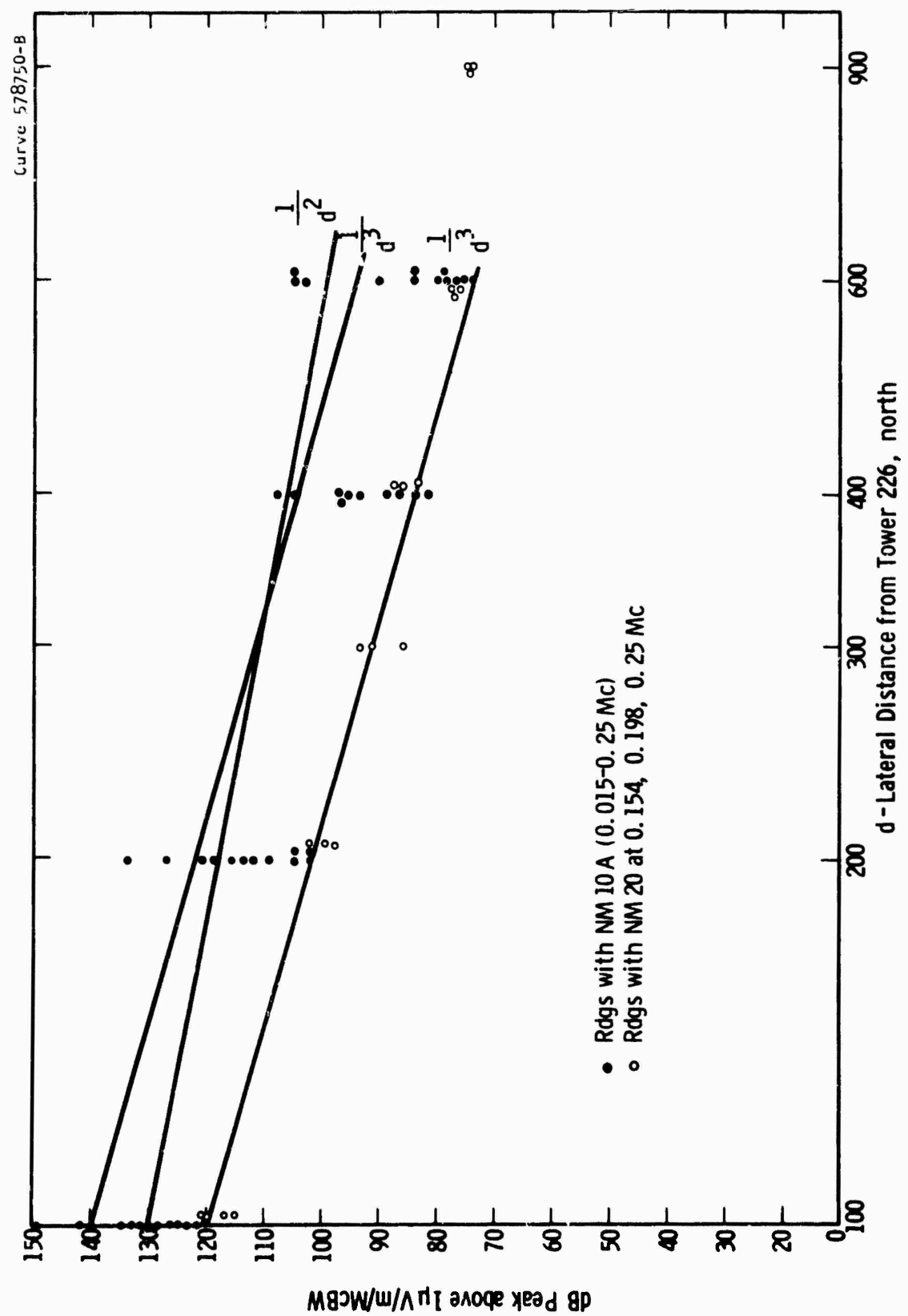


Fig. 93—161 kV HCST line attenuation 0.015-0.25 Mc with artificial gap on north phase

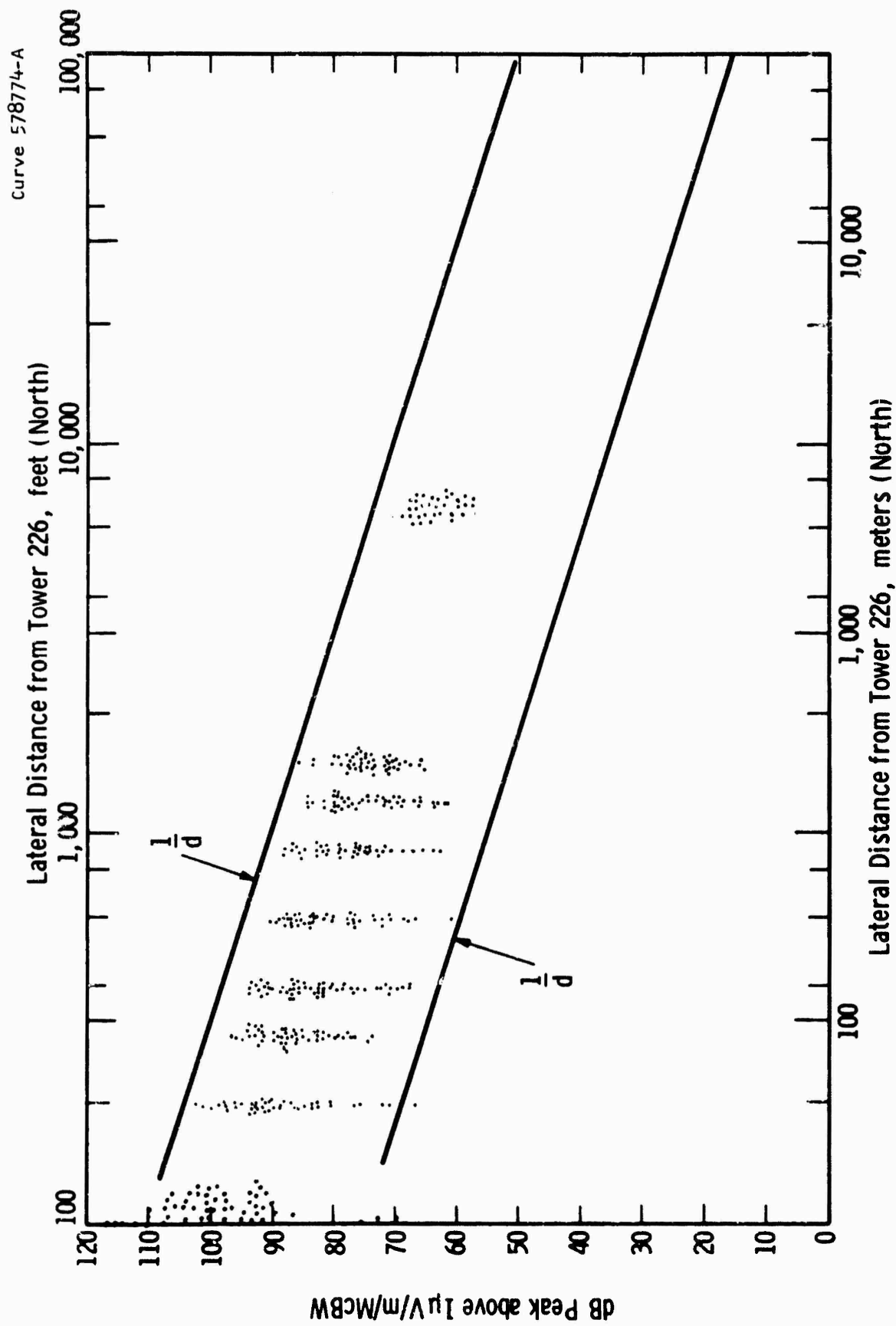


Fig. 94 - 161 kV HCST line lateral attenuation range 0.154-24 Mc with artificial gap

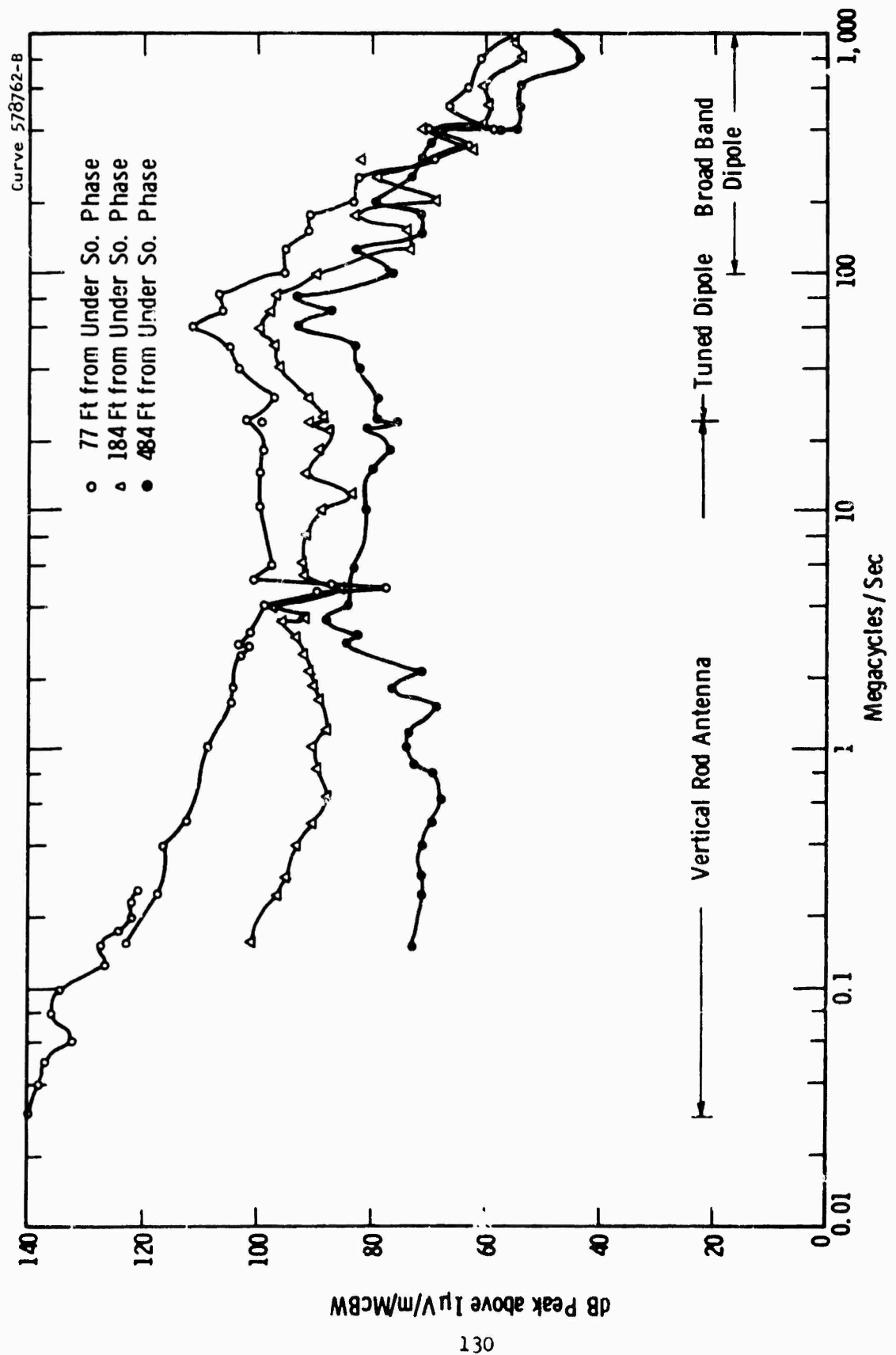


Fig. 95-110 kV HCWP line spectra with artificial gap

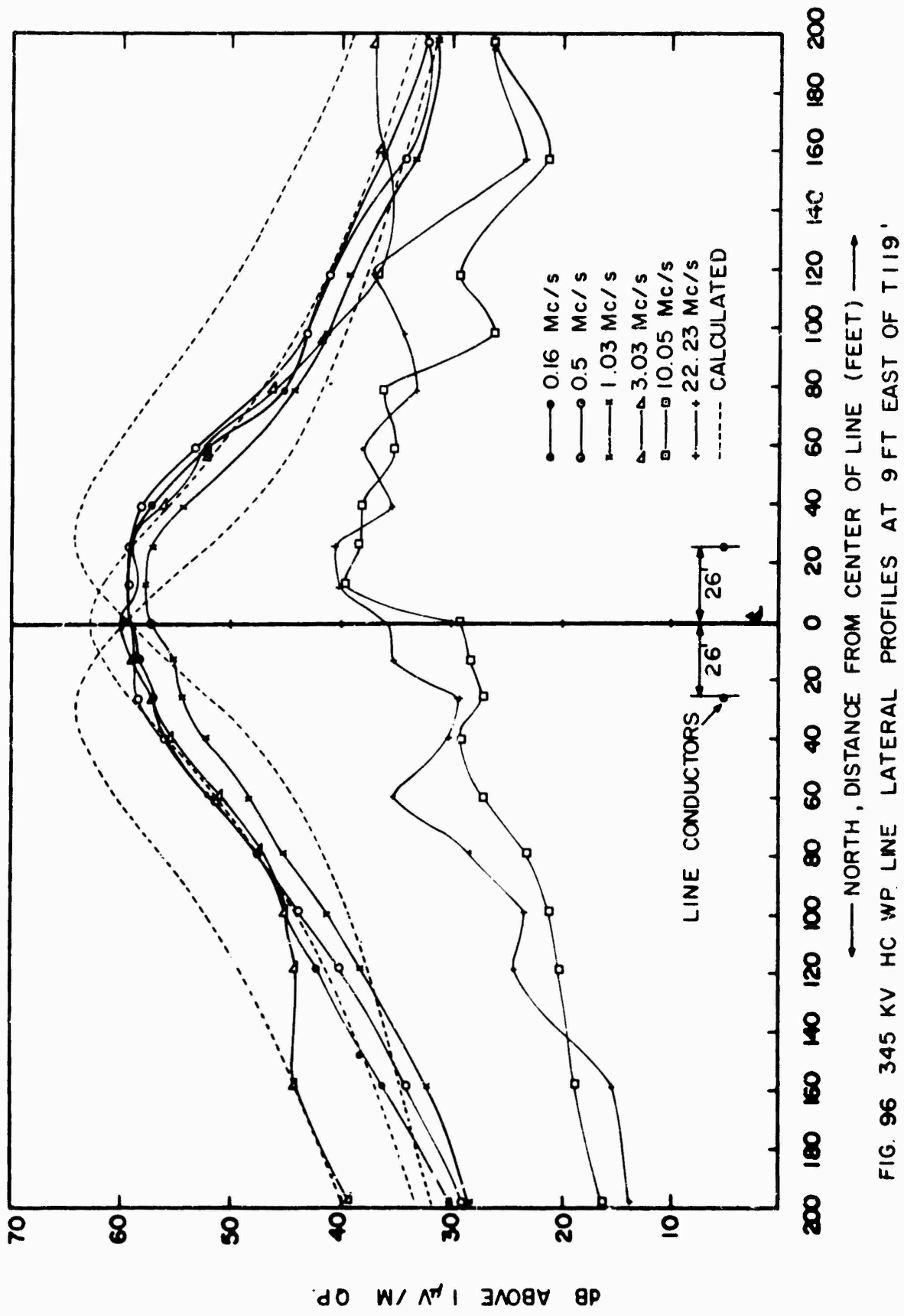


FIG. 96 345 KV HC WP LINE LATERAL PROFILES AT 9 FT EAST OF T119.

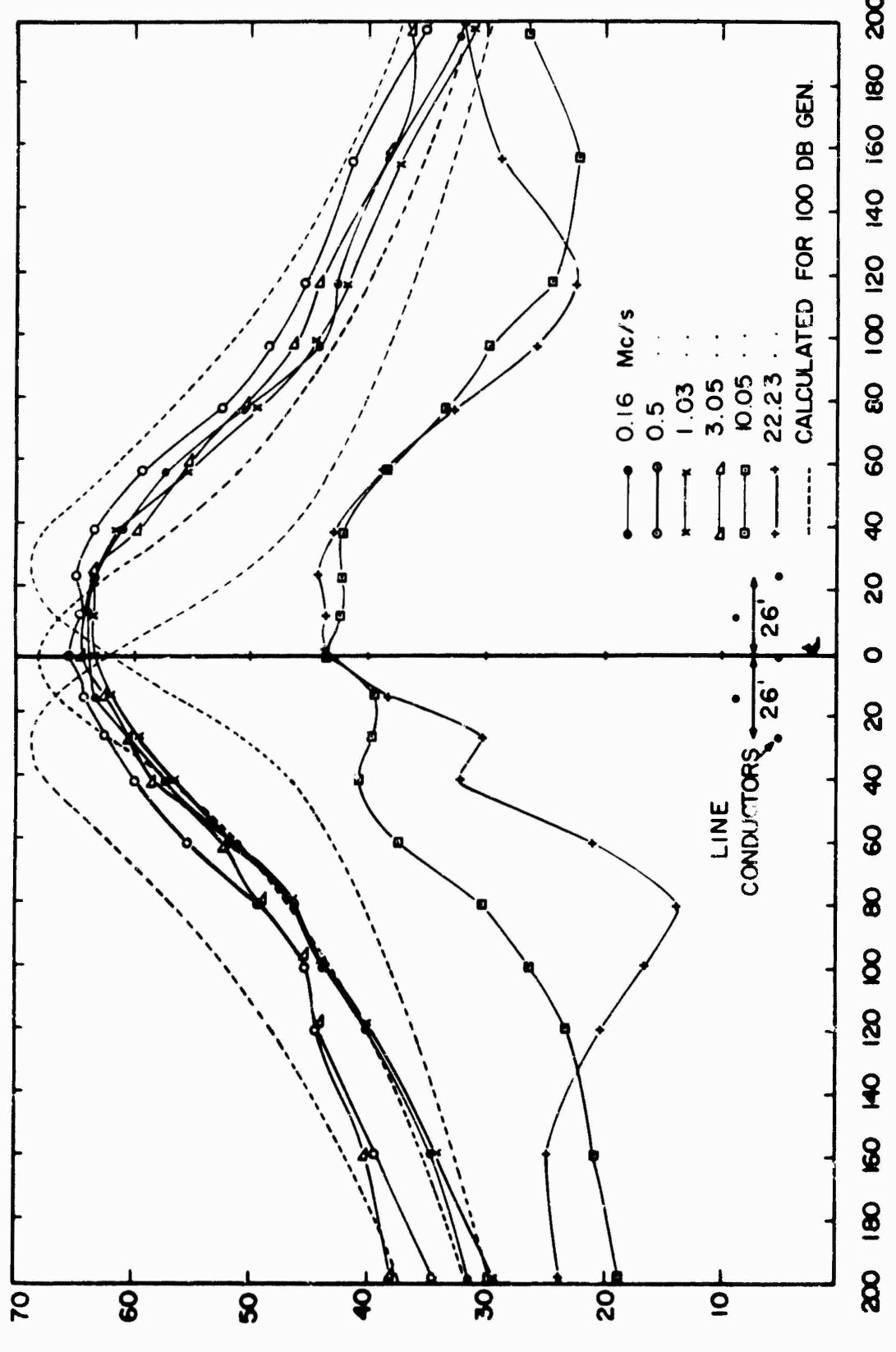


FIG. 97 345 KV HC WP LINE LATERAL PROFILES AT MID-SPAN WITH LINE NORMAL (TII8-119)

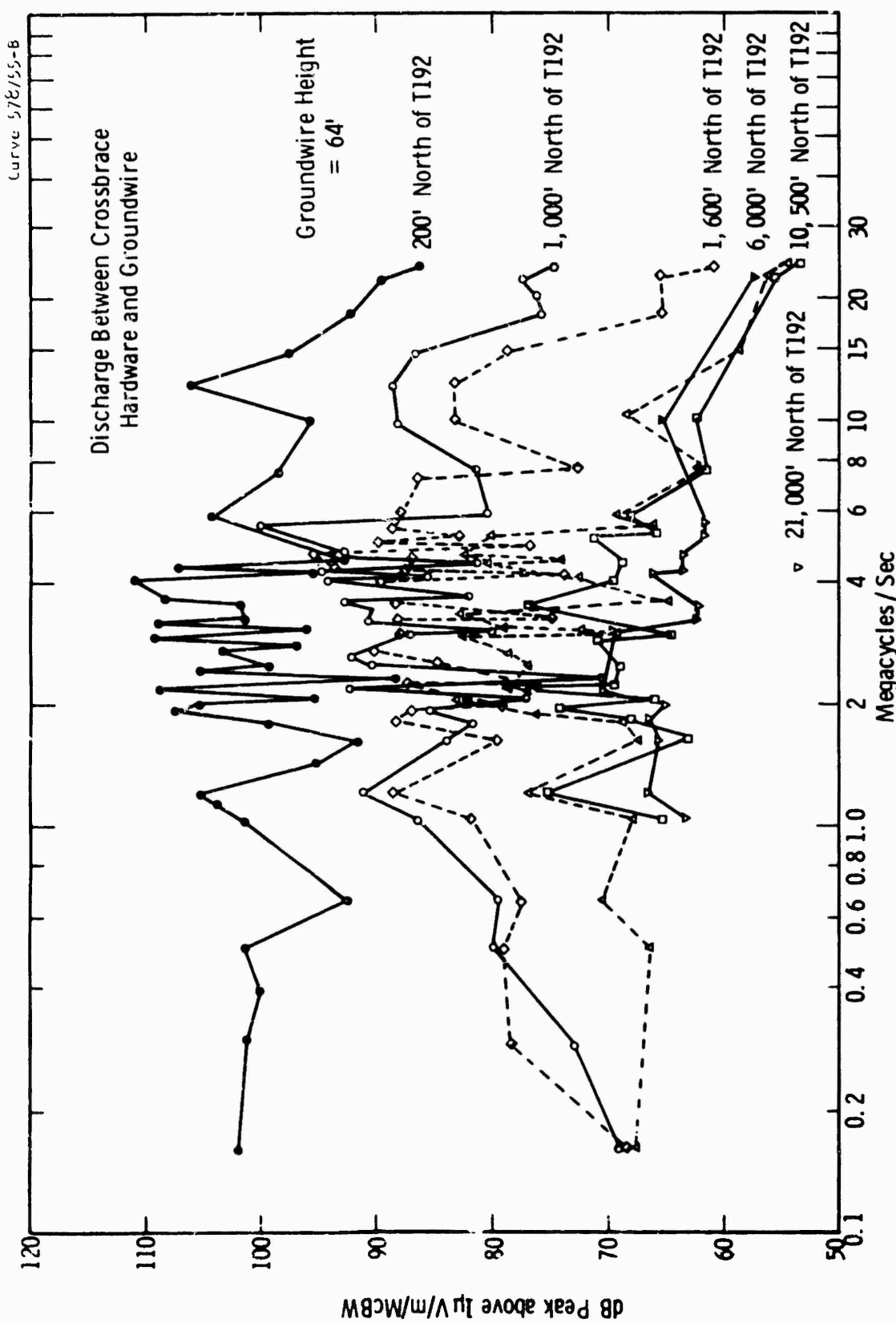


Fig. 98 - 345 KV HCWP line spectra from 200-21000 feet lateral to tower with natural gap

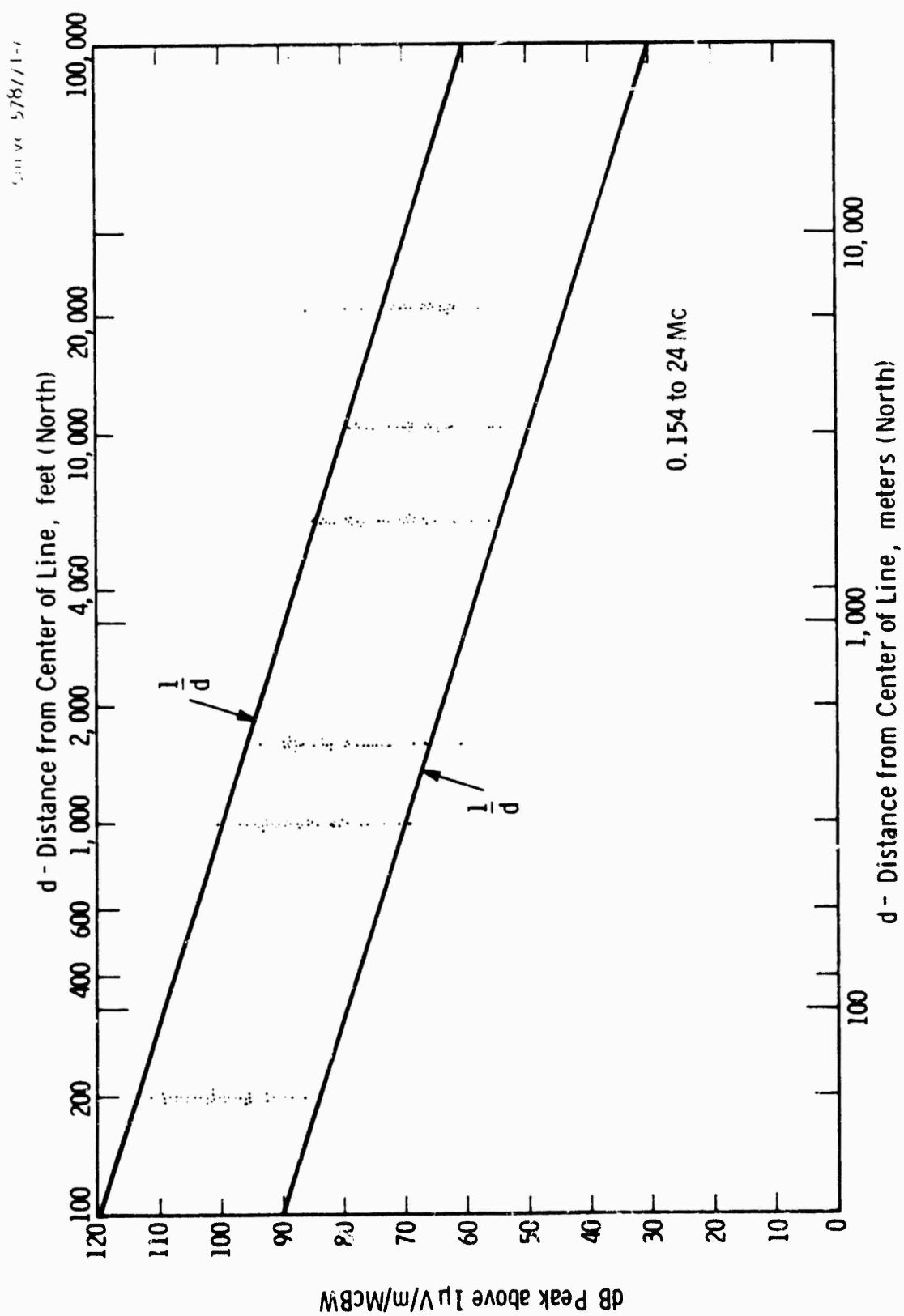


Fig. 99—345 kV HCWP line lateral attenuation 0.154-24 Mc with natural gap at T192

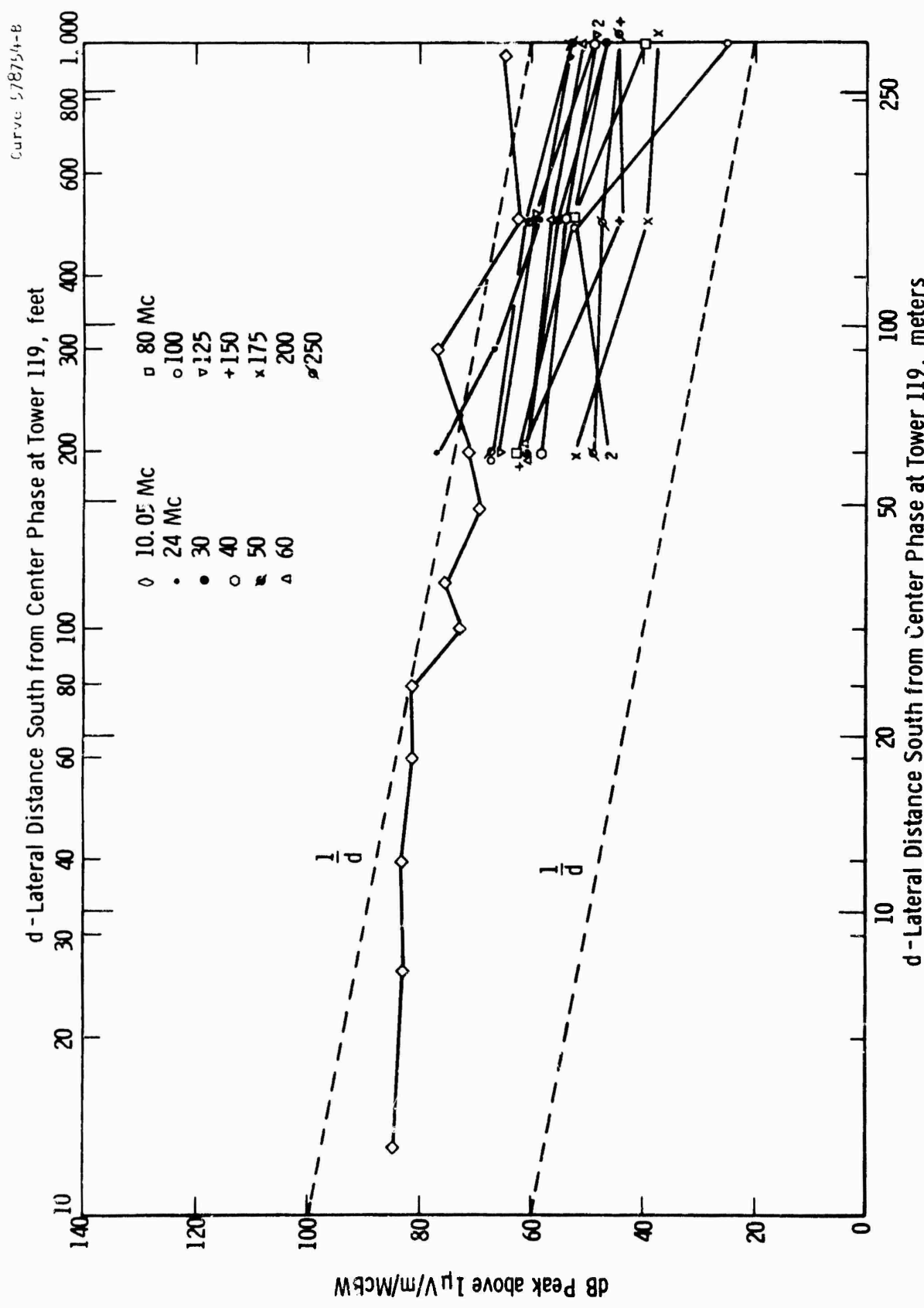


Fig. 100—345 kV HCWP line lateral attenuation 10-250 Mc with line normal

APPENDIX I - ANALYSIS OF LABORATORY TESTS TO DETERMINE
THE EFFECT OF CONDUCTOR DIAMETER AND THE SHAPE AND SIZE
OF CONDUCTOR PROTRUSIONS ON RADIO NOISE GENERATION

1. INTRODUCTION

Radio noise due to conductor corona (streamers) is caused by particles, such as raindrops, snow, dirt, insects, burrs, nicks etc. For the prediction of radio noise from conductor corona it is important to know what effect the conductor diameter and electric gradient have on the magnitude of the radio noise generated by corona. This Appendix describes tests made to obtain additional information as to the effect of conductor diameter and gradient. Three sizes of round-head rivets and three sizes of conical head rivets were mounted on twenty foot lengths of aluminum tubing of different diameters. The rivets were placed two feet apart along the conductor.

The conducted radio noise voltage was measured by means of the NEMA 107-1964 test circuit, starting at the highest 60 cycle voltage to ground and then decreasing the voltage in small steps until the critical or threshold voltage was passed.

Photographs were taken of each conductor protrusion (rivet) in corona thus enabling the corona plume or streamer length to be measured. The form of the plumes for the exposure time used can be seen from Figures I-2 and I-3. The plume is roughly defined by sketch on Fig. 4. The narrow or neck portion near the conductor was measured along with the total length of the plume.

These tests enabled a curve to be plotted between conductor diameter and conductor gradient for the same radio noise generation. Also the measurements of plume length showed a relationship between the plume length and conductor diameter and radio noise magnitude.

It was found that the magnitude of radio noise generation increases with some power of conductor diameter greater than unity for the same conductor surface gradient. This means that for the same radio noise generation the gradient should be reduced when the conductor diameter is increased. See Fig. I-8.

2. TEST EQUIPMENT AND TEST CIRCUIT

The test equipment consists of the following principal items: (This equipment is free of radio noise to voltages far above conductor ratings):

1 - 60 cycle, 500 kV test transformer with induction type motor driven voltage control.

1 - Two 4 inch diameter aluminum tubes placed side by side. These are used to connect the test transformer to the coupling capacitors.

4 - 0.005 mfd., Westinghouse capacitors rated 69 kV continuous, 100 kV for 7-1/2 minutes. Each capacitor is about 10 inches in diameter, and 30 inches long.

23 - Special low radio noise suspension insulators to support the conductor under test at one end.

1 each - Triple and single ring four foot diameter shields spun from aluminum. (One for each end of the test conductor, see Fig. 1).

1 - Polaroid camera and tripod with 2:1 telephoto lens.

1 - Stoddart NM20C receiver Sér. 305-4.

1 - Stoddart power supply for the above 90780-2. Serial No. 197-3.

1 - R.F. bridge. (General Radio Type 916 AL. Serial No. 2879).

1 - Signal generator. (Ferris Instrument Co. Model 22D. Serial No. 540).

2 - Radio frequency choke coils about 20,000 ohm impedance at 1 Mc/s.

1 - 150 ohm rf loading circuit.

1 - Microammeter. Weston Model 440. No. 11275 plus 1 - Westinghouse Micropot No. 1.

The test circuit is shown in Fig. I-1. The Stoddart radio noise meter is connected across an impedance of 150 ohms and this meter is protected by the radio frequency choke across the input end

of the 185 ohm coax. With a test conductor in place the impedance of the load to a corona generator is 146 ohms as measured with the G.R. 916 AL Bridge at 1.05 Mc/s. This gives a correction factor of $\frac{150}{146} = 1.03$ or 0.256 dB to the readings.

The correction factor used was determined by feeding a known signal from the signal generator into the circuit across the high voltage capacitors and noting the signal measured on the Stoddart meter. This gave a correction factor of 1.111 (0.914 dB), which was the one used and carried out by changing the gain of the Stoddart meter.

This correction factor assumes that corona current is essentially independent of the load impedance of 150 ohms which represents the loading to a corona generator located on a long line with 300 ohms surge impedance in each direction from the corona generator.

3. TEST PROCEDURES

The conductor diameters tested were 0.675, 1.05, 1.315, 1.66 and 2.375 inches. The rivet sizes were 0.05, 0.07 and 0.1 inches diameter and height.

Prior to commencement of the tests the length and diameter of the conductors were checked and holes drilled two feet apart for the location of the rivets which were to act as protrusions. All burrs on conductor were removed, the conductors checked for smoothness, degreased and finally cleaned with paper and from then on only handled using cotton gloves.

These precautions were to ensure that radio noise generation occurred due to the rivet protrusions and not due to dirt, burrs etc. on the conductor. The conductor was placed 12 feet 8 inches above and parallel to the ground plane. The walls of laboratory were several times this distance from the conductor under test.

All the conductors with protrusions (rivets) were tested at 1.0 Mc/s for conducted radio noise voltage, by starting at the

highest 60 cycle voltage to ground and then decreasing the voltage in small steps until the critical or threshold voltage was passed.

Six voltage runs were made on each conductor and average, quasi-peak and peak (FI, QP and PK) readings recorded for single rivet protrusions of the different shapes and sizes. Also for the purpose of picture taking the conductors were photographed with three sizes of conical rivets affixed and in corona and likewise for round head rivets.

A voltage run was made on the 2.375 in. diameter conductor without rivets and the readings noted. This confirmed the obvious that the previous readings were from corona due to the rivets and not from conductor corona.

During the test on the 0.675 in. diameter conductor with the 0.05 in. round head rivet a quasi-peak reading of 40 dB was recorded with only 20 kV on the conductor. Past experience judged this much too high and the fault was found to be a ladder and lift truck (used for placing the conductors) left too near the high voltage circuit. When these were removed 130 kV gave 38 dB quasi-peak.

Much time was spent determining the best arrangement for taking detailed pictures of the corona plumes. Eventually a polaroid camera with 3000 film, a one second exposure at 4.6, a 2:1 telephoto lens at a distance of 13.15 feet from the conductor was finalized upon.

Time did not permit pictures to be taken of streamers on the 0.675 in. diameter conductor under this final set up but all other conductors were photographed. The pictures for the 2.375 in. diameter conductor were of 2 and 5 second exposure but the size of a 1 second exposure picture was obtained by extrapolation, based on films exposed 2 and 5 seconds. Exposure time should be kept constant for plume measurements.

The polaroid pictures were enlarged later to approximately 9-1/2" x 7-1/2" (7 times by area) so that accurate measurements of streamer length could be made.

4. RESULTS AND ANALYSIS

4.1 Conductor Gradient Calculations

The conductor surface gradient is a very important criterion in any comparison of radio noise due to conductor corona. For the laboratory measurements made at the Trafford High Voltage Laboratory the gradient relation for a single conductor above a ground plane was used. This relation is

$$g = \frac{V}{r \log_e \frac{2h}{r}} \text{ kV/cm} \quad (1)$$

where r is radius of conductor in cms

h is height of conductor above ground plane is 386 cms, (12 ft. 8 in.)

V is the voltage in kilovolts to ground

The calculated gradient factors (kV/cm/kV) are tabulated in Table I for the conductors tested.

These conductor surface gradient factors are for the smooth conductors of aluminum tubing used for the laboratory measurements. The effect of conductor diameter, surface condition, and relative air density on the radio noise generation by conductor corona are discussed in Section 4.5 which is to follow.

Table I

Conductor Diameter Inches	Conductor Radius cms	Gradient Factor kV/cm/kV
0.675	0.857	0.1721
1.05	1.333	0.1185
1.315	1.67	0.0975
1.66	2.11	0.0805
2.375	3.02	0.0595

4.2 Photographs of Corona Plumes and Analysis

The photographs of the corona plumes from the rivets are shown in Figs. I-2, and I-3 for conductor sizes as indicated. The smaller the conductor diameter the smaller is the plume as shown on the photographs. The different size and shape rivets, on a specific conductor, do not give significant changes in the plume size with the measurement technique used. The plume dimensions were obtained from 8-1/2 x 11 inch glossy prints by means of a scale on clear glass, and a magnifying glass. The conductor dimension on the print was used to check the measurements. The plume dimensions measured from the photographs are shown by the sketch on Fig. I-4. It was found that the neck of the plume was about the same length for all conductor diameters. The brush part of the plume increased in length with increase in the conductor diameter. Amin gives data on streamer or plume lengths which are proportional to the point diameters of 0.1, 0.2 and 0.25 cms which he tested.

The curves of Fig. 5 were obtained by means of the relation

$$g_1 = \frac{v_1}{(r_1 + a_1) \log_e \frac{2h}{r_1}} \quad (2)$$

where a_1 is the distance in cms from the conductor surface. It can be shown that for the same gradient at the conductor surface for two conductors of radius r_1 and r_2

$$\frac{a_1}{a_2} = \frac{r_1}{r_2} \quad (3)$$

This relation indicates that the corona plume can propagate farther from the larger conductor and therefore the radio noise pulse magnitude would be expected to increase and be proportional to the radius. Measurements, see Fig. I-4, show that the plume length does increase approximately with the conductor radius. The current injected into the line conductor at the corona plume will depend on the size of the plume. If we assume the plume is spherical the electrostatic capacity of the plume to space will also increase with the conductor radius. It appears then that these two effects can result in a radio noise pulse magnitude proportional to the square of the radius. The curve marked "d²" on Fig. I-6 corresponds to this condition.

4.3 The Effect of Conductor Diameter on the Radio Noise Generation

The average radio noise levels, in dB peak above 1 μ v/ per Mc bandwidth, measured on the five conductor diameters with the three sizes of round head rivets and the average for the three sizes of conical head rivets are shown on Fig. I-7. It is obvious that the level increases with the conductor diameter for all sizes of rivets. From these curves it is possible to obtain the change in level with diameter. This was done at 20 kV_{rms}/cm and plotted in Fig. I-6. The 0.675 inch diameter conductor was omitted since it did not go into corona until a gradient of 24 kV_{rms}/cm was reached. The measurements show an increase very nearly proportional to the square of the conductor radius for the rivets tested. This figure also gives data^{1,2} obtained from other laboratory measurements. Artificial rain data are given on Fig. I-9 for four sizes of single and bundle ACSR conductors. Some of these conductors were also tested after artificial rain was turned off and the conductors were wet. Under this wet condition the radio noise level increased about 6 dB above the level in rain. There was no significant difference with rain between single and bundle conductors when maximum gradient on the sub-conductor of the bundle is used for comparison. The largest measured increase in radio noise

generation with conductor diameter is obtained with soil or mist on conductor surface. Under these conditions the number of possible sources on the conductor surface is near the maximum; whereas, in practice the number of sources would seldom be as great. For rain and wet the increase with conductor diameter is less than for soil or mist, probably because water collects on the bottom side of the conductor and this water determines the level of radio noise generation. The electric field distorts the water drops, more or less, into sharp points, which go into corona and probably produce a shielding effect. The effect of rivet shape and size is shown on Fig. I-10. The 0.05 inch rivets result in larger radio noise levels than the 0.1 inch rivets and the round head rivets give somewhat more than the conical rivets.

4.4 Conductor Gradients for the Same RN Level

From the measurements made it is possible to obtain conductor gradient to diameter relations for the same radio noise level. This can be done for only the four larger diameter conductors by means of the curves on Fig. I-7 for the tests with the conical head rivets. The gradient values for two levels, 131 dB and 135 dB, are shown on Fig. I-8. Curves from other laboratory measurements with conductors in artificial rain, wet from rain, and with soil sprinkled on surface are also shown on Fig. I-8.

It is of interest to see what form calculated curves would be. By means of equation 2 it is possible to obtain the relation:

$$\frac{g_{s1}}{g_{s2}} = \frac{r_2(r_1 + a_1)}{r_1(r_2 + a_2)} \quad (4)$$

where g_{s1} and g_{s2} are the surface gradients of the conductors 1 and 2. By making $a_1 = a_2$ the relative surface gradients of conductors 1 and 2 can be obtained, assuming the same radio noise generation. (This assumes that corona pulse magnitude and plume length are proportional to r_1 and a_2 .) From equation 4, a curve for $a_1 = a_2 = 1$ cm and $a_1 = a_2 = 5$ cm was obtained. These curves are plotted on Fig. I-8

along with points and curves obtained from measurements. It appears that gradient variation with conductor diameter depends on the value of "a" (plume length). The curves obtained from measurements are for practical gradient values, and empirical relations, such as shown on Fig. I-8, can be obtained for comparing radio noise generation of conductors. The value of γ used on Fig. I-8 is 3.5, an average constant based on experimental data. Actually γ probably varies slightly with conductor diameter and operating gradients as indicated by laboratory tests.

The length of plumes measured and reported herein are greater than is obtained by the theoretical relation, equation 4. If $a_1 = a_2$ in eq. 4 is made as large as the plume length measured then the conductor gradient to diameter curve is considerably out of line, (see 5 cm curve on Fig. I-8), with the curves obtained by measurement. This may be due to assuming that the effective radio noise length of the plume is as obtained from photographs; whereas, the effective length is only a fraction of this. (See result for $a_1 = a_2 = 1$ cm on Fig. I-8). It was found during tests that the plume length shown on photograph depended on the exposure time. The data on Fig. I-4 is for 1 second exposure. It is not known what the plume length would be on film exposed for 1/120 of a second. Some measurements made with exposure times of 1/2, 1, and 5 sec. gave plume lengths as measured on the photographs of 4.65, 6 and 7.5 inches, respectively. Further investigation is necessary to establish the effective plume length with respect to radio noise. For the purpose of this investigation and prediction of radio noise from conductor corona, the measured radio noise data as shown on Fig. I-6 and I-8 will be used.

4.5 Empirical Relations for Prediction of the Radio Noise Generation due to Conductor Corona

The prediction techniques to be described are based on laboratory measurements given and data in literature. They apply only to high voltage lines where conductor corona predominates. The

empirical relations are used principally as a means of comparing a line to another line for which test data are available. This comparison method is necessary since it is not possible to calculate the radio noise generation in terms of the known parameters.

The conductor gradient is the most important factor and its effect on the radio noise level due to corona is expressed as, using Peeks relation for the critical gradient, given in the denominator of eq. 5 below,

$$\Delta \text{dB}_{g12} = A \left[\frac{\frac{g_2}{21(1 + \frac{0.3}{\sqrt{r_2 \delta_2}}) \delta_2 m_2}}{\frac{g_1}{21(1 + \frac{0.3}{\sqrt{r_1 \delta_1}}) \delta_1 m_1}} \right] \quad (5)$$

If the effect of altitude is taken to be given by the $\sqrt{\delta}$ as explained in reference 45, Appendix VII, (Vol. III) Part 2, then approximately

$$\Delta \text{dB} = \gamma \left(\frac{\frac{g_2}{m_2 \sqrt{\delta_2}} - \frac{g_1}{m_1 \sqrt{\delta_1}}}{\frac{g_2}{m_2 \sqrt{\delta_2}} + \frac{g_1}{m_1 \sqrt{\delta_1}}} \right) = 3.5 \left(\frac{\frac{g_2}{m_2 \sqrt{\delta_2}} - \frac{g_1}{m_1 \sqrt{\delta_1}}}{\frac{g_2}{m_2 \sqrt{\delta_2}} + \frac{g_1}{m_1 \sqrt{\delta_1}}} \right) \quad (6)$$

where g_1 and g_2 are the gradients of conductors, δ_1 and δ_2 are the relative air density factors for altitudes considered and m_1 and m_2 are respective conductor surface factors. The value of γ for g in $\text{kV}_{\text{rms}}/\text{cm}$, is taken as 3.5, an average constant obtained from CIGRE 402, 1960, T. Yamada and H. Kondo.

For $m_1 = m_2 = 1$ and $\delta_1 = 1$, the effect of altitude referred to sea level:

$$\Delta \text{dB} = 3.5 g \left(\frac{1}{\sqrt{\delta}} - 1 \right) \quad (7)$$

The effect of conductor diameter is shown by Fig. I-6. Since rain conditions are the most important in this case, the following relation for diameter effect will be used:

$$\Delta \text{dB} = 20 \log_{10} \left(\frac{d_2}{d_1} \right)^{3/2} = 30 \log_{10} \frac{d_2}{d_1} \quad (8)$$

The overall radio noise generation change is then from eq. 6 and 8 as

$$\Delta dB_{21} = \gamma \left(\frac{g_2}{m_2 \sqrt{\delta_2}} - \frac{g_1}{m_1 \sqrt{\delta_1}} \right) + 30 \log_{10} \frac{d_2}{d_1} \quad (9)$$

If we make $dB_1 = dB_2$ the conductor gradient to diameter relation for the same radio noise generation is obtained for $\delta_1 = \delta_2 = 1$, and $m_1 = m_2 = 1$. From 9 under this condition,

$$g_2 = g_1 - \frac{20}{\gamma} \log_{10} \left(\frac{d_2}{d_1} \right)^{3/2} \quad (10)$$

If $g_1 = 18 \text{ kV}_{\text{rms}}/\text{cm}$, $d_1 = 1 \text{ inch}$, and $\gamma = 3.5$, a curve as shown on Fig. I-8 is obtained. A curve is also given for exponent 2 instead of 3/2 in order to see the difference in gradients. This difference is not large, amounting to only 4% between 1 and 2 inch diameter conductors.

The effect of increasing altitude is to reduce the critical gradient and thus to increase the radio noise. However, the environment (air) is usually cleaner at the higher altitudes and the surface factor will be higher and compensation for increasing altitude may occur.

5. REFERENCES

1. Miller, C. J., Jr., The Calculation of Radio and Corona Characteristics of Transmission Conductors, AIEE Trans., Vol. 76, Part III, Aug. 1957, pp. 461-475.
2. Stone, Louis N., Prof., Oregon State University, Corvallis, Oregon. (From unpublished data with kind permission of Prof. Stone).

Dwg. 852A004

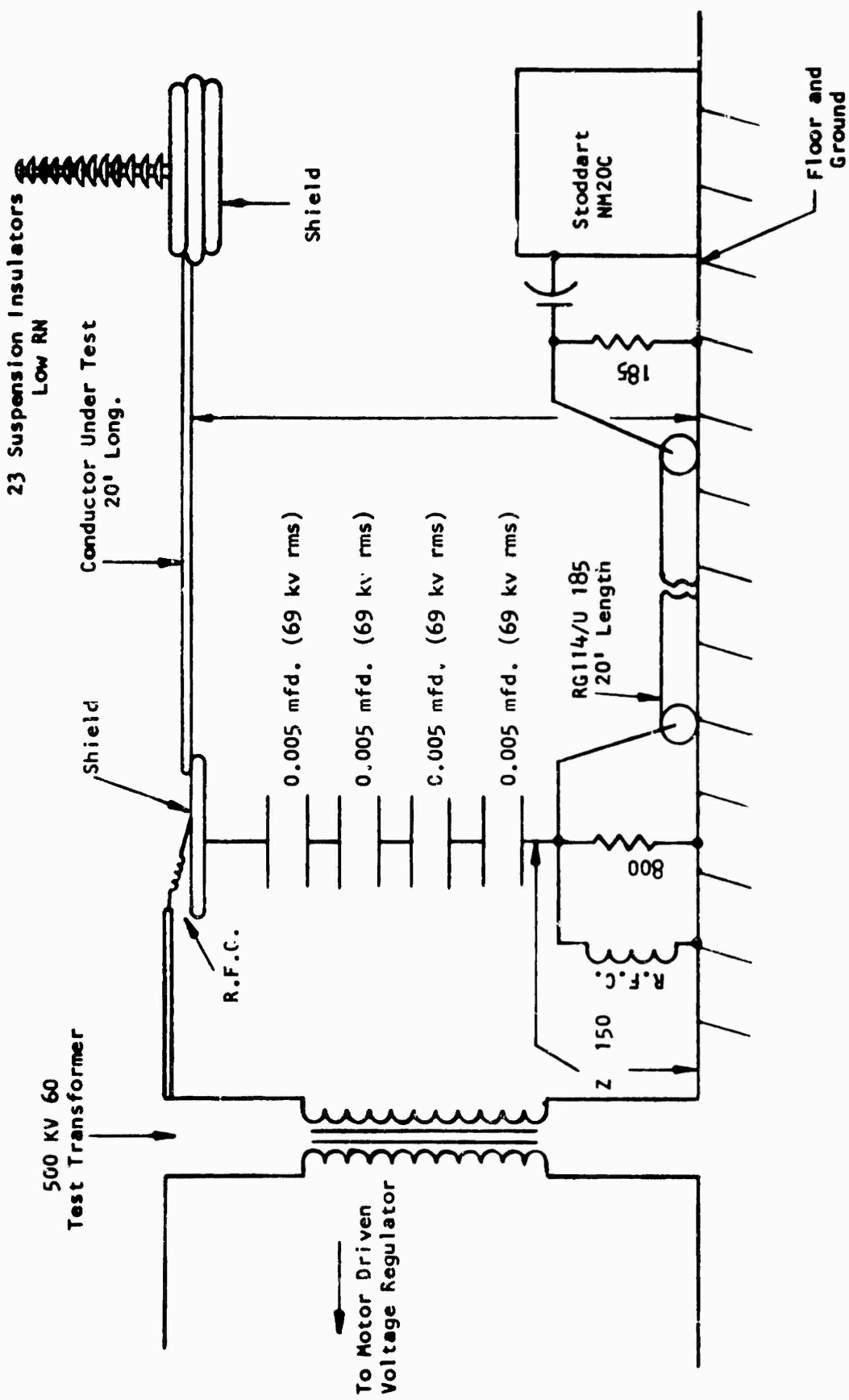


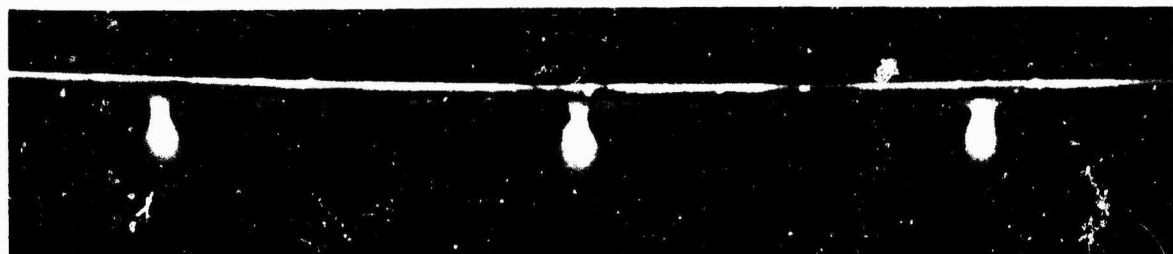
Fig. I-1 - Radio noise test circuit used for conductor tests in laboratory



a. Conductor Diameter 1.05 in (26.65 mm)



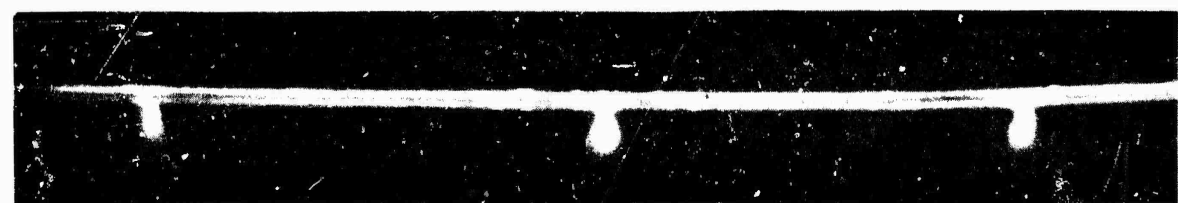
b. Conductor Diameter 1.315 in (33.4 mm)



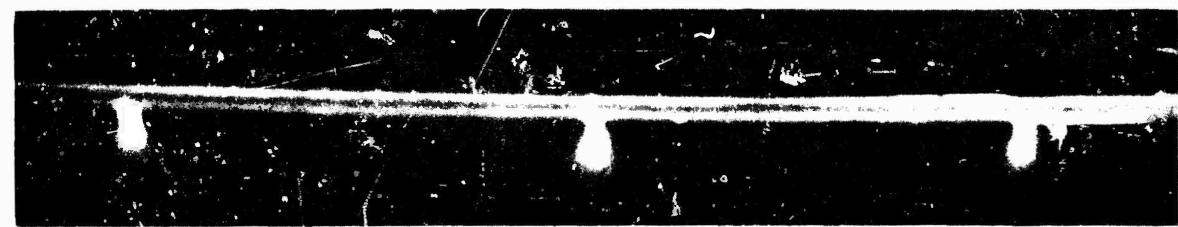
c. Conductor Diameter 1.66 in (42.15 mm)

Fig. I-2 Corona Streamers from Round headed aluminum rivets as protrusions
on smooth aluminum conductors of different diameters.

Left hand 0.1 in (2.5 mm) diam rivet. Center 0.07 in (1.75 mm) diam rivet.
Right hand 0.05 in (1.25 mm) diam rivet.



a. Conductor Diameter 1.05 in (26.65 mm)



b. Conductor Diameter 1.315 in (33.4 mm)



c. Conductor Diameter 1.66 in (42.15 mm)



d. Conductor Diameter 2.375 in (60.35 mm)

Fig. I-3 Corona Streamers from conical headed aluminum rivets as protrusions from smooth aluminum conductors of different diameters.
Left hand 0.1 in (2.5 mm) diam rivet. Center 0.07 in (1.75 mm) diam rivet.
Right hand 0.15 in (1.2 mm) diam rivet.

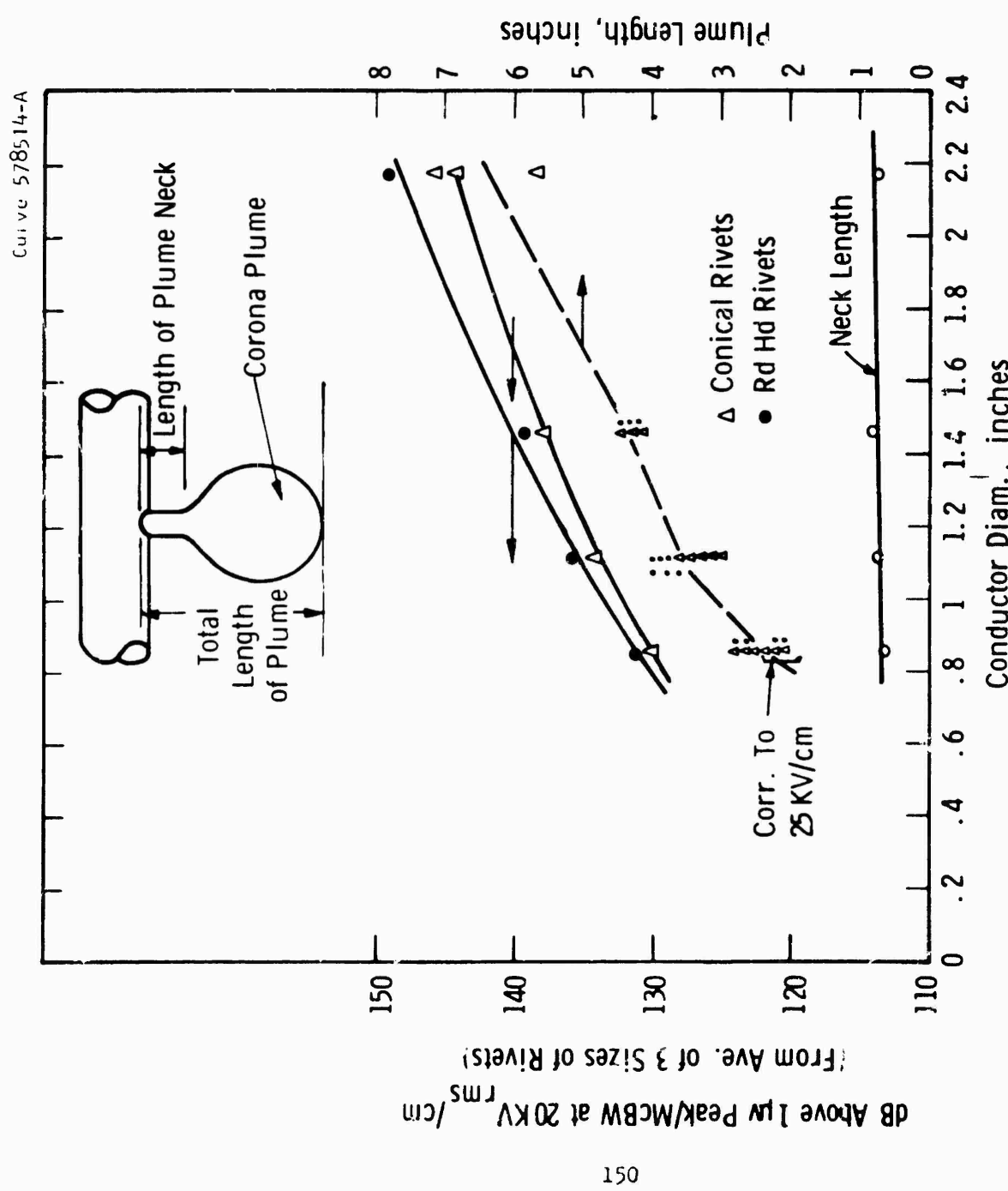


Fig. I-4—Radio noise generation and corona plume length of rivets

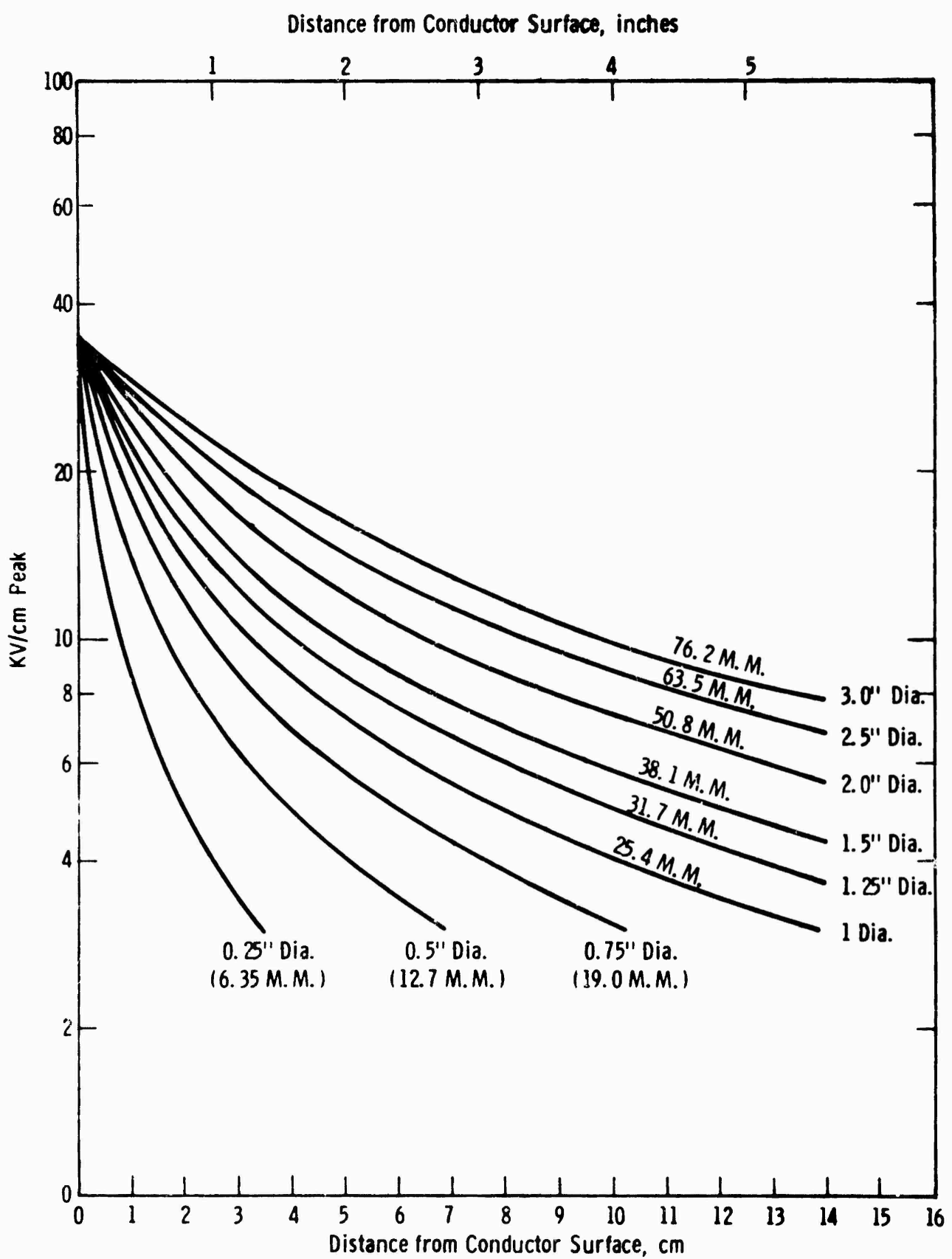


Fig. I-5 — Gradient change with distance from conductor surface

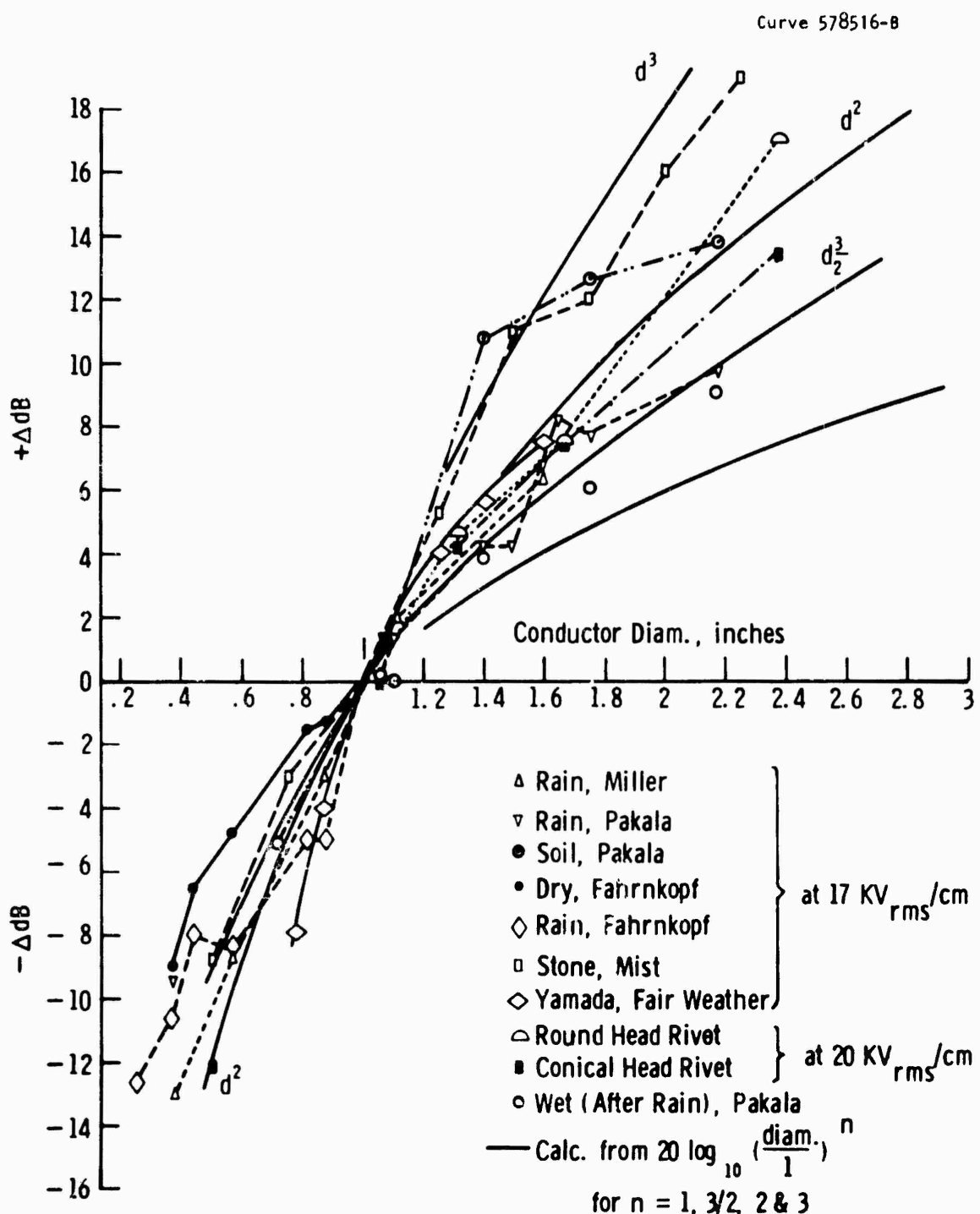


Fig. I-6 —Effect of conductor diam. on radio noise generation

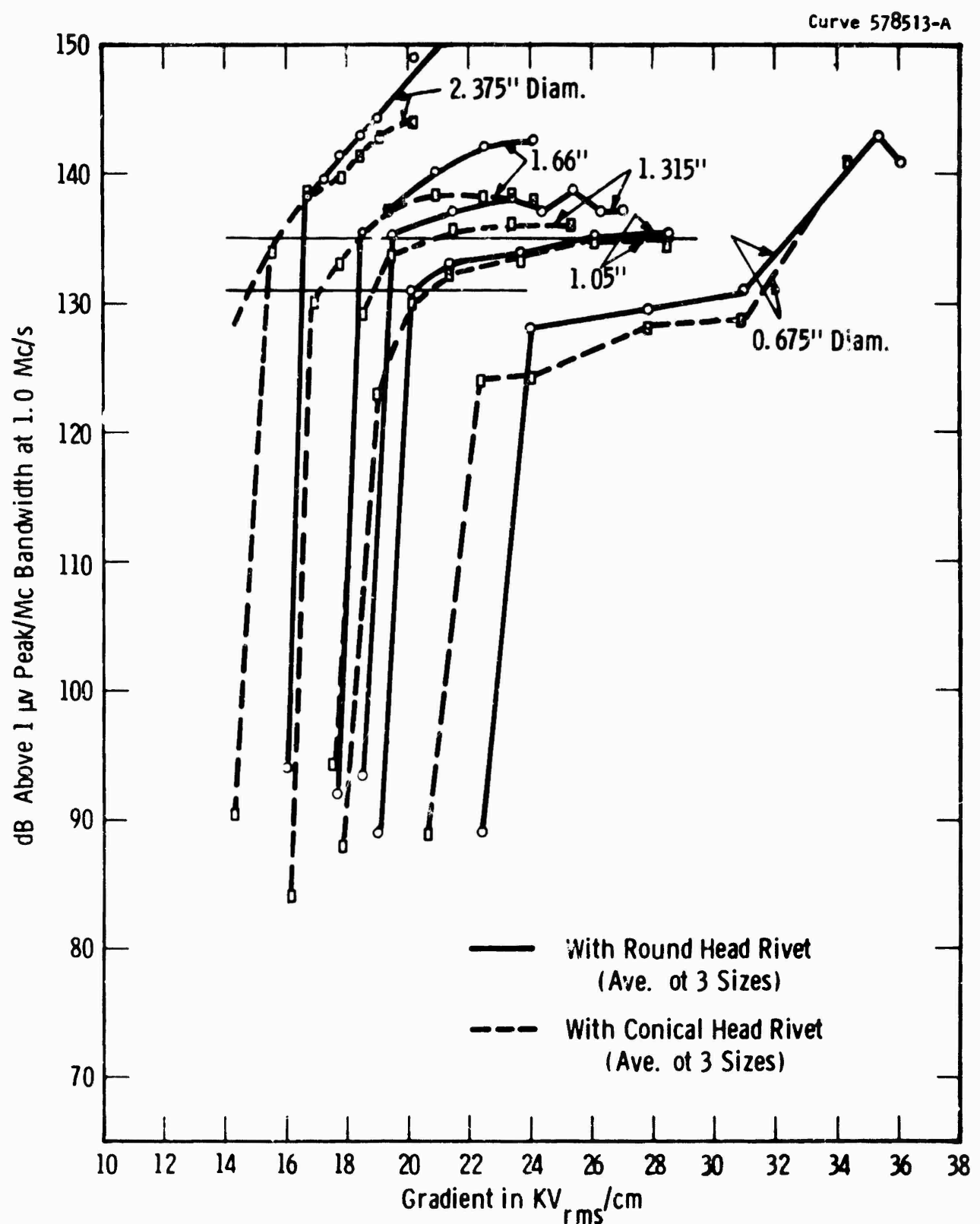


Fig. I-7 - Smooth conductors at 1 Mc/s with rivets

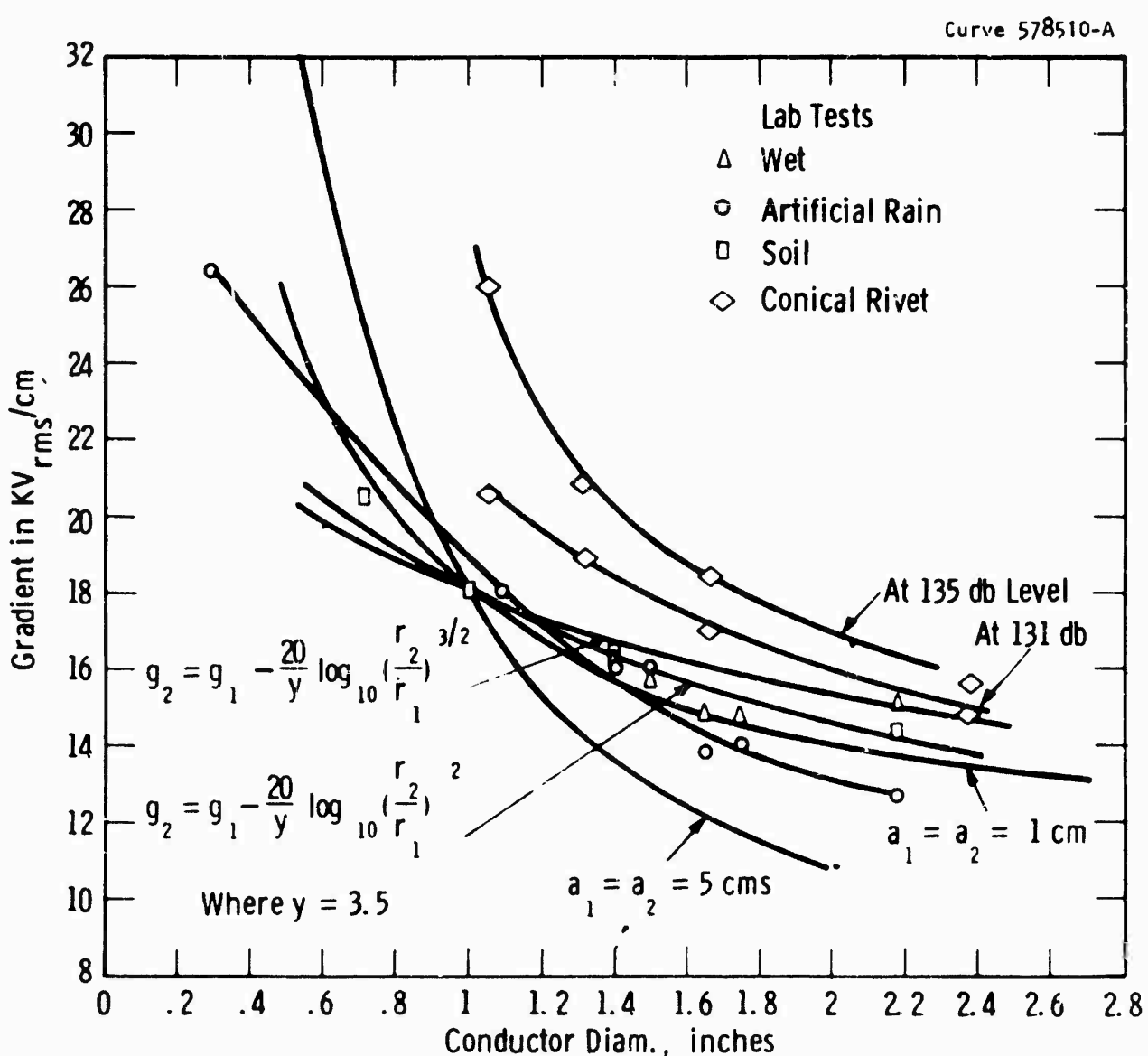


Fig. I-8 - Conductor gradient to diameter relation for same radio noise generation for 1 Mc/s

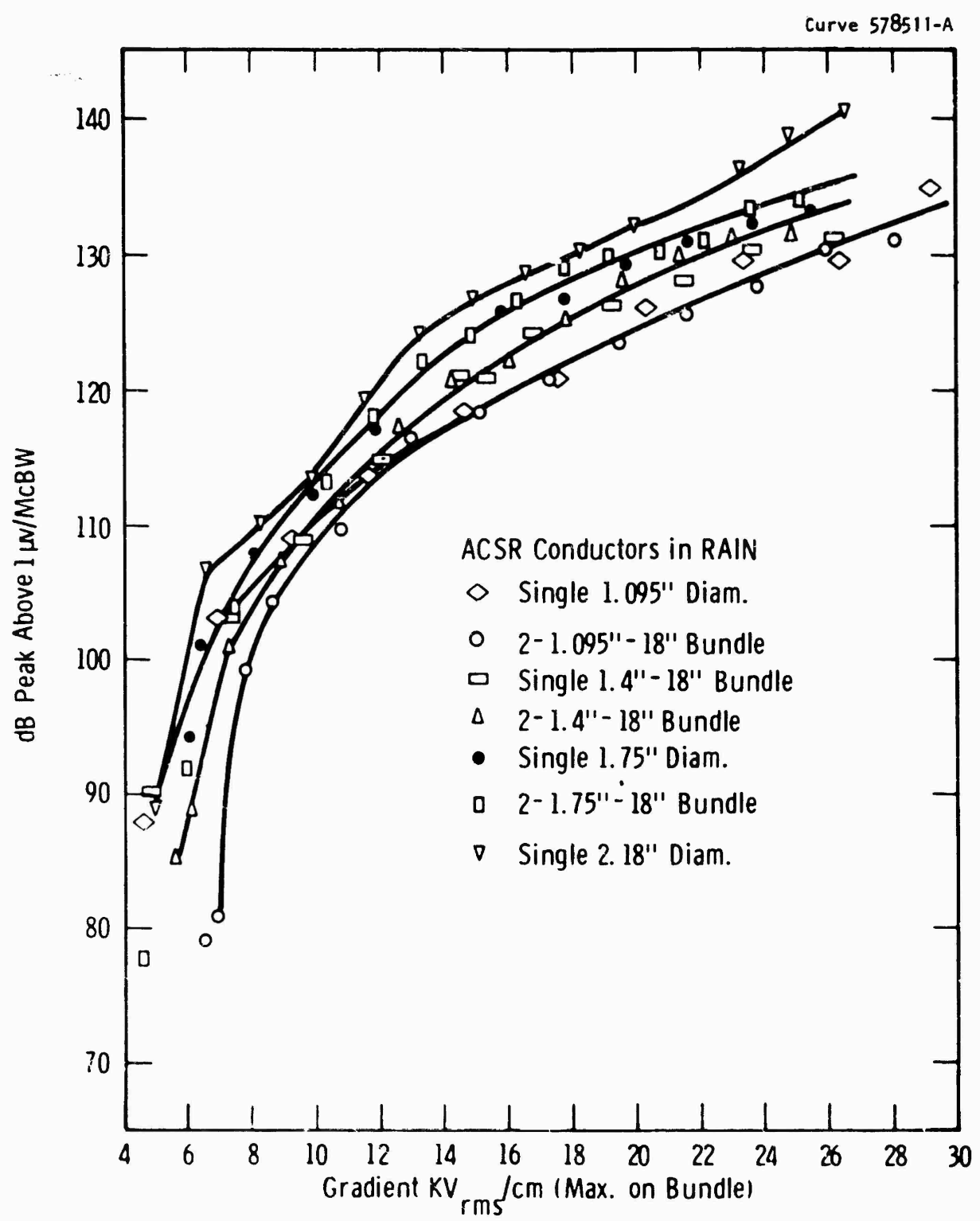


Fig. I-9 - ACSR conductors at 1.0 Mc/s in artificial rain

Curve 578512-A

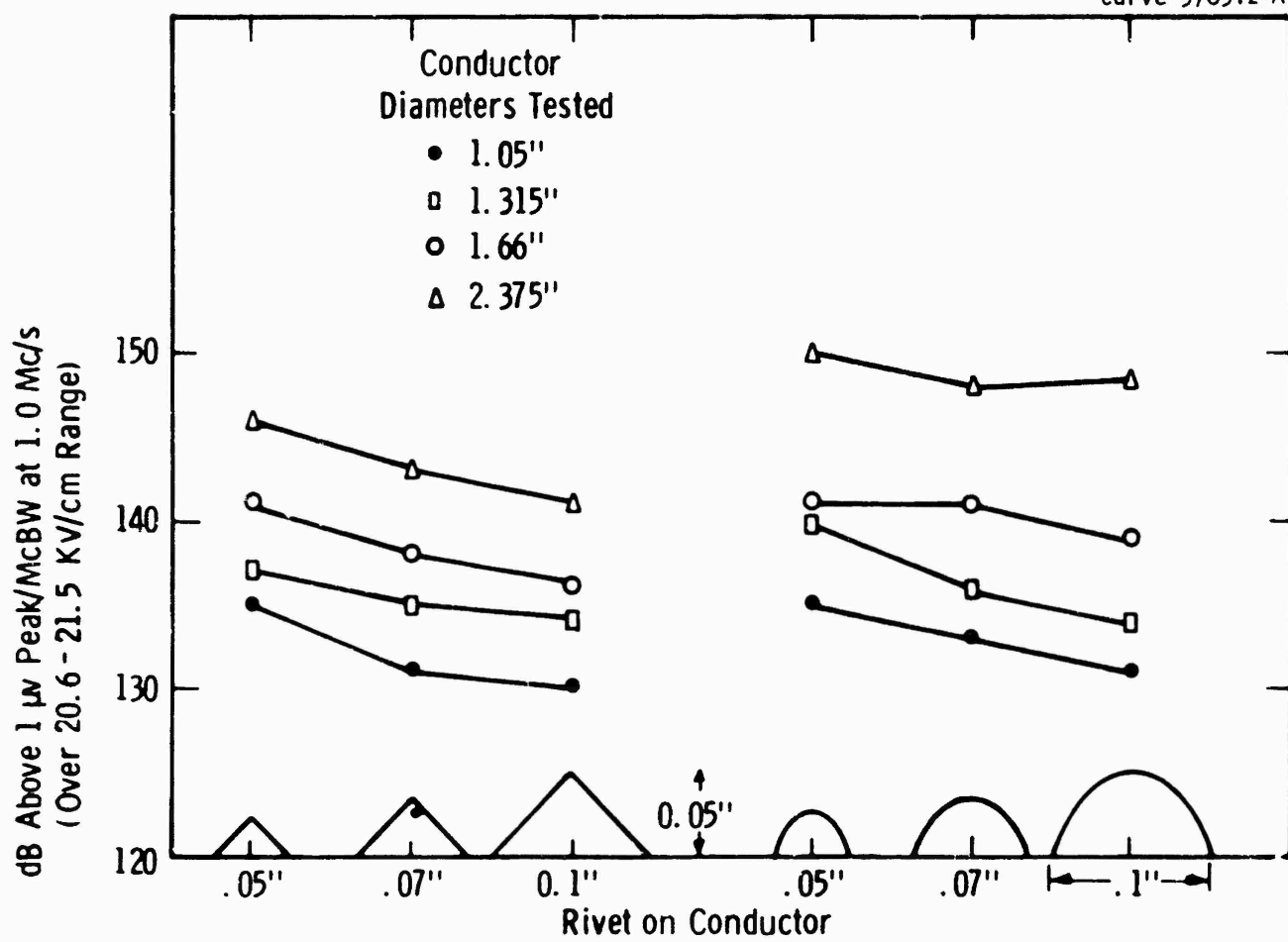


Fig. I-10-Radio noise for different sizes and shapes at rivets on four conductor diameters

Appendix II - Calculation of Electric Field Near a Transmission Line

1. Introduction

It is necessary to obtain a calculation of the field factors (ratios of E/V where E is field strength and V is conductor voltage), at various distances from a line and compare these with the measured results. The calculation reported herein is based on electrostatic fundamentals assuming the neutral plane at ground surface (effect of ground wires neglected).

2. Calculation of Field Strength E Relative to Conductor Voltage V

Referring to Figure II-1 the field strength at P due to charge q per cm on center conductor is in esu

$$E = \frac{q}{r^2} = \frac{VC}{r^2} \text{ statvolts/cm}$$

where V = conductor voltage and C is capacity per centimeter of conductor.

For comparison of measured fields with calculated fields the vertical components due to charge on conductor is required, this is

$$E_1 = \frac{VC}{r^2} \left(\frac{h-y}{r} \right) = \frac{VC (h-y)}{r^3} \quad (1)$$

Substituting $r^3 = [x^2 + (h-y)^2 + z^2]^{3/2}$ and integrating over length s of conductor

$$E_1 = 2 \int_0^{z=\ell} \frac{VC(h-y) dz}{[x^2 + (h-y)^2 + z^2]^{3/2}} \quad (2)$$

$$E_1 = \frac{2 VC (h-y) \ell}{[x^2 + (h-y)^2] \sqrt{x^2 + (h-y)^2 + \ell^2}} \quad (3)$$

The vertical field of image charge is obtained in similar manner, and is

$$E_2 = \frac{2 VC (h+y) \ell}{[x^2 + (h+y)^2] \sqrt{x^2 + (h+y)^2 + \ell^2}} \quad (4)$$

Since ℓ^2 will be many times larger than x^2 and $(h-y)^2$ both E_1 and E_2 simplify to

$$E_1 = \frac{2 VC (h-y)}{x^2 + (h-y)^2} \text{ statvolts/cm} \quad (5)$$

$$E_2 = \frac{2 VC (h+y)}{x^2 + (h+y)^2} \text{ statvolts/cm} \quad (6)$$

Equations 5 and 6 may be simplified without appreciable error since the value of y for field strength tests is only 2.5 feet, which is small compared to conductor heights. The field strengths for three conductors are, after multiplying by 100 to obtain statvolts/meters; (d = conductor spacing). V_1 , V_2 , V_3 are applied conductor voltages, after adding the vertical components of all the charges.

For conductor 1

$$E_{1r} = \frac{400 V_1 C_1 h_1}{x^2 + h_1^2} - \frac{400 V_{21} C_2 h_2}{(x + d)^2 + h_2^2} - \frac{400 V_{31} C_3 h_3}{(x + 2d)^2 + h_3^2} \quad (7)$$

For conductor 2

$$E_{2r} = -\frac{400 v_{12} C_1 h_1}{(x + d)^2 + h_1^2} + \frac{400 v_2 C_2 h_2}{x^2 + h_2^2} - \frac{400 v_{32} C_3 h_3}{(x - d)^2 + h_3^2} \quad (8)$$

$$E_{3r} = -\frac{400 v_{13} C_1 h_1}{(x + 2d)^2 + h_1^2} - \frac{400 v_{23} C_2 h_2}{(x + d)^2 + h_2^2} + \frac{400 v_3 C_3 h_3}{x^2 + h_3^2} \quad (9)$$

In terms of microvolts and microvolts per meter, x and h in feet and C in microfarads per foot equations 7, 8 and 9 are:

$$E_{1r} = \frac{3.86 \times 10^5 v_1 C_1 h_1}{x^2 + h_1^2} - \frac{3.86 \times 10^5 v_{21} C_2 h_2}{(x + d)^2 + h_2^2} - \frac{3.86 \times 10^5 v_{31} C_3 h_3}{(x + 2d)^2 + h_3^2} \quad (10)$$

For conductor 2 (center conductor):

$$E_{2r} = \frac{-3.86 \times 10^5 v_{12} C_1 h_1}{(x + d)^2 + h_1^2} + \frac{3.86 \times 10^5 v_2 C_2 h_2}{x^2 + h_2^2} - \frac{3.86 \times 10^5 v_{32} C_3 h_3}{(x + d)^2 + h_3^2} \quad (11)$$

For outside conductor 3:

$$E_{3r} = -\frac{3.86 \times 10^5 V_{13} C_1 h_1}{(x + 2d)^2 + h_1^2} - \frac{3.86 \times 10^5 V_{23} C_2 h_2}{(x + d)^2 + h_2^2} + \frac{3.86 \times 10^5 V_{33} C_3 h_3}{x^2 + h_3^2} \quad (12)$$

Calculated values of the lateral profile using these expressions give results which compare quite well with measured results. It should be realized that these expressions assume an ideal ground plane and that they are intended for use at short distances 200 feet or less, and at frequencies below 3 Mc/s.

For a single conductor the relations simplify to

$$E = \frac{73.3 VCh}{x^2 + h^2} \text{ microvolts per meter.}$$

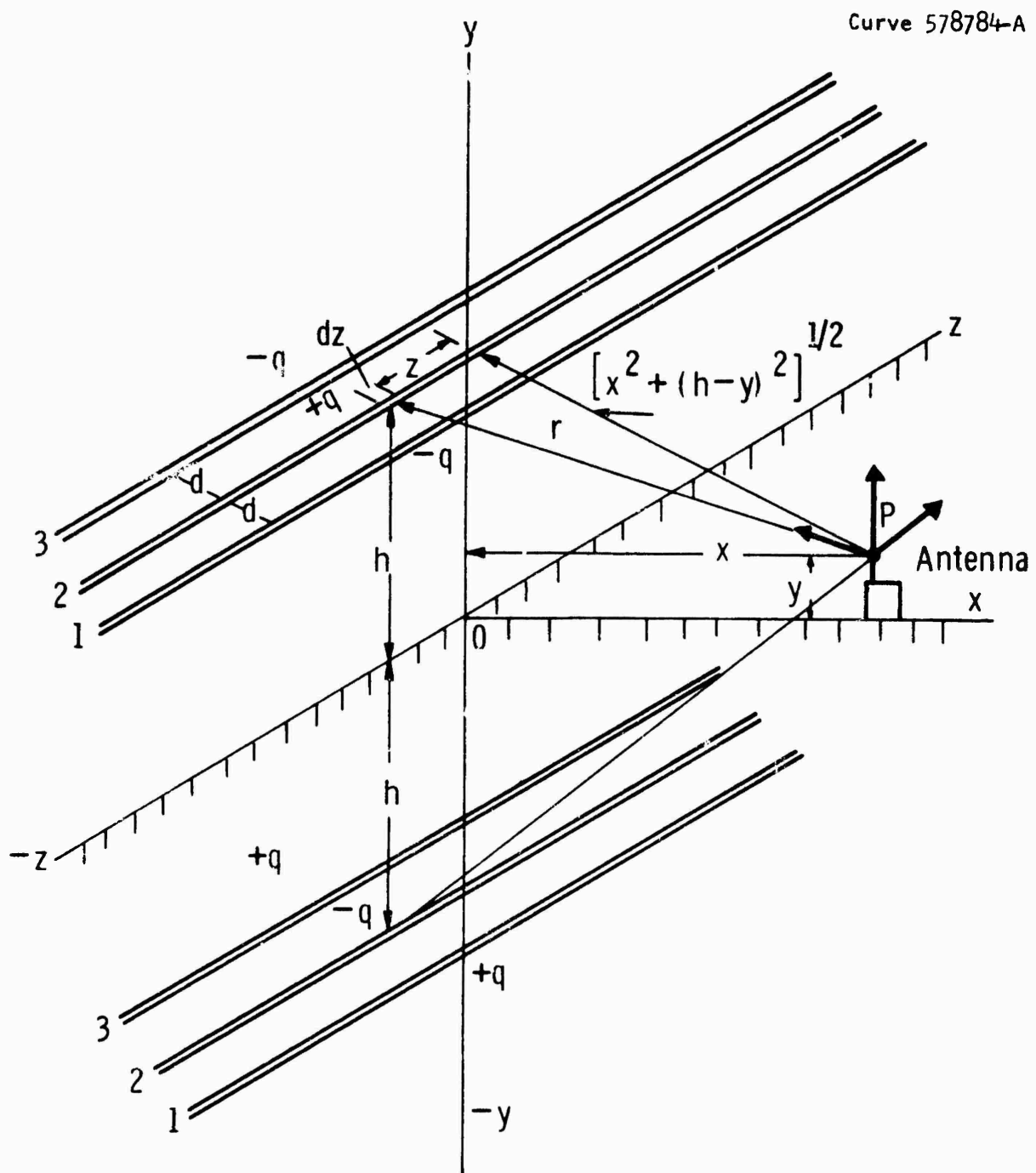


Fig. II 1-Electric field strength near conductors

Appendix III- Radio Noise - High Voltage Transmission Lines

Conductor Gradient Calculations

1. Introduction

In order to compare lines with respect to radio noise or to make any predictions of the radio noise generation by the line conductors, it is necessary to calculate the line conductor gradients. In this Appendix approximate methods of gradient calculation will be given and results compared with accurate computer calculations. It will be seen that simple approximate methods are satisfactory for transmission line radio noise problems.

2. Discussion of the Accurate Method

Gradient calculations can be made by setting up a system of equations¹ relating the conductor voltages as functions of the charge on the conductor by means of Maxwell's coefficients. After the charges have been calculated the electric gradient can be obtained by Coulomb's Law applied to an infinite straight line of charge.

The voltage in terms of all the conductor charges and the self and mutual coefficients is

$$V_a = A_{aa} Q_a + A_{ab} Q_b + \dots + A_{an} Q_n \quad (1)$$

with A_{aa} , the self coefficient = $2\ln \frac{h_{aa}}{r_a}$

A_{an} , the mutual coefficient = $2\ln \frac{h_{an}}{d_{an}}$

where h_{aa} = Distance of conductor "a" to its corresponding image in the ground

h_{an} = Distance of conductor "a" to the image corresponding to conductor "n"

r_a = Radius of conductor "a," or if a bundle, equivalent radius

d_{an} = Distance between conductor "a" and conductor "n"

The units for this set of equations are statvolts and statcoulombs/cm, and an equation is needed for every conductor or subconductor to be considered individually. The system of equations is then inverted to obtain the relations between charges and voltages in terms of capacitance coefficients, giving equations of the form:

$$Q_a = K_{aa} V_a - K_{ba} V_b - \dots - K_{na} V_n \quad (2)$$

This inversion and equation manipulation can be performed with matrix algebra, and is well-suited for digital-computer calculations. The capacitance coefficients so derived must be multiplied by 0.1786 to convert to practical units in microfarads per mile and the voltages in volts. The voltage relations are then inserted to obtain the complete equation for charge in coulombs/mile. (In this report the gradient will be in kV/cm, the conductor radius or diameter in inches and conductor charges will be in coulombs per mile. This procedure is not too consistent; however, it has developed in practice and it is not desirable to change at this time).

The gradients can be calculated manually by means of above equations for three phase three conductor line (no ground wires), in less than two hours. For lines with ground wires and double circuit lines computers have been and are being used. In this appendix approximate methods of calculation will be compared with the more accurate computer results.

The following example is given for a 345 kV line to illustrate the use of the equations given in reference 1. Figure 1 shows the line configurations used for example. The values of the capacitance coefficients are obtained first. The various constants are:

$$h_{aa}' = h_{bb}' = h_{cc}' = 80 \text{ feet} = 960 \text{ inches}$$

$$h_{ab}' = h_{bc}' = 84.4 \text{ feet} = 1016 \text{ inches}$$

$$h_{ac}' = 97.5 \text{ feet} = 1170 \text{ inches}$$

$$d_{ab} = d_{bc} = 28 \text{ feet}, d_{ac} = 56 \text{ feet}$$

Calculations are:

$$DK_{aa} = (2 \log_e \frac{960}{0.875}) (2 \log_e \frac{960}{0.875}) - (2 \log_e \frac{84.8}{28})^2$$

$$DK_{aa} = (14) (14) - (2.21)^2 = 191.1$$

$$DK_{bb} = (14) (14) - (1.1)^2 = 194.79$$

$$DK_{cc} = (14) (14) - (2.21)^2 = 191.1$$

$$DK_{ab} = (2 \log_e \frac{84.8}{28}) (2 \log_e \frac{960}{0.875}) - (2 \log_e \frac{97.5}{56}) (2 \log_e \frac{84.8}{28})$$

$$DK_{ab} = (2.21) (14) - (1.1) (2.21) = 28.56$$

$$DK_{ac} = (1.1) 14 - (2.21) (2.21) = 10.6$$

$$DK_{bc} = (2.21) 14 - (2.21) (1.1) = 28.56$$

$$\begin{aligned} D &= (14) (14) (14) + 2 (2.21) (1.1) (2.21) - (2.21)^2 (14) - \\ &\quad (1.1)^2 14 - (2.21)^2 (14) \\ &= 2745 + 10.7 - 68.5 - 17 - 68.5 = 2601.7 \end{aligned}$$

$$C_{nn} = 0.1786 \frac{K_{nn}}{D} \text{ in microfarads/mile}$$

$$C_{aa} = 0.1786 \times \frac{191.1}{2601.7} = 0.01316 \text{ mfd/mile}$$

$$C_{bb} = 0.0134$$

$$C_{cc} = 0.01316$$

$$C_{ab} = 0.00196$$

$$C_{ac} = 0.000728$$

$$C_{bc} = 0.00196$$

$$Q_a = 0.01316 \times 1 - 0.00196 (- .5 + i.866) - 0.000728 (- .5 - i.866) = 0.01454$$

$$Q_b = - 0.00196 \times 1 + 0.0134 (- .5 + i.866) - 0.00196 (- .5 - i.866) = 0.0154$$

$$Q_c = - 0.000728 \times 1 - 0.00196 (- .5 + i.866) + 0.01316 (- .5 - i.866) = 0.01454$$

From these charge values the gradient can be obtained. The electric intensity G in statvolts per cm at a distance r centimeters from an infinitely long line of charge of Q statcoulombs per cm length is

$$G_S = \frac{2Q_S}{kr} \text{ statvolts/cm} \quad (3)$$

In practical units this is for air dielectric, $k = 1$

$$G = \frac{1800 \times 10^9}{r} Q \text{ volts/cm} \quad (4)$$

For a mile long conductor with uniform charge density and r in inches

$$G = \frac{4404 Q}{r} \text{ kV/cm/kV to ground} \quad (5)$$

(This relation is used in units as indicated because transmission line radio noise investigators in USA and Canada have been using conductor radii in inches and line lengths in miles and the gradient in kV/cm.)

The calculated gradient factors and gradients for the example given will then be

$$G_a = \frac{4404 Q_a}{r} = \frac{4404 \times 0.01454 \times 10^{-6}}{0.875} = 73.1 \times 10^{-6} \text{ volts/cm/volt to gnd.} \quad (6)$$

= 0.0731 kV/cm/kV to gnd.

= 0.0422 kV/cm/kV L-L

$$G_b = 0.0447 \text{ kV/cm/kV L-L}$$

$$G_c = 0.0422 \text{ kV/cm/kV L-L}$$

For 345, $g_a = g_c = 0.0422 \times 345 = 14.55 \text{ kV/cm}$ and $g_b = 15.4 \text{ kV/cm}$

3. Approximate Method of Gradient Calculation

3.1 Single Conductor Above a Ground Plane - The gradient for a single conductor of radius r at a distance h above the ground at a voltage of V kilovolts from conductor to ground is for $(\frac{2h}{r})^2 \gg 1$

$$g = \frac{V}{r \log_e \frac{2h}{r}} \text{ kV/cm} \quad (6)$$

This relation is used in connection with laboratory testing for a conductor parallel to a flat ground plane.

Curves of the gradient factor in $\text{kV}/\text{cm}/\text{kV}$ to ground are given on Fig. 2 for single and bundle conductors at a height of 10 feet above the ground. This height is generally used in laboratory areas for testing conductors.

3.2 Three Phase Lines with Single Conductors

From eq. 4

$$G = \frac{1800 \times 10^9}{r} Q = \frac{1.8 V C}{r} \text{ kV/cm} \quad (7)$$

where C is the electrostatic capacity. The value of C for a three conductor line is approximately

$$C = \frac{i}{18 \log_e \frac{2h}{r \sqrt{\frac{2h}{D} + 1}}} \text{ farads/kilometer} \quad (8)$$

where h is average height of conductors above a perfect ground plane

r is the conductor radius in cms

D is the geometric mean phase spacing defined as

$$\sqrt[3]{d_{ab} d_{ba} d_{ac}}$$

From equation 7 and 8 the gradient factor becomes

$$G = \frac{1}{r \log_e \frac{2h}{\sqrt{(\frac{2h}{D})^2 + 1}}} \text{ kV/cm/kV} \quad (9)$$

For single circuit three phase lines of horizontal or vertical configuration with single conductors with phase spacing of d (outside phase to center phase) the gradients obtained by means of equation 8 will result in an average gradient which is somewhat higher than it is for the outside phase conductors, and somewhat lower than for the center phase conductor.

In order to obtain better accuracy for the gradient values for each of the line conductors the following changes are arbitrarily made. These changes give simple relations which will give quite accurate gradient values, especially for phase spacings greater than 20 feet. The only change is to take the geometric means of the two distances to the other two conductors instead of the geometric mean of the three distances as was done previously. For the outside conductors D is then

$$D_a = \sqrt{d_{ab} d_{ac}} \quad (10)$$

for $d_{ab} = \frac{d_{ac}}{2}$ which is nearly always the case.

$D_a = D_b = \sqrt{2} d_{ab}$ for the outside phase conductor, and for the center phase conductor D_c becomes d_{ab}

$$D_c = \sqrt{d_{ba} d_{bc}} = d_{ab} \quad (11)$$

The approximate gradient relations are now:

For the outside phase conductor (a)

$$G_a = \frac{1}{r \log_e \frac{2h}{\sqrt{\frac{2h^2}{d^2} + 1}}} \text{ kV/cm/kV gnd.} \quad (12)$$

and for the center phase conductor (b)

$$G_b = \frac{1}{r \log_e \frac{2h}{\sqrt{\frac{4h^2}{d^2} + 1}}} \text{ kV/cm/kV gnd.} \quad (13)$$

Calculations were made, assuming smooth conductors, by means of equations 11 and 12 for several values of conductor diameter and for phase to phase spacings of 20, 30, 40 and 50 feet and conductor height of 40 feet. The results have been plotted on Fig. 3 for the outside phase conductor and on Fig. 4 for the center phase conductor. This approximate method checks very well with the accurate method at spacings of 30, 40 and 50 feet. For the shorter spacing of 20 feet the error is greater but still it is less than 2 percent.

3.3 Three Phase Lines with Bundle Conductors

In 1909, P. H. Thomas presented an AIEE paper entitled "Output and Regulation in Long Distance Lines," AIEE, Vol. XXXVIII, Part I, 1909. In this paper he proposed dividing the transmission line conductors so as to increase the capacity and decrease the inductance and thus obtain more power transmission, better regulation and higher power factor. This idea was considered in Germany by O. Burger in Siemens-Zeitschrift, 1922. Later in 1932 and 1935 G. Markt and B. Mengela developed the fundamentals of conductor spacings, surge impedance and power transmission with divided conductors. They also called these divided or multiple phase conductors "bundle" conductors and this name is now generally accepted. When transmission voltages went above 345 kV it became apparent that bundle conductors had several advantages for ac transmission.

In this report the gradient relations for bundle conductors will be based on "Electrical Fundamentals of Bundle Conductors" by W. V. Mangoldt from "Bundelleitungen" (Siemens-Schuckertwerke 1942).

Several assumptions are made as follows:

1. It is assumed that the charges on the sub-conductors are equal and the total charge is assumed to be at the geometric center of the bundle at a height h above a perfect ground plane.

2. The approximate equations are considered good for sub-conductor spacing to conductor diameter ratios of 5 or greater. (Ratios for practical EHV lines are usually greater than 10).

3. A smooth conductor surface is assumed. (In practice the surface factor is less than for a smooth conductor because of stranding, but mainly because of dirt, insects, grass, burrs, nicks, scratches, water drops, snow, ice and etc. The surface factor varies from time to time because of weather, seasons, and no exact surface factor can be predicted.)

The following general relation for the gradient factor can be obtained from Mangoldt (see Fig. 5 for 2, 3 and 4 conductor bundle configurations)

$$G = \frac{1 + \frac{2(n-1)r \sin \frac{\pi}{n} \cos \theta}{s}}{n r \log_e \frac{2h}{r \frac{1}{n} s \frac{n-1}{n} \sqrt{\left(\frac{2h}{D}\right)^2 + 1}}} \quad (14)$$

where G = the gradient factor in kV/cm/kV to ground or neutral

n = number of sub-conductors in the bundle

θ = angle from point of max. gradient

s = distance between nearest sub-conductors

r = conductor radius in cms

h = conductor height above the ground plane

$S = \frac{n-1}{\sqrt{S_{12} S_{13} \dots S_{1n}}}$, is s for $n = 2$, s for $n = 3$, 1.12 s for $n = 4$

D = geometric mean phase spacing

3.3.1 The Two-Conductor Bundle

For a two-conductor bundle, $n = 2$. The maximum gradient factor, $\theta = 0$, from equation 14 is

$$G = \frac{1 + \frac{2r}{s}}{2r \log_e \frac{2h}{\sqrt{rs \left(\frac{2h}{d} \right)^2 + 1}}} \quad (15)$$

Defining D as was done for single conductors for the outside phase, equation 9, D is replaced by $2d$, where d is the phase spacing. The gradient factor for the outside phase will be

$$G_a = \frac{1 + \frac{2r}{s}}{2r \log_e \frac{2h}{\sqrt{rs \left(\frac{2h}{d} \right)^2 + 1}}} \text{ kV/cm/kV}_\text{gnd.} \quad (16)$$

For the center phase conductor, if D is replaced by d, as was done for single conductors, Eq. 10, the center phase gradient factor will be:

$$G_c = \frac{1 + \frac{2r}{s}}{2 r \log_e \sqrt{\frac{2h}{rs (\frac{4h^2}{d^2} + 1)}}} \text{ kV/cm/kV}_{\text{gnd.}} \quad (17)$$

These two relations, equations 16 and 17, were used to obtain the gradient factor with conductor diameter. The curves of Figures 3 and 4 show the gradient factors in $\text{kV}_{\text{rms}}/\text{cm}/\text{kV}$ of line to line voltage. It is only necessary to multiply the gradient factor by the three phase line rms voltage to obtain the conductor gradient in $\text{kV}_{\text{rms}}/\text{cm}$.

3.3.2 The Three-Conductor Bundle

For a three-conductor bundle, $n = 3$. The maximum gradient factor for sub-conductors ($\theta = 0$), is for the outside phase from equation 14

$$G_a = \frac{1 + 3.464 \frac{r}{s}}{3 r \log_e \sqrt[3]{\frac{rs^2}{rs^2 - \sqrt{\frac{2h^2}{d^2}} + 1}} \frac{2h}{}} \text{ kV/cm/kV}_{\text{gnd.}} \quad (18)$$

and for the center phase it is,

$$G_c = \frac{1 + 3.464 \frac{r}{s}}{3 r \log_e \sqrt[3]{\frac{rs^2}{rs^2 - \sqrt{\frac{4h^2}{d^2}} + 1}} \frac{2h}{}} \text{ kV/cm/kV}_{\text{gnd.}} \quad (19)$$

The curves marked 3-conductor bundle on Figures 3 and 4 were calculated from equations 18 and 19.

3.3.3 The Four-Conductor Bundle

For a four-conductor bundle $n = 4$. The maximum gradient factor, $\theta = 0$, is for the outside phase conductor,

$$G_a = \frac{1 + 4.242 \frac{r}{s}}{4 r \log_e \frac{2h}{\sqrt[4]{r (1.12s)^3} \sqrt[4]{\frac{2h^2}{d^2} + 1}}} \text{ kV/cm/kV}_{\text{gnd.}} \quad (20)$$

and for the center phase conductor,

$$G_c = \frac{1 + 4.242 \frac{r}{s}}{4 r \log_e \frac{4h}{\sqrt[4]{r (1.12s)^3} \sqrt[4]{\frac{4h^2}{d^2} + 1}}} \text{ kV/cm/kV}_{\text{gnd.}} \quad (21)$$

The gradient factors calculated by means of equations 19 and 20 are shown in Figures 3 and 4 in kV/cm/kV line to line.

4.0 Comparison of the Approximate Method with Computer Data Obtained by Accurate Method

A comparison of the gradient factors obtained by the simple relations given herein with computer data from more complicated expressions shows a gradual increase in the error as the phase spacing is decreased. At phase spacings 20 to 50 feet and conductor diameters from 0.8 to 2.8 inches the approximate method of gradient calculation gives results for single conductors which are in error from 0 to 1.4 percent for center phase and less than this for the outside phase. For the larger phase spacings 30 feet and above the error is negligible and of no consequence for radio noise considerations.

For bundle conductors the maximum error occurs for 20 foot spacing and is as high as 2 percent in some cases. However, it is less than this for spacings of 30 feet and higher. With the phase spacings required for EHV lines (20 feet or more) the approximate method presented herein for calculating the conductor gradient is satisfactory for radio noise and corona loss estimates and for the purpose of comparing EHV lines.

For single circuit lines with the conductors in a vertical configuration the curves on Figure 4 will give the center phase gradient. For double circuit vertical configuration the gradients will depend on the phase sequence of the conductors. For double circuit line with conductor sequences $a_1 a_2 a_3 - b_1 b_2 b_3$ the gradients on a_2 and b_2 obtained from Fig. 4 (center phase) will be the highest of the six conductors and within 2 percent for 22 foot vertical phase conductor spacing.

5.0 One Bundle Conductor Above a Ground Plane

For single phase tests on conductors in the laboratory it is necessary to know the conductor gradient factor. In this case the calculations for a single conductor are made as shown in section 3.1. For bundle conductor tests the gradient factor can be obtained from eq. 14 using the capacity for a bundle conductor above a ground plane

$$G = \frac{1 + \frac{2(n-1)r \sin \frac{\pi}{n} \cos \theta}{s}}{n r \log_e \frac{2h}{r \frac{1}{n} s \frac{n-1}{n}}} \text{ KV/cm/KV}_{\text{gnd.}} \quad (22)$$

Laboratory tests are often made with $h = 10$ feet. Also radio noise will be compared to the maximum gradient on the sub-conductor, $\theta = 0$. Figure 2 gives the gradient factors for single and bundle conductors when tested 10 feet above the ground plane.

References

1. Electrical Transmission and Distribution Reference Book, Fourth Edition 1950, pp. 749-752, Westinghouse Electric Corporation, East Pittsburgh, Pennsylvania.

Curve 577009-A

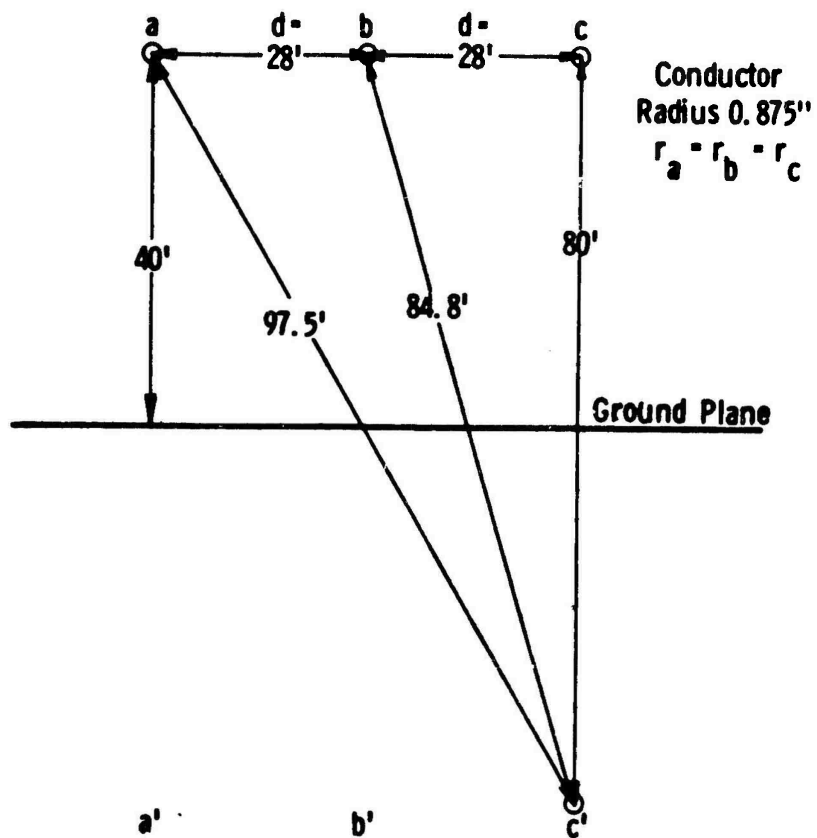


Fig. 1 Line configuration for sample calculation given in Appendix.

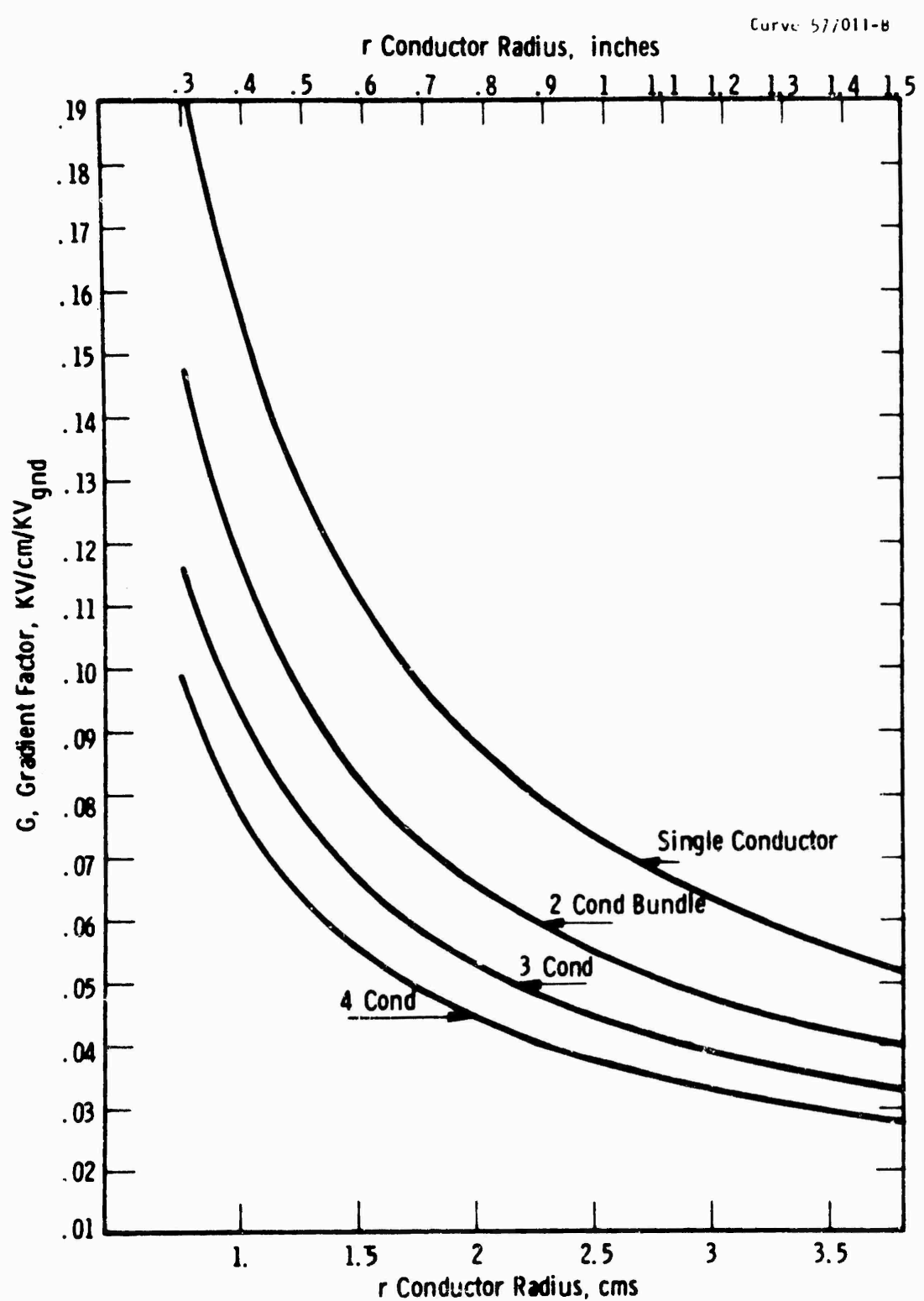


Fig. 2 Conductor gradient factors for single phase laboratory tests 10 feet above ground plane.

Curve 577012-B

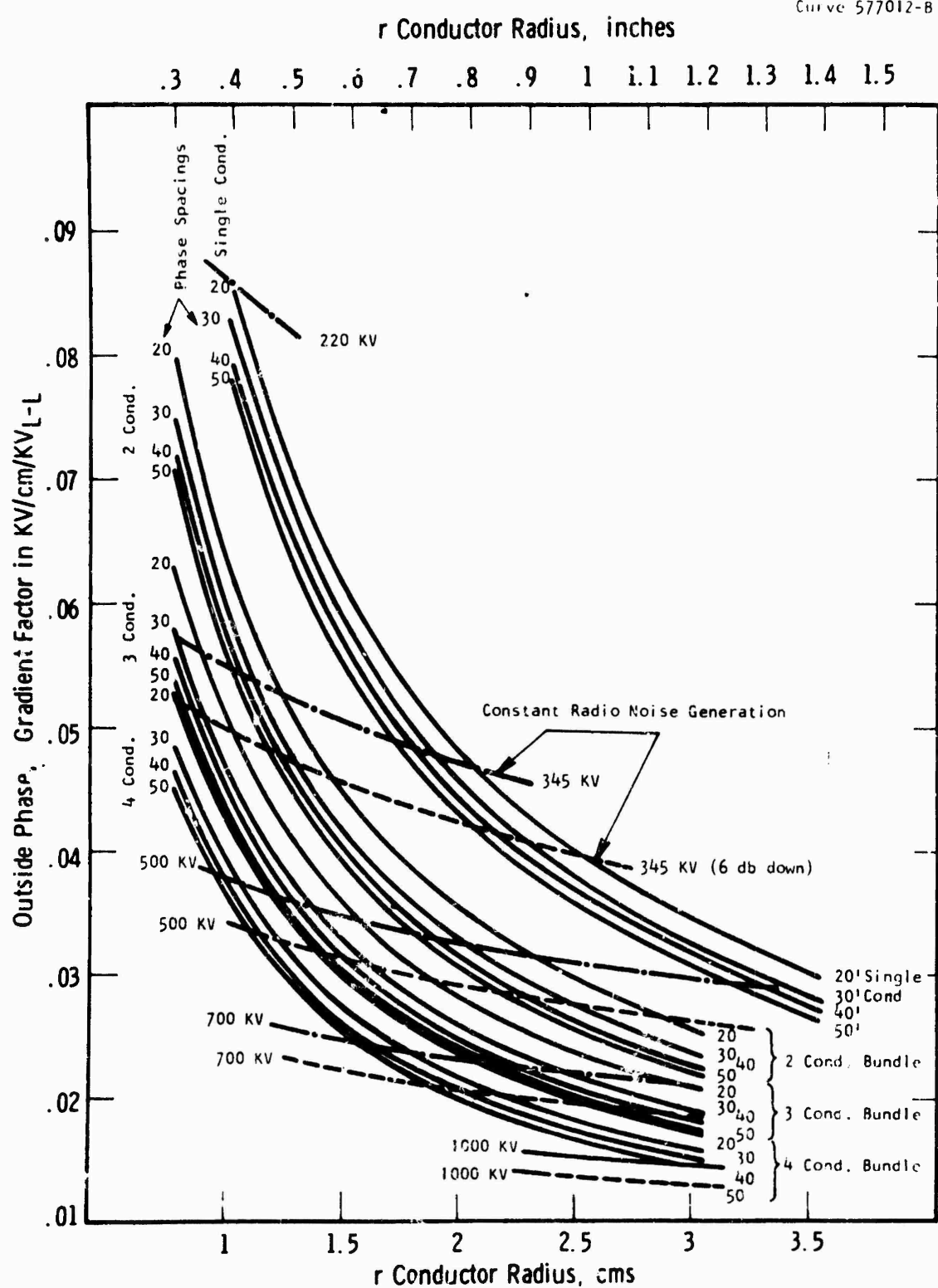


Fig. 3 Outside phase conductor gradient factors for single conductor and 2, 3, and 4 sub-conductor bundle conductors and conductors for same radio noise generation.

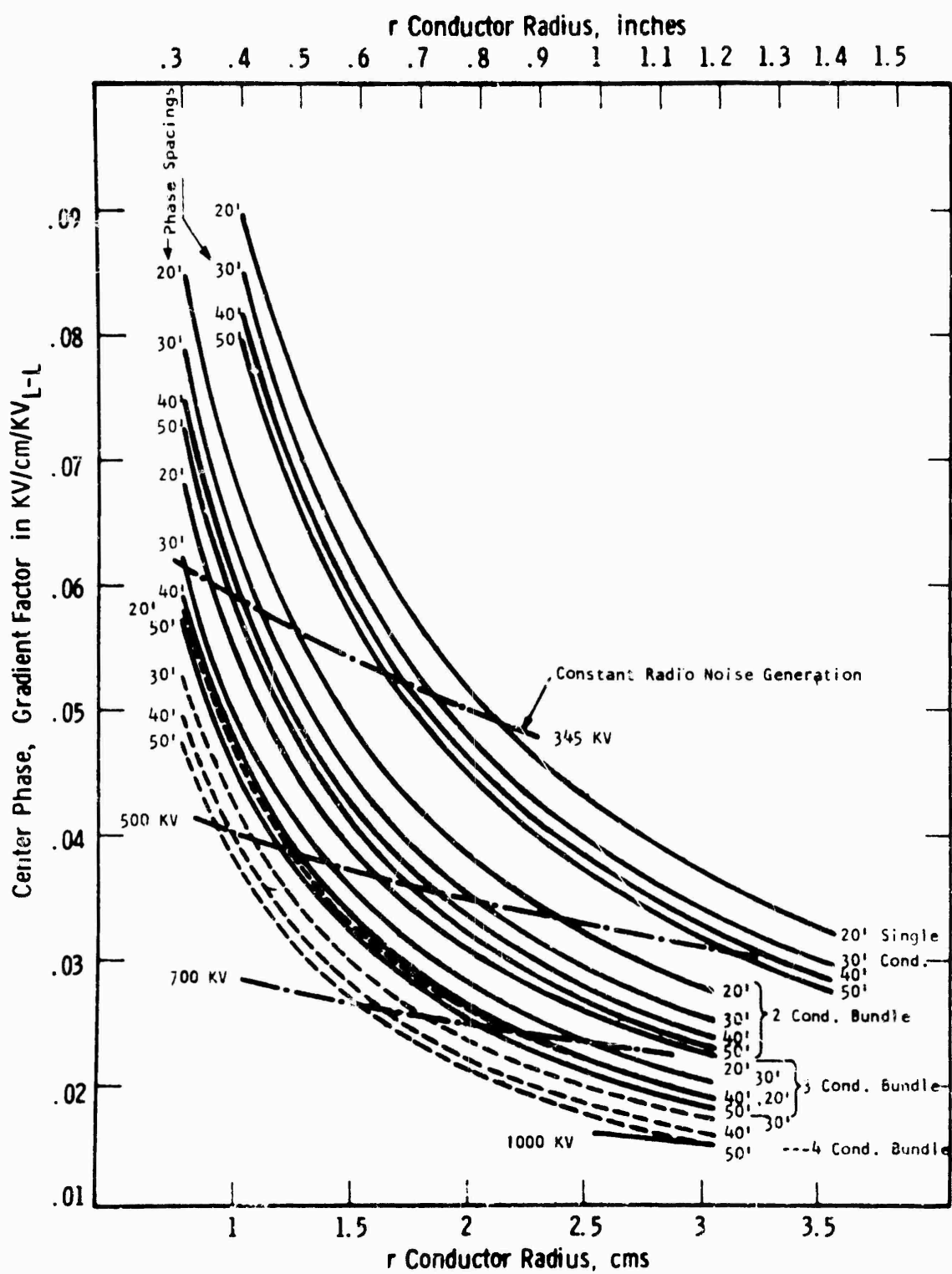


Fig. 4 Center phase-conductor gradient factors for single conductor and 2,3 and 4 sub-conductor bundle conductors.

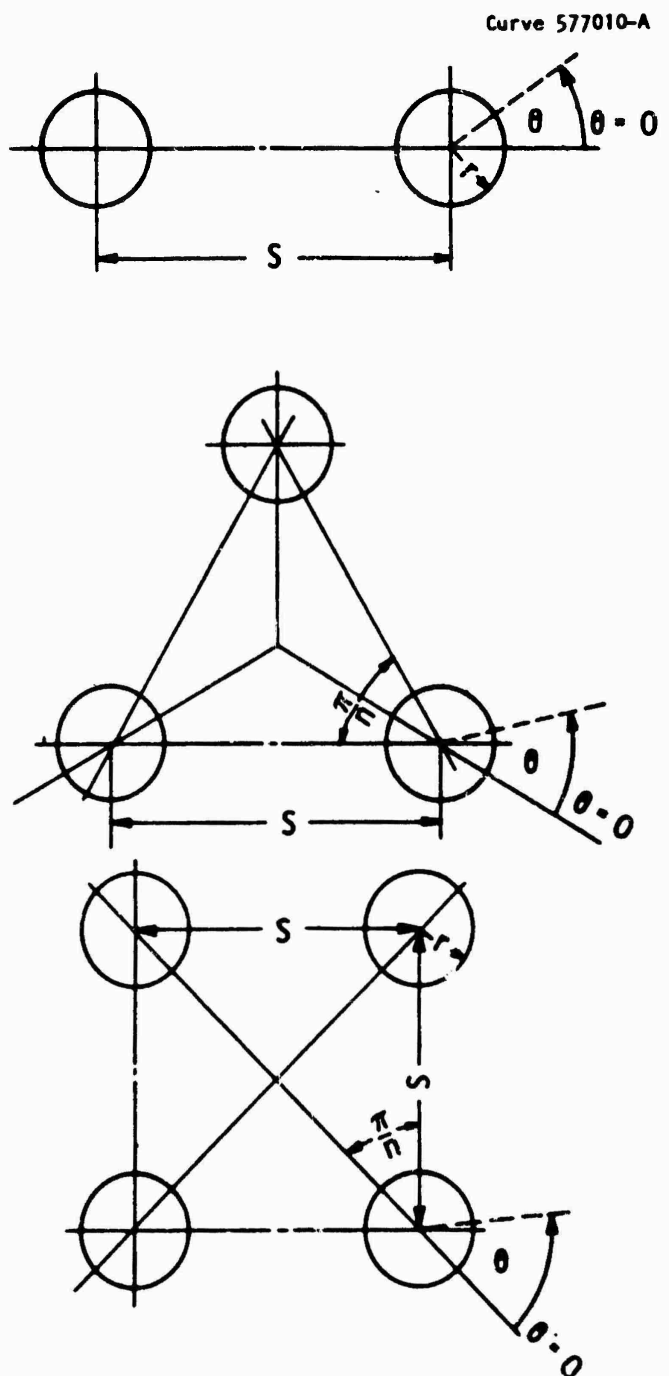


Fig. 5 Bundle conductor configurations.

HIGH VOLTAGE POWER LINE
SITING CRITERIA

Appendix IV of Vol. I

Application of Antenna Theory to
Radiation from Transmission Lines

30 December 1966

Westinghouse Electric Corporation
Electric Utility Headquarters Department
Research and Development Center
Pittsburgh, Pennsylvania

Rome Air Development Center (RADC)
Griffiss Air Force Base
Rome, New York 13442

Contract AF30(602)3822

Contents - Appendix IV of Vol. I

	<u>Page No.</u>
1. Introduction	183
2. Some Concepts from Antenna Theory	188
3. Effect of Terrain and Ground Conditions	194
4. Development Description of Computer Program	199
4.1 Equations Utilized	199
4.2 Development of Computer Equations for Reflection Factor, R	201
4.3 Development of Computer Equations for the Surface Wave Attenuation Factor, F	203
4.4 Equations for Components of Wave	205
4.5 Total Field Factor	206
5. Description of Computer Programs for Field Strengths at a Distance of Several Wavelengths	207
5.1 Simplified Propagation Calculation - Distance Variation	207
6. Programs with Effect of Ground Conditions - Distance Profile Calculations	208
6. Table I - Ground Constants	210
7. Height Variation Calculations	211
8. Near Field Program	211
9. Conclusions from Comparisons of Computer Results of Lateral Profiles	212
10. Description of Computer - Calculated Attenua- tion Curves	213
Figures 1 to 29 inclusive for this Appendix IV	215-243
References on Antenna and Propagation Theory	244-263
Fortran Statements for Near Field Calculation	264
Fortran Statements for Simplified Radiation Pro- pagation Calculations - Modified Equation	267
Fortran Statements for Radiation Propagation Calculations-Norton Equation-Distance Variation	270

Page No.

Fortran Statements for Radiation Propagation Calculations Modified Equation - Distance Variation	275
Fortran Statements for Radiation Propagation Calculations - Norton Equation - Height Variation	280
Fortran Statements for Radiation Propagation Calculations - Modified Equation - Height Variation	285

List of Figures - Appendix IV of Vol. I

	<u>Page No.</u>
Fig. 1b Illustrations of Quantities Used in Propagation Equations.	215
Fig. 1a Illustration of Relation Between Quantities Specifying Ground Conditions.	215
Fig. 2 Graphic Relationships Between Directions of Currents (or Voltage Polarities) for the Modal Sets.	216
Fig. 3 Gap on 345 kV Line - Vertical Antenna Norton's Dipole Equation Comparisons of Measured and Calculated.	217
Fig. 4 Lateral Perpendicular to Tower 119 with Artificial Gap, 30 Mc/s, Vertical Dipole Antenna. Comparisons of Measured and Calculated. Norton Equation for Vertical Dipole.	218
Fig. 5 Horizontal Field 30 Mc/s, 42 ft Conductor Ht., 20 feet Antenna Ht. Comparison of Measured and Calculated with Modified Norton Equation.	219
Fig. 6 Laterals Perpendicular to Tower 119 with Artificial Gap. (Frequency 50 Mc/s) Antenna Vertical Dipole. Comparison of Measured and Calculated.	220
Fig. 7 Horizontal Field 50 Mc/s. 20 ft. Antenna Ht. Comparison of Measured and Calculated with Modified Norton Equation.	221
Fig. 8 Horizontal Field 90 Mc/s. Comparison of Measured and Calculated with Norton's Modified Eq. 20 Ft. Antenna Ht.	222
Fig. 9 Laterals Perpendicular to Tower 119 with Artificial Gap. (Freq. 90 Mc/s) Antenna Vertical Dipole. Comparison of Measured and Calculated.	223
Fig. 10 Attenuation of Field with Distance for 3 Ft. Vertical Antenna at 0.96 Mc/s.	224
Fig. 11 Attenuation of Field with Distance for 3 Ft. Vertical Antenna at 1.92 Mc/s.	225

Page No.

Fig. 12 Attenuation of Field with Distance for Vertical Antenna 3.84 Mc/s.	226
Fig. 13 Attenuation of Field with Distance for 3 Ft. Vertical Antenna at 7.68 Mc/s.	227
Fig. 14 Attenuation of Field with Distance for 3 Ft. Vertical Antenna at 15.36 Mc/s.	228
Fig. 15 Attenuation of Field with Distance for Vertical Dipole at 30.72 Mc/s.	229
Fig. 16 Attenuation of Field with Horizontal Dipole Perpendicular to Line at 30.72 Mc/s.	230
Fig. 17 Attenuation of Field with Distance for Vertical Dipole at 61.44 Mc/s.	231
Fig. 18 Attenuation of Field with Distance for Horizontal Dipole Perpendicular to Line at 61.44 Mc/s.	232
Fig. 19 Attenuation of Field with Distance for Vertical Dipole at 122.88 Mc/s.	233
Fig. 20 Attenuation of Field with Distance for Horizontal Dipole at 122.88 Mc/s.	234
Fig. 21 Attenuation of Field with Distance for Vertical Dipole at 245.76 Mc/s.	235
Fig. 22 Attenuation of Field with Distance for Horizontal Dipole Perpendicular to Line at 245.76 Mc/s.	236
Fig. 23 Attenuation of Field with Distance for Vertical Dipole at 491.52 Mc/s.	237
Fig. 24 Attenuation of Field with Distance for Horizontal Dipole Perpendicular to Line at 491.52 Mc/s.	238
Fig. 25 Attenuation of Field with Distance for Vertical Dipole at 983.04 Mc/s.	239
Fig. 26 Attenuation of Field with Distance for Horizontal Dipole Perpendicular to Line at 983.04 Mc/s.	240

Page No.

- Fig. 27 Lateral Attenuation 0.015-0.96 Mc for 35 foot Conductor Height (Calc.) 241
- Fig. 28 Lateral Attenuation 0.015-0.96 Mc/s for 50 foot Conductor Height (Calc.) 242
- Fig. 29 Lateral Attenuation 0.015-0.96 Mc for 90 foot Conductor Height (Calc.) 243

APPENDIX IV

APPLICATION OF ANTENNA THEORY TO RADIATION FROM TRANSMISSION LINES

1. Introduction

1.1 The transmission line with sources of corona or electrical breakdown metal-to-metal ("gap sources") might be considered to be a complicated antenna structure with parasitic elements such as parts of towers, insulation strings, other phase-, static-, or ground-wires. The horizontal conductors of the transmission line act as long horizontal antennas, except that the conductors are supported at each tower with insulators which have some effective capacitive reactance that conductively couples the conductor to the tower should this be of metal. Where the tower structure is guyed, such as a guyed-V steel or aluminum tower, the lengths of these guys may be of a critical wavelength and act as radiators.

The sources of radio noise generation are also of complicated form. With conductor corona of the normal value, the radio noise voltage generated on the conductors induces a very small portion into the tower over the frequencies of importance for conductor corona. In the near field, the corona plume acts as a local "antenna" of the current source toward ground, and a loop antenna near a particularly strong corona plume on the surface of the conductor will point toward this plume as the field strength meter is moved around the plume.

In contrast, a high energy gap on a supporting metal structure (transmission line tower) within a high 60 cycle electric field may be of such energy and frequency content that sufficient energy may be coupled into the tower and any associated conductors and guys and then radiated.

1.2 A difference between transmission line propagation and antenna theory also exists in the fact that in a discussion of antennas one usually assumes a sinusoidal variation of signal on the antenna. In contrast, current pulses of varying frequency content are set up on a line (or tower) by a corona source or gap type source.

To satisfy electromagnetic field conditions at the conductors, electro-motive forces (emf's) must be induced along the conductors that are equal and opposite to the fields. (Reference 59 of Appendix VII, Vol. 3, by

C. F. Wagner). For a 30 meter conductor spacing, the electromagnetic disturbances at a conductor will not be felt until after a time of 0.1 microsecond. (30 meters divided by 300×10^6 meters per second, the speed of light.) If the emf's are integrated along the conductors, the voltage approaches the value that would be obtained using the conventional value of conductor surge impedance (414 ohms), which can be computed for this conductor spacing (30 meters). It takes about 1/3 the travel time between conductors (about 0.03 microsecond here) for this value of induced voltage to be reached by the buildup of conductor emf.

Thus, this analysis fixes the time limit for which the conventional conductor surge impedances are applicable which are used in computations, and shows that for power lines, their use is justified for all impulses greater than several tens of millimicroseconds. The utilization of surge impedances, therefore, is good at least to 30 megacycles, but for frequencies above this limit a different approach must be utilized.

The analysis of the propagation phenomena through space due to corona pulses on transmission lines is very complicated. Being an impulsive type of generation, a change in conditions of charge, current flow into space, etc. at a given point are not felt at another point until after the time necessary for the effect to travel between the two points with the speed of light.

1.3 For zero earth resistivity the electric field near a charged conductor can be determined by taking the sum of the fields due to line charges on the conductor or on its image in the earth, and the normal component of electric field at the earth's surface is inversely proportional to the sum of the square of the conductor height and the distance along the ground from under the conductor. (This is analogous to the ray theory to describe ground-reflections of radiation from antennas.)

Since the earth resistivity is not zero, an analysis considering ground could be modified to include its resistance. For a short distance behind the head of the traveling wave all of the charge resides on the surface of the earth, and the conductor image may be

taken at a depth equal to the conductor height. At each point immediately after the passage of the head of the traveling wave because of ground resistance, the charge on the surface of the earth begins to penetrate downward into the earth, and the equivalent depth of the image conductor can be adjusted to take this penetration of charge into account.

However, in many cases the effect of the finite ground is sufficiently small so that its effect on the equivalent image depth can be neglected. Lateral profiles of radio noise fields from transmission lines, calculated utilizing conductor images at depths equal to the conductor height, compare well with field tests in the broadcast frequency range (Appendix II). At lower and higher frequencies other approaches have to be taken in considering the effect of ground.

- 1.4 Several approaches to the propagation along the system of conductors have been undertaken by investigators, one of which is the so-called "modes" of propagation. (See references by Carson and others.) The modal-component approach represents a reduction of complicated coupled circuits (such as power line conductors) to elementary, uncoupled circuits. It is similar to the symmetrical component attack in the sense that resulting networks and their inputs are transformed into modal voltages, currents, and impedances with natural modal frequencies. Modal components thus solved from their corresponding modal networks are combined in a manner prescribed by the "transformation matrices" peculiar to the given circuit to obtain corresponding circuit components.

In the case of lumped circuit parameters, the resulting modal components can be finite totally uncoupled networks for any given input. However, as Wagner and Carson (Ref. 26 of this Appendix) point out, for distributed circuits such as transmission lines (a form of wave guide), pulse inputs may initially see uncoupled modal networks, but as the pulse progresses along the conductor of the transmission line, components which were, say, purely conductor to conductor break up into components involving the ground in addition to those of conductor to conductor, ad infinitum. It may be this introduction of "impurities" into the "purely" uncoupled components that is the reason why for a given location on a long line with corona sources the so-called line to line components do

not "pile up" and dominate the resulting radio noise patterns. Wagner (previous reference) also points out that, assuming effective grounding by the towers, the static wires grounded at each tower cause a further redistribution of modal components, effectively "coupling" the purely uncoupled circuits.

Guillemin* shows that for an infinitely long line or one properly terminated, the summation of discrete modal components goes over, in the subsequent limiting processes, into a continuous spectrum of components, the Fourier integral.

The physical picture usually taken of the modal set for a single-circuit three-phase line with static wires is as follows (refer to Fig. 2): the modal current directions in the phase wires or modal voltage polarities, for the "ground-return mode", here Mode 1, are all the same and return in the ground and static wires. The directions or polarities for Mode 2, the "outer-phase, line to line mode", are symmetrically opposite about the vertical center line of the test line. The modal current and voltage for Mode 2 are zero on the center phase and the outer phase magnitudes are equal as are the static conductor magnitudes, the magnitude on the outer phases being larger than that on the static conductors, Mode 3, the "center to outer-phase, line-to-line mode", has the largest magnitude of modal voltage and current on the center phase, and the direction and polarity are opposite to that on the outer phase and static conductors.

The remaining modes of academic interest (since normally no corona is on them) are related to the presence of the static conductors, and in each case the magnitudes on the static conductors are the largest. The static conductor directions or polarities are opposite to those of the phase conductors for Mode 4. Mode 5 corresponds to Mode 2 but has diametrically opposite directions and polarities, with the center phase currents and voltages being very small or zero. Mode 6, which results instead of Mode 4 for the higher frequency and higher ground resistivity has center phase current direction and voltage polarity.

*Communication Networks, Vol. II, Chapt. XIII, "The Transient Behavior of Long Lines," p. 576

1.5 In the 1920's a debate ensued as to whether there could be radiation from power transmission lines, the interest at that time being in radiation at 60 cps. This was shown to be insignificant, but Carson (Reference 27 of this Appendix) pointed out that radiation mainly occurs where discontinuities exist in the transmission line, such as at terminations, and some radiation would result theoretically if the spacing of the wires or the geographical direction of the line changed as the wave moved down the wires. Mathematically, this results in the formation of a multiplicity of modes of propagation, as discussed previously, which either 'rearrange' the field or subtract or contribute energy to the principal mode so as to establish continuity in the field pattern at the point of discontinuity in the line. Energy from pulses formed by corona or gaps will be radiated regardless of how uniform the line.

1.6 Recent field measurements have tended to bear out, at least from one to three Mc/s and below, that an analytical approach based on static charges and the resulting electric field may apply to transmission lines at least out to 150 to 200 feet. (See Appendix II.) Further, the only mode of major importance with uniform generation appears to be that associated with the ground return path for distances comparable to the usual rights-of-way. Too, the modal approach in its present state appears to be limited to spacings small compared with wavelength.

Therefore, it appears from the standpoint of the broadcast frequencies that a simplified approach may be taken in the analysis of the fields near a transmission line. It remains to be shown what analysis will give satisfactory answers for higher and lower frequencies. The most direct method is through a comparison of measured and calculated values.

The work of Koike, Oliver, et al (64 and 82 of this Appendix) indicates that for long wire antennas that coupling to the other wires is small, so that in analyzing the response of the power transmission line to high frequencies one may need be concerned with only the one wire with the corona source. The results of tests reported elsewhere in this report, however, shows this to be true only at the location of the corona source. As one moves down the transmission line in either direction more energy, depending on frequency, becomes coupled into the other conductors

and they must be considered in the calculation of the field pattern (lateral profile) near the line. In the case of several wires with uniformly distributed corona sources occurring at different points in time this leads one to conclude that the field due to each wire may be analyzed separately provided energy is coupled into the other conductors and its effect considered.

2. Some Concepts from Antenna Theory

2.1. The basic concept in estimating radio wave propagation, and its attenuation, is that applicable in free space, or in a hypothetical region free of all objects that would change the propagation from an ever uniformly expanding pattern. Antenna theory follows that of optics and takes the inverse square law of the attenuation of power. Since power is proportional to the square of the field strengths, the field strength in free space is attenuated or falls off inversely to the first power of distance from the antenna. The field intensity concept is frequently more convenient than power attenuation at frequencies below 30 Mc's since it is independent of frequency as opposed to that for power which has the term frequency squared involved. Antenna theory is generally discussed in terms of relatively small antennas or ones "isotropic" - radiating power uniformly in all directions.

Antenna theory usually assumes a small isotropic (one radiating equally in all directions) antenna (point source) of such dimensions that the field radiated is in the form of an outward propagating sphere. Energy is therefore being dissipated as the radius squared; that is,

$$P_r = \frac{P_t}{4\pi r^2}$$

where P_t is total radiated power at the antenna and r is the distance to the point in question. Since the field intensity is proportional to the square root of the power, in free space the field intensity will decrease as the first power of the distance " r ".

2.2 With an infinite line source in free space of constant generation the situation is complicated by the proximity of the changes along the line and the time of travel from succeeding points along the line. Without losses in the conductor the electric field is everywhere parallel to the wire without any radial component and the magnetic field is disposed in concentric circles centered on the conductor. However, from the above consideration of a small isotropic antenna one would expect, since the cylindrical area varies as the first power of the radius that the field from a small infinite wire will vary as $r^{-1/2}$, which mathematically can be shown to be the case, when the distance r is sufficiently large. (See, for example, Radio Aerials,(book), E. B. Moulin, Oxford Press, 1949.)

2.3 In practice, however, to be complete, one must be concerned with the effects of the earth; if the transmission path is long, the atmosphere, clouds, and the ionosphere; and if the frequency is high, trees and other irregularities in the path of propagation. It is, therefore, often expeditious to consider a division of the propagation into optical or line of sight and beyond the radio horizon depending upon the frequency. The radio horizon may be defined as that distance where the radio wave first touches the earth and is of course a function of the heights of the transmitting and receiving antennas, as well as the earth's curvature. The optical or line-of-sight distance is calculated as

$$d_{LS} = \sqrt{2Rh_1} + \sqrt{2Rh_2}$$

where R is the effective radius of the earth, and h_1 and h_2 are the heights of the two antennas. The refractive index of the air decreases with height above earth, which has the effect of refracting radio waves downward toward the earth. This effect is included in the field calculations by using an earth radius larger than the actual, experimental evidence (Reference 81 of this Appendix) indicating an effective radius about $4/3$ the actual, or about 5280 miles. A ray from an antenna of height h , therefore, is tangent to the earth, or its optical horizon, is at a distance

$$d_o = \sqrt{2Rh} = \sqrt{2 \cdot 5280 \cdot h} = 103 h$$

The limiting frequency for sky-wave transmission in the distance range here considered is usually not greater than 40 Mc/s. Sky-wave field intensities have been calculated in the literature for various distances up to and beyond those considered in this report below this limiting frequency. These are often calculated for a given antenna radiation at a specific distance, such as 300 millivolts per meter at 1 km. Values, such as this, exceed by a large amount the value generally measurable at this distance from power lines. Thus, the values given by these calculations greatly exceed any sky-wave radiation that would be measured as a result of power line radio noise. For example, the incident sky-wave field intensity (no ground-wave component included) for frequencies from 2 to 30 Mc/s approaches as a maximum 55 db above one microvolt per meter, depending upon the reflecting ionosphere layers and the number of "hops" made by the wave, for zero atmospheric absorption index. (See, for example, Department of the Army TM 11-499, Radio Propagation, August 1950.) A more appropriate value (with a gap-type source, see Fig. 75) might be 30 μ V per meter at 1 km, or a value one ten-thousandth the base value, 80 db lower. Thus, for this radiation level, the incident sky-wave field intensity would be some value less than 55 minus 80 or 25 db below one microvolt per meter. This is about 0.05 microvolts per meter and below levels normally considered. Therefore, the significant component of radio noise propagation to be considered for the distances here is the direct and ground-reflected components.

2.4 For the purposes of this report, because of the smaller distances of interest, the analysis is based on plane earth, and reflections from the sky are not considered.

With the presence of a reflecting earth, the simplest approach is again to return to the theory of optics, or more specifically to the theory of rays, with the direct and ground-reflected radiation represented by the rays.

McPetrie and Strickland (Reference 70 of this Appendix) in 1940 pointed out that the simple ray theory becomes inaccurate where the heights of the transmitting and receiving antennas are not comparable with the wavelength, as is the case for normal transmission line conductor heights. However, although the ray theory is incomplete in this

region, the field can be determined by the vector addition of the field given by the ray theory and by the (Sommerfeld) surface wave. This latter field depends on the electrical properties of the reflecting surface and the distance between the transmitter and receiver, but is independent of the heights of transmitter and receiver.

The ray theory also involves the assumption that the (Fresnel) reflection coefficient of the earth does not vary rapidly with angle of incidence, which is not true for glancing incidence (small angles of incidence) at broadcasting wavelengths.

Considering the ray theory, but representing the reflected ray by an image antenna, the electric field from short antennas varies inversely with the square of the distance between transmitter and receiver. However the ratio of the magnitudes of the surface wave to image fields is much less for horizontally than for vertically polarized waves. The ray theory is, therefore, theoretically applicable over a wider range of angles of incidence (hence, antenna heights) for horizontally than for vertically polarized areas. (Reference 70)

2.5 Another theory postulates that the radiation reflected from the ground is due to the re-radiation by the molecules in the ground which have been polarized by the field from the transmitter. The simple ray theory considers radiation from the transmitting antenna at the image position of the transmitting antenna in the reflecting surface. A true image, however, can be formed only if all the rays arriving at the receiver after reflection undergo the same change on reflection, which can only be exactly true if the transmitter and receiver antennas are very small.

2.6 Calculating procedures of propagation for dipole antennas have been developed over the past 30 years, culminating in an organized method by Norton (Reference 81 of this Appendix), taking into account the change in reflection factor with ground resistivity and polarization. As discussed previously, the expression for the vector electric field is divided into two terms, identified with a space wave, predominating at large distances above the earth, and a surface wave predominating near the surface of the earth.

Considering the earth a flat plane, the field intensity of a small dipole antenna at distances of several wavelengths is calculated by the following:

$$\frac{E}{E_0} = \frac{1}{d} (\cos^3 \psi_1 e^{j\frac{2\pi r_1}{\lambda}} + R \cos^3 \psi_2 e^{j\frac{2\pi r_2}{\lambda}} + (1 - R) F \cos^2 \psi_2 e^{j\frac{2\pi r_2}{\lambda}})$$

(See section on computer equation development for explanation of this equation.)

The above equation (hereafter referred to as Norton's equation) does not allow for diffraction loss due to earth curvature and the field strength calculated from it will therefore be increasingly higher - or more conservative - at particularly long distances. Gerks⁴⁹ and Norton⁸¹ give a rough rule for the distance limit of accuracy for this equation as $50/(f_{Mc})^{1/3}$ miles; hence, for 1000 Mc/s, a distance limit of 5 miles. Gerks also shows that up to 10 Mc/s, the difference between the value calculated by plane-earth equations and that calculated considering a spherical earth are within 5 dB, regardless of the earth conductivity and dielectric constant.

- 2.7 When the receiving antenna is high ($h > 2000/f_{Mc}^{2/3}$ ft.) the curvature of the earth will modify the approximations that are normally made in calculating field intensity both at areas within and beyond the line of sight. Norton states that at sufficiently large antenna heights beyond the line of sight, the field intensity increases exponentially with the height rather than linearly as occurs with medium antenna heights. ($h < 2000/f_{Mc}^{2/3}$ ft., which for 1000 Mc/s is only 20 feet, while for 125 Mc/s it is 80 ft.)

- 2.8 Within the line of sight, the curvature of the earth can still have several effects on the propagation of radio waves for high transmitting or receiving antennas. The reflection coefficient of the ground-reflected wave is different for the curved surface of the earth than for a plane surface. Also, since the ground-reflected wave is reflected against the curved surface of the earth, its energy is diverged more than would be indicated by the inverse-distance law discussed previously. This energy divergence can be taken into account by applying a divergence factor D. This factor has the effect of reducing the ground-reflected component

of the space wave, the effect on the reflection coefficient being small for moderate distances. The overall result is, therefore, a smaller oscillation of field intensity about the free-space value, but with maximum and minimum occurring at essentially the same distances as those if the divergence factor is not included. Thus, the decrease of the reflected wave for some frequencies can increase the total field at given locations beyond the plane-earth region so that the propagation approaches that of free space. Therefore, from a conservative standpoint, in this region, one may use the inverse-distance relation to obtain field intensities somewhat higher than will actually occur.

2.9 An expression for the height gain of antennas at a particular distance is quite complicated and various forms are given in the literature at large distances.^{12, 23, 81} At frequencies below 1.5 Mc/s no appreciable change in field strength occurs by elevating antennas above ground before roughly 200 feet,¹⁹ although there is an effect on the impedance of antennas used for these frequencies. For frequencies less than about 10 Mc/s an antenna must be elevated higher than about 25 feet before the effect is noticeable. For frequencies above 25 Mc/s (using dipole antennas), the received levels are very sensitive to changes in height because of the rapid change in phase angle and magnitude of the ground-reflected wave.

Burrows²³ derives height gain curves for antenna separation distances beyond those for which the received field strength begins to vary inversely with the square of the distance. For frequencies well above 1 Mc/s with the ground constants assumed here (dielectric of 30 and conductivity of 20 millimhos per meter), an analysis of his results indicates no increase with height until a height of $(123/f_{\text{Mc/s}})$ feet is reached for vertical polarization or $(4.1/f_{\text{Mc/s}})$ feet for horizontal polarization. The increase is then approximately 3 dB per decade of height until a height is reached of $(1000/f_{\text{Mc/s}})$ feet for vertical polarization or $(33.3/f_{\text{Mc/s}})$ feet for horizontal polarization. Above this height the increase is about 18 dB per decade of height.

Egli indicates that his analysis of test results above 40 Mc/s, the field strength for the receiving antenna varies as the square root

of the height for 6 to 30 feet and above this directly as the height where the reception is beyond line of sight. For line of sight reception the strength increases proportional to the height.

In addition to the effect of ground on the reflected and surface waves of propagation, the impedance of low antennas is caused to oscillate around the free space value for heights close to ground. Where the height is more than a quarter-wave above ground, this effect is insignificant compared to other effects.¹⁹

The effect of antenna height is considered further in Appendix V.

- 2.10 The gain of arrays of parasitic elements is not readily calculated but is more the result of practical experience and investigations. However, on the basis of this experience with practical antennas and ground measurements, gains of about 9 dB can be obtained with four-element arrays for spacings in the order of one-eighth wavelength, and front-to-back ratios upwards of 30 dB for frequencies for which the system is tuned. (For example, see Department of the Army and the Air Force, TM 11-486-6, Electrical Communication Systems Engineering, Radio, August 1956, pp. 14-75.)

The transmission line may consist of a set of three to five conductors (more, if phase conductors are in bundles). Tests with gap-type, radio-noise sources are described elsewhere in this report. For lines with steel towers, peaks and minimum values have been measured in an otherwise relatively smooth frequency spectrum which are comparable to the above dB gain.

3. Effect of Terrain and Ground Conditions

- 3.1 This study has not considered the effect of the earth's curvature or sky waves, since for the generally low noise levels from power lines the distances to be considered are short. Also for the frequencies under consideration the absorption in the atmosphere in the presence of rain, snow, or fog may be neglected. In addition, the effect of ground on the impedance of low antennas is not considered here. The ground conditions over which propagation of the electric field takes place affects this propagation in several ways; first, by multiple reflections from irregularities and obstacles, particularly at the high frequencies, and

second, by the effect of the ground conductivity and dielectric constant upon the reflected- and surface-wave components. Although no tests conducted under this study were specifically directed toward determining these effects, a brief review of the results from some of the references given in this Appendix pertinent to this subject, will be helpful in interpretation of the attenuation curves that will follow.

3.2 With regard to the effect of ground conductivity and dielectric constant, calculations were performed using a dielectric constant of 30 and a ground conductivity of 20 millimho-meters per square meter, this having given a reasonably good check of calculated with measured data through 90 mc/s. (See Section 9.) Gerks⁴⁹ gives these values for "good soil" and shows in his examples that attenuation out beyond a distance of one mile is greater with poorer ground conditions. Should, however, very good conductivity be present or the propagation of interest be over sea water, the curves given in this appendix may be expected to give a somewhat greater attenuation than will be experienced. In these instances, a relationship of attenuation inversely to the first power of distance should be used throughout the distance range of interest. Table I gives the range of constants for various ground conditions.

3.3 Colwell and Friend³⁵ have conducted propagation measurements at 59, 87 and 98 Mc/s over earth with varying degrees of moisture and over fresh water with antenna heights from 1.4 to 2.2 meters. The attenuating curves for values at 59 Mc/s for dry and damp earth and deep fresh water were very nearly the same, the attenuation changing from the inverse distance relationship to the inverse distance squared at about 50 meters. Similar results were found for 87 and 98 Mc/s over dry earth and deep fresh water, except the attenuation changes to the inverse distance squared relationship at about 37 meters.

3.4 Burrows²² has made measurements at 150 Mc/s with a vertical ground-wave doublet over deep fresh water having a dielectric constant of 82.1 and a conductivity of 4.05×10^8 electrostatic units. His data indicates the attenuation to follow the inverse distance relationship out to about 10 meters and to be following the inverse distance squared relationship by about 1000 meters. This may be compared to the calculated curves,

Fig. 20, for 122.9 Mc/s that follow, which shows nearly the same attenuation for the lowest antenna height but was calculated using a dielectric constant of 30 and a conductivity of 20 millimho-meters/meter squared.

3.5 Day and Trolese³⁷ have reported on their experiments for horizontal polarization on the propagation of short waves in the frequency range from 25 to 24,000 Mc/s over desert terrain. Although the terrain would ordinarily be considered uniform (terrain being plane within ± 10 feet), small scale irregularities were found to have appreciable effect at the higher frequencies (above 1000 Mc/s) but the low frequencies were fairly insensitive to small irregularities.

A marked difference was noted in the change of field strength over a 24 hour period for line-of-sight propagation for a 26.7 mile and a 46.3 mile path as contrasted with none-line-of-sight, particularly for microwave frequencies. The change in either case was attributed to changes in the atmospheric conditions, the air being mixed and showing a slightly smaller equivalent radius of earth curvature in the day-time, and experiencing a temperature inversion at night due to the warm ground. For frequencies 1000 Mc/s and below, for low antenna heights (25 feet) the change was in the order of 20 dB up during the night time. However, for this low antenna height, the propagation was not line-of-sight. For high antenna heights (190 feet) with line-of-sight propagation, the change was in the order of 5 dB. Likewise, height-gain curves for 170, 520 and 1000 Mc/s were only slightly modified at night time, the low-height values gradually shifting toward higher field strength as night progressed, but the high-height strengths being little changed.

3.6 Day and Trolese³⁷ also give height-gain measurements taken by means of an airplane for 170, 520, 1000 and 3300 Mc/s which indicate a high value of reflection coefficient over desert, the higher two frequencies showing the effect of ground irregularity. Their comparison of measured values for 170, 520 and 1000 Mc/s calculated values based on plane-earth and a unity reflection coefficient showed remarkable agreement.

3.7 Where propagation is over a rough surface, multipath reflections occur, especially at the higher frequencies, and the resultant field

pattern is no longer that determined by the combination of the direct wave with one reflected wave. For rough terrain, movement of the receiving antenna causes large variations at higher frequencies in the magnitude and phase of ground reflections. For high receiving antennas, such as in airplanes, the field pattern over mountainous terrain can show a complete absence of any interaction with the ground reflection.

- 3.8 A reflecting surface may be considered flat if surface irregularities are of such magnitude as not to cause path differences larger than some small fraction of the wavelength, and Day and Trolese³⁷ give the following limit definition:

$$\frac{H \cos \Theta}{\lambda} \ll 1$$

where H is the height of the surface irregularities, λ the wavelength, and Θ , the angle of incidence.

For the highest frequency covered by this study (1000 Mc/s), if $\cos \Theta$ is taken very nearly equal to 1.0 this definition would limit the height of the surface irregularities to something very much less than one foot. If the surface irregularity is limited to 10 feet, the surface may be considered flat only for frequencies less than 100 Mc/s by this definition.

- 3.9 Bullington¹⁹ gives an empirical nomogram which summarizes available data as to the effect of nearby hills. For 10 Mc/s this nomogram shows only a median "shadow loss" about 4 dB for variations in terrain of as much as 1000 feet. However, for 1000 Mc/s this loss varies from about 10 dB for a 50-foot variation to 30 dB for a 1000-foot variation.

- 3.10 Egli⁴¹ has taken the data given in FCC reports in terms of the distribution of received field strengths over irregular terrain and from a plot of this data in dB above the theoretical plane earth attenuation finds that they are "log-normally distributed". He shows the terrain distribution of field intensity to have a standard deviation of 8.3 dB at 127.5 Mc/s and of 11.6 dB at 510 Mc/s, the median being displaced 12 dB from theoretical plane-earth by his "terrain factor" for the two frequencies. From the data of References 69 and 93 he states that the vertical polarization is somewhat better directly behind hills but away from the hill shadow a higher signal is received with horizontally polarized waves.

In terms of the present problem, according to these findings, should the noise field be of such magnitude as to carry over a hill (generally not likely), a vertical antenna would be more susceptible to interference directly behind the hill; whereas, the horizontal antenna would be more susceptible in back of, but away, from the hill and in wooded areas.

- 3.11. Attenuation for antenna heights above one wavelength in wooded areas has been found to be somewhat less for horizontally polarized waves than for vertically polarized waves for frequencies below 300 to 500 Mc/s but independent of polarization above 300 to 500 Mc/s. For lower antenna heights, the reception is determined by the ground wave, and vertical polarization provides less attenuation than horizontal.

Attenuation at 30 Mc/s due to trees, is about 2 or 3 dB for vertical polarization but negligible for horizontal polarization, and increases with frequency.¹⁹

4. Development Description of Computer Program

4.1 Equations Utilized

The basic equation utilized is Norton's general equation⁸¹

$$\begin{aligned} \frac{E}{E_0} = & \frac{1}{d} \left[\cos^3 \Psi_1 \cdot e^{j2\pi r_1/\lambda} \quad \text{Direct wave component of space} \right. \\ & + R \cos^3 \Psi_2 e^{j2\pi r_2/\lambda} \quad \text{Ground-reflected component of} \\ & \left. + 1 - R F \cos^2 \Psi_2 e^{j2\pi r_2/\lambda} \right] \quad \text{Surface wave} \quad (1) \end{aligned}$$

where the quantities d , r_1 , r_2 , h_1 , h_2 , Ψ_1 and Ψ_2 are as indicated in Fig. 1a, being the wave length of the frequency of interest and $j = \sqrt{-1}$. R is the plane-wave reflection coefficient of the ground which is a function of the wave polarization, dielectric constant and conductivity of the reflection surface, and the angle of incidence of the wave. The surface-wave attenuation function, F , and R will be developed later. Gerks⁴⁷ has given the equations for the vertical component with F and R developed for use in the digital computer. The development here will follow Norton without the approximation of Gerks.

From Fig. 1, it can be shown that

$$r_1 = \sqrt{(h_1 - h_2)^2 + d^2}, \quad r_2 = \sqrt{(h_1 + h_2)^2 + d^2}$$

$$\cos \Psi_1 = \frac{d}{r_1}, \quad \cos \Psi_2 = \frac{d}{r_2}$$

$$\frac{2\pi r_{1,2}}{\lambda} = 2\pi \frac{(f_{Mc})}{984.2344} \quad r_{1,2} = 0.0063838 (f_{Mc}) \quad r_{1,2} = \underline{\text{ANG } 1,2*}$$

Bullington³ indicates terms to be added to the basic equation for the induction field and the secondary effects of the ground. Both he and Gerks (as have others) use the approximation:

$$4\pi \frac{h_1 h_2}{\lambda d}$$

for the Norton angle

$$\frac{2\pi r_2}{\lambda}$$

*Underlined quantities are symbols used in the Computer program.

Norton⁸¹ has shown that at the higher frequencies where the "numerical" distance (to be given shortly, when $p > 20$ and $p > 100 (q_1 + q_2)$

$$\frac{2\pi}{\lambda} (r_2 - r_1) \approx \frac{4\pi h_1, h_2}{\lambda d}$$

It is to be noted that the $\cos \psi_1$, and $\cos \psi_2$ terms in part reflect the directivity of the doublet antenna considered by Norton. The computer program has the option to assume essentially non-directivity by making these equal to one, if desired. Basic parameters not a function of distances used by Norton are:

$$X = \frac{17.9731 \times 10^{15} \sigma}{f_{Mc}} \text{ emu}$$

$$\cos b'' = \frac{X}{\sqrt{\epsilon^2 + X^2}} = \frac{1}{\sqrt{1 + \frac{\epsilon^2}{X^2}}}$$

as indicated by Fig. 1b, where σ is the ground conductivity expressed in millimho-meters/meter square and ϵ is the dielectric constant of the ground referred to air as unity.

Basic parameters which are functions, additionally, of distances as given by Norton are (see Fig. 1b):

$$1) \quad \cos b' = \frac{X}{\sqrt{\epsilon - \cos^2 \psi_2^2 + X^2}} = \frac{1}{\sqrt{1 + \left(\frac{\epsilon - \cos^2 \psi_2}{X}\right)^2}}$$

2) The "numerical distances"

a) for vertical polarization

$$p = \frac{\pi r_2}{\lambda} \frac{\cos^2 b''}{X \cos b'} = 0.0031919 (f_{Mc} r) \frac{\cos^2 b''}{X \cos b'}$$

b) for horizontal polarization

$$p = \frac{\pi r_2}{\lambda} \frac{X}{\cos b'} = 0.0031919 (f_{Mc} r) \frac{X}{\cos b'}$$

3) The "numerical" antenna heights

a) for vertical polarization

$$q_{1,2} = \frac{2\pi h_{1,2}}{\lambda} \left[\frac{\cos^2 b''}{X \cos b'} \right]^{1/2} = 0.0063838 (f_{mc} h_{1,2}) \left[\frac{\cos^2 b''}{X \cos b'} \right]^{1/2}$$

b) for horizontal polarization

$$q_{1,2} = \frac{2\pi h_{1,2}}{\lambda} \left[\frac{X}{\cos b'} \right]^{1/2} = 0.0063838 (f_{mc} h_{1,2}) \left[\frac{X}{\cos b'} \right]^{1/2}$$

4.2 Development of Computer Equations for the Reflection Factor, R

From Norton⁸¹, the reflection factor is given as:

$$R = \frac{\frac{(q_1 + q_2)}{2p} e^{-j(\pi/4 - b/2)} - 1}{\frac{(q_1 + q_2)}{2p} e^{-j(\pi/4 - b/2)} + 1}$$

Use computer program symbols:

$$Q = \frac{q_1 + q_2}{2p} \quad \text{and} \quad \text{THETA} = (\pi/4 - b/2) - 0.785398 - \frac{B_N}{2}$$

Then

$$\begin{aligned} R &= \frac{Q e^{-j(\text{THETA})} - 1}{Q e^{-j(\text{THETA})} + 1} = \frac{(Q \cos(\text{THETA}) - 1) + j Q \sin(\text{THETA})}{(Q \cos(\text{THETA}) + 1) + j Q \sin(\text{THETA})} \\ &= \frac{[(Q \cos(\text{THETA}) - 1)(Q \cos(\text{THETA}) + 1) + Q^2 \sin^2(\text{THETA}) +]}{(Q \cos(\text{THETA}) + 1)^2 + Q^2 \sin^2(\text{THETA})} \\ &= \frac{j Q \sin(\text{THETA}) \{ (Q \cos(\text{THETA}) + 1) - (Q \cos(\text{THETA}) - 1) \}}{(Q \cos(\text{THETA}) + 1)^2 + Q^2 \sin^2(\text{THETA})} \\ &= \frac{Q^2 \cos^2(\text{THETA}) - 1 + Q^2 \sin^2(\text{THETA}) + j 2 Q \sin(\text{THETA})}{Q^2 \cos^2(\text{THETA}) + 2 Q \cos(\text{THETA}) + 1 + Q^2 \sin^2(\text{THETA})} \\ &= \frac{(Q^2 - 1) + j 2 Q \sin(\text{THETA})}{RDEN} \end{aligned}$$

Where $\underline{RDEN} = Q^2 + 2 Q \cos(\text{THETA}) + 1$

If $\underline{QS} = Q^2$, $\underline{RDEN} = QS + 2Q \cos(\text{THETA}) + 1$

The real part of the numerator of R is then

$$\underline{RK} = (Q^2 - 1) = QS = 1$$

and the imaginary part

$$\underline{RI} = 2 Q \sin (\theta)$$

For horizontal polarization,

$$Q = \frac{q_1 + q_2}{2p} = \frac{\frac{2\pi}{\lambda} (h_1 + h_2) \left[\frac{X}{\cos b'} \right]}{\frac{2\pi}{\lambda} r_2 \left[\frac{X}{\cos b'} \right]}^{1/2} = \frac{h_1 + h_2}{r_2} \left[\frac{\cos b'}{X} \right]^{1/2}$$

$$= (\underline{HD}) (\underline{XB})$$

$$\text{if } \underline{HD} = \frac{h_1 + h_2}{r_2} \quad \text{and } \underline{XB} = \left[\frac{\cos b'}{X} \right]^{1/2}$$

$$\text{Also, } \underline{BN} = b = \pi - b' = 3.14159 - \cos^{-1} (\cos b')$$

For vertical polarization,

$$Q = \frac{q_1 + q_2}{2p} = \frac{\frac{2\pi}{\lambda} (h_1 + h_2) \left[\frac{\cos^2 b''}{X \cos b'} \right]^{1/2}}{\frac{2\pi}{\lambda} r_2 \left[\frac{\cos^2 b''}{X \cos b'} \right]} = \frac{(h_1 + h_2)}{r_2} \left[\frac{X \cos b'}{\cos^2 b''} \right]^{1/2}$$

$$= (\underline{HD}) (\underline{XB})$$

$$\text{If } \underline{HD} = \frac{h_1 + h_2}{r_2} \quad \text{and } \underline{XB} = \left[\frac{X \cos b'}{\cos^2 b''} \right]^{1/2}$$

$$\text{Also, } \underline{BN} = b = 2b'' - b' = 2 \cos^{-1} (\cos b'') - \cos^{-1} (\cos b')$$

$$\underline{BPCOS} = \cos b'$$

$$\underline{BPPCOS} = \cos b''$$

$$\underline{\underline{X}} = X$$

$$\underline{R2} = r_2, \underline{HC} = h_1, \underline{HA} = h_2$$

4.3 Development of Computer Equations for the Surface Wave Attenuation Factor, F

Norton⁸¹ gives the attenuation factor as

$$F = 1 + j\sqrt{\pi w} e^{-w} \operatorname{erfc}(-j\sqrt{w})$$

"erfc" being one minus the error function,
where for elevated antennas

$$w = \frac{4pe^{jb}}{(1-R)^2} = Pe^{jB} = P(\cos B + j \sin B)$$

Gerks² points out that for $0 < P \leq 10$,

$$F = 1 + j\sqrt{\pi w} e^{-w} - 2w + \frac{(2w)^2}{1 \times 3} - \frac{(2w)^3}{1 \times 3 \times 5} + \dots$$

converges fairly rapidly, whereas for $P > 10$,

$$F = - \left[\frac{1}{2w} + \frac{1 \times 3}{(2w)^2} + \frac{1 \times 3 \times 5}{(2w)^3} + \frac{1 \times 3 \times 5 \times 7}{(2w)^4} + \dots \right]$$

is more suitable.

It can be shown (Gerks²) that for $0 < P \leq 10$:

$$\begin{aligned} \text{the real part of } F = & 1 - \sqrt{\pi Pe^{-P}} \cos B \sin \left(\frac{B}{2} - P \sin B \right) - (2P) \cos B \\ & + \frac{(2P)^3}{1 \times 3} \cos 2B - \frac{(2P)^3}{1 \times 3 \times 5} \cos 3B + \dots + (-1)^n \frac{(2P)^n}{1 \times 3 \times 5 \times (2n-1)} \cos nB + \dots \end{aligned}$$

$$\text{and the imaginary part of } F = \sqrt{\pi Pe^{-P}} \cos B \cos \left(\frac{B}{2} - P \sin B \right) - (2P) \sin B$$

$$+ \frac{(2P)^2}{1 \times 3} \sin 2B - \frac{(2P)^3}{1 \times 3 \times 5} \sin 3B + \dots + (-1)^n \frac{(2P)^2}{1 \times 3 \times \dots \times (2n-1)} \sin nB + \dots$$

For $P > 10$,

$$\begin{aligned} \text{The real part of } F = & - \left[\frac{\cos B}{(2P)} = \frac{1 \times 3}{(2P)^2} + \cos 2B + \frac{1 \times 3 \times 5}{(2P)^3} \cos 3B + \dots \right. \\ & \left. \dots + \frac{1 \times 3 \times \dots \times (2n-1)}{(2P)^n} \cos nB + \dots \right] \end{aligned}$$

and the imaginary part

$$= - \left[\frac{\sin B}{(2P)} + \frac{1 \times 3}{(2P)^2} \sin 2B + \dots + \frac{1 \times 3 \times \dots \times (2n-1)}{(2P)^n} \cos nB + \dots \right]$$

In the computer program,

$$\text{Real } F = \underline{FR}$$

$$\text{Imaginary } F = \underline{FI}$$

$$\underline{HR} = (-1)^n (2P)^n \cos (nB)$$

$$\underline{HI} = (-1)^n (2P)^n \sin (nB)$$

$$\underline{A} = \sqrt{\pi P} / e^{PCos B}$$

$$B = \frac{B}{2} - P \sin B$$

And $P = \underline{PC}$ while $B = \underline{BC}$. It now remains to determine P and B .

$$\text{Again } Pe^{jB} = \frac{4pe^{jb}}{(1 - R)^2}$$

where ' p ' and ' b ' have been given already as ' PN ' and ' BN ', respectively, and R is the reflection factor, which has a real part ' $RR/RDEN$ ', and an imaginary part ' $RI/RDEN$ '.

Letting $\underline{RRM} = 1 - RR/RDEN$ and $\underline{RIM} = RI/RDEN$, expand the denominator:

$$(1 - R)^2 = (\underline{RRM} - j\underline{RIM})^2 = (\underline{RRM}^2 - \underline{RIM}^2) - j2x\underline{RRM}\times\underline{RIM}$$

Thus

$$\begin{aligned} Pe^{jB} &= \frac{4p(\cos b + j \sin b)}{(\underline{RRM}^2 - \underline{RIM}^2) - j2x\underline{RRM}\times\underline{RIM}} \quad \frac{(\underline{RRM}^2 - \underline{RIM}^2) + j^2 \times \underline{RRM} \times \underline{RIM}}{(\underline{RRM}^2 - \underline{RIM}^2) + j2x\underline{RRM}\times\underline{RIM}} \\ &= \frac{4(PN)}{(\underline{RRM}^2 - \underline{RIM}^2)^2 + 4 \times \underline{RRM}^2 \times \underline{RIM}^2} \left[(\underline{RRM}^2 - \underline{RIM}^2) \cos b - 2 \times \underline{RRM} \times \underline{RIM} \times \sin b \right. \\ &\quad \left. + j(2 \times \underline{RRM} \times \underline{RIM} \times \cos b + (\underline{RRM}^2 - \underline{RIM}^2) \sin b) \right] \end{aligned}$$

Let the denominator be

$$\begin{aligned} \underline{PBDEN} &= \underline{RRM}^4 - 2\underline{RRM}^2\underline{RIM}^2 + \underline{RIM}^4 + 4\underline{RRM}^2\underline{RIM}^2 \\ &= \underline{RRM}^4 + 2\underline{RRM}^2\underline{RIM}^2 + \underline{RIM}^4 = (\underline{RRM}^2 + \underline{RIM}^2)^2 \end{aligned}$$

Let the real part of the numerator be

$$\underline{PBRN} = (\underline{RRM}^2 - \underline{RIM}^2) \cos (BN) - 2 (\underline{RRM} \times \underline{RIM}) \sin (BN)$$

And the imaginary part be

$$\underline{PBIN} = (\underline{RRM}^2 - \underline{RIM}^2) \sin (BN) + 2 (\underline{RRM} \times \underline{RIM}) \cos (BN)$$

The program sets $\underline{RRM}^2 = \underline{RRMS}$ and $\underline{RIM}^2 = \underline{RIMS}$.

Then

$$B = \underline{BC} = \tan^{-1} \frac{\underline{PBIN}}{\underline{PBRN}}$$

and

$$P = \underline{PC} = \frac{4(PN)}{\underline{PBDEN}} \sqrt{\underline{PBRN}^2 + \underline{PBIN}^2}$$

4.4 Equations for Components of Wave

1) Direct Wave

$$\cos^3 \psi_1 e^{j \frac{2\pi r_1}{\lambda}} = \cos^3 \psi_1 (\cos \frac{2\pi r_1}{\lambda}) + j \sin \frac{2\pi r_1}{\lambda}$$

$$\underline{\text{DWCR}} = \left(\frac{D}{R_1}\right)^3 \cos \frac{2\pi r_1}{\lambda} = \underline{\text{DWK}} \times \cos (\underline{\text{ANG1}})$$

$$\underline{\text{DWCI}} = \left(\frac{D}{R_1}\right)^3 \sin \frac{2\pi r_1}{\lambda} = \underline{\text{DWK}} \times \sin (\underline{\text{ANG1}})$$

If flagged, DWK is set equal to one.

2) Ground Reflection

$$R \cos^3 \psi_2 e^{j \frac{2\pi r_2}{\lambda}} = \frac{(RR + jRI)}{RDEN} \cos^3 \psi_2 (\cos \frac{2\pi r_2}{\lambda} + j \sin \frac{2\pi r_2}{\lambda})$$

$$\cos \psi_2 = \frac{(d)}{r_2} = \underline{\text{COPH2}}, \quad \cos^2 \psi_2 = \underline{\text{SCOPH2}}$$

$$\frac{2\pi r_2}{\lambda} = \underline{\text{ANG2}}$$

Real part of the ground-reflected component = GRCR

$$= \underline{\text{SCOPH2}} \times \underline{\text{COPH2}} \times (RR \cos (\underline{\text{ANG2}}) - R1 \sin (\underline{\text{ANG2}})) / RDEN$$

Imaginary part of component = GRCI

$$= \underline{\text{SCOPH2}} \times \underline{\text{COPH2}} \times (RR \sin (\underline{\text{ANG2}}) + RI \cos (\underline{\text{ANG2}})) / RDEN$$

3) Surface Wave

$$(1 - R) F \cos^2 \psi_1 e^{j \frac{2\pi r_2}{\lambda}} = (1 - \frac{RR}{RDEN}) \times (FR + j FI) \times \underline{\text{SCOPH2}} \times (\cos (\underline{\text{ANG2}}) + j \sin (\underline{\text{ANG2}}))$$

$$= \underline{\text{SCOPH2}} \times (RRM - j RIM) \times (FR + j FI) \times (\cos (\underline{\text{ANG2}}) + j \sin (\underline{\text{ANG2}}))$$

$$\text{But } (RRM - j RIM) \times (FR + j FI) = (RRM \times FR + RIM \times FI) +$$

$$+ j (RRM \times FI - RIM \times FR) = \underline{\text{SWK1}} + j \underline{\text{SWK2}}.$$

The real part of the surface wave then becomes:

$$\underline{\text{SWR}} = (\underline{\text{SWK1}} \times \cos (\underline{\text{ANG2}}) - \underline{\text{SWK2}} \times \sin (\underline{\text{ANG2}})) \times \underline{\text{SCOPH2}}$$

and the imaginary part:

$$\underline{\text{SWI}} = (\underline{\text{SWK1}} \times \sin (\underline{\text{ANG2}}) + \underline{\text{SWK2}} \times \cos (\underline{\text{ANG2}})) \times \underline{\text{SCOPH2}}$$

In the above, if flagged, $\cos \psi_2$ is set equal to one.

4.5 Total Field Factor

The total field at some distance then becomes the vectorial sum of the real and imaginary parts of the three components.

$$\text{Sum of Real Parts} = \underline{T} = \text{DWCR} + \text{CRCR} + \text{SWR}$$

$$\text{Sum of Imaginary Parts} = \underline{U} = \text{DWCI} + \text{GRCI} + \text{SWI}$$

The magnitude of the total field factor is then

$$\underline{\text{FIELD}} = R^2 + U^2$$

or, calculated in decibels* is

$$\underline{\text{FIELD}} = 10 \log_{10} T^2 + U^2$$

This value is printed out for vertical and horizontal polarization as well as these values divided by the distance. In effect, these values are the ratio of the field intensity at a given distance to that of free space at a unit distance, or E/E_0 , for each polarization.

* Decibels = $20 \log_{10} E_1$ when referred to one microvolt per meter, E,
being in the same units.

5. Description of Computer Programs for Field Strengths at a Distance of Several Wavelengths

A number of computer programs have been written in FORTRAN IV for the IBM 7054 (or 360) to calculate field strength patterns at a distance of several wavelengths (the radiation field) laterally to the power line. The Fortran statements for these programs are given at the end of this appendix. It was anticipated that by comparing the calculated with measured field strength patterns, the characteristic and a measure of the magnitude of the noise source or a secondary radiator could be made and a method derived for predicting the propagation from this source. All programs assume the noise source to be an elevated transmitter and only a single phase conductor of the power line and its image are considered. The earth is considered to be a flat plane with no discontinuities. The equations utilized were for the electric field, and the horizontal field calculated is that for the antenna perpendicular to the line, which is usually the direction giving the highest magnitude.

5.1 Simplified Propagation Calculation - Distance Variation

This program was written for initial experimentation to determine the gross rate of change of relative field strength for a long radiating conductor. Noise sources or the generating voltages are presumed distributed uniformly along the conductor, but the time lag between sources is considered to be zero. Unless otherwise "inputted", the program assumes a ground reflection factor of one with zero phase shift. A value other than one, either positive or negative to reflect a 180 degree phase shift of the reflected wave, may be "inputted". Distances at which the calculation is to start and to stop and the distance increment must be stipulated.

The following input cards with their respective format must be specified for each case:

- 1) Title card (any title of 71 characters or less; first space a blank).
- 2) Card specifying:
 - (a) conductor height in feet
 - (b) receiving antenna height above ground or its effective height if on the ground, in feet
 - (c) frequency in megacycles per second, and
 - (d) the reflection factor if other than plus one.

The Fortran format is as follows: 2F5.1, F9.3, F4.3.

3) Card specifying:

- (a) The distance at which the calculation starts,
- (b) at which it ends, and
- (c) the incremental distance to be taken, all in feet, the Fortran format being 3F8.1.

The output consists of the inputted title, the data of cards 2) and 3) and the vertical and horizontal field in dB with respect to a "per unit" source RF voltage at each distance as determined by the starting and ending distances and the specified increment.

As an experimental variation in one other auxiliary program, this program was modified to give only the real part of the field calculations.

6. Programs with Effect of Ground Conditions - Distance Profile Calculations

Two more detailed computer programs were developed to include the effect of ground conductivity and the dielectric constant upon the reflection factor and to include the surface wave component of the total propagation wave. Logic has been incorporated to print-out the surface wave component, and the other components as well as the reflection factors at each distance where the surface wave component is larger than one one-hundredth of the largest of the other components.

The first of the two programs considers the noise source as a dipole and utilizes Norton's general equation for elevated antennas (see later) which includes the cube of the cosine of the angle (cosine Ψ_1 , and cosine Ψ_2 in the earlier description) made by the ray line connecting the source with the receiving antenna, either directly or by reflection, with a horizontal line through the noise source. The second of the two programs utilizes a modification of Norton's equation with the square of the cosine of these angles, which is more applicable to a long radiating conductor.

The vertical field calculation of the first program was checked by comparing results from this program with those given in Figures 4, 5 and 6 of Gerks' paper (Ref. 49 of this Appendix).

The following input cards with their respective format must be specified for each case for either program.

1) Title card (any title of 71 characters or less; first space a blank).

2) Card specifying:

- (a) conductor height in feet
- (b) the receiving antenna height above ground; or its effective height, if on the ground, in feet

- (c) frequency in megacycles per second
- (d) the dielectric constant, and
- (e) the ground conductivity in milli-mhos per meter or millimho-meters per square meter. (See Table I.)

The Fortran format for this card is as follows: 2F5.1, F9.3, 2F7.1.

3) Card specifying

- (a) the starting distance (do not start with zero) in feet
- (b) the ending distance in feet
- (c) the distance increment in feet
- (d) a "flag" character, and
- (e) a value for the divergence factor.

The items (d) and (e) may be omitted.

If a character number is inputted for item (d) the result depends on which program is being used. In the case of the first program (using cube of cosines), a "flag" will set the cosines to one and eliminate the surface wave in the calculation of the total wave. A "flag" in the input to the second program will cause the reflection factor, the direct-, reflected- and surface-wave components to be printed out, at each distance and polarization. This second program also has the feature that should the surface-wave components be equal to or greater than one-hundredth of either the direct- or reflected- waves, these calculated data will be printed out.

(A modification of the first program was also written, for check purposes, that prints out these data and certain other calculation values without the necessary flag or size requirements.)

TABLE I
GROUND CONSTANTS

<u>Type</u>	<u>Dielectric Constant</u>	<u>Ground Conductivity</u> (Millimho-meters/square meter)
Sea Water	81	3000 to 5000
Fresh Water	81	10 to 1
Wet Earth	5 to 30	100 to 1
Dry Earth	2 to 5	0.1 to 0.01

(Taken from Reference 88 of this Appendix. Other authors give other values; for example, Reference 49 gives for sea water: ϵ of 80 and σ of 4000; for "good soil": ϵ of 30 and σ of 20 (the value used in the calculation of the accompanying curves); for "poor soil": ϵ of 4 and σ of 1. Reference 23 tabulates measured values for various locations in the United States.)

7. Height Variation Calculations

Two programs were written based on the equations previously described to calculate the variation in field as antenna height is varied at a given distance from the transmission line. Inputted data is somewhat similar to that for the distance profile calculations except for Input Card 2 gives

- (a) conductor height in feet
- (b) distance from line in feet
- (c) the dielectric constant, and
- (d) the ground conductivity

with Format F5.1, F8.1, 2F7.1; and Input Card 3 gives

- (a) frequency in megacycles per second
- (b) antenna height to which calculation is to be made
- (c) height interval at which each calculation is to be made
- (d) a "flag" if components and reflection factors are to be printed out.

Calculations start at a zero antenna height and proceed to the height indicated on Card 3. Format for Card 3 is: F9.1, 2F7.1, I2.

8. Near Field Program

The calculations of the near and radiated fields have been incorporated in separate programs in order to facilitate computation.

The near field is calculated for a vertical antenna on the basis of a vertical dipole transmitter and its reflection or image under perfect ground conditions. Heights of the two antenna heights must be specified as well as distances over which the calculation is to be made. Also printed out is the direct- and reflected- wave components $1/fd$, $1/(fd)^2$, and $1/(fd)^3$ and their vector sum as given by

$$\sqrt{\left[\frac{1}{(fd)^3} - \frac{1}{fd} \right]^2 + \left[\frac{1}{(fd)^2} \right]^2}$$

in decibels above one microvolt.

Input to this program consists of the following cards:

- 1) Title card (any title of 71 characters or less; first space a blank).

2) Card specifying:

- (a) conductor height in feet
- (b) antenna height in feet
- (c) frequency in megacycles per second.

Format is 2F5.1, F9.3.

3) Card specifying:

- (a) distance at which calculation is to start in feet
- (b) distance to which calculation is to be taken in feet
- (c) distance interval at which calculations are to be made in feet.

Format is 3F8.1.

9. Conclusions from Comparisons of Computer Results of Lateral Profiles

A comparison of calculated profiles is made with chart recording measurements at 30, 50, and 90 Mc/s on Figs. 4 through 9, taken with the antennas mounted on the instrument van while an artificial gap was hung on the transmission line. The following conclusions can be drawn:

9.1 All profiles measured with the horizontal antenna 20 feet above ground exhibit oscillations of at most about 10 dB in magnitude (peak to minimum), which have not been reproduced in the calculations and could be attributable to contributions from the other line conductors, which are not taken into account in the equations. However, the major trend of the shape of the profiles, including large dips in the field strength, have been matched by calculations using the modification of the Norton equation. The best match, including the large dips, occurs if the calculation is made as if the gap were hung on the center phase, rather than the nearest outside phase.

At 30 and 50 Mc/s, calculations using the conductor height at the tower the best match; at 90 Mc/s, the height at midspan gives the best.

In the length of 80 to 200 feet, the profile, both measured (except with 10 dB oscillations) and calculated, is fairly flat, and the profile beyond this distance toward 1000 feet slopes off to $1/d^2$ for these three frequencies.

9.2 Profiles measured with the vertical antenna 20 feet above ground exhibit little of the minor oscillations noted above. This profile appears to be matched best, except for the major dips at 90 Mc/s, predicted by the modified equation, by the Norton equation for a dipole transmitting antenna. Attenuation out to 1000 feet is about as $1/d$ for the vertical antenna.

9.3 Based on the above, the computation methods appear adequate if the Norton equation is used for the vertical antenna and the modification of this equation for the horizontal dipole.

10. Description of Computer-Calculated Attenuation Curves

Figures 10 through 26 are calculated distance attenuation curves for frequencies from 0.96 to 983.04 Mc/s from 200 feet to 100,000 feet. Attenuation has been calculated for vertical antennas for this range of frequencies and for the horizontal tuned dipole perpendicular to the transmission line for frequencies 30.72 to 983.04 Mc/s for a combination of conductor and antenna heights spanning those values of interest. As indicated previously, ground dielectric of 30 and a conductivity of 90 milli-mho meters per meter square was assumed. The calculations do not reflect the minor oscillations noted previously as apparently due to other phase conductors.

As frequency is increased the interaction between the direct- and ground-reflected-waves become more pronounced, so that prominent minimum points appear in the curves, as indicated by Fig. 16 for 30.72 Mc/s. As indicated on this figure, and as has been noted from the calculations for other frequencies, a trend line along the crests between these minimum points follows the inverse distance relationship. This fact has been utilized in all the following attenuation curves, and the curves drawn to reflect the crest values as given by the line labeled "approximate" and as a basis for determining the reference value at 200 foot distance. Thus, as may be noted in Fig. 16 for 30.72 Mc/s, values for any given curve may be below this "approximate" base value at 200 feet, but the method is more appropriate for establishing attenuation over the range of distance. In some cases, the levels of noise near the line may be large enough to permit the use of a reference distance greater than 200 feet. In other cases, the level may be so low that closer distances must be used to establish an adequate reference level, and the curves should be extrapolated as appropriate.

Also, comparisons of attenuation between the lower antenna height of 10 feet or with this height and higher heights should not be made since in most instances the curves for 10 foot antenna height have been appreciably shifted to establish a starting point of 0 dB at 300 feet.

Depending on frequency and the combination of conductor and antenna heights, at some point in distance the calculated attenuation changes from the trend of inverse distance to the inverse-distance-squared relationship. The curves are, therefore, an aid in determining where this change takes place.

At 0.96 Mc/s the attenuation of the calculated radiation field for the vertical 3 ft. antenna is very nearly as the inverse distance relationship (Fig. 10) from 200 to 100,000 feet, being about 3 dB below the value given by this relation, with respect to 200; at 100,000 foot distance. Below 0.96 Mc/s and beyond a distance of the wavelength divided by the attenuation is also for all practical purposes inversely

with distance for the conductor heights of interest here. However, at distances less than this limiting value the induction and near field terms assume greater importance. Figures 27 through 29 give curves of attenuation as calculated by the vector sum of the inverse; inverse-square; and the inverse-cubed distance again related to a distance of 200 feet, and are an aid in determining the distance at which the attenuation changes its rate.

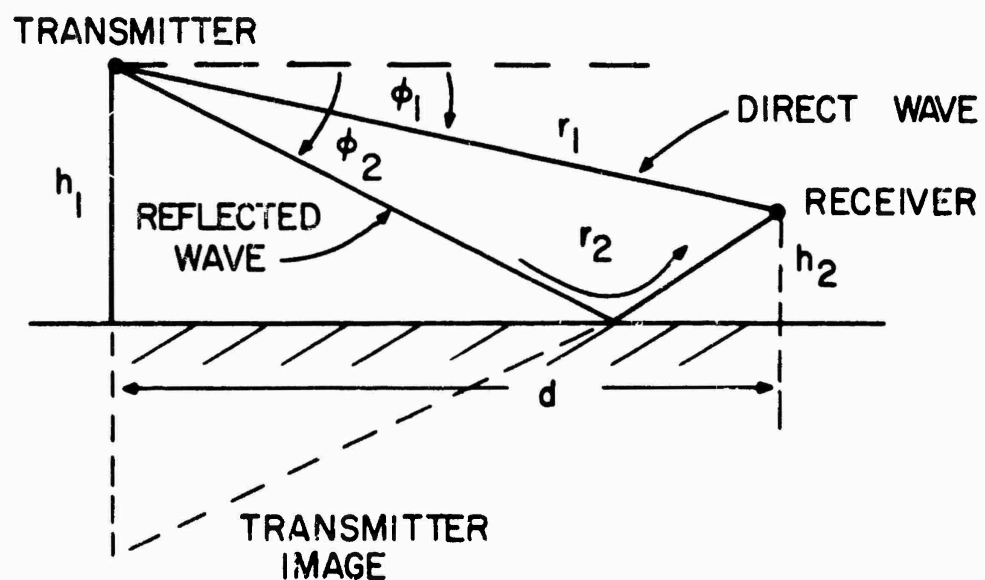


FIG. 1a ILLUSTRATIONS OF QUANTITIES USED IN PROPAGATION EQUATIONS

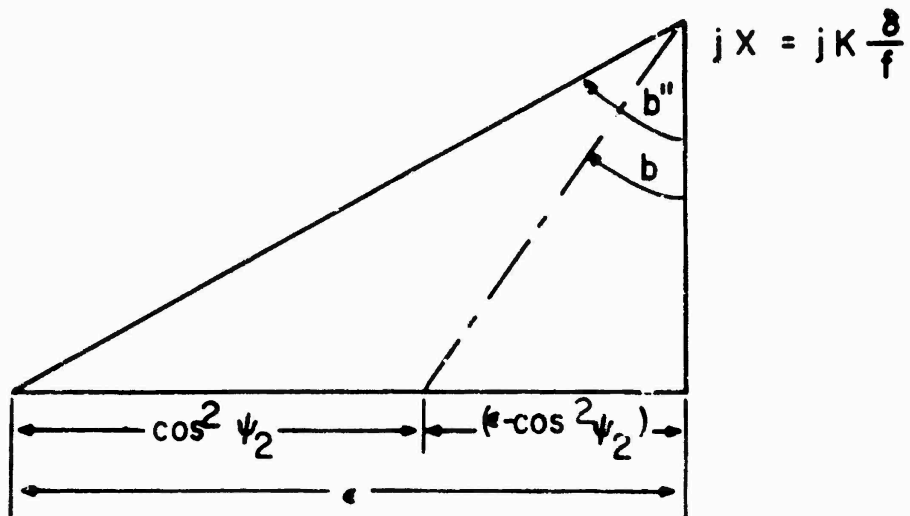


FIG. 1b ILLUSTRATION OF RELATION BETWEEN QUANTITIES SPECIFYING GROUND CONDITIONS

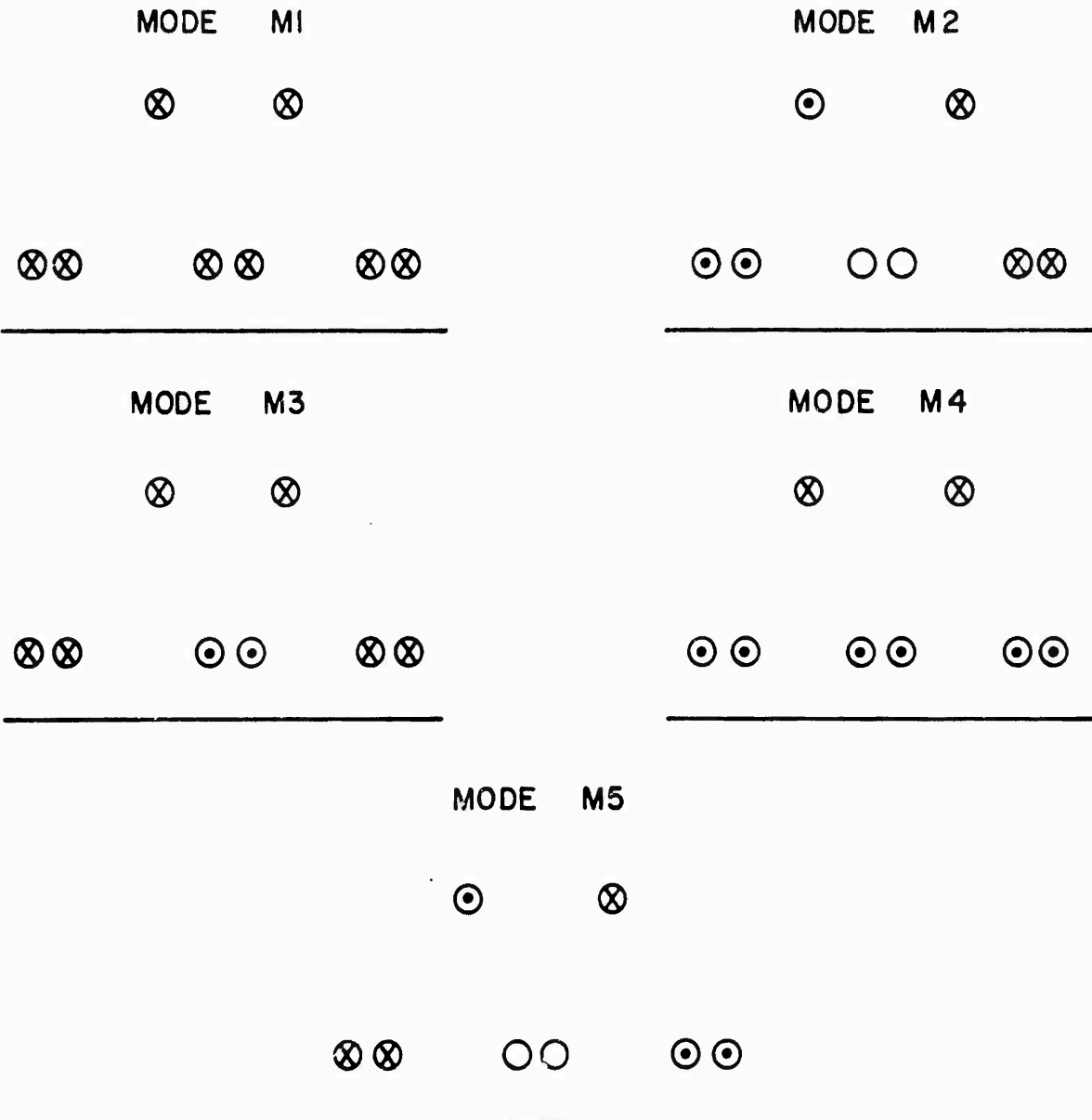


FIG. 2 GRAPHIC RELATIONSHIPS BETWEEN DIRECTIONS OF CURRENTS (OR VOLTAGE POLARITIES) FOR THE MODAL SETS.

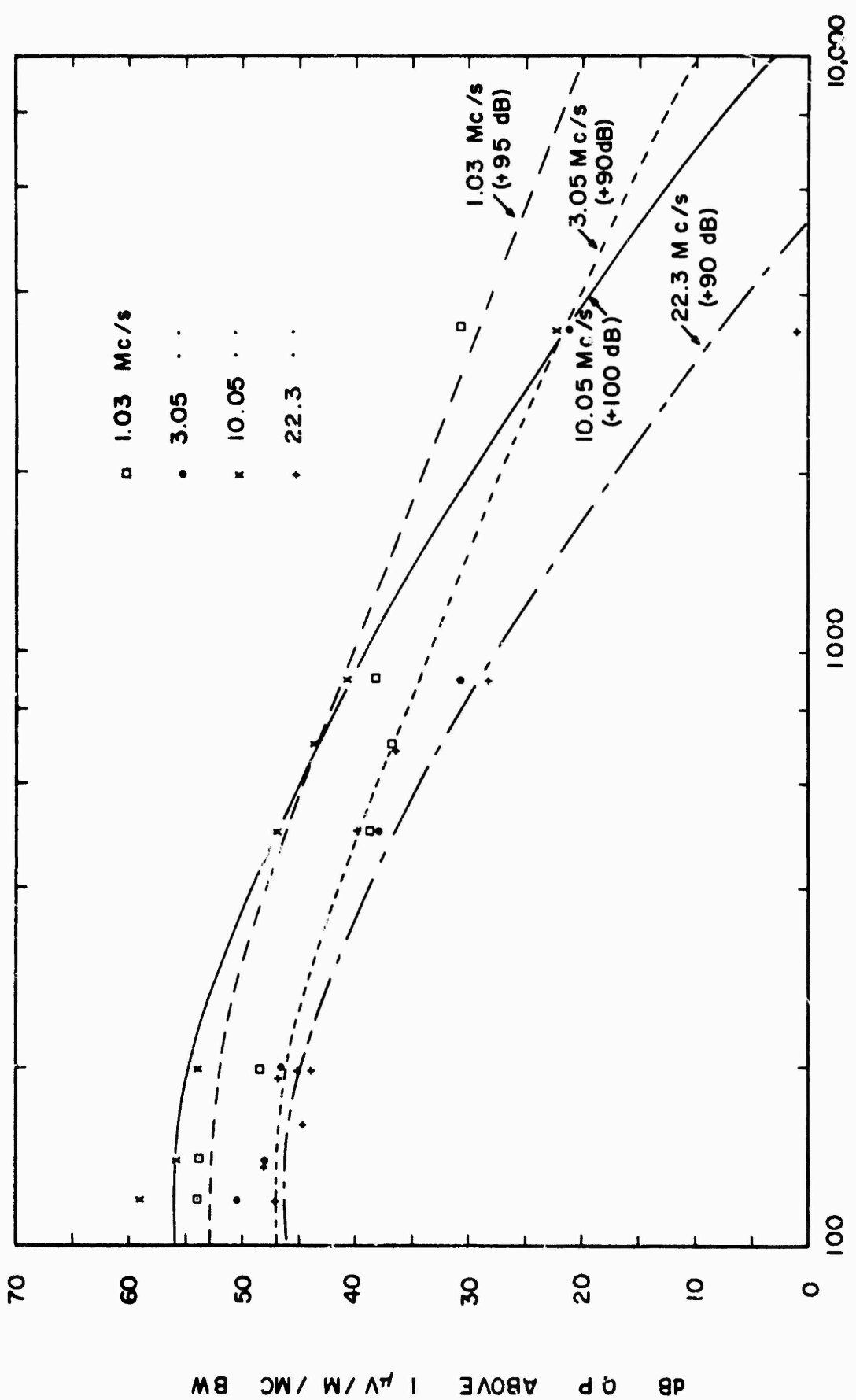


FIG. 3 GAP ON 345 KV LINE VERTICAL ANTENNA NORTON'S DIPOLE EQ'N
COMPARISONS OF MEASURED AND CALCULATED

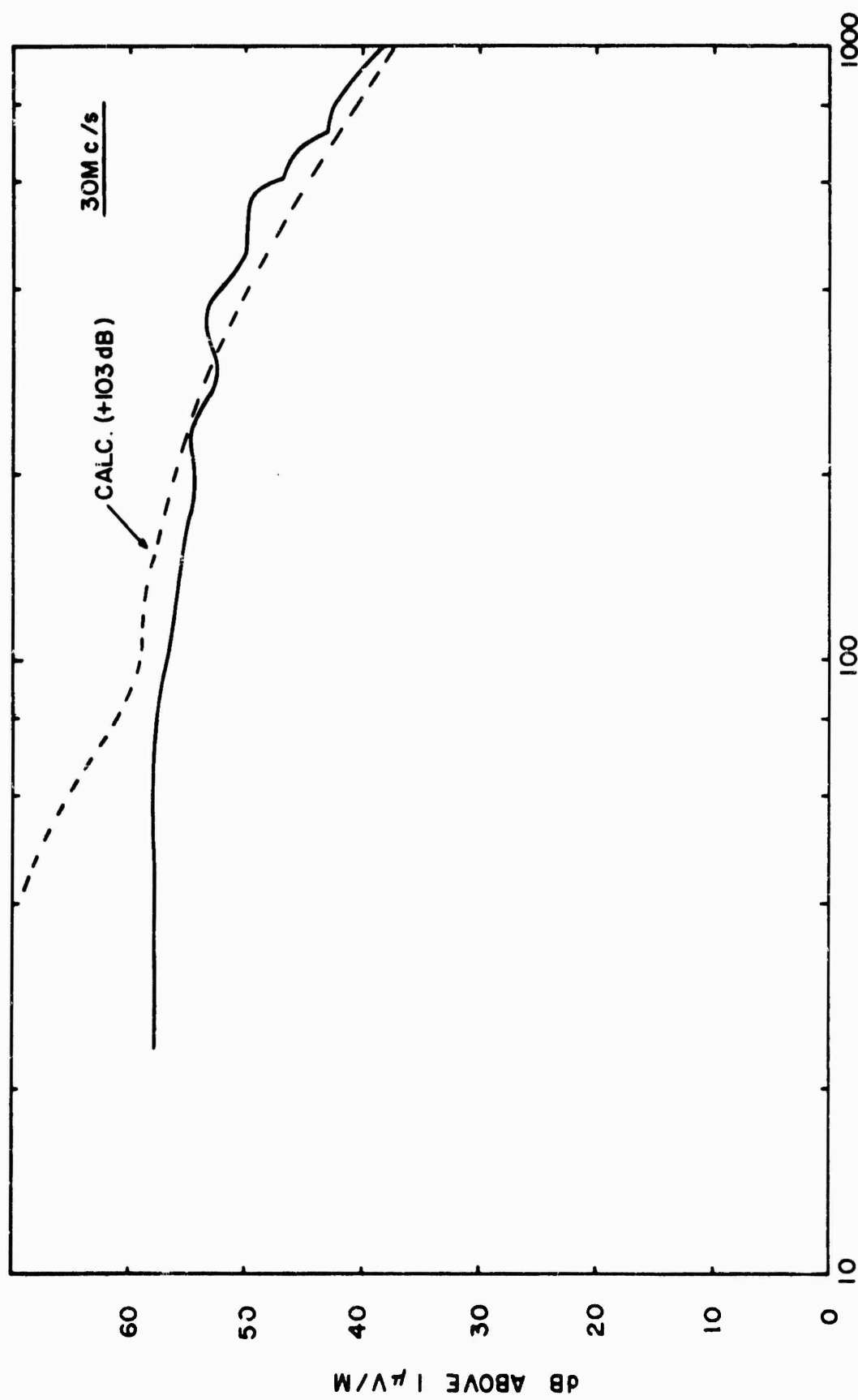


FIG. 4 LATERAL PERPENDICULAR TO TOWER 119 WITH ARTIFICIAL GAP.
 VERTICAL TUNED DIPOLE ANTENNA. COMPARISONS OF MEASURED AND CALCULATED.
 EQ'N FOR VERTICAL DIPOLE.

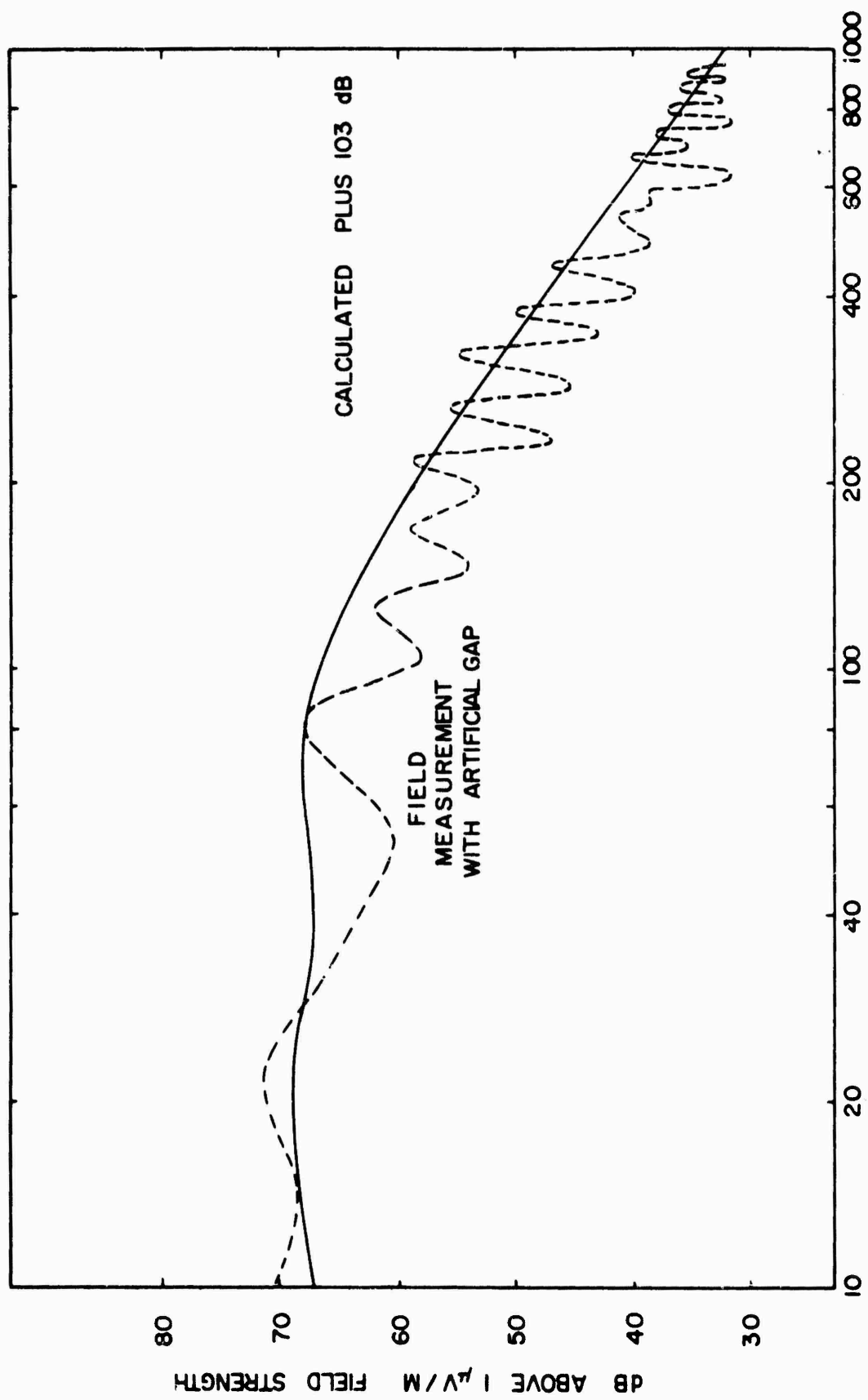


FIG. 5 HORIZONTAL FIELD 30 Mc/s. 42' CONDUCTOR HT. 20' ANTENNA HT. COMPARISON OF MEASURED AND CALCULATED WITH MODIFIED NORTON EQN.

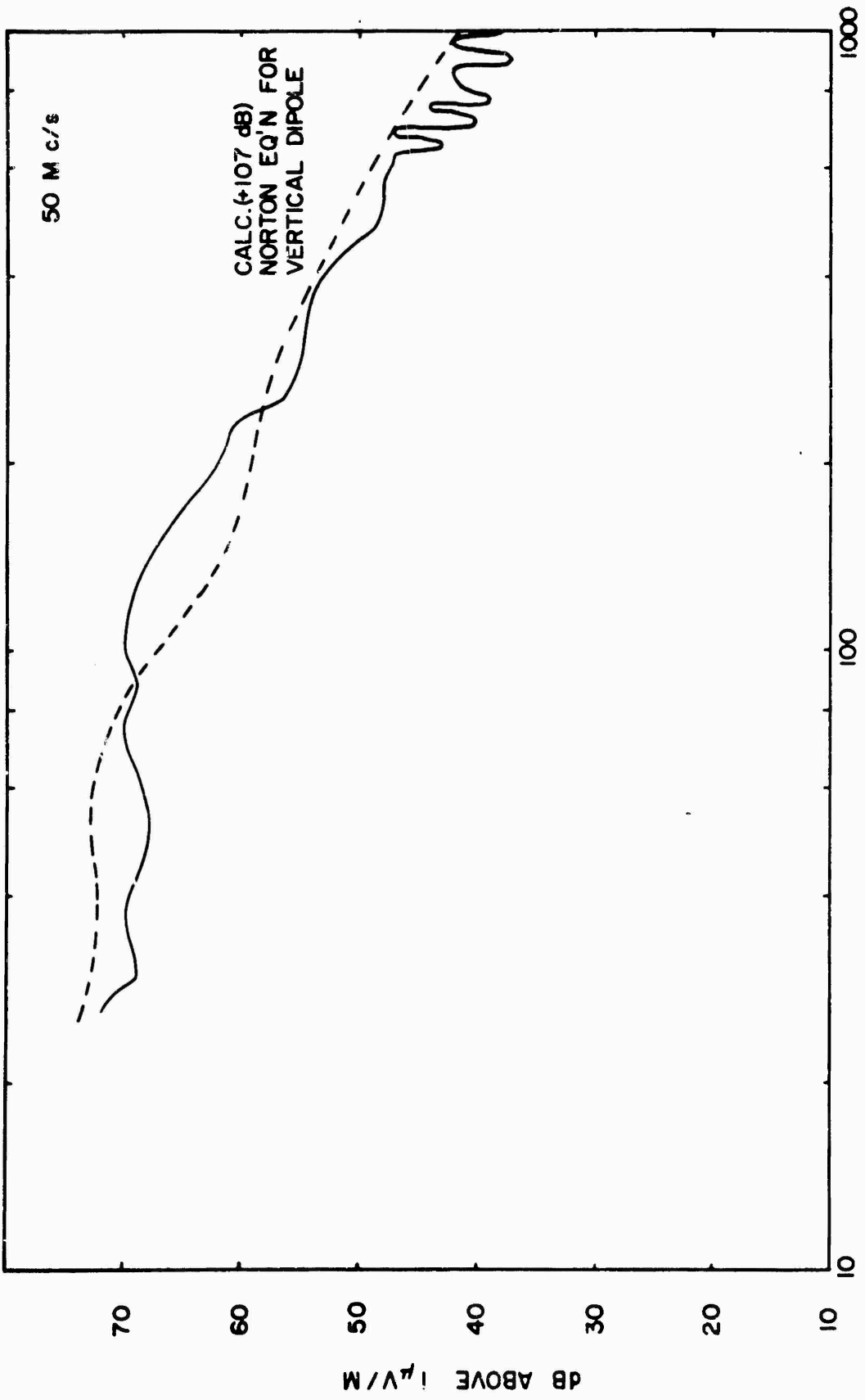


FIG. 6 LATERALS PERPENDICULAR TO TOWER 19 WITH ARTIFICIAL GAP (FREQUENCY 50 Mc/s)
ANTENNA VERTICAL TUNED DIPOLE. COMPARISON OF MEASURED AND CALCULATED

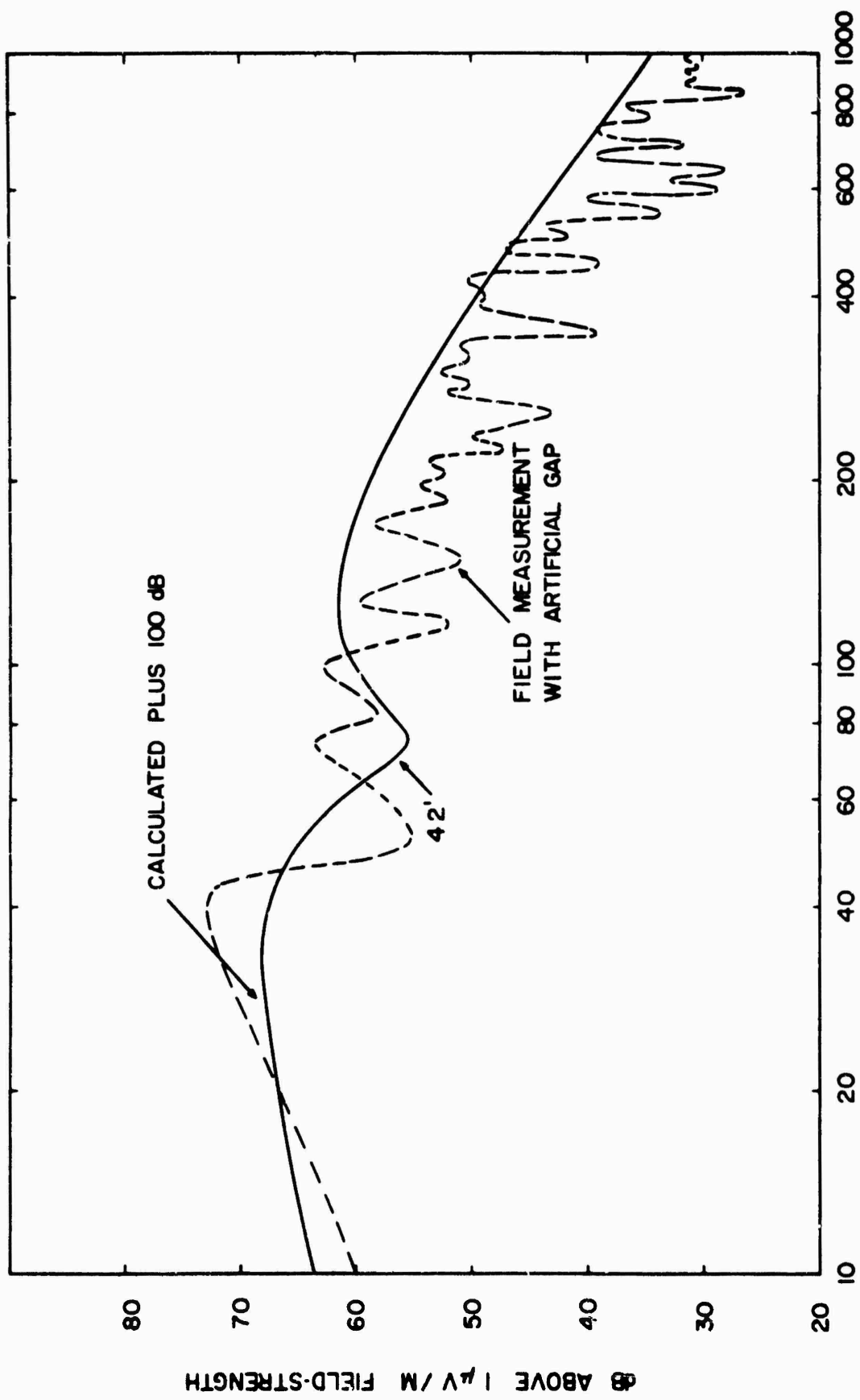


FIG. 7 HORIZONTAL FIELD 50 Mc/s. 20 FT ANTENNA HT. COMPARISON OF MEASURED AND CALCULATED WITH MODIFIED NORTON EQN.

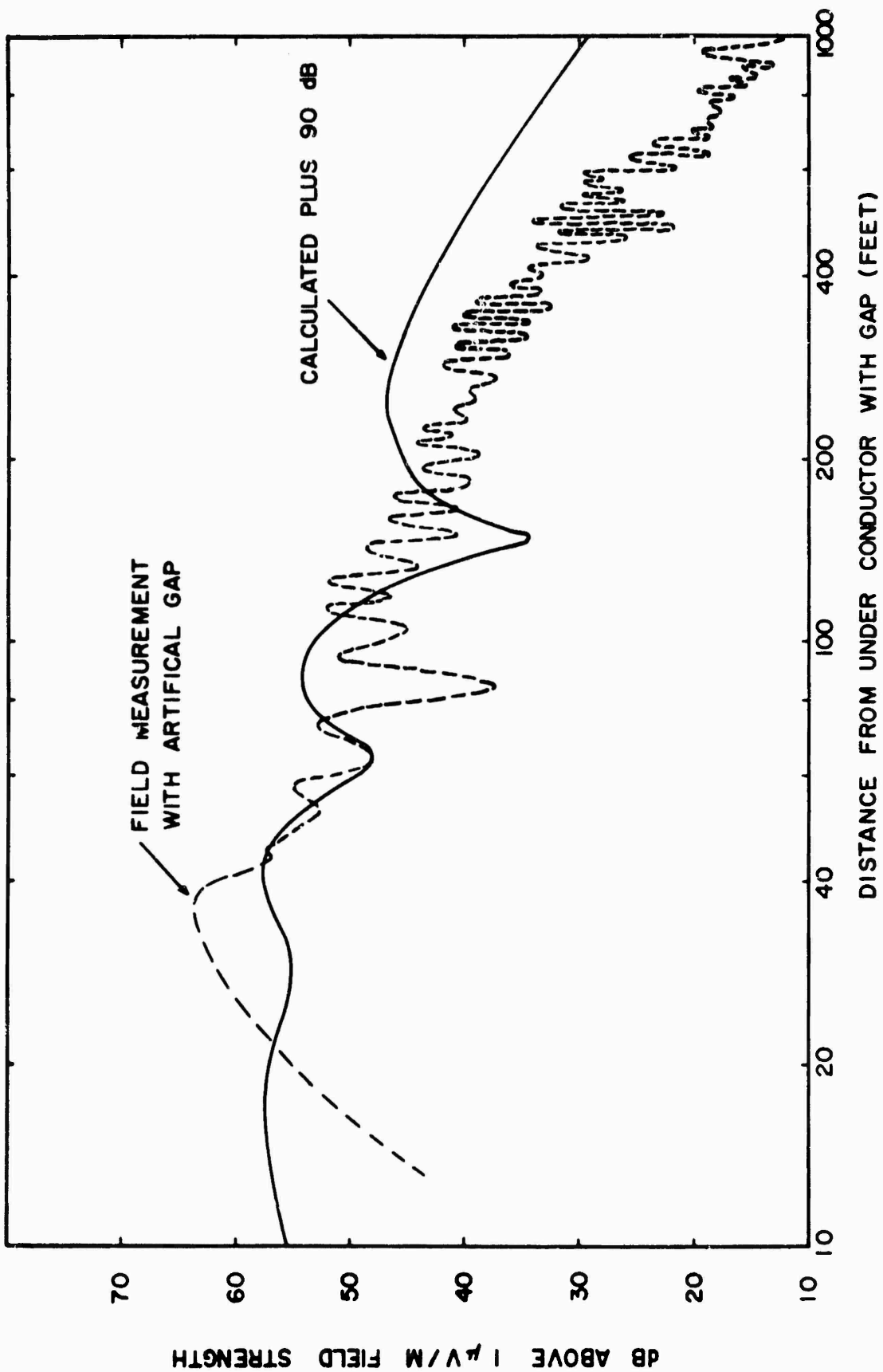


FIG. 6.8 HORIZONTAL FIELD 90 M c/s. COMPARISON OF MEASURED AND CALCULATED WITH NORTONS MODIFIED EQ'N. 20' ANTENNA HT.

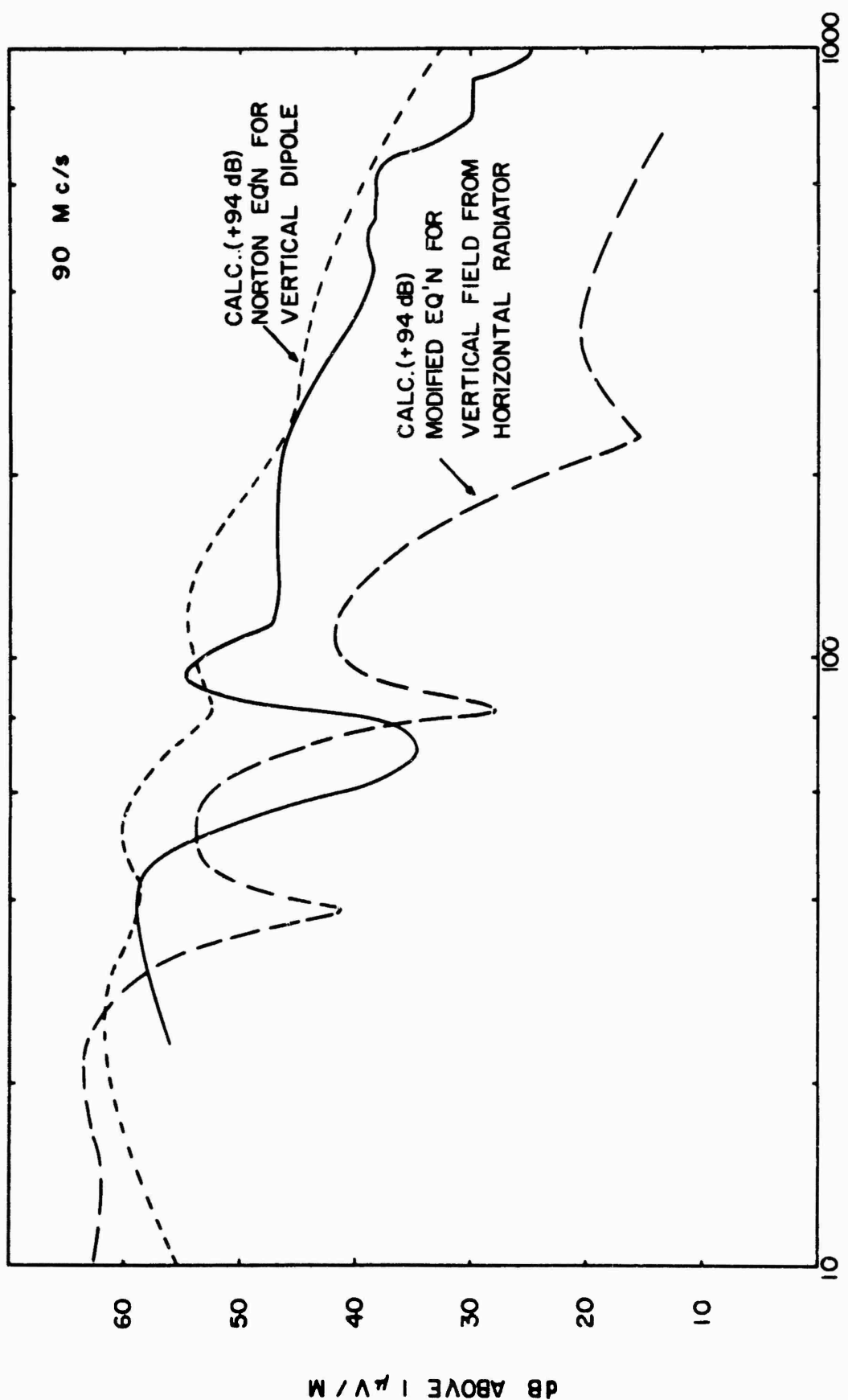


FIG 9 LATERALS PERPENDICULAR TO TOWER 119 WITH ARTIFICIAL GAP. (FREQUENCY 90M c/s)
ANTENNA VERTICAL DIPOLE. COMPARISON OF MEASURED AND CALCULATED

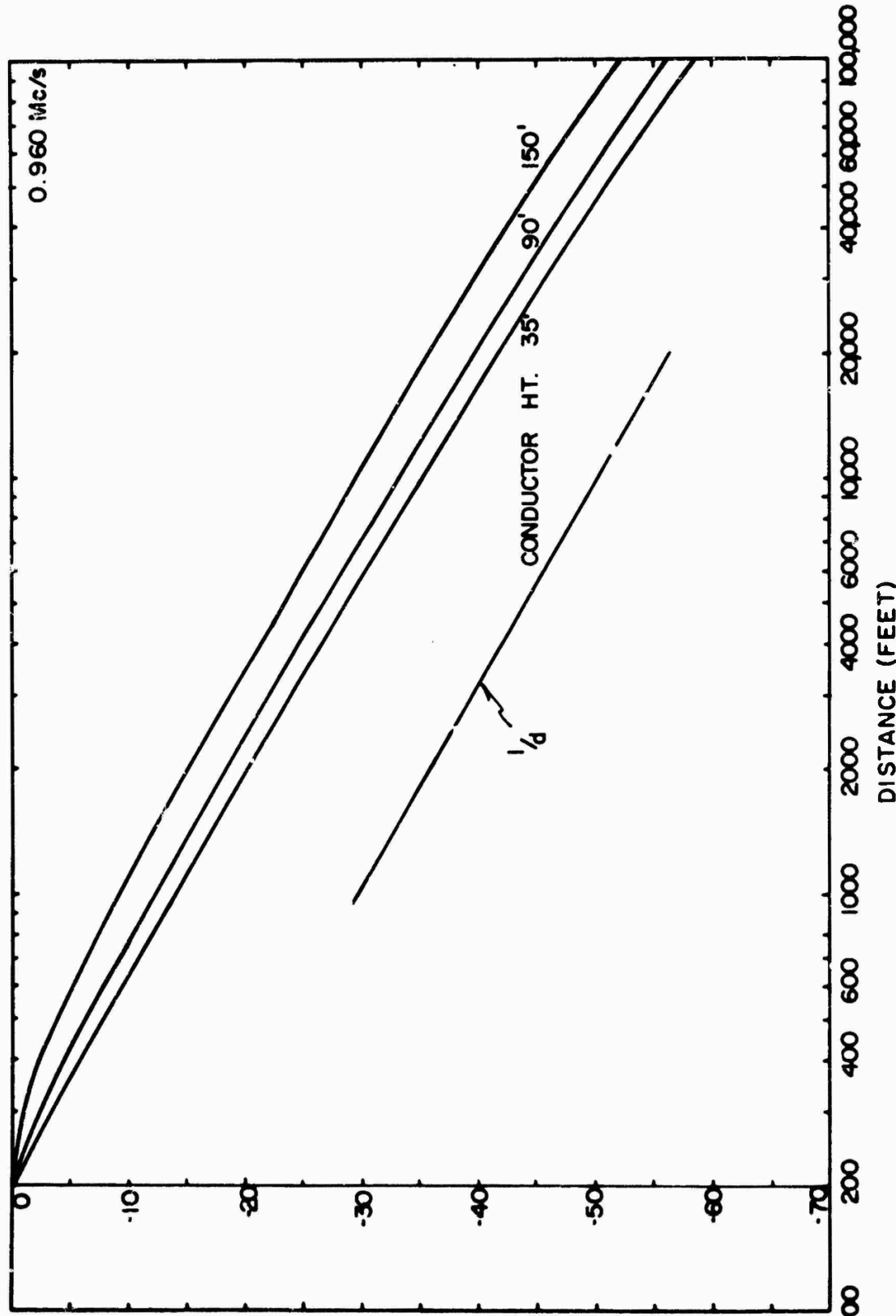


FIG. 10 ATTENUATION OF FIELD WITH DISTANCE FOR 3 FT.
VERTICAL ANTENNA AT 0.960 Mc/s

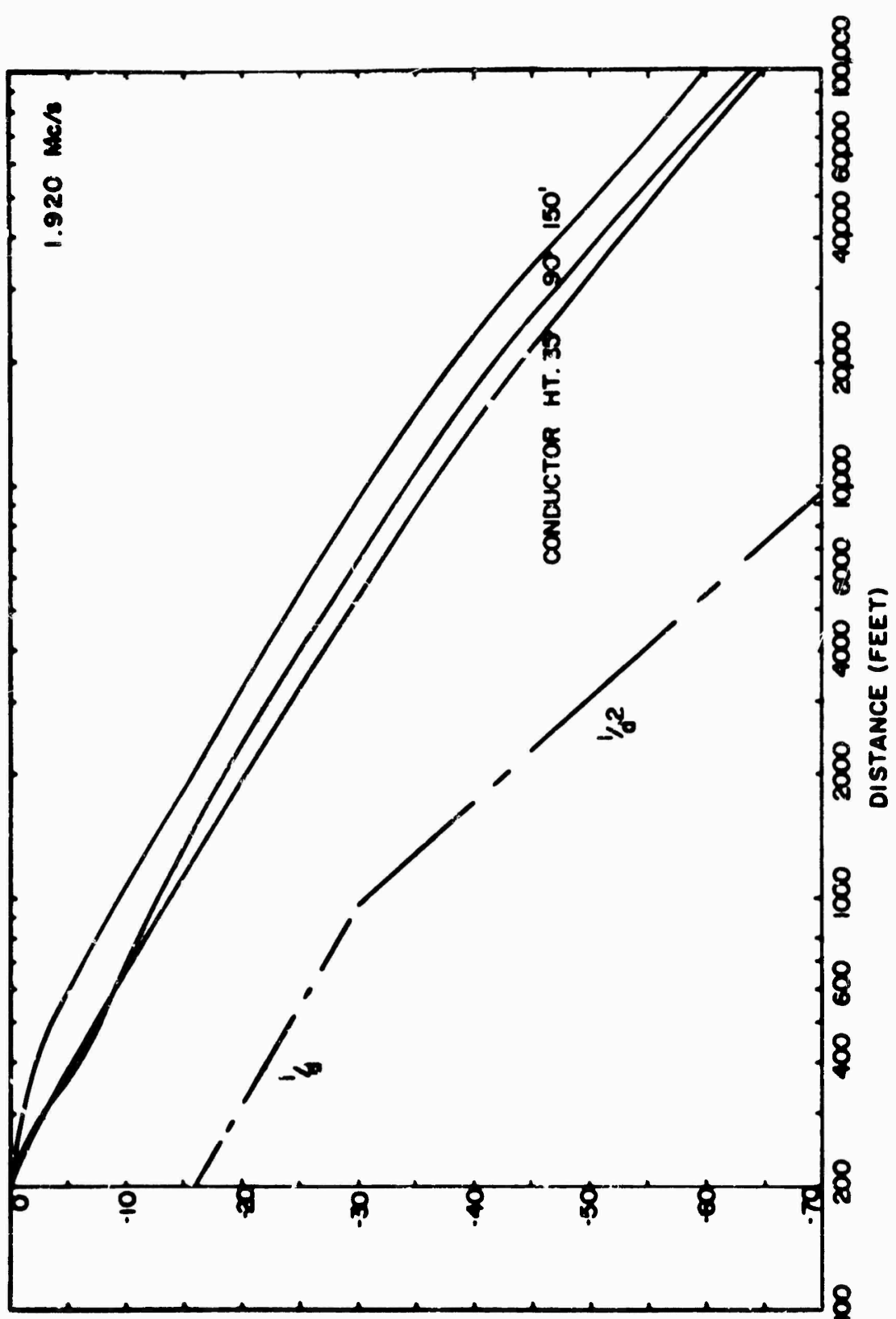


FIG. II ATTENUATION OF FIELD WITH DISTANCE FOR 3 FT.
VERTICAL ANTENNA AT 1.920 Mc/s.

ATTENUATION RELATIVE TO 200 (dB)

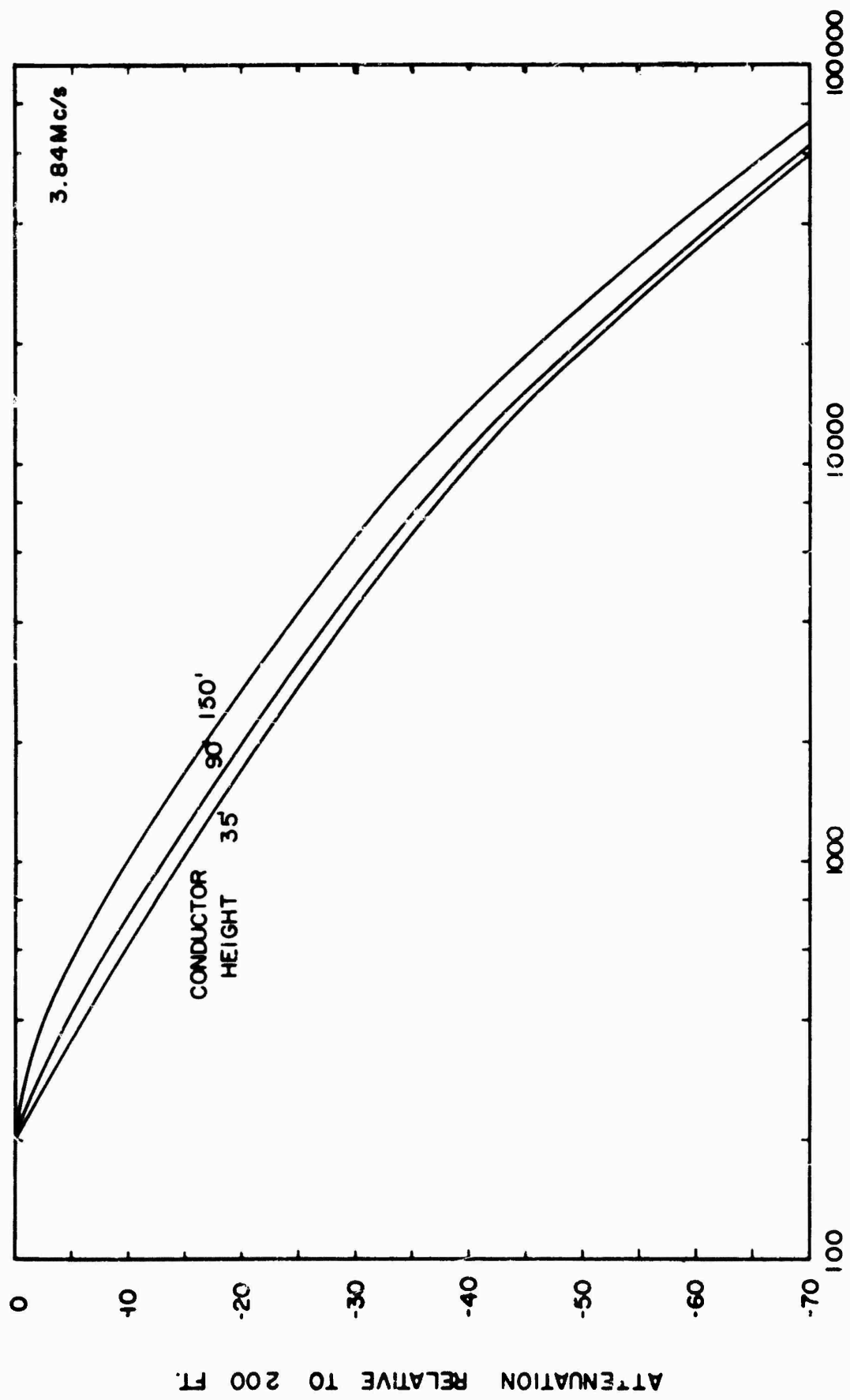


FIG. 12 ATTENUATION OF FIELD WITH DISTANCE FOR VERTICAL ANTENNA 3.84 Mc/s

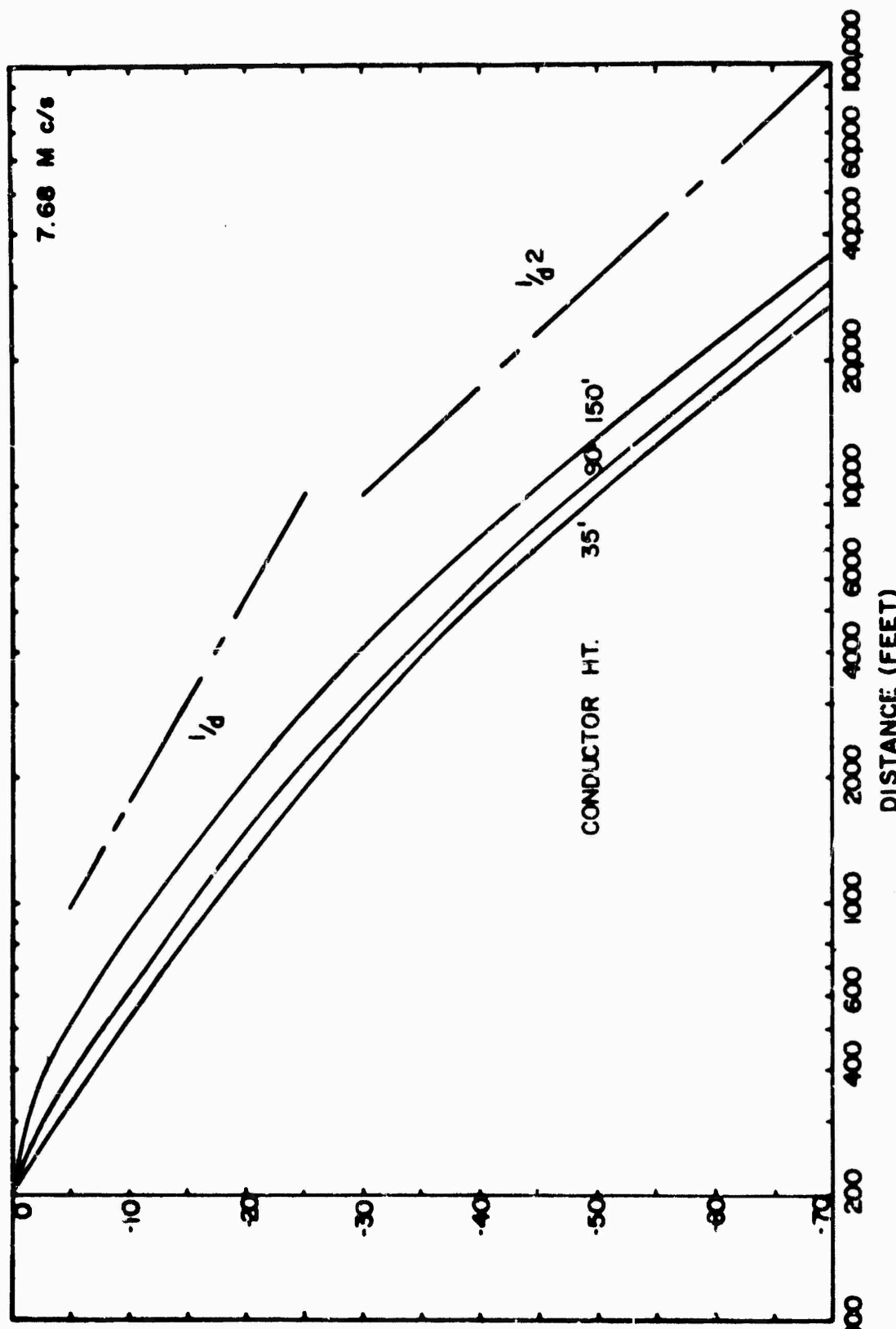


FIG. 13, ATTENUATION OF FIELD WITH DISTANCE FOR 3 FT
VERTICAL ANTENNA AT 7.68 M c/s

ATTENUATION RELATIVE TO 200, (dB)

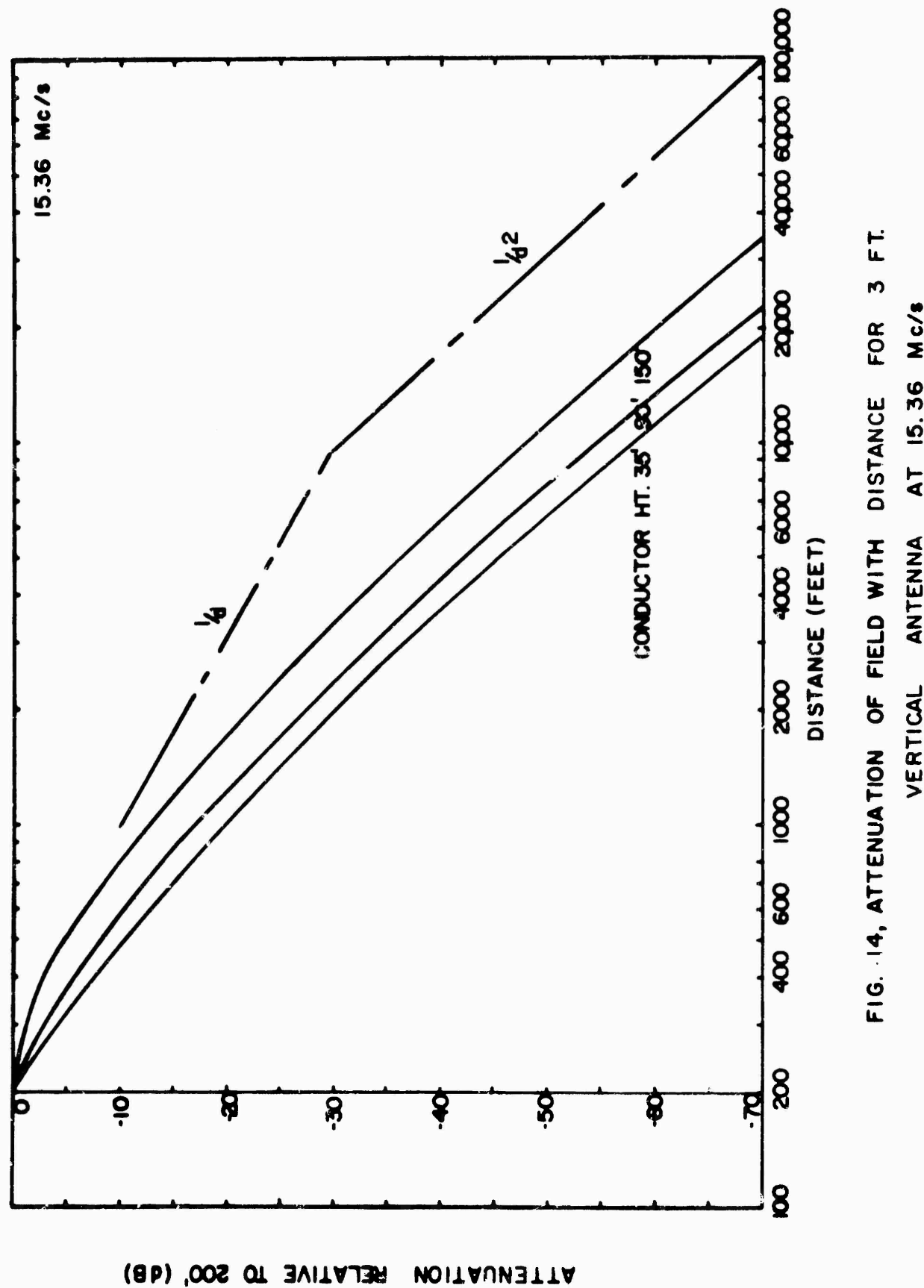


FIG. 14, ATTENUATION OF FIELD WITH DISTANCE FOR 3 FT.
VERTICAL ANTENNA AT 15.36 Mc/s

ATTENUATION RELATIVE TO 200, (dB)

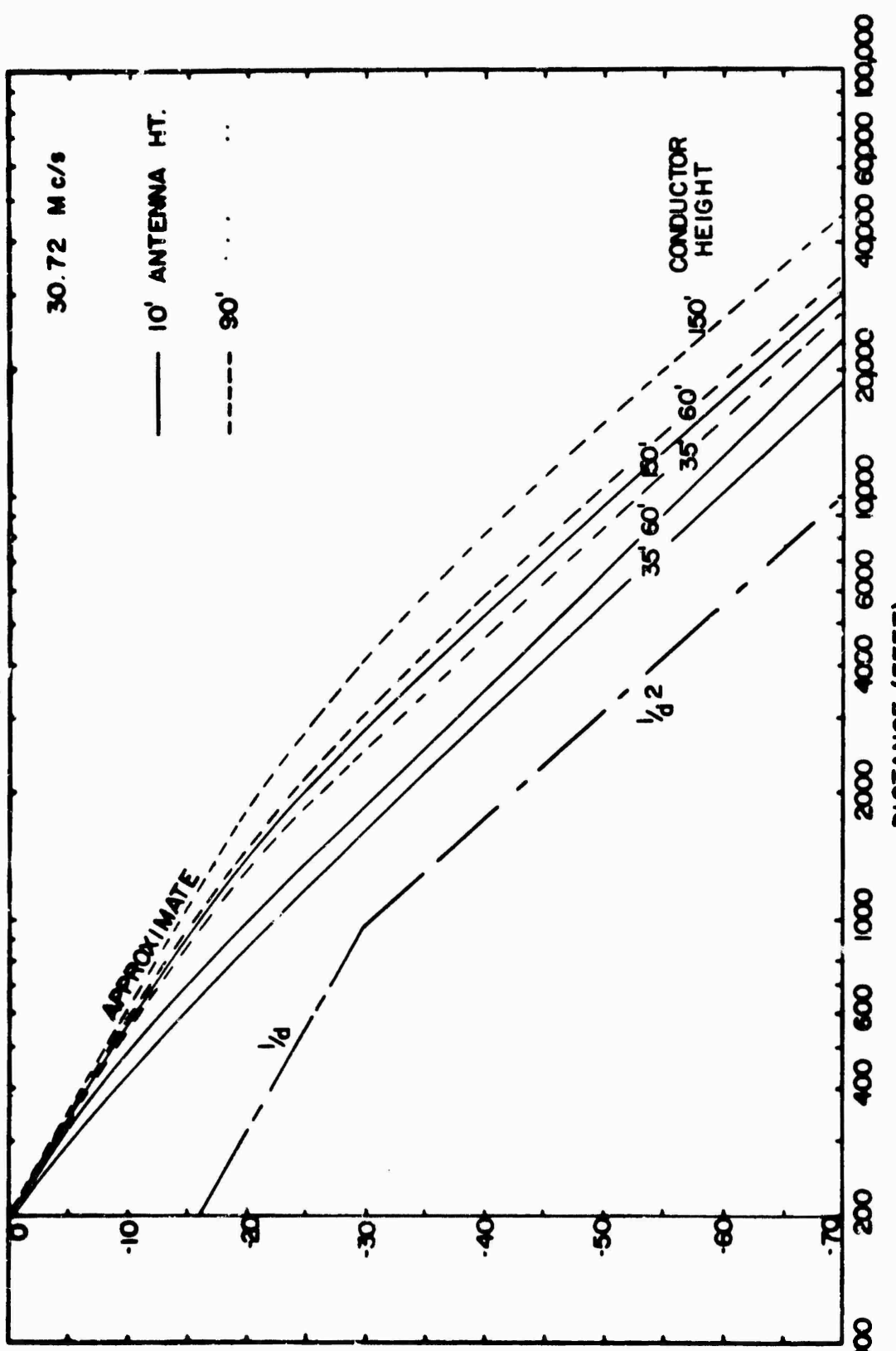


FIG. 15, ATTENUATION OF FIELD WITH DISTANCE FOR VERTICAL DIPOLE AT 30.72 Mc/s

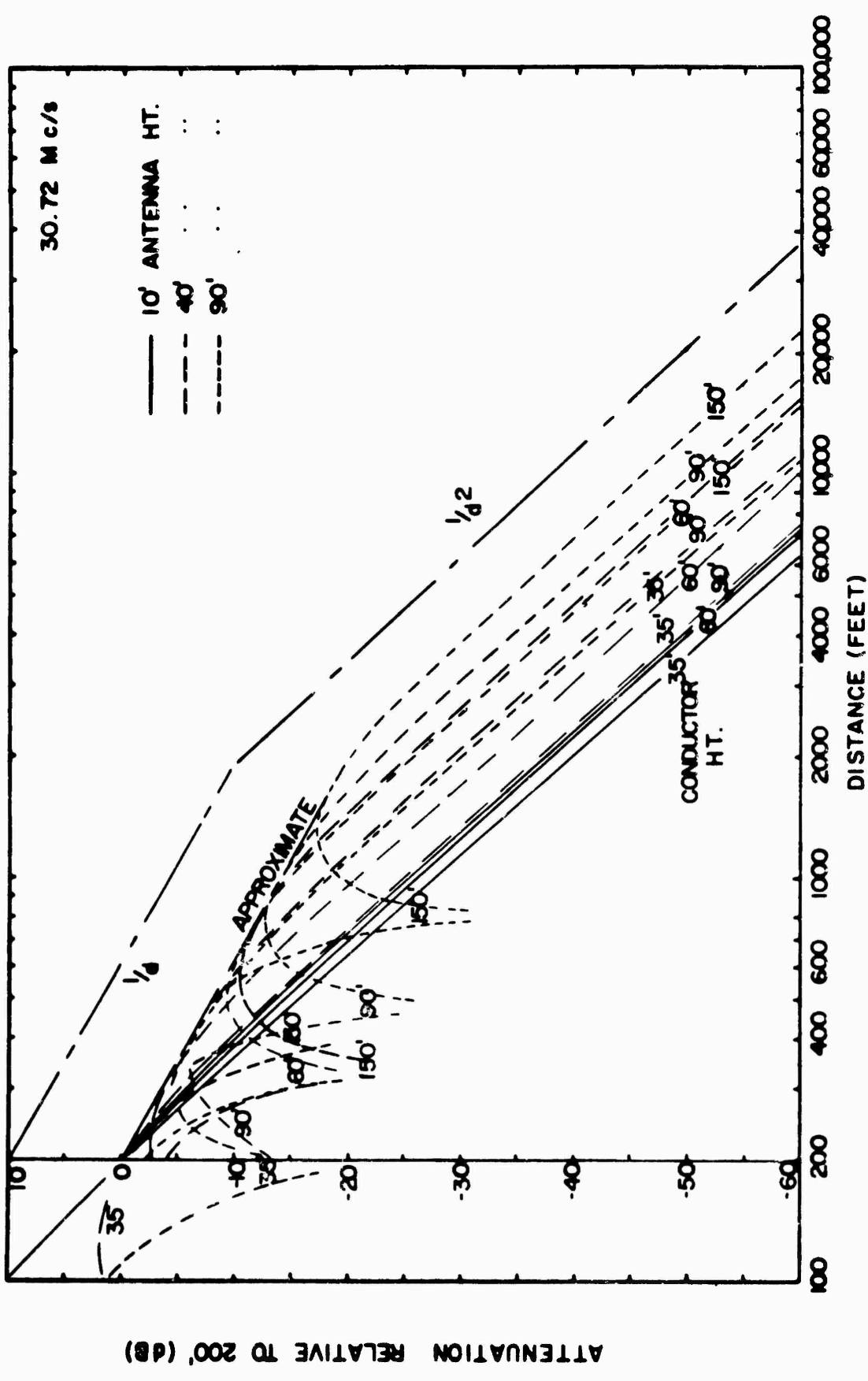


FIG. 16, ATTENUATION OF FIELD WITH HORIZONTAL DIPOLE
PERPENDICULAR TO LINE AT 30.72 Mc/s

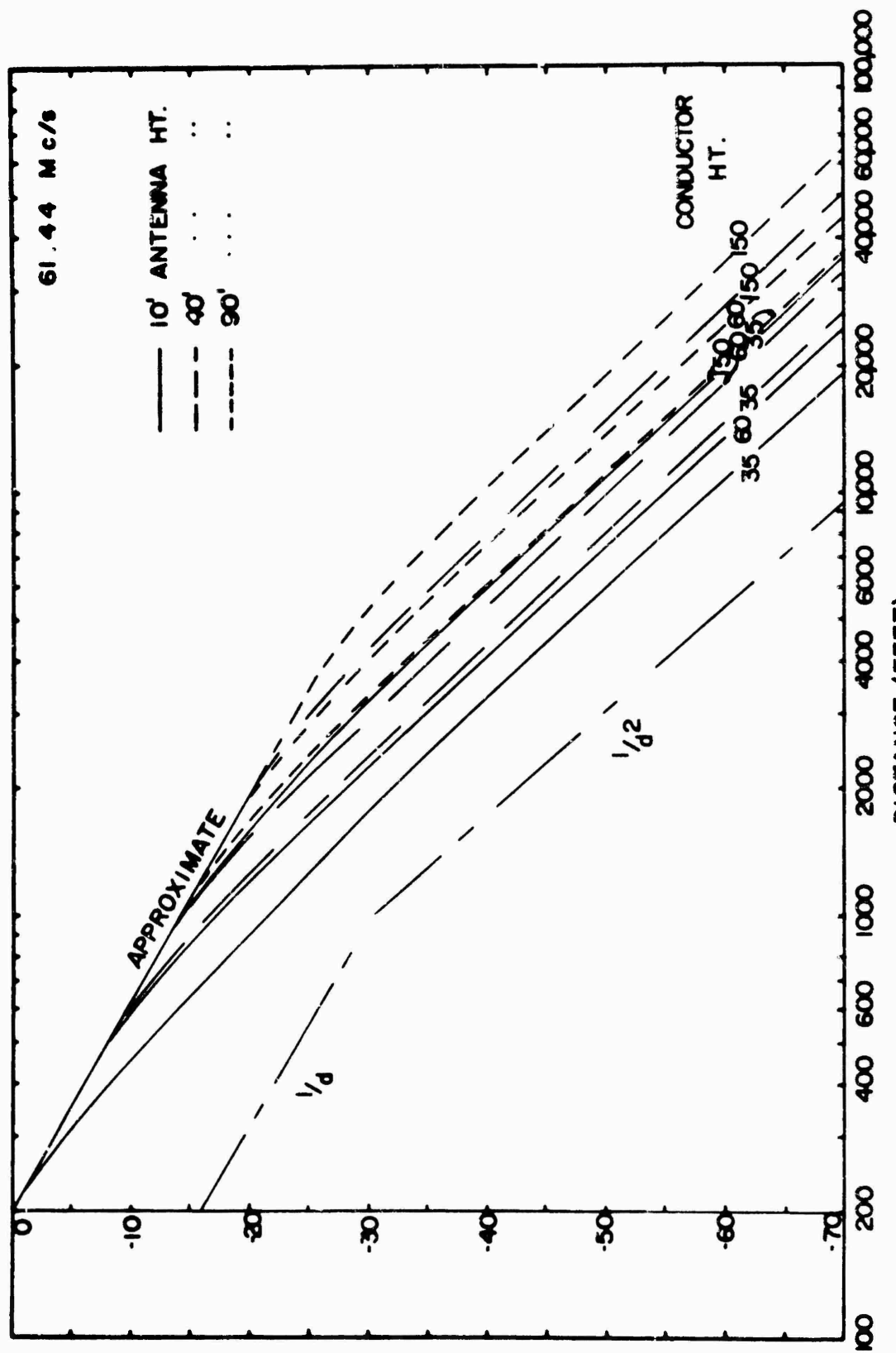
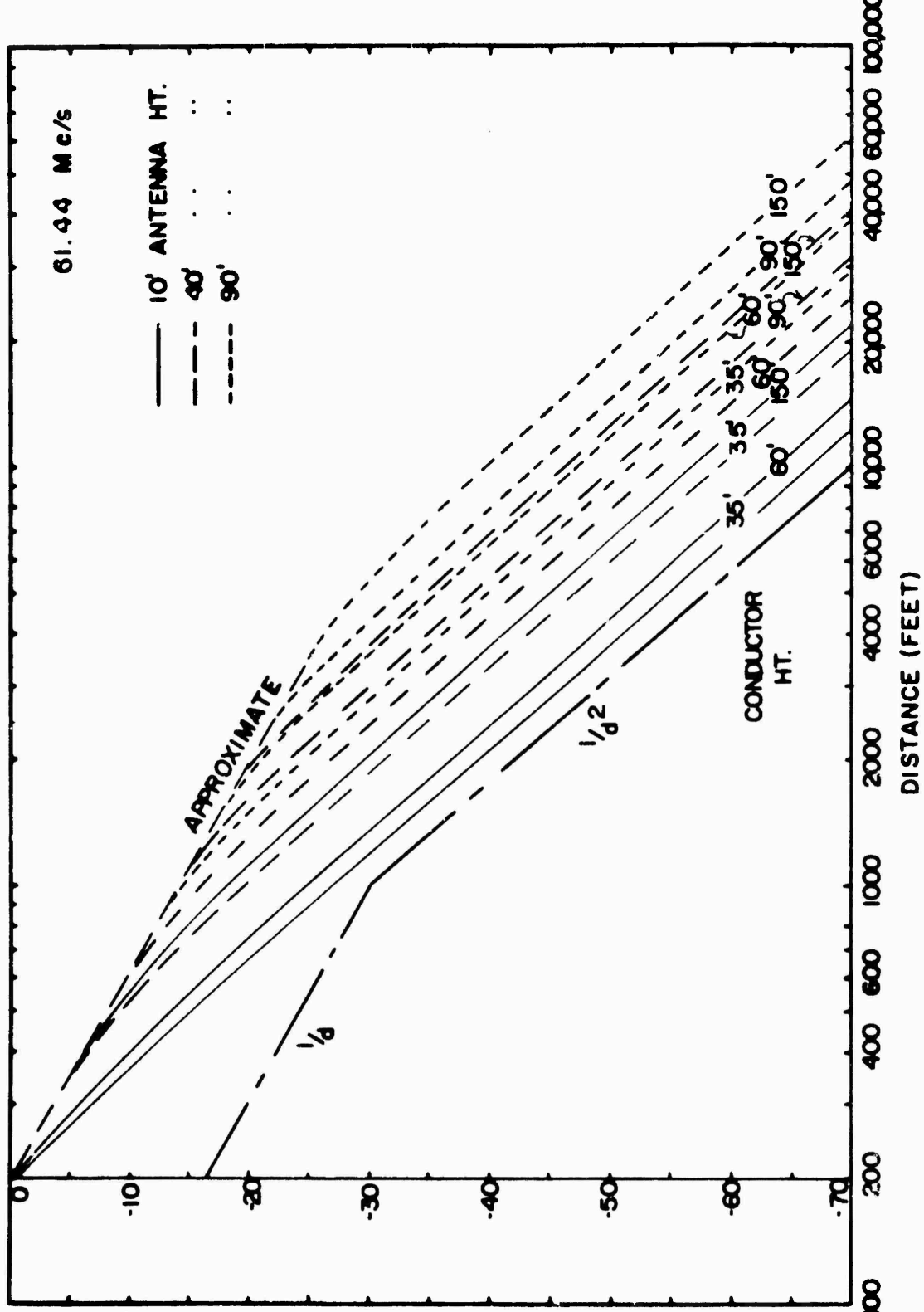


FIG. 17, ATTENUATION OF FIELD WITH DISTANCE FOR VERTICAL
DIPOLE AT 61.44 Mc/s



ATTENUATION RELATIVE TO 200^(dB)

FIG. 18 ATTENUATION OF FIELD WITH DISTANCE FOR HORIZONTAL DIPOLE
PERPENDICULAR TO LINE AT 61.44 Mc/s

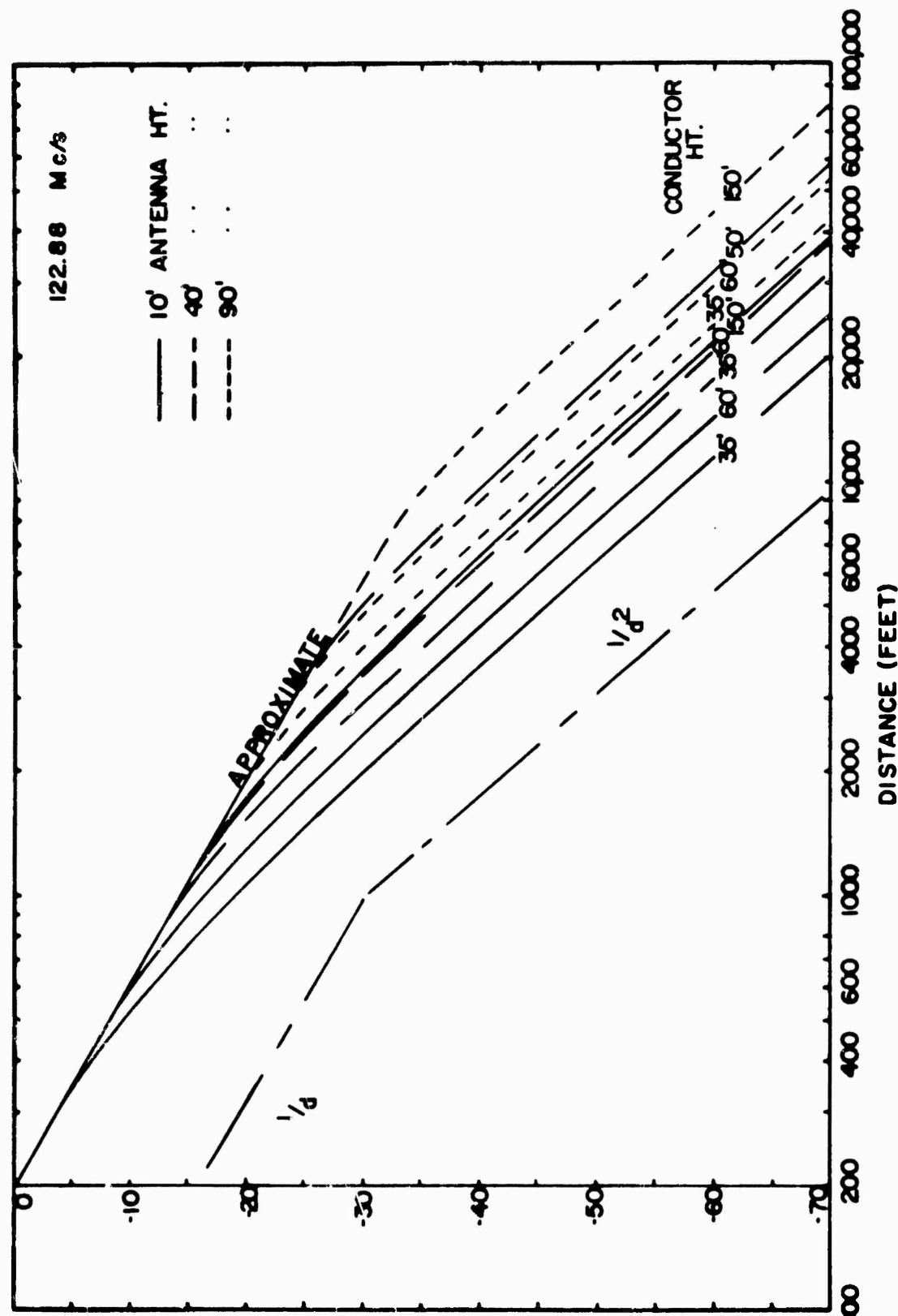
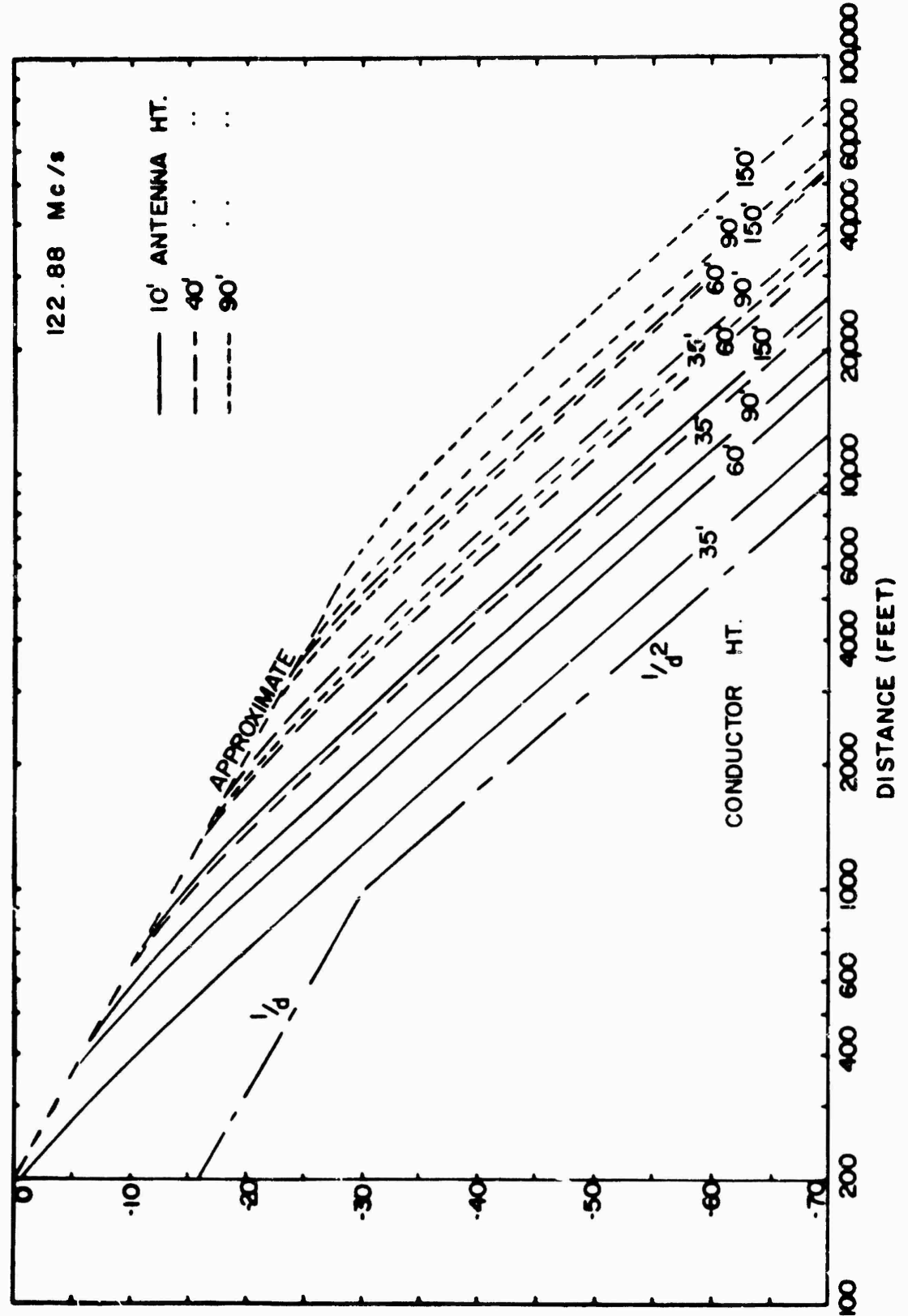


FIG. 19. ATTENUATION OF FIELD WITH DISTANCE FOR
VERTICAL DIPOLE AT 122.88 Mc/s



ATTENUATION RELATIVE TO 200, (dB)

FIG. 20, ATTENUATION OF FIELD WITH DISTANCE FOR HORIZONTAL DIPOLE AT 122.88 Mc/s

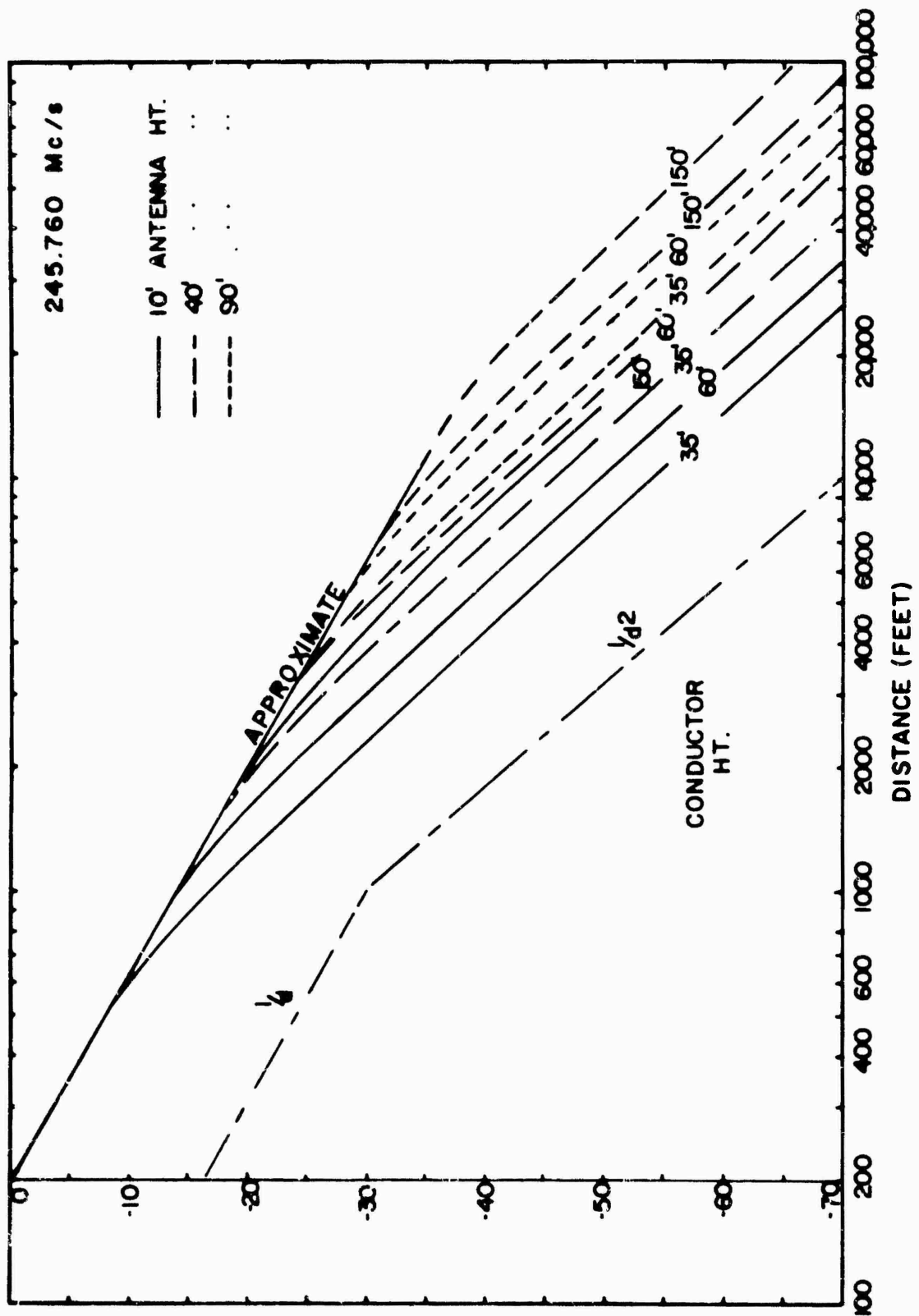


FIG. 2: ATTENUATION OF FIELD WITH DISTANCE FOR
VERTICAL DIPOLE AT 245.760 Mc/s

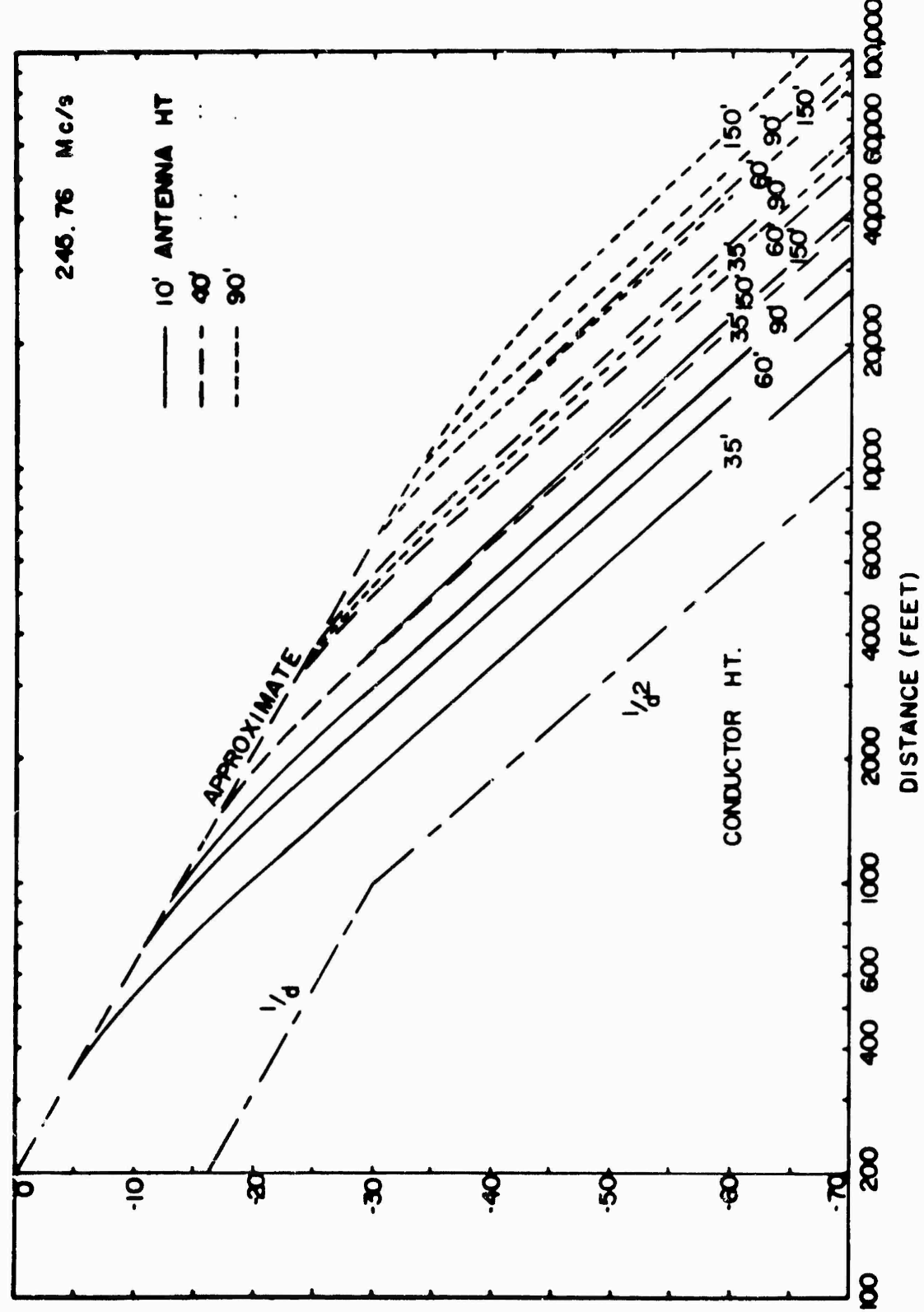
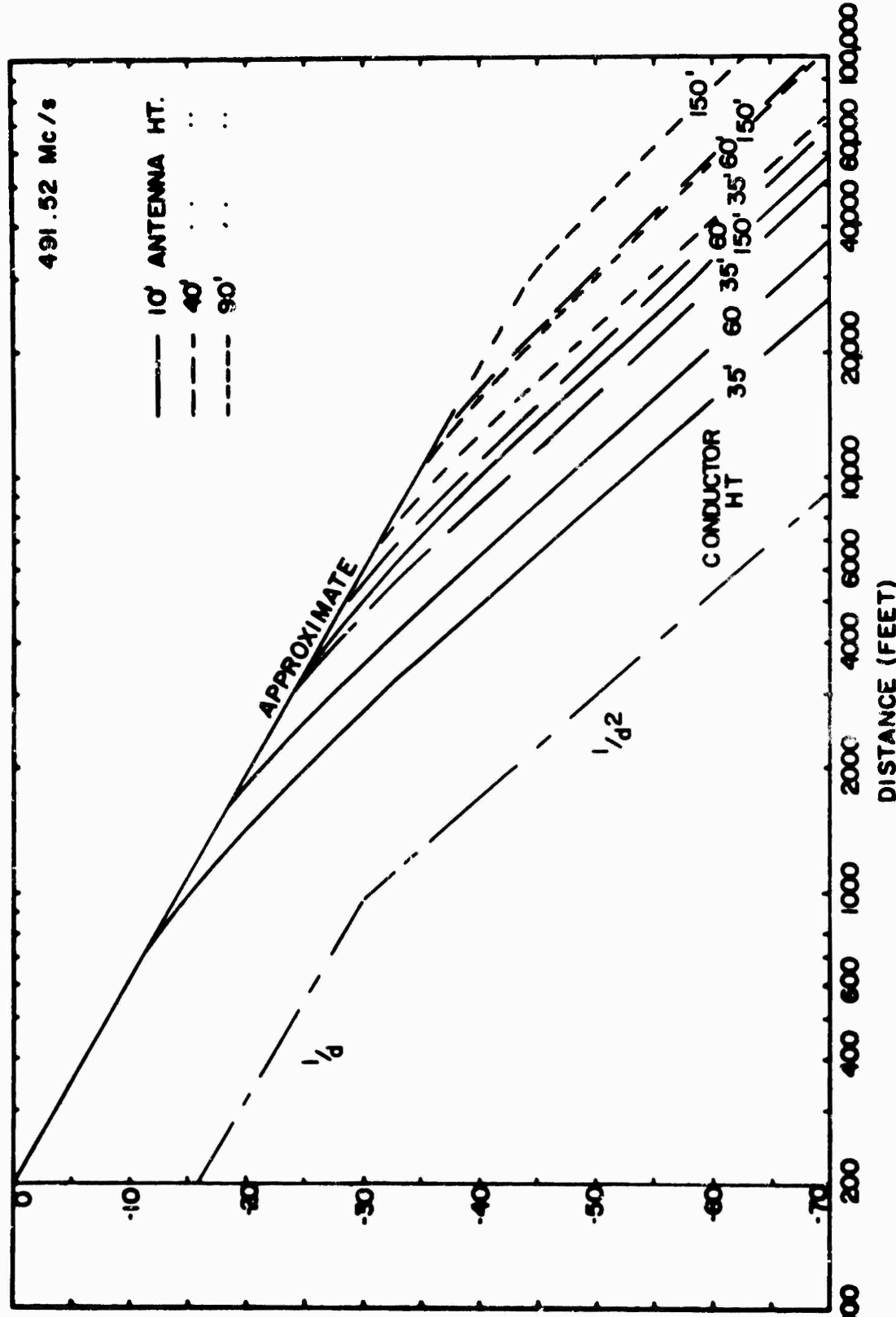


FIG. 22 ATTENUATION OF FIELD WITH DISTANCE FOR HORIZONTAL DIPOLE PERPENDICULAR TO LINE AT 245.76 Mc/s



ATTENUATION RELATIVE TO 200' (dB)

FIG. 23, ATTENUATION OF FIELD WITH DISTANCE FOR VERTICAL DIPOLE AT 491.52 Mc/s

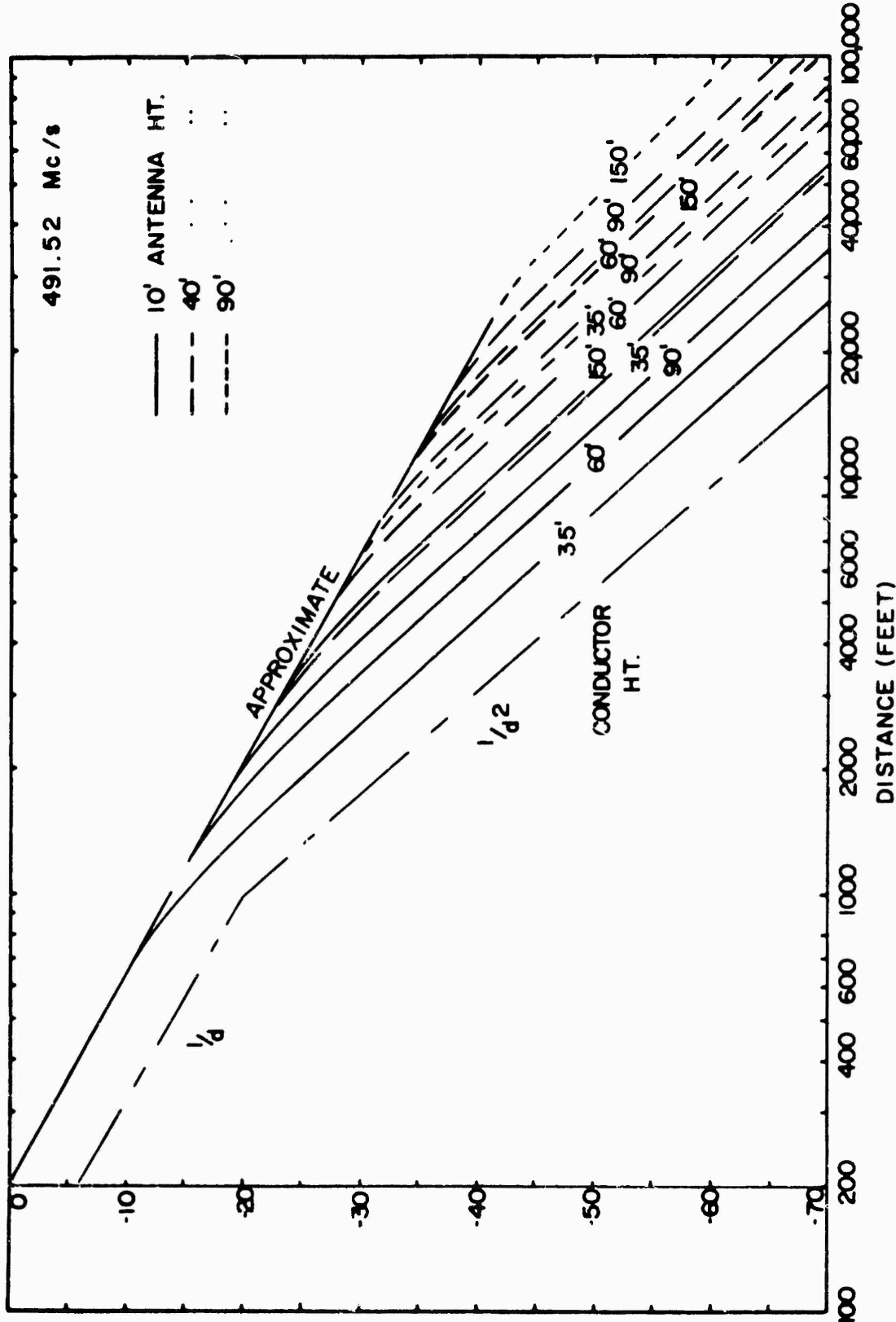


FIG. 24, ATTENUATION OF FIELD WITH DISTANCE FOR HORIZONTAL DIPOLE
PERPENDICULAR TO LINE AT 491.52 Mc/s

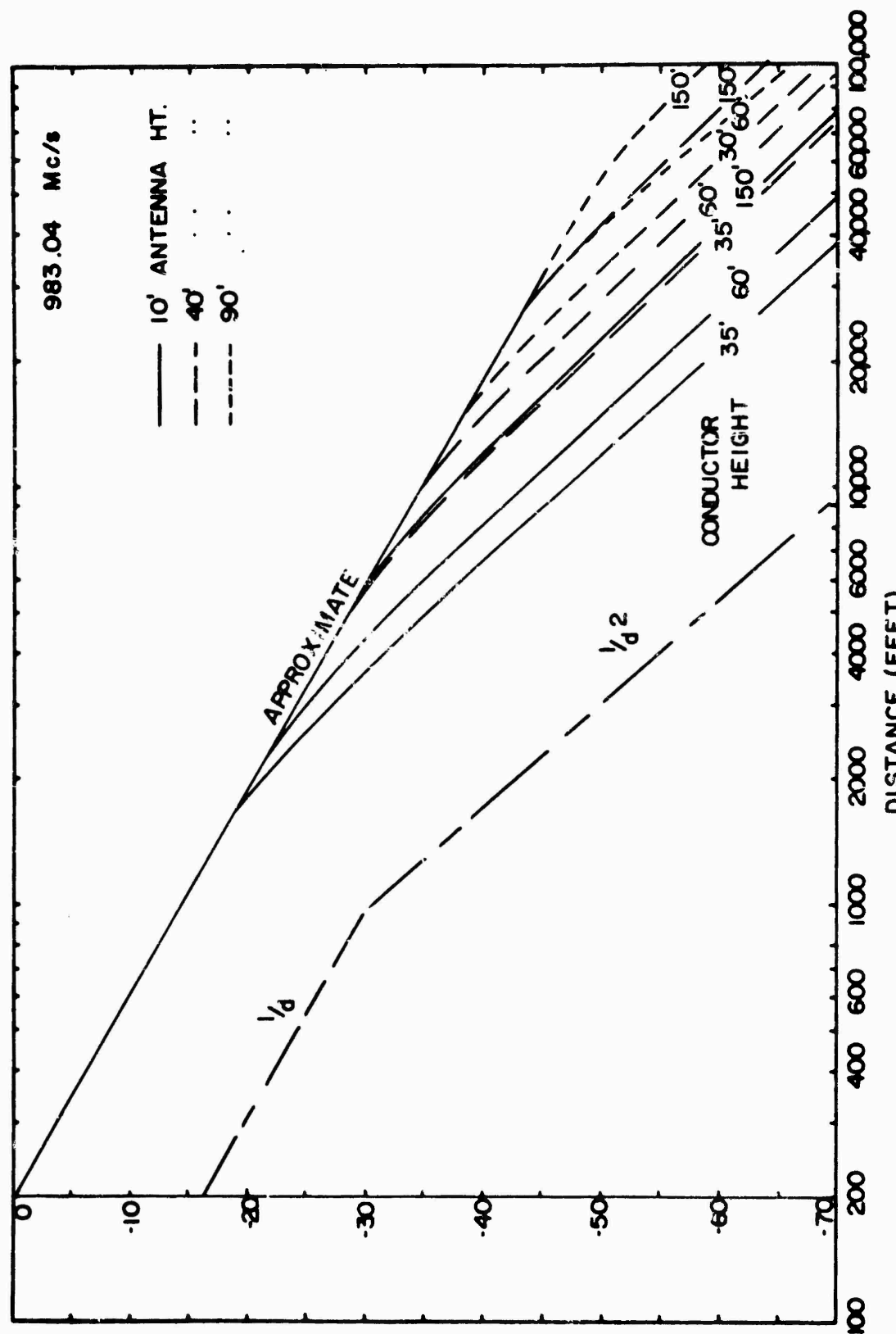


FIG. 25, ATTENUATION OF FIELD WITH DISTANCE FOR VERTICAL DIPOLE AT 983.04 Mc/s

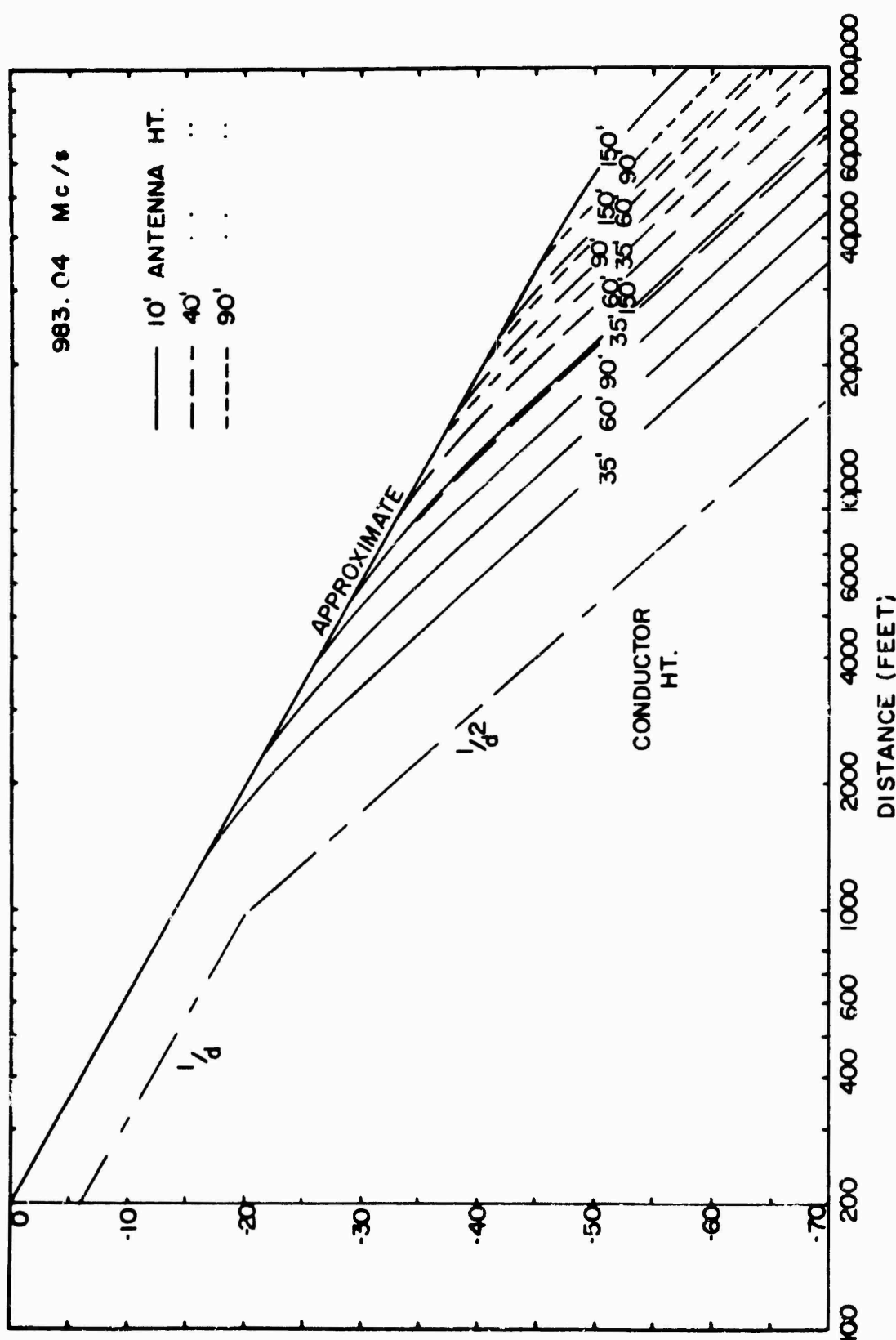


FIG. 26, ATTENUATION OF FIELD WITH DISTANCE FOR HORIZONTAL DIPOLE
PERPENDICULAR TO LINE AT 983.04 Mc/s

Curve 579281-A

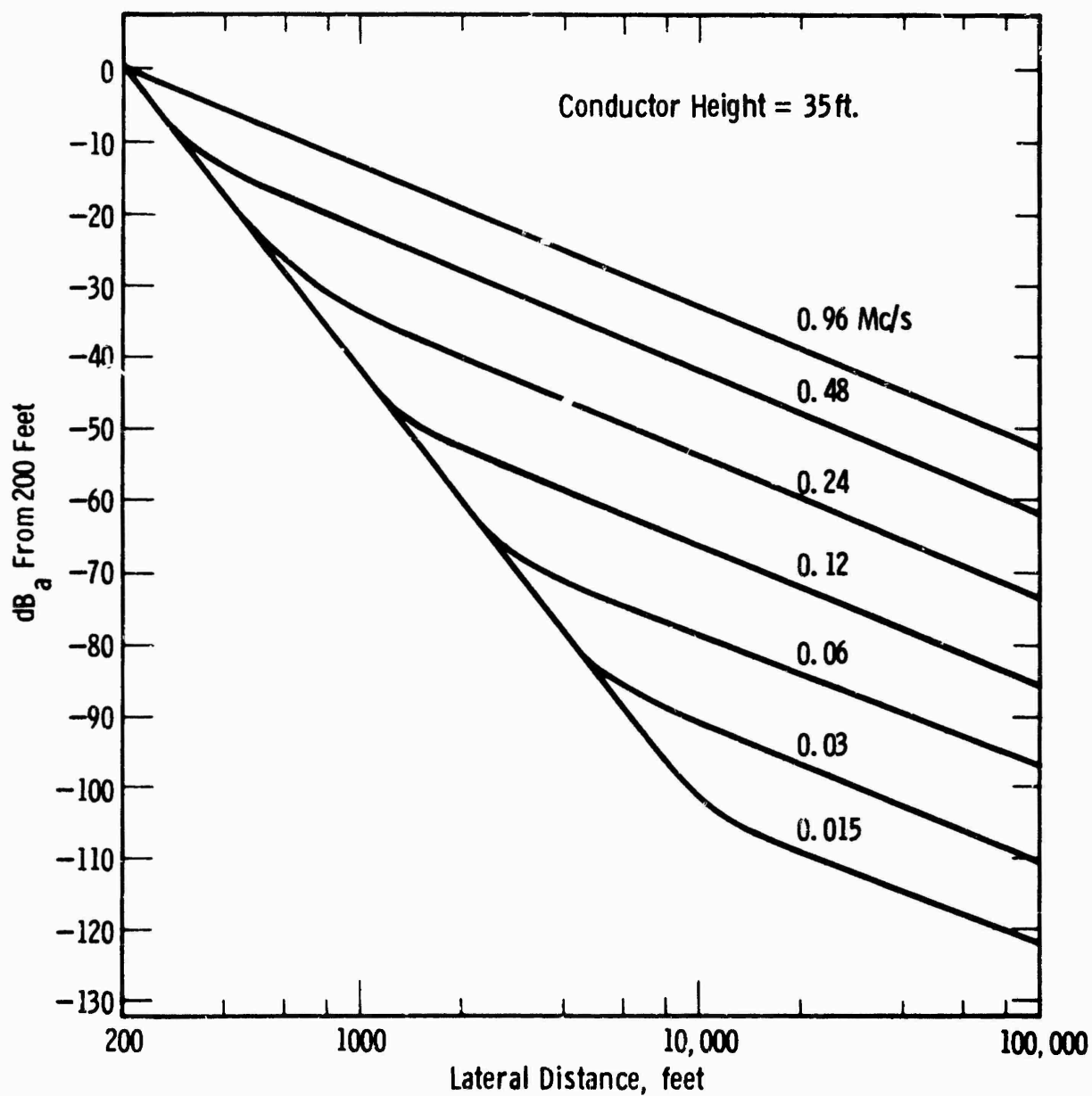


Fig. 27—Lateral attenuation 0.015 - 0.96 Mc for 35 foot conductor height (Calc.)

Curve 579282-A

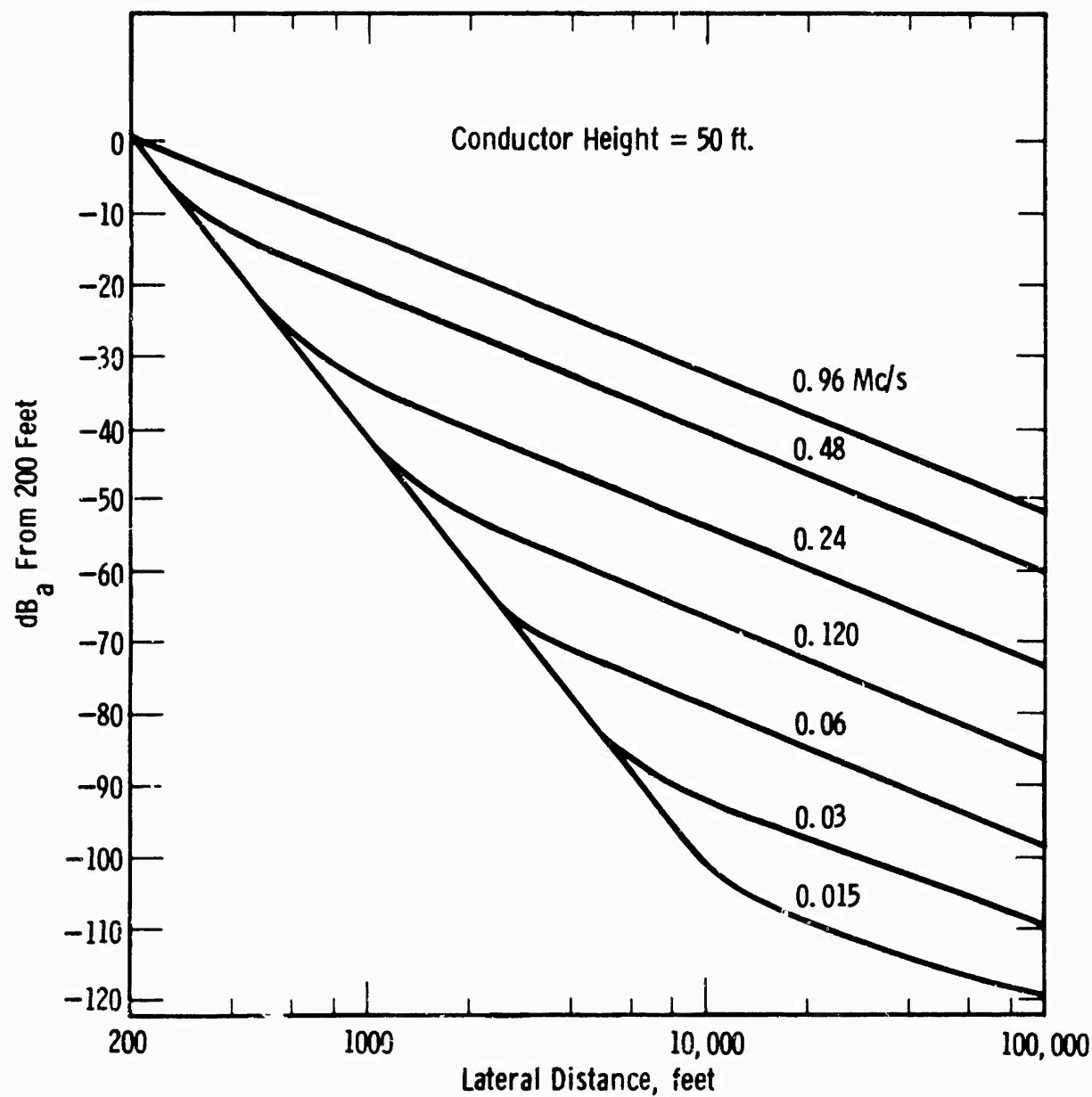


Fig. 28—Lateral attenuation 0.015-0.96 Mc/s for 50 foot conductor height (Calc.)

Curve 579283-A

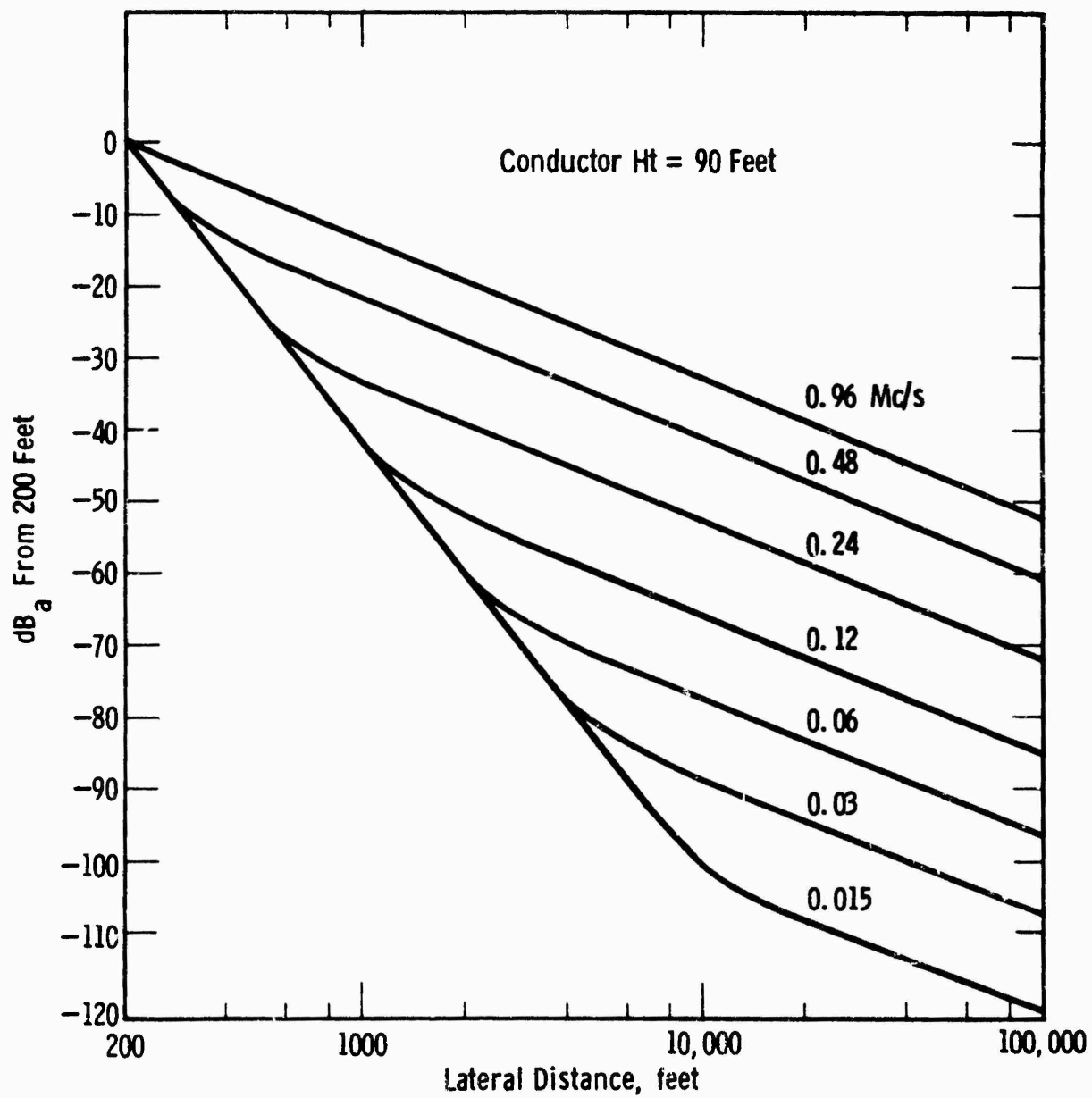


Fig. 29—Lateral attenuation 0.015-0.96 Mc for 90 foot conductor height (Calc.)

REFERENCES ON ANTENNA AND PROPAGATION THEORY

1. Aiken, C. B., "Two Mesh Tuned Coupled Circuit Filters," Proc. IRE, Vol. 25, Feb. '37, pg. 230-272.

Circuits tuned alike and coupled by pure reactance. Universal resonance curves are developed for pair of isochronous circuits. Formulas for band width, ratio of height of peaks to valleys. Critical coupling when ckt resistances are unequal. Shift of peaks with changes in coupling reactance. Form of primary current of impedance across primary.

Circuits tuned to slightly different frequencies. General expression for secondary current. Unsymmetrical resonance curve as result of detuning.

Coupling by complex impedance.

2. Alford, Andrew, "Coupled Networks in RF Circuits," Proc. IRE, Vol. 29, Feb., '41, pp. 55-70.

Develops equations for coupled networks in RF circuits.

3. Alian, E. W., Jr., "UHF Propagation Characteristics," ELECTRONICS, Vol. 22, pp. 67-87, Aug. '47.

Curves and equations for propagation.

4. Bechmann, R., "Calculation of Electric and Magnetic Field Strengths of Any Oscillating Straight Conductors," Proc. IRE, Vol. 19, pp. 461-466, March, '31.

General theoretical formulas for finite length conductors.

5. Beverage, H. H.; Rice, C.W.; Kilroy, F.W., "The Wave Antenna, A New Type of Highly Directive Antenna," Trans. AIEE, p. 42, 215, 1923.

Show growth of signal currents in long horizontal (receiving) antenna with axis in direction of signals. Effect of damping resistance. Mechanical model. Gives directivity curves for various lengths. Input impedance.

6. Beverage, H. H., "Some Notes on UHF Propagation," RCA Rev., Vol. 1, pp. 76-87, Jan., '37.

Discussion of propagation within optical distance, ground wave propagation beyond horizon and sky wave propagation. Gives measured and calculated values.

7. Bray, W. J.; Hopkins, H. G.; Kitchen, F. A.; Saxton, J. A., "Review of Long-Distance Radio Wave Propagation above 30 Mc/S," Proc. IRE, Jan, '55, pp. 97-95.

Covers freq. band from 30 Mc/S to 100 Gc/S.
Normal propagation - Radio-Horizon Distance = $\sqrt{2h_1} + \sqrt{2h_2}$ statute miles
where $h_1 + h_2$ are aerial heights in feet. Distance given by equation is
about 15% greater than the geometrical horizon distance. Diffraction
around earth's surface with standard atmospheric refraction - for both
horizontal and vertical polarization $0.152 f^{1/3}$ db per statute mile or
 $0.095 f^{1/3}$ db per kilometer, f in Mc/S. Applies to diffraction around
smooth earth. Effects of surface roughness. Effects of large obstacles.
Attenuation due to oxygen, etc., at SHF. Special propagation mechanisms.
(Extensive bibliography.)

8. Boese, W. C., and Fine, Harry. FCC-TRR Report #2.4 15, Oct. 7, 1955 (Revised Nov. 15, 1955), "Present Knowledge of Propagation in the VHF and UHF TV Bands."

Presents conclusions based on experimentation and calculation.

9. Bolljohn, J. R., and G. L. Matthew, "A Study of the Phase and Filter Properties of Arrays of Parallel Conductors between Ground Planes," Proc. IRE, Vol. 50, Mar., '62, p. 299.

Characteristics of conductors of finite and tuned lengths.

10. Booker, H. G., and P. C. Clemmow, "A Relation between Sommerfeld Theory of Radio Propagation over a Flat Earth and the Theory of Diffraction at a Straight Edge," Proc. IRE, Pt. III, Vol. 97, pp. 18-27, Jan., '50.

Points out that ray theory of propagation from a source in presence of a flat, imperfectly reflecting earth is only an approximation since involves assumption that Fresnel reflection coefficient of earth does not vary rapidly with angle of incidence, which is not satisfied for glancing incidence of vertically polarized waves over earth's surface at broadcasting wavelengths.

11. Booker, H. G. and P. C. Clemmow, "The Concept for Angular Spectrum of Plane Waves," Proc. IRE, Vol. 97, Pt. 3, pp. 11-17, Jan. '50.

Development leading up to other reference on pp. 18-27 of same volume.

12. Brown, G. H., "Directional Antennas," Proc. IRE, Vol. 25, Jan. '37, pp. 78-145.

Methods applicable to array design. Cases of both driven and parasitic arrays treated and some experimental results. Effective and total radiated power of arrays. Radiation patterns. Parasitic reflectors.

Cont'd.

12. (Con.) Antenna parallel to an infinite sheet. Method of measuring mutual impedance between antennas and of adjusting array. Method of computing mutual between a tower and a 'T' antenna. Expressions for electromagnetic field in vicinity of a straight wire, end-loaded and of arbitrary length and vertical radiation characteristics at any great distances.
13. Brown, G. H., and King, R., "High Frequency Models in Antenna Investigation," Proc. IRE, Vol. 22, 471, Apr., '34.
Discussion of modeling for antenna design.
14. Brown, J., "A Theoretical Analysis of Some Errors in Aerial Measurements," Proc. IRE, Vol. 105C, pp. 343-351, Sept. '58.
Use of idea of spectrum of plane waves introduced by Booker and Clemmow. Shows that size of receiving aerial can influence errors in measured radiation patterns and power gains.
15. Brown, J. and E. V. Jull, "The Prediction of Aerial Radiation Patterns from Near-Field Measurements," Proc. IRE, Vol. 108B, pp. 635-644, Nov., '61.
Method described of predicting aerial radiation pattern from near-field measurements. Expansion of radiated field in terms of a series of radially expanding modes. For cylindrical (2-dimensional) aerial and way in which method can be extended to 3-dimensional. Method similar in many aspects to plane-wave-spectrum approach of Booker and Clemmow using Fourier series except here surface is closed cylinder instead of infinite plane, and total field found as Fourier series.
16. Bullington, K., "Radio Propagation of Frequencies above 30 Mc/S," Proc. IRE, Waves and Electrons Section, Vol. 35, Oct., 1947, pp. 1122-1136.
Calculations and measurements above 30 Mc/S.
17. Bullington, K., "Radio Propagation Variations at VHF and UHF," Proc. IRE, Vol. 38, pp. 27-32, Jan., 1950.
Gives measured and theoretical field intensities in 40 to 50 Mc range over 10 to 1000 miles for antenna heights of 500 and 30 feet. Effects of atmospheric fading. Effect of hills; gives nomograph of feet of valley depth, freq. (10 to 2000 Mc/S) and "median shadow loss" in db and ratio of shadow loss exceeded in 90% of locations to median shadow loss. (Very low below 50 feet and 10 Mc/S.)

18. Bullington, K., "Reflection Coefficients of Irregular Terrain," Proc. IRE, Aug., 1954, pp. 1258-1262,
- Experimental results at 4000 mc. Gives theoretical curves of reflection coefficients for sawtooth, sine-wave and random terrains versus phase angle.
19. Bullington, K., "Radio Propagation Fundamentals," Bell System Tech. Journal, Vol. 36, pp. 573-626, May, 1957.
- Theory and experiment in all frequency bands of current interest are summarized. Ground wave and sky wave transmission are considered. Good summary of all factors in propagation theory.
20. Burrows, C. R.; H. Decimo; L. E. Hunt, "Ultra Short-Wave Propagation: Mobile Urban Transmission Characteristics," Elec. Eng., Vol. 54, p. 115-124, Jan., '35.
- Field measurements of mobile reception.
21. Burrows, C. R.; H. Decimo; L. E. Hunt, "Ultra Short-Wave Propagation over Land," Proc. IRE, Vol. 23 #12, Dec. '35, p. 1507-1535.
- Gives method of estimating received field for case where ground is substantially level except for slope of hill supporting antenna.
22. Burrows, C. R., "The Surface Wave in Radio Propagation over Plane Earth," Proc. IRE, Vol. 25 No. 2, Feb., '37 pp. 219-229.
- Experiments show that Sommerfeld's surface wave is not set up by simple antennas, for conditions which dielectric constant cannot be neglected. Experiments made over deep fresh water (Seneca Lake) at 150 Mc/S with loaded $\lambda/4$ vertical doubled. Variation of field strength with distance (1 to 2000 meters) with antenna heights 0.52 to 0.60 m. above surface of water. $\epsilon = 82.1$ and $\sigma = 4.05 \times 10^8$ electrostatic units.
- Variation of field strength with antenna height: vertical at 24.8 and 25 meters above water. Larger heights for vertical for 1800 meters.
23. Burrows, C. R., "Radio Propagation over Plane Earth - Field Strength Curves," Bell System Tech. Journal, Vol. 16, pp. 45-75, Jan., '37.
- Development of propagation equations and calculation of distance loss.

24. Burrows, C. R., and M. C. Gray, "The Effect of the Earth's Curvature on Ground-Wave Propagation," Proc. IRE, Vol. 29, pp. 16-24, Jan., '41.

25. Burrows, C. R., "Radio Propagation over Spherical Earth," Proc. IRE, Vol. 23, pp. 470-480, May, 1935.

Development of propagation equations.

26. Carson, John R., "The Guided and Radiated Energy in Wire Transmission," Trans., AIEE, pp. 908-913, Oct., '24.

Preliminary study to earlier work (Oct., '21). Points out engineering theory of guided transmission along wires based on transmission equation with prop. constant and characteristic of line represents actual wave with theoretical exactness only at great distance from physical terminals of line. Ignores accompanying waves which must be taken into account in order to directly explain radiation and scattering of energy from system. Complete wave must in general be represented by expression: (Complimentary waves)

$$V(z) = V_0 * (z) + \int_0^{\infty} K(u) i(z, u) du, \quad I(z) = I_0(z) + \int_0^{\infty} i(z, u) du$$

In addition to the principal wave, corresponding to wave of energy theory, there is an infinite number of waves (expressible as an infinite series or an infinite integral depending on whether system is radially bounded or unbounded) which indirectly satisfies Maxwell's equations and geometry of conducting system and which therefore can exist independently. The complete system is therefore built up out of all particular solutions, unknown constants of integration being determined from boundary conditions at physical terminals or system and at points of discontinuity. Each wave of current (and voltage) accompanied by characteristic field distribution of E and H. Thus, at energy point of discontinuity, represented say by a change in direction of line or by a change in electrical constants or structure, both direct and reflected complementary waves are called into existence. Complementary waves may either merely rearrange field or may subtract from or contribute energy to principal or guided wave. In this way, possible to account for radiation, while recognizing fact that principal wave is not attended by radiation.

"Suppose that we ignore not only complementary wave but its associated electromagnetic field, and attempted to calculate direction and character of energy flow in field from characteristic elementary field of principal wave alone. In neighborhood of wires and at some distance from terminals (or points of discontinuity in the line) the result of such a calculation would not be greatly in error, but at a great distance from the wires the results would be entirely incorrect, and would in fact lead to totally

Cont d.

- 26.(Cont.) incorrect conclusion that no radiation from system takes place. On other hand, if we calculate field at a great distance from wires by means of retarded vector potential of principal wire current while ignoring complementary wire current wave, this error is avoided and except in very extreme cases radiation is thereby calculable to a very high degree of approximation."
27. Carson, John R., "Radiation from Transmission Lines," Jour. AIEE, Vol. 40, pp. 789-790, Oct., 1921 (listed further thoughts in JAIRE, Oct., 1924).
 Short discussion. "It follows that for any number of parallel wires along which waves are traveling, the rate of radiation across any parallel cylindrical surface vanishes." Since current is not attenuated by radiation, the energy losses due to radiation from the system as a whole must appear as terminal impedance corrections or reflection effects. If at any point the spacing of the wires is changed or the geographical direction of the line is changed, the amount of radiation is modified and this must appear as a reflection effect in the current wave which our formulas do not take into account. For ideal line consisting of two straight parallel wires of perfect conductivity of length X and separation Y between wires, freq. of $P/2$ is transmitted along the line without attenuation and with velocity of light C , line so terminated that there is no appreciable reflection of current, letting $\delta \equiv X/Y$, γ being wave length,

$$S = 30(PyI/c)^2(1 - [\sin 4\pi\delta]/4\pi\delta)$$
 in practical units.
 For single Hertzian oscillator of moment yI , $S_0 = 10(PyI/c)^2$ and

$$S = 3S_0(1 - [\sin 4\pi\delta]/4\pi\delta)$$

 For very short lines radiation is prop. to $(\text{freq.})^4$ while for very long lines prop. to $(\text{freq.})^2$ and as length of line is increased approaches

$$S \sim 30(PyI_0/c)^2 = 3S_0$$
. If $y = 1 \text{ ft.}$ and f_{mc}/s , $S = 0.0051(1 - [\sin 4\pi\delta]/4\pi\delta)$ in watts/ampères.
28. Carson, John R. "Wave Propagation over Parallel Wires, The Proximity Effect," Phil. Mag., April, 1921.
 Similar discussion to previous references.
29. Carson, John R., "The Present Status of Wire Transmission Theory and Some of Its Outstanding Problems," Bell System Jour., Vol. 7, 1928, pp. 268-80.
 Discussion of generalized 'n' parallel wires as having 'n' possible modes of propagation, with corresponding characteristic impedances
 Distribution of wave energy among modes determined by boundary conditions.
 Discussion of limitations of theory for arbitrary impressed field and of velocity of classical form of differential equations. Classical theory all right where small losses in conductor dielectric and have a plane EH wave and system can be specified by classical Z's and Y's.
 "In general (if do not limit), for n parallel conductors there

Cont'd.

29. (Con) exist, in addition to the "n" principal modes of propagation, an n-fold infinity of other modes of propagation,....differing from the principal waves in that they are not quasi-plane and are very rapidly attenuated. For fields near the conductor, complementary waves usually appreciable only in neighborhood of physical terminals of system, so that at distances from terminals, usually small, they (currents, charges and fields) are represented with sufficient accuracy by principal waves alone. At a great distance from the conductors, however, it appears that the errors resulting from ignoring fields of complementary waves may be large, in fact the complementary waves must be expressly included to take into account phenomena of radiation. Explanation of his method of using retarded potentials and calculating principal modes as first approx. method; first calc. first Q's by elementary theory; second, calculate fields by retarded potentials.

30. Carson, John R., "The Rigorous and Approximate Theories of Electrical Transmission Along Wires," Bell Sys. Tech. Jour., Vol. 7, 1928, pp. 11-25.

"Investigate the conditions under which the specification of the system by means of its self and mutual impedances is valid and to provide a general method for calculating these circuit parameters from the geometry and electrical constants of the system." Specs. by means of Z's is valid if other conductors or dielectric are too imperfect. However, valid to high degree of approx. for all "efficient" systems.

Shows that classical two dimension transmission theory assumes $(\mu^2 - \delta^2)$ is negligible in dielectric.

31. Carson, John R., "The Statistical Energy-Frequency Spectrum of Random Disturbances," Bell Sys. Tech. Jour., Vol. 10, 1931, p. 374.

32. Carson, John R., "Wave Propagation in Overhead Wires with Ground Return," Bell Sys. Tech. Jour., Vol. 5, 1926, p. 539 (Nov. '26, Reprint B-219).

Gives equations for wave propagation.

33. Carson, J. R. and Hoyt, R. S., "Propagation of Periodic Wave Over a System of Parallel Wires," Bell Sys. Tech. Jour., 1927, #4, p. 495.

Further development of wave equations.

34. Carter, P. S., "Circuit Relations in Radiating Systems and Applications to Antenna Problems," Proc. IRE, Vol. 20, #6, June '32, pp. 1004-1041.

Discussion of radiating systems on basis of circuit analysis.

35. Colwell, R. C. and A. W. Friend, "Ultra High Frequency Wave Propagation over Plane Earth and Fresh Water," Proc. IRE, Vol. 25 #1, Pt. I, Jan., '37, pp. 32-37.

59 to 98 Mc/S, $\lambda/2$ vertical rod antenna for transmitter and receiver. For 59 Mc/S field intensity beyond 50 meters. Prop. follows $(IA/d^2)K$ and before 50 meters becomes IH/d . Same for 87 and 98 Mc/S except breaking point at 36 meters. For 59 Mc/S antenna heights $h_1 = 1.6$ meters, $h_2 = 2.1$ m. For 87 and 98, $h_1 = 1.4$ m and $h_2 = 2.2$ m. Curves vary nearly same for damp earth, dry sod and deep fresh water.

For any type of antenna we may use $E = IA/d$, letting $A = 60\pi h/\lambda$ where H = "effective ht." of antenna, I = transm. antenna current in amperes, λ = wave length in meters and d = distance in meters. By inserting constant K in free space equation to correct for apparent value of I , $E = IKA/d^2$ for field strength at any distance (over a plane) when $d/h_1 h_2 > 10$.

Burrows, Decimo and Hunt have deduced and experimentally verified an equation for field strength at much greater distances for conditions which can still be assumed to approximate plane earth:

$$E = 240 \pi^2 HI \frac{h_1 h_2}{\lambda^2 d^2} . \quad (1) \text{ from which } K = \pi \frac{h_1 h_2}{\lambda} \text{ of } A = 60\pi H/\lambda$$

36. Committee Report, "Report on Committee on Radio Wave Propagation," Proc. IRE, Vol. 26, pp. 1193-1134, Oct. '38.

Review of "state of art" in propagation prediction by 1938.

37. Day, J. P. and L. G. Trolese, "Propagation of Short Radio Waves over Desert Terrain," Proc. IRE, Feb., '50, pp. 165-175.

Measurements of the vertical distribution of field strength over a 190-ft. interval were made under two meteorological conditions for frequencies of 25, 63, 170, 520, 1000, 3300, 9375 and 24000 Mc. Two meteorological conditions: in daytime atmosphere well mixed with index of refraction distribution nearly standard; at night small scale duct was formed due to temperature inversion arising from cooling of the ground by radiation. Prop. over an optical path of 26.7 miles and non-optical 46.3 mile path. A few measurements were made by means of an airplane to altitudes of 8000 feet. Transmitters and receivers were located in elevator cabs mounted on 200 foot towers. Most measurements with horizontal polarization.

Gives height-gain curves during various times of the day.

38. DeWitt, John H., Jr., "The Relation of the Carrying Car to the Accuracy of Portable Field-Intensity Measuring Equipment," Proc. IRE, Vol. 27, Jan., '39, p. 1.
- Shows photographically field pattern about various cars and trucks.
39. Eckersly, T. L., "Ultra-Short-Waves Refraction and Diffraction," Jour. IRE, Vol. 80, pp. 286-304, Mar., '37 (Dec., '37.)
40. Eckersly, T. L., and G. Milligen, "Experimental Verification of the Diffraction Analysis of the Relation between Height and Gain for Radio Waves of Medium Lengths," Proc. Phys. Soc. (London), Vol. 51, pp. 805-809 (1939)
41. Egli, John J., "Radio Propagation above 40 Mc over Irregular Terrain," Proc. IRE, Vol. 45, #10, Oct., 1957, pp. 1383-1391.
- Effect of uneven terrain on frequencies above 40 Mc/S and methods of estimating. Analysis of data from FCC Reports and others to determine distribution of received field strengths over irregular earth to come up with a "terrain distribution" standard deviation and median. Some remarks about reception in vicinity of hills and wooded areas and effect of polarization.
42. Englund, C. R.; Crawford, A. B., and W. W. Mumford, Proc. IRE, Vol. 21, pp. 464-492, Mar., '33.
43. Feldman, C. B., Proc. IRE, Vol. 21, pp. 764-802, Jan., '33.
44. Fine, Harry, "An Effective Ground Conductivity Map for Continental United States," Proc. IRE, Vol. 42, #9, Sept. '54, pp. 1405-1408.
- Provides a map of ground conductivity values for the U. S.
45. Fine, H., UHF Propagation within Line of Sight," FCC, TRR Rep. No. 2.4.12; June 1, 1951.
- Analysis of available data for determination of empirical attenuation curves.

46. Firestone, W. L., "Analysis of Transmission Line Directional Couplers," Proc. IRE, Vol. 42, Oct. '54, pp. 1529.

General development. Makes reference in power line carrier. Gives results cal. and exp. for 25 to 2000 kc/s at very small distances for two to four wire systems.

47. Frederick Research Corporation, Handbook on Radio Frequency Interference, Vol. I, "Fundamentals of Electromagnetic Interference," copyright 1962.

General summary with nomographs and curves for propagation prediction.

48. Fris, H. T., "A Note on a Simple Transmission Formula," Proc. IRE, 34, pp. 254-256, May, 1946.

Emphasis utility of simple transmission formula to a radio circuit made up of transmitting and receiving antennas in free space:

$$\frac{P_r}{P_t} = \frac{ArAt}{d^2 \lambda^2} \quad (1)$$

where Ar = effective area of receiving
At = effective area of transmission

Effective area of any antenna is defined for condition in which antenna is used to receive a linearly polarized, plane electromagnetic wave.

A. Small Dipole with no heat loss: $A_{dip.} = 0.1193 \lambda^2$
 $A = 0.1305 \lambda^2$

B. Isotropic Antenna with no heat loss: $A_{isot} = \lambda^2 / 4$

C. Broadside Arrays (Pine Tree Antennas) with reflector that doubled gain $A \approx n \times 0.5 \lambda \times 0.5 \lambda$ where n is total number of half-wave dipoles in front curtain.

D. Parabolic reflector: 2/3 projected area of reflector

E. Electric horns Aperture Sides $\gg \lambda$: (very long horns) 81% aperture area.

Derives (1) from above. States that (1) is correct with a few per cent when $d = 2a^2 / \lambda$
where 'a' is largest linear dimension of either of antennae.

49. Gerks, T. H., "Use of a High-Speed Computer for Ground Wave Calculations," IRE Trans. on Antennas and Propagation, May, '62, pp. 292-299.
50. Gracely, F. R., "Temperature Variations of Ground Wave Signal Intensity Standard Broadcast Frequencies," Proc. IRE, Vol. 37, pp. 360-363, April, 1949.
Measurements over 6 paths of lengths from 76 to 558 miles at frequencies from 640 to 1170 Gc. Show that variations of ground-wave signal intensity appear to be more closely related to changes in temperature than to changes in any other single commonly observed meteorological quantity. Decreases in intensity at higher temperature and decrease is approx. prop. to path length in wave lengths.
51. Gray, M. C., "Diffraction and Refraction of a Horizontally Polarized Electromagnetic Wave over a Spherical Earth," Phil. Mag., Vol. 27, pp. 421-436, April, '39.
52. Hamberger, F., C. V. Larich, and M. Jones, "High-Freq. Prop. Characteristics," Proc. IRE, April, '40, Vol. 28, pp. 175-179.
53. Holmes, R. S. and Turner, A. H., "An Urban Field Strength Survey at Thirty and One Hundred Megacycles," May '36, Proc. IRE.
Measurement in urban areas of signal strengths and effects of uneven terrain, buildings, etc.
Discussion by C. R. Burrows, Proc. IRE, Jan., '37, p. 146.
54. Johler, J. R., "Propagation of the Low-Frequency Radio Signal," Proc. IRE, Vol. 50, Pt. 1, pp. 404-427, Apr., '62. (Correction, Proc. IRE, Oct., '62, p. 2092.)
Review of theoretical work, extensive reference list on subject.
55. Jones, L. F., "A Study of the Propagation of Wavelengths between Three and Eight Meters," Proc. IRE, Vol. 21, #3, pp. 349-386, March, '33.
Used an airplane, autogiro, dirigible and automobile and in house. Antenna on top of Empire State Building. Interference range approximately 100 miles. Observations made at a distance of 280 miles.

56. Jull, E. V., "An Investigation of Near -Field Radiation Patterns Measured with Large Antennas," p. 363, Vol. AP-10, No. 4, Antennas & Propagation, July, '62.
- Expression for measured Near-field antenna radiation pattern using concept of an angular spectrum of plane waves. Antennas sandwiched between two infinite, perfectly conducting parallel plates, separation equal to thickness of antennas and less than $\lambda/2$ so that only TEM mode propagates so that electric field is everywhere normal and magnetic field everywhere parallel to plates. Explores problem of distortion of near-field pattern by measuring antenna.
57. Kuhan, T. and G. Eckart, "Propagation of Electromagnetic Waves above the Ground. Solution of the Problem of the Surface Wave," Jour. Phys. Radium, Vol. 10, pp. 165-176, May '49. (Digest in Proc. IRE, Nov. '49, p. 1356, 1892.)
- Detailed discussion of Sommerfeld's treatment of radiation of dipole: Sommerfeld overlooked a factor which completely annuls so-called surface wave. Epstein's argument shows that surface wave cannot be included in the solution. (4007 of 1947; Jan. '48, p. 173. Experimental results confirm these theoretical conclusions. (See also 951 of May '49, p. 520.)
58. Kift, F., "The Propagation of High Frequency Radio Waves to Long Distances," Proc. IRE, Pt. B, Vol. 107, pp. 127-140, Mar., '60.
59. King, R., "A Generalized Coupling Theorem for UHF Circuits," Proc. IRE, Feb. '40, pp. 84-87.
60. King, R., "Application of Low-Frequency Circuit Analysis to the Problem of Distributed Coupling in UHF Circuits," Proc. IRE, Vol. 27, Nov. '39, p. 715-724.
61. King, R. and K. Tomiyasu, "Terminal Impedance and Generalized Two-Wire Line Theory," Proc. IRE, Oct. '49, p. 1134-39.
- Deals with end effects but some discussion of points outside of terminal zones. ("where conventional line theory is adequate.")

62. King, R. W. P. and H. J. Schmitt, "The Transient Response of Linear Antennas and Loops," IRE Trans., Ant. & Prop., May '62, p. 222-28.

Short pulses studied experimentally and theoretically. Initial response is always that of an infinitely long antenna at a frequency near upper limit of frequencies contained in pulse provided this is short enough so that reflection not superimposed.

Two parallel conductors behave like a transmission line only as long as they are sufficiently close together. So that a positive pulse traveling along one conductor is influenced by the presence of the "similar" negative pulse traveling in the second conductor. This means that the length of the pulse must be long compared with the time of travel with the velocity of light of a signal from the pulse on one conductor to the pulse on the other. If the two conductors are separated further, the presence of the pulse in the second one can have no effect on the pulse in the first one and it must behave just as if isolated, that is, like an antenna. Also applies to image plane. Response is then that of an antenna of radius a with an impedance which becomes constant.

63. Kirke, H. L., "Calculation of Ground-Wave Field Strength over a Composite Land and Sea Path," Proc. IRE, Vol. 37, pp. 489-496, May, '49.

Experiment conducted at 537, 922 and 1240 KC over a land-sea path to 460 KM giving extremes on conductivity from badly conductive land to sea. Discusses several empirical methods of calculating for distance as of about 10 to 400 kilometers and shows data from about 8 Km out.

64. Koike, R., "Recent Advances in the Use of Coupled Transmission Lines as Directional Couplers," Proc. IRE, Vol. 108, Pt. B 1961, p. 120-124.

Experiments and developments concerned with coaxial lines but discusses also in general.

65. LaGrane, A. H., and C. W. Chapman, "Some Propagation Characteristics of High UHF Signals in the Immediate Vicinity of Trees," Antennas & Prop. #9, No. 5, Sept., '61, p. 487, IRE Trans.

Measurements made at very low angles of 2880 Mc/S vertically-polarized signals of single tree and wooded area.
(Gives references to other such investigations.)

66. MacLean, K. G. and G. S. Wickizer, "Notes on Random Fading of 50 Mc/S over Non-Optical Paths," Proc. IRE, Aug., '39, p. 501.

Fig. 9: Comparison of calculated and observed field strengths on 52.75 Mc/S. Up to optical horizon calculated from level ground, grazing-incidence formula. Beyond optical distances, slope of calculated line was obtained from empirical curve published by H. H. Beveridge. Agreement between calculated and observed average field within 3 db.

67. Mannelack, C., "Radiation from Transmission Lines," Trans. AIEE, Vol. XIII, 1923, pp. 289-301 (same as '23 Jan. AIEE, pp. 95 and 981.)

Along a perfect line, without ohmic or leakage losses, plane electromagnetic traveling waves are propagated without distortion and without attenuator; hence, there is no radiation. Showed that radiation energy is much smaller than ohmic losses. The flow of energy in the dielectric is parallel to the pair of wires. However, near the source of a disturbance or near the end of the line where reflection occurs, or in general near any place where there is a change in the geometrical or electrical behavior of the line, the field cannot be plane. Shows that the classical theory of waves (neglecting radiation) gives a "theoretical" distribution of current along the line that is a very close approximation to "true" distribution, i.e., the unknown distribution taking place when the radiation is considered. Works out for finite line lengths: the power radiated by an oscillating transmission line open at both ends is proportional to the square of the ratio of distance between wires to the wave length of the oscillation.

68. Mathews, W. E., "Transmission Line Equivalent of Electronic Traveling Wave System," J. Appl. Phys. 22, pp. 310-316, 1951. (Proc. IRE to be published.)

Parallel plane and coaxial cylindrical systems. Gives equivalent circuits.

69. McPetrie, J. S. and J. A. Saxton, "An Experimental Investigation of the Propagation of Radiation Having Wavelengths of 2 and 3 Metres," Jour. IRE, Vol. 87, 1940, pp. 146-153.

70. McPetrie, J. S. and A. C. Strickland, "Reflection Curves of Propagation Characteristics of Radio Waves Along the Earth's Surface," Jour. IRE, Vol. 87, 1940, pp. 135-145.

71. McPetrie, J. S., "Reflection Coefficient of Earth's Surface for Radio Waves," Jour. IRE, Vol. 82, pp. 214-218, Feb. '38.

72. Millington, G., "Ground Wave Propagation over an Inhomogenous Smooth Earth," Jour. IEE, Part III, Vol. 96, p. 53, Jan. '49.

Develops method for prediction of long distance propagation.

73. Millington, G. and N. Elsen, "Ground Wave Propagation across a Land-Sea Boundary," Nature, Vol. 164, pp. 114-115, July 16, '49, Digest Proc. IRE, Dec. '49, p. 1493.

Increase of field strength observed on crossing the coastline for 3.13 Mc radiation along a path passing for about 100 Km overland and then across the English Channel. Field strength shown graphically. Also measurements at 1.122 Mc in an aircraft flying at a height of 1000 feet. At frequency used both land and sea are essentially conducting. A major recovery of field strength was noted 25 miles beyond the coast line.

74. Millington, G., "The Diffraction of Wireless Waves Around the Earth," Phil. Mag., vol. 27, pp. 517-542, May, '39.

75. Monteath, G. D., "Coupled Transmission Lines as Symmetrical Directional Couplers," Proc. IRE, May, '55 (102B), p. 383.

Two similar unbalanced transmission lines coupled together by strong common outer conductor for part of their length.

76. Nagy, A. W., "An Experimental Study of Parasitic Wire Reflectors on 2.5 Meters," Proc. IRE, Vol. 24, p. 240, Feb. '36.

77. Nergaard, L. S. and B. Salzberg, "Resonant Impedance of Transmission Lines," Proc. IRE, Vol. 27, pp. 579-583, Sept., '39.

78. Norton, K. A., "Propagation of Radio Waves over a Plane Earth," Nature, Vol. 135, pp. 954-955, June 8, 1935.

Discussion of development of surface wave.

79. Norton, K. A., "Physical Reality of Space and Surface Waves in the Radiation Field of Radio Antennas," Proc. IRE, Vol. 25, pp. 1192-1202, Sept., '37.

Equations for electric and magnetic dipoles.

80. Norton, K. A., "Propagation of Radio Waves over the Surface of the Earth and in the Upper Atmosphere, Part I," Proc. IRE, Vol. 24, p. 1367-1387, Oct., '36.

Mathematical development for propagation.

Part II - Proc., Vol. 25, pp. 1203-1236, Sept., '37.

More general formulas for effective ht. and effect of finite conductivity and formulas for attenuation factor.

81. Norton, K. A., "The Calculation of a Ground Wave Field Intensity Over a Finite Conducting Spherical Earth," Proc. IRE, Vol. 29, pp. 623-639, Dec., '41.

A complete development of equations for dipoles.

82. Oliver, B. M., "Directional Electromagnetic Couplers," Proc. IRE, Nov., '54 Vol. 42, pp. 1686-1692.

Develops equations neglecting attenuation, assuming conductor sizes and spacings are infinitesimal. Compared with wavelength and that lines are balanced and coupling is symmetrical. Thus only TEM waves are considered.

83. Page, H., and G. D. Monteath, "The Vertical Radiation Patterns of Medium-Wave Broadcasting Aerials," Proc. IRE, Vol. 102, Pt. B, 1955, pp. 279-295.

Deals with vertical mast antennas.

84. Peters, C. L., "Accuracy of the Earth-Flattening Approximation in the Theory of Microwave Propagation," Phy. Rev., Vol. 70, pp. 518-522, Oct., '46.

85. Pierce, J. R., "Coupling of Modes of Propagation," J. App. Phys., 25, pp. 179-183, Feb., '54.

86. Podszech, Heinrich-Karl (book) "Carrier Communication over Power Lines," Third Edition, Springer-Verlay 1963.

Gives attenuation characteristic for lines to carrier signals.

87. Ramo, S., Proc. IRE 27, p. 757-763 (1939)
88. Reed, H. R. and C. M. Russell, "Ultra High Frequency Propagation," (book), John Wiley & Sons, Inc.
- Equations and constants for propagation prediction.
89. Rice, P. L. and R. T. Daniel, "Radio Transmission Loss versus Distance and Antenna Height at 100 Megacycles," Trans. IRE, PGAP, Vol. AP-3, Apr., '55.
FCC Report 2.4.15 by Boise and Fine points out error in referring to FCC Report.
90. Rice, S. O., "Reflection of Electromagnetic Waves from Slightly Rough Surfaces," Communications on Pure and Applied Mathematics, Aug., '51, pp. 351-378.
91. Rocco, M. D. and J. B. Smyth, "Diffraction of High-Frequency Radio Waves around the Earth," Proc. IRE, Oct. '49, pp. 1195-1203.
Reports non-optical ht.-gain measurements on uniform desert link at frequencies of 25, 63, 170, 520, 1000, 3300 and 9375 MC using horizontal polarization.
92. Saxton, J. A., "Basic Ground-Wave Propagation Characteristics in the Frequency Band 50-800 Mc/S," Proc. IRE, pt. III, Vol. 101, pp. 211-214, July, '54. Disc. pp. 221-224.
At distances such that variations in atmospheric reflective index are of little significance. Empirical correction for irregular terrain. If earth be regarded as a plane
- $$E_0 \approx 7 \frac{\sqrt{P_G}}{d} \frac{4\pi h_T h_R}{\lambda d} \quad \text{provided that } \sin \psi \approx \psi; \text{i.e.}$$
- When $d \gg (h_T + h_R)$ P - power radiated; G = Gain of radiator
 d = distance in meters.
 with respect to λ/z dipole,
93. Saxton, J. A. and B. N. Hardin, "Ground Wave Field-Strength Surveys at 100 and 600 Mc/S," Proc. IRE, Pt. III, Vol. 101, pp. 215-221, July, '54, Disc. 221-224.

94. Schelkunoff, S. A. and C. B. Feldman, "On Radiation from Antennas," Proc. IRE, Nov., '42, pp. 511-516.

Some theoretical remarks and experimental data relating to applications of transmission-line theory to antennas as pertains to field along surface and impedance.

95. Schelkunoff, S. A., "Principal and Complementary Waves in Antennas," Proc. IRE, Vol. 34, 1946, p. 23P-32P.

Presents details of analysis of cylindrical and other conical and non-conical antennas as a supplement to "Theory of Antennas of Arbitrary Size and Shape." Gives equations for voltage and current distributions for antennas of small transverse dimensions.

96. Schelkunoff, S. A., "Theory of Antennas of Arbitrary Size and Shape," Proc. IRE, 492-521, 1941.

General discussion of existing approaches and their limitations. Discussion of multiple modes of transmission. Resonance effects of various shapes.

Wave propagation along part of perfectly conducting wires; gives equation for current distribution in two thin infinitely long perfectly conducting parallel wires, energized in "push-pull" in form of complex differential.

97. Schilling, J. C., C. R. Burrows, F. B. Fennell, "Ultra-Short Wave Propagation," Proc. IRE, Vol. 21, pp. 427-462, March, '33.

98. Schonland, B. F. J., "The Pilot Streamer in Lightning and the Long Spark," Proc. of Royal Society, A, 61.220, pp. 25-38, 1953.

Discusses other observations of pilot streamer. "No observable stepped electrostatic field change during the downward course of a nearby stepped code." "The step electrostatic field changes are of magnitude less than 1/10 of the continuous field changes in the intervals between steps." "Proves" that change in bright step is small and di/dt compared with return streamer is low.

99. Trever, B. and P. S. Carter, "Notes on Propagation of Waves, Below 10 Meters in Length," Proc. IRE, Vol. 21, p. 387, Mar., '33.

100. Trever, B., "UHF Propagation Through Woods and Underbrush," RCA Review, Vol. 5, pp. 97-100, July, '40.
101. Van der Pol, B. and H. Bremmer, "Further Notes on the Propagation of Radio Waves over a Finitely Conducting Spherical Earth," Phil. Mag., Vol. 27 pp. 261-275, Mar., '39.
102. Vergara, W. C., J. L. Levatich, and T. J. Carroll, "VHF Air-Ground Propagation for Beyond the Horizon and Tropospheric Stability," IRE Trans., Antennas and Propagation, Vol. 10, No. 4, Sept.'62, p. 608.
103. von Handel, P. and Wolfgang Pfister, "Ultra-Short Wave Propagation along the Curved Earth's Surface," Proc. IRE, Vol. 25, No. 3, Pt. 1, Mar. '37, p. 346-363.
Practical application of calculation of diffraction by curves which give decrease of field intensity with distance for various elevations in whole range of wavelengths. Curves substantiated by airplane measurements for transmitter antenna 30 and 135 meters high.
104. Wait, James R., "Average Decay Laws for ULF Fields," Proc. IRE, Jan. '62, Pages 53-56.
Assumes parallel plate waveguide with homogeneous isotropic walls for propagation in earth-ionosphere waveguide. If square of field amplitude is averaged over width of waveguide the averaged intensity is obtained. In intermediate distance region $d < 3000 \text{ Km.}$, $|E^2|$ varies as $d^{-3/2}$ when ground losses are negligible (such as over sea water). Ground conductivity results in additional attenuation per unit distance. (Source taken to be a vertical electric dipole located in lower surface, i.e., the ground.)
105. Wait, James, R., "Introduction to Theory of V.L.F. Propagation," Proc. IRE, July, '62, pp. 1624-1647.
"Self-contained exposition of conventional theory of propagation of VLF radio waves."
106. Watson, G. N., "The diffraction of Electric Waves by the Earth," Proc. Roy. Soc., (London) Vol. 95, pp. 83-99, Oct. 7, 1918 and pp. 546-563 July 1919.
107. Watt, A. D., and E. L. Maxwell, "Characteristics of Atmospheric Noise from 1 to 100 Kc/s," Proc. IRE, Vol. 45, pp. 787-795, June, '57.

108. Wise, W. Howard, "Potential Coefficients for Ground Return Circuits," Bell Sys. Tech. Jour., Vol. 27, 1948, pp. 365-371.

Discussion of earlier work by Carson and further development.

"Ordinarily $4(M + iN)$ will not be an important correction to $2 \log P'/P$, but if freq. is high and height is small it can be a worthwhile correction." Gives curves for "self's" M and N.

109. Wise, W. H., "The Grounded Condenser Antenna Radiation Formula," Proc. IRE, pp. 1684-1689, Sept. '31.

110. Wise, W. H., "Propagation of High-Frequency Currents in Ground Return Circuits," Proc. IRE, 1934, Vol. 22, p. 522.

111. Wu, T. T., "Theory of Dipole Antenna and the Two Wire Transmission Line," J. Math. Phys., Vol. 2, pp. 550-574, July-Aug., 1961.

**FORTRAN Statements
for
Near Field Calculation**

```
RADC - EFN  SNUKC: START.1 - IFN(5) -
```

```

32000 FORMAT (1H1)
32100 WRITE (6,32000)
31000 FORMAT(46HO RF PROP. CALC. = MFC. FMT: VERTICAL DIST.)
      WRITE (6,31000)
30000 FORMAT (72H
      )
1      READ (5,3000C)
      WRITE(6,3000)
2      10000 FORMAT (2F5.1,F3.3)
      READ (5,10000) HC,HA,FREQ
10001 FORMAT(1SH CONDUCTOR HT. ,F5.1,1H. MFT. ,F5.1,1H. FREQ.
      ,F9.3,5H MHz.
      ,WRITE(6,10001)HC,HA,FREQ
10003 FORMAT (3F8.1)
      READ (5,10003) SD,ED,DI
10004 FORMAT(44H FT TOTAL (CB). C. NO. OF TS AND TOTAL
      ,)
      WRITE(6,10004)
D=SD
      NI=INT((ED-SD)/0.1)+1
265      DO 500 K=1,NI
      R1=SQRT((HC-HA)**2.0*D*D)
      R2=SQRT((HC+HA)**2.0*D*D)
      SNPH1=(HC-HA)/R1
      SNPH2=(HC+HA)/R2
      COPH1=D/R1
      COPH2=D/R2
      ANG1=0.0063839*FREQ*R1
      ANG2=0.0063839*FREQ*R2
      ANG11=1.0/ANG1
      ANG12=ANG11*ANG11
      ANG13=ANG11*ANG112
      ANG21=1.0/ANG2
      ANG212=ANG21*ANG21
      ANG213=ANG21*ANG21
      C DIRECT WAVE COMPONENT CALC.
      DWCR=(ANG11-ANG11)*COS(ANG1)-ANG112*SIN(ANG1)*SNP41*COPH1
      DMC1=(ANG113-ANG11)*SIN(ANG1)*ANG112*COPH1*SNP41*COPH1
      C GROUND-REFLECTED WAVE
      GRCR=(ANG213-ANG21)*COS(ANG2)-ANG212*SIN(ANG2)*SNP42*COPH2
      GRC1=(ANG213-ANG21)*SIN(ANG2)*ANG212*COPH2*SNP42*COPH2
      C TOTAL FIELD CALC.
      T=DWCR+GRCR

```

```

PAGE 2
RADC - EFN SOURCE STATEMENT - IFN( < ) -
U=DMCI+GRCI
FIELD=10.0*ALCG10(I*I+J*U*U)
COMPT1=SQRT((ANG1I3-ANG1I)**2+0.0+ANG1R,(I**2+0.0))
COMPT2=SQRT((ANG2I3-ANG2I)**2+0.0+ANG2R,(I**2+0.0))
COMPT1=20.0*ALCG10(COMPT1)
COMPT2=20.0*ALCG10(COMPT2)
10022 FORMAT(1X,F8.1,2PE12.2,1PHE10.3)
WRITE(6,10022) D,FIELD,ANG1I,ANG1R,CHMPT1,ANG2I,ANG2R,
1213,COMPT2
500 D=D+DI
501 GO TO 32100
END

```

266

FORTRAN Statements
for
Simplified Radiation Propagation Calculation -
Modified Equation

RADC - FFN SOURCE STATEMENT - FILE(S) -

09/07/66

```

DWCHR=DKH*CUS(ANG1)
DCHI=DKH*SIN(ANG1)
CRKH=COPH2*CIPH2
CRCHR=CRKH*COS(ANG2)
CRCHI=CRKH*SIN(ANG2)
TH=DWCHR-(P*CKCHR;
UH=DCMCHI-(R*CRCHI)
HFIELD=10.0*ALNG10((TH*TH+UH*UH)-20.*PI*AT.G10(D))
10006 FORMAT(1X,F9.1,2P2E12.1)
      WRITE(6,10006) U,VFIELD,HFIELD
500 D=D+0.1
501 GO TO 32100
END
  
```

269

FORTRAN Statements

for

Radiation Propagation Calculations -

Norton Equation

Distance Variation

RADC - EFN SOURCE STATEMENT - IFN(S) -

08/31/66

PAGE 1

```
32000 FORMAT (1H)
32100 WRITE (6,32000)
31000 FORMAT (72H) RADIO HIGH - FREQUENCY PROPAGATION CALCULATIONS
1(PLANE - EARTH)
WRITE(6,31000)
30000 FORMAT (72H)
1
READ (5,30000)
WRITE(6,30000)
10000 FORMAT (2F5.1,F9.3,2F7.1)
READ (5,10000) IHC,HA,FREQ,DIELC,COND
10001 FORMAT (1SH CONDUCTOR HT. ,F5.1,1.14H ANTENNA HT. ,F5.1, 8H FREQ.
1,F9.3,4H MHZ )
WRITE(6,10001) IHC,HA,FREQ
10002 FORMAT (20H DIELECTRIC CONSTANT,F7.1,18HEARTH CONDUCTIVITY ,F6.1)
WRITE(6,10002) DIELC,COND
10003 FORMAT (3F6.1,1,F6.3)
READ (5,10003) SD,ED,DI,L,DIVF
271 800 DIVF=1.0
801 CONTINUE
10007 FORMAT(72H)
10008 FORMAT(70H FT) VERTICAL VERT/DIST. HORIZONTAL MORIZ/DIST OUTPUT
1. FIELD (0.6)
1. IF (LI) 210,210,211
211 WRITE (6,10007)
210 WRITE (6,10004)
X=17.9731*COND/FREQ
BPPUS=1.0/SQRT(1.0+((DIELC/X)*(DIELC/X)))
D=SD
MI=INT((ED-SD)/DI)+1
DO 500 K=1,MI
R1=SQRT((IHC-HA)**2.0+0*D)
R2=SQRT((HC+HA)**2.0+0*D)
ANG1=0.0063838*FREQ*R1
ANG2=0.0063838*FREQ*R2
PK=0.5*ANG2
HD=(IHC+HA)/R2
IF (LI) 400,400,401
400 COPH2=D/R2
60 TO 402
```

RADC - EFM SOURCE STATEMENT - IFM(SI) -

```

401 COPMH2=1.0
402 SCOPMH2=(COPMH2)*(COPMH2)
        BPCOS=1.0/ SQRT(1.0+(DIELC-SCOPMH2)/X)**2.0!
C DIRECT WAVE COMPONENT CALC.
    IF (LI) 403,403,404
403 DNK=(D/R1)**3.0
    GO TO 405
404 DNK=1.0
405 DNCR=DNK*COS(ANG1)
        DNCL=DNK*SIN(ANG1)
C GROUND-REFLECTED WAVE COMP. CALC.-VERTICAL POLARIZED
406 X8=SQRT(X*BPCOS/(BPPCOS*BPPCOS))
        BN=2.0*ARCOS(BPPCOS)-ARCOS(BPCCS)
        J=1
    GO TO 200
C GROUND-REFLECTED WAVE COMP. CALC.-HORIZONTAL POLARIZED
207 X8=SQRT(BPCOS/X)
        BN=3.14159-ARCOS(BPPCOS)
200 THETA=0.785399-0.5*BN
        Q=HDX8
QS=Q*Q
PH=PK/(X8*X8)
RDEN=QS+2.0*QCOS(THETA)+1.0
        AR=QS-1.0
        RI=2.0*QSIN(THETA)
GCR=SCOPMH2*COPMH2*(IRR*COS(ANG2)-RI*SIN(ANG2))/RDEN
GRCI=SCOPMH2*COPMH2*(IRR*SIN(ANG2)+RI*COS(ANG2))/RDEN
GCR=DIVF*GCR
GRCI=DIVF*GRCI
    IF (LI) 601,601,300
300 SWR=0.
        SWI=0.
    GO TO 602
C SURFACE-WAVE COMPONENT
601 RNM=1.0*(RR/RDEN)
        RIM=(RI/RDEN)
        RRMS=RNM*RR
        RIMS=RIM*RIM
        PBDEN=(RRMS+RIM)**2.0
        PRBN=(RRMS-RIM)*COS(BN)-2.0*RIM*RIM*SIN(BN)
        PBIN=2.0*RRIM*RIM*COS(BN)+(RRMS-RIM)*SIN(BN)
        BC=ATAN(PBIN/PRBN)
        PC=4.0*PI*SQRT(PBN*PRBN+PBIN*PBIN)/PBDEN

```

30	31		
34			
38			
39			
41			
42	43		
46			
47			
49			
50			
51			
52			
53			
54			
59			
60			
61			
62			
63			
64			
65			

```

C SURFACE ATTENUATION FACTOR
201 HR=0.0
    MI=0.0
    C=1.0
    SN=1.0
    COM=1.0
    DO 2011 I=1,35
        E=I
        C=(2.0*E-1.0)
        COM=(2.0*PC)*COM/C
        SN=-SN
        HR=SIN(CM*COSIE*BC)+HR
        HI=SIN(COM*COSIE*BC)+HI
        A=SQRT(1.14159*PC/EXP(IPC*COSIE*BC))
        B=PI*SQRC-PC*SIN(HB)
        IR=1.0+ASIN(HB)+IR
        FI=ACOS(SB)+HI
        GO TO 204
202 HR=0.0
    MI=0.0
    C=1.0
    COM=1.0
    DO 2021 I=1,20
        E=I
        C=(2.0*E-1.0)
        COM=C/(2.0*PC)*COM
        HR=COM*COSIE*BC)+HR
        HI=COM*SINIE*BC)+HI
        2021 HI=COM*SINIE*BC)+HI
        2023 HI=-HR
        FI=-HI
    204 SMX1=RRM*FR+RMF1
        SMX2=RRM*FI-RMF1
        SMR="SCOPH2*(SMKL1*COSI(ANG2))-SMK2*S
        SM1="SCOPH2*(SMK2*COSI(ANG2)+SMK1*S
        C TOTAL FIELD CALC.
    602 T=DMCR+GCR+SM
        U=DRCI+GRCI+SMI
        FIELD=10.0*ALOC10(T*U*U)
        FIELD=FIELD-20.0*ALOC10(D)
        FORMAT(LX,F8.1,4P2E12.1)
        10005 FORMAT(IH+,33X,4P2E12.1)
        10006 FORMAT(IH+,33X,4P2E12.1)

```

08/31/66

RADC - EFN SOURCE STATEMENT - IFN(S) -

```
IF (J) 206,206,205  
205 WRITE (6,10005) D,FIELD•FIELD  
      J=J-1  
      GO TO 207  
206 WRITE (6,10006) FIELD•FIELD  
500 D=D+1  
501 GO TO 32100  
END
```

PAGE 4

FORTRAN Statements

for

Radiation Propagation Calculations -

Modified Equation

Distance Variation

RADC - HFN SOURCE STATION - HF(S) -

```

' L A N K
' TITLE
30000 FORMAT(172H
1
      READ(15,30000)
      WRITE(6,30000)
10000 FORMAT(12F5.1,F9.3,2F7.1)
      READ(15,10000)HC,HA,FREQ,DIELC,CJND
10001 FORMAT(11SH CONDUCTOR HT.,F5.1,14H ANTENNA HT.,F5.1, 8H FFLW.)
1, F9.3,4H MHZ )
      WRITE(16,10001)HC,HA,FREQ
10002 FORMAT(120H DIELECTRIC CONSTANT,F7.1,14HFARTH CONDUCTIVITY ,F6.1)
      WRITE(16,10002)DIELC,CJND
10003 FORMAT(3F8.1,1,1,F6.3)
      READ(15,10003)SD,ED,DI,L,DIVF
      IF(LDIVF) 800,800,801
800 DIVF=1.0
801 CONTINUE
10004 FORMAT(170H FT
1.   FIELD (DB)
1.   VERTICAL   VERT/DIST.  HORIZONTAL  HORIZINTL  HORIZ/DIST  OUTPUT
210 WRITE(6,10004)
X=17.9731*COND/FREQ
BPPCOS=1.0/SQRT(1.0+((DIELC/X)*(DIELC/X)))
276
      O=SD
      NI=INT((ED-SD)/DI)+1
      DO 500 K=1,NI
      R1=SQRT((HC-HA)**2.0+D*D)
      R2=SQRT((HC+HA)**2.0+D*D)
      ANG1=0.0063938*FREQ*R1
      ANG2=0.0063938*FREQ*R2
      PX=0.5*ANG2
      SNPH1=(HC-HA)/R1
      HD=(HC+HA)/R2
      COPH1=D/R1
      COPH2=D/R2
400 SCOPH1=COPH1*COPH1
      SCOPH2=(COPH2)*(COPH2)
      BPCOS=1.0/ SQRT(1.0+((DIELC-SC1PH2)/X)**2.0)
C GROUND-REFLECTED WAVE COMP. CALC.-VERTICAL POLARIZED

```

```

RADC - EFN SOURCE STATEMENT - IFNSI -
          09/15/60

600 XB=SQRT(X*BPCOS/(BPPCOS*BPPCOS))
BN=2.0*ARCOS(BPPCOS)-ARCOS(BPPCOS)
DNK=SNPH1*COPH1
GRCK=HD*COPH2
J=1
GO TO 200
C GROUND-REFLECTED WAVE COMP. CALC.-HORIZONTAL POLARIZED
207 XB=SQRT(BPCOS/X)
BN=3.14159-ARCUS(BPPCOS)
DNK=SCOPH1
GRCK=SCOPH2
200 THETA=0.705398-0.5*BN
C DIRECT WAVE COMPONENT CALC.
405 DMCR=DNK*COS(ANG1)
DMCI=DNK*SIN(ANG1)
Q=HD*X0
QS=Q*Q
PN=PK/(XB*X0)
RADEN=QS+2.0*Q*COS(THETA)+1.0
RR=QS-1.0
RI=2.0*Q*SIN(THETA)
277
C GROUND-REFLECTED WAVE
GRCA=GRCK*(RR*COS(ANG2)-RI*SIN(ANG2))/RDEN
GRCI=GRCK*(RR*SIN(ANG2)+RI*COS(ANG2))/RDEN
GRCA=DIVF*GRCA
GRCI=DIVF*GRCI
C SURFACE-WAVE COMPONENT
601 RRM=1.0-(RR/RDEN)
RIM=(RI/RDEN)
RRMS=RRM*RRM
RIMS=RIM*RIM
PDDEN=(RRMS+RIM)*2.0
PRN=(RRMS-RIM)*COS(BN)-2.0*FIM*RRM*SIN(BN)
PBIN=2.0*FIR*RRM*COS(BN)+(RIMS-RIM)*SIN(BN)
BC=ATAN(PBIN/PBRN)
PC=4.0*PN*SQRT(PBRN*PBIN)/RDEN
C SURFACE ATTENUATION FACTOR
IF (PC<10.0) 201,201,202
201 HR=0.0
FI=0.0
C=1.0
SN=1.0
COM=1.0
PCEOTEN

```

RADC - EFN SOURCE STATEMENT - IFN(S) -

```

DO 2011 I=1,35
E=1
C=(2.0*E-1.0)
COM=(2.0*PC)*COM/C
SN=-SN
HR=SN*COM*COS(E*AC)+HR
2011 HI=SN*COM*SIN(E*AC)+HI
A= SORT(3.14159*PC)/EXP(IPC*COS(HC))
B=0.5*BC-PC*SIN(BC)
FR=1.0-A*SIN(B)+HR
FI=A*COS(B)+HI
GO TO 204
202 HR=0.0
HI=0.0
C=1.0
COM=1.0
901 00 2021 I=1,20
E=1
C=(2.0*E-1.0)
COM=C/(2.0*PC)*COM
HR=COM*COS(E*BC)+HR
2021 HI=COM*SIN(E*BC)+HI
2023 FR=-HR
FI=-HI
C SURFACE WAVE CALC.
204 SWK1=RRM*FR+RIM*FI
SWK2=RRM*FI-RIM*FR
SW1 =SCOPH2*(SWK1*COS(LANG2))-SWK2*SIN(LANG2)
SW1 =SCOPH2*(SWK2*COS(LANG2))-SWK1*SIN(LANG2)
C TOTAL FIELD CALC.
602 T=DWCR+GRCR+SWR
U=DMCI+GRCI+SWI
DIMENSION FIELD(2),FIELD(2)
FIELD(J+1)=10.0*ALNG10(T*U*U)
FIELD(J+1)=FIELD(J+1)-20.0*ALNG10(U)
K=L
TEST=AMAX1(ABS(DWCR),ABS(DWCI),ABS(GPCH),ABS(GRCI))
TESTC=AMAX1(ABS(SWK1),ABS(SWI))
IF (TEST-100.0*TESTC) 10054,10054,10054
10054 K=1
10053 CONTINUE
IF (K) 10020,10020,10021
10021 RR=RR/RDEN

```

09/15/66

RADC - EFN SOURCE STATEMENT - IFN(S) -

```
DWCR=DWCR/D  
DWCI=DWCI/D  
GRCR=GRCR/D  
GRCI=GRCI/D  
SWR=SWR/D  
SWI=SWI/D  
10022 FORMAT (2F7.3,1P6E10.2)  
      WRITE(6,10022) RRW,RIM,DWCR,DWCI,GRCR,GRCI,SWR,SWI  
10020 CONTINUE  
      IF (J) 206,206,205  
205 J=J-1  
      GO TO 207  
10005 FORMAT(1X,F8.1,2P4E12.2)  
206 WRITE(6,10005) D,FIELD(2),FIELD(1),FIELD(1),FIELD(1)  
500 D=D+DI  
501 GO TO 32100  
END
```

94

99

FORTRAN Statements
for
Radiation Propagation Calculations -
Norton Equation
Height Variation

RADC - EFN SOURCE STATEMENT - IFN(S) -

09/13/66

PAGE 1

```
32000 FORMAT (1H1)
32100 WRITE(6,32000)
31000 FORMAT (72H RADIO HIGH - FREQUENCY PROPAGATION CALCULATIONS MAIN
1-HEIGHT VARIATION)
      WRITE(6,31000)
30000 FORMAT (72H
1      READ (5,30000)
      WRITE(6,30000)
10000 FORMAT (F5.1,F3.1,2F7.1)
      READ (5,10000)HC,DIELC,COND
10007 FORMAT (F9.3,2F7.1,12)
      READ (5,10007)FREQ,HL,HIN,L
10001 FORMAT (15H CONDUCTOR HT. ,F5.1,12H DISTANCE ,F8.1,8H FREQ.
      WRITE(6,10001)HC,D,FREQ
10002 FORMAT (20H DIELECTRIC CONSTANT,F7.1,20H EARTH CONDUCTIVITY ,F7.1)
      WRITE(6,10002)DIELC,COND
10004 FORMAT (70H HT.(FT) VERTICAL VERT/DIST. HORIZONTAL HORIZ/DIST
1. FIELD (DB)
      FIELD (DB)
210  WRITE (6,10004)
      X=17.9731*COND/FREQ
      BPPCOS=1.0/SQRT(1.0+((DIELC/X)*(DIELC/X)))
      NI=INT(HL/HIN)+1
      NI=INT(HL/HIN)+1
      HA=0.0
      DO 500 K=1,NI
      R1=SQRT((HC-HA)**2.0+D**2)
      R2=SQRT((HC+HA)**2.0+D**2)
      ANG1=0.0063838*FREQ*k1
      ANG2=0.0063838*FREQ*k2
      PK=0.5*ANG2
      HD=(HC+HA)/R2
      COP=D/R2
      402 SCOPH2=(COPH2)*(COPH2)
      BPCOS=1.0/ SQRT(1.0+((DIELC-SCCPH2)/X)**2.0)
      C DIRECT WAVE COMPONENT CALC.
      403 DWK=(D/R1)*3.0
      405 DWR=DWK*COS(ANG1)
      DWC=DWK*SIN(ANG1)
      C GROUND-REFLECTED WAVE COMP. CALC.-VERTICAL POLARIZED
      600 XB=SQRT(X*BPCOS/(BPCOS*APPCL))
      BN=2.0*ARCOS(BPCOS)-ARCCOS(BPCOS)
```

09/13/66

```

J=1
GO TO 200
C GROUND-REFLECTED WAVE COMP. CALC.-HORIZONTAL POLARIZED
207 XB=SQR(THPCOS/K)
BN=3.14159-ACOS(THPCOS)
200 THETA=0.78539-0.5E-4
Q=HD*XB
QS=0*0
PN=PK/(XH*XH)
RDEN=QS+2.0*Q*COS(THETAT)+1.0
RR=QS-1.0
RI=2.0*Q*SIN(THETAT)
GRCP=SCCPH2*COPH2*(PC*COS(ANG2)-1*SIN(ANG2))/E24
GRCI=SCUPH2*COPH2*(PC*SIN(ANG2)+1*COS(ANG2))/RDEN
C SURFACE-WAVE COMPARISON
601 RRM=1.0-(KR/RDEN)
RIM=(RI/RDEN)
RRMS=RP*ERRQ
RIMS=RIM*RIM
PBDEN=(RRMS-RIM)**2.0
PBRN=(RRMS-RIM)*COS(BRN)-2.0*SIN(BRN)*SIN(RM)
PBIN=2.0*RIM*(PC*COS(ANG)+(RMS-RIM)*SIN(ANG))
BC=ATAN(PBRN/PBIN)
PC=4.0*PN*SQRT(PBRN*PBIN*PHIN*PHIN)/PBDEN
IF (PC<10.0) 201,201,202
C SURFACE ATTENUATION FACTOR
201 HR=0.0
HI=0.0
C=1.0
SN=1.0
COM=1.0
DO 2011 I=1,35
E=I
C=(2.0*E-1.0)
COM=(2.0*PC)*CINV/C
SN=-SN
HR=SN*COS(E*HC)+HP
2011 HI=SN*COS(SINE*HC)+HI
A=SORT(3.14159*PC)/EXP(PC+COS(HC))
B=0.5*BC-PC*SIN(HC)
FR=1.0-A*SIN(B)+HR
FI=A*COS(HI)+HI
GO TO 204

```

	REALFACT	56
IMAGFACT	58	
REALATTN	60	61
IMAGATTN	63	62
	64	
	65	

09/13/66

RADC - FFN SOURCE STATEMENT - FIN(S) -

```

202 HR=0.0          71
HR=0.0
C=1.0
COM=1.0
901 DO 2021 I=1,20   71
E=1
C=(2.0*E-1.0)
COM=C/(2.0*PC)*COM
HR=COM*COS(E*B1)+HR
2021 HI=COM*SIN(E*B1)+HI
2023 FR=-HR
FI=-HI
C SURFACE WAVE CALC.
204 SWK1=RR*FR+RIM*FI
SWK2=RR*FI-RIM*FR
SMR = SCOPH2*(SWK1*COS(ANG2)-SWK2*SIN(ANG2))
SMI = SCOPH2*(SWK2*COS(ANG2)+SWK1*SIN(ANG2))
C TOTAL FIELD CALC.
602 T=DWCR+GKCR+SMR
U=DMCI+GRCI+SMI
FIELD=10.*ALOG10(T*T*U*U)
283 FIELD=FIELD-20.*ALOG10(D)
IF (ABS(DMCI)-ABS(LU).GT.SWK1)10054,10050
10050 IF (ABS(GRCR)-ABS(LU).GT.SMR)10054,10051
10051 IF (ABS(DWCR)-ABS(LU).GT.SMI)10054,10052
10052 IF (ABS(GRCR)-ABS(LU).GT.SMI)10054,10053
10054 L=1
10060 FORMAT(126H SIGNIFICANT SURFACE WAV )
WRITE (6,10060)                                     92
10053 CONTINUE
IF (J>206,206,205
10005 FORMAT(1X,FF9.1,4P2E12.1)
10006 FORMAT(1H+,33X,4P2E12.1)
205 WRITE (6,10005) HA,FIELD,FIELD
J=J-1
IF (L>10020,10020,10021
10021 RR=RR/RDF1
DMCR=DMCR/D
DMCI=DMCI/D
GKCR=GKCR/D
GRCI=GRCI/D
SMR=SMR/D
SMI=SMI/D

```

PAGE 4

09/13/66.

```
RADC - FHN STATUS = FHN - FHN -  
10022 FORMAT (F7.3,1P6E10.2)  
    WRITE(6,10022) RHN,RIN,DWCI,DWCE,DRCI,DRCF,SWR,SWI  
10061 FNCWRITE(10,1)  
    WRITE(6,10041)  
10020 CONTINUE  
    GO TO 207  
206 WRITE (6,10041)  
    IF (L) 10025,10026,10026  
10026 RRW=RR/RDN  
    DWCR=DWCF/D  
    DWCI=DWC1/F  
    GRCR=GACK/D  
    GRCI=GRC1/D  
    SWR=SWR/D  
    SWI=SWI/D  
10027 FORMAT (2F7.3,1P6E10.2)  
    WRITE(6,10027) RHN,RIN,DWCE,DWCI,DRCI,DRCF,SWR,SWI  
10025 CONTINUE  
500 HA=HA+HIN  
501 GO TO 32100  
END
```

103

106

106

FORTRAN Statements

for

Radiation Propagation Calculations -

Modified Equation

Height Variation

26/15/64

RADC - EFN SOURCE STATEMENT - IFN(S) -

```

32000 FORMAT (1H1)
32100 WRITE(6,32000)
31000 FORMAT (90H0 RADIO HIGH-FREQUENCY PROPAGATION CALCULATIONS - HIGH
1T VARIATION NORTON'S MODIFIED FREQ.
      WRITE(6,31000)
30000 FORMAT (72H
1      READ (5,30000)
      WRITE(6,30000)
10000 FORMAT (F5.1,F8.1,2F7.1)
      READ (5,10000)HC,D,DIELC,COND
10007 FORMAT (F9.3,2F7.1,I2)
      READ (5,10007)FREQ,HL,HIN,L
10001 FORMAT (15H CONDUCTOR HT.,F5.1,1?H  DISTANCE ,F3.1,PH  FREQU.
1,F9.3,4H MHZ )
      WRITE(6,10001)HC,D,FREQ
10002 FORMAT (20H DIELECTRIC CONSTANT,F7.1,20H EARTH CONDUCTIVITY ,F7.1)
      WRITE(6,10002)DIELC,COND
10004 FORMAT (17H HT.(FT) VERTICAL   VERT/CLST.  HORIZONTAL  HORIZ/DIST
1. FIELD (DB) )
210  WRITE (6,10004)
286   X=17.9731*COND/FREQ
     BPPCOS=1.0/SQRT(1.0+((DIELC/X)*(DIFLC/X)))
     NI=INT(HL/HIN) +1
     HA=0.0
     DO 500 K=1,NI
       R1=SQRT((HC-HA)**2.0*D*D)
       R2=SQRT((HC+HA)**2.0*D*D)
       ANG1=0.0063838*FREQ*R1
       ANG2=0.0063838*FREQ*R2
       PK=0.5*ANG2
       SNPH1=1HC-HA)/R1
       HD=(HC+HA)/R2
       COPH1=D/R1
       COPH2=D/R2
       SCOPH1=COPH1+COPH1
402   SCOPH2=(COPH2)*(COPH2)
       BPCOS=1.0/ SQRT (1.0+((DIFLC-SCCPH2)/X)*#7.0)
C GROUND-REFLECTED WAVE COMP. CALC. -VFRICAL P.MAFIZFD
600   XB=SQRT(X*BPCOS/(BPPCOS*BPPCOS))
     BN=2.0*ARCOS(BPPCOS)-ARCSIN(BPPCOS)
     DWK=SNPH1*COPH1
22    23
25    26
26    27

```

PAGE 7

DEC/15/87

RADC - EFN SOURCE STATT-NR - IF(J(S) -

GRCK=HD*COPH2
J=1

GO TO 200

C GROUND-REFLECTED WAVE COMP. CALC.-HORIZONTAL POLARIZED
207 XB=SQRT(BPCOS/X)
BN=3+14159-ARCOS(BPCOS)

DWK=SCOPH1
GRCK=SCOPH2

200 THETA=0.785398-0.5*BN

C DIRECT WAVE COMPONENT. CALC.

405 DWCR=DWK*COS(ANG1)

DWC1=DWK*SIN(ANG1)

Q=HD*X_B

QS=Q*Q

PN=PK/(XB**XB)

RDEN=QS+2.0*Q*COS(THETA)+1.0

RR=QS-1.0

RI=2.0*Q*SIN(THETA)

C GROUND-REFLECTED WAVE

GRCK=GRCK*(RR*COS(ANG2)-RI*SIN(ANG2))/RDEN

GRCI=GRCK*(RR*SIN(ANG2)+RI*COS(ANG2))/RDEN

C SURFACE-WAVE COMPONENT

601 RRM=1.0-(RR/RDEN)

RIM=(RI/RDEN)

RRMS=RRM*RRM

RIMS=RIM*RIM

PBDEN=(RRMS+RIMS)**2.0

PBRN=(RRMS-RIMS)*COS(BN)-2.0*RIM*RRM*SIN(BN)

PBIN=2.0*RIM*RRM*COS(BN)+(RRMS-RIMS)*SIN(BN)

BC=ATAN(PBIN/PBRN)

PC=4.0*PN*SQR(T(PBRN*PRIN+PRIN*PRIN))/PBDEN

C SURFACE ATTENUATION FACTOR

IF (PC<10.0) 201,201,202

201 HR=0.0

HI=0.0

C=1.0

SN=1.0

COM=1.0

DO 2011 I=1,35

E=1

C=(2.0*E-1.0)

COM=(2.0*PC)*COM/C

SN--SN

PFL FCT
FACT DR

CONSTANT
34
35

36
37
38
39
40
41

42
43
44
45
46
47
48
49
PCEQTEN

```

RAOC      -   TFM      SURCF STATE AT(I) -  FN(S) -
          HI=SN*COM*COS(E*HC)+HR
          A=SQRT(3.14159*PC)/EXP(PC*CONS(HC))
          B=0.5*BC-PC*SIN(BC)
          FR=1.0-A*SIN(B)+HR
          FI=A*COS(B)+HI
          GO TO 204
202      HR=0.0
          HI=0.0
          C=1.0
          COM=1.0
          DO 2021 I=1,20
          E=I
          C=(2.0*E-1.0)
          COM=C/(12.0*PC)*CIM
          HR=COM*COS(E*HC)+HR
          HI=COM*SIN(E*BC)+HI
2021      FR=-HR
          FI=-HI
          C SURFACE WAVE CALC.
          SWK1=RRM*FR+RM*FI
          SWK2=RRM*FI-RM*FR
          SWR =SCOPH2*(SWK1*COS(ANG2)-SWK2*SIN(ANG2))
          SWI =SCOPH2*(SWK2*CUS(ANG2)+SWK1*SIN(ANG2))
          C TOTAL FIELD CALC.
          204      T=DMCR+GRCR+SMR
          U=DMCI+GRCI+SMI
          DIMENSION FIELD(2),FIELD(2)
          FIELD(J+1)=10.0*ALOG10(T*T+U*U)
          FIELD(J+1)=FIELD(J+1)-20.0*ALOG10(U)
          K=L
          TEST=AMAX1(ABS(DMCR),ABS(GFCR),ABS(GFCI))
          TESTC=AMAX1(ABS(SMR),ABS(SWI))
          IF (TEST-100.0*TESTC) 10054,10054,10054
10054      K=1
          10053  CONTINUE
          IF (K) 10020,10020,10021
10021      RR=RR/RDEN
          DMCR=DMCR/D
          DMCI=DMCI/D
          GRCR=GRCR/D
          GRCI=GRCI/D
          SMR=SMR/D
          REALFACT 44
          MAGFACT 44
          REALATTN 61
          MAGATTN 61
          OCCUTEN
          SURFACE
          WAVE
          TEST

```

92/15/64

RADC - EFN SNUFCF STATIST - IF(5) -
SWI=SWI/D
10022 FORMAT(2F7.3,1P6E10.2)
 WRITE(6,10022) RHW,RI4,DmCR,DmCL,IFC1,IFC2,SUR,SWI
10020 CONTINUE
 IF (J) 206,205
205 J=J-1
 GO TO 207
10005 FORMAT(1X,F3.1,2P4F12.?)
206 WRITE(6,10005) HA,FILEU(2),FILEU(3),FILEU(1),FILEDD(1)
500 HA=HA+HIN
501 GO TO 32100
END

HIGH VOLTAGE POWER LINE
SITING CRITERIA

Appendix V of Vol. I

Effect of Antenna Height

30 December 1966

Westinghouse Electric Corporation
Electric Utility Headquarters Department
Research and Development Center
Pittsburgh, Pennsylvania

Rome Air Development Center (RADC)
Griffiss Air Force Base
Rome, New York 13442

Contract AF30(602)3822

List of Figures for Appendix V

	<u>Page No.</u>
Fig. 1 Van Used for Instruments and Antenna Mounting.	297
Fig. 2 Horizontal Tuned Dipole Comparisons at 93 ft from 110 kV Line Tower.	298
Fig. 3 Horizontal Tuned Dipole Comparisons at 200 ft from 110 kV Line Tower.	299
Fig. 4 Horizontal Tuned Dipole Comparisons at 500 ft from 110 kV Line Tower.	300
Fig. 5 Vertical Tuned Dipole Comparisons at 93 ft from 110 kV Line Tower.	301
Fig. 6 Vertical Tuned Dipole Comparisons at 200 ft from 110 kV Line Tower.	302
Fig. 7 Vertical Tuned Dipole Comparisons at 500 ft from 110 kV Line Tower.	303
Fig. 8 Average Difference Between Tripod and Van Roof Antennas Referred to Tripod Mtg.	304
Fig. 9 Antenna Used for Tests from 24 ft to 90 ft Height.	305
Fig. 10 Effect of Horizontal Dipole Height at 30 Mc/s at Three Distances from Line.	306
Fig. 11 Effect of Horizontal Dipole Height at 100 Mc/s at Three Distances from Line.	307
Fig. 12 Effect of Vertical Dipole Height at 100 Mc/s at Three Distances from Line.	308
Fig. 13 Effect of Receiver Antenna Height at 200, 600 and 1998 ft Opposite Line Tower.	309
Fig. 14 Horizontal Fields 200 ft from Source at 30 Mc/s.	310
Fig. 15 Horizontal Field 2000 ft from Source, 30 Mc/s.	311
Fig. 16 Horizontal Fields 200 ft from Source at 150 Mc/s.	312

APPENDIX V - EFFECT OF ANTENNA HEIGHT

I. INTRODUCTION

In the beginning of the project on power lines siting criteria it was realized that the most efficient method of making extensive measurements, in the field with dipole antennas, was to mount these antennas on the roof of the test van. This mounting location offered the advantages of a more stable antenna mount in high winds than the tripod, lateral profile recordings could be made by simply moving the van, the antenna could be rotated from inside the van during inclement weather and instrumentation could be used inside the van. This method is quite adequate for the comparison of the relative field strengths produced by lines and the effect of lateral distance from a line.

It is recognized that the field strength values obtained using the van antenna mounting method would be different from those obtained when using the standard method of mounting the antennas on a tripod. The antenna factors supplied by the instrument manufacturer are based on an antenna height of 8.5 and 10 feet above ground; whereas, the antenna height when mounted on the test van roof is 20.5 feet. The phase relationship of signals received through direct radiation to those received from reflections from ground are different for the two antenna heights.

In order to determine the amount of difference involved, comparison measurements of field strength were obtained with the dipole antennas mounted according to manufacturer's specifications and with the antennas mounted on the van roof. These measurements were initially made using the artificial gap-type radio noise generator as the signal source and later with commercial TV or FM broadcast stations as the signal source.

Measurements were also made to determine the effect of changing dipole antenna height near a power line from twenty-four feet

to ninety feet. This was done on a 345 kV line with the artificial gap-type radio noise generator as the signal source.

This appendix details the procedures followed and the results obtained in performing these antenna comparison measurements.

2. METHODS OF MEASUREMENT AND RESULTS

2.1 Comparison of Antennas Near Power Line

The artificial gap-type radio noise source was connected to the outside phase conductor of a horizontal configuration 110 kV wood pole line shown in Figures 17 and 30d.* Field strength measurements were made at lateral distances of 77 feet, 184 feet, and 484 feet from the line conductor to which the gap was connected. The line conductor is 39 feet above ground level.

The frequency range under investigation requires the use of three separate tuned dipole antennas. The frequency ranges covered by individual antennas are 30 - 90 Mc/s, 90 - 400 Mc/s and 400 - 1000 Mc/s.

Measurements were completed for one of the tuned dipole antennas mounted on a tripod and then repeated with that antenna mounted on the van roof at each of the three test locations, see Fig. 1. For the measurements made with antennas mounted on the tripod, the test van and instruments were located 200 feet from the antenna and connection to the antenna was made with 200 feet of RG 9/U coaxial cable. Corrections were made to compensate for cable attenuation.

The results of these measurements can be seen in Figs. 2 through 8. Because of the low radio noise in the 400 to 1000 Mc/s range, particularly at 200 and 500 feet, comparisons are limited to the 30 to 400 Mc/s range. From Fig. 8 it can be seen that the average dB difference between the two antenna mounting locations is minimum at the location nearest the source and approaches the value, $20 \log_{10} \frac{h_2}{h_1}$,

*Figures of Vol. I.

as distance from the source is increased, h_1 and h_2 being the two receiver antenna heights.

Figures 2 through 7 show a direct comparison of the two antenna mounting locations at different distances from the source. From these figures it is evident that measurements made with antennas mounted on the van roof are practically always higher than those with the antennas mounted on a tripod.

2.2 Commercial Broadcast Stations as Source for Antenna Comparisons

The antenna mounting locations were compared on commercial broadcast signals. A test location was selected which was more than ten miles from transmitting antennas, and was a local high point in elevation, free of reflecting surfaces such as buildings, trees, etc. For the measurement of television signals, the signal was viewed on a portable television set to assure that the signal was not affected by reflections while on either the tripod or van roof.

With the tuned dipole antenna mounted on the tripod, measurements were made at one frequency at five randomly selected points on a straight line 100 feet long. The antenna was then moved to the van roof and the measurements repeated.

Within the frequency range of 50 Mc/s to 206 Mc/s four stations were measured; three of which were TV stations and one was an FM station. Of the four stations measured, two of the television stations and the FM station appeared in the frequency range between 50 and 100 Mc/s. The average difference between the field strength measured, with the antenna mounted on the van, was within 1 dB of the difference due to height change calculated by $20 \log_{10} (h_2/h_1)$. Variations between tripod and van roof mounting locations for the five measurement locations were within 1.5 dB.

For the remaining TV station at 206 Mc/s, variations between tripod and van roof amounted to 6 dB for the different locations, and the average difference between the two antenna mounting locations was 6 dB less than the calculated difference.

2.3 Effect of Antenna Height From 24 Feet to 90 Feet

These investigations into the effect of dipole antenna height for a dipole near a power line were made jointly with the Air Force. Field strength measurements were applied to a strip chart recorder while the height of antennas was varied from 24 feet to 90 feet above ground level.

For this series of measurements the radio noise source was the artificial gap-type radio noise generator connected to the outside phase of a bundle conductor of 345 kV horizontal configuration steel tower line. Measurements were made over the frequency range of 30 Mc/s to 200 Mc/s at lateral distances of 200, 600 and 2000 feet from a point directly beneath the radio noise generator.

A horizontal tuned dipole was used in measurements in the frequency range of 30 to 80 Mc/s and a broad-band dipole was used both vertically and horizontally over the frequency range of 100 to 200 Mc/s.

The tower on which the antenna was mounted was a five-section telescoping steel tower of triangular construction, Figure 9. Raising or lowering the tower was accomplished through a cable being wound or unwound on a motor driven drum. The tower height was varied at a linear rate and required approximately four and a half minutes to be raised or lowered over the height range of 24 to 90 feet. A motor driven rotator mounted on top of the tower was used to vary the antenna azimuth. A micro-switch was actuated once each revolution of the cable drum and was used to obtain an indication of tower height.

At a height of 24 feet the antenna was rotated to obtain a maximum value on the field strength meter which was indicating the quasi-peak level. This value was also fed to a graphic recorder from the recorder output jack on the meter. Upon locating the angle of maximum value, the antenna azimuth was noted and the tower was then raised to a height of 90 feet. During motion of the tower the previously mentioned micro-switch actuated a capacitive discharge

circuit which caused an instantaneous change in the meter output level, thereby placing a mark on the recorder chart for each sixteen inch change in tower height. Upon attaining a height of 90 feet the antenna was again rotated for maximum value on the field strength meter. If the azimuth of maximum signal found at 90 feet differed significantly from that at 24 feet, a second chart was made as the tower was being lowered. From the strip chart recordings it is possible to determine the effect of antenna height directly.

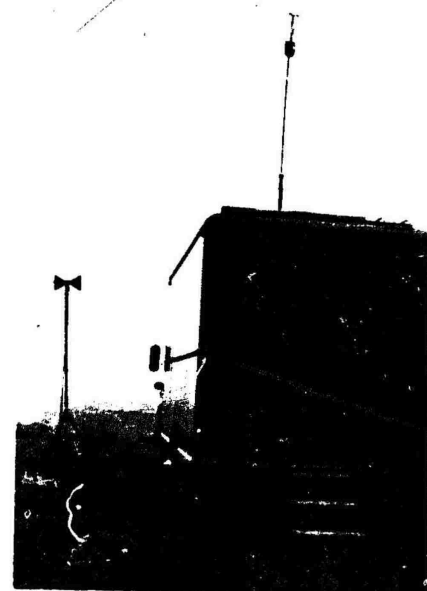
Figures 10, 11 and 12 are representative of the charts obtained. From Figure 13 it can be seen that at a frequency of 100 Mc/s the maximum deviation of the signal level with height from the signal level at a height of 24 feet is +8 dB and -9 dB 200 feet from the source, +2 dB and -14 dB at 600 feet from the source, and +3 dB and -6 dB 2000' feet from the source. For the purpose of communication receiver siting with respect to power lines only the increase in radio noise level is of importance. Figure 13 is a graphic representation of the maximum deviation versus frequency for the three lateral measurement locations. These results indicate a general decrease in the amount of variation with antenna height as the distance from the source is increased.

2.4 Comparison of Measurements with Calculations

Field strength variations with height were calculated with the equations of Appendix IV from ground to a height of 200 feet above ground, at distances of 200 feet, 600 feet, and 2000 feet from a source similar to the one used in the measurements. Comparisons of the calculated and measured values are shown in Figures 14, 15 and 16. To compare the data, approximate corrections have been made for changes in elevation of the terrain where measurements were made. Considering the irregularity of the terrain in the near vicinity of the measurement locations, the calculated variations compare quite well with measurement results.



(a) Tunable Dipole Antenna



(b) Broadband Antennas

Fig.1 . Van Used for Instruments and Antenna Mounting.

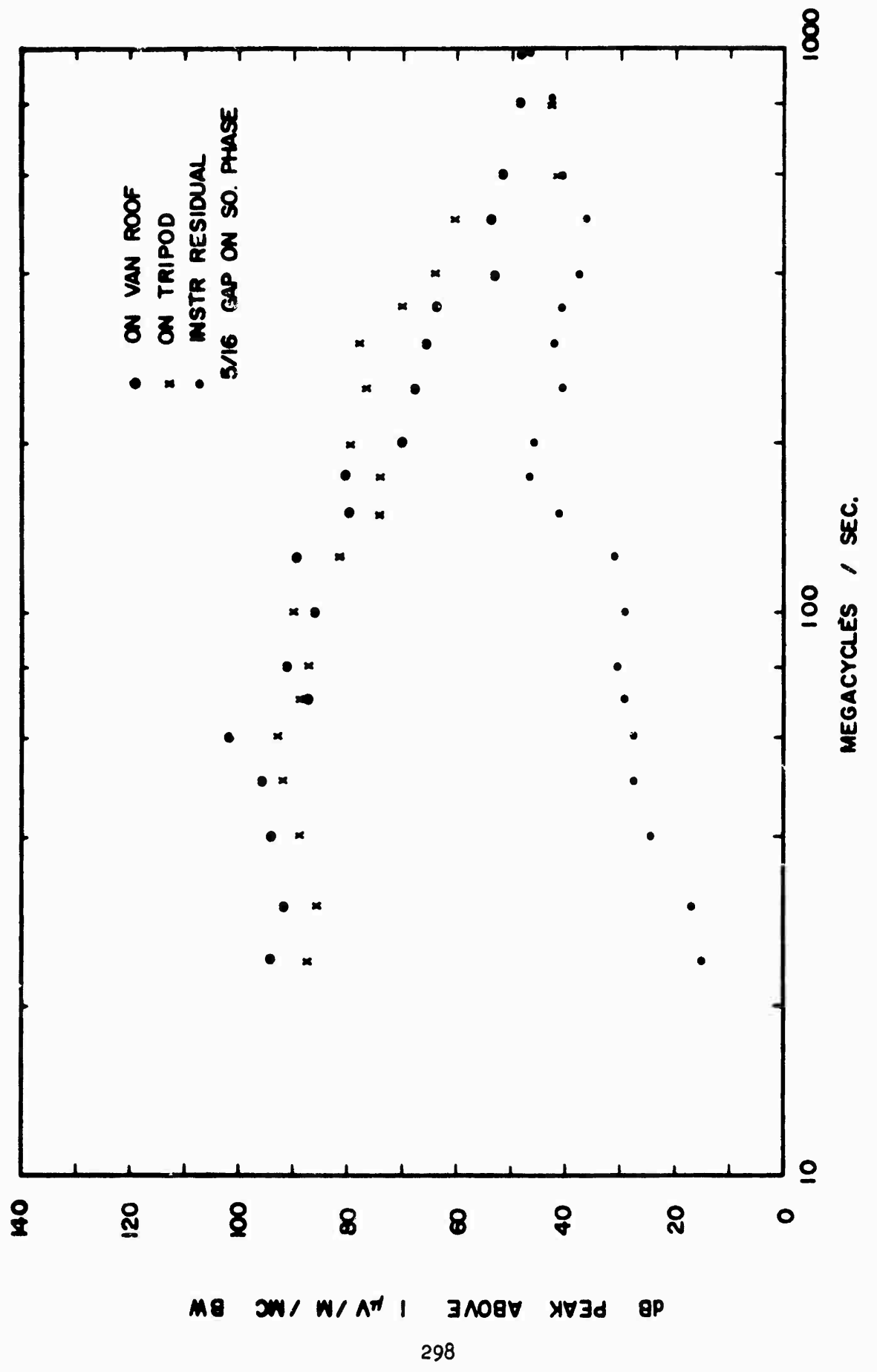


FIG. 2. HORIZONTAL TUNED DIPOLE COMPARISONS AT 93' FROM 110 KV LINE TOWER

FIG. 3 HORIZONTAL TUNED DIPOLE COMPARISONS AT 200 FEET FROM
110 KV LINE TOWER

MEGACYCLES / SEC.



• ON VAN ROOF
 ✕ ON TRIPOD
 • INSTR. RESIDUAL
 5/16" GAP ON SO. PHASE

140

120

100

80

60

40

20

0

dB PEAK ABOVE 1 μ V/M / MC BW

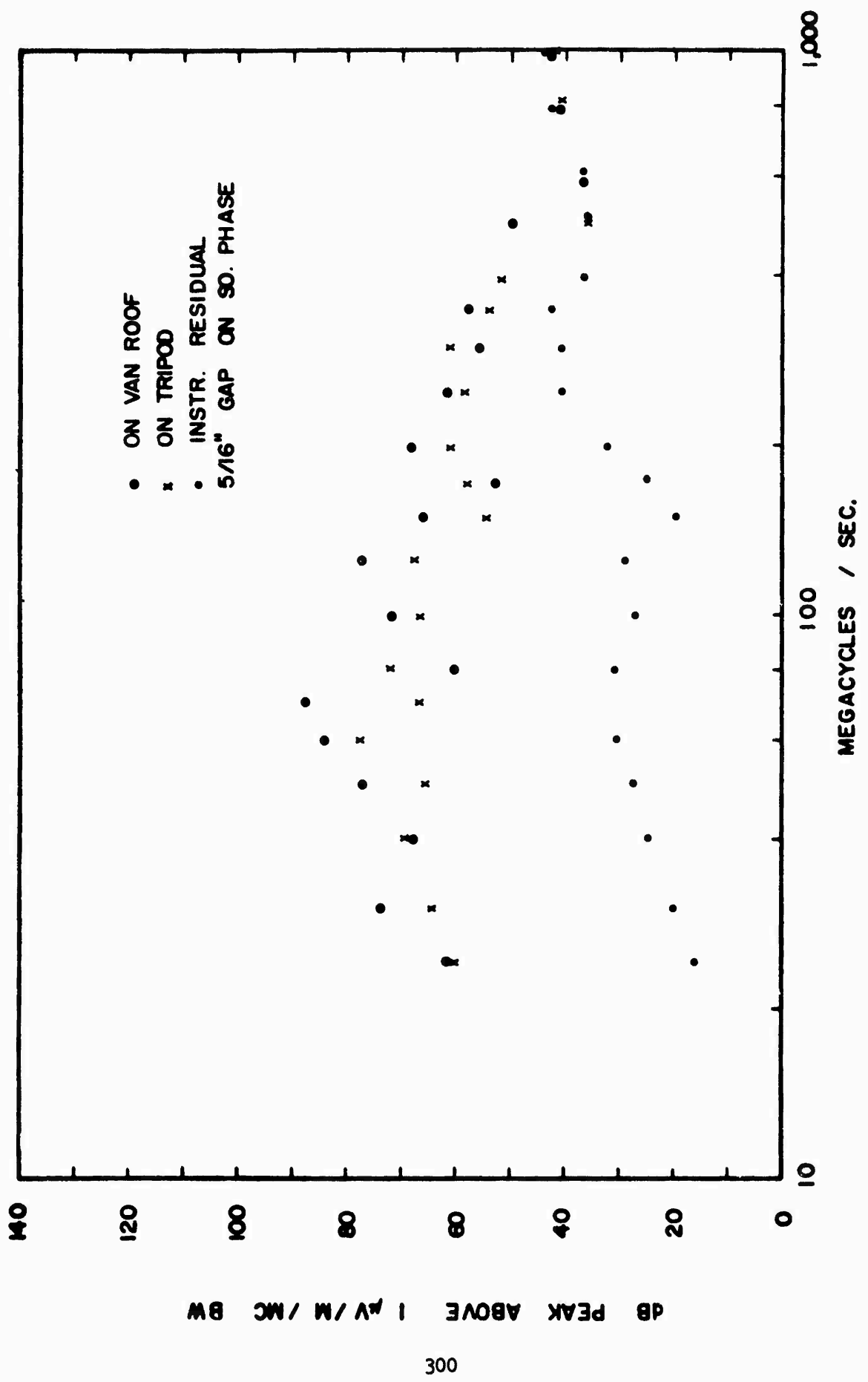


FIG. 4 HORIZONTAL TUNED DIPOLE COMPARISONS AT 500 FEET FROM 110 KV LINE TOWER

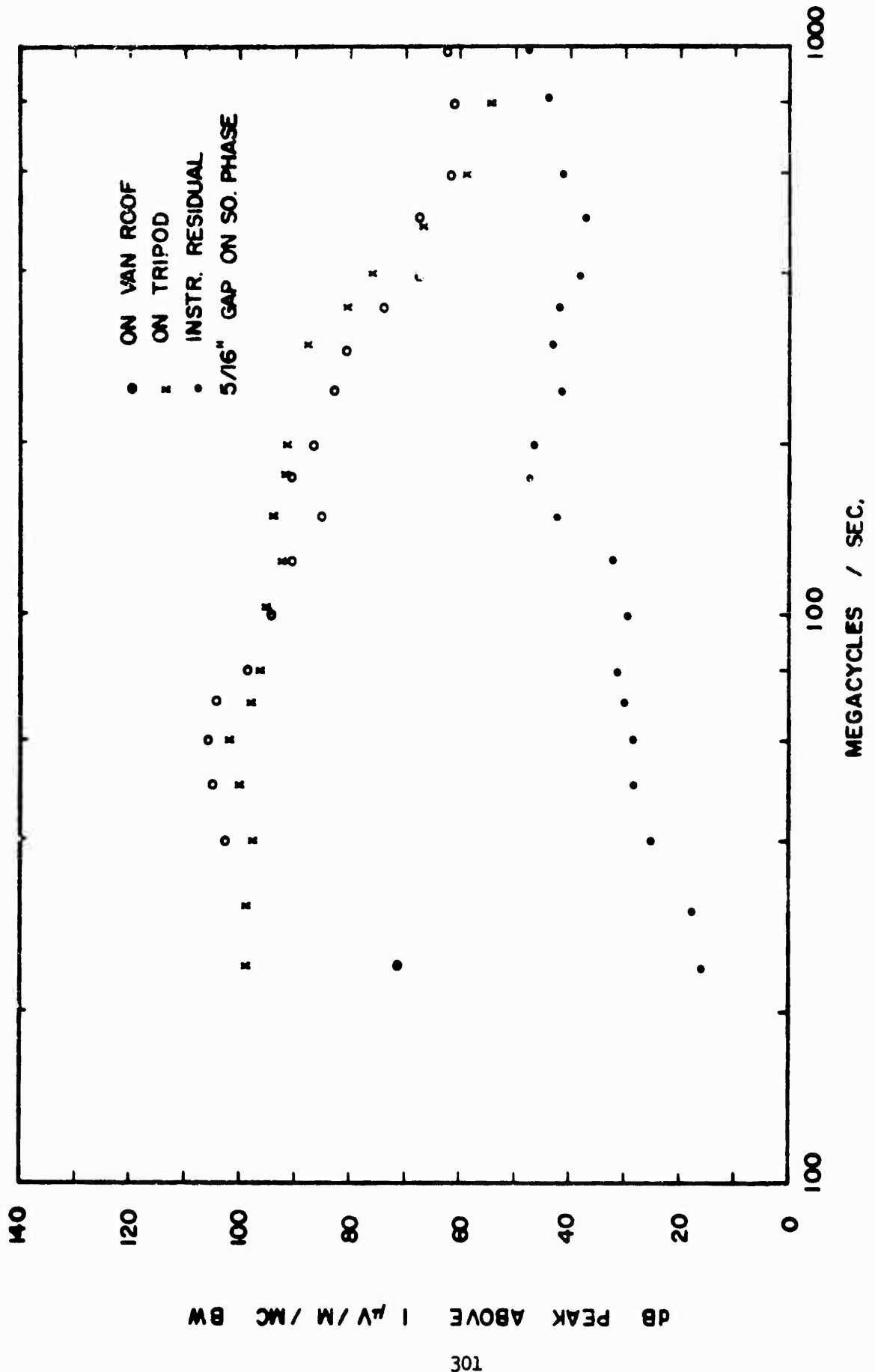


FIG. 5 VERTICAL TUNED DIPOLE COMPARISONS AT 93 FT. FROM 110 KV LINE TOWER

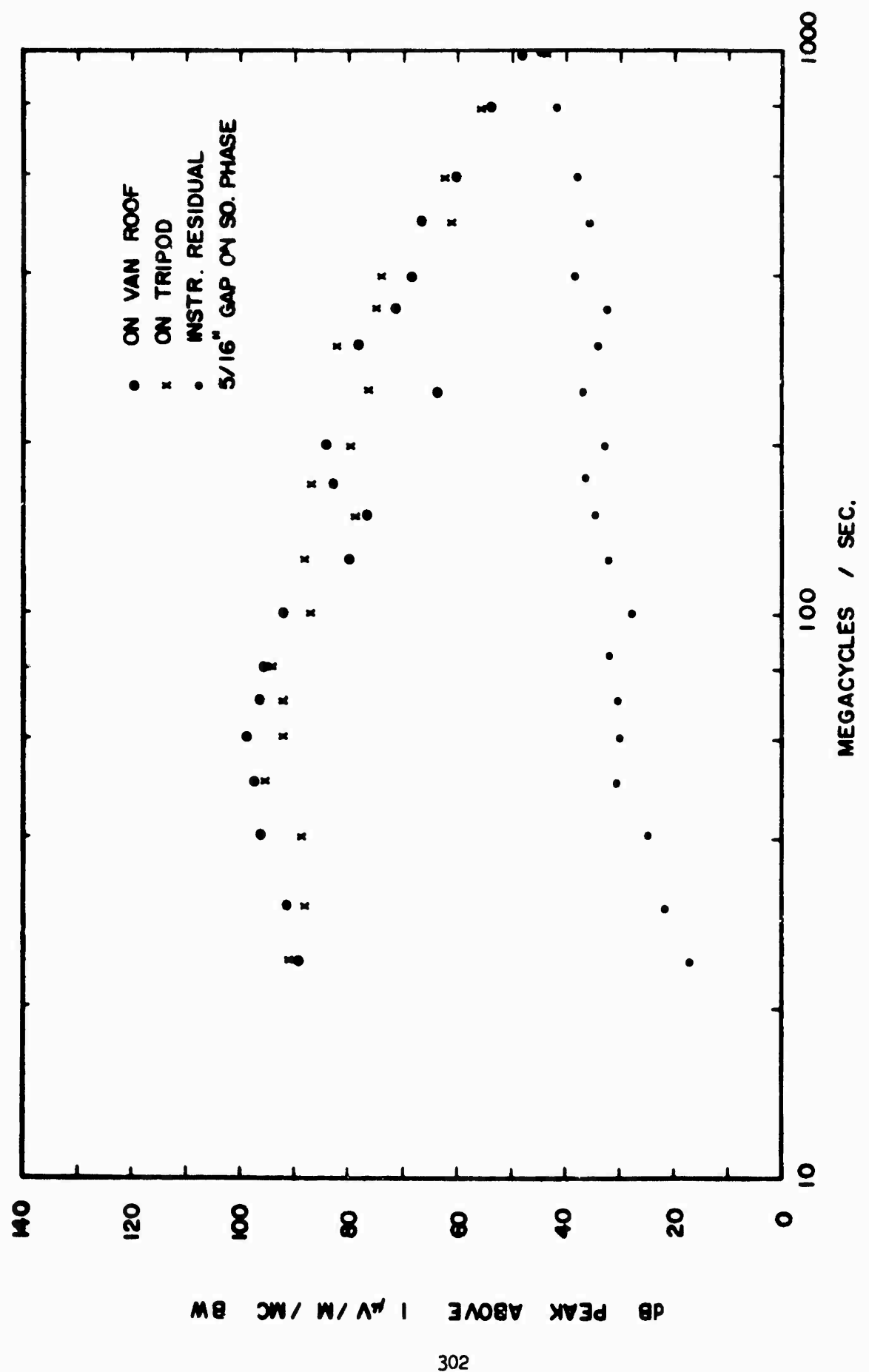
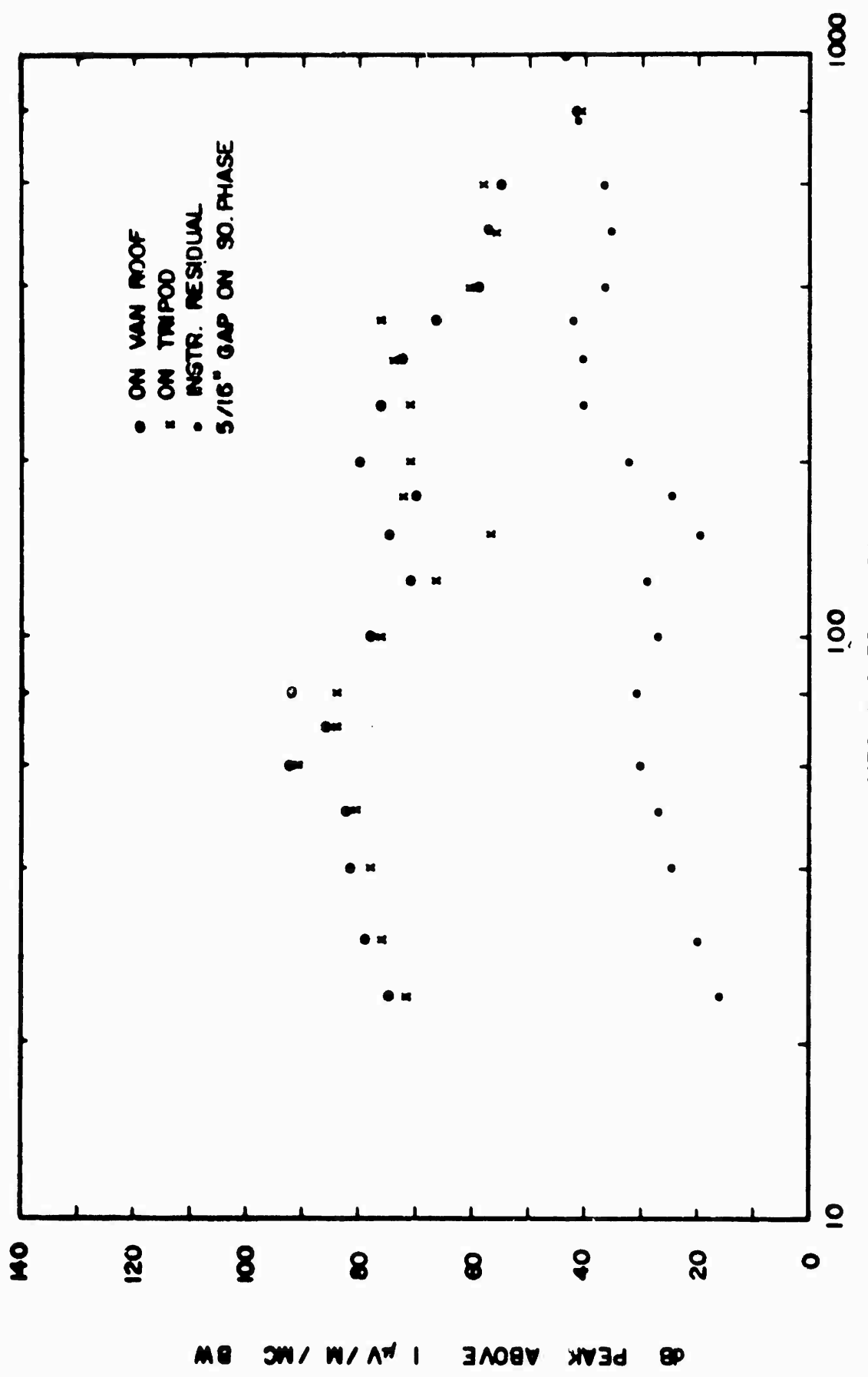


FIG. 6 VERTICAL TUNED DIPOLE COMPARISONS AT 200' FROM 110 KV LINE TOWER

FIG. 7 VERTICAL TUNED DIPOLE COMPARISONS AT 500' FROM 110KV TOWER



Curve 579058-8

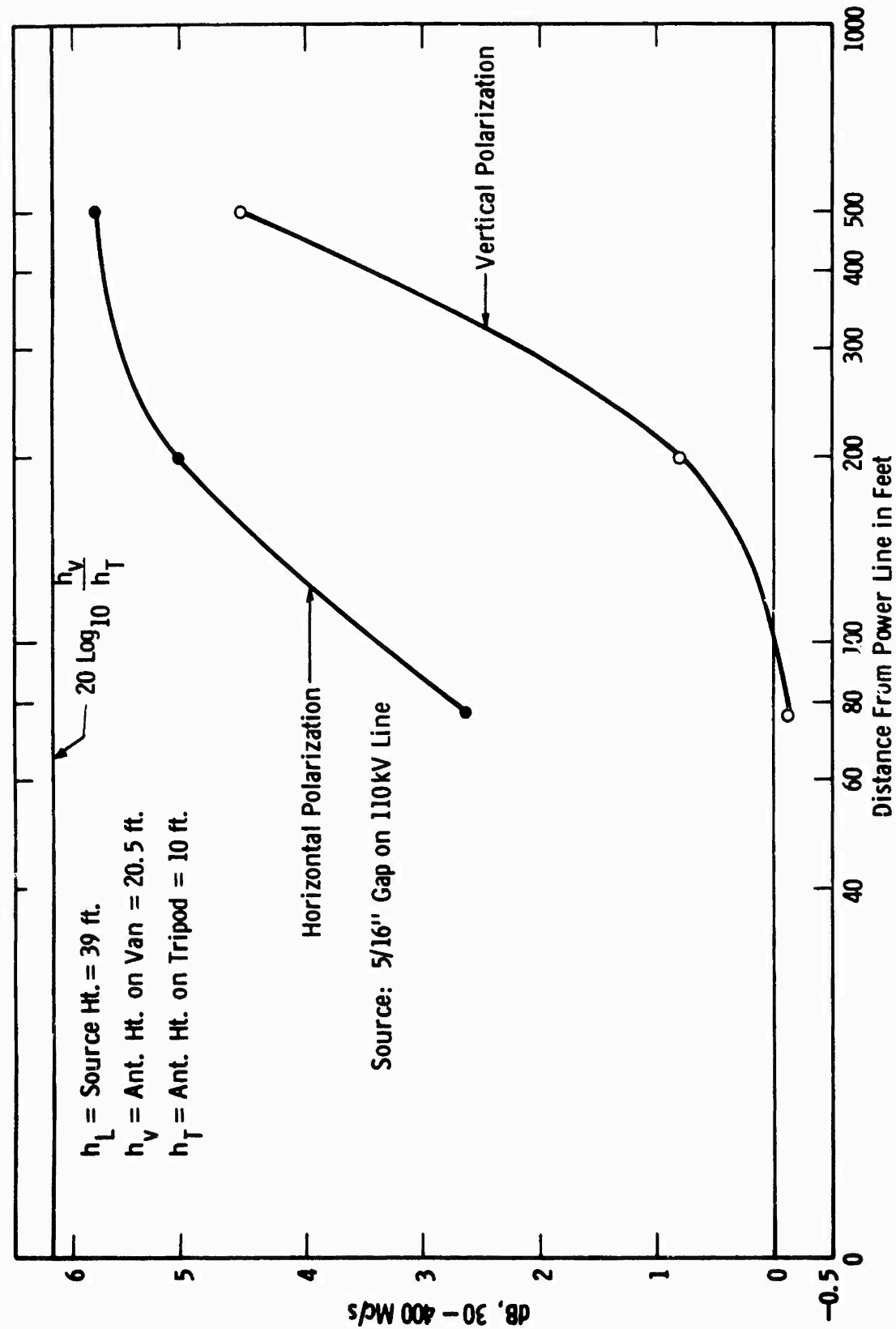
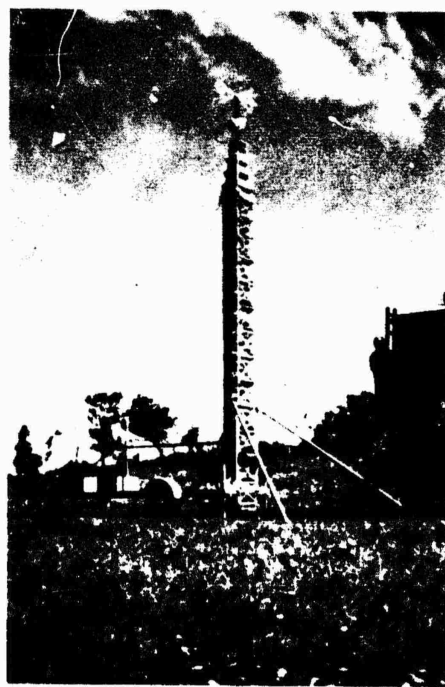


Fig. 8—Average difference between tripod and Van Roof antennas referred to tripod htg



(a) Antenna at 24 Feet



(b) Antenna at 90 Feet

FIG. 9

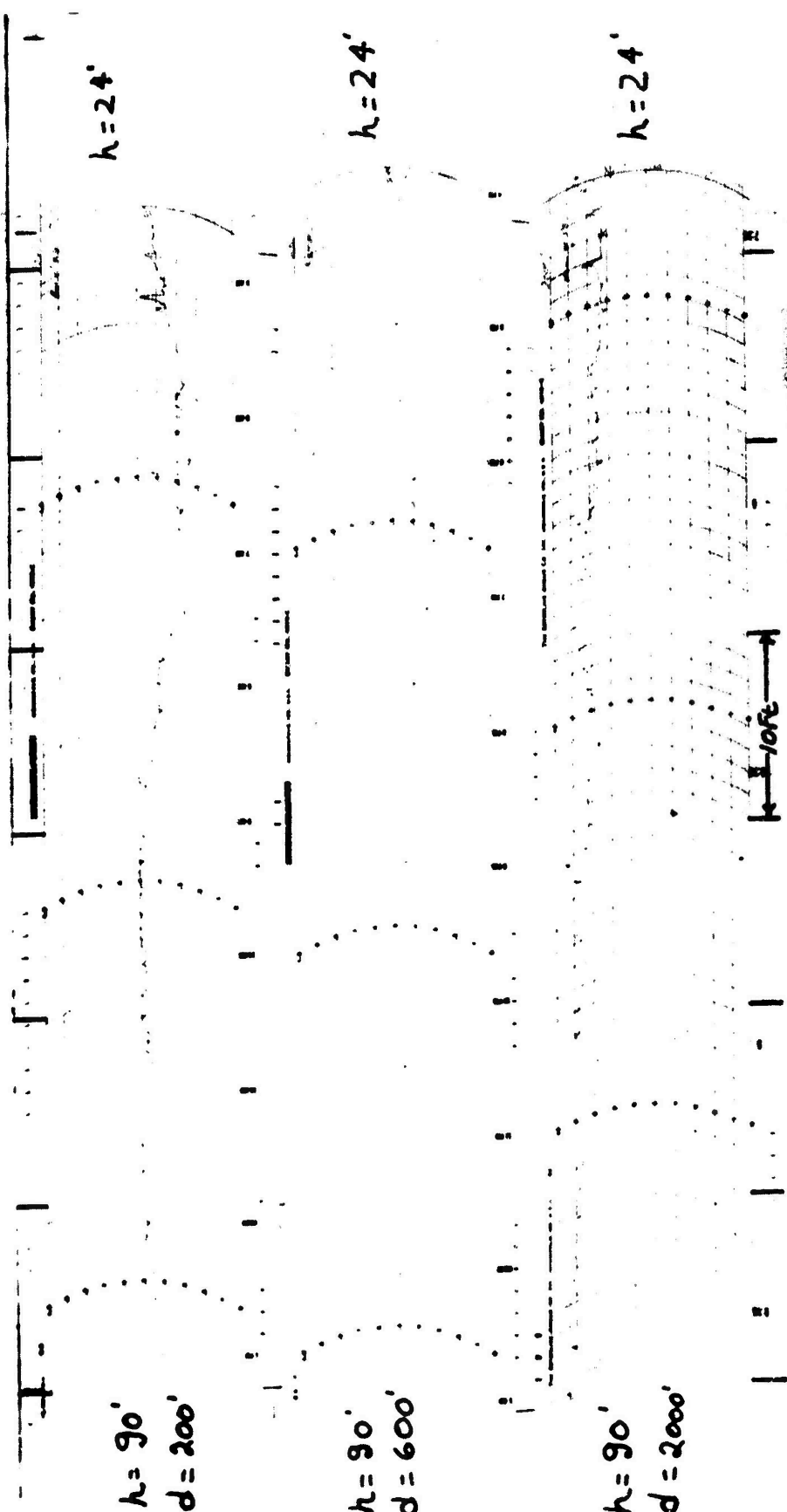


Fig. 10 Effect of Horizontal Dipole Height at 30 Mc/s at Three Distances From Line. (Vertical Scale = Approx. 1 db/Minor Division).

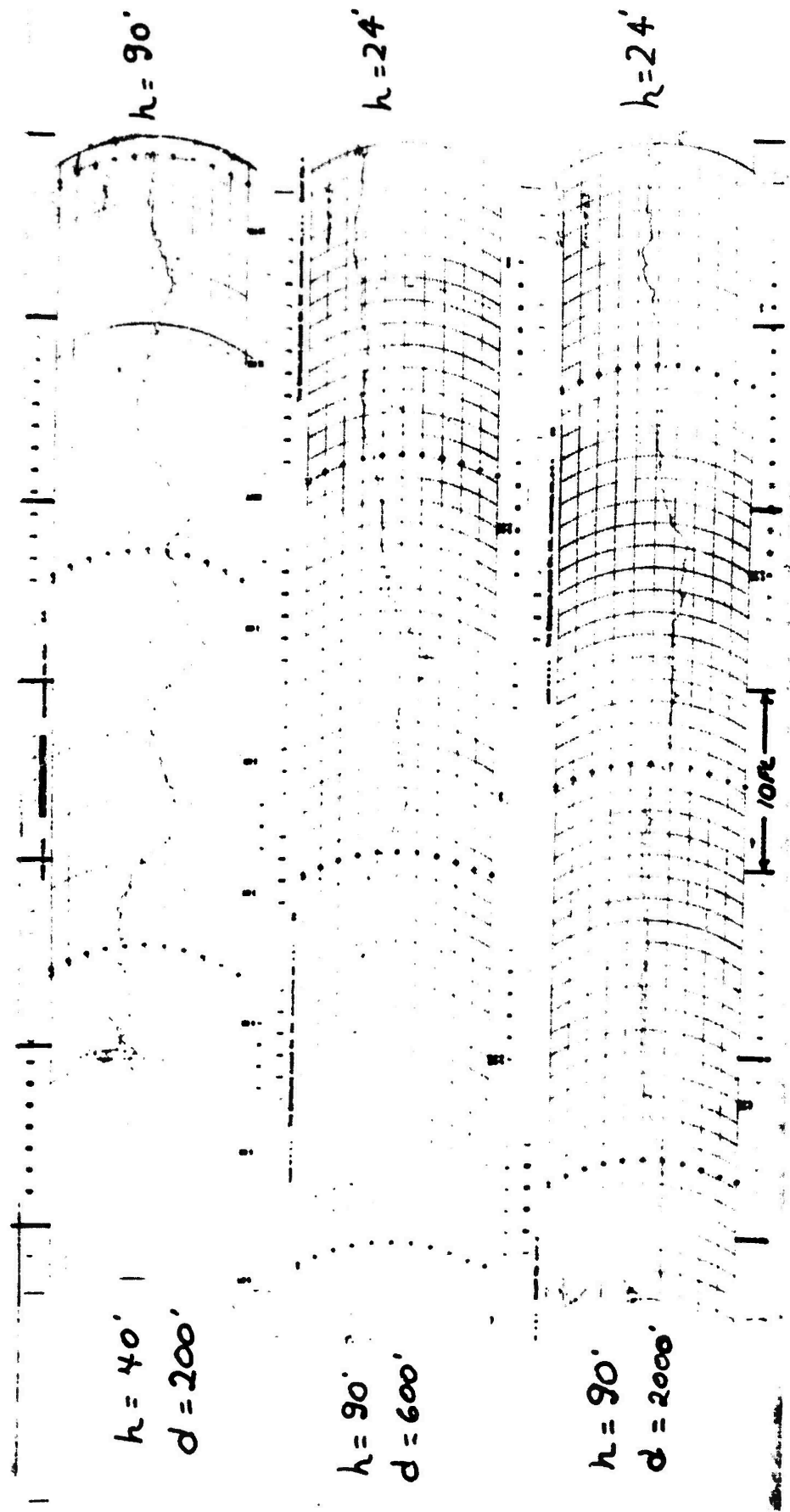


Fig. 11 Effect of Horizontal Dipole Height at 100 Mc/s at Three Distances From Line. (Vertical Scale = Approx. 1 db/Minor Division).

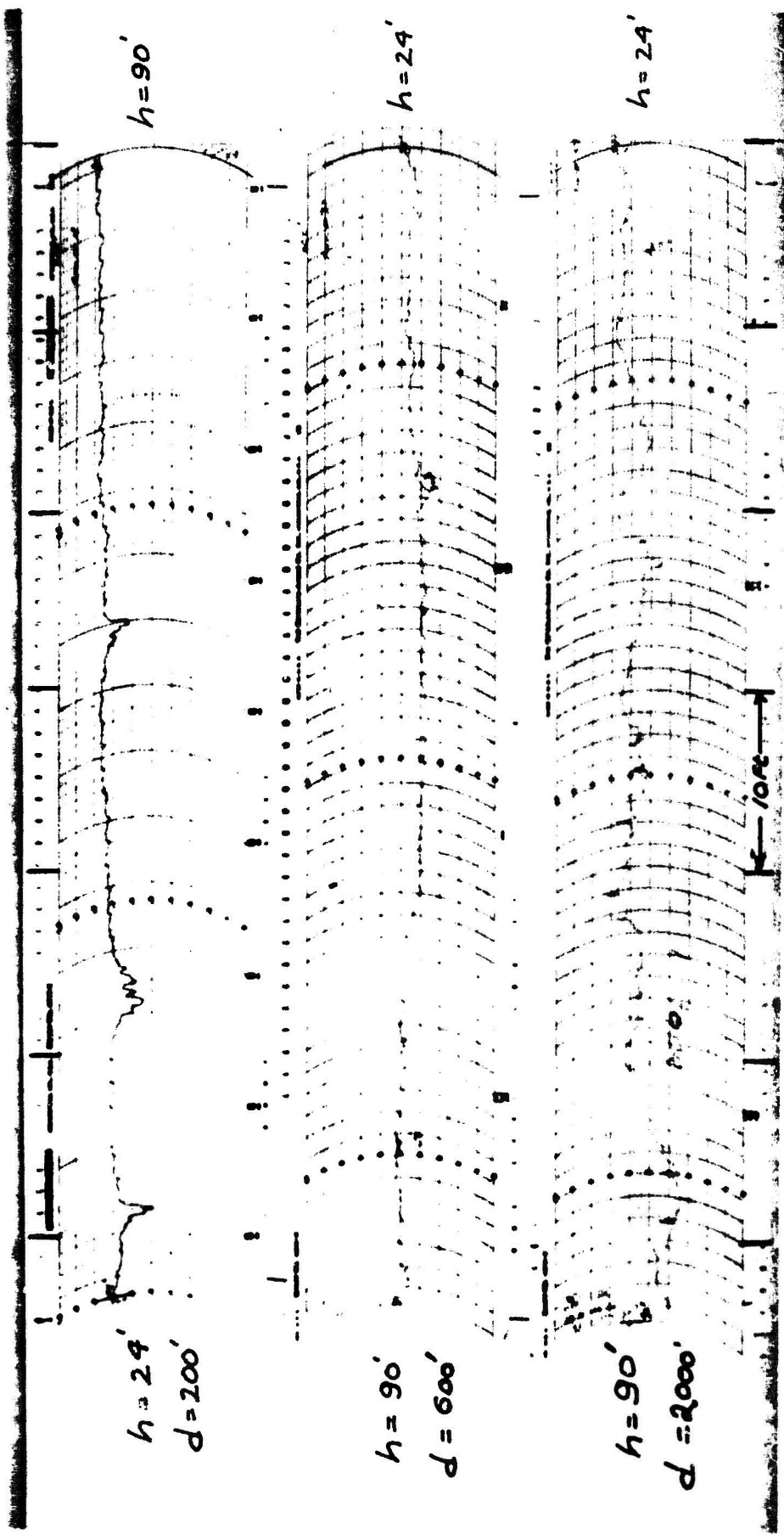


Fig. 12 Effect of Vertical Dipole Height at 100 Mc/s at Three Distances From Line. (Vertical Scale = APPROX. 1 db/Minor Division).

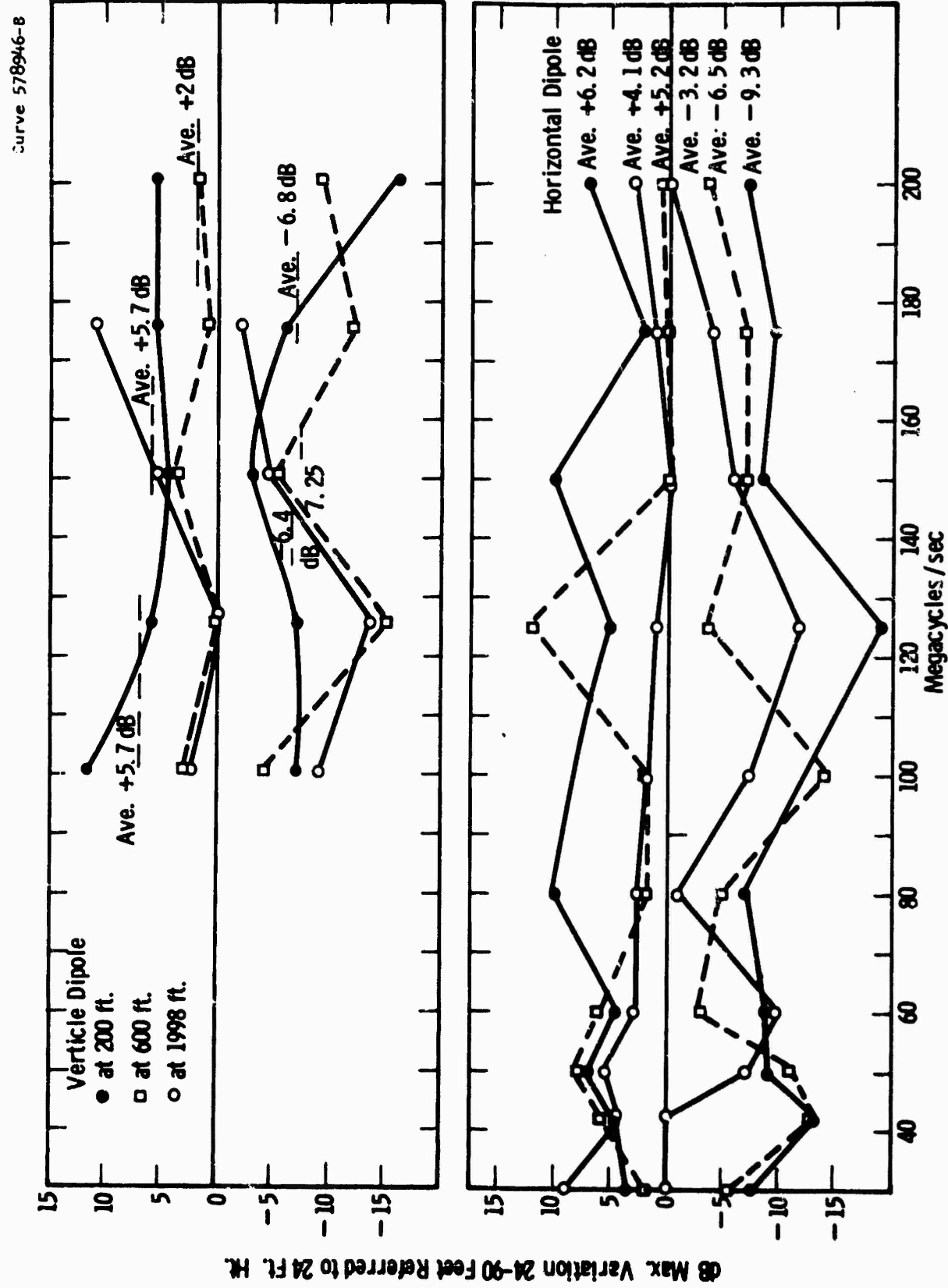


Fig. 13—Effect of receiver antenna height at 200, 600 & 1998 feet opposite line tower

Curve 579111-A

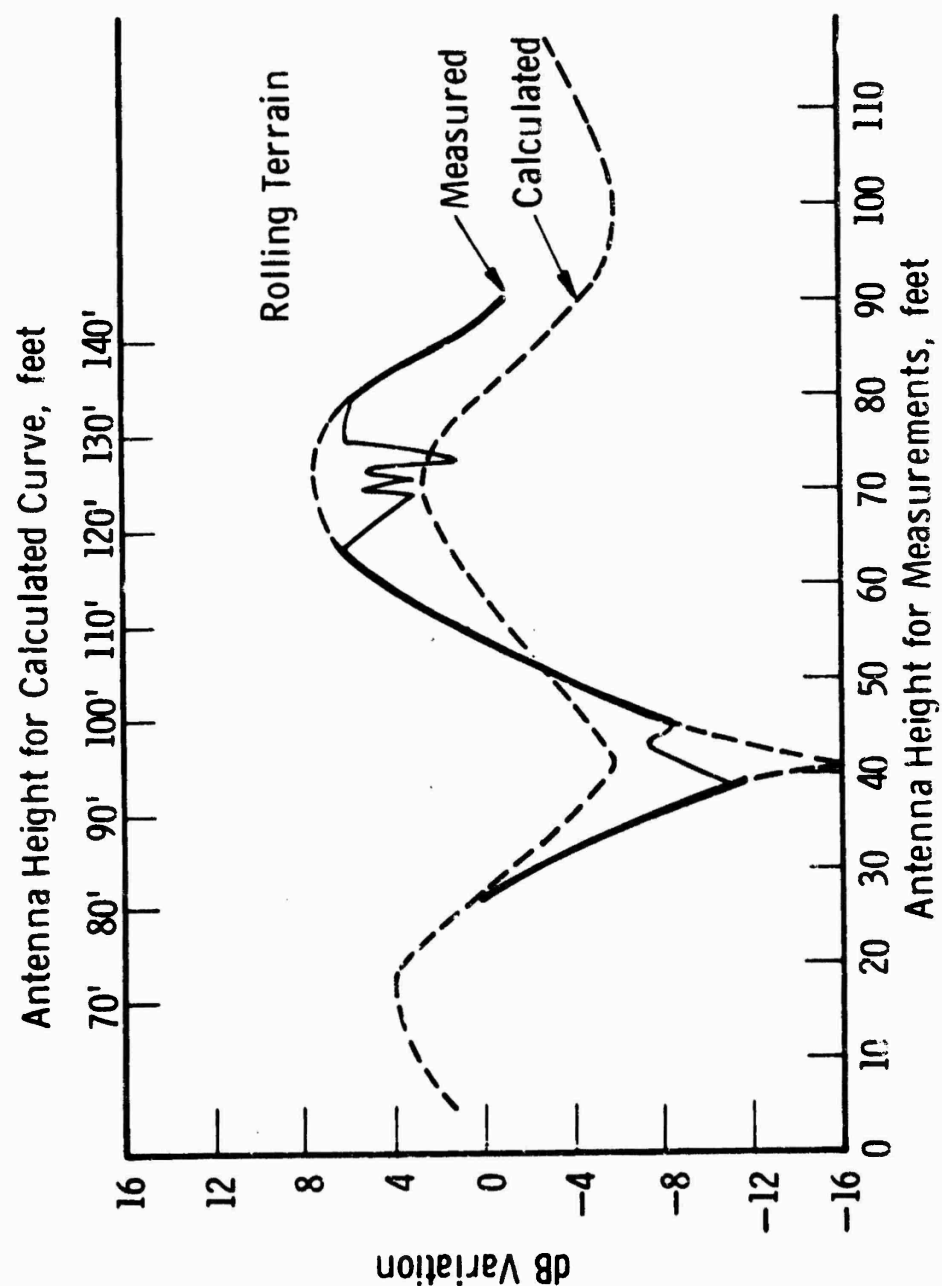


Fig. 14—Horizontal fields 200 feet from source at 30 Mc/s

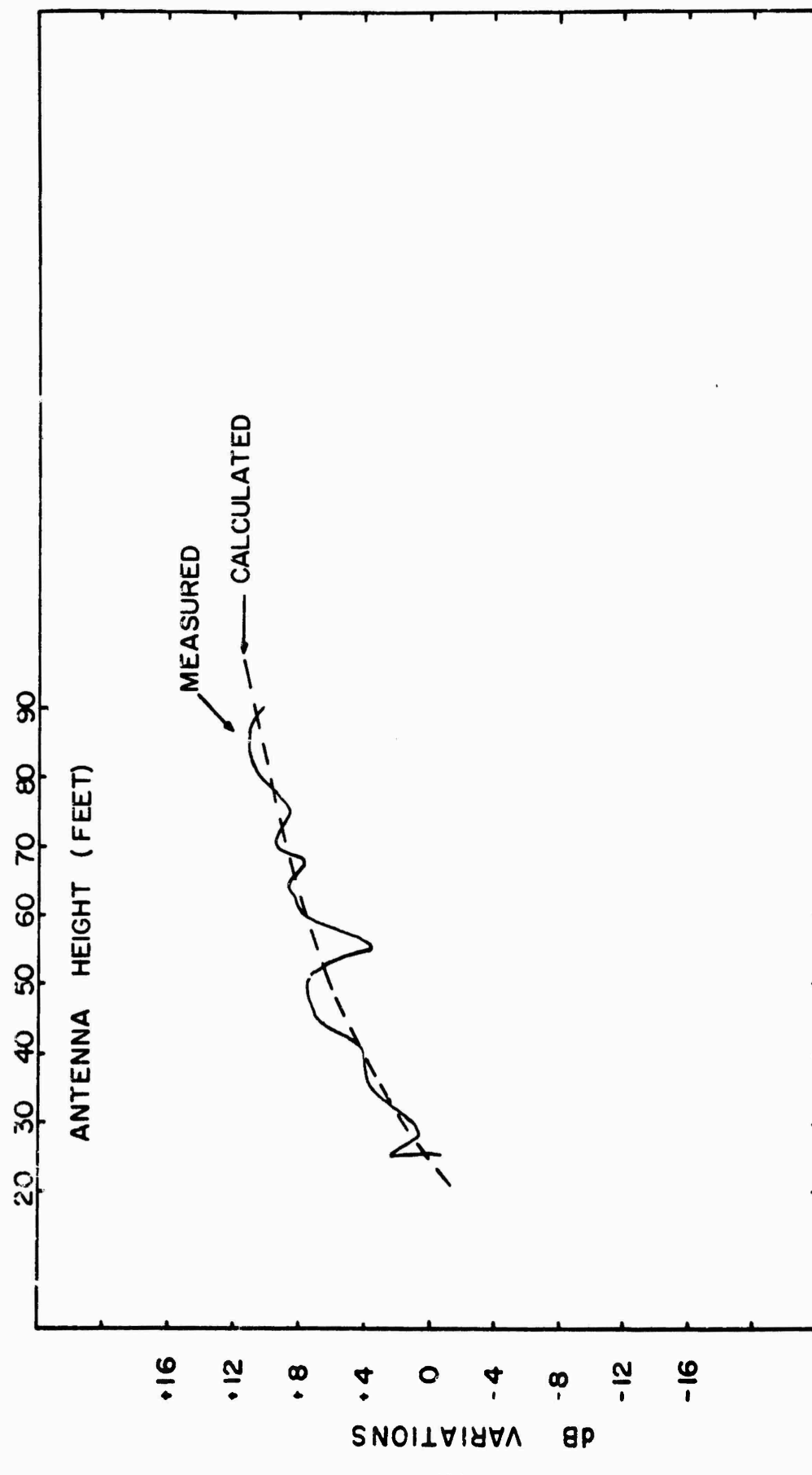


FIG. 15, HORIZONTAL FIELD 2000' FROM SOURCE. 30 Mc/s.

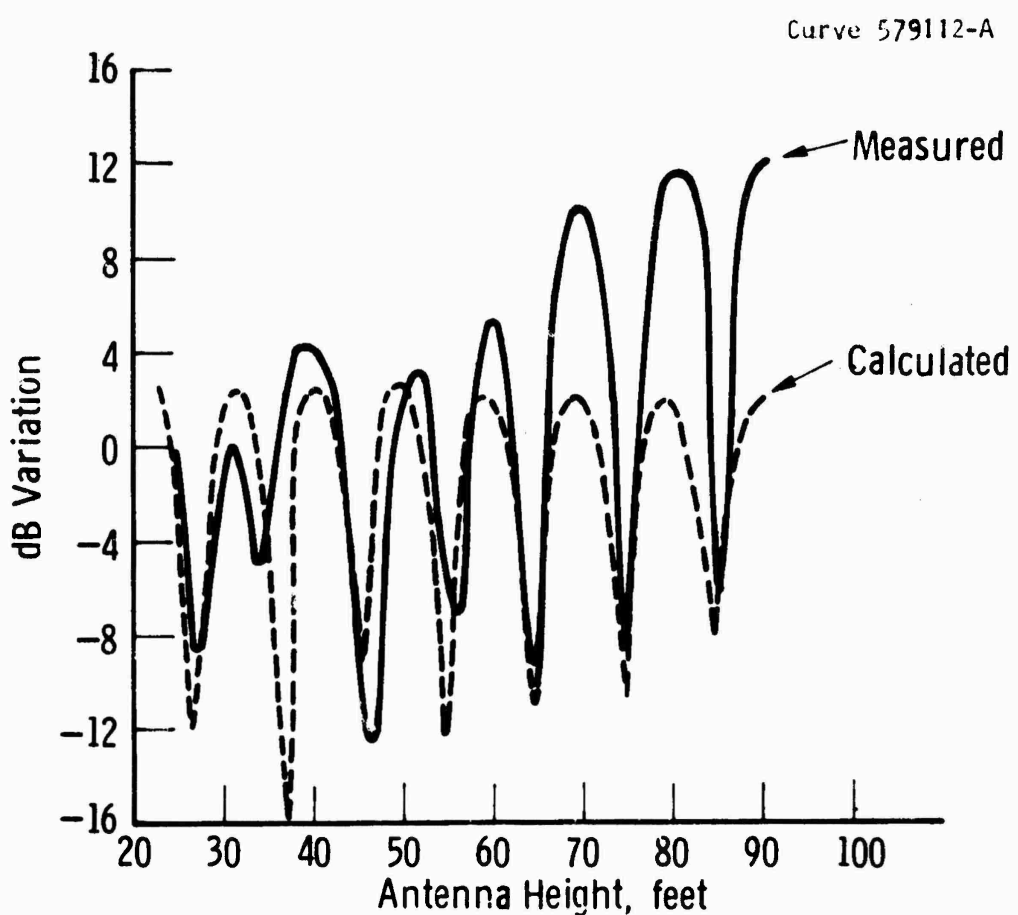


Fig. 16—Horizontal fields 200 feet from source at 150 Mc/s

HIGH VOLTAGE POWER LINE
SITING CRITERIA

Appendix VI of Vol. I

Low Frequency Measurements
60 Cycles/sec to 15 Kilocycles/sec

30 December 1966

Westinghouse Electric Corporation
Electric Utility Headquarters Department
Research and Development Center
Pittsburgh, Pennsylvania

Rome Air Development Center (RADC)
Griffiss Air Force Base
Rome, New York 13442

Contract AF30(602)3822

Contents - Appendix VI of Vol. I

	<u>Page No.</u>
1. Introduction	
1.1 The Low Frequency Induction Problem	316
1.1.1 The Nature of the Problem	
1.1.2 History of Low Frequency Interference Coordination	
1.1.3 Definitions	
1.2 The Low Frequency Induction Model	318
1.2.1 Metallic Cross	
1.2.2 Ground Potential	
1.2.3 Magnetic Induction	
1.2.4 Electric Induction	
1.3 Balanced and Residual Components	321
1.3.1 Balanced Currents	
1.3.2 Residual Currents	
1.3.3 Balanced Voltages	
1.3.4 Residual Voltages	
1.3.5 Symmetrical Components and Coupling Factors	
1.4 The Generation of Power System Harmonic Voltages and Currents	323
1.4.1 Transformers	
1.4.2 Rotating Machinery	
1.4.3 Power Factor Correcting Capacitors	
1.4.4 Polyphase Rectifier and Inverter Systems	
1.5 The Propagation of Power System Harmonic Voltages and Currents	325
1.5.1 Power Line Characteristics	
2. Measurements	328
2.1 Instrumentation	
2.2 Magnetic Field Measurements	
2.3 Electric Field Measurements	
2.4 Conclusions	
Table I - Non-triple Odd 60 cycle Harmonics	333
References	334

List of Figures - Appendix VI of Vol. I

	<u>Page No.</u>
Fig. 1 Rise in Station Ground Potential under Fault Conditions.	337
Fig. 2 Magnetic Induction Model.	338
Fig. 3 Electric Induction Model.	339
Fig. 4 Phase to Neutral Reactances of a Typical Transmission Line.	340
Fig. 5 Sending End Phase to Neutral Impedance of Typical Transmission Line with Far End Open and Short-Circuited.	341
Fig. 6 Ratio of Current at Far End to Current at Near End with Far End Short-Circuited and Ratio of Voltage as Far End to Voltage at Near End with Far End Open.	342
Fig. 7 345 kV Line Harmonics 200 Feet from Tower.	343
Fig. 8 244 kV Line Harmonics at 78 and 200 Feet from Tower.	344
Fig. 9 161 kV Line Harmonics at 200, 400, 600, 1500 Feet from Towers.	345
Fig. 10 69 kV Line Harmonics at 200 Feet from Tower.	346
Fig. 11 46 kV Line 60 Cycles and Harmonics at 200 Feet from Pole.	347
Fig. 12 8 kV Line Harmonics at 50 and 200 Feet from Pole.	348
Fig. 13 8 kV Line Harmonics with Receiver Set for 60 Cycle Bandwidth.	349
Fig. 14 161 kV Line Harmonic Att. Lateral to Line.	350
Fig. 15 Odd Harmonic Levels to Nominal 60 Cycle Line to Line kV.	351
Fig. 16 60 Cycle Electric Field 200 Feet from Center-Line.	352

APPENDIX VI - LOW FREQUENCY MEASUREMENTS 60 CYCLES/SEC. TO 15 KILOCYCLES/SEC.

1. Introduction

1.1. The Low Frequency Induction Problem

1.1.1. The Nature of the Problem

When a power and a communication circuit are operated in close proximity, the power circuit may interfere with the normal operation of the communication circuit as a result of mutual conductive or inductive effects. The portion of the frequency spectrum which this section of the report covers begins with the power system fundamental of 60 Cps and extends to 15 Kc. The power system elements which may produce these frequencies in various amounts are generators, transformers, the load and their interrelationship. Among the communication systems which may be affected are wire line telephone and telegraph, and, to a small extent, geophysical, and scientific instrumentation.

1.1.2. History of Low Frequency Interference Coordination

Shortly after the first alternating current transmission system went into service in 1886, inductive interference problems occurred between power and telephone industries. Telephone and power lines served the same customers and therefore became inseparable companions. At the turn of the century it was a common sight to observe mazes of open-wire telephone lines converging in industrial areas with paralleling power lines. The transmission of alternating current power at high voltages became possible with the iron core transformer, thus giving rise to the generation of harmonics caused by the magnetization of the iron.^{1*}

In 1891, two French inventors, Huting and Leblanc,⁴ had demonstrated that carrier transmission was possible, but separation of voice and carrier frequencies was not possible until the separation filter was invented in 1915.

* References are given at the end of this Appendix.

Shortly after the First World War, the power and telephone industries coordinated their efforts in working out corrective procedures that would be mutually satisfactory to each other. This led to the formation of the Joint Subcommittee on Development and Research of the National Electric Light Association and the Bell Telephone System.² The Subcommittee assigned specific problem areas to eleven project committees, each working on a principle of cooperation for a solution.

By 1918 the first practical carrier system was placed in service between Baltimore and Pittsburgh, which supplied four additional voice channels to a physical wire circuit. The carrier channels were virtually immune to low frequency induction, except when physical interruption occurred due to a power line cross, protective fuse opening, or to other causes. High density carrier systems soon began to appear and the noisy physical circuit became a subordinate channel; thus, power line harmonic induction was of less consequence. Over a period of about 20 years a number of reports were released to the industries which formed the basis for solutions to inductive coordination problems.³

The density of wire telephone systems during the first World War had grown to considerable proportions and to some extent congested areas were alleviated by telephone cables. However, cables at that time were costly and transmission over long distances was impractical. Voice frequency telephone repeaters also improved long distance communications. However, power line induction was still one of the limiting factors. Great improvements were made in wire line, cable carrier, and coaxial cable systems, but power line induction was still possible. Radio and microwave systems now avoid this completely, but the problem is still a consideration at the telephone subscriber level.

With increasing complexity and sensitivities of sophisticated military and commercial electronics systems it is necessary to consider the aspects of inductive coordination, the basic principles of which are still applicable.

1.1.3. Definitions

Interference, as discussed here, is the effect which arises from the characteristics and interrelation of power and communication systems, which is of such character and magnitude as would prevent the communication system from rendering satisfactory and economical service if methods of coordination were not applied.

Coordination deals with the location, design, construction, operation, and maintenance of power and communication systems which will prevent interference.

Inductive Influence are those characteristics of a communication circuit with its associated apparatus which determine the extent to which it is capable of being adversely affected by a given inductive field.

Inductive Coupling is the interrelation of neighboring power with communication circuits whereby voltages or currents or both are induced into the communication circuit.

Inductive Susceptiveness are those characteristics of a communication circuit with its associated apparatus which determine the extent to which it is capable of being adversely affected in giving service by a given inductive field.

1.2. The Low Frequency Induction Model

Extraneous voltages in communication circuits are generally classified as being caused by one or more of four effects. In this section we will briefly explain each effect. Two caused by conducting processes are (1) metal cross and (2) ground potential and the other two by induction processes are (3) magnetic induction and (4) electric induction.⁷

1.2.1. Metallic Cross

When a power and communication circuit are operated in close proximity, such as when each share a common mechanical support on the same right-of-way or when crossing each other at right angles on separate right-of-ways, a metallic cross can occur due to failure of the mechanical support or to physical metallic contact of the two circuits.

1.2.2. Ground Potential

Another method of impressing extraneous voltages on a communication circuit is through conduction from common use of a grounding system. Power systems frequently employ the earth as a means of protection from lightning, for stabilizing the power system neutral, and under fault conditions, to limit the voltages. When a fault current flows into a power plant grounding system, the rise in station ground potential above distant earth can become considerable in proportion to normal conditions. A communications circuit, which serves the plant utilizing the local station ground, can be subjected to the same rise in potential. The communication circuit also being connected to distant ground (referred to as remote ground in reference to the power station) at the distant exchange, will be subjected to failure if the potential rise exceeds its protector gap break-down voltage. This also can be a hazard to personnel using or in contact with the communication circuit. Figure 1 illustrates the effect of rise in station ground potential under fault conditions.

1.2.3. Magnetic Induction

Magnetic induction is the process involving the induction of voltages and currents into a communication circuit due to the magnetic field produced by the flow of power line currents. Figure 2A illustrates a simple model of the magnetic induction process. In actuality, two communication conductors are involved but for simplicity, one is shown. As shown, the current flowing in the power conductor sets up a magnetic field which induces another current of opposite direction in the communication conductor. A voltage is also induced in the communication conductor as a result of the induced current. The induction process is analogous to simple transformer action where a secondary voltage is induced due to a primary current. In a similar manner, the voltage is proportional to the rate of change of the magnetic flux of the current producing it. The induced voltage appears as a small voltage, E , in series with the conductor in the figure.

In Figure 2B, the process is further amplified by grounding one end of the communication conductor. In this case the open-end voltage equals the sum of all the infinitesimal series voltage generators down the total exposure length.

In Figure 2C, the magnetic induction model shows a more realistic approach to induction on a communication circuit, such as would occur when the ends of the communication wire are terminated in loads similar to central offices, conductor impedance being neglected. This circuit can also be envisioned as a loop antenna which lies in the magnetic field of the power current.

1.2.4. Electric Induction

Electric induction is the process involving induction of voltages in a communication circuit due to the electric field produced by power circuit voltages. Figure 3A illustrates a simple model of the electric induction process. Again only one communication conductor is shown. This is better visualized by showing the capacitance between the conductors and each conductor to ground. The voltage on the power conductor to ground is directly proportioned to this admittance (inversely to their capacitance values) in series to ground. The voltage on the communication wire is always less than on the power wire by the obvious "voltage divider" action.

Figure 3B shows the termination of the communication wire in its longitudinal impedance characteristic such as would be in the case of central office equipment. In the practical case the impedance of the capacitance C_{pc} is very much greater than the impedance terminating the communication wire, therefore the current I_{ind} is practically independent of Z_1 and Z_2 . However, the total induced current is divided between the ends of the communication wire in proportion to the end admittances. The voltage to ground due to electric induction is the product of the current i , and the impedance to ground Z_1 , or the current i_2 and Z_2 . Since the value of C_{pe} is proportional to the length of the exposure, the magnitude of I_{ind} is also proportional to the length of the exposure. The value of I_{ind} is also directly proportional to the frequency of the power voltage (or harmonic of

the power voltage) since the admittance of C_{pe} is directly proportional to frequency (fundamental or harmonic). The effects of electric induction are consequently directly proportional to the voltages-to-ground on the power wire, the frequency of these voltages, and the length of the exposure between the power and communication wires.

1.3. Balanced and Residual Components

The process of induction of harmonic voltages and currents into a communication circuit is more clearly understood and analyzed by separately classifying the power circuit induction components into balanced and residual.

1.3.1. Balanced Currents

Balanced currents are those components of the actual phase currents whose vector sum is zero. Most power lines at the transmission level are operated with nearly balanced line currents. The net effect from the standpoint of magnetic induction in a communication conductor at a distance large with respect to phase spacing is almost zero, under perfect conditions with all power circuit phase currents equal in magnitude and 120 degrees apart in phase. At distribution levels, balance of phase currents rarely exists because of unbalanced loads and unsymmetrical conductor arrangement. In rare cases 60 Cps components can be balanced but harmonic currents can become unbalanced because of unsymmetrical power circuit impedances to the harmonics. One example would be in the case of one phase transformer of differing size or type than the other two phases. In an isolated single-phase ungrounded 2-wire line fed from an isolating transformer, the currents in the two conductors are equal but flow in opposite directions.

1.3.2. Residual Currents

Residual currents are the vector sum of the actual currents in the phase wires which in a three-phase circuit, if other than zero, must return through a ground connection. In a power circuit having a neutral or overhead ground wires the circuit residual current is the vector sum of the currents in the phase conductors, while the line residual current is the vector sum of the currents in all the conductors of the

line. The line residual is also defined as the ground return current, since this part of the current must return through the earth. In visualizing residual or ground return currents, one may envision an equivalent single-phase current in the circuit with the phase wires paralleled as one conductor, the current returning through ground and neutral as the other conductor.

1.3.3. Balanced Voltages

Balanced voltages are those components of the actual phase-to-ground voltages whose vector sum is zero. Again, as with balanced currents discussed above, when the phase-to-ground voltages are equal and 120 degrees apart in phase, the net effects of electric induction in a communication conductor is zero.

1.3.4. Residual Voltages

Residual voltage is the vector sum of the voltage-to-ground of all the phase conductors. In a three phase transmission line, the effect of residual voltage in causing the flow of residual current is equivalent to a single-phase voltage (equal to 1/3 the residual voltage) applied between the wires in multiple and ground.

1.3.5. Symmetrical Components and Coupling Factors

Symmetrical three-phase systems can be analyzed by symmetrical components. (Details in the use of symmetrical components are found in References 8 and 9.) Power engineers generally use symmetrical components to define balanced and residual components, which were discussed in the preceding paragraphs. Balanced voltages and currents are those of positive or negative-sequence and residual voltages or currents correspond to the sum of the phase quantities or to three times the zero-sequence quantities. Analytical consideration must be given to these components in terms of two (and sometimes three) separate and distinct circuits, since induction in a communication conductor is different for each component. For example, coupling factors for residual or zero sequence components are much greater than for balanced or positive and negative-sequence

components. The ratio of these coupling factors may be as high as 50 to 1 and is dependent upon the power circuit configuration and the separation between the power and communication conductors. If under ideal operating conditions a power system is symmetrical, only positive- and negative-sequence voltages are generated, then only positive- and negative-sequence currents flow. However, seldom is this the case, and unbalanced conditions exist. The flow of positive and negative-sequence currents through unbalanced series impedances or shunt admittances produce unbalanced voltages which introduce zero-sequence components. From the standpoint of induction these components may be many times that of the original balanced currents. Frequently, the conductor system is transposed to reduce the unbalance.

1.4. The Generation of Power System Harmonic Voltages and Currents

1.4.1. Transformers

When a sinusoidal voltage is impressed across a transformer winding with all other windings open circuited, the transformer draws a magnetizing current sufficient to induce a flux in the core to generate a back EMF equal to the applied voltage except for a very small leakage drop.¹⁰ This magnetizing current is made up in addition, to a 60 Cps component, of components of odd multiples of 60 Cps of different magnitudes.¹²

The predominant harmonic is the third, and this can be as high as 50 to 60 percent of the fundamental exciting current. The magnitude of the harmonic content decreases as the order of harmonic increases.

1.4.2. Rotating Machinery

Rotating machinery includes rotary condensers, frequency changers, converters, motors, and generators. Present-day designs of these machines take into consideration the need for a reduction of harmonics. Harmonics generated in the synchronous machine are due to the nature of the machine, such as the variation of reluctance of the magnetic path because of the need for slots to support the windings, saturation effects at tooth tips

and at other points within the magnetic path, and saliency of the rotor field poles. The machine designer controls the harmonics by proper shaping of the magnetic structure, by skewing of poles or slots, by selection of the number of slots, and by design of the winding (chording, fractional slotting, etc.)

Harmonics produced in induction motors are rarely important. Those frequencies that are present again are generally caused by reluctance changes in the magnetic paths, and are related to the speed of the induction motor, and therefore may vary with load.

Harmonics in dc machines or ac commutating machines can be caused also by the commutators.

1.4.3. Power Factor Correcting Capacitors

Capacitors do not generate harmonics.^{13,14} However, they often reduce the effects of harmonic voltages because of their filtering action. Since they are generally connected across line conductors and their impedances are inversely proportioned to frequency, they offer lower impedance as frequency increases. Capacitor banks can reduce harmonic voltages when connected close to the source of harmonics. Their prime function, however, is not to reduce the harmonics but to correct power factor. Under certain conditions capacitor banks can set up resonant conditions which may greatly accentuate harmonic currents, thereby increasing the power system influence to communication circuits. Severe cases of telephone influence have been recorded in areas where resonance effects have been established between power system harmonic inductive reactances resonating with power factor correction banks. Corrective measures taken for such instances are to slight shift the system resonances off the harmonic by relocating the capacitor bank, or by adding or removing a small amount of capacity to the bank.

1.4.4. Polyphase Rectifier and Inverter Systems

For a number of years chemical, metallurgical and traction systems have made extensive use of polyphase grid controlled

and non-grid controlled rectifying systems. Some systems derive as many as 72 phases from a three-phase ac supply source. Inductive coordination problems arise from the commutation of the three-phase supply system, which may be situated in dense industrial areas served by wire and cable communication facilities. As a result of the commutation processes, the rectifier systems are potential generators of power system harmonics; the lower the number of phases, the greater the values of harmonics being produced. Odd order harmonics are produced on the ac side while even order harmonics are produced on the dc side. The ac side order of harmonics present with balanced operation are $n = (ps + 1)$, and on the dc side $n = ps$, where n = harmonic order, p = number of phases (in multiples of 6) and s is any whole number. The greatest concern in inductive coordination problems with rectifying systems is due to the ac side harmonics since dc side harmonics are generally confined to the dc side.^{15, 16, 17, 19, 20, 21, 22, 23, 24}. On traction systems however, dc-side harmonics are distributed over wide areas as well as the ac-side, and both can cause coordination problems.

1.5. The Propagation of Power System Harmonic Voltages and Currents

1.5.1. In order to understand the propagation of power circuit harmonic currents and voltages and to determine coupling factors at the various frequencies into a communication circuit, it is necessary to determine the impedances at those frequencies. Figure 4 depicts the phase-to-neutral reactances of a typical transmission line. The reactances at both the 60 Cps fundamental and at the 25th harmonic are shown divided into one mile sections.

It can be seen that the shunt capacitive reactances are very large compared to the series inductive reactances at the 60 Cps fundamental however, at the 25th harmonic the shunt impedances are decreased by 25 to 1 while the series impedances are increased by the same ratio. For a 19.1 mile length of line the series and shunt impedances are equal at the 25th harmonic (viz., $19.1 \times 20 = 382 = 7,300/19.1$); however, at the 60 Cps fundamental the line would have to be about 480 miles long.

To obtain an idea of how, quantitatively, the difference affects line performance, consider Figure 5, which shows the sending-end impedance of a typical transmission line with the far end open and with it short circuited as a function of length and frequency neglecting losses. These curves are computed from the formulas:

$$\text{Sending-end impedance with far end open} = jZ_0 \cot \theta$$

$$\text{Sending-end impedance with far end short circuited} =$$

$$jZ_0 \tan \theta$$

where Z_0 is the characteristic impedance to neutral (380 ohms in the example)

θ is the line angle (or phase shift) in degrees = frequency times length times 360 divided by velocity of propagation.

Since in a smooth circuit without losses (a good approximation for power transmission circuits at low harmonic frequencies), the velocity is independent of frequency, the curves can be plotted using length times frequency, that is, kilocycles-miles, as abscissas.

For example, a 100-mile line at 60 Cps is $.06 \text{ kc} \times 100 \text{ miles} = 6 \text{ kc-miles}$; a 20 mile line at 1,500 Cps is 30 kc-miles, and so forth. For such lines the velocity of propagation is about 180,000 miles per second.

With a velocity of 180,000 miles per second, θ , or phase shift is two degrees per mile per kc, which can be derived as follows:

$$\text{Wavelength at frequency } f = \frac{180,000 \text{ miles}}{f}$$

$$\text{One wavelength} = 360 \text{ degrees}$$

$$\text{Whence } \frac{180,000 \text{ miles}}{f} = 360 \text{ degrees}$$

$$\text{Degrees per mile} = \frac{360f}{180,000} = 2^\circ \times \frac{f}{1,000}$$

* If f is in kc, degrees per mile = 2 degrees $\times f$ (in kc).

With respect to Figure 5:

With the far end open, the impedance looking into the near end is capacitive reactance up to 45 kc-miles; with the far end short circuited it is inductive reactance up to that length. Above 45 kc-miles the signs are reversed.

At 22.5 and 67.5 kc-miles, the impedances with the far end open and then short-circuited are the same in magnitude but opposite in sign.

At 45 kc-miles, the impedance with the far end open is very low; with the far end short-circuited, it is very high. That is, at this length a short-circuit on the far end tends to look like an open-circuit at the near end; an open-circuit at the far end tends to look like a short-circuit at the near end. Actually, the near end impedances would go to zero or infinity except for the losses in the circuit. The significance of 45 kc-miles is that it is "one-quarter wavelength". That is, 45×2 degrees = 90 degrees, which is one-quarter of 360 degrees. The effects at this length are sometimes referred to as "natural line resonance" because a line of this length with the far end open looks from the sending end like a series resonant circuit; with the far end short-circuited, it looks from the sending end like a parallel resonant circuit.

- 1.5.2. Another factor of importance in considering propagation is what happens to harmonic currents and voltages as they traverse the line from the sending end to the far end. Figure 6 shows, for the same line as used in Figures 4 and 5, the ratio of voltage at the far end to that at the near end with the far end open, and the ratio of current at the far end to that at the near end with the far end short-circuited. This curve is based on the formula:

$$R = \frac{1}{\cos \theta}$$

where R = ratio of voltage at the far end to that at the near end with the far end open, or the ratio of current at the far end to that at the near end with the far end short-circuited.

θ = line angle in degrees - two degrees times kc-miles.

The abscissas are again in terms of kc-miles. It is of some interest to note that these two ratios are shown by the same curve; that is, the voltage ratio with the far end open is the same as the current ratio with the far end short-circuited. The quarter wavelength effect is again evident. Here again the difference between the way a line performs at 60 Cps and at harmonic frequencies may be noted.

In most practical cases the far end of a line is not open nor short-circuited. While the treatment of the general case is beyond the scope of this report, it may be said that for short transmission circuits the impedance at harmonic frequencies across the far end is frequently almost pure inductive or capacitive reactance. In such cases the effects shown in Figures 5 and 6 occur, but for different line lengths than shown there. Treatment of actual cases can be found in literature references.

2. Measurements

2.1. Instrumentation

The instrument used in all measurements from 60 cycles/sec. to 15 kilocycles/sec. was a Radio Interference Field Intensity Meter, Model NM-40A, serial number 310-46, manufactured by the Stoddart Aircraft Radio Company, Inc.

Laboratory tests were made on this instrument to assure that the 60 cycle harmonics indicated were not a result of spurious response to the fundamental frequency.

In one test, a 60 cycle signal of 0.515 volts (114 db above 1 μ volt) was fed into the input of the instrument and the 60 cycle, 120 cycle and 180 cycle components of the input wave

shape were measured. A 20 db resistive attenuator was then inserted between the voltage source and the input of the instrument and the three frequency components were measured again. The resulting reduction in each of the three frequency components was 20 db.

In a second test the instrument was used to make a harmonic analysis of two separate 60 cycle/sec. sources of equal amplitude (.32 volts rms). Both of these sources appeared sinusoidal when viewed on an oscilloscope. The result of the two analyses indicated the differences between the harmonic content of the two sources as 8 db at the second harmonic, 25 db at the third harmonic and 9 db at the fourth harmonic. This conclusively illustrated that the indicated harmonic levels were actually a measure of the harmonic content of the input voltage wave rather than spurious response of the instrument.

Power for this instrument was supplied from a portable, gasoline engine driven, 110-volt 60-cycle generator. The ignition system of the gasoline engine is shielded to prevent interference. Also, great care was taken in positioning the generator and connecting cables to assure that they were not influencing the measurements.

2.2. Magnetic Field Measurements

The strength of the magnetic field produced by a power line, in the 60 cycle/sec. to 15 kilocycle/sec. frequency range, is primarily proportional to the power current and its harmonics flowing in the power line. Therefore, the strength of the magnetic field in the vicinity of a low voltage line could be greater than that in the vicinity of a high voltage line.

Due to this fact, comparisons of power lines of different voltage levels cannot be made on a basis of magnetic field strength measurements in this frequency range.

2.3. Electric Field Measurements

All measurements were made with the electric antenna mounted on a tripod at a height of approximately four-and-one-half feet above ground and oriented for maximum indication on the field strength meter. At each location the portable generator and power leads were positioned to assure that they were not influencing the measurements. The results of these measurements can be seen in Figures 7 through 16.

Measurements were made with and without gap-type radio noise sources. For the 244-kV line (Figure 8), a gap-type noise generator was connected to the line on the east phase for the measurements 200 feet east of Tower 161. No generator was connected for the west side measurements. No difference in harmonic levels can be seen with or without the gap. The gap-type noise on the other lines (a natural gap for the 345-kV line of Figure 7 and for the 48-kV line of Figure 11, and a gap-type noise generator for the 161-kV line of Figure 9) could not be measured. Only the harmonics of 60 Cps were detected in this frequency range for all voltage ratings.

The measurements were made on all lines except one, with the instrument bandwidth adjustment set to the narrowest bandwidth of 8 cycles/sec. This very narrow bandwidth was employed in an effort to detect frequencies between the 60 cycle/sec. harmonics. None were detected. Unless specific interest is in the amplitude of individual harmonics, measurements may be made in less time with the maximum bandwidth of 60 cycles and still obtain the same spectrum envelope. Compare Figures 12 and 13.

Even order harmonics were observed in some measurements. (Figures 7, 10, 11, 12.) No definite answer can be given as to the source of these harmonics, although some possibilities, such as utilization equipment, are mentioned in the introduction.

Figures 12 and 13 also indicate that the field strength was varying with time at frequencies of the higher order harmonics. This may be due to slight shifting of the fundamental frequency which results in a shift in the harmonic frequency equal to the fundamental frequency shift multiplied by the harmonic number. For example: the 200th harmonic of 60.0 cycles/sec. is 12,000 cycles/sec. If the fundamental frequency should change to 60.1 cycles/sec. the 200th harmonic would then become 12,020 cycles/sec. These variations were occurring at a frequency of less than 1 cycle/sec. and are most pronounced when the instrument bandwidth is narrowest.

The lateral attenuation at several harmonic frequencies for a high-voltage line can be seen in Figure 14. It appears that this lateral attenuation is dependent on both frequency and distance from the line. However, the general attenuation trend is between $1/d^2$ and $1/d^3$. However, there is also a possibility that the harmonic content of the voltage wave may have changed due to load changes, within the period of time in which the measurements were made.

Figure 15 indicates that the field strength of odd order harmonics taken as a group is proportional to the nominal 60 cycles/sec. line to line voltage at a distance of 200 feet from centerline. However, the 60 cycle field strength 200 feet from centerline decreases more rapidly than the nominal 60 cycle line to line voltage as shown by Figure 16. This is most likely largely due to the increased conductor heights and phase spacings necessary for higher voltage levels. However, it is also possibly dependent on the effect of load on the harmonic voltages, and the physical location of the neutral conductor. On low voltage lines the neutral conductor is ground in some cases and in other cases it is a separate conductor located on the pole with the phase conductors.

2.4. Conclusions

- 2.4.1. The gap-type noise generator has no measurable effect on the electric field strength from a transmission line in the frequency range of 60 cycles/sec. to 15 kilocycles/sec.
- 2.4.2. The 60 cycle/sec. fundamental and associated harmonics are the main sources of the electric field produced by a transmission line in the 60 cycle/sec. to 15 kilocycle/sec. frequency range.
- 2.4.3. The 60 cycle and some of the lower frequency harmonics are very powerful compared to broadband radio noise on the line.
- 2.4.4. These low frequencies can be measured without difficulty several hundred feet from a high voltage line and the probability is remote that any broadband noise will hinder these measurements.
- 2.4.5. Protection from these low frequency fields from the power line to a communication site requires that the power line be in shielded cable and underground for sufficient distance from the overhead part of the power line. At what distance would depend on the voltage and current conditions and type of wiring inside the communication site.
- 2.4.6. In any prediction where power frequency harmonics are important the effect of other utilization devices, not discussed here, which generate appreciable harmonics should be considered.
- 2.4.7. The measured field strengths of the odd non-triple harmonics, expressed as a percentage of the 60 cycle/second field strength, are within the order of magnitude of previous voltage measurements made by others (Table I).

TABLE I
NON-TRIPLE ODD 60 C/S HARMONICS
 (In Percent of 60 Cps Voltage or Field Strength)

		Frequency (Cps)							
		300	420	660	780	1020	1140	1300	1500
8 Measured	1.0	.14-.22		.045	.08	.045	.04	-	.028
	Av.	1.0	.29	.12	.09	.05	.04	-	.07
11-13.8 Reference	Max.	2.7	.71	.69	.60	.26	.56	-	.25
	Av.								
46 Measured	.61	.25	.32	.58	.70	.032	.018	.045	
	Av.	1.2	.44	.09	.04	.04	.03	.06	.06
19-44 Reference	Max.	4.1	1.16	.42	.14	.29	.20	.22	.43
	Av.								
69 Measured	.125	.05	.095	.07	.07	.018	.07	.05	
	Av.	1.1	.35	.13	.17	.04	.03	.03	.03
60-69 Reference	Max.	3.2	.97	.65	1.0	.23	.18	.15	.11
	Av.								

* Reference data is taken from Table 6, page 772 of the fourth edition of Electrical Transmission and Distribution Reference Book, Westinghouse Electric Corporation, 1950.

Measured values shown are percent of the 60 C/s field strength as measured two hundred feet from center of line.

REFERENCES

1. Electrical Transmission and Distribution Reference Book, Fourth Edition, Westinghouse Electric Corporation, 1960, Chapter 1, p. 1.
2. Reports of Joint General Committee of National Electric Light Association and Bell Telephone System on Physical Relations between Supply and Signal System.
 - (a) "Principles and Practices for the Inductive Coordination of Supply and Signal Systems," December 9, 1922.
 - (b) "Principles and Practices for the Joint Use of Wood Poles by Supply and Communication Companies," February 15, 1926.
 - (c) "Inductive Coordination - Allocation of Costs between Supply and Communication Companies," October 15, 1926.
3. Engineering Reports of Joint Subcommittee on Development and Research, National Electric Light Association (Edison Electric Institute), and Bell Telephone System.
 - (a) Engineering Report Nos. 1 to 8, vol. 1, published March, 1930.
 - (b) Engineering Reports Nos. 9 to 15, vol. II, published April, 1932.
 - (c) Engineering Reports Nos. 16 to 25, vol. III, published January, 1935.
 - (d) Engineering Reports Nos. 26 to 38, vol. IV, published January, 1937.
 - (e) Engineering Reports Nos. 39 to 49, vol. V, published January, 1942.
4. Encyclopedia Britannica, vol. 21, 1961, Telephone, 6. Carrier Systems, p. 899.
5. Loc. cit.
6. Bell System Practices, Transmission Engineering and Data, Inductive Coordination Practices, Outside Plant Engineering, Structural Coordination, Section AB63.061, AC17.001.

7. Electrical Transmission and Distribution Reference Book, etc., op. cit.
Chapter 23, p. 741.
8. Engineering Reports of Joint Subcommittee on Development and Research, etc.,
Engineering Report No. 4, Appendix I, pp. 38-42. (See Reference 3.)
9. C. F. Wagner and R. D. Evans, Symmetrical Components, (McGraw Hill Book Company, 1933).
10. Electrical Transmission and Distribution Reference Book, etc., op. cit.
Chapter 5, pp. 96-98.
11. Ibid, p. 125.
12. Loc. cit.
13. Inductive Coordination Aspects of Shunt Capacitor Installations, Edison Electric Institute Bulletin, (1938), pp. 382-3.
14. W. E. Feaster and E. L. Harder, "System Lower Harmonic Voltages - Methods of Calculation and Control by Capacitors," Transactions AIEE, (1941), pp. 1066-
15. R. D. Evans, "Harmonics and Load Balance of Multiphase Rectifiers: Considerations in the Selection of the Number of Rectifier Phases," AIEE Transactions, vol. 62, (1943) (April Section), pp. 182-8.
16. H. D. Brown, J. J. Smith, "Current and Voltage Wave Shape of Mercury Arc Rectifiers," AIEE Transactions, vol. 52, (1933), pp. 973-84.
17. P. W. Blye, H. E. Kent, "Effects of Rectifiers on System Wave Shape," AIEE Transactions, vol. 53, (1934), (January Section), pp. 54-63.
18. R. D. Evans, H. N. Miller, Jr., "Harmonics in the AC Circuits of Grid Controlled Rectifiers and Inverters," AIEE Transactions, vol. 58, (1939), pp. 861-70.
19. E. F. Christensen, C. H. Williams, C. C. Herskind, "Analysis of Rectifier Circuits," AIEE Transactions, vol. 63, (1944), pp. 1048-
20. Engineering Reports of Joint Subcommittee on Development and Research, etc.
Engineering Report 22. (See Reference 3.)

21. Reports of Joint General Committee of Edison Electric Institute and Bell Telephone System on Physical Relations between Electrical Supply and Signal Systems, Publication M5, (Edison Electric Institute, New York, New York, July, 1945).
22. R. D. Evans, "Rectifier Circuit Power Factors, Harmonics, and Wave Shapes," Electrical World, (October, 1943).
23. Rectifier Wave Shape, Publication El, Edison Electric Institute, (New York, New York, April, 1937).
24. D. C. Prince, P. B. Vodges, Principles of Mercury Arc Rectifiers and Their Circuits, (McGraw Hill Book Company, New York, New York, 1927).
25. "Inductive Co-ordination Aspects of Rectifier Installations. Condensation of: Appendix II, Propagation of Harmonic Currents and Voltages," AIEE Transactions, vol. 62 (1946), pp. 431-2.
26. Engineering Reports of Joint Subcommittee on Development and Research, etc.
Engineering Report 23. (See Reference 3.)
27. Engineering Reports of Joint Subcommittee on Development and Research, etc.
Engineering Report 24. (See Reference 3.)

Dwg. 852A385

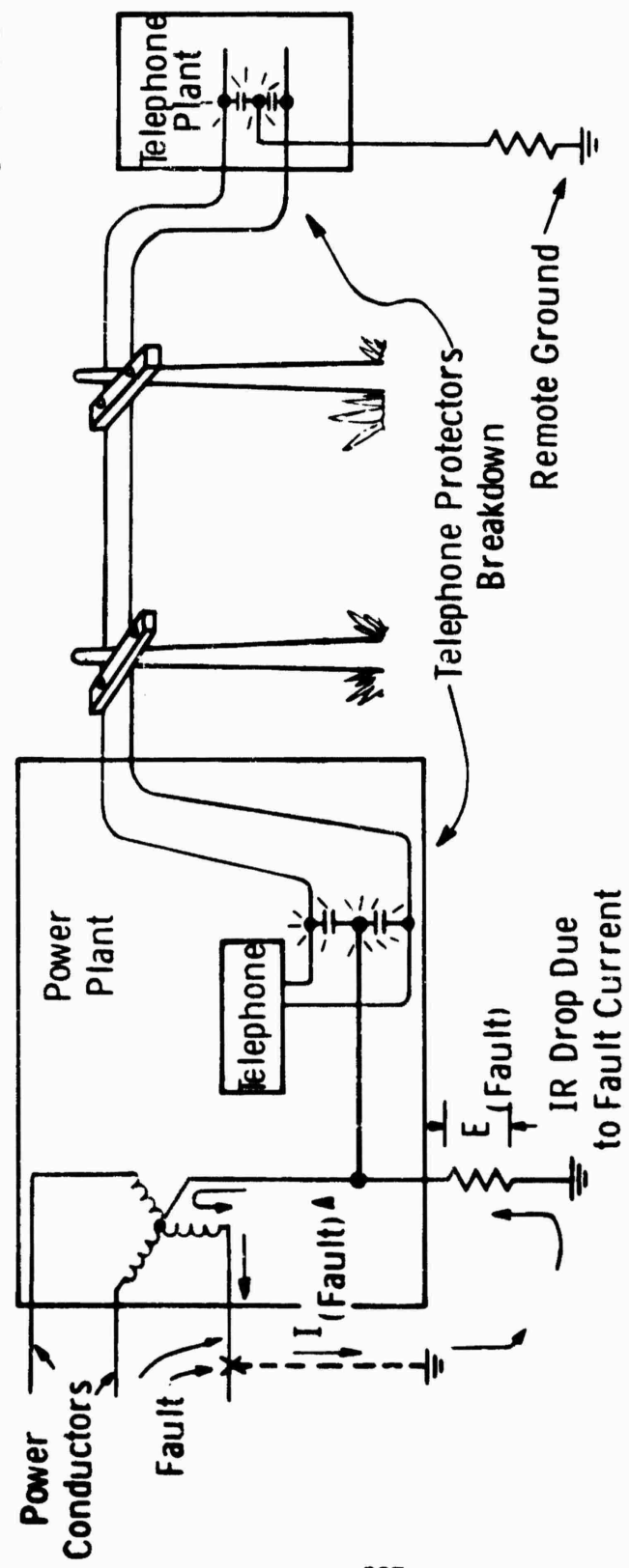
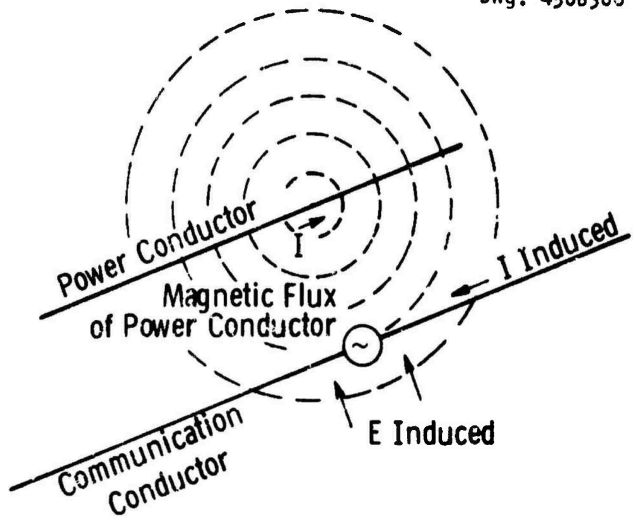
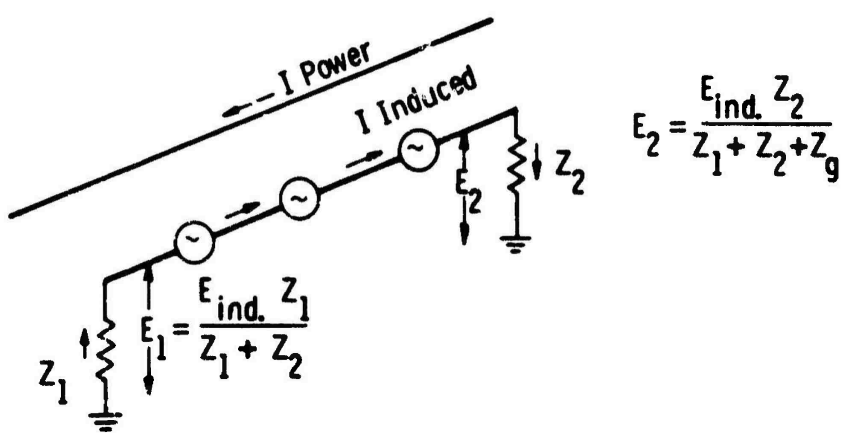
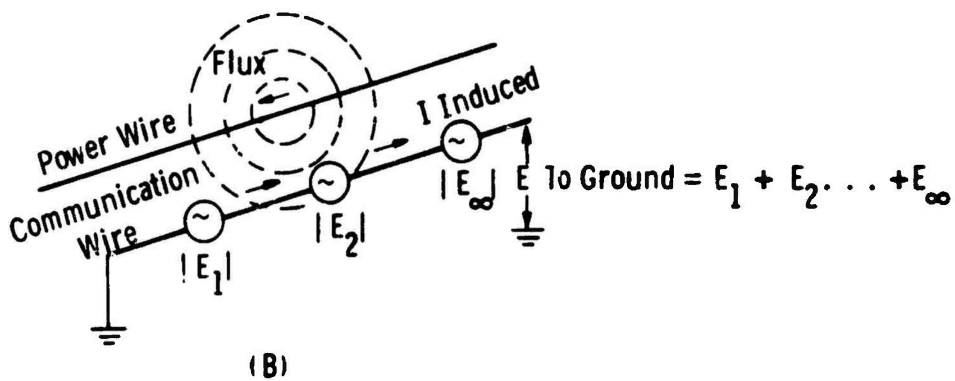


Fig. 1—Rise in station ground potential under fault conditions

Dwg. 4508306



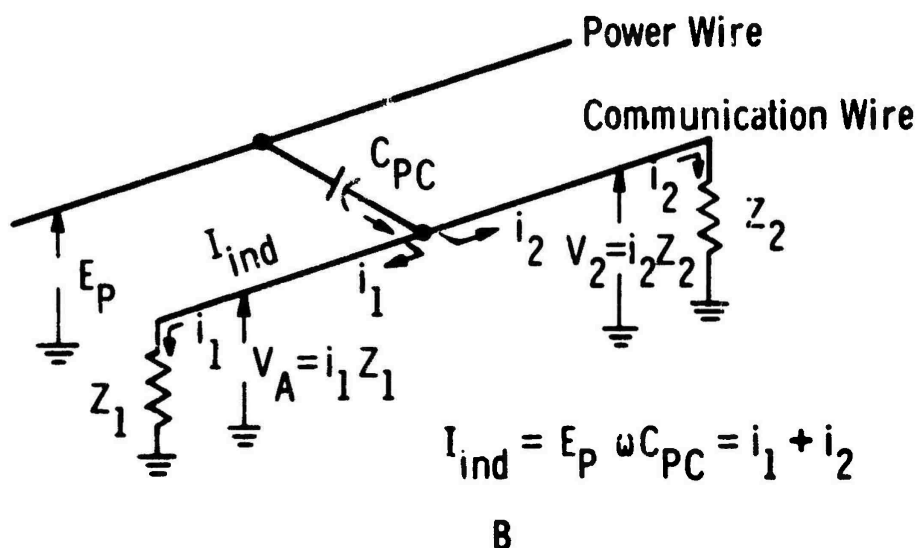
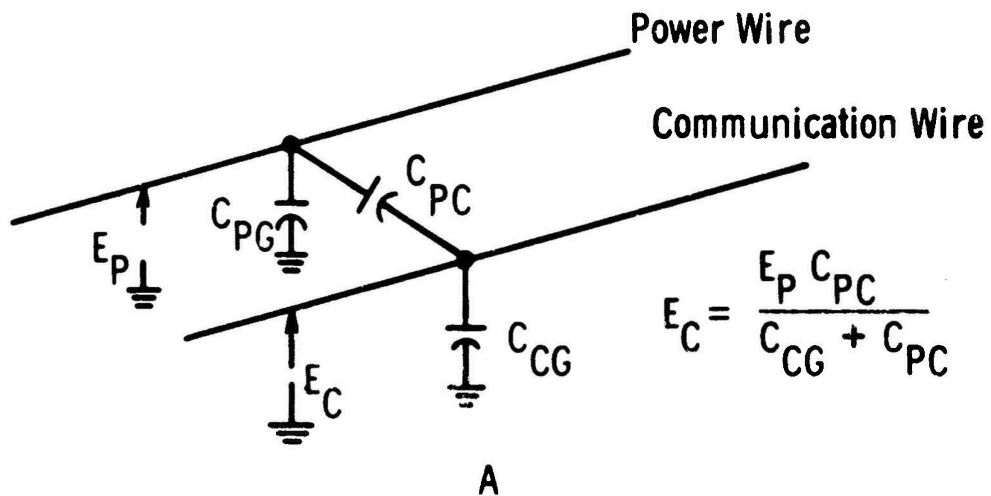
(A) Magnetic Induction Model



(C) Longitudinal Induction of Current Due to Power Wire Currents

Fig. 2-Magnetic induction model

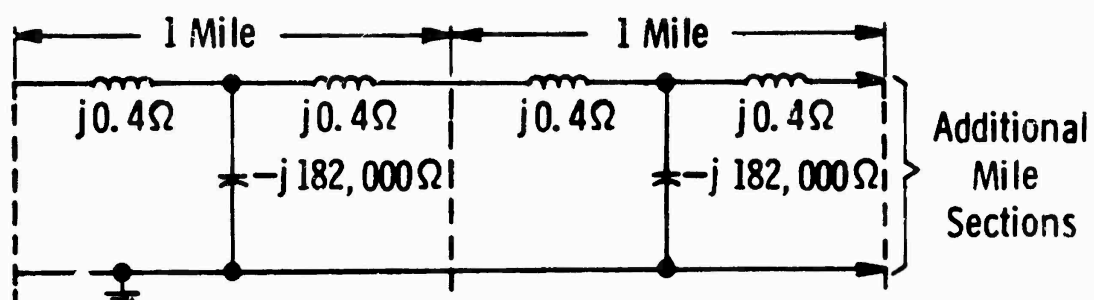
Dwg. 852A386



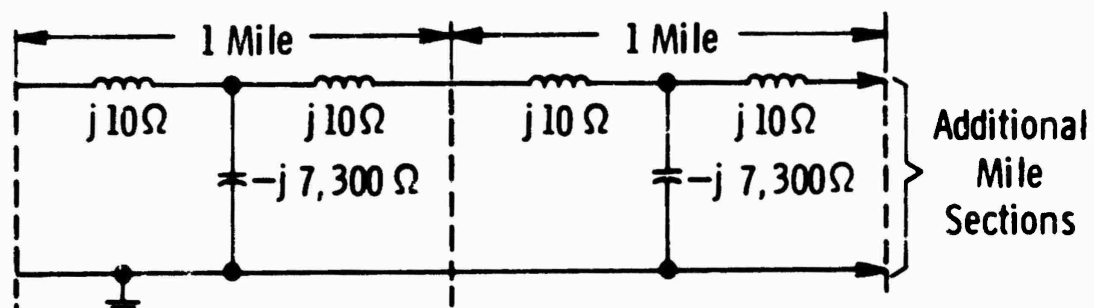
Longitudinal induction of current due to power wire voltages

Fig. 3-Electric induction model

Dwg. 852A387



(A) 60 Cycle Line Reactances



(B) 25th Harmonic Reactances

Fig. 4—Phase-to-neutral reactances of a typical transmission line

Curve 579109-A

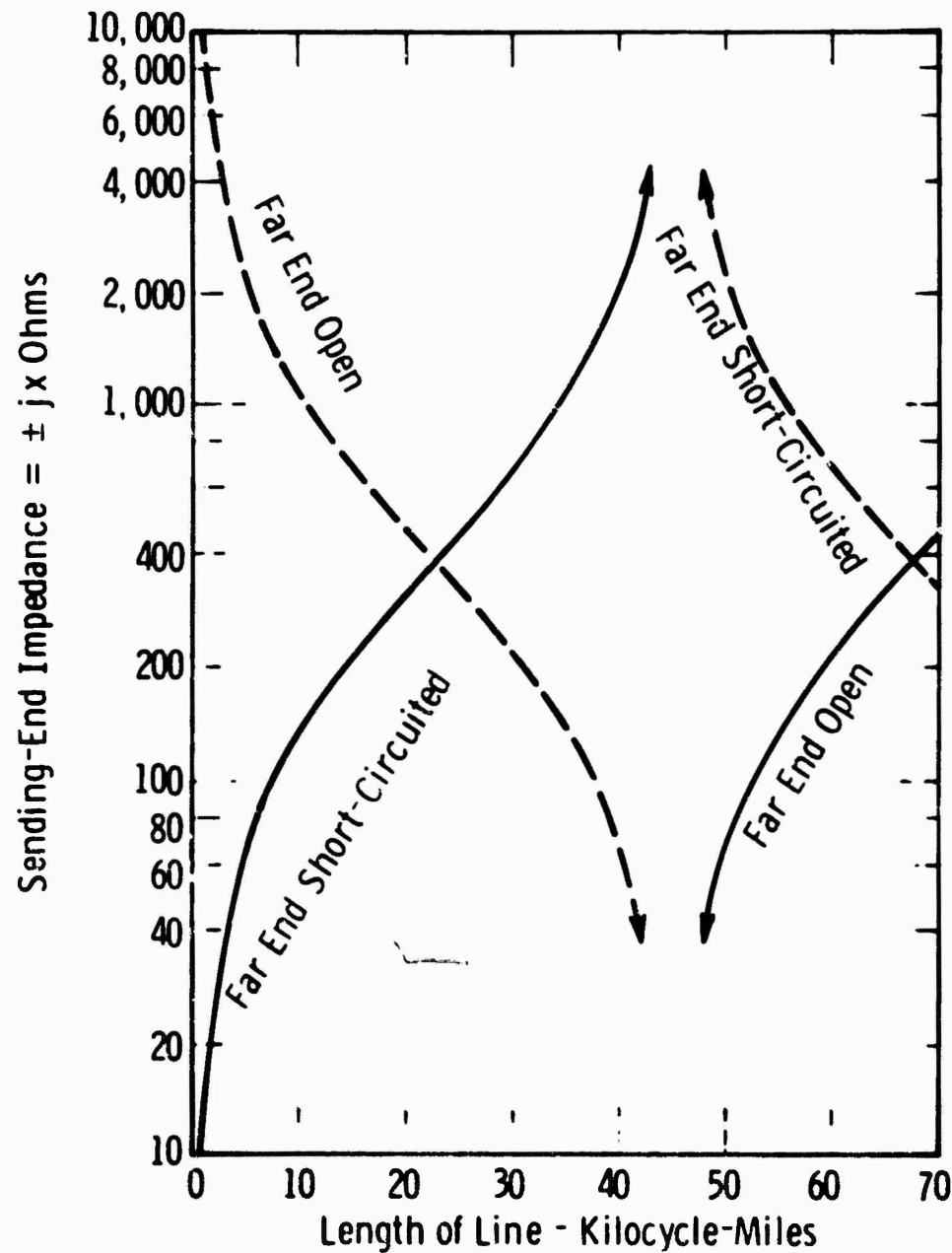


Fig. 5—Sending-end phase-to-neutral impedance of typical transmission line with far end open and short-circuited

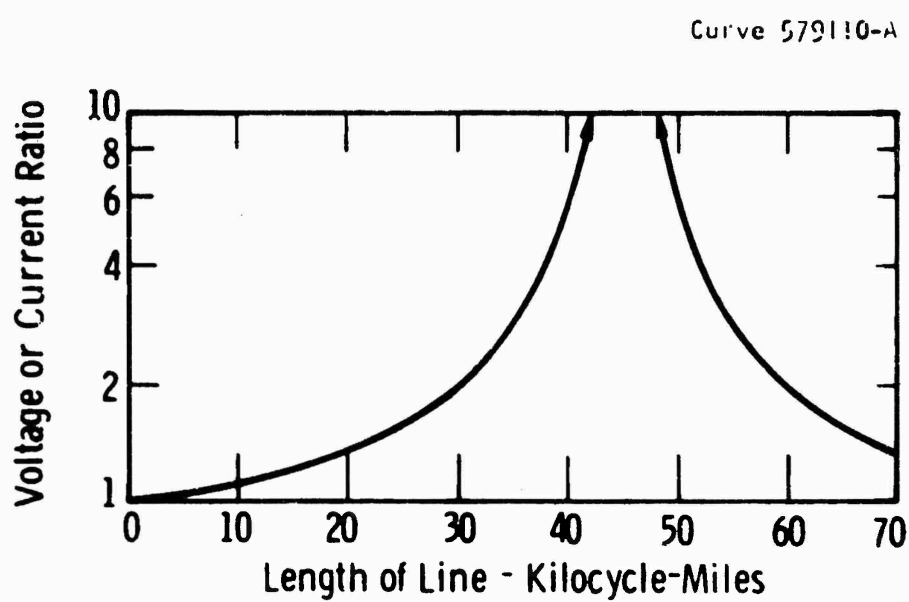


Fig. 6—Ratio of current at far end to current at near end with far end short-circuited and ratio of voltage at far end to voltage at near end with far end open

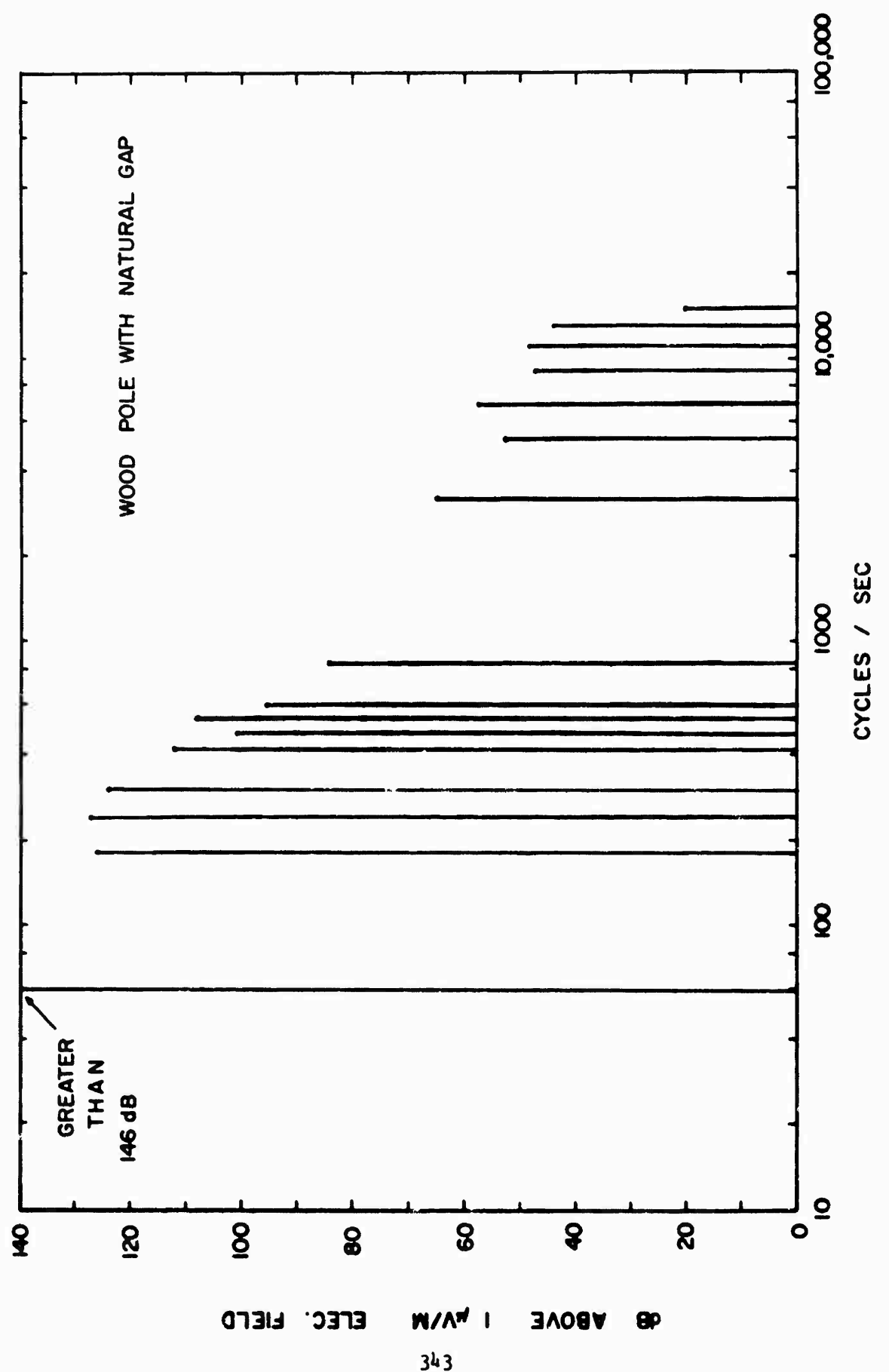


FIG 7 345 KV LINE HARMONICS 200 FEET FROM TOWER

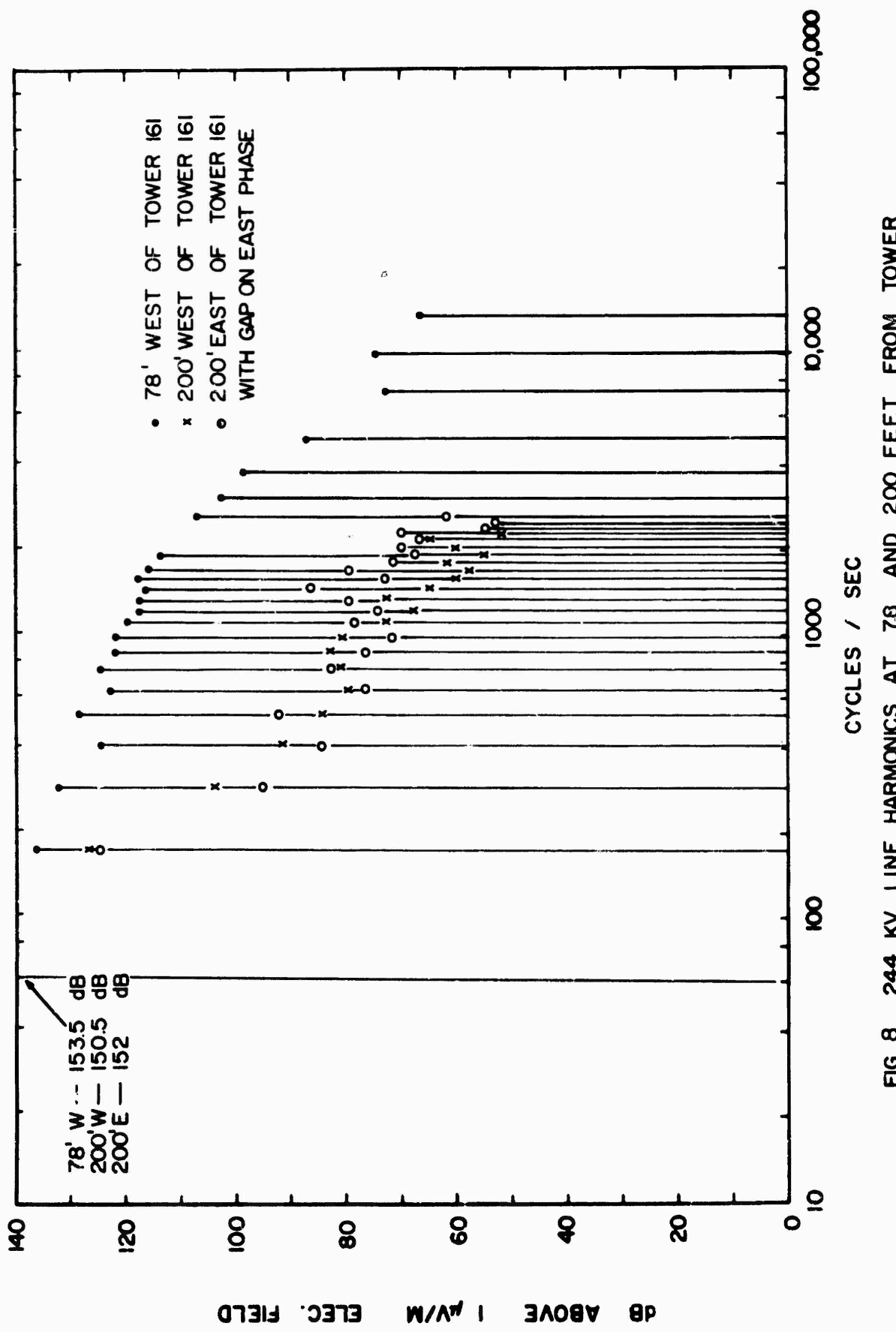


FIG. 8 244 KV LINE HARMONICS AT 78 AND 200 FEET FROM TOWER

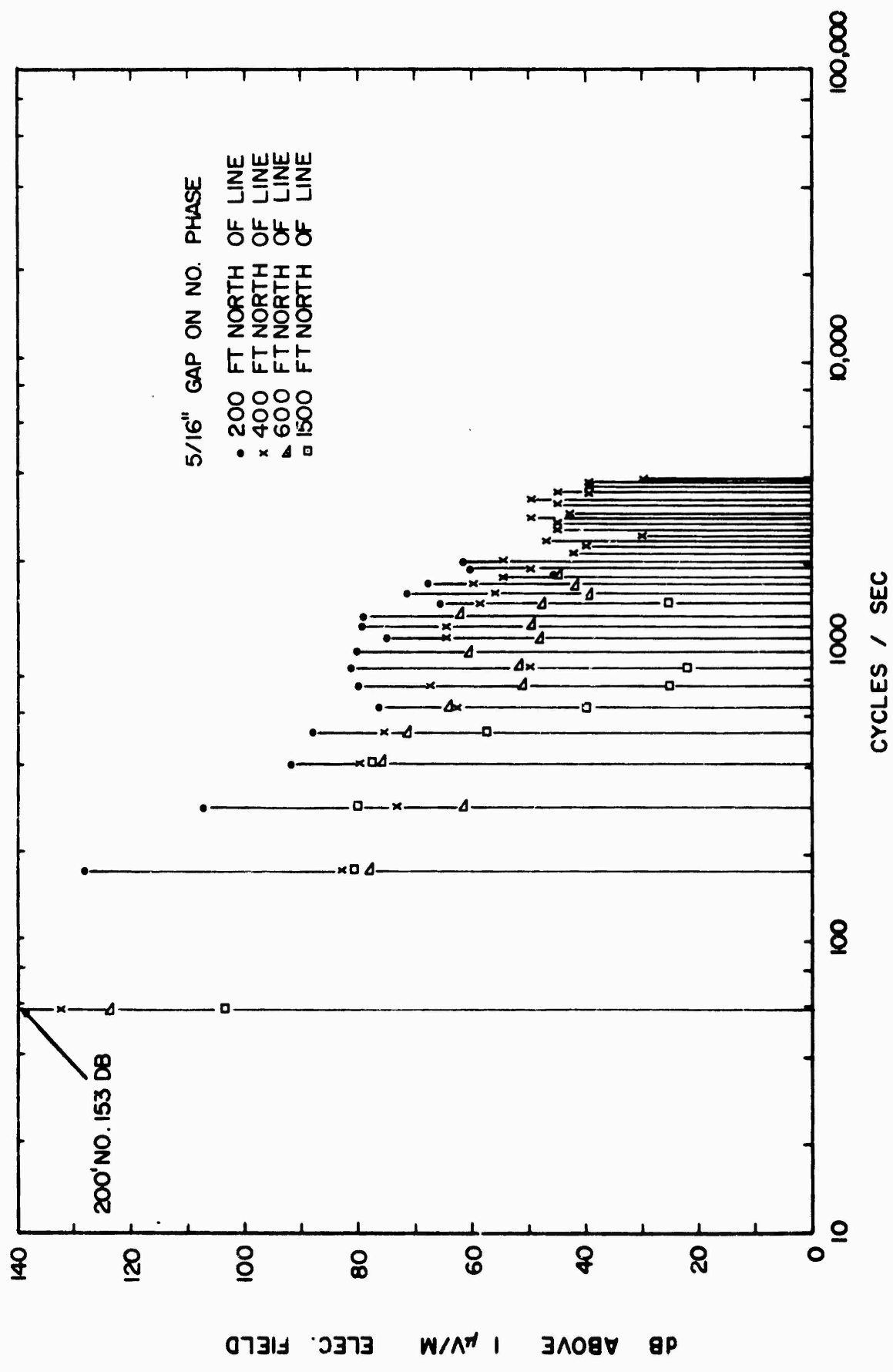


FIG 9 161 KV LINE HARMONICS AT 200, 400, 600, 1500 FEET FROM TOWERS LINE

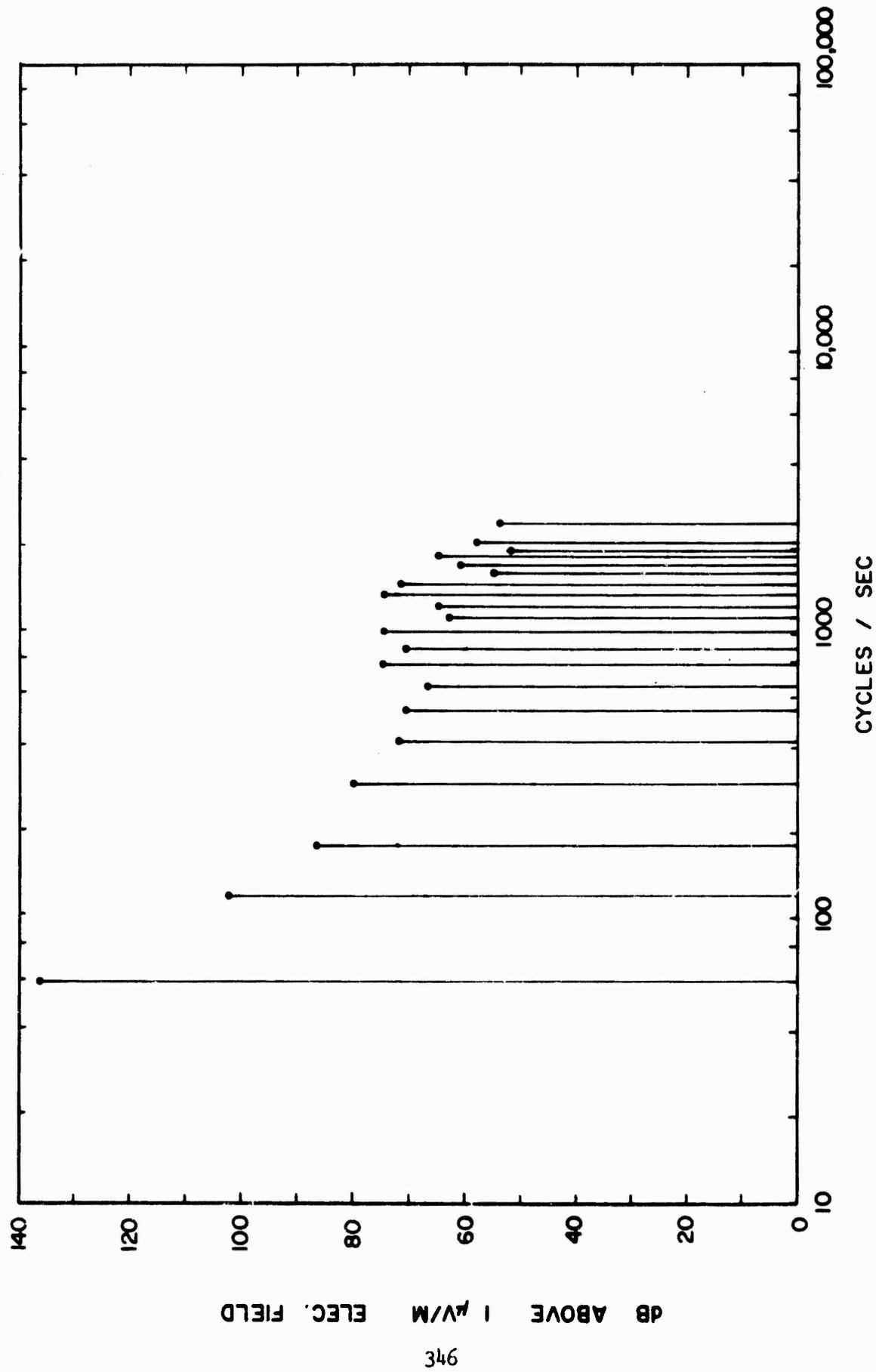


FIG. 10 69 KV LINE HARMONICS AT 200 FEET FROM TOWER

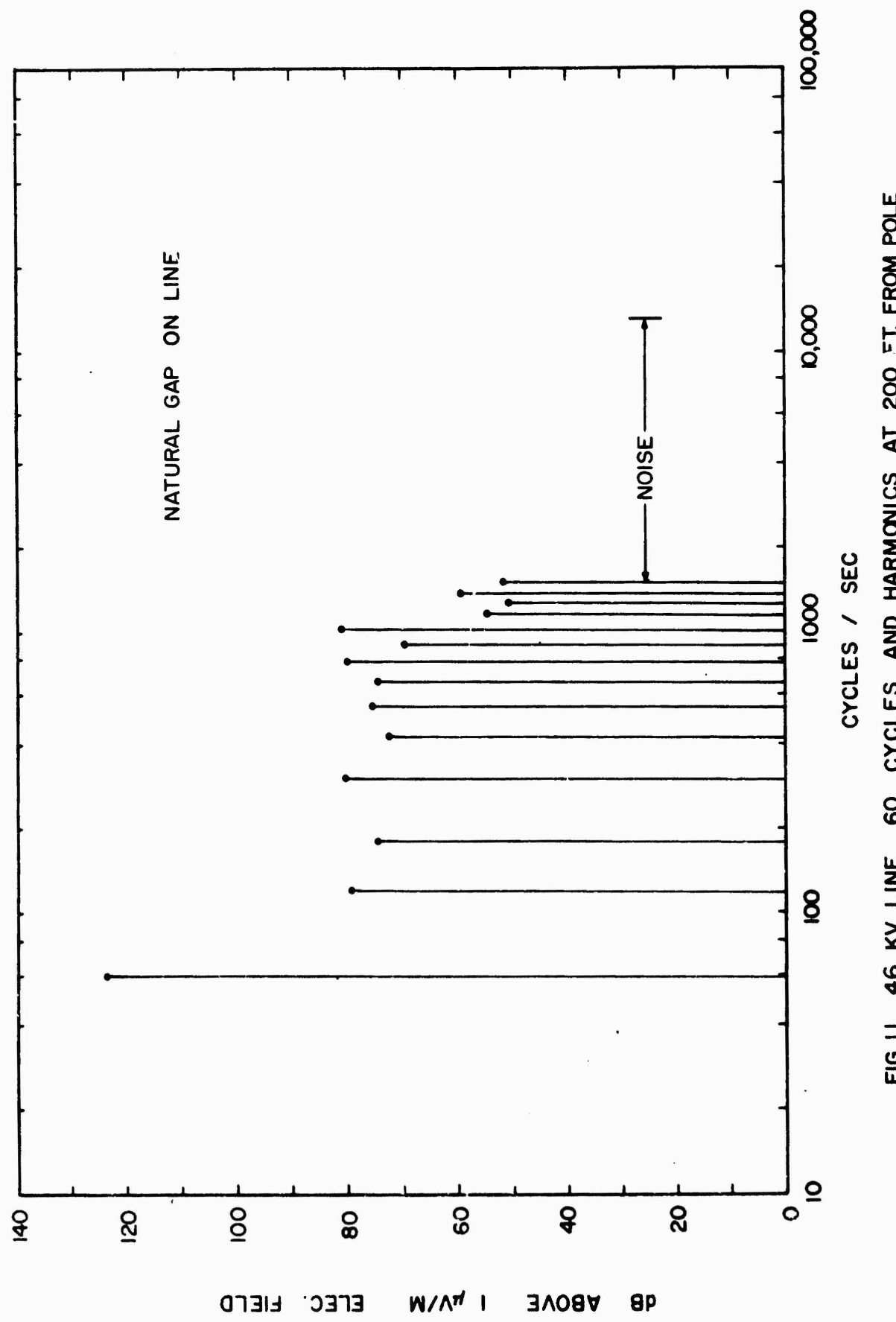


FIG. 11 46 KV LINE 60 CYCLES AND HARMONICS AT 200 FT. FROM POLE

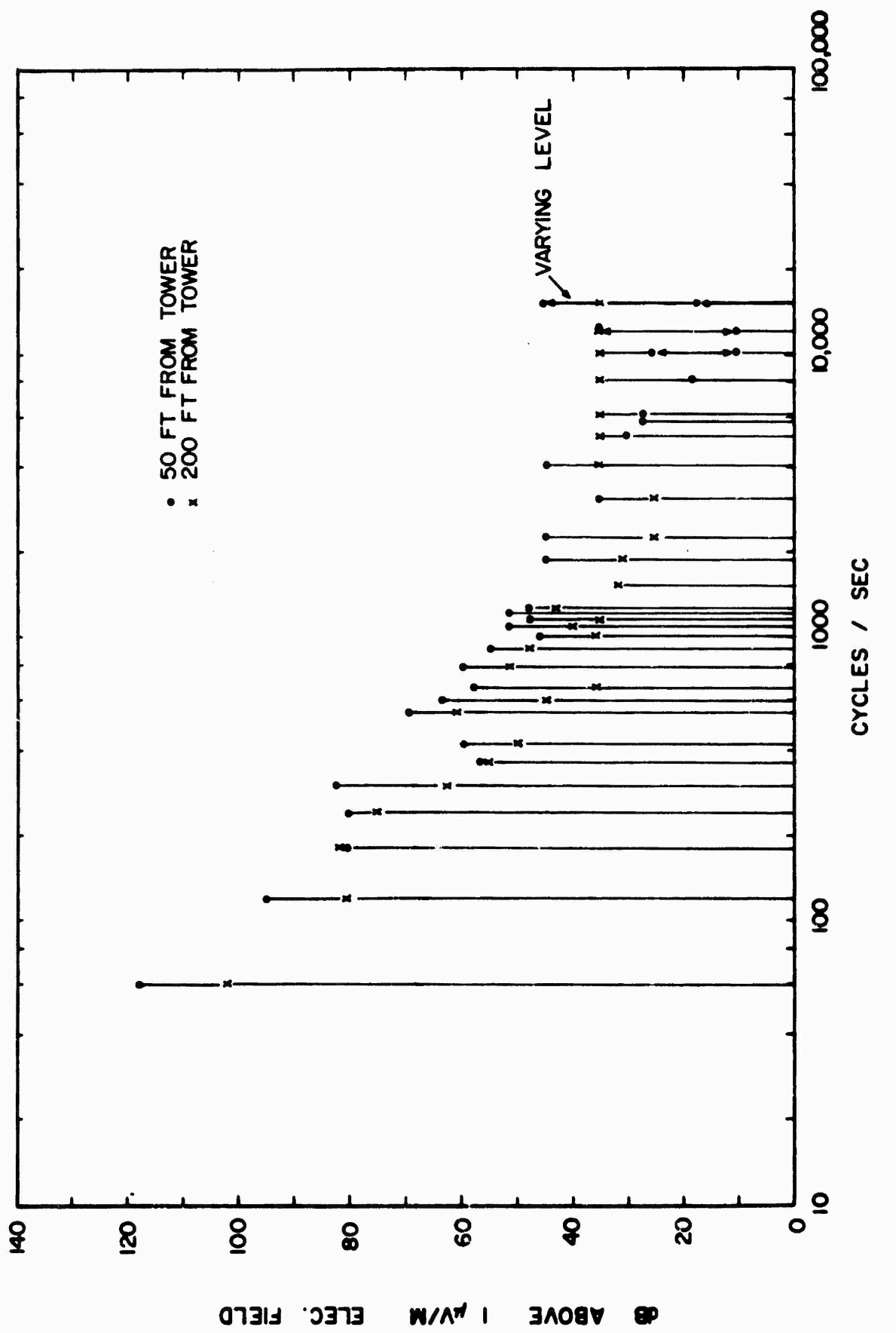


FIG.12 8 KV LINE HARMONICS AT 50 AND 200 FEET FROM POLE

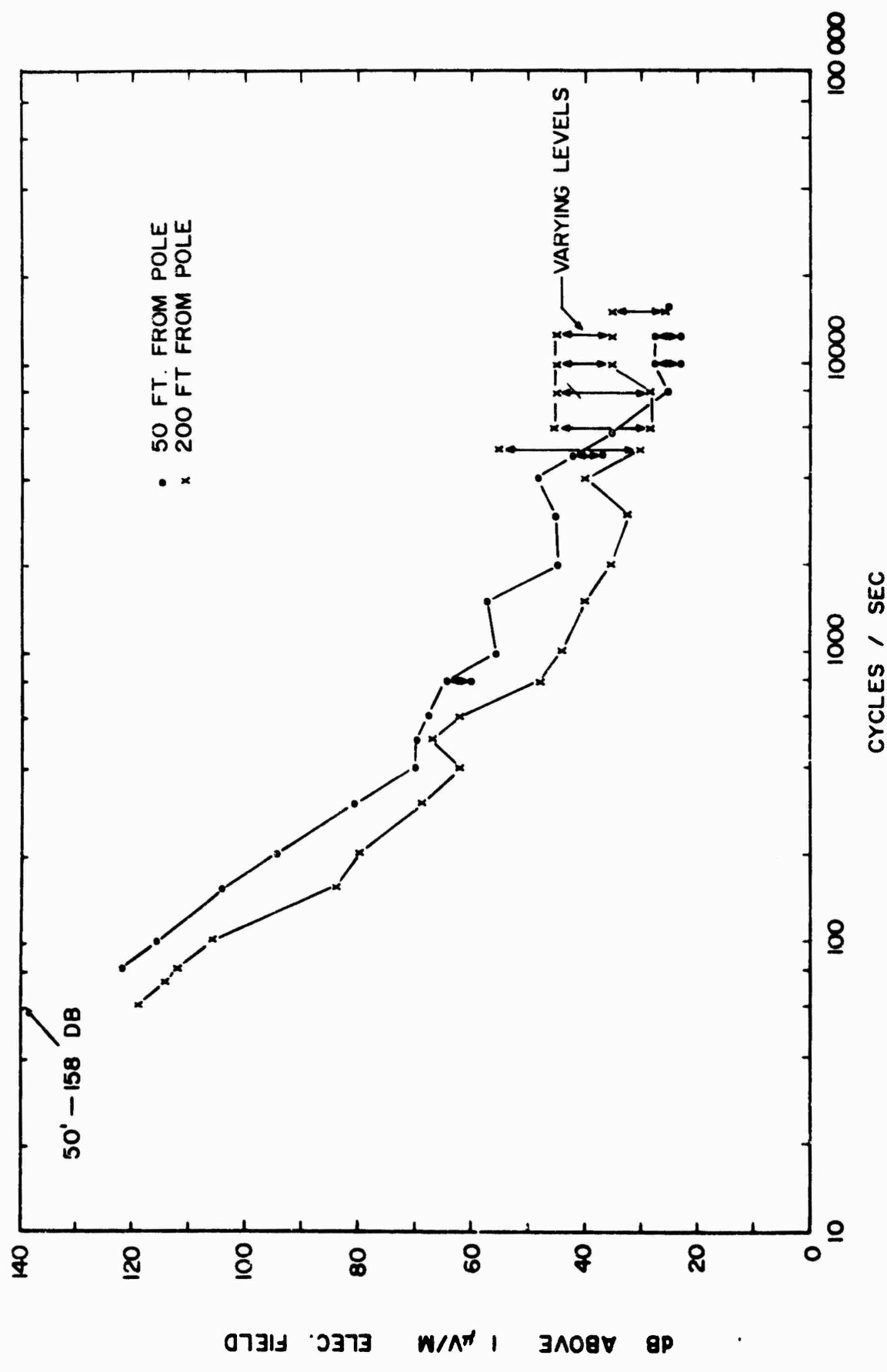


FIG 13 8 KV LINE HARMONICS WITH RECEIVER SET FOR 60 c/s BANDWIDTH

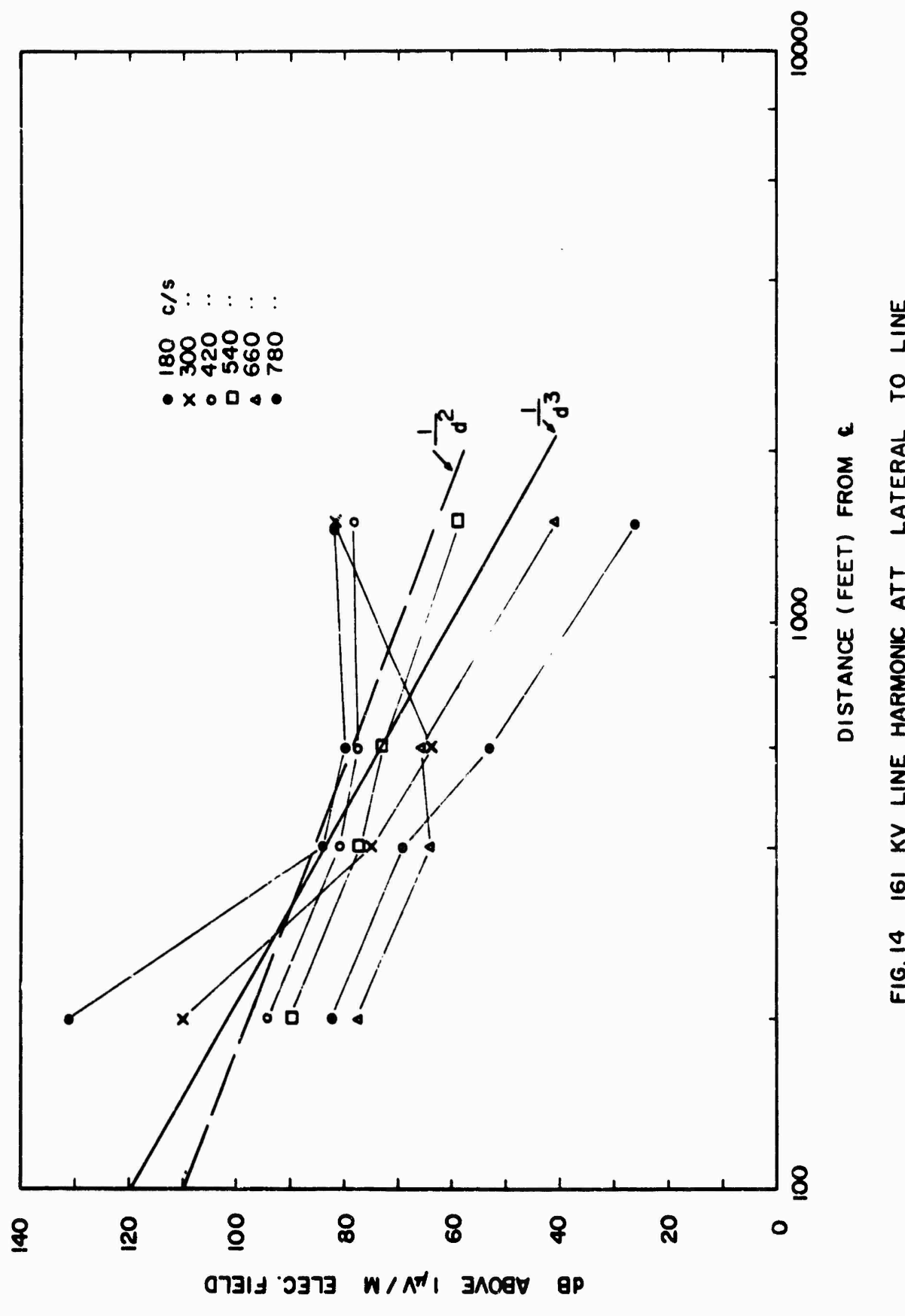


FIG. 14 161 KV LINE HARMONIC ATT LATERAL TO LINE

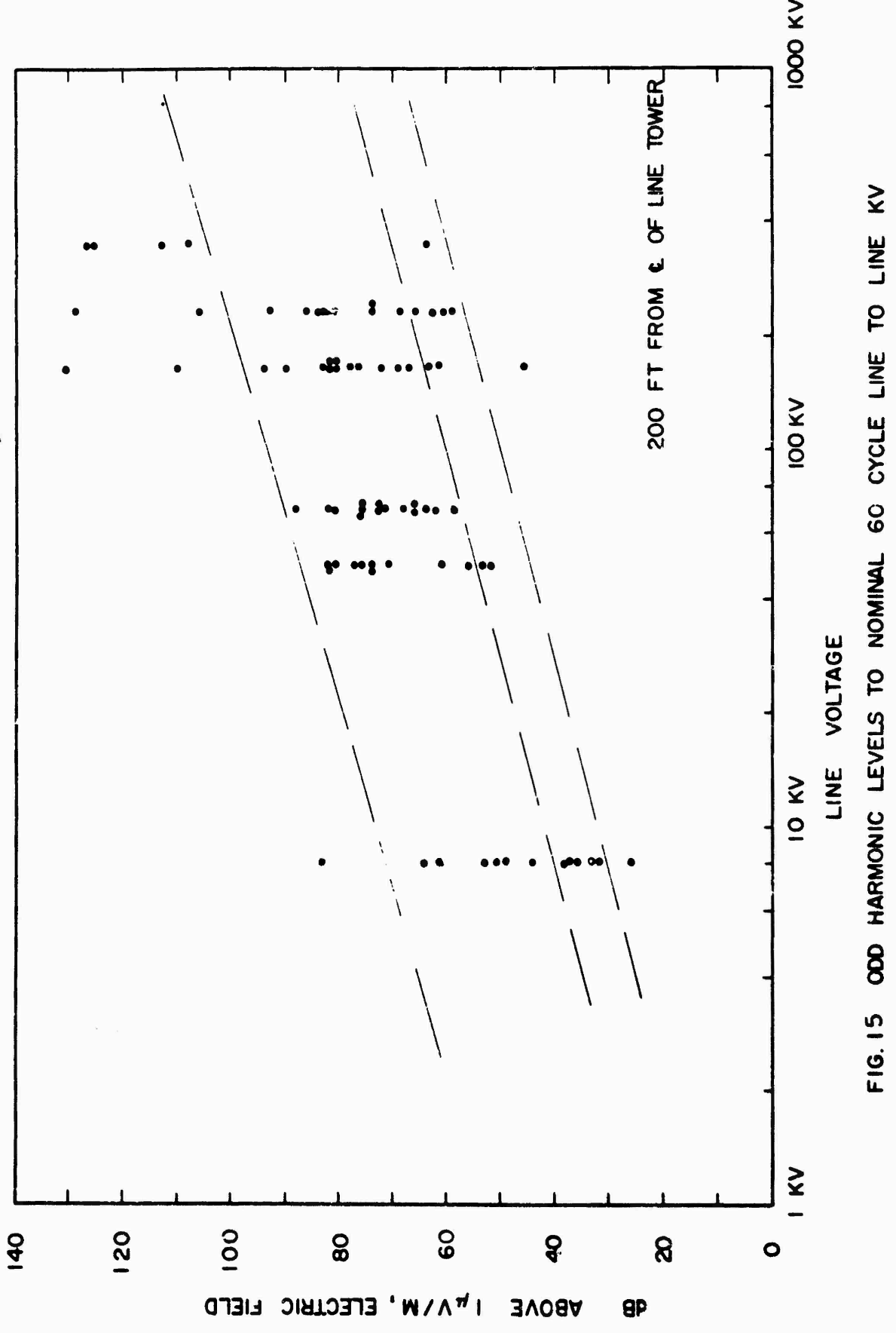


FIG. 15 ODD HARMONIC LEVELS TO NOMINAL 60 CYCLE LINE TO LINE KV

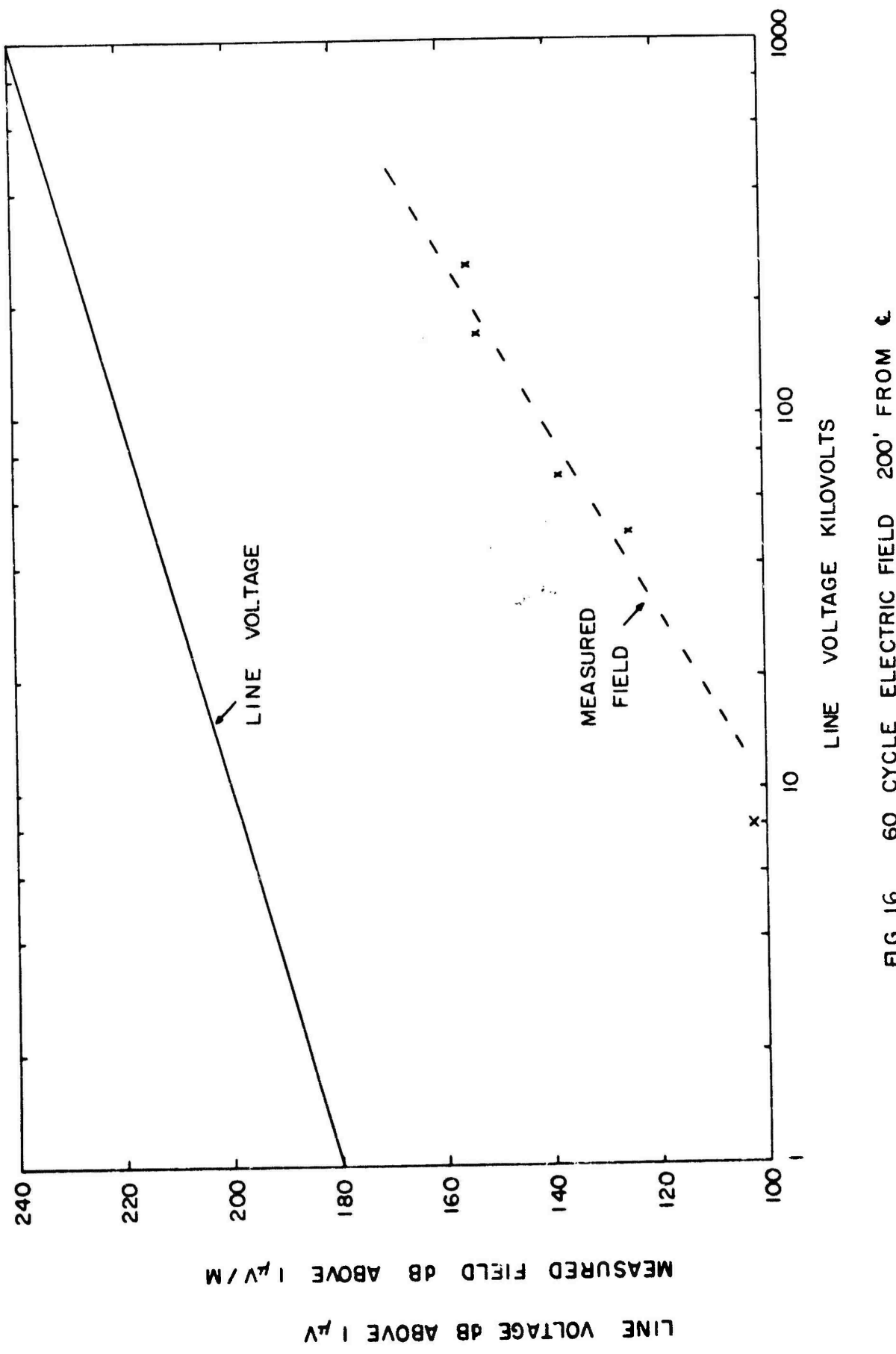


FIG. 16 60 CYCLE ELECTRIC FIELD 200' FROM L

UNCLASSIFIED

Security Classification

DOCUMENT CONTROL DATA - R&D

(Security classification of title, body of abstract and indexing annotation must be entered when the overall report is classified)

1. ORIGINATING ACTIVITY (Corporate author) Westinghouse Electric Corporation		2a. REPORT SECURITY CLASSIFICATION UNCLASSIFIED
		2b. GROUP
3. REPORT TITLE High Voltage Power Line Siting Criteria		
4. DESCRIPTIVE NOTES (Type of report and inclusive dates) Final		
5. AUTHOR(S) (Last name, first name, initial) W. E. Pakala E. R. Taylor, Jr. R. T. Harrold		
6. REPORT DATE March 1967	7a. TOTAL NO. OF PAGES 564	7b. NO. OF REPS 130
8a. CONTRACT OR GRANT NO. AF30(602)-3822 & PROJECT NO. 4540 c. Task 454002 d.	8b. ORIGINATOR'S REPORT NUMBER(S) 66-8EO-RADIO-RI 8d. OTHER REPORT NO(S) (Any other numbers that may be assigned to report) RADC-TR-66-606 Vol I-III	
10. AVAILABILITY/LIMITATION NOTICES This document is subject to special export controls and each transmittal to foreign governments, foreign nationals or representatives thereto may be made only with prior approval of RADC (EMLI), GAFB, N.Y. 13440		
11. SUPPLEMENTARY NOTES	12. SPONSORING MILITARY ACTIVITY Rome Air Development Center (EMCVI-1) Griffiss AFB NY 13440	

13. ABSTRACT

The purpose of this contract on High Voltage Power Line Siting Criteria is to determine the various factors involved and their effects on radio noise from power lines so that a communication site can be selected which will not be seriously affected by radio interference from existing lines or from proposed lines in the vicinity of the communication site.

Field strength measurements were made from 60 hertz to 1000 MHz on both wood pole and steel tower lines from 2.4 kV to 345 kV inclusive. Some measurements were attempted below 60 hertz without success. Measurements were also made with an artificial gap connected to a phase conductor at the tower. This was done in order to have a controllable and powerful radio noise generator for the measurement of spectra at various distances from the line. These measurements have been applied to estimation or prediction of radio noise with respect to the most important factors of distance from line and the frequency and to other factors such as line height, and antenna height and polarization.

The report also includes (1) laboratory measurement of conductor corona type radio noise with conductors of different diameters and different surface conditions (These measurements are applicable in the estimation of the magnitude of radio noise generation by extra high voltage line conductor corona.), (2) laboratory measurements of the frequency spectra of artificial gap-type radio noise generator and corona, (3) a bibliography of American and Foreign literature of importance

DD FORM 1473 JAN 64

UNCLASSIFIED

Security Classification

UNCLASSIFIED

Security Classification

14.	KEY WORDS	LINK A		LINK B		LINK C	
		ROLE	WT	ROLE	WT	ROLE	WT
	Power Line Interference Power Line Siting Criteria Power Line Corona Radio Frequency Interference Electric Discharge Electric Cables Electrical Corona						

INSTRUCTIONS

1. ORIGINATING ACTIVITY: Enter the name and address of the contractor, subcontractor, grantee, Department of Defense activity or other organization (corporate author) issuing the report.

2a. REPORT SECURITY CLASSIFICATION: Enter the overall security classification of the report. Indicate whether "Restricted Date" is included. Marking is to be in accordance with appropriate security regulations.

2b. GROUP: Automatic downgrading is specified in DoD Directive 5200.10 and Armed Forces Industrial Manual. Enter the group number. Also, when applicable, show that optional markings have been used for Group 3 and Group 4 as authorized.

3. REPORT TITLE: Enter the complete report title in all capital letters. Titles in all cases should be unclassified. If a meaningful title cannot be selected without classification, show title classification in all capitals in parenthesis immediately following the title.

4. DESCRIPTIVE NOTES: If appropriate, enter the type of report, e.g., interim, progress, summary, annual, or final. Give the inclusive dates when a specific reporting period is covered.

5. AUTHOR(S): Enter the name(s) of author(s) as shown on or in the report. Enter last name, first name, middle initial. If military, show rank and branch of service. The name of the principal author is an absolute minimum requirement.

6. REPORT DATE: Enter the date of the report as day, month, year, or month, year. If more than one date appears on the report, use date of publication.

7a. TOTAL NUMBER OF PAGES: The total page count should follow normal pagination procedures, i.e., enter the number of pages containing information.

7b. NUMBER OF REFERENCES: Enter the total number of references cited in the report.

8a. CONTRACT OR GRANT NUMBER: If appropriate, enter the applicable number of the contract or grant under which the report was written.

8b. &c. & 8d. PROJECT NUMBER: Enter the appropriate military department identification, such as project number, subproject number, system numbers, task number, etc.

9a. ORIGINATOR'S REPORT NUMBER(D): Enter the official report number by which the document will be identified and controlled by the originating activity. This number must be unique to this report.

9b. OTHER REPORT NUMBER(S): If the report has been assigned any other report numbers (either by the originator or by the sponsor), also enter this number(s).

10. AVAILABILITY/LIMITATION NOTICES: Enter any limitations on further dissemination of the report, other than those

imposed by security classification, using standard statements such as:

- (1) "Qualified requestors may obtain copies of this report from DDC."
- (2) "Foreign announcement and dissemination of this report by DDC is not authorized."
- (3) "U. S. Government agencies may obtain copies of this report directly from DDC. Other qualified DDC users shall request through .."
- (4) "U. S. military agencies may obtain copies of this report directly from DDC. Other qualified users shall request through .."
- (5) "All distribution of this report is controlled. Qualified DDC users shall request through .."

If the report has been furnished to the Office of Technical Services, Department of Commerce, for sale to the public, indicate this fact and enter the price, if known.

11. SUPPLEMENTARY NOTES: Use for additional explanatory notes.

12. SPONSORING MILITARY ACTIVITY: Enter the name of the departmental project office or laboratory sponsoring (paying for) the research and development. Include address.

13. ABSTRACT: Enter an abstract giving a brief and factual summary of the document indicative of the report, even though it may also appear elsewhere in the body of the technical report. If additional space is required, a continuation sheet shall be attached.

It is highly desirable that the abstract of classified reports be unclassified. Each paragraph of the abstract shall end with an indication of the military security classification of the information in the paragraph, represented as (TS), (SI), (C), or (F).

There is no limitation on the length of the abstract. However, the suggested length is from 150 to 225 words.

14. KEY WORDS: Key words are technically meaningful terms or short phrases that characterize a report and may be used as index entries for cataloging the report. Key words must be selected so that no security classification is required. Identifiers, such as equipment model designation, trade name, military project code name, geographic location, may be used as key words but will be followed by an indication of technical content. The assignment of links, roles, and weights is optional.

UNCLASSIFIED

Security Classification

SUPPLEMENTARY

INFORMATION

1 December 1969

DISTRIBUTION AND AVAILABILITY CHANGES

IDENTIFICATION	FORMER STATEMENT	NEW STATEMENT	AUTHORITY
AD-812 266 Westinghouse Electric Corp., Pittsburgh, Pa. Final rept. Rept. no. 66-8EO- RADIO-R1-Vol-1, RADC-TR-66-606- Vol-1 Mar 67 Contract AF 30(602)- 3822	No Foreign without approval of Rome Air Development Center, Attn: EMLI, Griffiss AFB, N. Y.	No limitation	RADC, USAF ltr, 14 Jul 69